

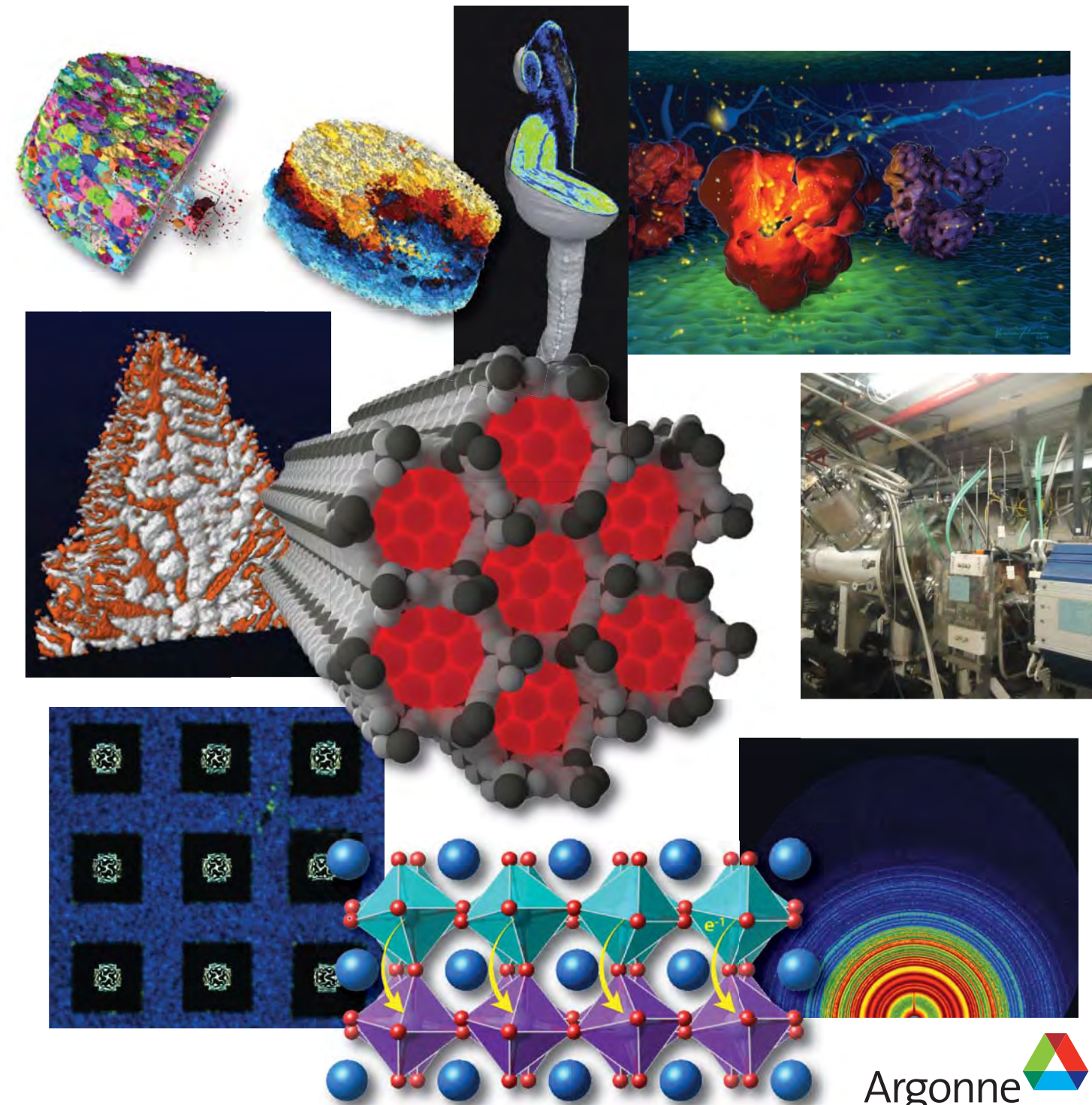
APS SCIENCE 2016  
May 2017 ANL-17/09

Argonne National Laboratory

# APS SCIENCE 2016

RESEARCH AND ENGINEERING HIGHLIGHTS FROM THE  
ADVANCED PHOTON SOURCE AT  
ARGONNE NATIONAL LABORATORY

ANL-17/09  
ISSN 1931-5007  
May 2017





# APS SCIENCE 2016

**RESEARCH AND ENGINEERING HIGHLIGHTS FROM THE  
ADVANCED PHOTON SOURCE AT  
ARGONNE NATIONAL LABORATORY**

# TABLE OF CONTENTS

## **ACCESS TO BEAM TIME AT THE ADVANCED PHOTON SOURCE**

2 WELCOME

4 THE ADVANCED PHOTON SOURCE UPGRADE PROJECT

## **5 APS ORGANIZATION CHART**

## **7 PALEONTOLOGY**

8 THE TALE OF THE TULLY MONSTER: A WEIRD WONDER FOSSIL FINDS A HOME

## **10 AROUND THE APS: AWARDS & HONORS**

## **11 ELECTRONIC & MAGNETIC MATERIALS**

12 THE TWISTED LIAISON BETWEEN MAGNETISM AND SUPERCONDUCTIVITY

14 CAN WE FLIP OUR UNDERSTANDING OF HIGH- $T_c$  SUPERCONDUCTORS?

16 SEEING STRIPES IN NICKELATES

18 A NOVEL ROUTE TO QUANTUM SPIN LIQUIDS

20 ANOMALOUSLY LARGE CHARGE TRANSFER IN AN ATOMIC LAYER CAKE OF TRANSITION METAL OXIDES

22 THE INNER RUMBLINGS OF NEW PHOTOVOLTAIC CHAMPION MATERIALS

24 ASYMMETRIC CLOSE ENCOUNTERS OF THE MAGNETIC KIND

26 SQUEEZING OUT A NOVEL CONFINED METAL IN AN INSULATOR

28 INDUCING POLARIZATION IN SUPERLATTICES BY ALTERNATING NON-FERROELECTRIC OXIDE LAYERS

30 A LINK BETWEEN CUPRATE LATTICE VIBRATIONS AND HIGH-TEMPERATURE SUPERCONDUCTORS

31 AN ATOMIC CONTRADICTION

33 SAMARIUM HEXABORIDE CONTINUES TO AMAZE

34 PROBING THE EFFECTS OF REDUCED STRAIN ON PSMO FILMS

36 WHAT'S A NICE PYROCHLORE LIKE YOU DOING WITH A SOC LIKE THAT?

38 STUDYING THE MAGNETIC BEHAVIOR OF SUPERCONDUCTING EUROPIUM

39 HOW A MULTIFERROIC STOPPED BEING FERROIC AND BECAME GLASSY

## **41 ENGINEERING MATERIALS & APPLICATIONS**

42 MODELING TEMPERATURE-DEPENDENT STRUCTURE IN SODIUM BORATE MELTS

44 COATING POROUS CRYSTALLINE FRAMEWORKS TO REPEL WATER AND OIL

46 PUTTING THE SQUEEZE ON HYDROGEN AND SODIUM FOR SUPERCONDUCTIVITY

48 COMPARING 3-D SHOCK DAMAGE IN COPPER TO ITS PRE-DAMAGED STATE

50 REVEALING GROWTH PATTERNS IN EUTECTIC MIXTURES

52 A HIGH-PERFORMANCE, LOW-TEMPERATURE SOLID OXIDE FUEL CELL

54 IMPROVING THE BRAIDS THAT BIND URANIUM FROM SEAWATER

56 ELECTRODES DISTORT THE PROPERTIES OF QUANTUM WELLS

58 AN ABUNDANT ALTERNATIVE TO LITHIUM-ION BATTERIES

60 ELECTRODE OPTIONS FOR LITHIUM-ION BATTERIES

62 BUILDING BETTER BATTERIES WITH SELENIUM AND SULFUR

63 GETTING THE MOST OUT OF MULTICRYSTALLINE SILICON

64 PUTTING A COAT ON A HOT TURBINE

67 IMPROVING THE DEVELOPMENT OF NEW MATERIALS FOR NUCLEAR ENERGY

68 THE WAY MAGNESIUM ALLOY STRESSES

70 DESIGNING MORE DURABLE MATERIALS WITH A 3-D-PRINTED TITANIUM ALLOY

71 SEEKING A LESS-EXPENSIVE, SAFER MEANS OF TRAPPING NOBLE GASES

## **73 SOFT MATERIALS & LIQUIDS**

74 IMAGING DRUG DISTRIBUTION FROM METERED-DOSE INHALERS

76 LOOKING AT THE LAG IN ROOM-TEMPERATURE IONIC LIQUIDS

77 GROWING INORGANIC CRYSTALS ON ORGANIC SELF-ASSEMBLED MONOLAYERS

78 TWO FOR ONE: SIMULTANEOUS X-RAY MEASUREMENTS OF DISSOLVED GAS AND CAVITATION BUBBLES

80 MEASURING THE MICROSTRUCTURE OF NATURAL GUMS

82 USING PRESSURE TO INTERROGATE THE BUNDLING BEHAVIOR OF AMPHIPHILES

84 SQUISHY POLYMER BALLS DON'T ALWAYS CONFORM

## **85 CHEMICAL SCIENCE**

86 NEON YIELDS SECRETS IN FIRST LOCK-UP

88 WHEN YOUR LATTICES DON'T LINE UP: CHARGE INVERSION NEAR WET CHARGED SURFACES

90 FAKING PHOTOSYNTHESIS TO MAKE HYDROGEN FUEL

92 THE MODEL CATALYST

94 NATURAL BUILDING BLOCKS FOR NEW CATALYSTS

96 PEPTIDE WRAPPING AIDS CATALYSIS

98 TRACKING THE ACTIVE COPPER SITES IN A CATALYTIC MINERAL

99 CARBON-ENCAPSULATED IRON PARTICLES FOR LESS EXPENSIVE, MORE EFFICIENT FUEL CELLS

101 BUBBLES GET IN THE WAY OF ELECTROLYSIS

102 A MATERIALS SOLUTION TO BREAKING THE OXYGEN-HYDROGEN BOND

104 TRANSFORMING HOW WE LIGHT THE WORLD

106 STRAINING IS BETTER FOR CATALYTIC REACTIONS

107 WHAT MAKES A GIANT MOLECULE STABLE?

109 IN THIS CONTAMINATION-RESISTANT CATALYST, EVERY PT ATOM IS AN ACTIVE SITE

110 BETTER THAN PERFECT

## **113 LIFE SCIENCE**

114 UNEARTHING THE MECHANISM OF THE FRANK-STARLING LAW, A CENTRAL REGULATOR OF HEART FUNCTION

116	HUNTING FOR TRACE ELEMENTS IN THE ZEBRAFISH EMBRYO
118	SILICON BIOMIMICRY
120	TAPBPR: A NOVEL PROTEIN CHAPERONE WITH A ROLE IN PEPTIDE EDITING IN IMMUNE RECOGNITION
122	AN UNUSUAL SHAPE CHANGE TO DELIVER SELENOCYSTEINE TO PROTEINS
124	CANCER RISK OF CHROMIUM SUPPLEMENTS FOR DIABETES
126	<b>DATA</b>
127	<b>STRUCTURAL BIOLOGY</b>
128	IS THE GATE LOCKED OR JUST SHUT?
130	NEW INSIGHTS INTO THE MECHANISMS UNDERLYING LYSOSOMAL DISEASE AND EBOLA INFECTION
132	FIGHTING EBOLA WITH AN ANTIBODY COCKTAIL
134	HOW A ZIKA PROTEIN COULD GUIDE VACCINE DEVELOPMENT
136	STRUCTURAL INSIGHTS INTO CANNABIS RECEPTORS COULD LEAD TO NEW THERAPIES
138	FROM TRASH TAG TO MAJOR CELLULAR MEDIATOR: THE EMERGING ROLE OF THE UBIQUITIN SYSTEM
140	A PROMISING NEW TOOL FOR DRUG DESIGN
144	STRUCTURE OF THE HUMAN SEROTONIN TRANSPORTER ELUCIDATES AN ANTIDEPRESSANT MECHANISM
142	THE STRUCTURE OF A PROTEIN THAT FACILITATES CANCER SPREAD
146	AN INSIDE LOOK AT A NOTORIOUS HOSPITAL-ACQUIRED INFECTION
148	HOW BACTERIA GET THEIR SUGAR FIX
150	OUTSMARTING ANTIBIOTIC-RESISTANT BACTERIA
152	BATTLING BACTERIAL RESISTANCE
154	WATCHING THE COMPLETE CYCLE OF CELLULOSE BIOSYNTHESIS
156	BEGINNING TO SEE THE LIGHT
158	LESSONS FROM IMPERFECT ATTEMPTS TO REPLICATE DAMAGED DNA
160	MODULATING A MAJOR DRIVER OF DEVELOPMENT
162	A NOVEL ROUTE TO A RNA CAP
164	HOW CELLS DISTRIBUTE GENETIC MATERIAL DURING CELL DIVISION
165	LEARNING THE TRICKS OF A DOUBLE-TIMING ENZYME
167	<b>ENVIRONMENTAL, GEOLOGICAL &amp; PLANETARY SCIENCE</b>
168	DISCOVERY OF A NEW MANTLE IRON OXIDE
170	REDUCING THE UNDERGROUND MIGRATION OF URANIUM
172	ENHANCING OUR UNDERSTANDING OF MANTLE MELT FRACTION
174	ICE WITH HYDROGEN STUFFING
176	OXYGEN FUGACITY IN CHROMITE: UNDERSTANDING THE SOLAR SYSTEM
178	THE RELATIONSHIP OF METAL IONS TO MANGANESE DEPOSITS IN WATER PIPES
179	<b>NANOSCIENCE</b>
180	BUILDING WITH DNA TINKER TOYS
182	CREATING BONDS FOR PROGRAMMABLE ATOMS
184	PEEKING INTO A MICROWAVE REACTOR
186	SOUNDING OUT THERMAL CONDUCTORS
188	<b>DATA</b>
189	<b>NOVEL ACCELERATOR &amp; X-RAY TECHNIQUES &amp; INSTRUMENTATION</b>
190	SUCCESSFUL INSTALLATION AND OPERATION OF SCU 18-2 AT APS SECTOR 6
191	FIRST TEST OF THE APS UPGRADE PROTOTYPE FEEDBACK CONTROLLER
192	A FAST-CORRECTOR POWER SUPPLY AND CONTROLLER FOR APS-U
193	SOLID-STATE RF AMPLIFIER R&D AT THE ADVANCED PHOTON SOURCE
194	NANODIAMOND BALLS GENERATE UNPRECEDENTED TERAPASCAL STATIC PRESSURE
196	FLUID TOPOLOGY IN REAL TIME
198	A NEW X-RAY BRAGG COHERENT DIFFRACTION 3-D IMAGING METHOD
199	STUDYING ULTRAFAST PHOTO-INDUCED MESOSCOPIC PHASE TRANSITIONS
201	PROBING THE MECHANICS OF PROTEIN FUNCTION
202	AN X-RAY VISION OF A METAL 3-D PRINTING PROCESS
204	A GRAPHENE WINDOW TO BETTER MICROFLUIDICS
206	FAST FIND FOR POLYMER GRATING ROUGH EDGES
208	ADDING WHITE X-RAYS FOR IMPROVED BRAGG COHERENT DIFFRACTION IMAGING
210	PRECISELY MEASURING SMALL STRAINS IN TINY VOLUMES
212	MAKING MORE-PERFECT THIN FILMS
213	A NEW IMAGING MODE USING A GERMANIUM ENERGY-DISPERSIVE STRIP DETECTOR
214	QUICK-SCANNING XAFS AT APS BEAMLINE 9-BM
215	NANO-CALORIMETRY FOR THE CONCURRENT DETERMINATION OF THERMODYNAMIC STATES OF X-RAY PROBED VOLUMES
216	A NEW BENT BRAGG-LAUE MONOCHROMATOR AT APS BEAMLINE 17-BM-B
217	THREE DIMENSIONAL, VARIABLE-WAVELENGTH, X-RAY BRAGG COHERENT DIFFRACTIVE IMAGING
219	MODELING WAVE PROPAGATION THROUGH NON-IDEAL OPTICS
220	STREAMING IMAGES TO POWDER PATTERNS AND PAIR DISTRIBUTION FUNCTIONS WITH GSAS-II
221	AERODYNAMIC LEVITATOR FOR HIGH-ENERGY X-RAY SCATTERING FROM HIGH-TEMPERATURE NUCLEAR MATERIALS
222	A NEW ERA FOR X-RAY FLUORESCENCE MICROSCOPY: FASTER, BETTER, MORE-AUTOMATED ANALYSIS
224	GENERAL-PURPOSE RECIPROCAL SPACE MAPPING SOFTWARE FOR USE AT THE APS
226	<b>TYPICAL APS MACHINE PARAMETERS</b>
226	<b>APS SOURCE PARAMETERS</b>
228	<b>ACKNOWLEDGMENTS</b>



# ACCESS TO BEAM TIME AT THE ADVANCED PHOTON SOURCE

Five types of proposals are used at the Advanced Photon Source (APS): general user, partner or project user, collaborative access team (CAT) member, CAT staff, and APS staff. All beam time at the APS must be requested each cycle through the web-based Beam Time Request System. Each beam-time request (BTR) must be associated with one of the proposals mentioned above.

## GENERAL USER PROPOSALS AND BTRs

Proposals are peer reviewed and scored by a General User Proposal Review Panel, and time is allocated on the basis of scores and feasibility. A new BTR must be submitted each cycle; or each cycle, allocation is competitive. Proposals expire in two years or when the number of shifts recommended in the peer review has been utilized, whichever comes first.

## PARTNER OR PROJECT USER PROPOSALS AND BTRs

Proposals are peer reviewed by a General User Proposal Review Panel and reviewed further by a subcommittee of the APS Scientific Advisory Committee and by APS senior management. Although a new BTR must be submitted each cycle, a specific amount of beam time is guaranteed for up to three years.

## CAT MEMBER PROPOSALS

Proposals from CAT members are typically much shorter and are reviewed by processes developed by individual CATs. Allocation/scheduling is determined by the CAT management.

## CAT AND APS STAFF MEMBER PROPOSALS AND BTRs

These proposals are also very short and are reviewed through processes developed by either the CAT or the APS. Each CAT/beamline determines how beam time is allocated/scheduled. Collaborative access team and/or APS staff may submit general user proposals, in which case the rules for general user proposals and BTRs are followed.

In addition to the above, the APS has developed an industrial measurement access mode (MAM) program to provide a way for industrial users to gain rapid access for one-time measurements to investigate specific problems. A MAM proposal expires after one visit.

The APS User Information page (<https://www1.aps.anl.gov/Users-Information>) provides access to comprehensive information for prospective and current APS users.





## THE ADVANCED PHOTON SOURCE FACILITY AT ARGONNE NATIONAL LABORATORY

The Advanced Photon Source (APS) occupies an 80-acre site on the Argonne National Laboratory campus, about 25 miles from downtown Chicago, Illinois. It shares the site with the Center for Nanoscale Materials and the Advanced Protein Characterization Facility.

For directions to Argonne, see <http://www.anl.gov/directions-and-visitor-information>.

The APS, a national synchrotron radiation research facility operated by Argonne for the U.S. Department of Energy (DOE) Office of Science, provides this nation's brightest high-energy x-ray beams for science. Research by APS users extends from the center of the Earth to outer space, from new information on combustion engines and microcircuits to new drugs and nanotechnologies whose scale is measured in billionths of a meter. The APS helps researchers illuminate answers to the challenges of our high-tech world, from developing new forms of energy, to sustaining our nation's technological and economic competitiveness, to pushing back against the ravages of disease. Research at the APS promises to have far-reaching impact on our technology, our economy, our health, and fundamental knowledge of the materials that make up our world.

### CONTACT US

For more information about the APS send an email to [apsinfo@aps.anl.gov](mailto:apsinfo@aps.anl.gov) or write to APS Info, Bldg. 401, Rm. A4115, Argonne National Laboratory, 9700 S. Cass Ave., Argonne, IL 60439.

To order additional copies of this, or previous, issues of *APS Science* email to [apsinfo@aps.anl.gov](mailto:apsinfo@aps.anl.gov).



To download PDF versions of *APS Science*  
back issues go to  
[www.aps.anl.gov/Science/Reports/](http://www.aps.anl.gov/Science/Reports/)

Visit the APS on the Web at  
[www1.aps.anl.gov/](http://www1.aps.anl.gov/)





# WELCOME



Stephen K. Streiffer

May 2017

Those of us who are fortunate enough to be entrusted with operation of a research facility such as the Advanced Photon Source (APS) like to mark the passing of time with milestones. As you can see from the chronology on the facing page, the APS has had a lot of them. For instance, in 1995, the first x-ray light from our accelerator was cheered (and we made sure to celebrate the 20th anniversary).

But the milestone we use as our touchstone is the one in 1996 when our sponsor, the U.S. Department of Energy (DOE), gave the APS official sanction to begin operations and the first high-brightness x-ray beams flashed down a beamline to users waiting enthusiastically in our experiment hall.

Today, thousands of users, more than 20,000 (and counting) peer-reviewed publications, and myriad discoveries about our world later, we are tightening our focus on the future of the APS and synchrotron x-ray science with great excitement.

While free-electron lasers, such as our sister DOE Office of Science facility the Linac Coherent Light Source at SLAC National Accelerator Laboratory, have opened exciting new vistas for x-ray science, new ideas for particle accelerators, x-ray beamline instrumentation, and experimental techniques are

revolutionizing the future of storage ring-based x-ray sources like the APS here at Argonne National Laboratory. We plan on taking full advantage of those new ideas.

At the age of 21, the APS is, in people years, just entering maturity. We'll buy that. Twenty-one years on from those first x-rays, we like to think we have this light source business figured out. We routinely deliver x-rays dependably, on schedule; those x-ray beams are stable (they hit where they are needed); and we know, as we've always known, that the well-being and productivity of our customers, the users, drive everything we do.

So, now it is time to look toward building (literally) on the lessons learned and knowledge gained. We have embarked on a plan supported by our sponsor, the DOE, that will prepare the APS for the next phase in x-ray science and discovery. This plan, the APS Upgrade, will couple a vastly improved x-ray source to innovative, cutting-edge beamline instruments. The immediate beneficiaries of this plan will be our staff, who get to build and operate an exciting new machine, and our users, who will do as they have always done: produce a torrent of new research while expanding the possibilities afforded by new technologies.

Long-term, the winners will be our fellow citizens, whose lives will be further enriched by the breakthroughs that the APS Upgrade will enable, just as they have benefited from the science already produced at the present APS.

Jim Kerby, at the time of this writing the APS Upgrade Interim Project Director, follows this "Welcome" with an eloquent appreciation of Stuart Henderson, who successfully shepherded the APS Upgrade before leaving us to take the well-deserved job as Director of the DOE's Jefferson Lab. Working with Stuart has been a highlight of my time at the APS.

We think the Upgrade is well regarded in the places that matter. We like it a lot. You could even go so far as to say we are thrilled by the possibilities it presents; you would be correct.

But the Upgrade itself is only one part of our goal for the APS.

Every successful organization needs a vision. This is ours: Operate and develop hard x-ray user facilities and advance the forefront of x-ray science, transforming exploration of energy, biological, and other functional materials, chemistries, and systems, to overcome global challenges to sustainable energy, health, and national security.

We want to play a central role in advancing hard x-ray science and technology as we exploit the APS Upgrade x-ray energy, brightness, and coherence. We aim to leverage the leadership computing, math, and computer science resources at Argonne in order to meet the computational challenges presented by an ever-increasing torrent of research data that can only grow in the time of the Upgrade. We will leverage Argonne leadership in hard x-ray science across the Lab to ensure that the Upgrade fulfills its research mission. And we will create an atmosphere where our people can develop concepts for future x-ray sources and accelerator technologies. All this, while we sustain excellence, improve efficiency in day-to-day APS operations, operate in a manner that assures the safety of our staff and users and respects the environment, maintain a diverse and nurturing workplace, and prepare the next generations of scientists.

These are the very definition of lofty goals, but my time at the APS has given me great confidence in the ability of our people; I know they will deliver.

I hope you will read the highlights in this 15th edition of *APS Science* with an appreciation for the remarkable research enabled by our staff and produced by our users. At the same time, look at these highlights as preludes to the great science still to come.

*Stephen K. Streiffer*

*Argonne National Laboratory*

*Associate Laboratory Director,*

*Photon Sciences;*

*and Director, Advanced Photon Source*

# ADVANCED PHOTON SOURCE CHRONOLOGY

**March 14, 1984:** "Planning Study for Advanced National Synchrotron-Radiation Facilities," sponsored by the U.S. Department of Energy (DOE) Office of Basic Energy Sciences (Peter Eisenberger and Michael L. Knotek, co-chairs), gives first priority to construction of synchrotron-radiation facility optimized for insertion devices

**July 24, 1984:** "Major Facilities for Materials Research and Related Disciplines," sponsored by the Major Materials Facilities Committee of the Commission on Physical Sciences, Mathematics, and Resources of the National Research Council (Dean E. Eastman and Frederick Seitz, co-chairs), gives highest priority to construction of facility with undulator radiation in the hard x-ray region of spectrum

**February 1986:** "6-GeV Synchrotron X-Ray Source Conceptual Design Report" published by Argonne National Laboratory

**April 1987:** "7-GeV Advanced Photon Source Conceptual Design Report" published by Argonne National Laboratory

**May 1988:** DOE approves new-project start

**October 1, 1989:** First construction funds released by DOE

**June 4, 1990:** Groundbreaking ceremony and start of Advanced Photon Source (APS) facility construction

**October 7, 1993:** Begin linac commissioning (50-MeV electron beam)

**April 17, 1994:** First electron beam stored in particle accumulator ring

**July 31, 1994:** Linac positron-current performance specifications met

**January 22, 1995:** First 7-GeV electron beam in booster synchrotron

**February 20, 1995:** First injection of 7-GeV electron beam from booster synchrotron to storage ring

**March 18, 1995:** First turn of 7-GeV electron beam in storage ring

**March 25, 1995:** First stored electron beam (4.5 GeV)

**March 26, 1995:** First storage ring bending magnet radiation detected in Sector 1 (beamline 1-BM-A)

**April 15, 1995:** First stored 7-GeV electron beam

**August 9, 1995:** First x-ray beam from APS undulator in Sector 1 (beamline 1-ID)

**October 11, 1995:** Attain DOE storage-ring commissioning milestone of 20-mA operation, minimum 10 hours of beam lifetime

**January 12, 1996:** First 100-mA stored electron beam

**January 26, 1996:** First undulator operated with 100-mA stored electron beam

**May 1, 1996:** APS dedication ceremony in APS experiment hall

**July 30, 1996:** First stored 7-GeV positron beam

**July 31, 1996:** First stored positron beam at 100-mA current

**August 8, 1996:** Secretary of Energy signs Key Decision #4 declaring project completion milestone





# The Advanced Photon Source Upgrade Project



Stuart Henderson

This is a bittersweet update for me to finish. As many of you may know, I have left Argonne National Laboratory and the Advanced Photon Source to serve as the next Director of Jefferson Laboratory.

It is hard to believe that I came to the APS just three years ago to continue the great work done earlier on the APS Upgrade (APS-U). It has been a real pleasure and a tremendously satisfying experience for me to lead the great team that we've assembled toward delivering a state-of-the-art facility to support the needs of the scientific community for the foreseeable future.

Importantly, the project's timeline remains on track, thanks to the tremendous efforts of many people at the APS and within the broader APS community.

Last fall, the Department of Energy approved Critical Decision 3B for the APS-U. This important step provides the authority to begin procurement of long-lead components, and we are working toward the first procurements of production hardware later this year. The procurement plan calls for placing an order for the first set of the APS-U quadrupole magnets, which is an important step in the trajectory of the APS-U.

In addition, in mid-March DOE's Basic Energy Sciences (BES) Program held a status review of the project to assess our progress toward the next major milestone – the preparation of the proposed “baseline” for the project, which is the firm scope, cost and

schedule for the APS-U. This is a critical next step. To that end, project staff are hard at work to complete the preliminary design and document the technical design in a Preliminary Design Report, one of the key deliverables for approval of the project's baseline.

We know we are moving in the right direction toward completing the Upgrade, so as to meet the scientific needs of our more than 5000 academic, laboratory and industrial researchers – while also driving the discoveries and processes that will make life better for everyone.

Lastly, the project remains in very capable hands: at the time of writing, Jim Kerby is serving as Interim Project Director, providing the experience and continuity required to keep the project on track. In addition, Mark Beno was named Technical Director for the APS-U, a newly created position in which he will offer high-level technical expertise, with an emphasis on integrating APS-U investments with the overall APS beamline strategy. Meanwhile, the search process for the next APS-U Project Director is under way.

I am grateful for all the hard work and support that so many people have shown for this important project.

Thank you, and onward!

*Stuart Henderson*  
*former APS-U Project Director*



Jim Kerby

I believe I speak for everyone on the APS-U Project in expressing our thanks to Stuart and wishing him the

very best at Jefferson Laboratory. His leadership of the APS-U has been exceptional, as can be seen by the facts that the Project is on very solid ground.

That said, the Project is continuing to move forward. Later this year, the APS-U Preliminary Design Report will be complete, and will show the evolution of our design over the course of the past several years. In the accelerator systems area, the largest single change has been improvement of the storage ring emittance to 42-picometers, more than 30% lower than the previous design. In the experimental systems area, we have engaged the community to further develop our science case, and develop the requirements for insertion devices, front ends and feature beamlines to enable the exploration of that science. Thanks are due to everyone, staff and users, who helped in this process.

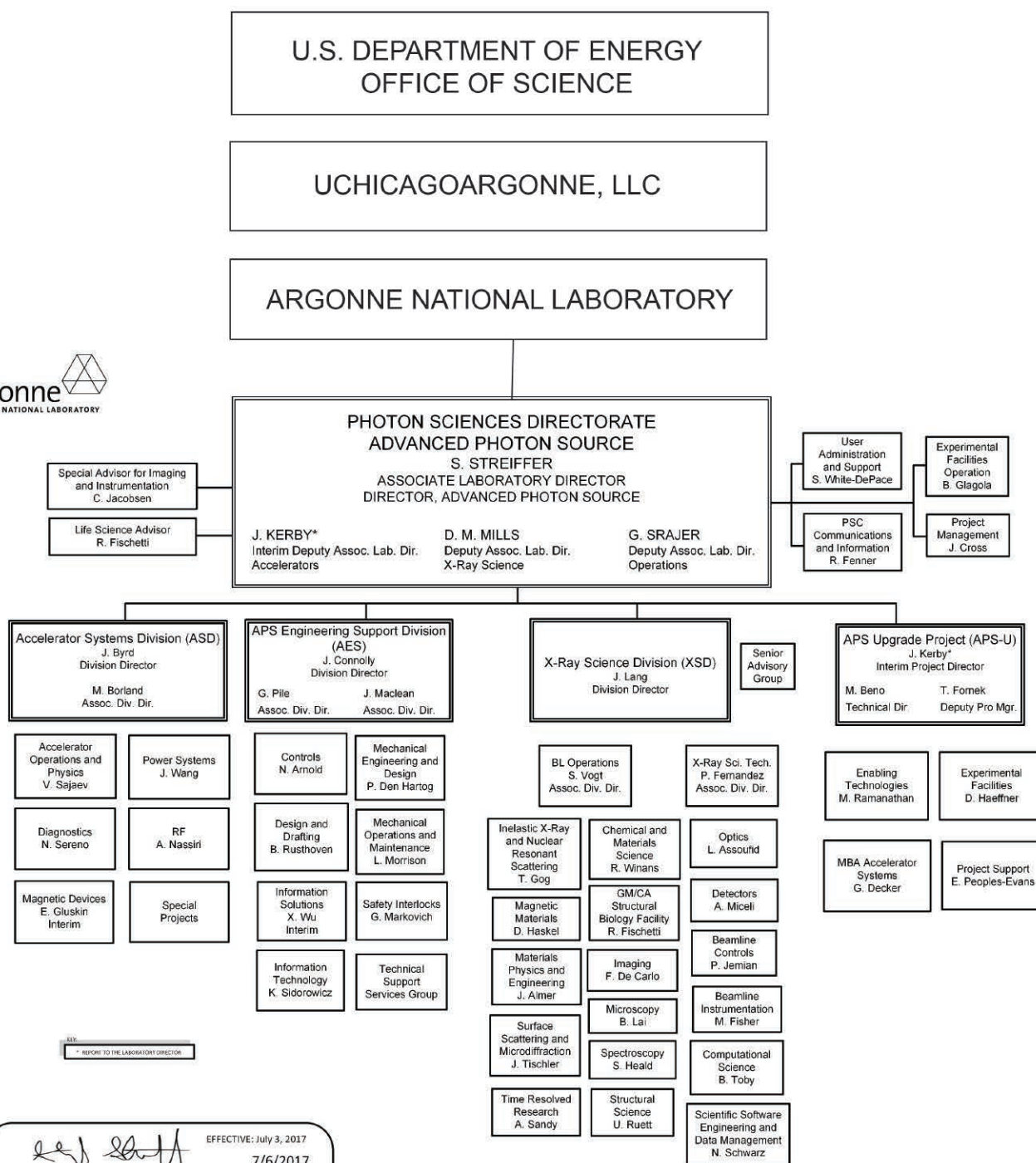
In late June of 2017, we received a vote of confidence from the Scientific Facilities Division in the Basic Energy Sciences (BES) Program of the Office of Science. They concurred on our first purchases of several production items, including 160 of the 1320 magnets needed for the multi-bend achromat storage ring phase of the APS-U. While we have far to go, it is gratifying to receive this first go-ahead from BES.


Though we have a Project Director position to fill, the APS-U team as a whole has been strengthened in the past months by several key additions. The team is working hard, we have a fine design, and we look forward to creating the best facility possible and enabling the scientific explorations of the APS user community for decades to come.

*Jim Kerby*  
*APS Upgrade Interim Project Director*

The APS Upgrade Project is funded by the U.S. Department of Energy Office of Science under Contract No. DE-AC02-06CH11

# APS ORGANIZATION CHART




 EFFECTIVE: July 3, 2017  
 7/6/2017  
 Approved: S. Streiffer  
 Associate Laboratory Director

## ACRONYMS FOR ARGONNE DIVISIONS USED IN THIS BOOK

- AES - APS Engineering Support Division
- ASD - Accelerator Systems Division
- CEP - Communications, Education, and Public Affairs Division
- MSD - Materials Science Division
- XSD - X-ray Science Division



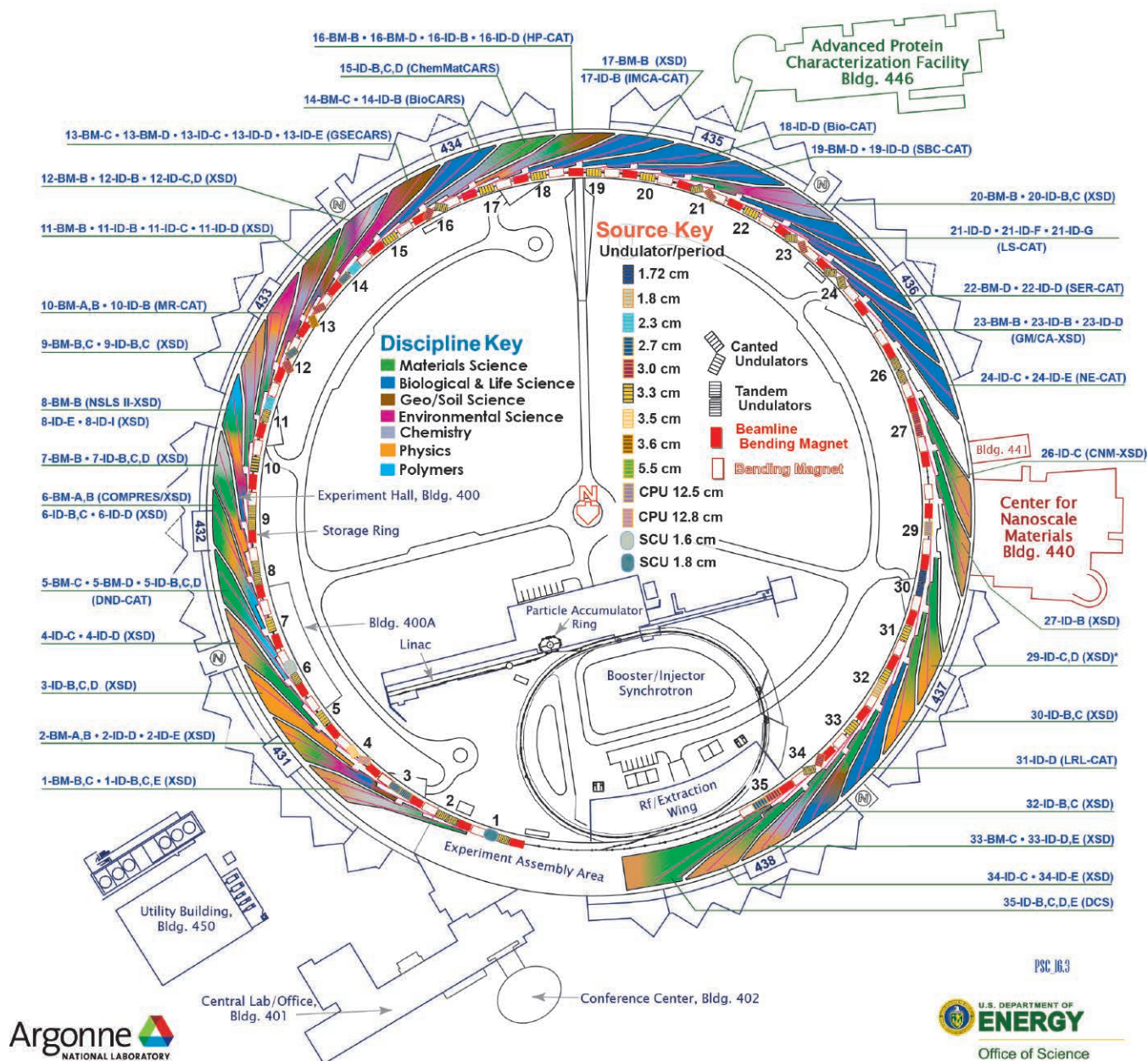
# ARGONNE NATIONAL LABORATORY 400-AREA FACILITIES

## ADVANCED PHOTON SOURCE

(Beamlines, Disciplines, and Source Configuration)

## ADVANCED PROTEIN CHARACTERIZATION FACILITY

## CENTER FOR NANOSCALE MATERIALS



Argonne  
NATIONAL LABORATORY

U.S. DEPARTMENT OF  
**ENERGY**  
Office of Science

**APS SECTORS:** At the APS, a “sector” comprises the radiation sources (one bending magnet and nominally one insertion device, although the number of insertion devices in the straight sections of the storage ring can vary), and the beamlines, enclosures, and instrumentation that are associated with a particular storage ring sector. The APS has 35 sectors dedicated to user science and experimental apparatus. **X-ray Science Division (XSD)** sectors comprise those beamlines operated by the APS. **Collaborative access team (CAT)** sectors comprise beamlines operated by independent groups made up of scientists from universities, industry, and/or research laboratories.

**Key to the beamline descriptions that accompany science highlights:** Beamline designation • Sector operator • Disciplines • Techniques • Radiation source energy • User access mode(s) • General-user status •

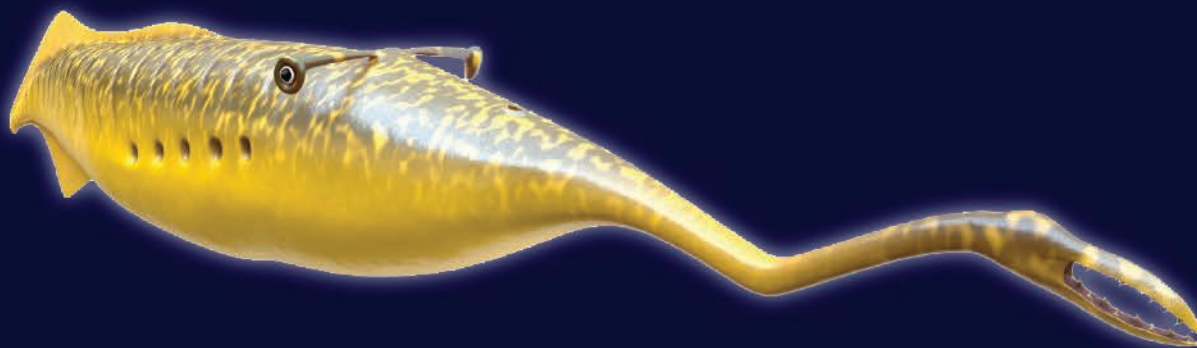




# THE TALE OF THE TULLY MONSTER: A WEIRD WONDER FOSSIL FINDS A HOME

**T**he soft-bodied *Tullimonstrum gregarium*, or Tully Monster, lived over 300 million years ago during the Pennsylvanian Period in an ocean that covered much of what we now call the State of Illinois in the U.S. An amateur fossil hunter, Mr. Francis Tully, first discovered its traces in 1958 in a pile of shale discarded by coal miners, and copious other similar discoveries soon testified that the Tully monster was once abundant. But by modern standards the animal looks so strange that no one has been quite sure what it was. In this extensive review, researchers analyzed over 1200 specimens with a variety of experimental tools such as optical and electron imaging, and x-ray imaging at the APS in order to place the fossil on the correct limb of Earth's family tree. The research team found that the Tully Monster belongs with the lampreys—modern, eel-like animals that attach to fish and extract blood with circular rows of teeth. Beyond the long awaited classification of Illinois' official state fossil, this work shows that lamprey morphology was once much more diverse, extending the definition of what these animals can be and challenging the idea that lampreys represent a “primitive” and relatively unchanged animal group.

*Note: A video about the Argonne Tully Monster research is at <http://bit.ly/2ilt3Qw>*



Scientists have struggled for over 50 years to classify the Tully Monster into a known phylum. Was it related to snails, or eels? Maybe it was a kind of worm? The Tully Monster resembles, in part, a cucumber, a crab, and a rubber torpedo. Its mouth opened like a claw at the end of a long proboscis. Its eyes attached not to its face, but capped a thin bar that ran perpendicular to its body at the top of its head (Fig. 1).

Earlier analyses had pegged the Tully Monster as a swimming gastropod, or snail, based on a line running down the animal's body believed to be its gut. But this line, commonly called a "gut trace," usually ends at the anus just before the tail, and often appears dark. This gut-trace line was light-colored and extended into the tail. Also odd for a gut, it began not at the mouth, but at the fossil's eye bar. The researchers re-classified this line as a notochord—a cartilaginous rod that formed the basis of the backbone. The line was not plumbing used for digestion, but infrastructure for nerves and electrical signals. The researchers found a true gut trace in some specimens, and as expected, it ended just short of the tail. Unlike gastropods, the Tully Monster is a vertebrate.

To determine what the fossilized structures were made of, the researchers in this study, from Yale University, the American Museum of Natural History, the Field Museum of Natural History, Argonne National Laboratory, and the Yale Peabody Museum of Natural History used energy-dispersive spectroscopy on the scanning electron microscope at the Field Museum of Natural History in Chicago, Illinois, and synchrotron images collected at XSD x-ray beamline 8-BM-B of the

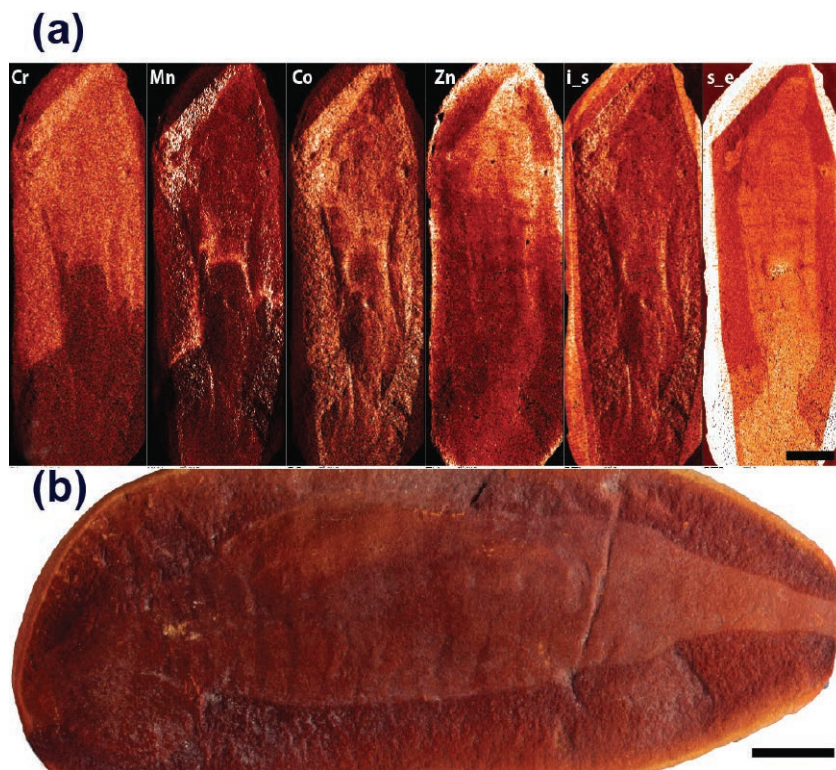


Fig. 1. (a). Synchrotron elemental mapping of a Tully Monster fossil, showing variable preservation that helped to identify tissues (scale bar 1 cm). (b). A fossil Tully Monster, showing the notochord and other features (scale bar 1 cm). Facing page: A reconstruction, by Sean McMahon, of the Tully Monster in life.

APS. This enabled the researchers to create elemental maps of the Tully Monster fossils. Among other findings, these maps showed that the fossils' rows of pointy cone-shaped teeth were composed of keratin (the protein that protects epithelial cells from damage or stress) like those of lampreys, not chitin (the major constituent in the exoskeleton of arthropods and the cell walls of fungi) found in gastropods. Further evidence affirming the Tully Monster's lamprey lineage included gill pouches, a tongue-like organ, a dorsal fin, a single nostril, and a lamprey-like three-lobed brain. The examination also found that the proboscis was not flexible, as previously thought, but characterized by three articulations.

The Tully Monster fossil has been "problematic" for half a century, but with the aid of hundreds of specimens and modern microscopy techniques, this work settles the animal into its proper place. Perhaps most surprising is that the Tully Monster shares its lineage with a group of organisms believed to have evolved from a common ancestor that exhibits such little diversity today.

Modern lampreys demonstrate so little variation in how they look and function, that some perceive them as a kind of largely un-evolved living fossil. This research demonstrates that throughout the millions of years they have existed, lampreys have in fact undergone extensive evolutionary diversification, only a small amount of which remains in the form we now see.

— Jenny Morber

**See:** Victoria E. McCoy<sup>1\*</sup>, Erin E. Saupe<sup>1</sup>, James C. Lamsdell<sup>1,2</sup>, Lidya G. Tarhan<sup>1</sup>, Sean McMahon<sup>1</sup>, Scott Lidgard<sup>3</sup>, Paul Mayer<sup>3</sup>, Christopher D. Whalen<sup>1</sup>, Carmen Soriano<sup>4</sup>, Lydia Finney<sup>4</sup>, Stefan Vogt<sup>4</sup>,

Elizabeth G. Clark<sup>1</sup>, Ross P. Anderson<sup>1</sup>, Holger Petermann<sup>1</sup>, Emma R. Locatelli<sup>1</sup>, and Derek E.G. Briggs<sup>1,5</sup>, "The 'Tully monster' is a vertebrate," *Nature* **532**, 496-513 (2016).

DOI: 10.1038/nature16992

**Author affiliations:** <sup>1</sup>Yale University, <sup>2</sup>American Museum of Natural History, <sup>3</sup>Field Museum of Natural History, <sup>4</sup>Argonne National Laboratory, <sup>5</sup>Yale Peabody Museum of Natural History

**Correspondence:**

\* victoria.mccoy@yale.edu

Funding was provided by a Field Museum visiting scholarship to V.E.M. and by the NASA Astrobiology Institute (NNA13AA90A) Foundations of Complex Life, Evolution, Preservation and Detection on Earth and Beyond. This research used resources of the Advanced Photon Source, a U.S. Department of Energy (DOE) Office of Science User Facility operated for the U.S. DOE Office of Science by Argonne National Laboratory under contract number DE-AC02-06CH11357.

8-BM-B • NSLS-II/XSD • Chemistry, life sciences, environmental science, materials science • Transmission x-ray microscopy • 5.5-20 keV, 9-18 keV • On-site • Accepting general users •



## WEN OF XSD WINS DOE EARLY CAREER AWARD

Haidan Wen of XSD received a DOE Early Career Award, a prestigious research grant for \$2.5 million over five years. The effort, now in its seventh year, is designed to bolster the nation's scientific workforce by providing support to exceptional researchers during the crucial early career years, when many scientists do their most formative work. The grant will fund Wen's research to develop a new imaging technique to catch dynamic snapshots of materials as they're changing and performing unusual phenomena, using x-rays at the APS.

## SHU OF XSD SHARES IN R&D 100 AWARD

Deming Shu, senior engineer for nanopositioning with XSD, was one of the recipients of a 2016 R&D 100 Award, which annually recognize the 100 most innovative technologies and services of the past year. The award was for development of the Hard X-Ray Scanning Microscope with Multilayer Laue Lens (MLL) Nanofocusing Optics, a high-throughput scientific imaging tool that routinely provides sub-20-nm spatial resolution imaging. This novel MLL-based, vacuum-compatible microscope is a general-purpose x-ray microscopy tool that is suitable for a broad range of imaging experiments. For example, imaging techniques currently supported are: x-ray fluorescence, ptychography, diffraction, differential phase contrast, and x-ray absorption spectroscopy. The system is installed at the Hard X-ray Nanoprobe beamline at the National Synchrotron Light Source II facility at Brookhaven National Laboratory.

## JACOBSEN IS A 2016 ARGONNE DISTINGUISHED FELLOW

Chris Jacobsen, special advisor to the Director of the APS for imaging and instrumentation, and professor in the Department of Physics and Astronomy (and member of the Applied Physics Program and the Chemistry of Life Processes Institute) at Northwestern University, was named a 2016 Argonne Distinguished Fellow. Jacobsen's research focuses on developing new optics and computation methods in x-ray microscopy and applying them to problems in biology, environmental science, and materials science. Argonne Distinguished Fellows represent only 3% of research staff at the Lab, making the award the highest scientific and engineering rank at Argonne. Argonne Fellows are recognized internationally for their work and show the type of leadership that impacts Argonne's future and its mission.

## LI IS THE RECIPIENT OF THE 2016 APSUO ROSALIND FRANKLIN YOUNG INVESTIGATOR AWARD

The APS Users Organization (APSUO) awarded the 2016 APSUO Rosalind Franklin Young Investigator Award to Ling Li (Harvard University) for his work using high-resolution synchrotron-based tomography techniques at the APS to develop a fundamental understanding of the mechanical and multifunctional design of biological materials. Li's research is motivated by the fact that our ability to rationally develop multifunctional engineering structural materials without compromising their

mechanical performance is currently limited. This is due to the lack of a comprehensive understanding of the interplay between multiple distinct and potentially conflicting properties, and the underlying structure. For example, the design of transparent structural materials is still primarily based on laminated glasses, which is a century-old technology.

## USERS OF APS RECEIVE DOC SILVER MEDAL

Two scientists from the National Institute of Standards and Technology, Andrew Allen and Lyle Levine, were awarded the Department of Commerce Silver Medal for their groundbreaking work on the microstructure and dynamics in materials over many length scales and under real-world conditions. The scientists used the USAXS (ultra-small-angle x-ray scattering) instrument on the XSD beamline 9-ID-C at the APS in their discoveries. They closely examined their samples' microstructure and dynamics at different temperature, atmosphere, and pressure conditions. The USAXS instrument can determine the size or structure of a sample's components across multiple length scales from angstroms to about 20  $\mu\text{m}$ . The Silver Medal is the second-highest award granted by the Secretary of Commerce for distinguished and exceptional scientific/engineering achievement.

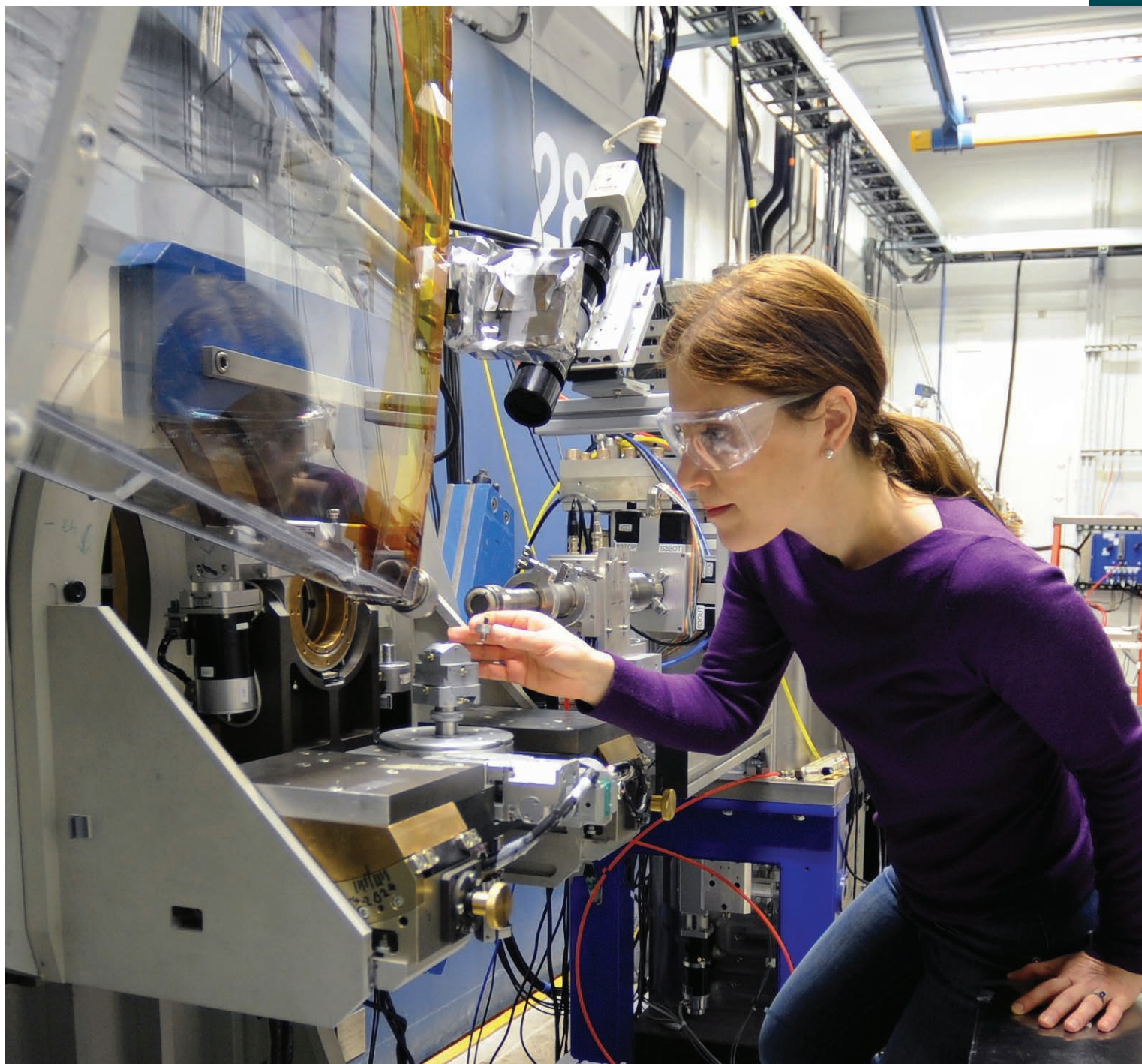
## TWO APS USERS NAMED "BREAKTHROUGH PRIZE" WINNERS

Two users of the APS, Harry F. Noller, Director of the Center of Molecular Biology of RNA at the University of Southern California, and Stephen J. Elledge, Gregor Mendel Professor of Genetics and Medicine in the Department of Genetics at Harvard Medical School, were named "Breakthrough Prize" winners in life sciences. Both have used the high-brightness x-ray beams at the APS in their work, Noller at the GM/CA-XSD structural biology facility and Elledge at the NE-CAT facility. Elledge was honored for "elucidating how eukaryotic cells sense and respond to damage in their DNA and providing insights into the development and treatment of cancer." Noller was honored for "discovering the centrality of RNA in forming the active centers of the ribosome, the fundamental machinery of protein synthesis in all cells, thereby connecting modern biology to the origin of life and also explaining how many natural antibiotics disrupt protein synthesis."

## APS USER MARKS WINS THE 2017 PRIESTLEY MEDAL

Tobin J. Marks, the Charles E. and Emma H. Morrison Professor of Chemistry, Professor of Materials Science & Engineering, and the Vladimir N. Ipatieff Professor of Catalytic Chemistry at Northwestern University, and a user of the grazing-incidence x-ray scattering instrument at APS beamline 8-ID-E, was selected as the 2017 winner of the Priestley Medal for "pioneering research in catalytic polymerization, organometallic chemistry, organic opto-electronic materials, and electronically functional metal oxides." The Priestley Medal is the American Chemical Society's highest honor, which recognizes distinguished services to chemistry.

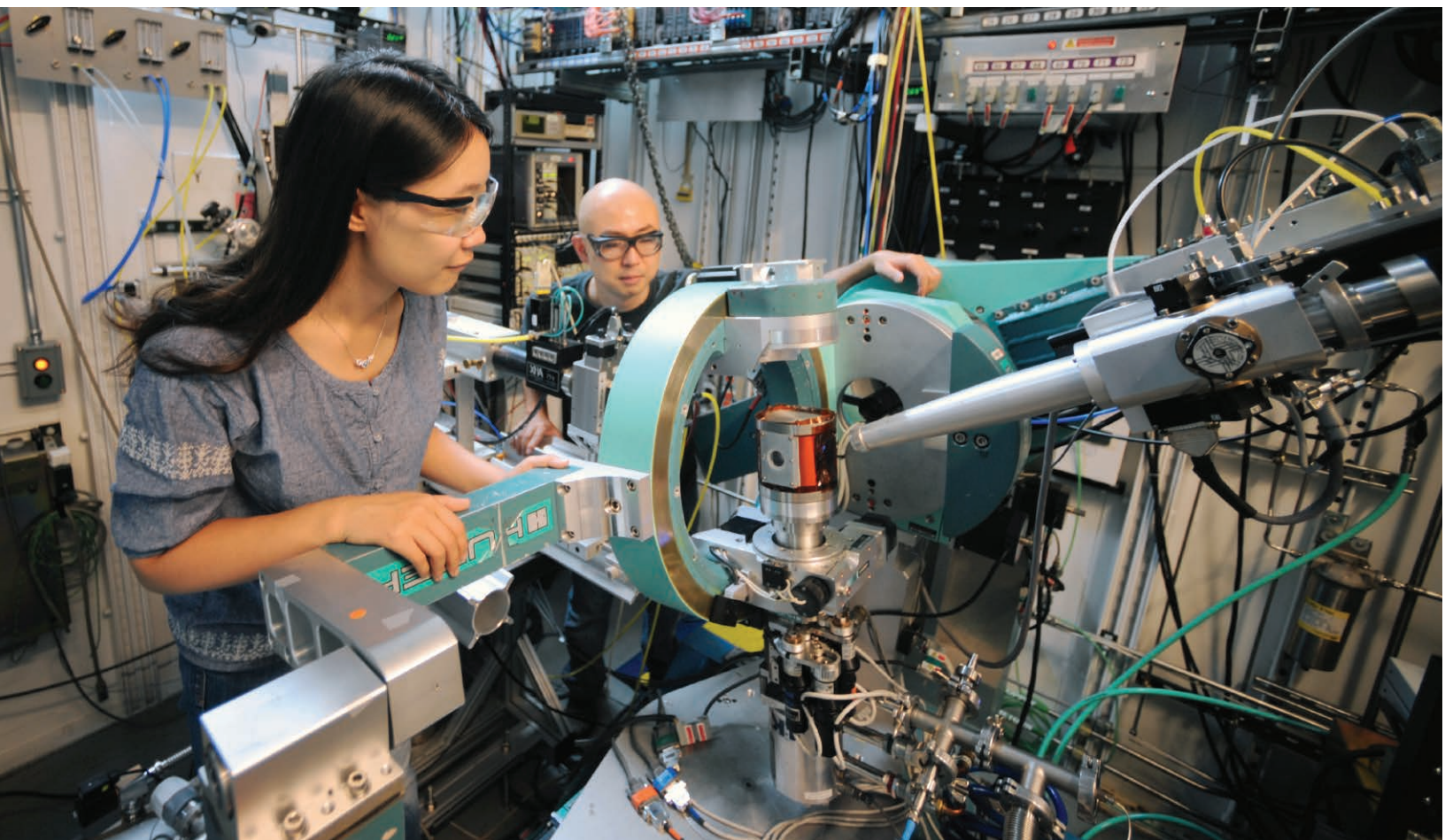
# ELECTRONIC & MAGNETIC MATERIALS



Mary Upton, physicist and beamline scientist with the XSD Inelastic X-ray & Nuclear Resonant Scattering Group at the APS, places a sample in the resonant inelastic x-ray scattering spectrometer at the APS 27-ID-B x-ray beamline. This instrument is used to measure the intrinsic properties of electronic excitations, which are key to understanding the electrical and magnetic behaviors of materials.



# THE TWISTED LIAISON BETWEEN MAGNETISM AND SUPERCONDUCTIVITY

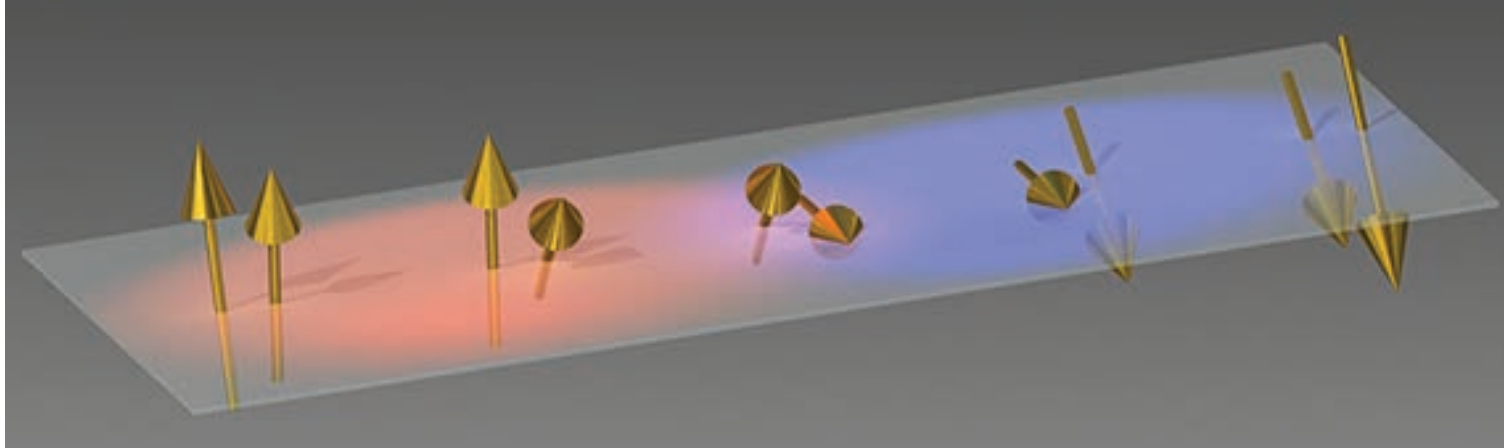


APS user and first author Yishu Wang (California Institute of Technology) at the 6-circle diffractometer in the research station of the XSD 4-ID-D insertion device x-ray beamline. A cryostat is mounted on the sample stage of the diffractometer. The sample being studied is inside a high pressure cell, set inside the cap at the end of the cryostat. Both the optical windows (transparent circle on the side) and the x-ray windows (brown kapton tape) on that cap are visible. Physicist and beamline scientist Yejun Feng of the XSD Magnetic Materials Group can be seen behind the instrument.

In various materials that show unusual forms of superconductivity, including the rare earth cuprates, heavy electron metals, and iron based pnictides, superconductivity typically emerges from a magnetically ordered state. Despite more than three decades of research, however, the precise mechanism by which superconductivity takes hold remains unclear for all these systems. By means of magnetic x-ray diffraction studies at the APS researchers have investigated the magnetic characteristics of a helical spin-order phase preceding a recently discovered pressure-induced superconducting phase in manganese phosphide (MnP). The work suggests that electron pairing in the superconducting states could be triggered by spin fluctuations of helical character (Fig. 1), retained from the adjacent ordered state. Furthermore, MnP and related transition metal compounds form a family of model systems for exploring the interaction between magnetic and superconducting states with spin character of a helical form.

The discovery of a high-pressure superconducting phase in MnP in 2015 was motivated by knowledge of the material's complex magnetic properties. Researchers already knew that MnP shows a helical spin ordering at ambient pressure and at temperatures below 50K, which gives way to a ferromagnetic phase at a pressure of about 1 GPa. The ferromagnetic phase is replaced by a new phase, thought to be antiferromagnetic, at about 2 GPa, and superconductivity sets in at about 7 GPa.

A team of researchers from the California Institute of Technology, Argonne National Laboratory, and the



Chinese Academy of Sciences using the XSD 4-ID-D x-ray beamline sought to clarify the character of the intermediate magnetic state between 2 to 7 GPa in order to understand its connection with the adjacent superconducting state.

Helical ordering means exactly what it says: the spins of electrons situated along a line in the lattice have a fixed turn angle, or pitch, from one to the next. To detect this spin pattern, the researchers conducted non-resonant magnetic x-ray diffraction experiments on a sample of MnP held at 4K in a specially designed high-pressure diamond anvil cell. Each anvil had wide perforations on one side so that x-rays could pass in and out of the sample with as little interference as possible from the environment. This was important because the diffraction signal the researchers were looking for was weak, 10<sup>-8</sup> of the signal from Bragg diffraction by the lattice.

In general, a diffraction peak indicates periodic patterns of charges or spins (Fig. 1) since they both have interaction cross sections with x-rays. Here the pattern of observed peaks, mirror symmetric along one lattice axis on both sides of an ordered arrangement of charges, suggested that the observed diffraction is associated with a superlattice. The absence of peaks at half the value of transferred momentum value indicated the observed peaks to be fundamental. Moreover, both the low diffraction angles and the low intensity rule out the possibility of charge origin. Since the non-resonant interaction of x-rays with spins at low diffraction angles are predominantly sensitive to the spin component out of the diffraction plane, the researchers concluded that observed peaks most likely originated from a helical magnetic order.

Fig. 1. In spiral magnets (with local spins pictured as golden arrows), a pair of itinerant electrons (red and blue clouds) can be bound together through their individual interaction with the spiral spin wave. The itinerant electron pair forms a superconducting state with unusual symmetry that is different from phonon-mediated superconductivity. X-ray diffraction at the APS revealed the spiral pitch distance a key factor in controlling the nature of magnetically mediated superconductivity.

A helical arrangement of spins has both ferromagnetic and antiferromagnetic characteristics, with their relative influence depending on the pitch angle. At ambient pressure, the helical order in MnP possesses a fairly large pitch, meaning that spins of nearest neighbor electrons are not too far apart in orientation, giving them a ferromagnetic character. At higher pressure, though, the newly discovered helical ordering has a much smaller pitch. Nearest-neighbor spins in this arrangement have a substantial angle between them, producing an overall character that is closer to antiferromagnetic, even though the ferromagnetic nature is preserved locally. As the MnP lattice shrank under pressure, the helical pitch decreased proportionately, implying that superconductivity of different types can be facilitated by spin fluctuations of various pitch angles after the static magnetic order has been suppressed.

In comparison to ordinary period-doubling antiferromagnetism, the presence of a ferromagnetic component in helimagnetic materials will suppress the formation of conventional phonon-based superconductivity. Thus, the superconductivity in MnP is more likely to be unconventional. This finding opens the door to experiments on materials related to MnP. For example, chromium arsenide (CrAs) also has helical order with a relatively short pitch, and transitions to a superconducting state under high pressure, whereas manganese silicide (MnSi) exhibits a larger pitch helix and does not show high-pressure superconductivity even down to tempera-

tures of 10 mK above absolute zero. Many other compounds with the same form as MnP exist, where the first element is V/Cr/Mn/Fe/Co/Ni and the second P/As/Sb, all of which show helical magnetic ordering. Careful examination of this family of materials would illuminate the connection between superconducting states and the magnetic state from which they arise.

— David Lindley

**See:** Yishu Wang<sup>1</sup>, Yejun Feng<sup>1,2\*</sup>, J.-G. Cheng<sup>3</sup>, W. Wu<sup>3</sup>, J.L. Luo<sup>3,4</sup>, and T.F. Rosenbaum<sup>1\*\*</sup>, "Spiral magnetic order and pressure-induced superconductivity in transition metal compounds," *Nat. Commun.* **7**, 13037 (6 October 2016). DOI: 10.1038/ncomms13037

**Author affiliations:** <sup>1</sup>California Institute of Technology, <sup>2</sup>Argonne National Laboratory, <sup>3</sup>Chinese Academy of Sciences, <sup>4</sup>Collaborative Innovation Center of Quantum Matter

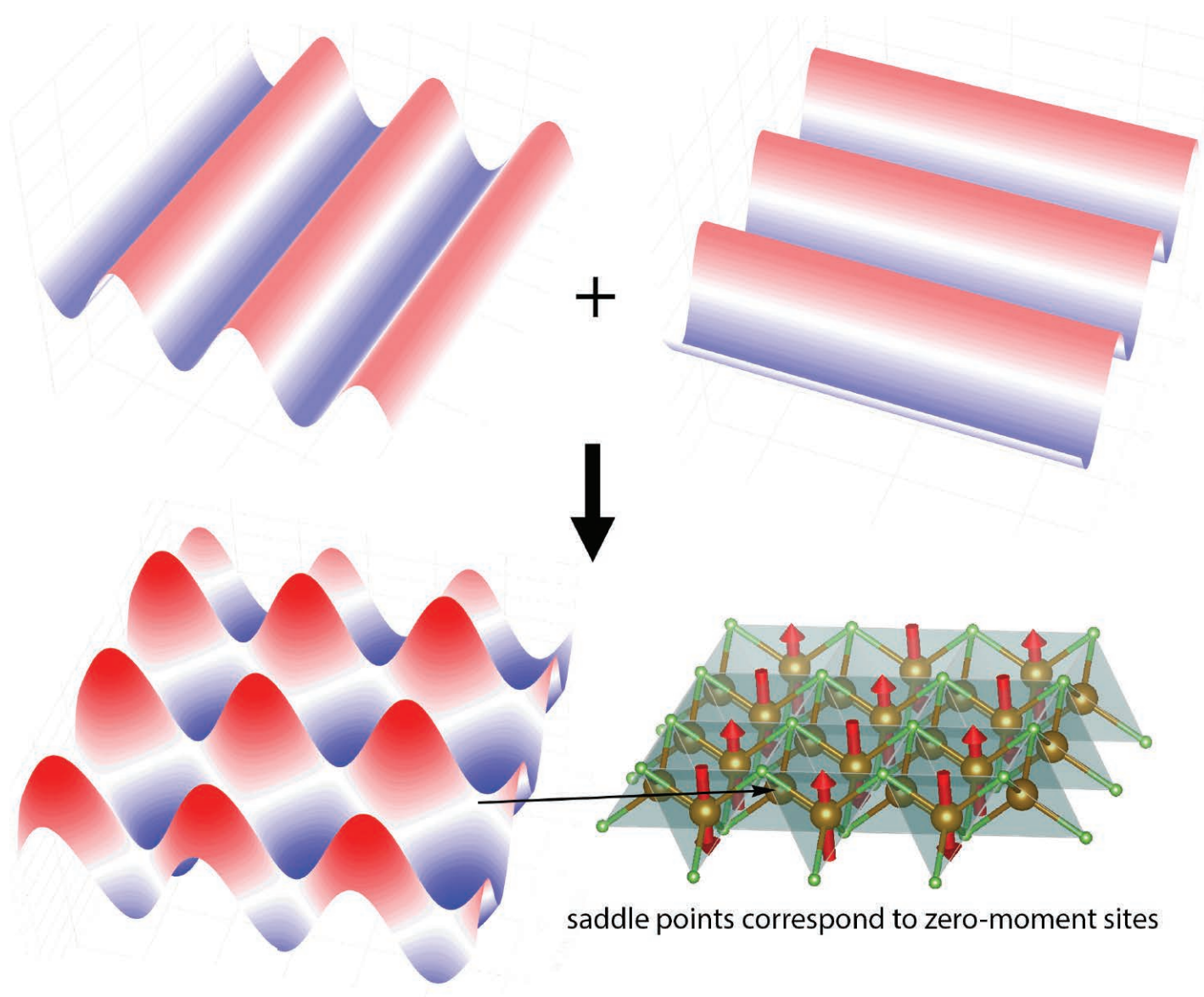
**Correspondence:** \* yejun@anl.gov  
\*\* tfr@caltech.edu

J.-G.C. and J.L.L. were supported by the MOST and NSF of China, and the Strategic Priority Research Program of the Chinese Academy of Sciences. Sample preparation at the MRSEC facilities of the University of Chicago was supported by NSF Grant No. DMR-1420709. The work at the California Institute of Technology was supported by U.S. Department of Energy Basic Energy Sciences Award DE-SC0014866. The use of the Advanced Photon Source and the Center for Nanoscale Materials at Argonne National Laboratory was supported by the U.S. Department of Energy Office of Science User Facilities under contract No. DE-AC02-06CH11357.



# CAN WE FLIP OUR UNDERSTANDING OF HIGH- $T_C$ SUPERCONDUCTORS?

**S**uperconductors have applications as diverse as medical devices and high-speed trains, with the potential to impact electricity transmission and power grids in the future. So the magnetic ground state of one class of superconducting materials—those which superconduct at high temperatures and are iron-based—is an area of active scientific research. A fuller understanding of these materials would allow intentional application of their superconducting abilities. Recent results from studies by an international team working at the APS reveal a new magnetic state for these materials, a state with non-uniform magnetization, which manifests at a temperature very close to the one at which superconductivity occurs, thus pointing toward possibilities for new superconducting materials.



Superconductors are materials, usually non-magnetic, which produce zero electrical resistance when cooled below a critical temperature. Individual electrons within the superconducting material form bound pairs rather than moving like a free-flowing stream, as in the plumbing analogy commonly used to visualize electricity. Iron-based superconductors, which also exhibit magnetism, are rare so characterizing the magnetic ground state of these materials would give scientists important clues to the quantum underpinnings that produce their superconductive behavior. To gain that insight, a team of scientists investigated the families of iron spin ordering found within these materials.

The team of researchers from Argonne, Northern Illinois University, Northwestern University, the University of Minnesota, Ruhr-Universität Bochum (Germany), and the National University of Science and Technology MISiS (Russia) used a variety of processes to analyze high-temperature iron-based superconductive materials in order to learn more about their magnetic ground state. They synthesized a compound for testing,  $\text{Sr}_{(0.63)}\text{Na}_{(0.37)}\text{Fe}_2\text{As}_2$ , and characterized its magnetic properties using x-ray diffraction, neutron diffraction, and Mössbauer spectroscopy. They took powder x-ray diffraction data at the XSD 11-BM-B beamline at the APS, which showed that the material behaves as other iron-based superconductors do, changing from tetragonal to orthorhombic symmetry at approximately 105 K. However, the sample material also transitions back to tetragonal symmetry at approximately 73 K. The team also gathered powder neutron diffraction data at Oak Ridge National Laboratory using beamline HB-1A at the High Flux Isotope Reactor and the

POWGEN diffractometer at the Spallation Neutron Source to confirm that the tetragonal and orthorhombic phases were magnetically ordered.

However, there are two ways to model the spins based on the diffraction data. The two models differ by the number of domains in a phase and whether the spins in each domain are superposed coherently or incoherently. To distinguish between these two options, the team used Mössbauer spectroscopy to probe the local magnetic structures of the material.

The team took Mössbauer spectra over a range of temperatures, from 5 K to 125 K. The spectra at high temperature show evidence for the paramagnetic phase of the material. At lower temperatures, such as 30 K, the spectrum consists of more than a single peak; it shows the presence of non-magnetic sites as well as magnetic sites whose effective field is larger than expected. Further statistical analysis by the team shows this spectrum implies that half of the sites are magnetic while the remaining half are not, supporting the single-domain, coherent-superposition model as the one which represents the physics of the sample. Figure 1 shows a cartoon representation of how the component spin-waves from the single-domain model add together to produce spin-waves whose amplitudes alternate between twice as high (as the initial spin-wave) over certain sites and zero. The figure also shows how the zero amplitude spin-waves correlate to the sites in the sample lattice with zero magnetic moments.

The team concluded that this tetragonal phase—the phase with both magnetic and non-magnetic sites—is best understood in terms of itinerant spin-density waves rather than localized spins. Itinerant spins are ones that have fluctuating amplitudes and cannot be localized to a single lattice site. Additionally, they concluded that the magnetism for this material is consistent with modulation of the polarization of spins grouped into correlated bands, rather than magnetism due to localized spin interactions.

By showing data which supports a non-uniform magnetic state and itinerant spins rather than localized spins, these new results emphasize that these materials hold a lot of promise for expanding our understanding of magnetism as well as new avenues for superconductive materials.

— Mary Alexandra Agner

**See:** J.M. Allred<sup>1\*</sup>, K.M. Taddei<sup>1,2</sup>, D.E. Bugaris<sup>1</sup>, M.J. Krogstad<sup>1,2</sup>, S.H. Lapidus<sup>1</sup>, D.Y. Chung<sup>1</sup>, H. Claus<sup>1</sup>, M.G. Kanatzidis<sup>1,3</sup>, D.E. Brown<sup>2</sup>, J. Kang<sup>4</sup>, R.M. Fernandes<sup>4</sup>, I. Eremin<sup>5,6</sup>, S. Rosenkranz<sup>1</sup>, O. Chmaissem<sup>1,2</sup>, and R. Osborn<sup>1</sup>, “Double-Q spin-density wave in iron arsenide superconductors,” *Nat. Phys.* **12**, 493 (May 2016).

DOI: 10.1038/NPHYS3629

**Author affiliations:** <sup>1</sup>Argonne National Laboratory, <sup>2</sup>Northern Illinois University, <sup>3</sup>Northwestern University, <sup>4</sup>University of Minnesota, <sup>5</sup>Ruhr-Universität Bochum, <sup>6</sup>National University of Science and Technology MISiS

**Correspondence:** \* jmallred@ua.edu

Work at Argonne (J.M.A., K.M.T., D.E. Bugaris, M.J.K., D.Y.C., H.C., M.G.K., S.R., O.C., and R.O.) was supported by the U.S. Department of Energy (DOE) Office of Science, Materials Science and Engineering Division. R.M.F. and J.K. were supported by the U.S. DOE Office of Science-Basic Energy Sciences, under award number DE-SC0012336. The work of I.E. was supported by the Focus Program 1458 Eisen-Pniktide of the DFG, and by the German Academic Exchange Service (DAAD PPP USA no. 57051534). I.E. also acknowledges the financial support of the Ministry of Education and Science of the Russian Federation in the framework of Increase Competitiveness Program of NUST MISiS (N 22014015). The High Flux Isotope Reactor and Spallation Neutron Source are DOE Office of Science User Facilities operated by the Oak Ridge National Laboratory. This research used resources of the Advanced Photon Source, a U.S. DOE Office of Science User Facility operated for the DOE Office of Science by Argonne National Laboratory under Contract No. DE-AC02-06CH11357.

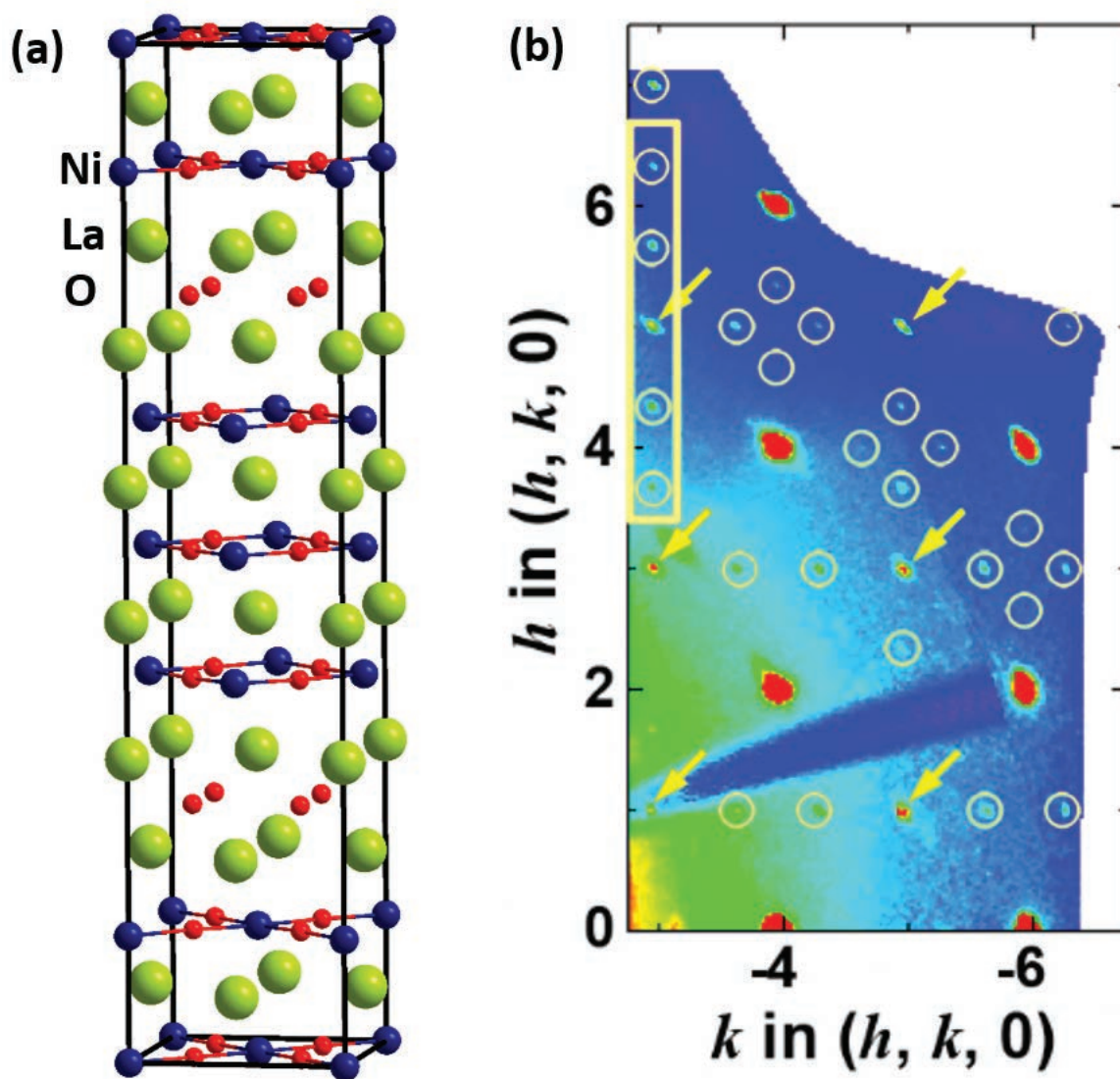
11-BM-B • XSD • Chemistry, materials science, physics • Powder diffraction • 22-33 keV • On-site, mail-in • Accepting general users •

< Fig. 1. How the component spin-waves add together to produce spin-waves whose amplitude alternates between double the initial amplitude and zero, and how those zero amplitude points correspond to zero-moment sites within the lattice of the superconducting material.



# SEEING STRIPES IN NICKELATES

One way researchers are trying to untangle the still mysterious workings of the high-temperature cuprate superconductors is by studying the behavior of electrons in materials with related crystal and electronic structures. An Argonne, University of Chicago team used x-ray diffraction measurements at the APS, to probe a phase transition in one such material, a lanthanum nickelate  $\text{La}_4\text{Ni}_3\text{O}_8$  (La-438), whose electronic properties change markedly on cooling below 105 K. They found that in the low temperature state, the charge distribution developed a stripe ordering, but with an unexpected pattern, hinting at novel lattice-electron interactions that may have counterparts in the cuprates. The formation of in-phase charge stripes points to the existence of novel phenomena in this complex lattice and suggests strategies for creating new materials that may have implications for the mechanism of superconductivity in cuprates or that may lead to entirely new superconductors themselves.



The compound La-438 has a unit cell containing trilayer structures in which nickel ions are arranged in squares, stacked in sets of three, perpendicular to the long axis (Fig. 1a). La-438, a semiconductor at room temperature, undergoes a phase transition on cooling below 105 K, when its resistivity abruptly increases. It has been suggested that suitable doping might cause nickelates with this general structure to become superconductors at low temperatures [1], like their cuprate cousins, although no examples have been found so far.

Investigating the phase transition in La-438 has been difficult because researchers had not been able to obtain single crystals of the material, so structural studies could be performed only on powder samples. The team of researchers in this study, from Argonne and The University of Chicago, developed a method to create crystals of La-438 by first growing a boule of a parent phase,  $\text{La}_4\text{Ni}_3\text{O}_{10}$ , in a high-pressure oxygen environment within a furnace. They then cleaved pieces from the parent material and heated them in a reducing hydrogen-argon mix. Although the transformation into La-438 was accompanied by a significant lattice distortion, the team succeeded in obtaining large (about 1 cubic millimeter) although fragile single crystals of La-438. Observation of the phase change in these crystals closely tracked previous measurements, including a pronounced heat capacity peak at the transition temperature.

Using the ChemMatCARS 15-ID-ID-B,C,D beamline at the APS, the team carried out x-ray diffraction measurement of La-438 single crystals; their result showed evidence of only small changes to the lattice dimensions through the phase transition. Below the transition temperature, however, a number of weak diffraction spots appeared, indicating the formation of a superlattice with three times the normal lattice parameter in the plane of the nickel layers

< Fig. 1. (a) Crystal structure of  $\text{La}_4\text{Ni}_3\text{O}_8$  at 300 K. (b) Charge superlattice peaks of  $\text{La}_4\text{Ni}_3\text{O}_8$  below phase transition. Yellow circles and arrows indicate superlattice peaks and leakage intensity from neighboring layer Bragg peaks, respectively.

(Fig. 1b). No such signals had been seen in earlier powder diffraction studies.

To interpret their measurements, the researchers were guided by similar changes seen in the better-understood material LSNO-1/3 ( $\text{La}_{2-x}\text{Sr}_x\text{NiO}_4$ , with  $x = 1/3$ ). This compound also develops a threefold superlattice at low temperature, accompanied by the formation of charge stripe ordering in which the valence of metal ions in two-dimensional layers within the lattice departs from uniformity in a “corrugated” manner. Accordingly, the team sought to reproduce the superlattice diffraction pattern from La-438 by calculating the behavior of model structures in which the charge attributed to nickel ions in each trilayer structures was allowed to vary slightly from the notional average.

The team found strong evidence for the formation of charge stripes (Fig. 2), but that finding came with a surprise. In LSNO-1/3, the stripes adopt a staggered pattern, so that a charge excess in one layer is above and below a charge deficit in adjacent layers. This pattern reduces Coulombic repulsion between the layers and thus contributes to the stability of the superlattice. In La-438, a similar staggered arrangement was found between adjacent trilayers of nickel ions, but within each trilayer, the charge stripes stack up in phase (Fig. 2). That arrangement undoubtedly increases Coulombic repulsion forces within the trilayers, the researchers say, implying that some other force or forces are stabilizing the in-phase stacking. Recent theoretical studies by Argonne staff implicate a charge-lattice coupling as this stabilizing force [2].

— David Lindley

## REFERENCES

- [1] V. I. Anisimov, D. Bukhalov, and T. M. Rice, *Phys. Rev. B* **59**, 7901 (1999). DOI: 10.1103/PhysRevB.59.7901
- [2] Antia S. Botana, Victor Pardo, Warren E. Pickett, and Michael R. Norman, *Phys. Rev. B* **94**, 081105(R) (2016). DOI: 10.1103/PhysRevB.94.081105

See: Junjie Zhang<sup>1\*</sup>, Yu-Sheng Chen<sup>2</sup>, D. Phelan<sup>1</sup>, Hong Zheng<sup>1</sup>, M.R. Norman<sup>1</sup>, and J.F. Mitchell<sup>1\*\*</sup>, “Stacked

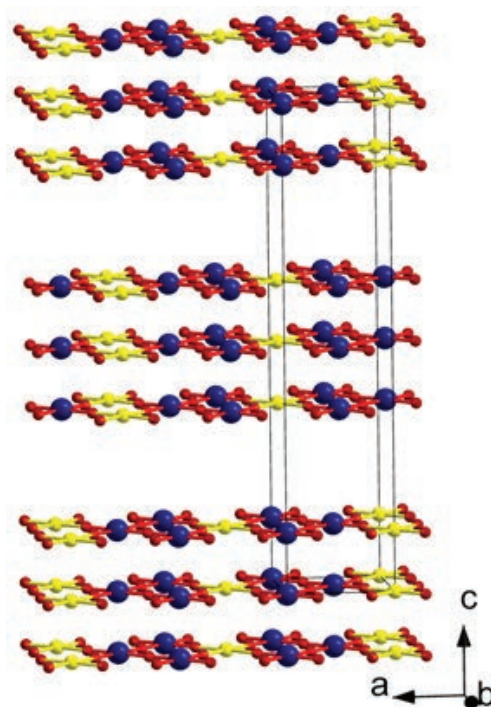


Fig. 2. Real-space charge stripe model. Yellow (blue) spheres represent areas of higher (lower) Ni valence than the average of 1.33+. Red spheres represent oxygen atoms.

charge stripes in the quasi-2D trilayer nickelate  $\text{La}_4\text{Ni}_3\text{O}_8$ ,” *Proc. Nat. Acad. Sci.* **113**(32), 8945 (August 9, 2016). DOI: 10.1073/pnas.1606637113

**Author affiliations:** <sup>1</sup>Argonne National Laboratory, <sup>2</sup>The University of Chicago

**Correspondence:** \* junjie@anl.gov, \*\* mitchell@anl.gov

This work was supported by the U.S. Department of Energy (DOE) Office of Science-Basic Energy Sciences, Materials Science and Engineering Division. ChemMatCARS is principally supported by the Divisions of Chemistry (CHE) and Materials Research (DMR), National Science Foundation, under grant number NSF/CHE-1346572. This research used resources of the Advanced DOE Office of Science User Facility operated for the DOE Office of Science by Argonne National Laboratory under contract number DE-AC02-06CH11357.

15-ID-B,C,D • ChemMatCARS • Materials science, chemistry • Single-crystal diffraction, anomalous and resonant scattering (hard x-ray), microdiffraction, liquid surface diffraction, high-pressure diamond anvil cell, x-ray reflectivity • 6-32 keV, 10-70 keV • On-site • Accepting general users •



# A NOVEL ROUTE TO QUANTUM SPIN LIQUIDS

Observed only in the past decade, quantum spin liquids (QSLs) are currently the focus of intense research. Potential applications range from quantum computing and electronic data storage, to high-temperature superconductivity. A multi-national research team working at the APS and the European Synchrotron Radiation Facility (ESRF) has demonstrated that an unusual form of quantum spin dynamics suggestive of a QSL is present at low temperatures in the iridium-based compound  $\text{Na}_2\text{IrO}_3$ . In a first for the field of QSL research, the team unequivocally showed that the iridium compound achieves its quantum state through “bond-directional interactions,” wherein the electronic spin interactions of the compound are intertwined with its crystallographic directions. By establishing that these bond-directional interactions can suppress the iridium compound’s magnetic ordering, the scientists have provided a new path for realizing the QSL state in a variety of materials.

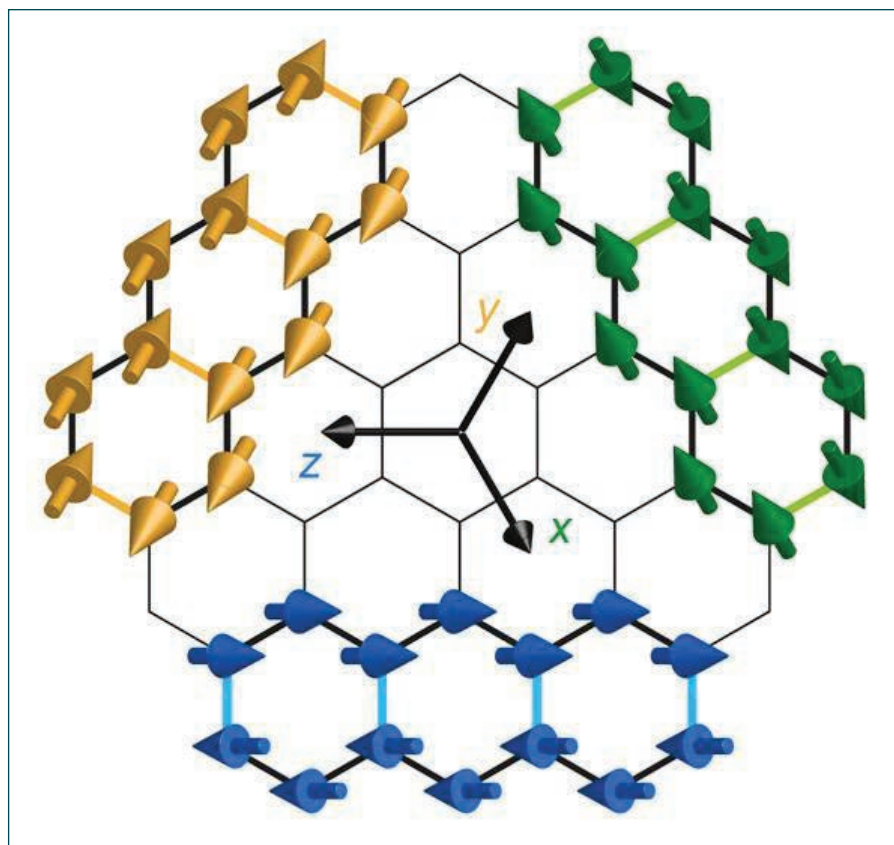


Fig. 1. Zigzag spin patterns propagating along three equivalent directions in the honeycomb lattice, each pattern rotated  $120^\circ$  from the other two.

In the 1970s, the American physicist Phil Anderson proposed the concept of a quantum spin liquid as a distinct electronic state of matter in which the usual long-range order of magnetic moments is avoided and magnons — a quantum of magnetic excitation — break up into fractional excitations. The most rudimentary geometrical arrangement producing a QSL is a triangular lattice, with a single interacting electron appearing at each vertex. Due to the triangular geometry, there is not a unique arrangement of electron spins producing a lowest energy: an arrangement of two electrons with up spin and one with down spin is energetically equivalent to one electron with up spin and two with down. Such a quantum system is frustrated, meaning there is no single quantum state uniquely possessing the lowest energy.

Because of the frustration, the spin arrangements in quantum spin liquids continuously shift, unlike the more-or-less fixed spin ordering in conventional magnetic materials. One such example of quantum spin liquids occurs in the Kitaev model, named after the theoretician who first described it. Highly unusual magnetic orderings, such as zigzag and spiral patterns, can appear around a Kitaev QSL state (Fig. 1).

In the Kitaev model, the bond-directional nature of the spin interactions in a honeycomb-like geometry produces a QSL. The  $\text{Na}_2\text{IrO}_3$  compound

features an (approximately) two-dimensional honeycomb lattice of iridium ions ( $\text{Ir}^{4+}$ ) sandwiched between layers of oxygen atoms. Theoretical considerations point toward a quantum spin liquid state arising in the  $\text{Na}_2\text{IrO}_3$  compound at low temperatures. Unfortunately, it is notoriously difficult to experimentally demonstrate the presence of a QSL. The first experiment demonstrating the existence of a quantum spin liquid utilized inelastic neutron scattering (INS). However, considerable time and effort was required to produce a crystalline sample large enough and pure enough to allow the use of INS.

The two iridium-based samples were too small for single-crystal INS, so diffuse magnetic x-ray scattering (a new technique for this type of study) was performed at the XSD 9-ID-B,C, 27-ID-B, and 30-ID-B,C beamlines of the APS. In the diffuse magnetic scattering measurements, the electromagnetic fields of the x-rays interacted with the spins of the electrons in the samples providing a Fourier transform of the spin arrangement (Fig. 2). Earlier studies indicated that at low temperatures, the honeycomb structure of  $\text{Na}_2\text{IrO}_3$  should support conventional magnetic interactions (Heisenberg interactions) as well as exotic (Kitaev) interactions. The Heisenberg interactions are isotropic in nature (i.e., the same in all directions), whereas the Kitaev interactions are highly direction-dependent (anisotropic). To reveal the anisotropy of the spin interactions at temperatures from near-absolute 0 to around 70 K, the diffuse magnetic x-ray scattering experiments at the APS were complemented with resonant magnetic x-ray diffraction measurements performed at XSD beamline 6-ID-B. Additionally, resonant inelastic x-ray scattering measurements were gathered at beamline ID20 at the ESRF.

Collectively, the measurements showed that bond-directional magnetic interactions dominated over much of the low-temperature range. Because each pair of spins on a bond tend to point along the bond, the presence of three types of bonds in the honeycomb lattice leads to frustration in much the same way as the three electron spins on a triangle are frustrated. This real-

space and spin-space entanglement indicated the presence of the rare Kitaev phase in  $\text{Na}_2\text{IrO}_3$ .

These findings highlight the benefits of using diffuse magnetic x-ray scattering to uncover bond-directional interactions that give rise to the QSL state.

— Philip Koth

**See:** Sae Hwan Chun<sup>1</sup>, Jong-Woo Kim<sup>1</sup>, Jungho Kim<sup>1</sup>, H. Zheng<sup>1</sup>, Constantinos C. Stoumpos<sup>1</sup>, C.D. Malliakas<sup>1</sup>, J.F. Mitchell<sup>1</sup>, Kavita Mehlawat<sup>2</sup>, Yogesh Singh<sup>2</sup>, Y. Choi<sup>1</sup>, T. Gog<sup>1</sup>, A. Al-Zein<sup>3</sup>, M. Moretti Sala<sup>3</sup>, M. Krisch<sup>3</sup>, J. Chaloupka<sup>4</sup>, G. Jackeli<sup>5,6</sup>, G. Khaliullin<sup>5</sup>, and B.J. Kim<sup>5\*</sup>, “Direct evidence for dominant bond-directional interactions in a honeycomb lattice iridate  $\text{Na}_2\text{IrO}_3$ ,” *Nat. Phys.* **11**, 462 (2015).

DOI: 10.1038/NPHYS3322

**Author affiliations:** <sup>1</sup>Argonne National Laboratory, <sup>2</sup>Indian Institute of Science Education and Research (IISER) Mohali, <sup>3</sup>European Synchrotron Radiation Facility, <sup>4</sup>Masaryk University, <sup>5</sup>Max Planck Institute for Solid State Research, <sup>6</sup>University of Stuttgart  
**Correspondence:** \* bjkim@fkf.mpg.de

Work in the Argonne Materials Science Division (sample preparation, characterization, and contributions to data analysis) was supported by the U.S. Department of Energy (DOE) Office of Science-Basic Energy Sciences, Materials Science and Engineering Division. K.M. acknowledges support from UGC-CSIR, India. Y.S. acknowledges DST, India, for support through Ramanujan Grant #SR/S2/RJN-76/2010 and through DST grant #SB/S2/CMP-001/2013. J.C. was supported by ERDF under project CEITEC (CZ.1.05/1.1.00/02.0068) and EC 7th Framework Programme (286154/SYLICA). This research used resources of the Advanced Photon Source, a U.S. DOE Office of Science User Facility operated for the DOE Office of Science by Argonne National Laboratory under Contract No. DE-AC02-06CH11357.

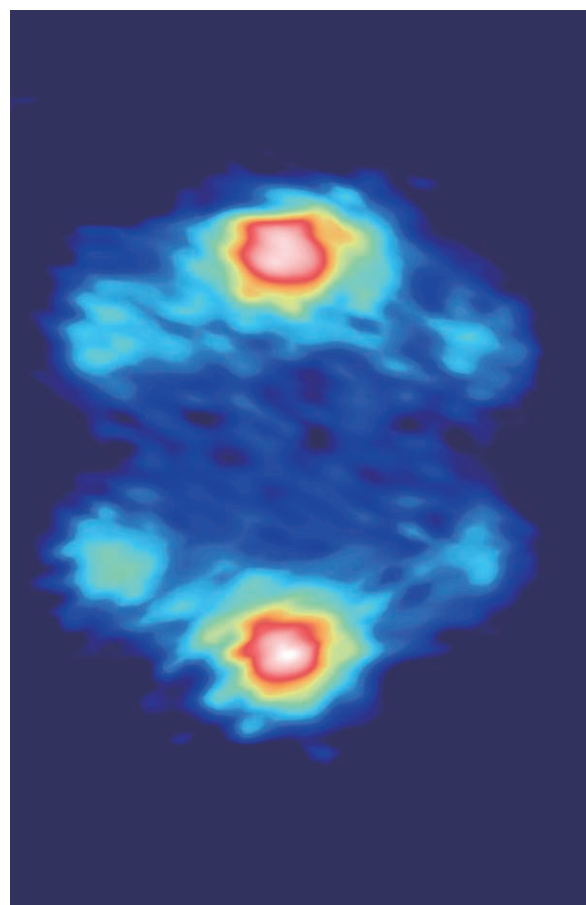


Fig. 2. Three pairs of diffuse magnetic x-ray scattering intensities associated with three short-range zigzag states fluctuating into one another in  $\text{Na}_2\text{IrO}_3$ . The distinct magnetic anisotropy of each state manifests bond-directional interactions that lead to strong magnetic frustration.

6-ID-B,C • XSD • Physics, materials science • Magnetic x-ray scattering, anomalous and resonant scattering (hard x-ray), general diffraction, grazing incidence diffraction • 3.2-38 keV • On-site • Accepting general users •

9-ID-B,C • XSD • Chemistry, materials science, life sciences • Nano-imaging, microfluorescence (hard x-ray), coherent x-ray scattering (hard x-ray), ultra-small-angle x-ray scattering • 4.5-30 keV • On-site • Accepting general users •

27-ID-B • XSD • Physics • Resonant inelastic x-ray scattering • 5-14 keV, 5-30 keV • On-site • Accepting general users •

30-ID-B,C • XSD • Physics, materials science • Inelastic x-ray scattering • 23.7-23.9 keV • On-site • Accepting general users •



# ANOMALOUSLY LARGE CHARGE TRANSFER IN AN ATOMIC LAYER CAKE OF TRANSITION METAL OXIDES

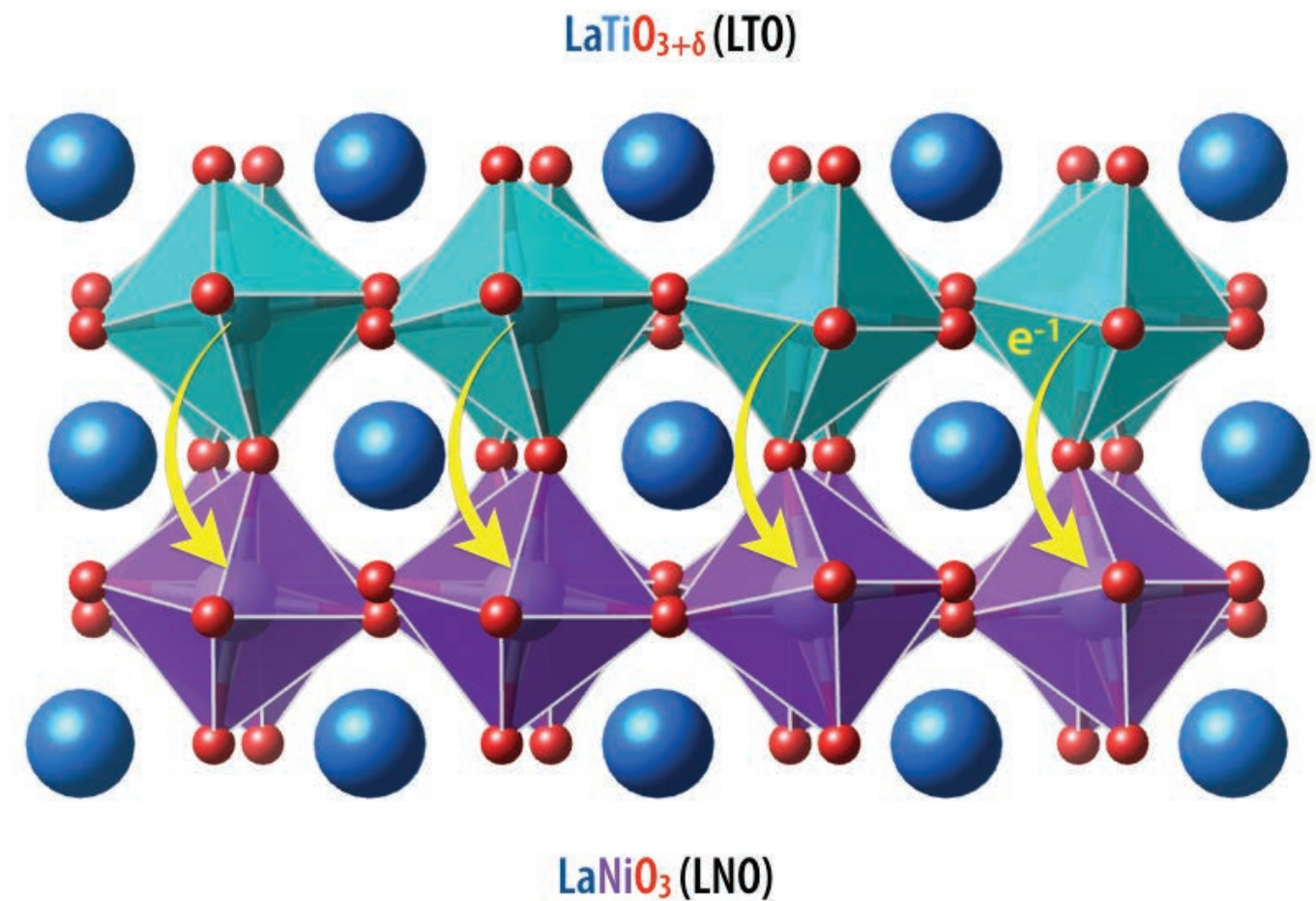


Fig. 1. Schematic of interfacial charge-transfer (yellow arrows) at the atomic scale in a heterostructure between doped Mott insulator  $\text{LaTiO}_{3+\delta}$  (top) and negative charge-transfer metal  $\text{LaNiO}_3$  (bottom).

**A**long with the critically important goal of making the next generations of electronics devices ever smaller, designers and developers also strive for multi-functionality. Traditional semiconductor-based microelectronic devices exploit interfacial charge transfer between different materials to create and manipulate electronic and magnetic states. The spintronic approach to electronics, based not just on electric charge but on spin as well, requires further rethinking materials and structures. Designing technologically relevant materials and understanding how charge transfer occurs at their interfaces is a continuing challenge for heterojunctions based on strongly correlated electronic materials. A team of researchers carried out studies at the APS that demonstrate how massive charge transfer occurs in a synthesized heterostructure of transition metal oxides to create an unusual Mott insulating ground state at the atomic scale. The work shows a path toward the development of electronics devices that are substantially more versatile and multifunctional than traditional semiconductors using various materials that could easily transition between a variety of electronic, magnetic, and spin states to achieve a wide range of functionalities in a single device.

Complex oxide interfaces have been found to offer tremendous possibilities for electronic and magnetic states that are unattainable with conventional semiconductors. Recent work has pointed toward a prominent role of partially filled d-shell transition metal ions in the phenomena connected to strongly correlated insulator behavior. The current work builds upon those ideas to examine an interface between a charge-transfer metal,  $\text{LaNiO}_3$  (LNO) and a doped Mott-Hubbard insulator,  $\text{LaTiO}_{3+\delta}$  (LTO). The team from the University of Arkansas, along with collaborators from the Indian Institute of Technology and Argonne, synthesized atomically thin Mott-Hubbard insulator/charge-transfer metal heterostructures and investigated them with resonant soft x-ray spectroscopy at XSD beamline 4-ID-C and diffraction at XSD beamline 6-ID-B, both of the APS.

The structure referred to as an LTO/LNO superlattice, was studied by x-ray absorption spectroscopy (XAS) and *in situ* x-ray photoemission spectroscopy (XPS) to determine how charge transfer operated in the novel interface. The experiment revealed an unexpected massive charge flow across the interface from titanium (Ti) to nickel (Ni) ions. Thus, the final state of Ni in the superlattice shows a state very close to  $\text{Ni}^{2+}$  within the chemical matrix originally supporting  $\text{Ni}^{3+}$ .

The team next investigated how this modified interfacial band structure alters the physical properties. X-ray absorption spectroscopy revealed an unusual electronic configuration of  $\text{Ni } 3d^8$ ,  $d^7$ , and  $d^8L$  states at the interfacial  $\text{NiO}_2$  layer. A reconstruction of the band structure near the interface was also confirmed, with the splitting of the Ni eg band gap of about 0.20 eV. Another bandgap of about 1.3 eV is seen between the Ti 3d and Ni  $e_g$  bands. Such a gap splitting has not been observed in other LNO-based heterojunctions.

The unusual insulating Mott ground state of the LTO/LNO heterostructure is an example of how manipulation of charge transfer can create exotic states in the electronic domain and also with orbital and spin degrees of freedom.

The researchers expect that further research involving other types of charge-transfer interfaces will open up even more intriguing possibilities for the eventual realization of electronics components with capabilities far beyond those in current semiconductors.

— Mark Wolverton

**See:** Yanwei Cao<sup>1\*</sup>, Xiaoran Liu<sup>1</sup>, M. Kareev<sup>1</sup>, D. Choudhury<sup>1,2</sup>, S. Middey<sup>1</sup>, D. Meyers<sup>1</sup>, J.-W. Kim<sup>3</sup>, P.J. Ryan<sup>3</sup>, J.W. Freeland<sup>3</sup>, and J. Chakhalian<sup>1\*\*</sup>, “Engineered Mott ground state in a  $\text{LaTiO}_{3+\delta}/\text{LaNiO}_3$  heterostructure,” *Nat. Commun.* **7**, 10418 (21 January 2016).

DOI: 10.1038/ncomms10418

**Author affiliations:** <sup>1</sup>University of Arkansas, <sup>2</sup>Indian Institute of Technology Kharagpur, <sup>3</sup>Argonne National Laboratory

**Correspondence:** \* yc003@uark.edu  
\*\* jak.chakhalian@rutgers.edu

J.C. and X.L. were supported by the Department of Energy grant DE-SC0012375 for synchrotron work at the Advanced Photon Source and material synthesis. D.M. was primarily supported by the Gordon and Betty Moore Foundation EPiQS Initiative through grant number GBMF4534. Y.C. and S.M. were supported by the DOD-ARO under grant number 0402-17291. This research used resources of the Advanced Photon Source, a US Department of Energy (DOE) Office of Science User Facility operated for the DOE Office of Science by Argonne National Laboratory under contract number DE-AC02-06CH11357.

4-ID-C • XSD • Physics, materials science • Magnetic circular dichroism (soft x-ray), x-ray magnetic linear dichroism, x-ray photoemission spectroscopy, x-ray photoemission electron microscopy, anomalous and resonant scattering (soft x-ray) • 500-2800 eV • On-site • Accepting general users •

6-ID-B,C • XSD • Physics, materials science • Magnetic x-ray scattering, anomalous and resonant scattering (hard x-ray), general diffraction, grazing incidence diffraction • 3.2-38 keV • On-site • Accepting general users •



# THE INNER RUMBLINGS OF NEW PHOTOVOLTAIC CHAMPION MATERIALS

Organolead halide perovskites have gained significant attention within the photovoltaic community as a potential next-generation solar-energy-harvesting platform. These materials show promise in the production of inexpensive solar power while offering the positive attributes of high efficiency, very light weight, and low cost. However, one limitation has been instability. A team of researchers working at the APS investigated the low-energy lattice dynamics of the organolead halide perovskites methylammonium lead iodide and methylammonium lead bromide. Their goal was to determine whether the atomic structure of the real material deviates from the ideal structure, which has so far been assumed in all theoretical models. Their findings reveal important discrepancies with the idealized structure of organolead halide perovskites in the temperature range relevant for the operation of perovskite solar cells. With even higher efficiencies and further reductions in production costs foreseen in the future, this study provides key insights to guide the understanding, optimization, and ultimately the commercial implementation of perovskite solar cells.

Organolead halide perovskites consist of a hybrid organic-inorganic lead halide material, which is the light-absorbing active layer. The heightened attention given to devices made out of these materials, commonly known as perovskite solar cells, is primarily due to their excellent and surging power-conversion efficiencies (well over 20%), along with the ability to use cheap, earth-abundant materials and low-cost fabrication methods in their production.

This special class of materials belongs to the category of hybrid (indicating their mixed organic-inorganic nature) lead (Pb) halides, with the chemical formula  $\text{MAPbX}_3$ , where MA stands for methylammonium ( $\text{CH}_3\text{NH}_3$ )

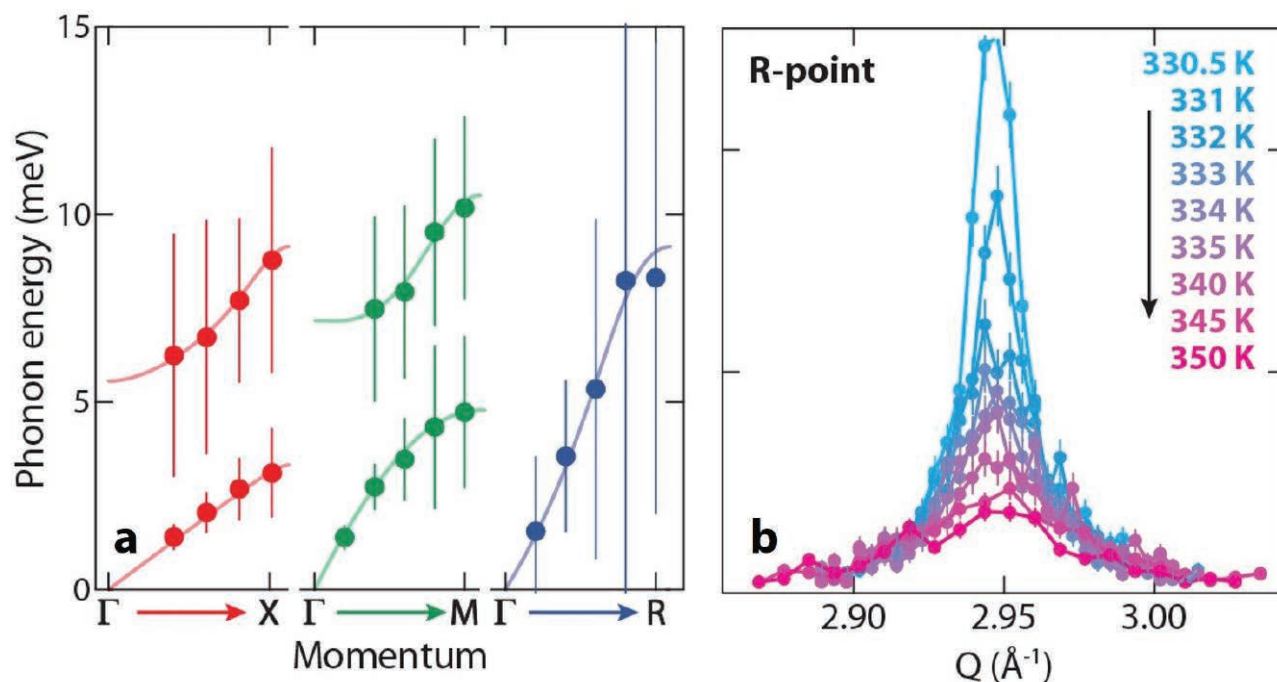


Fig. 1 (a). Momentum-energy dispersions of the lowest acoustic (red and green curves) and optical (transverse, blue curve) phonons in the cubic hybrid perovskite  $\text{CH}_3\text{NH}_3\text{PbBr}_3$ . The branches below are acoustic; the ones above are optical. The colors label different crystallographic directions. (b). Elastic diffraction signal at the R-point ( $3/2, 1/2, 1/2$ ), showing persistence of tetragonal domains even in the cubic phase above the structural transition point  $T_s = 327.5 \text{ K}$ .

and X represents either iodine (I), bromine (Br), or chlorine (Cl).

The team of researchers from the University of Toronto (Canada), DuPont Central Research and Development, DuPont Electronics and Communication Technologies, the University of Delaware, Argonne, Oak Ridge National Laboratory, and Carnegie Mellon University sought to answer the question: Are the structural deviations within organolead halide perovskites merely

dynamic or can they become static in the neighborhood of symmetry-breaking defect, forming “nano-puddles” with a different structure? They focused their attention on  $\text{MAPbI}_3$  and  $\text{MAPbBr}_3$ .  $\text{MAPbI}_3$  and  $\text{MAPbBr}_3$  crystallize at ambient temperatures in a tetragonal and cubic phase, respectively. Both compounds undergo a tetragonal-to-cubic structural transition upon warming above 327.5 K ( $\text{MAPbI}_3$ ) and 236.9 K ( $\text{MAPbBr}_3$ ).

The researchers' mission was to detail the nanoscale mechanics involved with the tetragonal-to-cubic phase transition. Inelastic x-ray scattering (IXS) measurements were performed at the HERIX spectrometer at XSD beamline 30-ID-B,C of the APS.

The team synthesized  $\text{MAPbI}_3$  and  $\text{MAPbBr}_3$  crystals using room-temperature solution processing routes. Inelastic x-ray scattering scans were measured in the cubic phase at temperatures of 350 K ( $\text{MAPbI}_3$ ) and 300 K ( $\text{MAPbBr}_3$ ). The scans allowed the team to resolve the phonon dispersions (Fig. 1a) within both compounds for their longitudinal and transverse modes, along the three high-symmetry directions connecting the zone center to specific zone-edge points ( $X$ ,  $M$ ,  $R$ ). From the experimental data, the team derived phonon frequencies and lifetimes.

Next, an investigation concerning the nature of the phase transition was conducted using neutron diffraction for a deuterated  $\text{MAPbI}_3$  crystal ( $d_6$ - $\text{MAPbI}_3$ ) and x-ray powder diffraction for a hydrogenated  $\text{MAPbI}_3$  polycrystal ( $h_6$ - $\text{MAPbI}_3$ ). Superlattice Bragg peak intensity and tetragonal distortion were measured to determine the phase-transition behavior. The neutron diffraction investigation was performed at the Spallation Neutron Source TOPAZ instrument at the U.S. DOE's Oak Ridge National Laboratory, while x-ray powder diffraction was conducted at the DND-CAT 5-BM-C beamline at the APS.

The researchers detected Bragg reflections from a different structural phase even in the (nominally) cubic regime (Fig. 1b). This finding demonstrates that nano-puddles with lower-than-cubic symmetry persist up to temperatures well above the structural phase transition (Fig. 2) and suggests that symmetry-breaking islands likely

nucleate around defects, and progressively grow larger over time. Eventually, they coalesce into nanoscopic-ordered structures that become macroscopically large below the phase transition.

The researchers established that lattice instability exists along the  $R$ -direction, triggered by a particular lattice mode that becomes progressively softer until the associated atomic displacements freeze out into a new structural configuration. They also explained that the cubic-to-tetragonal phase transition is positioned close to the tricritical point; while discovering the existence of pseudo-static, symmetry-breaking nano-regions above the cubic phase. Especially important is the fact that they determined  $\text{MAPbI}_3$  and  $\text{MAPbBr}_3$  perform well at a temperature range suitable for efficient photovoltaic operations.

Their work sheds new light on the inner workings of solar-energy-harvesting organolead halide perovskites. Exciting new possibilities in solar cell research exist due to the unusual, but attractive, photophysical properties of perovskite solar cells.

— William Arthur Atkins

**See:** Riccardo Comin<sup>1\*</sup>, Michael K. Crawford<sup>2,3</sup>, Ayman H. Said<sup>4</sup>, Norman Herron<sup>5</sup>, William E. Guise<sup>2</sup>, Xiaoping Wang<sup>6</sup>, Pamela S. Whitfield<sup>6</sup>, Ankit Jain<sup>1</sup>, Xiwen Gong<sup>1</sup>, Alan J. H. McGaughey<sup>7</sup>, and Edward H. Sargent<sup>1\*\*</sup>, “Lattice dynamics and the nature of structural transitions in organolead halide perovskites,” *Phys. Rev. B* **94**, 094301 (2016).

DOI: 10.1103/PhysRevB.94.094301

**Author affiliations:** <sup>1</sup>University of Toronto, <sup>2</sup>DuPont Central Research and Development, <sup>3</sup>University of Delaware, <sup>4</sup>Argonne National Laboratory, <sup>5</sup>DuPont

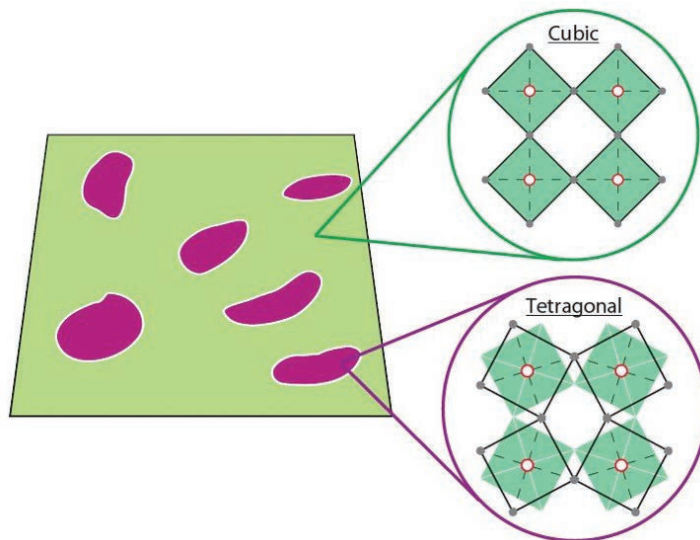


Fig. 2. Schematic of the structure of  $\text{MAPbX}_3$  perovskites above the tetragonal-to-cubic transition temperature, showing the presence of tetragonal nano-puddles inside the cubic phase. The insets show the cubic and tetragonal structural motifs with rotated octahedral in the tetragonal phase.

Electronics and Communication Technologies, <sup>6</sup>Oak Ridge National Laboratory, <sup>7</sup>Carnegie Mellon University

**Correspondence:** \* rcomin@mit.edu

\*\* ted.sargent@utoronto.ca

E.H.S. acknowledges the Natural Sciences and Engineering Research Council of Canada under the Discovery Grant program. A portion of this research at Oak Ridge National Laboratory's Spallation Neutron Source was sponsored by the Scientific User Facilities Division, Basic Energy Sciences, U.S. Department of Energy (DOE). The DuPont-Northwestern-Dow Collaborative Access Team beamlines are supported through E.I. duPont de Nemours & Co., Northwestern University, The Dow Chemical Co., the State of Illinois through the Department of Commerce and the Board of Education (HECA), the U.S. DOE Office of Energy Research, and the U.S. National Science Foundation Division of Materials Research. This research used resources of the Advanced Photon Source, a U.S. DOE Office of Science User Facility operated for the DOE Office of Science by Argonne National Laboratory under Contract No. DE-AC02-06CH11357.

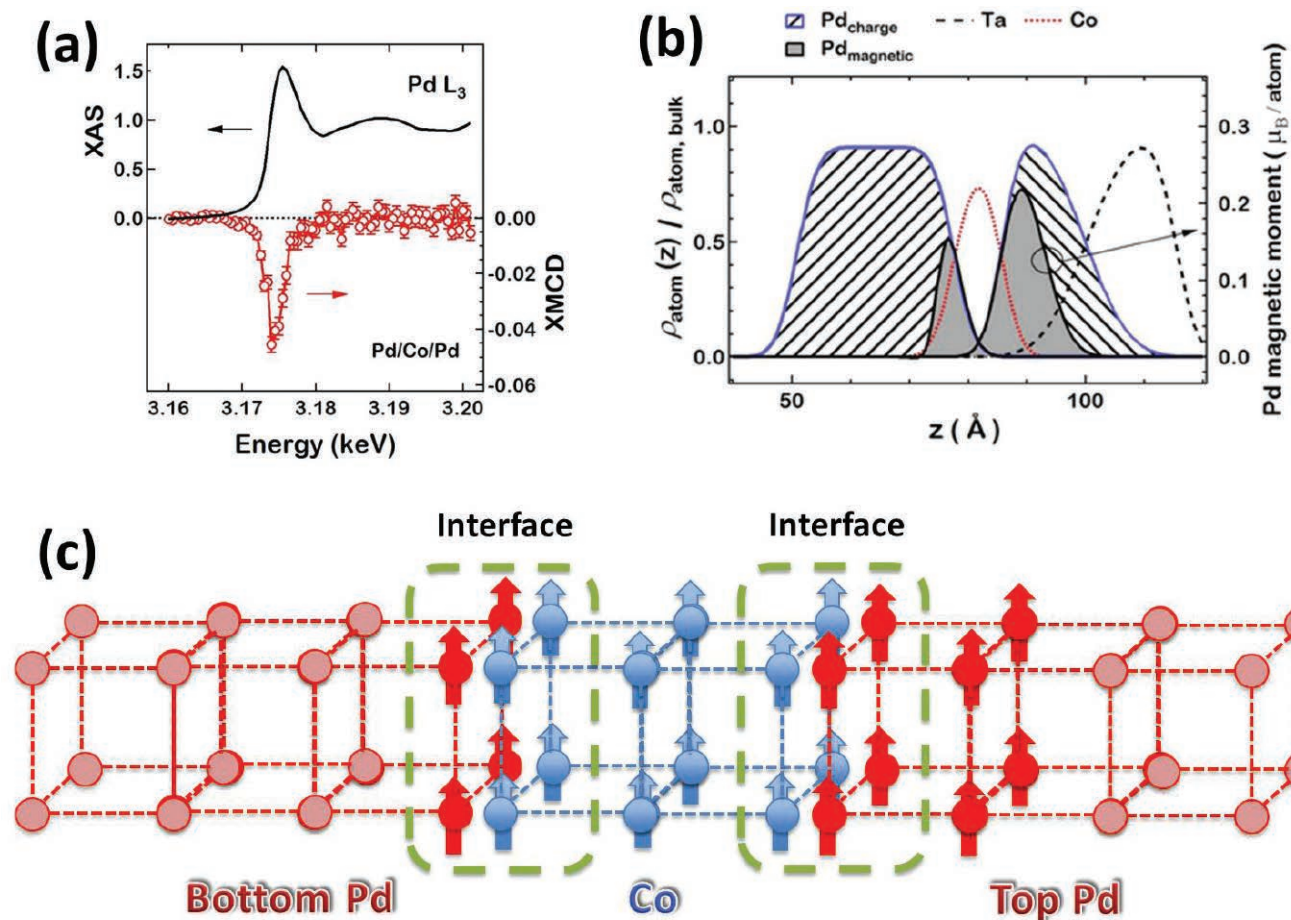
5-BM-C • DND-CAT • Materials science, polymer science • Powder diffraction, tomography, wide-angle x-ray scattering • 10-42 keV • On-site • Accepting general users •

30-ID-B,C • XSD • Physics, materials science • Inelastic x-ray scattering • 23.7-23.9 keV • On-site • Accepting general users •



# ASYMMETRIC CLOSE ENCOUNTERS OF THE MAGNETIC KIND

**T**raditional electronics is all about the movement of electric charge, but because spintronics adds the crucial element of electron spin, a whole new range of new phenomena must be considered. One of these is the magnetic moment in spintronic devices that use ferromagnetic/nonmagnetic (FN/NM) systems, which can greatly affect spin transport properties and thus the functionality of the device. This arises from a magnetic proximity effect at the FN/NM interface, in which the ferromagnetic material induces a magnetic moment in the adjoining nonmagnetic layer. Yet this magnetic proximity effect can vary in a tri-layer system consisting of both FM and NM layers. A group of researchers using the APS investigated this asymmetric effect to better understand how it affects spin transport properties. Achieving a better understanding of the precise origins of the effect through further studies will not only allow better and more efficient design of future spintronics-based devices, but may even lead to ways to exploit it to enhance and improve the promise of spintronics.



The team studied palladium (Pd)/cobalt(Co)/Pd thin-film structures, examining their microstructure and elemental distribution with high resolution transmission electron microscopy (HRTEM) and scanning transmission electron microscopy (STEM) and investigating magnetic effects with x-ray magnetic circular dichroism (XMCD) and x-ray resonant magnetic reflectivity (XRMR) at the XSD 4-ID-D x-ray beamline. Although the differences in microstructure between layer interfaces in such FM/NM systems have been studied previously, properly measuring magnetic asymmetries at the FM/NM interfaces has proven challenging, since it requires the ability to distinguish magnetic characteristics with both element- and depth-based resolution. Such measurements have been beyond the capabilities of most available scattering beamlines.

The HRTEM and STEM studies revealed a multigrained, mostly (111) texture in the Pd/Co/Pd films. Although a great deal of interfacial roughness was seen between the various film layers, the Co and Pd layers were clearly distinguishable.

Resonant x-ray reflectivity (RXR) measurements conducted at the APS provided a highly detailed depth profile with clearly contrasted, elementally specific resolution. The RXR studies also provided more information on the interfacial roughness of the film structures, showing it to be nearly identical between the top Co/Pd and the bottom Pd/Co interfaces. These measurements fit quite well with models that demonstrate very little difference in roughness at the top and bottom interfaces.

< Fig 1. (a) XAS and XMCD measured from the samples Pd/Co/Pd. The energy of circularly polarized x-rays were tuned to the Pd L3 edge to extract element specific information of the induced magnetic moment of Pd atoms. (b) Magnetic density profile of the Pd magnetic moment from the best fit model of the XRMR data measured at the Pd L3 edge. (c) Schematic diagram of induced magnetic region of the Pd. The spatial extent of the magnetic region and the total magnetic moment [gray area in (b)] is greater for the top Pd.

The x-ray magnetic circular dichroism (XMCD) observations tuned to Pd L edges showed direct evidence of a magnetic proximity effect with induced magnetic moments of nonmagnetic Pd in contact with ferromagnetic Co. Moreover, the quantitative magnetic moments of the top and bottom Pd layers could be distinguished by analyzing the XRMR data. Surprisingly, the induced Pd magnetic moments at the top Co/Pd interfaces were much larger than those at the bottom Pd/Co interfaces. The difference in magnetic proximity effect was present despite the nearly identical structural properties at the top and bottom interfaces.

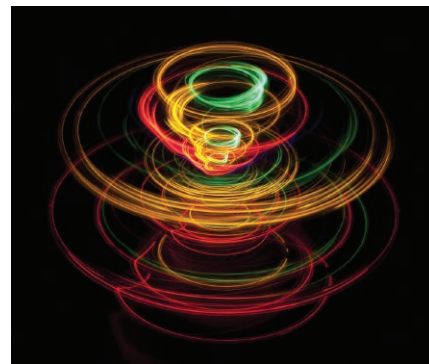
The team proposes two possible origins for this observed asymmetric magnetic effect in Pd. Differences in thickness between the top (1.5 nm) and bottom (2.5 nm) Pd film layers could create different magnetic moments, a possibility that might be resolved with a more detailed thickness-dependent study of the Pd/Co/Pd system. Alternatively, the asymmetric magnetic effect might be due to structural differences between the top and bottom Pd layers. Because the bottom Pd layer is deposited on a metallic tantalum buffer while the top Pd layer rests upon the Co layer, differences in the lattice constant properties could result with a concomitant effect on the overall magnetic moment.

It is known that the magnetic proximity effect modifies spin transport in FM/NM systems with possible increased resistivity, spin Hall effect, and increased domain wall velocity. Therefore, whatever its origins, the observed asymmetric magnetic proximity effect could potentially greatly affect the spin transport properties in the NM/FM/NM systems. — *Mark Wolverton*

**See:** Dong-Ok Kim<sup>1,2</sup>, Kyung Mee Song<sup>2,3</sup>, Yongseong Choi<sup>4</sup>, Byoung-Chul Min<sup>2</sup>, Jae-Sung Kim<sup>3</sup>, Jun Woo Choi<sup>2\*</sup>, and Dong Ryeol Lee<sup>1,4\*\*</sup>, “Asymmetric magnetic proximity effect in a Pd/Co/Pd trilayer system,” *Sci. Rep.* **6**, 25391 (2016). DOI: 10.1038/srep25391

**Author affiliations:** <sup>1</sup>Soongsil University, <sup>2</sup>Korea Institute of Science and Tech-

## The Discovery of Spintronics



An I.B.M. research fellow largely unknown outside a small fraternity of physicists, [Stuart] Parkin pattered for two years in a lab in the early 1990s, trying to find a way to commercialize an odd magnetic effect of quantum mechanics he had observed at supercold temperatures. With the help of a research assistant, he was able to manipulate the alignment of electronics to alter the magnetic state of tiny areas of a magnetic data storage disc, making it possible to store and retrieve information in a smaller amount of space. The huge increases in digital storage made possible by giant magnetoresistance, or GMR, made consumer audio and video iPods, as well as Google-style data centers, a reality.

“Redefining the Architecture of Memory,”

*The New York Times*

September 11, 2007

Graphic: <http://www.creativity103.com/design-packs/index.htm#rotate>

nology, <sup>3</sup>Sookmyung Women’s University, <sup>4</sup>Argonne National Laboratory

### Correspondence:

\* junwoo@kist.re.kr \*\* drlee@ssu.ac.kr

This work was supported by the KIST Institutional Program (2E26380), the Pioneer Research Center Program (2011-0027905), and NRF grants 2010-0004614, 2013R1A1A2011326, 2014K2A1A2048433, and 2013R1A2000245 funded by the Korean Government (MSIP and MOE). This research used resources of the Advanced Photon Source, a U.S. DOE Office of Science User Facility operated for the DOE Office of Science by Argonne National Laboratory under Contract No. DE-AC02-06CH11357.

4-ID-D • XSD • Physics, materials science • Anomalous and resonant scattering (hard x-ray), magnetic x-ray scattering, magnetic circular dichroism (hard x-ray) • 2.7-40 keV • On-site • Accepting general users •



# SQUEEZING OUT A NOVEL CONFINED METAL IN AN INSULATOR

Condensed-matter physicists find 5d perovskite iridates fascinating because of exotic states that arise during interplay among electron interaction, spin-orbit coupling, and crystal-field effect. These compounds can transform from an insulator to a confined metal during an applied stimulus. Past experiments have shown significant promise in the ability of 5d perovskite iridates to form functional materials that possess unique chemical and physical properties (including energy storage, ferroelectricity, and magnetism) that can respond to changes in their surroundings, owing to its tiny band gaps (as small as 0.1 eV) that can easily close by varying the doping, magnetic field, or temperature. Experiments show this material transforms consistently to a metal from doping and magnetic fields, while transition inconsistencies have arisen due to pressure. For that reason, a multi-institutional team of researchers successfully squeezed, for the first time, the insulating strontium iridium oxide ( $\text{Sr}_3\text{Ir}_2\text{O}_7$ ) using a diamond anvil cell (DAC) at the APS to produce a confined metal at around 60 GPa. Because a distinct pressure effect appears when compared to doping or magnetic field, their study indicates a new alternative approach is possible for synthesizing novel functional materials.

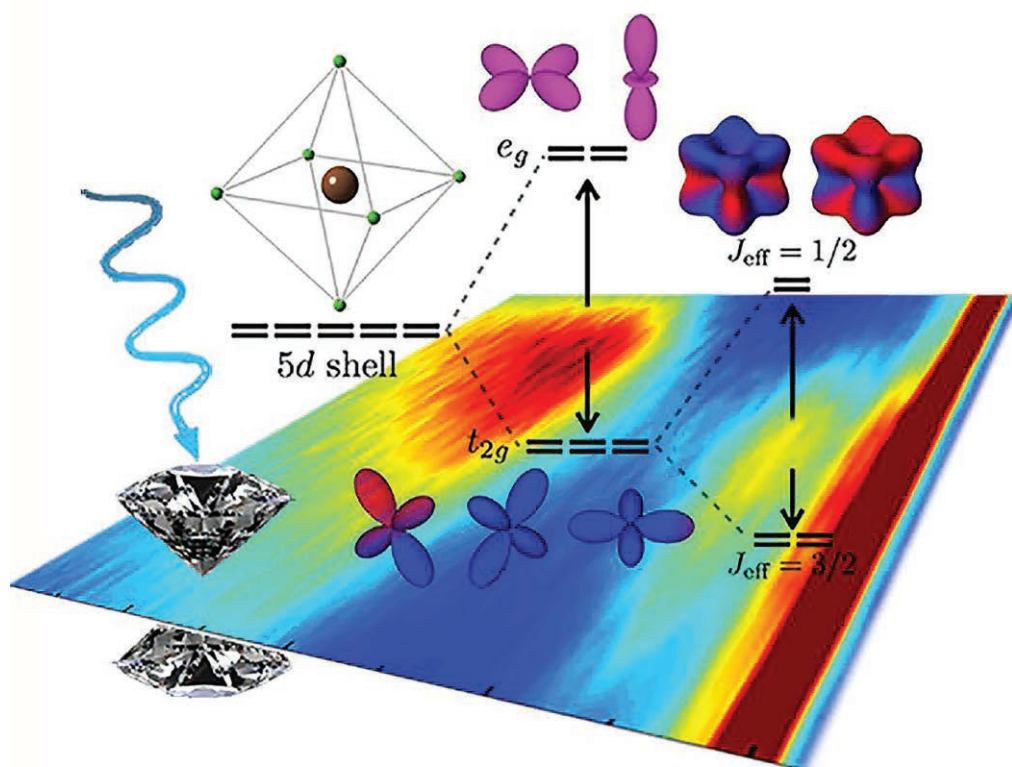


Fig. 1. Schematic of the RIXS experiment. The colored map shows the excitation events within the valence band of material  $\text{Sr}_3\text{Ir}_2\text{O}_7$ , which is obtained from RIXS measurements. The cartoon shows the energy levels in the materials that are related to these excitation events.

Such unique behaviors are of interest to the development of technically advanced systems for such actions as actuating, feedback, self-diagnosis, self-recovery, and sensing because the manipulation of such “smart” systems can mimic biochemical processes.

The team aspired to determine the actual transition pressure for  $\text{Sr}_3\text{Ir}_2\text{O}_7$ , as well as the underlying mechanisms. Using XSD beamlines 27-ID-B and 30-ID-B,C at APS, the team used measurements from electric resistance and resonant inelastic x-ray scattering (RIXS; Fig. 1) on single-crystal  $\text{Sr}_3\text{Ir}_2\text{O}_7$  under high pressure with the use of DAC experimental techniques. (Single crystals, which had never been used in previous high-pressure experiments, were used instead of powder.)

At pressures reaching upwards from about 63 GPa to 65 GPa and at a temperature of 300 K, the team used a four-probe sensing method (Fig. 2) to measure electric resistances within the ab-plane and along

the *c*-axis. Their results showed that  $\text{Sr}_3\text{Ir}_2\text{O}_7$  has insulating features at lower pressures (18.4 GPa and 43.15 GPa); however, at higher pressures (59.5 GPa and 63.0 GPa) it has metallic characteristics.

Considering its small charge gap, the team initially expected an insulator-metal transition should occur within  $\text{Sr}_3\text{Ir}_2\text{O}_7$  at relatively low pressure (30–40 GPa). However, the resulting insulator-metal transition occurs at a nearly doubled pressure value. The team concluded that it is the tilting and rotating of  $\text{IrO}_6$  octahedral sites within the compound that suppresses the electron mobility while trying to maintain an insulating state until tilting and rotating motions reach their limits.

Intriguingly, the high-pressure phase indicates a unique confinement phenomenon; that is,  $\text{Sr}_3\text{Ir}_2\text{O}_7$  became a confined metal with metallic behavior in the crystal's *ab*-plane, but with insulating behavior along its *c*-axis.

The team concluded that the novel behavior observed within this confined metal,  $\text{Sr}_3\text{Ir}_2\text{O}_7$  under high pressure is similar to the “strange metal” phase in a cuprate before the superconductivity appears. This makes it promising that superconductivity can be found in doped iridates.

Further, the team states that an important interplay exists between the electronic and structural properties of  $\text{Sr}_3\text{Ir}_2\text{O}_7$ . That same interplay exists generally within the Ruddlesden-Popper series of iridates, inferring the emergence of analogous novel behaviors that can reasonably be expected in these materials.

( $\text{Sr}_3\text{Ir}_2\text{O}_7$  is a type of Ruddlesden-Popper series of perovskite iridates whose chemical formula is  $\text{Sr}_{n+1}\text{Ir}_n\text{O}_{3n+1}$ , where *n* represents the number of  $\text{SrIrO}_3$  perovskite layers linking additional  $\text{SrO}$  layers; with Sr the chemical symbol for strontium and O for oxygen.)

Research in insulator-metal transitions represents an important challenge in modern condensed-matter physics. This important study adds credence to the fact that 5*d* perovskite iridates are at the threshold of a scientific frontier for studying exotic states of matter emerging from the interplay of electron interaction, spin-orbit cou-

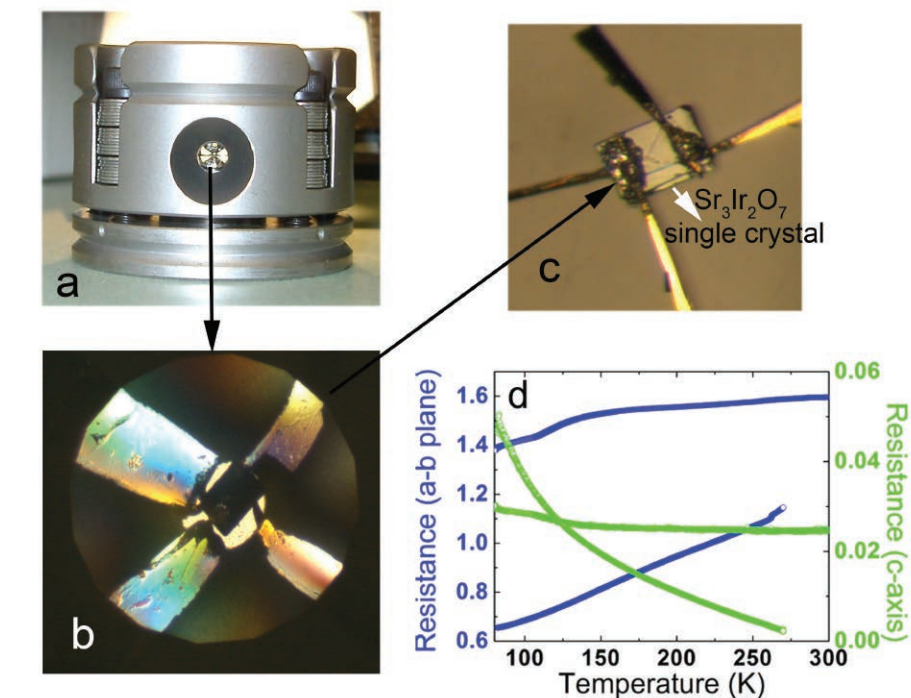


Fig. 2. Schematic of the 4-probe electric resistance experiment. (a) The diamond anvil cell that is used to generate the pressure; (b) The sample is confined in a chamber of diamond anvil cell with four electric probes attached; (c) The enlarged sample, a single-crystal of  $\text{Sr}_3\text{Ir}_2\text{O}_7$  with four electric probes, before it is put into diamond anvil cell; (d) The electric resistance of  $\text{Sr}_3\text{Ir}_2\text{O}_7$  above 59.5 GPa, which shows a metallic feature within the *a-b* plane but an insulating feature along the *c*-axis.

pling, and crystal-field effect. Such a discovery within these compounds could lead to new methods of synthesizing novel states of matter, those that are currently impossible with other methods. — William Arthur Atkins

**See:** Yang Ding<sup>1,2,3\*</sup>, Liuxiang Yang<sup>1,3</sup>, Cheng-Chien Chen<sup>2,4</sup>, Heung-Sik Kim<sup>5</sup>, Myung Joon Han<sup>5</sup>, Wei Luo<sup>6</sup>, Zhenxing Feng<sup>2</sup>, Mary Upton<sup>2</sup>, Diego Casa<sup>2</sup>, Jungho Kim<sup>2</sup>, Thomas Gog<sup>2</sup>, Zhidan Zeng<sup>1,3</sup>, Gang Cao<sup>7</sup>, Ho-kwang Mao<sup>1,3</sup>, and Michel van Veenendaal<sup>2,8</sup>, “Pressure-Induced Confined Metal from the Mott Insulator  $\text{Sr}_3\text{Ir}_2\text{O}_7$ ,” *Phys. Rev. Lett.* **116**, 216402 (2016). DOI: 10.1103/PhysRevLett.116.216402

**Author affiliations:** <sup>1</sup>Center for High Pressure Science and Technology Advanced Research, <sup>2</sup>Argonne National Laboratory, <sup>3</sup>Carnegie Institution of Washington, <sup>4</sup>University of Alabama at Birmingham, <sup>5</sup>Korea Advanced Institute of Science and Technology, <sup>6</sup>Uppsala University, <sup>7</sup>University of Kentucky, <sup>8</sup>Northern Illinois University

**Correspondence:**

\* yang.ding@hpstar.ac.cn

C.C.C. is supported by the Aneesur Rahman Postdoctoral Fellowship at Argonne. H.-S.K. and M.J.H. were supported by the Basic Science Research Program through NRF (Grant No. 2014R1A1A2057202) and by Samsung Advanced Institute of Technology (SAIT). G.C. acknowledges National Science Foundation support via Grant No. DMR1265162. H.-k. M. acknowledges the support of U.S. Department of Energy (DOE) Office of Science-Basic Energy Sciences under Award No. DE-FG02-99ER45775 and NSFC Grant No. U1530402. M.v.v. is supported by the U.S. DOE under Award No. DE-FG02-03ER46097, and by the Institute for Nanoscience, Engineering, and Technology at Northern Illinois University. This research used resources of the Advanced Photon Source, a U.S. DOE Office of Science User Facility operated for the DOE Office of Science by Argonne National Laboratory under contract number DE-AC02-06CH11357.

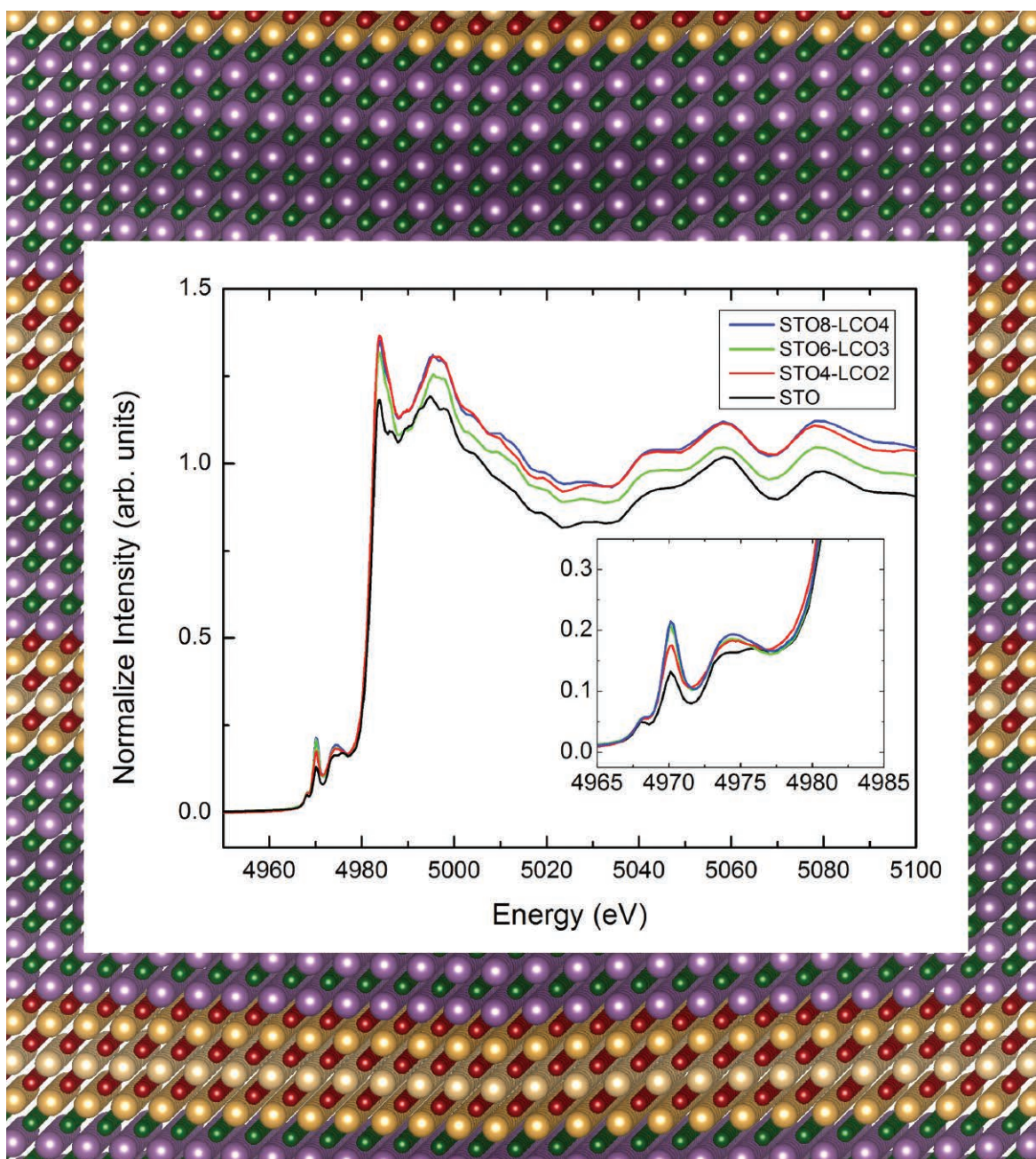
27-ID-B • XSD • Physics • Resonant inelastic x-ray scattering • 5-14 keV, 5-30 keV • On-site • Accepting general users •

30-ID-B,C • XSD • Physics, materials science • Inelastic x-ray scattering • 23.7-23.9 keV • On-site • Accepting general users •



# INDUCING POLARIZATION IN SUPERLATTICES BY ALTERNATING NON-FERROELECTRIC OXIDE LAYERS

The novel properties of superlattices make them ideal candidates for electronic applications that benefit from a separation of electrons and holes, such as generating electricity or photoelectrochemical hydrogen for fuel cells. While the abilities of superlattices composed of ferroelectric oxides have been previously examined, there has been little work done looking at non-ferroelectric oxides. A new study at the APS investigated a non-ferroelectric superlattice composed of two perovskite oxides— $\text{SrTiO}_3$  and  $\text{LaCrO}_3$ —to characterize its properties. The results include strong polarization, comparable to that of ferroelectric systems, which opens up new material options for photochemical and photovoltaic applications.



Superlattices are composed of alternating layers of two or more materials, each layer usually about one nanometer thick, built on top of a crystalline substrate. The large number of interfaces within a superlattice creates intriguing electronic properties. Recent work by a team with members from the Pacific Northwest National Laboratory, Argonne National Laboratory, and the SciTech Daresbury Campus (UK) assessed how the non-ferroelectric oxides SrTiO<sub>3</sub> and LaCrO<sub>3</sub> behave in a superlattice and whether they induce polarization across the superlattice. The studies showed that the charged interfaces between the superlattice layers produce built-in electric fields and potential gradients.

The team began by modeling from first principles, using density functional theory to describe the electronic structure of the superlattice. Their model predicted built-in electric fields across the two layers due to the differing distribution of charge at the interface on each side of a layer. The model predicted the fields across the SrTiO<sub>3</sub> and LaCrO<sub>3</sub> layers were of opposite sign. Additionally, both of the layers in the model reacted to the repetition of alternately-charged interfaces by distorting the shape of their oxygen octahedra, thus changing the bond lengths for Ti-O and Cr-O.

To create sample superlattices, the team laid down alternating layers of SrTiO<sub>3</sub> and LaCrO<sub>3</sub> on a crystalline substrate of (La,Sr)(Al,Ta)O<sub>6</sub>, beginning with SrTiO<sub>3</sub>. The samples varied the width of the SrTiO<sub>3</sub> and LaCrO<sub>3</sub> layers. The background of Fig. 1 shows a computer-generated depiction of a superlattice alternating an eight-atom-thick layer

of SrTiO<sub>3</sub> with a three-atom-thick layer of LaCrO<sub>3</sub>. The samples were grown with alternating, oppositely-charged interfaces between the SrTiO<sub>3</sub> and LaCrO<sub>3</sub>, e.g., when one interface had a termination of LaO-TiO<sub>2</sub> with a positive charge, the next one had a termination of SrO-CrO<sub>2</sub> with a negative charge.

The team measured the core-level and valence band photoemission spectra of the samples; they detected evidence of built-in electric potentials using x-ray photoelectron spectroscopy. The core peak measurements and modeled peak-broadening (using flat-band reference spectra for each layer) showed built-in potential gradients at SrTiO<sub>3</sub>-LaCrO<sub>3</sub> interfaces. The features measured in the valence band spectrum imply no large-scale charge transfer, bolstering the conclusion of built-in electric fields within both layers of the superlattice.

The team used XSD beamlines 20-BM-B and 20-ID=B,C at the APS to examine the bonding environment with x-ray absorption near-edge spectroscopy (XANES). The data showed a higher-than expected pre-edge peak, which indicates cation displacement perpendicular to the interface; this data is shown as part of Fig. 1. The unexpected pre-edge peak implies a distortion of the titanium octahedra that is in agreement with the team's models. Most exciting, though, is that this is a result previously only seen in ferroelectric superlattices.

The team made scanning-transmission electron microscope-high angle annular dark field measurements to create a visual representation of the displaced ions in the superlattice. From these measurements they could calculate the polarization across each unit cell in the superlattice, showing polarization is greatest near the interface between the SrTiO<sub>3</sub> layer and the crystalline base of the superlattice, decreases near the middle of the SrTiO<sub>3</sub> layer, and is the least strong at the SrTiO<sub>3</sub>-LaCrO<sub>3</sub> interface. These results again reinforce the idea that built-in potential differences between the superlattice layers create polarization through the SrTiO<sub>3</sub> layers.

Taken together, these results show that the alternation of polar and non-polar layers in a perovskite oxide superlattice induce polarity as strong as that induced in ferroelectric materials, opening

up a range of applications for these non-ferroelectric materials.

— Mary Alexandra Agner

**See:** Ryan B. Comes<sup>1\*</sup>, Steven R. Spurgeon<sup>1</sup>, Steve M. Heald<sup>2</sup>, Despoina M. Kepaptsoglou<sup>3</sup>, Lewys Jones<sup>4</sup>, Phuong Vu Ong<sup>1</sup>, Mark E. Bowden<sup>1</sup>, Quentin M. Ramasse<sup>3</sup>, Peter V. Sushko<sup>1</sup>, and Scott A. Chambers<sup>1\*</sup>, "Interface-Induced Polarization in SrTiO<sub>3</sub>-LaCrO<sub>3</sub> Superlattices," *Adv. Mater. Interfaces* **3**, 1500779 (2016).

DOI: 10.1002/admi.201500779

**Author affiliations:** <sup>1</sup>Pacific Northwest National Laboratory, <sup>2</sup>Argonne National Laboratory, <sup>3</sup>SciTech Daresbury Campus, <sup>4</sup>University of Oxford

**Correspondence:**

\* ryan.comes@pnnl.gov

\*\* sa.chambers@pnnl.gov

R.B.C. was supported by the Linus Pauling Distinguished Postdoctoral Fellowship at Pacific Northwest National Laboratory (PNNL LDRD PN13100/2581). S.R.S., M.E.B., and S.A.C. were supported by the U.S. Department of Energy (DOE) Office of Science-Basic Energy Sciences (BES) Division of Materials Sciences and Engineering under Award No. 10122. P.V.S. and P.V.O. were supported by the LDRD Program at PNNL. PNNL work was performed in the Environmental Molecular Sciences Laboratory, a National Science User Facility sponsored by the U.S. DOE Office of Biological and Environmental Research. The research leading to these results received funding from the European Union Seventh Framework Programme under Grant Agreement No. 312483—ESTEEM2 (Integrated Infrastructure Initiative (I3)). This research used resources of the Advanced Photon Source, an Office of Science User Facility operated for the U.S. DOE Office of Science by Argonne National Laboratory, and was supported by the U.S. DOE under Contract No. DE-AC02-06CH11357, and of the Canadian Light Source and its funding partners.

20-BM-B • XSD • Materials science, environmental science, chemistry • X-ray absorption fine structure, microfluorescence (hard x-ray), diffraction anomalous fine structure • 2.7-32 keV, 2.7-35 keV • On-site • Accepting general users •

20-ID-B,C • XSD • Materials science, environmental science, chemistry • X-ray absorption fine structure, x-ray Raman scattering, micro x-ray absorption fine structure, microfluorescence (hard x-ray), time-resolved x-ray absorption fine structure, x-ray emission spectroscopy • 4.3-27 keV, 7-52 keV • On-site • Accepting general users •

Fig. 1. Both XANES data and a computational depiction of the perovskite oxide superlattices investigated in this work are shown. The XANES data, especially the peaks in the 4000-eV range (see inset), show that the superlattices exhibit a polarization response similar to ferroelectric superlattices. The computational model of the superlattice shows the alternating layers of SrTiO<sub>3</sub> and LaCrO<sub>3</sub>; strontium atoms are purple, titanium green, lanthanum gold, and chromium red. The x-ray data was taken by Steve Heald at Sector 20-BM of the APS; the computational model depiction was created by Peter Sushko.



# A LINK BETWEEN CUPRATE LATTICE VIBRATIONS AND HIGH-TEMPERATURE SUPERCONDUCTORS

One of the key phenomena that marks high-temperature superconductors (HTSC) is the electron pairing mechanism displayed by such materials. In cuprates such as LCO ( $\text{La}_2\text{CuO}_4$ ), this can involve electron-phonon interaction (EPI) and electron-electron interaction (EEI). Non-equilibrium quasiparticles (QP) can lead to a strong lattice response for probing EPI and EEI effects in unconventional HTSCs and similar effects in materials such as SIO ( $\text{Sr}_2\text{IrO}_4$ ), which if confirmed, may help researchers to more fully understand EPI and EEI effects in HTSCs. Using photon-induced QPs and the high-brightness x-rays from the APS, a team of investigators explored similarities between the cuprate HTSC material LCO and the Mott insulator SIO. The work shows that SIO demonstrates striking similarities with cuprates such as LCO with a strong EPI effect that persists even in non-equilibrium conditions. This electron-phonon coupling can provide a new window into the understanding of cuprate lattice vibrations that are closely involved in various phase states important in high-temperature superconductivity. Such insights will be crucial in the development of materials for HTSC devices.

Quasiparticles are a type of emergent phenomenon observed in solid matter that approximate the actions or movements of particles such as electrons, but are not actually fermions or bosons. Their behavior can reveal important clues about fine structural, electronic, and magnetic characteristics and the nature of the coupling between these degrees of freedom in a solid. Toward that end, the researchers in this study, from Michigan State University, Tulane University, and Argonne National Laboratory, subjected SIO thin films to optical-pump x-ray diffraction from 0.5 eV to 3.0 eV at the XSD 7-ID-B,C,D beamline of the APS.

Although as a Mott insulator SIO features a quite different electronic structure than cuprates such as LCO, along with a different active orbital, the SIO thin films displayed a similar, unexpectedly strong lattice correlation to the optical excitation, possibly due to the presence of quasiparticles consisting of an electron at the bottom of the upper Hubbard band and a hole at the top of the lower Hubbard band. The crystallographic (0 0 12) diffraction peak showed the QP effect on lattice dynamics, with a structural recovery that was strongly dependent on film thickness, taking longer with thicker films.

Such optically-induced lattice expansion is known to sometimes result from photostriction in piezoelectric materials, but the investigators exclude this because SIO is not piezoelectric. They also rule out thermal expansion because the SIO lattice parameter is insensitive to temperature and thermal diffusion in SIO quickly dissipates the laser heating effects.

Transient absorption spectroscopy (TAS) measurements show a thickness-dependent photon-induced transparency immediately after excitation with both a fast and a slow component, with the slow component matching the lattice recovery dynamics.

*"Vibrations" cont'd. on page 32*

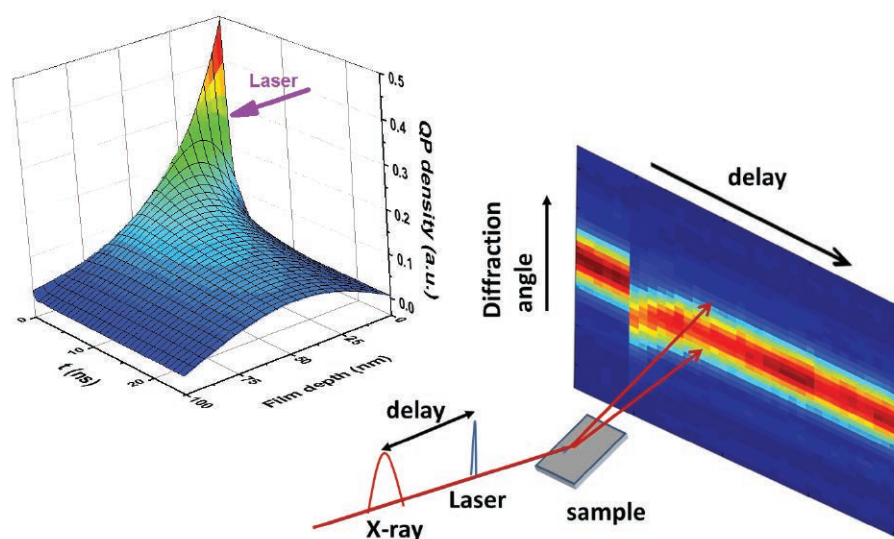


Fig.1. Schematic setup of the laser pump-x-ray probe experiment at APS beamline 7-ID-B,C,D showing a typical x-ray diffraction pattern as a function of the delay between the pump laser and the probing x-ray. *Insert:* the space and QP diffusion dynamics in a 100-nm film reconstructed from the time-dependent x-ray diffraction data.

# AN ATOMIC CONTRADICTION

How can a material conduct and impede the flow of electrons at the same time? Scientists created just such a material—a polar metal—by stabilizing a thin film on a slightly skewed supporting lattice, and then used the APS to study and refine this seemingly contradictory new substance. This research will make possible the development of new materials with unusual coexisting properties, such as those with anisotropic thermoelectric responses and magnetoelectric multiferroics, which could in turn stimulate the development of devices capable of performing electrical, magnetic, and optical functions simultaneously.

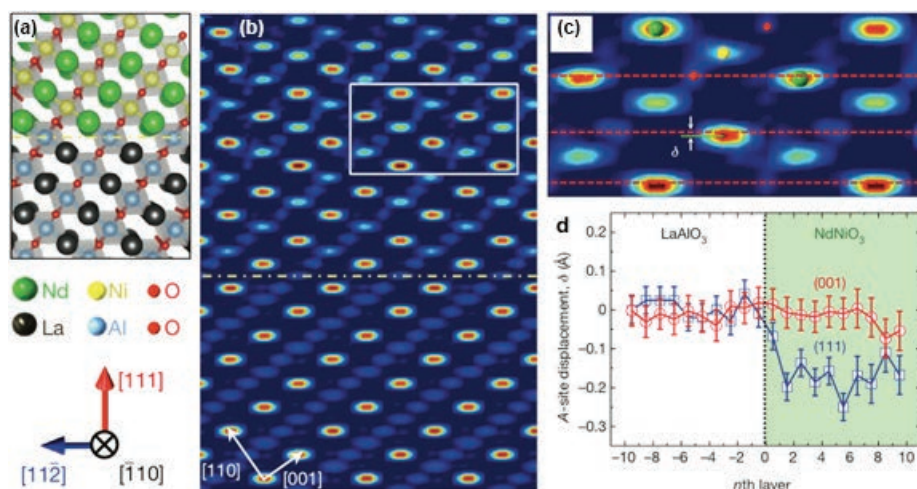


Fig. 1. Non-centrosymmetric NdNiO<sub>3</sub> thin films on LaAlO<sub>3</sub> (111) substrates. (a) Schematic illustration of the atomicscale thinfilm heterostructure. (b) Twodimensional electron density maps sliced through the pseudocubic (110) plane reconstructed through synchrotron CTR measurements and subsequent COBRA analyses. (c) Magnified images of electron density maps for the regions indicated by open rectangles in (b). Red broken lines in (c) represent the positions of oxygen atoms, which are taken as references to measure relative offcentre displacements ( $\delta$ ) of Nd atoms. (d) Layerdependent evolution of the A-site relative polar displacements across the interface in NdNiO<sub>3</sub>/LaAlO<sub>3</sub> (111) thin films. The 0th layer represents the NdNiO<sub>3</sub>/LaAlO<sub>3</sub> interface. In the twodimensional electron density map of (b), the A-site acentric displacements shown in (d) are measured with respect to oxygen atoms as displayed in (c). Image: C. B. Eom

A word can have two opposite meanings: One can bolt quickly away or bolt something down; dust the furniture by removing small particles or dust pesticides on a crop by adding them. A person, at least a fictional one, can have two conflicting personalities: Dr. Jekyll and Mr. Hyde. It turns out that a substance can have two incompatible properties: It can be at once a metal that conducts electricity and a polar material that insulates against electricity. These

polar metals were first proposed by P.W. Anderson and E.I. Blount some 50 years ago and they previously existed only serendipitously, but researchers from the University of Wisconsin–Madison, Northwestern University, Pennsylvania State University, the University of California, Irvine, Nanjing University, Argonne National Laboratory, and Cornell University synthesized these materials at room temperature in a laboratory and carried out a variety of studies.

To create the Jekyll-Hyde polar metal (Fig. 1), the researchers devised a new approach to molecular synthesis. Using a quantum mechanical design, they painstakingly grew a thin film, atom by atom, onto a supporting lattice. To keep the equal and opposite charges of the electrons from cancelling each other out, the structure of the supporting lattice was slightly skewed. The lattice was made of ternary ABO<sub>3</sub> perovskite  
*“Atomic” cont’d. on page 32*



*“Vibrations” cont’d. from page 30*

The researchers thus conclude that the lattice expansion is driven by long-lived electronic structure change associated with quasiparticles that diffuse and recombine at the surfaces and interfaces, with a continuous-time random walk diffusive dynamics. Differences in the dynamics observed at different photon energies can be explained by variations in initial QP distribution and thus confirm the QP diffusion picture, since the 1.5-eV pump has greater penetration depth than the 3.0-eV pump.

Considering the pump photon data and the band structure of SIO compared to the structure of LCO, the experimenters attribute the QPs to the formation of doublons and holons with zero spin in a background of spin 1/2. Excitation in SIO occurs in CT p-d and d-d transitions, whereas in LCO it primarily involves p-d charge transfer, although a d-d CT instability has also been suggested as a cause for lattice expansion in LCO. — *Mark Wolverton*

**See:** Yuelin Li<sup>1\*</sup>, Richard D. Schaller<sup>1</sup>, Mengze Zhu<sup>2</sup>, Donald A. Walko<sup>1</sup>, Jungho Kim<sup>1</sup>, Xianglin Ke<sup>2</sup>, Ludi Miao<sup>3</sup>, and Z.Q. Mao<sup>3</sup>, “Strong lattice correlation of non-equilibrium quasiparticles in a pseudospin-1/2 Mott insulator Sr<sub>2</sub>IrO<sub>4</sub>,” *Sci. Rep.* **6**, 19302 (20 January 2016). DOI: 10.1038/srep19302

**Author affiliations:** <sup>1</sup>Argonne National Laboratory, <sup>2</sup>Michigan State University, <sup>3</sup>Tulane University

**Correspondence:** \* ylli@aps.anl.gov

M.Z. and X.K. acknowledges start-up funds from Michigan State University. Work at Tulane University was supported by the NSF under Grant DMR-1205469 and U.S. Department of Defense Army Research Office under Grant No. W911NF0910530. This research used resources of the Advanced Photon Source and the Center for Nanoscale Materials, both U.S. Department of Energy (DOE) Office of Science-Basic Energy Sciences user facilities operated for the DOE Office of Science by Argonne National Laboratory under Contract No. DE-AC02-06CH11357.

**7-ID-B,C,D • XSD • Materials science, atomic physics, chemistry • Time-resolved x-ray scattering, time-resolved x-ray absorption fine structure, phase contrast imaging • 6-21 keV • On-site • Accepting general users •**

*“Atomic” cont’d. from page 31*

oxides, which were chosen for their electronic characteristics. The B cations in the structure created a sublattice that contributed to conduction, while the A cations created another sublattice that could undergo polarization.

To determine the best composition for the thin film, the team calculated that rare-earth (R) nickelates, RNiO<sub>3</sub>, specifically NdNiO<sub>3</sub>, with a non-equilibrium tilt pattern, would be best for generating polar displacements. Therefore, using pulsed laser deposition, the scientists deposited high-quality NdNiO<sub>3</sub> films on a LaAlO<sub>3</sub> substrate to provide increased bond connectivity. By clamping the film onto the rare-earth nickelate lattice, the internal structure of the molecules remained asymmetric, with the tilt angle varying between 4° and 8°, and kept the polarity of the material.

When the experiment was complete, the researchers demonstrated that the material had both polar and metallic properties, at room temperature, by using optical, electronic, and structural measurements. The cooperative polar neodymium and nickel displacements were verified using high-resolution synchrotron x-ray diffraction and near-edge x-ray absorption fine structure at XSD beamlines 4-ID-D, 6-ID-B,C and D, 12-ID-C,D and 33-ID-D,E at the APS. Hall measurements located mobile charge carriers in concentrations high enough to produce metallic conductivity. The researchers also experimented with a LaNiO<sub>3</sub> thin film, which is more conducting, and discovered that it too exhibited a polar metallic state. Since their initial models predicted that the material would not remain polar, the researchers needed to reevaluate and refine their models continually.

Beyond the discovery of these potentially useful polar materials, the team developed the new technique of geometric stabilization as a way to accelerate the discovery of new multifunctional materials with unusual coexisting properties. — *Dana Desonie*

**See:** T.H. Kim<sup>1</sup>, D. Puggioni<sup>2</sup>, Y. Yuan<sup>3</sup>, L. Xie<sup>4,5</sup>, H. Zhou<sup>6</sup>, N. Campbell<sup>7</sup>, P.J. Ryan<sup>6</sup>, Y. Choi<sup>6</sup>, J.-W. Kim<sup>6</sup>, J.R. Patzner<sup>1</sup>, S. Ryu<sup>1</sup>, J.P. Podkaminer<sup>1</sup>, J. Irwin<sup>1</sup>, Y. Ma<sup>1</sup>, C.J. Fennie<sup>7</sup>, M.S. Rzchowski<sup>1</sup>, X.Q. Pan<sup>4</sup>, V. Gopalan<sup>3</sup>, J.M.

Rondinelli<sup>2</sup>, and C.B. Eom<sup>1\*</sup>, “Polar metals by geometric design,” *Nature* **533**, 68 (5 May 2016).

DOI: 10.1038/nature17628

**Author affiliations:** <sup>1</sup>University of Wisconsin-Madison, <sup>2</sup>Northwestern University, <sup>3</sup>Pennsylvania State University, <sup>4</sup>University of California, Irvine, <sup>5</sup>Nanjing University, <sup>6</sup>Argonne National Laboratory, <sup>7</sup>Cornell University

**Correspondence:** \* ceom@wisc.edu

This work was supported by the National Science Foundation (NSF) under DMRE Work at the University of Wisconsin–Madison was supported by the U.S. Department of Energy (DOE) Office of Science-Basic Energy Sciences (BES) under award number DE-FG02-06ER46327. Work at Pennsylvania State University was supported by the DOE–BES under award number DE-SC0012375 (Y.Y., V.G.). The work at Northwestern University was supported by the Army Research Office under award numbers W911NF-15-1-0017 (J.M.R.), and DOE–BES DE-SC0012375 (D.P.). The work at Argonne is supported by the DOE–BES under contract number DE-AC02-02-06CH11357 (H.Z., P.J.R., Y.C., J.W.K.). The computational work made use of the Haise and Kilrain clusters at the Navy Department of Defense (DOD) Supercomputing Resource Center under the High Performance Computing Modernization Program initiative of the U.S. DOD and NSF XSEDE (ACI-1053575). The work at Cornell University was funded by DMR-1056441 (C.J.F.). This research used resources of the Advanced Photon Source, a U.S. DOE Office of Science User Facility operated for the DOE Office of Science by Argonne National Laboratory under Contract No. DE-AC02-06CH11357.

**4-ID-D • XSD • Physics, materials science • Anomalous and resonant scattering (hard x-ray), magnetic x-ray scattering, magnetic circular dichroism • 2.7-40 keV • On-site • Accepting general users •**

**6-ID-B,C • XSD • Physics, materials science • Magnetic x-ray scattering, anomalous and resonant scattering (hard x-ray), general diffraction, grazing incidence diffraction • 3.2-38 keV • On-site • Accepting general users •**

**6-ID-D • XSD • Physics, materials science • magnetic x-ray scattering, high-energy x-ray diffraction, powder diffraction, pair distribution function • 50-100 keV, 70-130 keV • On-site • Accepting general users •**

**12-ID-C,D • XSD • Chemistry, physics, materials science • Small-angle x-ray scattering, grazing incidence small-angle scattering, wide-angle x-ray scattering, surface diffraction • 4.5-40 keV • On-site • Accepting general users •**

**33-ID-D,E • XSD • Materials science, physics, chemistry, environmental science • Anomalous and resonant scattering (hard x-ray), diffuse x-ray scattering • general diffraction, surface diffraction, surface diffraction (UHV), x-ray reflectivity • 4-40 keV, 6-25 keV • On-site • Accepting general users •**

# SAMARIUM HEXABORIDE CONTINUES TO AMAZE

**S**amarium hexaboride ( $\text{SmB}_6$ ) is an intriguing intermediate-valence compound in which samarium lies in a murky middle ground between nonmagnetic  $\text{Sm}^{2+}$  and magnetic  $\text{Sm}^{3+}$  ions, due to different occupancy states of its  $f$ -electrons. At room temperature, it behaves as if it consisted of an array of independent localized magnetic moments interacting with itinerant conduction electrons, whereas at temperatures ranging between 70 and 5 K, bulk  $\text{SmB}_6$  becomes electrically insulating while electrically conducting states form at the surface, creating the possibility that  $\text{SmB}_6$  may be a technologically valuable topological insulator. Topological insulators have become one of the hottest topics in condensed matter physics since their discovery in 2007 because of their potential use in quantum computers and other novel devices. Although it is generally thought that the low-temperature properties of  $\text{SmB}_6$  arise from hybridization of  $f$ -band electrons with conduction electrons, experimental and theoretical efforts over the last 50 years have failed to yield a clear picture of what is going on. But researchers working at the APS reported findings that challenge conventional understanding of intermediate-valence insulators, in that they contradict the view that valence fluctuations destabilize spins on long time scales, thus demanding a new model of  $f$ -electron valence stability. This unprecedented discovery implies that neither the metallization nor the onset of magnetic order below 12 K are associated with a simple integer valence, but are characteristics of a robust intermediate-valence state.

Because the electronic states of intermediate-valence systems are sensitive to small changes in interatomic separation, the researchers from the University of Maryland, Columbia University, National Institute of Standards and Technology, and the Lawrence Livermore and Lawrence Berkeley national laboratories used resonant x-ray emission spectroscopy (RXES) at the HP-CAT 16-ID-D x-ray beamline of the APS to determine  $f$ -electron occupancy in  $\text{SmB}_6$  under a range of pressures. It was expected that increased pressure would reduce  $f$ -electron occupancy at some point, causing a shift to an overall integer valence of +3. Applied pressure stabilized metallic and magnetic ground states over the range 4-10 GPa and did reduce the  $f$ -electron occupancy, but surprisingly, the material maintained a significant divalent character up to the highest applied pressure of about 35 GPa and showed no signs of tending toward a single valence state (Fig. 1).

Next, the researchers sought one of the major causes of the persistent intermediate-valence state. It has long been known that the lattice constant of a compound may play a role in intermediate-valence phenomenology. This can be intuitively visualized as being due to ions contracting in radii upon increasing in valence. Therefore, a general shift toward a valence of +3 should be accompanied by a shrinking of the lattice constant, as occurs with samarium monosulfide.

Yet, amazingly, high-resolution x-ray diffraction experiments, again conducted at the HP-CAT beamline, told a much different story. At 10 GPa, the experimentally determined lattice constant was found to be 4.05 Å, which is far smaller than the hypothetical 4.115 Å value for trivalent  $\text{SmB}_6$ , if ion size alone determined valence.

*"Samarium" cont'd. on page 35*

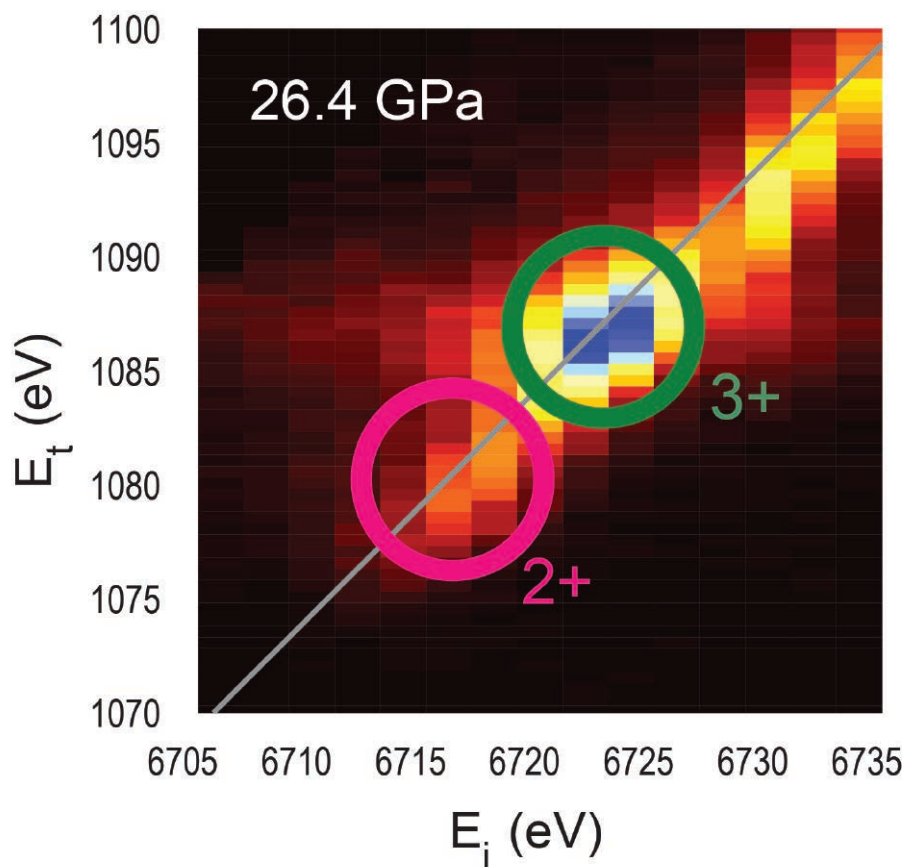
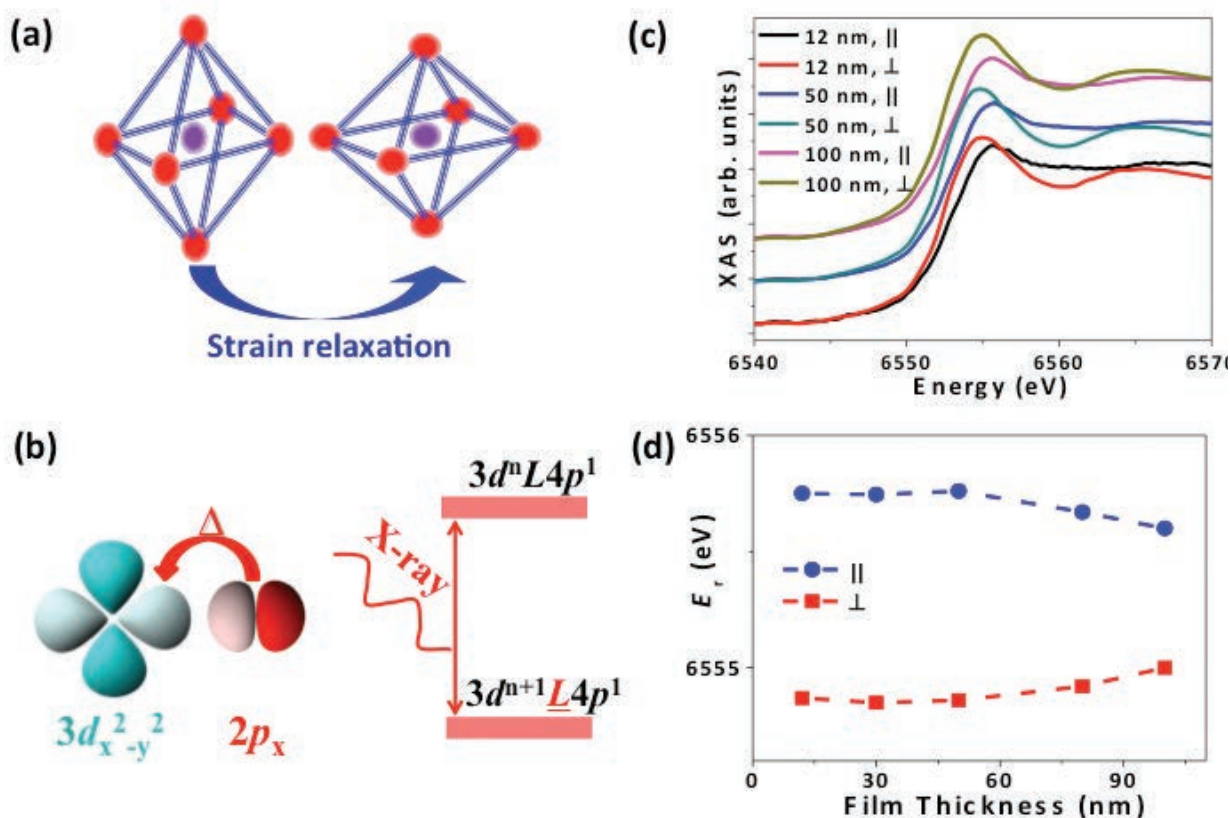


Fig. 1. RXES resonant emitted x-ray intensity is observed at energies corresponding to both 2+ and 3+ configurations, indicating that an intermediate-valence Sm state persists to high pressures in  $\text{SmB}_6$ . This contradicts previous expectations that Sm has a largely 3+ character, with negligible 2+ contribution, once  $\text{SmB}_6$  is metallic and magnetically ordered by a pressure of 10 GPa.



# PROBING THE EFFECTS OF REDUCED STRAIN ON PSMO FILMS

More efficient and higher-capacity memories for our various microelectronic devices require ever more sophisticated and precisely crafted materials for their components. Among the promising candidates for the next generation of non-volatile memory are perovskite manganites, which feature various useful properties including high spin polarization and colossal magnetoresistance. But many questions about their fine electronic structural characteristics remain to be resolved before their utility can be determined. A team of researchers probed the electronic structure of the perovskite manganite  $\text{Pr}_{0.67}\text{Sr}_{0.33}\text{MnO}_3$  (PSMO) films using the APS, concentrating specifically on the behavior of PSMO under strain relaxation. They found that strain relaxation occurred as film thickness increased, creating definite changes in PSMO charge transport and magnetic properties. The work demonstrates a strong correlation between the thickness of perovskite manganites and their electronic and magnetic properties, probed by the polarization-dependent x-ray absorption near-edge structure (XANES) synchrotron x-ray technique, which has important implications in the design and use of resistance random access memory (RRAM) devices with these materials. Continued study along the lines suggested by the present research promises to reveal even more intriguing characteristics of manganites that can be useful in the next generation of RRAM technologies. >>



<< The investigators, from the National University of Singapore and Argonne National Laboratory, studied PSMO films in various thicknesses from 12 nm to 100 nm deposited on LaAlO<sub>3</sub> (LAO) substrates using XANES at the XSD 20-ID-B,C x-ray beamline of the APS. XANES provides an excellent window into the structure of the absorbing atom, which in manganites such as PSMO is manganese (Mn) in the MnO<sub>6</sub> octahedron, as shown in Fig. 1b. The team collected data at the Mn K edge, at which the absorption structure is particularly sensitive to strain effects.

The PSMO films displayed two different forms of strain, an in-plane compressive strain and an out-of-plane tensile strain. Polarization-dependent XANES measurements revealed different peak absorption energy ( $E_r$ ) with the different strains, with anisotropic structural characteristics. However, as film thickness increased, these differences as well as the difference in  $E_r$  diminished (Fig. 1c-d).

X-ray diffraction studies showed definite effects not only on the lattice constant of the PSMO films, but also on rotation of the MnO<sub>6</sub> octahedron. With increasing film thickness and the resulting strain relaxation, the out-of-plane lattice parameter decreased and MnO<sub>6</sub> rotation was observed (Fig.1a). This is evidence of marked change in the PSMO crystal structure with corresponding effects on the film properties.

As one example, the experimenters conclude that these changes in PSMO

crystal structure are responsible for several subpeaks in the  $E_r$  energies observed under XANES studies, which could result from splitting in Mn energy levels due to changes in charge transfer between Mn 3d and Oxygen 2p orbitals. While in-plane charge transfer was more prominent in the thinnest films studied (12 nm), both in-plane and out-of-plane transfer increased with film thickness. The effect on  $E_r$  confirms that both charge transfer and crystal structure are affected by the strain relaxation, with the differing  $E_r$  values seen to converge as film thickness increases, as summarized in Fig. 1d.

These researchers suggest that as strain relaxation increases with film thickness, local structural anisotropy decreases in both the in-plane and out-of-plane directions with resulting changes in the probability of charge transfer and change in  $E_r$ . These changes also affect the PSMO magnetoresistance and the Curie temperature.

— Mark Wolverton

**See:** Bangmin Zhang<sup>1</sup>, Jingsheng Chen<sup>1</sup>, Ping Yang<sup>1</sup>, Xiao Chi<sup>1</sup>, Weinan Lin<sup>1</sup>, T. Venkatesan<sup>1</sup>, Cheng-Jun Sun<sup>2\*</sup>, Steve M. Heald<sup>2</sup>, and Gan Moog Chow<sup>1\*\*</sup>, “Effects of strain relaxation in Pr<sub>0.67</sub>Sr<sub>0.33</sub>MnO<sub>3</sub> films probed by polarization dependent X-ray absorption near edge structure,” *Sci. Rep.* **6**, 19886 (2016). DOI: 10.1038/srep19886

**Author affiliations:** <sup>1</sup>National University of Singapore, <sup>2</sup>Argonne National Laboratory

**Correspondence:** \* cjsun@aps.anl.gov, \*\* msecgm@nus.edu.sg

Work at the National University of Singapore is supported by the Singapore National Research Foundation under CRP Award No. NRF-CRP10-2012-02. P.Y. is supported by SSLS via NUS Core Support C-380-003-003-001. This research used resources of the Advanced Photon Source, an Office of Science User Facility operated for the U.S. Department of Energy (DOE) Office of Science by Argonne National Laboratory, and was supported by the U.S. DOE under Contract No. DE-AC02-06CH11357, and of the Canadian Light Source and its funding partners.

20-ID-B,C • XSD • Materials science, environmental science, chemistry • X-ray absorption fine structure, x-ray Raman scattering, micro x-ray absorption fine structure, microfluorescence (hard x-ray), time-resolved x-ray absorption fine structure, x-ray emission spectroscopy • 4.3-27 keV, 7-52 keV • On-site • Accepting general users •

“Samarium” cont’d. from page 33

These experimental results highlight the need for new theoretical insight into why SmB6 valence is sensitive to temperature but less so to applied pressure, and the nature of the underlying interactions that are responsible for the metallization and the onset of magnetic order. — Vic Comello

**See:** Nicholas P. Butch<sup>1,2,3\*</sup>, Johnpierre Paglione<sup>1</sup>, Paul Chow<sup>4</sup>, Yuming Xiao<sup>4</sup>, Chris A. Marianetti<sup>5</sup>, Corwin H. Booth<sup>6</sup>, and Jason R. Jeffries<sup>3</sup>, “Pressure-Resistant Intermediate Valence in the Kondo Insulator SmB6,” *Phys. Rev. Lett.* **116**, 156401 (2016).

DOI: 10.1103/PhysRevLett.116.156401

**Affiliations:** <sup>1</sup>University of Maryland, <sup>2</sup>National Institute of Standards and Technology, <sup>3</sup>Lawrence Livermore National Laboratory, <sup>4</sup>Carnegie Institute of Washington, <sup>5</sup>Columbia University, <sup>6</sup>Lawrence Berkeley National Laboratory

**Correspondence:**

\* nicholas.butch@nist.gov

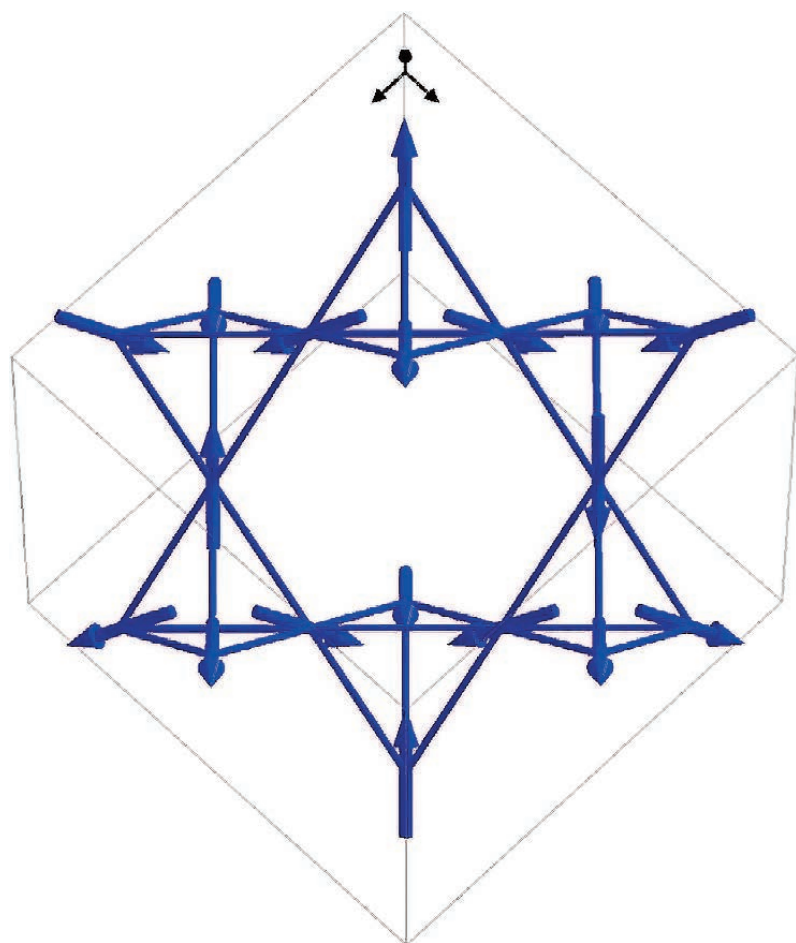
N.P.B. was supported by CNAM and the Lawrence Livermore National Laboratory Physical and Life Sciences directorate. J.R.J. was partially supported by the Science Campaign. HP-CAT operations are supported by the U.S. Department of Energy National Nuclear Security Administration (DOE-NNSA) under Award No. DE-NA0001974 and DOE-Basic Energy Sciences under Award No. DE-FG02-99ER45775, with partial instrumentation funding by the National Science Foundation (NSF). Lawrence Livermore National Laboratory is operated by Lawrence Livermore National Security, LLC, for the DOE-NNSA under Contract No. DE-AC52-07NA27344. C.A.M. was supported by the NSF MRSEC program through Columbia in the Center for Precision Assembly of Superstratic and Superatomic Solids (DMR1420634). Work at Lawrence Berkeley National Laboratory was supported by the Director, DOE Office of Science, Office of Basic Energy Sciences, Chemical Sciences, Geosciences, and Biosciences Division of the DOE under Contract No. DE-AC02-05CH11231. This research used resources of the Advanced Photon Source, a U.S. DOE Office of Science User Facility operated for the DOE Office of Science by Argonne National Laboratory under contract number DE-AC02-06CH11357.

< Fig. 1. (a) Illustration of strain relaxation in tetragonal ratio of MnO<sub>6</sub> octahedron with increasing Pr<sub>0.67</sub>Sr<sub>0.33</sub>MnO<sub>3</sub> film thickness on (001) LaAlO<sub>3</sub> substrate; (b) illustration of charge transfer ( $\Delta$ ) between Mn 3d and O 2p orbitals (left), and final electronic configuration (right) after x-ray absorption. L refers to the O ligand and surrounding the Mn ion; L indicates O ligand with one hole, resulting from the electron transfer from O 2p to empty Mn 3d orbitals; (c) polarized Mn K edge XANES for Pr<sub>0.67</sub>Sr<sub>0.33</sub>MnO<sub>3</sub> films with different thicknesses; in parallel measurement ( $\parallel$ ), the polarization vector ( $E$  vector) of the x-rays was in the film plane; in the perpendicular case ( $\perp$ ), the polarization vector was perpendicular to the film plane; (d) summary of  $E_r$  from the parallel and perpendicular measurements with varying film thickness. The dashed lines are viewing guides.



# WHAT'S A NICE PYROCHLORE LIKE YOU DOING WITH A SOC LIKE THAT?

Over the past few decades, certain classes of compounds, such as the pyrochlores and perovskites, have been found to exhibit unusual and complex electronic and magnetic behavior. Pyrochlores feature oxygen (O) atoms bound to a pair of transition or rare-earth metal elements (denoted here A and B), with the chemical form  $A_2B_2O_7$ . The cadmium-osmium-oxygen compound  $Cd_2Os_2O_7$  is a pyrochlore with its own set of interesting electronic and magnetic properties. Explaining the origin of these properties has proven to be a difficult task; however, recent research has now resolved the mystery. Neutron diffraction revealed an all-in/all-out (AIAO) magnetic structure, the first time this magnetic ordering has been demonstrated using this method. Additionally, resonant inelastic x-ray scattering, performed at the APS indicated an unexpected role for spin-orbit coupling (SOC) driving the compound's magnetic behavior. Besides revealing the subtle interplay of mechanisms responsible for the electronic and magnetic structure of  $Cd_2Os_2O_7$ , this research may provide insight into the origins of similar phenomena in other compounds where SOC was thought to be negligible.



Under the right conditions,  $Cd_2Os_2O_7$  will exhibit a metal-insulator transition (MIT). This phenomenon manifests as an abrupt transition from an electrically-insulating state to a conducting state. First described by Nevill Mott in 1949, MITs have been found in a wide variety of materials including transition metal oxides, a family of compounds that encompasses many of the pyrochlores, among them  $Cd_2Os_2O_7$ .

The metal-insulator transition observed in  $Cd_2Os_2O_7$ , unlike that originally proposed by Mott, is linked to its microscopic magnetic structure. This makes the compound a rare and potentially technologically-important material wherein these two properties (magnetism and electric conduction) can be coupled together. Neutron powder diffraction was enlisted to determine the material's magnetic structure. Normally, neutron diffraction would prove ineffective because the cadmium in  $Cd_2Os_2O_7$  readily absorbs neutrons instead of diffracting them. This problem was addressed by incorporating an isotope of cadmium,  $^{114}Cd$ , that resists neutron absorption. The subsequent neutron diffraction measurements revealed the compound's ground-state magnetic structure (i.e., its lowest-energy magnetic state). This magnetic structure is inextricably linked to the compound's crystalline structure.

The crystalline lattice of  $Cd_2Os_2O_7$  forms adjacent tetrahedra, like little pyramids, with atoms at the vertices and faces. Some of the unpaired electrons in the outer subshells of the osmium atoms, located at the vertices of each tetrahedron, give rise to a local magnetic ordering. This ordering occurs

< Fig. 1. Illustration of the all-in/all-out magnetic ground state observed in the  $Cd_2Os_2O_7$  pyrochlore. Individual tetrahedra represent the bonds between osmium (Os) atoms. Blue arrows depict the spins of outer, unpaired electrons in the Os atoms of each tetrahedron, with all spins either pointing inwards towards the tetrahedral center, or outwards away from it.

when the spins of these electrons (with their associated magnetic moments) either all point inward towards the center of the tetrahedron, or all point outwards (Fig. 1).

Resonant inelastic x-ray scattering (RIXS), performed on the MERIX instrument at the 30-ID-B,C beamline of the APS, an Office of Science user facility at Argonne National Laboratory, was used to probe the compound's electronic structure. X-rays were tuned to promote core electrons (those close to the nucleus) to the valence orbitals (the outermost electrons) in the osmium atoms. When these promoted electrons fell back to a lower atomic energy state, a photon was emitted which provided information about the compound's overall electronic arrangement, which in turn affects its magnetic structure.

Previous research using RIXS and other methods revealed the magnetic/electronic structures of certain iridium-based pyrochlores. As with  $\text{Cd}_2\text{Os}_2\text{O}_7$ , these iridium (Ir) pyrochlores exhibit metal-insulator transitions and other technologically-important characteristics which arise from a complex interplay of microscopic phenomena, for instance the electrostatic charges between ions in the material's crystalline lattice. Another contributing factor to the behavior of the iridate pyrochlores is spin-orbit coupling (SOC), which results from the interaction between the spins of certain electrons to their movement (or orbit) around the atomic nuclei.

While SOC plays a significant role in driving Ir-pyrochlore behavior, it was thought to only appear weakly in  $\text{Cd}_2\text{Os}_2\text{O}_7$ . This was disproven by the RIXS spectral data (Fig. 2), which reveals a magnetic excitation indicating significant spin-orbit coupling in the compound.

This research provides important insights into the factors driving the behavior of  $\text{Cd}_2\text{Os}_2\text{O}_7$ . The all-in/all-out magnetic ground state of this compound, which has only been inferred for the Ir pyrochlores, was directly ob-

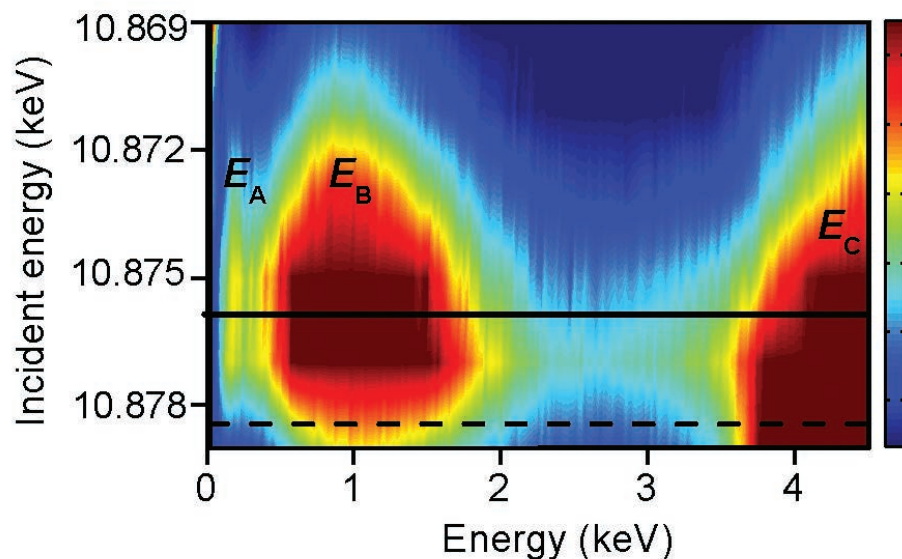


Fig. 2. X-ray scattering data for osmium atoms in  $\text{Cd}_2\text{Os}_2\text{O}_7$ . The vertical axis indicates the energy of incoming (incident) x-rays from the synchrotron beamline. The horizontal axis represents the inelastic energy loss, which is the energy difference between the incident and emitted x-ray photons associated with the RIXS process. Three distinct features appear, labeled  $E_A$ ,  $E_B$ , and  $E_C$ . The  $E_A$  feature indicates a magnetic excitation in  $\text{Cd}_2\text{Os}_2\text{O}_7$  due to spin-orbit coupling. (Solid horizontal line indicates the incoming x-ray energy that most strongly elicits features  $E_A$  and  $E_B$ , while the dashed line is the energy most associated with  $E_C$ )

served via neutron diffraction. Furthermore, RIXS spectral data demonstrated that spin-orbit coupling is a major factor in the appearance of its AI/AO magnetic ordering. These results also provide new information about the potential factors driving the magnetic and electronic characteristics of similar pyrochlores, indicating new pathways to drive and control the exotic metal-insulator transitions within these materials.

— Philip Koth

**See:** S. Calder<sup>1\*</sup>, J.G. Vale<sup>2</sup>, N.A. Bogdanov<sup>3</sup>, X. Liu<sup>4,5</sup>, C. Donnerer<sup>2</sup>, M.H. Upton<sup>6</sup>, D. Casa<sup>6</sup>, A.H. Said<sup>6</sup>, M.D. Lumsden<sup>1</sup>, Z. Zhao<sup>1,7</sup>, J.-Q. Yan<sup>1,7</sup>, D. Mandrus<sup>1,7</sup>, S. Nishimoto<sup>3,8</sup>, J. van den Brink<sup>3,8</sup>, J.P. Hill<sup>4</sup>, D.F. McMorrow<sup>2</sup>, and A.D. Christianson<sup>1,7</sup>, "Spin-orbit-driven magnetic structure and excitation in the 5d pyrochlore  $\text{Cd}_2\text{Os}_2\text{O}_7$ ," *Nat. Comm.* 7, 11651 (2016).

DOI: 10.1038/ncomms11651

**Author affiliations:** <sup>1</sup>Oak Ridge National Laboratory, <sup>2</sup>University College London, <sup>3</sup>IFW Dresden, <sup>4</sup>Brookhaven National Laboratory, <sup>5</sup>Chinese Academy of Sciences, <sup>6</sup>Argonne National Laboratory, <sup>7</sup>University of Tennessee, Knoxville, <sup>8</sup>Technische Universität Dresden

**Correspondence:** \* caldersa@ornl.gov

Work at Oak Ridge National Laboratory's High Flux Isotope Reactor was supported by the Scientific User Facilities Division, Office of Basic Energy Sciences, U.S. Department of Energy (DOE). Work in London was supported by the EPSRC. Work in Dresden was supported by the German Research Foundation (SFB 1143 of the Deutsche Forschungsgemeinschaft). Work performed at Brookhaven National Laboratory was supported by the U.S. DOE under Contract No. DE-AC02-98CH10886. X.L. acknowledges financial support from MOST (No. 2015CB921302) and CAS (No. XDB07020200) of China. D.M. and J.-Q.Y. acknowledge support from the U.S. DOE Office of Science-Basic Energy Sciences, Materials Sciences and Engineering Division. Z.Z. was partially supported by the CEM and National Science Foundation MRSEC under Grant No. DMR-1420451. This research used resources of the Advanced Photon Source, a U.S. DOE Office of Science User Facility operated for the DOE Office of Science by Argonne National Laboratory under Contract No. DE-AC02-06CH11357.

30-ID-B,C • XSD • Physics, materials science  
• Inelastic x-ray scattering • 23.7-23.9 keV •  
On-site • Accepting general users •



# STUDYING THE MAGNETIC BEHAVIOR OF SUPERCONDUCTING EUROPIUM

Europium, an unassuming silvery solid reminiscent of crumpled aluminum foil, may be best known for being one of the least abundant elements in the universe—but that is about to change. Research by an international team utilizing two x-ray beamlines at the APS has shown this element offers some insight into what occurs during the onset of superconductivity. Europium is superconductive at high pressures but recent results from studies carried out at the APS show that it retains its strong local magnetic moments while superconducting and without changing its valence state. This combination of superconductivity and magnetic moment indicates that europium's superconductivity results from magnetic fluctuations, unlike that which occurs in many other superconductors. The results demonstrate that superconductivity in europium may occur in a way similar to heavy fermions and iron pnictides, two types of materials whose own superconducting behavior challenges currently-accepted theories about the underlying role of magnetism in superconductivity.

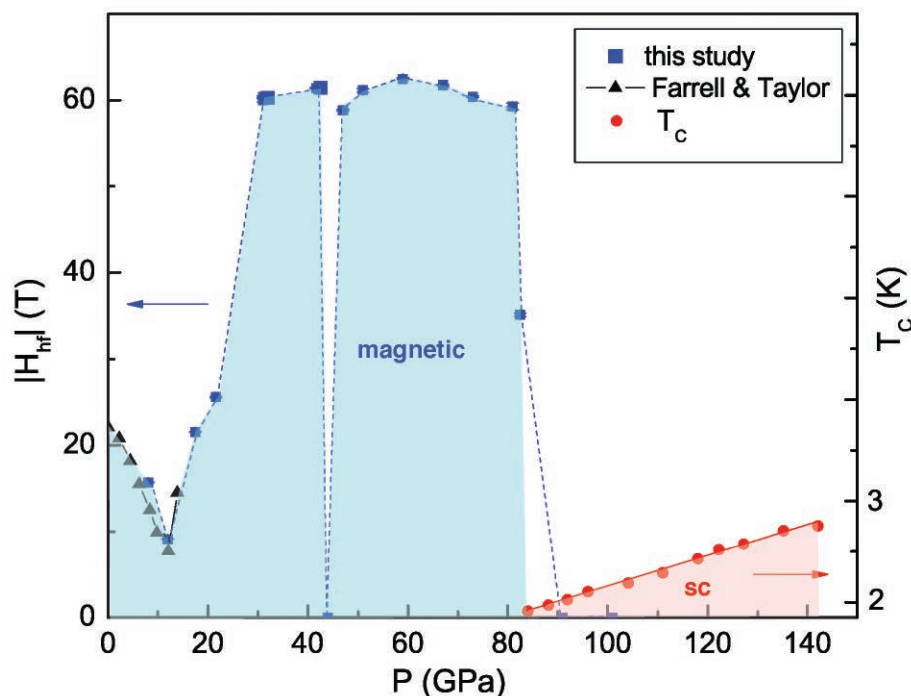


Fig. 1. The magnetic (left, shaded in blue) to superconductive (right, shaded in pink) transition in europium as a function of pressure. The left-hand Y-axis shows the non-zero magnitude of the magnetic hyperfine field when europium is magnetic. The right-hand Y-axis shows the critical temperature while europium is superconducting. Europium transitions from magnetic behavior to superconductivity at approximately 80 GPa.

Superconducting materials are usually non-magnetic and produce zero electrical resistance when cooled below a critical temperature. Instead of moving in a free flow, the electrons in a superconductor are bonded together into Cooper pairs. Most of the previous research that studied the relationship between magnetic ordering and superconductivity used materials that required charge doping, an added complexity that makes investigating the relationship more difficult.

The team chose to scrutinize europium, a lanthanide, which becomes superconducting without chemical doping. Most lanthanides—metallic elements also part of the set of rare earth elements—have strong magnetic properties. But only two, europium and cerium, superconduct, and only while under pressure. Previous research involving cerium showed that it superconducts while somewhat persisting in the 4f magnetic state, but also showed a significant increase in f-d hybridized orbital shells. The team analyzed europium to determine if it might react the same way.

To understand the relationship between magnetism and the onset of superconductivity in europium, the team

*"Europium" cont'd. on page 40*

# HOW A MULTIFERROIC STOPPED BEING FERROIC AND BECAME GLASSY

**M**ultiferroic materials could make vastly better information storage devices than the ones we currently use. A hard drive made from a multiferroic could be written on using electricity, with less energy and a more stable structure that wouldn't degrade from random accidents or stray magnetic fields. Such a hard drive could use four-state logic; each bit could be a 0 or 1 in two different ways; up or down electric polarization and up or down magnetically. This would allow much more information to be written on much smaller devices. But multiferroic materials are not well understood, and the best ones work only at inconveniently low temperatures. Researchers used the APS to explain why one such multiferroic, erbium manganese oxide, undergoes a phase transition from ferroic (magnetic) to glassy, and what this might mean for other multiferroic materials.

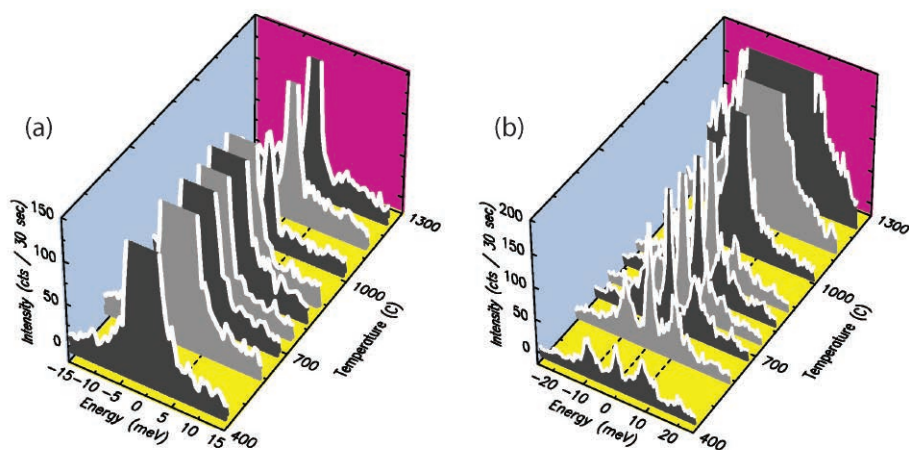


Fig. 1. Quasi-elastic scattered x-rays show a large peak in intensity at temperatures below about 880° C [middle peak in both (a) and (b)], suggesting the material is frozen in a glassy state.

Electricity and magnetism are linked; a stream of moving electrical charges—a current—creates a magnetic field. Conversely, a moving magnet can induce an electrical current. But some special materials such as iron, nickel and cobalt have their own permanent magnet moment, even without an electrical current running through them. We call them ferromagnets. Refrigerator magnets are ferromagnets, and they're also found in electrical generators, loudspeakers and transformers. There are also materials that have an intrinsic electrical field. These are called

ferroelectrics. Then there are some materials, called multiferroics, that have both a magnetic moment and an intrinsic electrical field; most usefully, these two qualities are linked. If we learn how to reliably manipulate one, we can use it to change the other. And if we learn how and why these materials' unusual atomic structures lead to their multiferroic properties, we can potentially design better multiferroics that are more amenable to commercialization.

Erbium manganese oxide develops ferroelectricity at temperatures less than 1195° C. The ferroelectricity

strengthens with a promising fast pace as temperature decreases. Then, the ferroelectricity suddenly degrades at ~800° and does not recover. Over decades, the exact reason for the degradation has been the subject of numerous studies. A team of researchers from Argonne, the Rochester Institute of Technology, and Rutgers University suspected a shift in the material's local symmetry—how the atoms are arranged—might be the reason for the change. The team used three different x-ray techniques to illuminate erbium manganese oxide's structural shifts between 20° and 1300° C. They found something very surprising: at lower temperatures, erbium manganese oxide behaved more like a glass than a crystalline solid (the vast majority of metals are crystalline). The manganese atoms each combined with three oxygen atoms to make little pyramid-like structures, and these pyramids were shifted around in a disordered way. When their positions were averaged the pyramids looked as if they were arranged in an orderly way, but this was an illusion. Each individual pyramid was a little off from where it should have been, as if a band of rampaging nano-children had run through and randomly kicked each pyramid out of place in a different direction. But at high temperatures, the material shaped right up.

*"Ferroic" cont'd. on page 40*



### *“Europium” cont’d. from page 38*

needed to measure the magnetic properties of the element across a range of pressures. They used synchrotron Mössbauer spectroscopy and x-ray emission spectroscopy—and a diamond anvil cell to provide pressure in both cases—to watch the evolution of the magnetic properties of europium as the pressure increased high enough to induce superconductivity. The synchrotron Mössbauer spectroscopy was performed during five experimental runs at the XSD 3-ID-B,C,D beamline at the APS; the team used the high-brightness x-rays to probe the M1 nuclear transition  $7/2 \rightarrow 5/2$  in  $^{151}\text{Eu}$ . The x-ray emission spectroscopy was performed at the HP-CAT 16-ID-D beamline at the APS; the team monitored the nonresonant Eu  $\text{L}\gamma_1$  line for changes that would indicate the presence of  $f$ - $d$  hybridization.

The team found that the onset of superconductivity occurred above 80 GPa and coincided with the disappearance of magnetic order. Figure 1 shows the change from the magnetic phase (below approximately 80 GPa) to the superconducting phase (above approximately 80 GPa). As the pressure increased, so did the magnetic hyperfine field, until approximately 80 GPa was reached. However, strong local magnetic moments persisted near the Eu cations after the onset of superconductivity. The team found no change in the  $\text{L}\gamma_1$  spectral line of europium, meaning that the  $4f$  magnetic state stayed intact with no measurable increase in  $f$ - $d$  hybridized orbital shells.

The team concluded that magnetic fluctuations may play a role in europium’s superconductivity because the effect of magnetic fluctuations on Cooper pairing has been shown to occur in other  $4f$  heavy fermion materials where superconductivity occurs near a quantum critical phase transition, as was shown in these results for europium. — *Mary Alexandra Agner*

**See:** W. Bi<sup>1,2,\*</sup>, J. Lim<sup>3,4</sup>, G. Fabbri<sup>1,3,5</sup>, J. Zhao<sup>1</sup>, D. Haskel<sup>1</sup>, E.E. Alp<sup>1</sup>, M.Y. Hu<sup>1</sup>, P. Chow<sup>6</sup>, Y. Xiao<sup>6</sup>, W. Xu<sup>7</sup>, and J.S. Schilling<sup>3</sup>, “Magnetism of europium under extreme pressures,” *Phys. Rev. B* **93**, 184424 (2016).

DOI: 10.1103/PhysRevB.93.184424

**Author affiliations:** <sup>1</sup>Argonne National

Laboratory, <sup>2</sup>University of Illinois at Urbana-Champaign, <sup>3</sup>Washington University in St. Louis, <sup>4</sup>Washington State University, <sup>5</sup>National Laboratory, <sup>6</sup>Carnegie Institution of Washington, <sup>7</sup>Chinese Academy of Sciences, **Correspondence:** \* wbi@aps.anl.gov

Support by Consortium for Materials Properties Research in Earth Sciences (COM-PRES), the National Science Foundation (NSF) through Grant No. DMR-1104742, and by the Carnegie/Department of Energy (DOE) Alliance Center (CDAC) through the National Nuclear Security Administration (NNSA)/Department of Energy (DOE) Grant No. DEFC52-08NA28554 is gratefully acknowledged. HP-CAT operations are supported by the DOE-NNSA under Award No. DE-NA0001974, with partial instrumentation funding by the NSF. This research used resources of the Advanced Photon Source, a U.S. DOE Office of Science User Facility operated for the DOE Office of Science by Argonne National Laboratory under Contract No. DE-AC02-06CH11357.

3-ID-B,C,D • XSD • Physics, geoscience, life sciences, chemistry, materials science • Nuclear resonant scattering, inelastic x-ray scattering, high-pressure diamond anvil cell • 7-27 keV, 14.41-14.42 keV • On-site • Accepting general users •

16-ID-D • HP-CAT • Materials science, geoscience, chemistry, physics • Nuclear resonant scattering, inelastic x-ray scattering (1-eV resolution), x-ray emission spectroscopy, high-pressure diamond anvil cell • 5-37 keV, 14.41-14.42 keV • On-site Accepting general users •

### *“Ferroic” cont’d. from page 39*

Because the structure was complicated and the difference subtle, the researchers used three different techniques at three different beam lines to figure it out. They used XSD beamline 11-ID-D to perform high-resolution x-ray diffraction to measure the lattice constants—the size of repeating units of atoms in the material—very precisely. At a separate XSD beamline, 3-ID-B,C,D, there is equipment that can resolve the energy of quasi-elastic scattered x-rays. These are x-rays scattered by atomic vibrations. This showed the team that the atoms in the erbium manganese oxide were shifted and frozen somewhat randomly in space, not in a perfectly ordered lattice (Fig. 1). At XSD beamline 8-ID-E, the team used x-ray speckles to measure the atoms’ move-

ment over time. They found the atomic shifts were frozen over time. APS is one of only three synchrotrons in the world that can do all three of these measurements. Its brilliance is especially valuable, making the x-ray speckle measurement possible.

Erbium manganese oxide’s glassy behavior at low temperatures is undesirable. It disrupts the useful ferroelectricity and magnetism of the material. Now that they know the structure, materials scientists may be able to re-design the material to decrease the glassy behavior by adding in additional elements, or substituting the existing elements with something different that is less likely to shift in this disordered way.

— *Kim Krieger*

**See:** A. Barbour<sup>1,\*</sup>, A. Alatas<sup>1</sup>, Y. Liu<sup>1</sup>, C. Zhu<sup>1</sup>, B.M. Leu<sup>1</sup>, X. Zhang<sup>1</sup>, A. Sandy<sup>1</sup>, M. S. Pierce<sup>2</sup>, X. Wang<sup>3</sup>, S.-W. Cheong<sup>3</sup>, and H. You<sup>1\*</sup>, “Partial glass isosymmetry transition in multiferroic hexagonal  $\text{ErMnO}_3$ ,” *Phys. Rev. B* **93** (5), 054113 (2016). DOI: 10.1103/PhysRevB.93.054113

**Author affiliations:** <sup>1</sup>Argonne National Laboratory, <sup>2</sup>Rochester Institute of Technology, <sup>3</sup>Rutgers University <sup>†</sup>Present address: Brookhaven National Laboratory

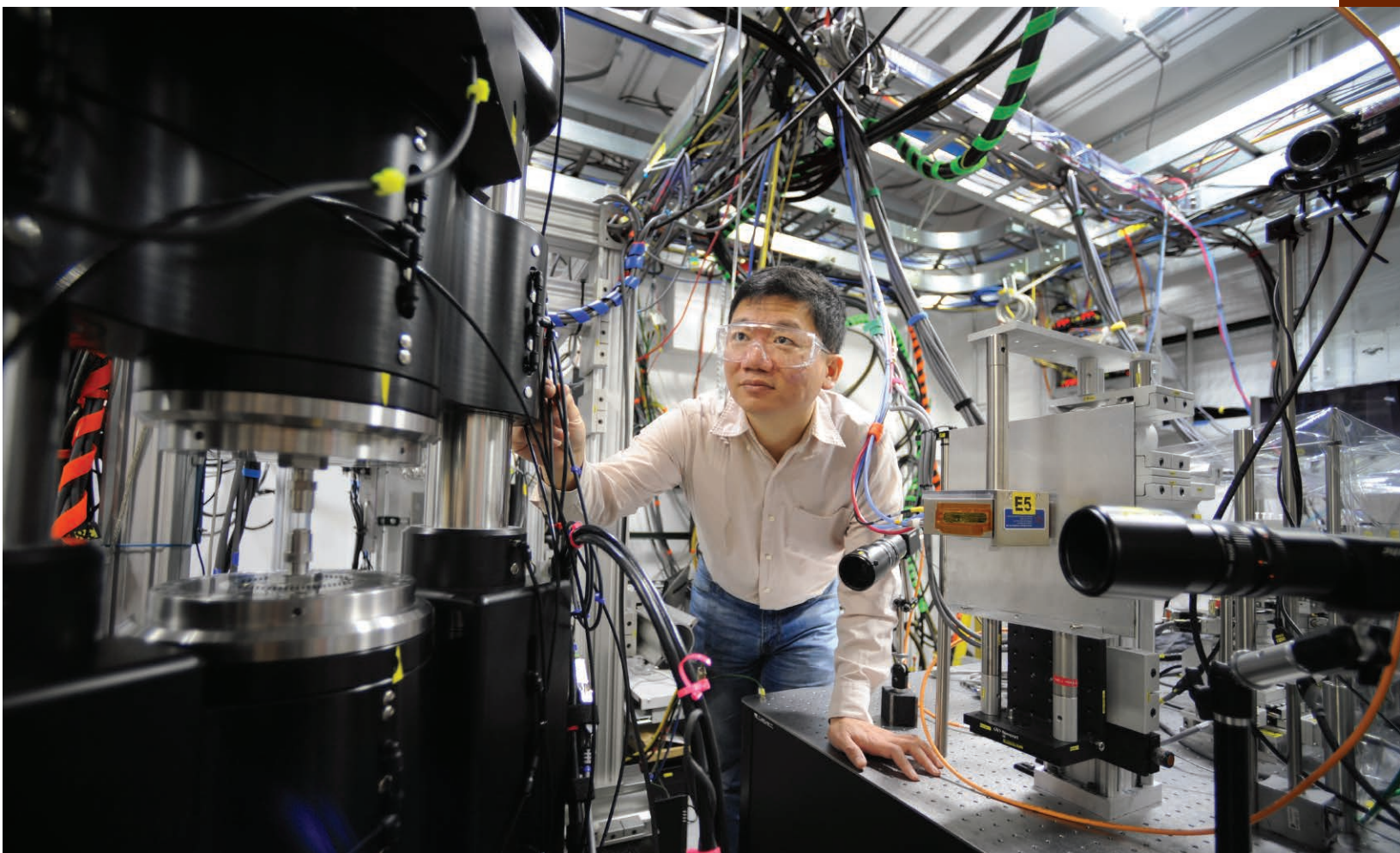
**Correspondence:** \* hyou@anl.gov

The work of A.B., C.Z., and H.Y. at the Argonne Materials Science Division was supported by the U.S. Department of Energy (DOE)-Basic Energy Sciences (BES), Materials Sciences and Engineering Division (MSED), and the work of A.A., B.L., A.S., and X.Z. at the APS by the DOE-BES Scientific User Facilities Division under Contract No. DE-AC02-06CH11357. This research used resources of the Advanced Photon Source, a U.S. DOE Office of Science User Facility operated for the DOE Office of Science by Argonne National Laboratory under Contract No. DE-AC02-06CH11357.

3-ID-B,C,D • XSD • Physics, geoscience, life sciences, chemistry, materials science • Nuclear resonant scattering, inelastic x-ray scattering, high-pressure diamond anvil cell • 7-27 keV, 14.41-14.42 keV • On-site • Accepting general users •

8-ID-E • XSD • Materials science, polymer science, physics • Grazing incidence small-angle scattering, x-ray photon correlation spectroscopy • 7.35-7.35 keV • On-site • Accepting general users •

# ENGINEERING MATERIALS & APPLICATIONS



Andrew Chuang, physicist and beamline scientist with the Materials Physics & Engineering Group of XSD, in the XSD 1-ID-E high-energy x-ray beamline preparing an x-ray tomography experiment for the three-dimensional characterization of advanced casting alloys for heavy duty engine applications.

# MODELING TEMPERATURE-DEPENDENT STRUCTURE IN SODIUM BORATE MELTS



Fig. 1. A spherical bead of borate suspended in an aerodynamic levitation furnace.



For decades, scientists have altered the chemical composition and structure of glass to improve performance. That's why brownies can be baked in Pyrex and the screen on a dropped smartphone often doesn't break. To discover glasses that are more functional and/or less expensive, scientists model the melt properties of glass-forming liquids. Researchers in this study used the thermodynamic model of ideal associated solutions to predict the temperature dependent properties of sodium borate glasses and then tested their model experimentally using high-intensity, high-energy x-rays from the U.S. Department of Energy's Advanced Photon Source (APS). The model predicted the structural transition found in molten  $\text{Na}_2\text{B}_4\text{O}_7$ , suggesting that it provides a much more computationally inexpensive method of structure prediction than molecular dynamics, covering the equilibrium melt, supercooled liquid, and glassy states.

As an amorphous material, the structure of glass is affected not just by its composition, but also by its thermal history. Modeling allows researchers to better understand the properties of different compositions of glasses and thus drive the development of novel glasses that propel technological advances forward. Glass modeling is increasingly done by topological constraint theory: the idea that these materials are created by nodes (atoms) that are constrained by rigid rods (chemical bonds). However, while this model works well at ambient temperature, it is not always effective at higher temperatures. For example, the model does not predict the sodium borate glass transition temperature plateau, at 20–40 mol %  $\text{Na}_2\text{O}$ , which is important, as sodium borosilicate glasses are in widespread use as Pyrex and optical glasses.

The researchers, from Materials Development, Inc. (MDI); Argonne National Laboratory; the Alexander Dubček University of Trenčín and RONA (Slovak Republic); the Institute of Chemical Technology Prague (Czech Republic); and Northwestern University set out to determine whether the thermodynamic model of ideal associated solutions could predict important temperature dependent structural changes, which can greatly affect the glass transition temperatures and melt properties important during glass making. This model describes an oxide liquid as an ideal solution of end member oxides and any crystalline compounds forming within the system. The model has no free parameters and requires as input

the melt composition and the free energies of formation, and local structure, of each compound; it outputs their relative amounts based on the laws of mass action and mass balance. The thermodynamic model predicts temperature dependence of the B–O coordination in the composition region 20–50 mol %  $\text{Na}_2\text{O}$ —in line with the glass transition temperature plateau.

To test the predictions, the team created borate ( $\text{Na}_2\text{B}_4\text{O}_7$ ) spherical beads that they suspended in an aerodynamic levitation furnace (Fig. 1) and then supercooled them from equilibrium liquid through the glass transition. The team used high-energy x-ray diffraction measurements made at XSD beamline 6-ID-D of the APS, which revealed a continuous structural transition in the network liquid, evolving from a low-density, depolymerized melt at about 300 K above the melting temperature, to a dense polymerized melt close to the glass transition. Thereby, the thermodynamic model of ideal associated solutions was shown to be able to predict temperature-driven structural rearrangements at different temperatures.

These results will help researchers to improve industrial glass design and manufacture, a process that will continue as MDI begins a four-year, NASA-funded project. The researchers will measure the thermophysical properties of molten metal oxides as they supercool in low gravity conditions—keeping the fluid free from convection—to more accurately measure physical properties. Initially, the researchers will use MDI and NASA levitation instruments and

then will perform experiments on the International Space Station. To better understand glass formation at the atomic level, the researchers will also continue to use the APS. — Dana Desonie

**See:** O.L.G. Alderman<sup>1,2\*</sup>, M. Liška<sup>3</sup>, J. Macháček<sup>4</sup>, C.J. Benmore<sup>2</sup>, A. Lin<sup>1,5</sup>, A. Tamalonis<sup>1</sup>, and J.K.R. Weber<sup>1,2</sup>, “Temperature-Driven Structural Transitions in Molten Sodium Borates  $\text{Na}_2\text{O}$ – $\text{B}_2\text{O}_3$ : X-ray Diffraction, Thermodynamic Modeling, and Implications for Topological Constraint Theory,” *J. Phys. Chem. C* **120**, 553 (2016).

DOI: 10.1021/acs.jpcc.5b10277

**Author affiliations:** <sup>1</sup>Materials Development, Inc., <sup>2</sup>Argonne National Laboratory, <sup>3</sup>Alexander Dubček University of Trenčín and RONA, <sup>4</sup>Department of Glass and Ceramics, Institute of Chemical Technology Prague, <sup>5</sup>Northwestern University

**Correspondence:**

\* o.alderman@gmail.com

O.L.G.A., J.K.R.W., A.L., A.T., and C.J.B. were supported by U.S. Department of Energy (DOE) Grant No. DE-SC0007564. This research used resources of the Advanced Photon Source, a U.S. DOE Office of Science user facility operated for the DOE Office of Science by Argonne National Laboratory under contract no. DE-AC02-06CH11357.

6-ID-D • XSD • Physics, materials science • Magnetic x-ray scattering, high-energy x-ray diffraction, powder diffraction, pair distribution function • 50-100 keV, 70-130 keV • On-site • Accepting general users •

# COATING POROUS CRYSTALLINE FRAMEWORKS TO REPEL WATER AND OIL

Porous materials appear in numerous industrial applications, where their range of topologies and internal cavities provide exceptionally high surface area for functions ranging from the absorption of toxins to catalyzing chemical reactions. Unfortunately, the efficiency and lifespan of these materials are often degraded by exposure to water, oils, and other solvents. While specialized coatings can resist such solvents, only limited success has been achieved in satisfactorily applying these coatings to porous materials. In this study, researchers have for the first time successfully coated tiny porous particles to make them both water- and oil-resistant, without degrading their functionality. The particles were composed of a metal-organic framework (MOF), which is both highly crystalline and highly porous. Several techniques, including x-ray diffraction measurements performed at the APS, were utilized to gauge the efficacy of the solvent-resistant coating. Effectively protecting MOFs and other porous materials from harsh chemical environments is expected to benefit a variety of applications, including molecular separation, carbon sequestration, and gas storage.

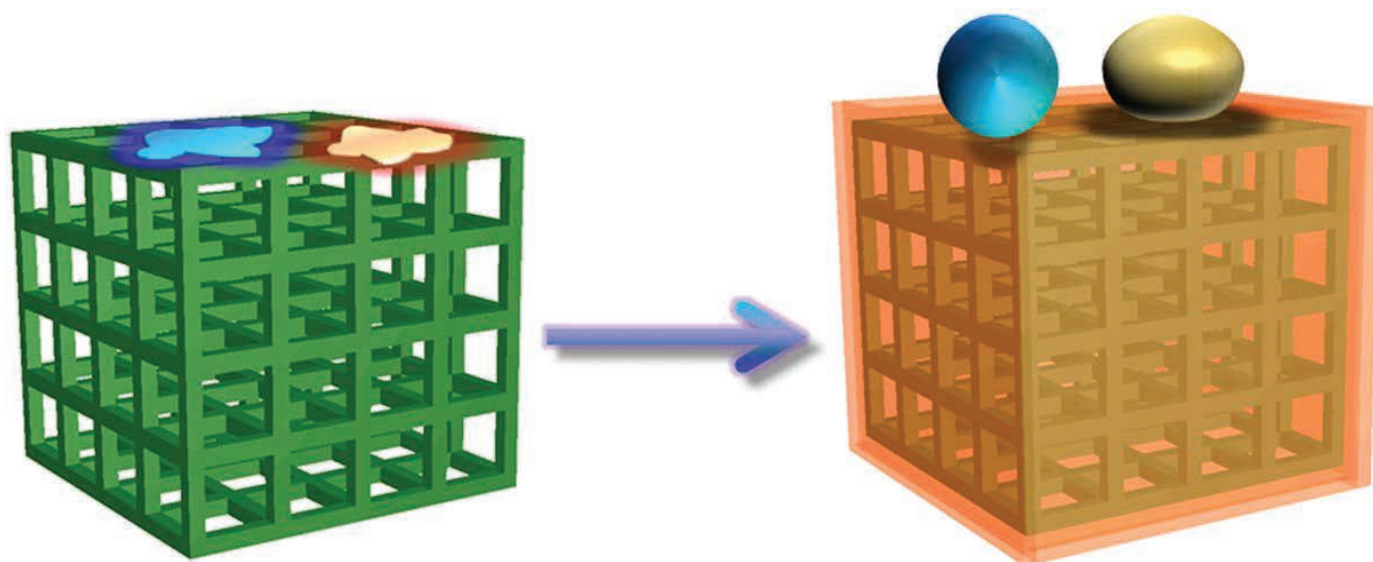


Fig. 1. Illustrations of a MOF before and after treatment. The left-hand side depicts water and oils adhering to the surface of an untreated MOF. After the MOF is chemically coated (right-hand side), water and oil bead up on its surface.

Among the most widely used porous compounds are the zeolites, which occur both as natural minerals and as commercially-synthesized compounds. MOFs also form highly porous crystallites with many favorable attributes such as adjustable pore size, large surface areas, and easy structural modification.

The porous material examined for this research was a zeolitic imidazolate framework (ZIF), which is a type of MOF that mimics the structure of a zeolite. Water and oil normally adsorb onto

the surfaces of ZIF particles. The researchers' task was to coat ZIF particles with a water- and oil-repellant compound while allowing other types of molecules to enter their pores. Figure 1 schematically illustrates the concept.

Particle coating was accomplished using a two-step process. First, the researchers, from Zhejiang University (China), the University of South Florida, and The University of Chicago, synthesized vinyl-functionalized ZIF particles. This means that vinyl molecules ( $C_2H_3$ ) were embedded throughout the

pores and cavities of the ZIF particles without disrupting their underlying single-crystalline lattice. The embedded vinyl molecules provided chemical 'handles' for attaching the final hydrophobic (water-repellant) and oleophobic (oil-repellant) coating. These modified particles were designated ZIF-8-V; the particular MOF crystalline structure is "ZIF-8," while "V" indicates the attached vinyl groups.

The final step in creating the amphiphobic ZIF particles was to utilize a chemical that would adhere to the embedded vinyl groups without blocking the particles' pores. A fluorinated organic molecule (1H,1H,2H,2H-perfluorodecanethiol) was chosen for being

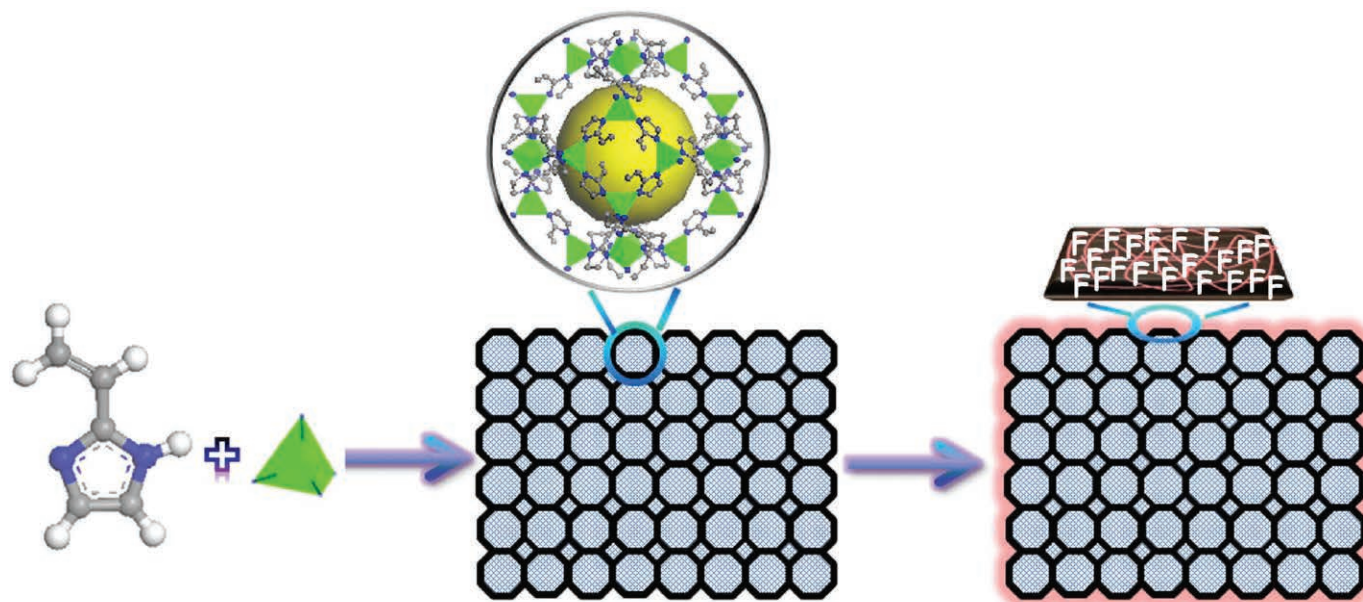


Fig. 2. Schematic depiction of the coating process. The left-hand side of the figure indicates that vinyl molecules have been distributed throughout the porous structure of the MOF particle. The inset at the middle top is a magnified view showing vinyl molecules encircling an individual component of the MOF particle. The right-most view depicts the fluorine-based compound applied to the outside of the entire MOF particle.

both highly amphiphobic as well as too large to enter the tiny ZIF-8-V pores. Following application of the amphiphobic compound, the newly-treated particles were designated ZIF-8-VF, where the appended "F" indicates the fluorine-based coating (Fig. 2)

A series of tests characterized both the coated and uncoated ZIF particles. Powder X-ray diffraction (PXRD) measurements indicated that the coated ZIF-8-VF particles retained their original porous structure and crystallinity. Additionally, infrared and x-ray photoelectron spectroscopy, nuclear magnetic resonance, nitrogen sorption isotherms, and scanning electron microscopy all indicated that the fluorine-based compound successfully adhered to the ZIF-8-VF particles, without degrading porosity or structural integrity.

The next step was to determine how well the coated ZIF-8-VF particles repelled water and oils. Contact angle experiments (measuring how far a fluid creeps up a particle's sides) demonstrated that the coated ZIF-8-VF particles were much more hydrophobic and oleophobic than the untreated ZIF-8-V particles. Additionally, vapor adsorption tests showed that the coated ZIF-8-VF particles adsorbed far less water vapor and hydrocarbon vapor than did the untreated ZIF-8-V particles.

As a final test, ZIF particles were exposed to 100% humidity along with CO<sub>2</sub>. After 240 h, the uncoated ZIF-8-V particles were markedly degraded, while the coated ZIF-8-VF particles appeared pristine even after tripling the exposure duration (720 h).

To demonstrate the applicability of these coating techniques to other porous materials, the researchers chose MOF-5, a crystalline form of MOF that is highly unstable in humid CO<sub>2</sub> environments. Coated and uncoated MOF-5 particles were examined by powder X-ray diffraction following exposure to humid CO<sub>2</sub> conditions. The PXRD data were collected at beamline 15-ID-B,C,D of ChemMatCARS at the APS. After 4 h, pores of the uncoated MOF-5 particles disappeared completely, while the coated (MOF-5-VF) particles retained their pores and crystallinity even after 7 days of continuous exposure.

These results show that the coating techniques demonstrated in this research not only render highly-crystalline MOF particles amphiphobic, but they also provide a kind of chemical shielding from the humid and acidic CO<sub>2</sub> environments found in many industrial processes. — Philip Koth

See: Qi Sun<sup>1,2</sup>, Hongming He<sup>2</sup>, Wen-

Yang Gao<sup>2</sup>, Briana Aguila<sup>2</sup>, Lukasz Wojtas<sup>2</sup>, Zhifeng Dai<sup>1</sup>, Jixue Li<sup>1</sup>, Yu-Sheng Chen<sup>3</sup>, Feng-Shou Xiao<sup>1\*</sup>, and Sheng-qian Ma<sup>2\*\*</sup>, "Imparting amphiphobicity on single-crystalline porous materials," Nat. Commun. **7**, 13300 (2016).

DOI: 10.1038/ncomms13300

Author affiliations: <sup>1</sup>Zhejiang University, <sup>2</sup>University of South Florida, <sup>3</sup>The University of Chicago

Correspondence: \* fsxiao@zju.edu.cn  
\*\* sqma@usf.edu

This work was supported by the National Natural Science Foundation of China (21273197, 21333009 and 21422306) and National High-Tech Research and Development programme of China (2013AA065301). Financial support from the University of South Florida and the U.S. National Science Foundation (DMR-1352065) is also acknowledged (S.M.). ChemMatCARS is supported by the National Science Foundation under grant number NSF/CHE-1346572. This research used resources of the Advanced Photon Source, a U.S. Department of Energy (DOE) Office of Science User Facility operated for the DOE Office of Science by Argonne National Laboratory under Contract Number DE-AC02-06CH11357.

15-ID-B,C,D • ChemMatCARS • Materials science, chemistry • Single-crystal diffraction, anomalous and resonant scattering (hard x-ray), microdiffraction, liquid surface diffraction, high-pressure diamond anvil cell • 6-32 keV, 10-70 keV • On-site • Accepting general users •



# PUTTING THE SQUEEZE ON HYDROGEN AND SODIUM FOR SUPERCONDUCTIVITY

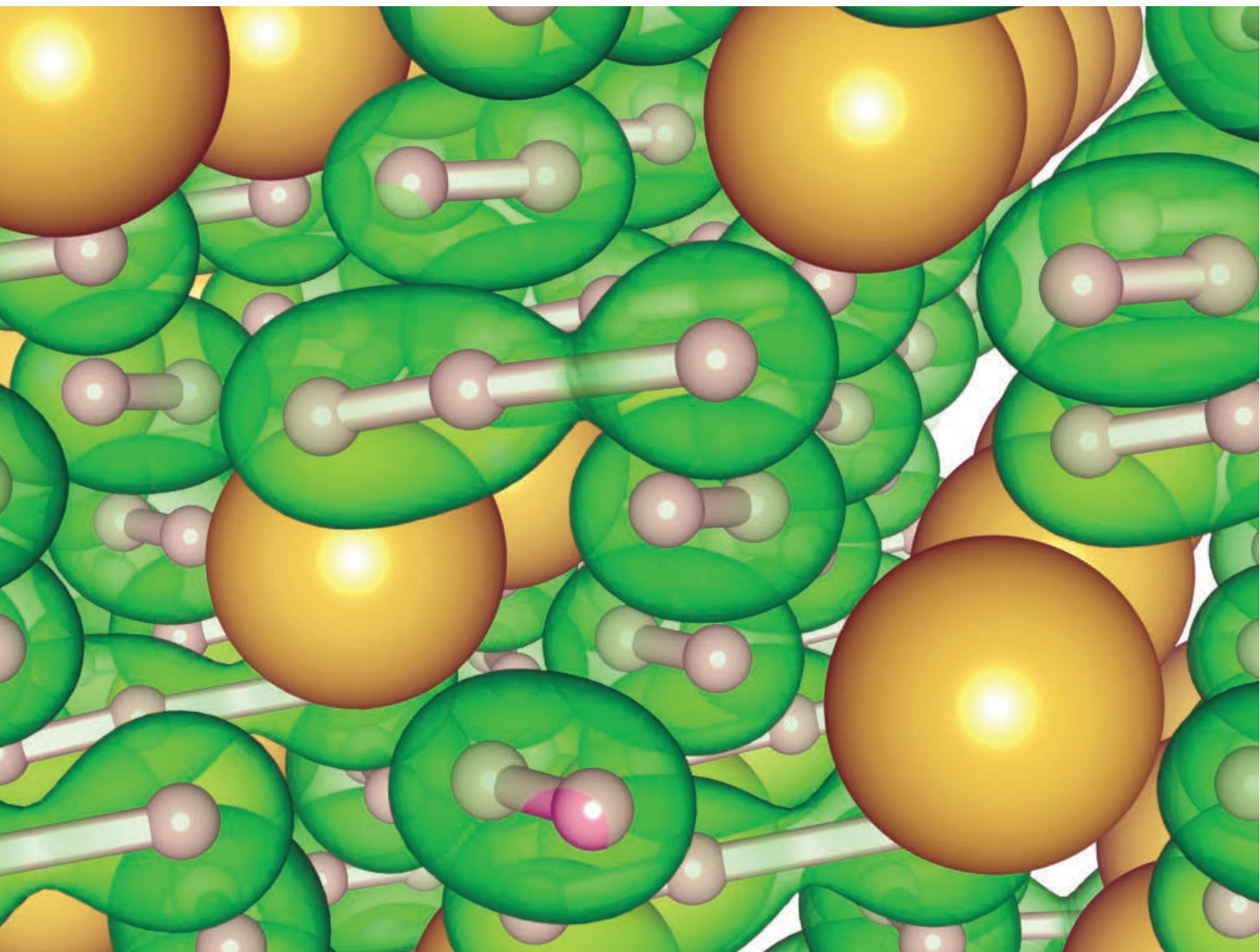


Fig. 1. Structure of  $\text{NaH}_7$ , with the three-atom hydrogen chain in center.

13-ID-C,D • GSECARS • Geoscience, environmental science • Microdiffraction, x-ray standing waves, x-ray absorption fine structure, resonant inelastic x-ray scattering, x-ray emission spectroscopy, high-pressure diamond anvil cell, high-pressure multi-anvil press • 4.9-45 keV, 10-75 keV • On-site • Accepting general users •

**S**uperconductivity is a hot phenomenon that occurs only at very cold temperatures. Finding ways to change that and make superconductivity practical at higher temperatures is a major goal for physicists and engineers. One possibility involves the metallic phase of hydrogen, theorized to be superconducting at ambient temperatures but yet to be achieved in practice. By synthesizing a compound of hydrogen with sodium using the APS, experimenters have achieved a new class of sodium polyhydrides, taking a highly promising first step toward achieving practical high-temperature, ambient pressure superconductivity. The unusual linear electronic structure of these polyhydrides lends itself to the creation of new metallic materials with superconducting properties at higher temperatures than previously possible. They may also be useful for hydrogen storage applications in fuel cells.

For years, polyhydride compounds, in which hydrogen atoms are combined with alkali metals such as sodium, lithium, or potassium atoms, have been predicted to display unusual properties and structures under high temperatures and pressures, including the possibility that superconducting properties might remain even at ambient temperatures and pressures. Such metallic hydrogen compounds would feature several H<sub>3</sub><sup>-</sup> ions in a linear configuration that would resemble a one-dimensional phase of hydrogen. But these intriguing theoretical predictions have eluded experimental confirmation. Recent reports of the production of Li polyhydrides seemed to favor theoretical models, but the resulting samples were not fully characterized to confirm their structure.

The research team in this experiment, from the Carnegie Institution of Washington, the Center for High Pressure Science and Technology Advanced Research (China), Lawrence Livermore National Laboratory, University College London (UK), the University of Cambridge (UK), Cavendish Laboratory (UK), The University of Chicago, and the Chinese Academy of Sciences set out to synthesize sodium and lithium polyhydrides using a laser-heated diamond anvil cell (DAC) at the GSECARS 13-ID-C,D x-ray beamline at the APS. Experiments at pressures up to of 70 GPa at room temperature showed no polyhydride phase in either Na or Li, but upon laser heating up to temperatures of about 2000° K at pressures of approximately 30 to 40 GPa, the researchers observed the formation of NaH polyhydrides (Fig. 1).

They investigated the newly-formed material using both x-ray diffraction (XRD) and Raman spectroscopy at GSECARS, both of which confirmed that the material's structure was quite different from pure hydrogen. Two stable phases were identified, NaH<sub>3</sub> and NaH<sub>7</sub>, although the former was far more dominant. Even higher polyhydrides might be present in the synthesized samples, although the data for them are inconclusive. The team's results match very well with their own theoretical calculations, which used the ab initio random structure searching method and predicted the NaH<sub>3</sub> phase and several others more favorable than those theorized in previous work.

Since the experiments involved very high pressures and temperatures confined to a small space inside the DAC at GSECARS, the experimenters faced some special challenges in obtaining their data. Laser heating of hydrogen under such conditions can result in breaking and failure of the DAC, and the team experienced this problem during most of their experiments, requiring repeated runs to ensure the collection of sufficient data for measurements and characterization. The researchers note that while prolonged laser heating is likely the best method for producing good single-phase samples, the susceptibility of DACs to failure in the presence of hydrogen makes this difficult at present.

The researchers plan to extend this work into the investigation of new classes of alkali metal polyhydrides, particularly the possibility of synthesizing them more easily at lower temperatures and pressures. The present work

is a significant step in creating the materials to eventually make superconductivity practical and accessible.

— Mark Wolverton

**See:** Viktor V. Struzhkin<sup>1\*</sup>, Duck Young Kim<sup>1,2</sup>, Elissaios Stavrou<sup>1,3</sup>, Takaki Muramatsu<sup>1</sup>, Ho-kwang Mao<sup>1,2</sup>, Chris J. Pickard<sup>4,5</sup>, Richard J. Needs<sup>6</sup>, Vitali B. Prakapenka<sup>7</sup>, and Alexander F. Goncharov<sup>1,8</sup>, "Synthesis of sodium polyhydrides at high pressures," Nat. Comm. **7**, 12267 (26 July 2016).

DOI: 10.1038/ncomms12267

**Author affiliations:** <sup>1</sup>Carnegie Institution of Washington, <sup>2</sup>Center for High Pressure Science and Technology Advanced Research, <sup>3</sup>Lawrence Livermore National Laboratory, <sup>4</sup>University College London, <sup>5</sup>University of Cambridge, <sup>6</sup>Cavendish Laboratory, <sup>7</sup>The University of Chicago, <sup>8</sup>Chinese Academy of Sciences

**Correspondence:**

\* vstruzhkin@carnegiescience.edu

High-pressure experiments were supported by the U.S. Department of Energy-Basic Energy Sciences (DOE-BES) under Contracts no. DE-FG02-02ER45955 and DE-FG02-99ER45775. D.Y.K. and T.M. acknowledge salary support by Energy Frontier Research in Extreme Environments Center, an Energy Frontier Research Center funded by the U.S. DOE Office of Science under Award Number DE-SC0001057. C.J.P. and R.J.N. were supported by the Engineering and Physical Sciences Research Council of the UK. E.S. and A.F.G. acknowledge support of DARPA under contracts no. W31P4Q1310005 and W31P4Q1210008. R.J.N. acknowledges financial support from the Engineering and Physical Sciences Research Council of the U.K. [EP/J017639/1]. C.J.P. acknowledges financial support from EPSRC [EP/G007489/2]. E.S. has performed parts of the work under the auspices of the U.S. DOE by Lawrence Livermore National Security, LLC, under Contract no. DE-AC52-07NA27344. A.F.G. acknowledges support of National Science Foundation of China (no. 21473211). GSECARS is supported by the National Science Foundation-Earth Sciences (EAR-1128799) and DOE-Geosciences (DE-FG02-94ER14466). This research used resources of the Advanced Photon Source, a U.S. DOE Office of Science User Facility operated for the DOE Office of Science by Argonne National Laboratory under contract no. DE-AC02-06CH11357.

# COMPARING 3-D SHOCK DAMAGE IN COPPER TO ITS PRE-DAMAGED STATE

Fuel cells efficiently convert chemical energy into electrical power while generating few if any polluting emissions. Like batteries, they consist of three parts: an electrolyte, an anode, and a cathode. Unlike batteries, which run down periodically, fuel cells can continue running as long as they are supplied with fuel. Today's solid oxide fuel cells (SOFCs) are an important type of fuel cell whose electrolyte—the layer separating the anode from the cathode—is a solid-state metal oxide. Most SOFCs can use a wide variety of fuels because their electrolytes conduct oxygen ions, but these SOFCs require high temperatures (500-750° C) to operate, which makes the fuel cells expensive and slow to start. Much research is aimed at developing SOFCs that operate at lower temperatures (300-500° C) by exploiting proton-conducting electrolytes, but such electrolytes that have high ionic conductivities are also often good conductors of electrons. Electron conduction needs to be suppressed during operation to force the electrons to pass through the external electrical circuit connected to the fuel cell (Fig. 1). Recently researchers developed an electron doping strategy that yields a high-performance SOFC having a proton-conducting electrolyte that achieves an ionic conductivity comparable to the best performing electrolytes operating at similar temperatures, while suppressing electronic leakage at the same time. The operating principles of the strategy were validated in separate experiments conducted at two APS beamlines.

The response of materials to dynamic loading varies according to their properties. For instance, the type, shape, and arrangement of grains and grain boundaries within a polycrystalline metal or alloy can dramatically affect how it deforms under load. These and other features of a material's microscopic structure are represented by numerical models utilized to predict dynamic loading behavior. To improve dynamic modeling accuracy, empirical data are needed that reveal how samples actually deform under shock loading conditions. However, at the microscopic level this empirical data has been incomplete. The experimental techniques demonstrated in this study will help reduce this knowledge gap.

High-energy diffraction microscopy is used increasingly as a non-destructive method for imaging materials at the grain and sub-grain levels. The high-energy x-rays required for HEDM are produced at synchrotron x-ray facilities like the APS. Both near-field and far-field HEDM exist; the two methods are used

to image different structural properties of a material. For this study, near-field was more appropriate for imaging the copper's orientation field with high spatial resolution.

The experimental target chosen for shock loading was a small disk of high-purity copper. Electron backscatter diffraction revealed an average grain size approximately 30  $\mu\text{m}$  across. Slightly less than one cubic millimeter of the copper sample was mapped using nf-HEDM. For three-dimensional (3-D) imaging, monochromatic x-rays were focused into a thin ribbon 1.4-mm wide by 2- $\mu\text{m}$  thick. This thin x-ray beam was used to render 170 individual "slices" of the sample that were assembled to form a 3-D image approximately 0.8  $\text{mm}^3$  in volume.

The 3-D imaging described above is not new. Instead, the novel achievement of this study is the direct comparison of pre- and post-shock conditions within the same exact region. This was accomplished by identifying and removing (via micromachining) a tiny region of

the copper disk that had been imaged by nf-HEDM. The extracted region was embedded in a copper target assembly, which was subsequently impacted by a high-speed copper plate to induce shock loading.

Following impact, the target assembly was taken to the XSD 1-ID-B,C,E beamline at the APS where the embedded copper region was again mapped using nf-HEDM. Figure 1 shows the pre- and post-shocked copper. The impact deformed the region's grains and grain boundaries, accompanied by spalling and formation of gaps (voids) between grains. Analysis confirmed that, as expected, most voids appeared at grain boundaries and other microstructural features.

On the other hand, the finding that voids showed no statistical correlation to any particular type of grain boundary was somewhat surprising and points to the presence of additional complicating variables affecting void position. Subsequent research (by Lieberman et al.) has examined some of these variables.



While considerable insight into the microscopic effects of shock loading has been gleaned from the experimental data, additional data analysis should provide an even better picture of shock loading within the copper specimen. For future experiments, the researchers anticipate that these techniques will be applied to shock loading phenomena in a variety of materials. Furthermore, by utilizing both near-field and far-field HEDM measurements, researchers expect a far more complete data set for further refinement of dynamic modeling programs.

— Philip Koth

**See:** David B. Menasche<sup>1\*</sup>, Jonathan Lind<sup>2</sup>, Shiu Fai Li<sup>2</sup>, Peter Kenesei<sup>3</sup>, John F. Bingert<sup>4</sup>, Ulrich Lienert<sup>5</sup>, and Robert M. Suter<sup>1</sup>, "Shock induced damage in copper: A before and after, three-dimensional study," *J. Appl. Phys.* **119**, 154902 (2016). DOI: 10.1063/1.4947270

**Author affiliations:** <sup>1</sup>Carnegie Mellon University, <sup>2</sup>Lawrence Livermore National Laboratory, <sup>3</sup>Argonne National Laboratory, <sup>4</sup>Los Alamos National Laboratory, <sup>5</sup>Deutsches Elektronen-Synchrotron

**Correspondence:**

\* david.menasche@hamiltonian-group.com

Work at Carnegie Mellon University was supported by the Los Alamos National Laboratory Laboratory-Directed Research and Development-Directed Research (LDRD-DR Project No. 20140114DR "Mesoscale Materials Science of Ductile Damage in 4 Dimensions"). J.F.B. acknowledges the support of the Joint Department of Defense/Department of Energy Munitions Program and the National Nuclear Security Administration's Science Campaign 2. This research used resources of the Advanced Photon Source, a U.S. Department of Energy (DOE) Office of Science User Facility operated for the DOE Office of Science by Argonne National Laboratory under Contract No. DE-AC02-06CH11357.

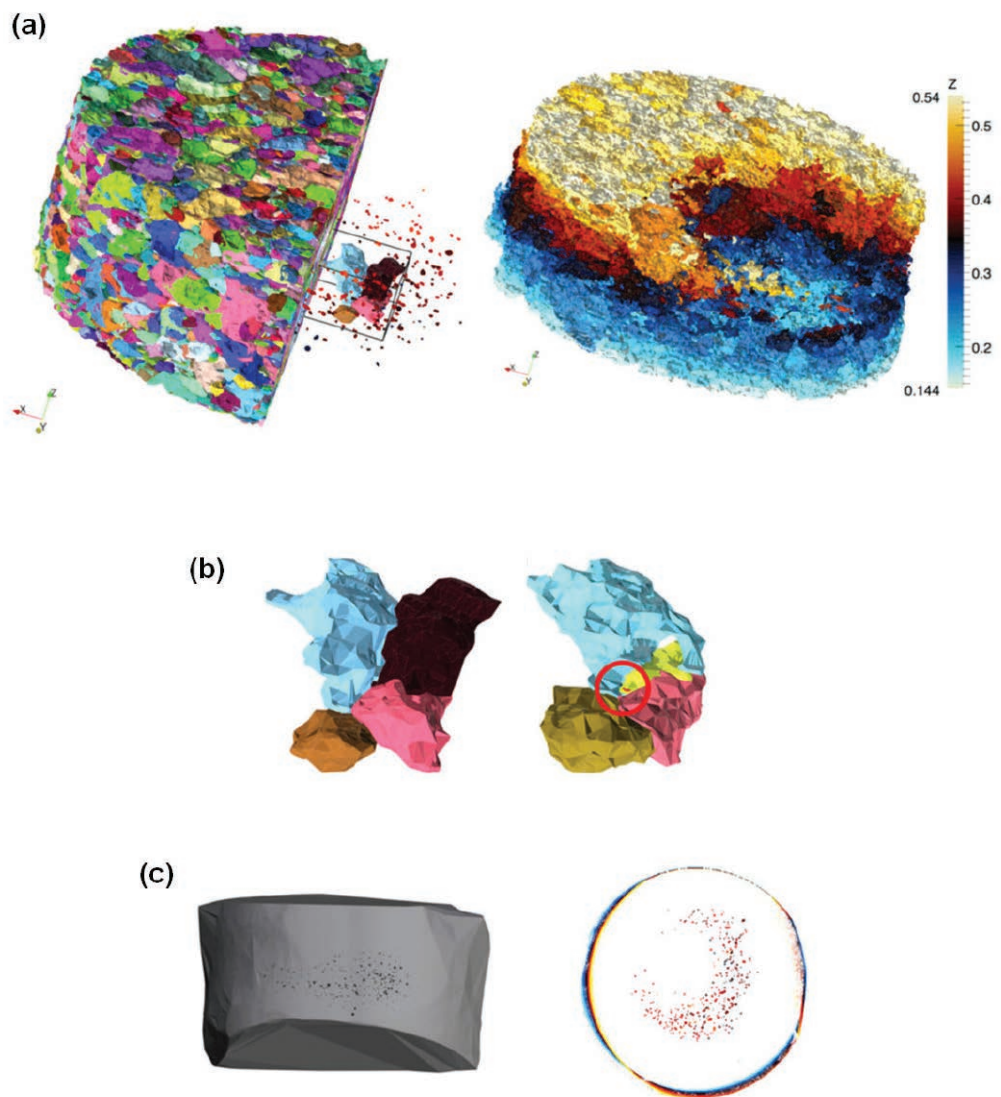


**Fig. 1.** Visual representation of the experimental data. Panels (a) and (b) show side-by-side comparisons of the pre- and post-shocked copper sample. The left-hand side of panel (a) presents a cutaway view of the copper sample prior to impact, with colors used to indicate each grain's crystalline orientation. The right-hand side of panel (a) is post-impact, with the color scheme indicating the amount that the center of mass of each grain has moved in the shock loading (z) direction. Colored bar on far right quantifies the center-of-mass displacements in the z-direction. (Missing grains in right-hand image actually exist, but were so distorted by impact they could not be reconstructed from the x-ray data.) Panel (b) shows close-up view of four copper grains, before (left) and after (right) impact. Location of this four-grain group within the sample is shown by the inset of panel (a). The sizes and shapes of the four color-coded grains are significantly altered by the impact. Rotation of the dark maroon grain at left is so severe that its post-shock orientation is represented by the yellow regions at right. Red circle indicates that a post-impact void has emerged where the four grains meet.

Panel (c) shows the emergence of voids following impact. Left side shows a cutaway view of the sample, with voids appearing black. Right side is a top-down view of the sample's edges showing a crescent-shaped spall/void field produced by impact.

1-ID-B,C,E • XSD • Materials science, physics, chemistry • High-energy x-ray diffraction, tomography, small-angle x-ray scattering, fluorescence spectroscopy, pair distribution function, phase contrast imaging • 41-136 keV, 45-116 keV • On-site • Accepting general users •

# REVEALING GROWTH PATTERNS IN EUTECTIC MIXTURES

The crystallized state of many materials arises from the repetition of a microscopic unit cell. In contrast to such a perfect crystalline lattice, the patterns formed by some solids display a much more complex ordering. In the case of “irregular eutectics,” highly complicated structures can arise at the mesoscale, including needles, plates, branches, and other convoluted shapes. Such complex structures appear frequently in nature, as well as in man-made materials ranging from organic solids to metallic and semi-metallic alloys. To gain additional insights into the underlying mechanisms responsible for the formation of these complex structures, x-ray microtomography performed at the APS was utilized to image the three-dimensional evolution of a representative irregular eutectic alloy. The experimental results have shed new light on the solidification pathways of the complex shapes arising from a eutectic system. These new insights should improve the modeling of such systems, allowing scientists and engineers to better predict and control their resulting morphologies, including enhancing the engineering of stronger and more resilient alloys.

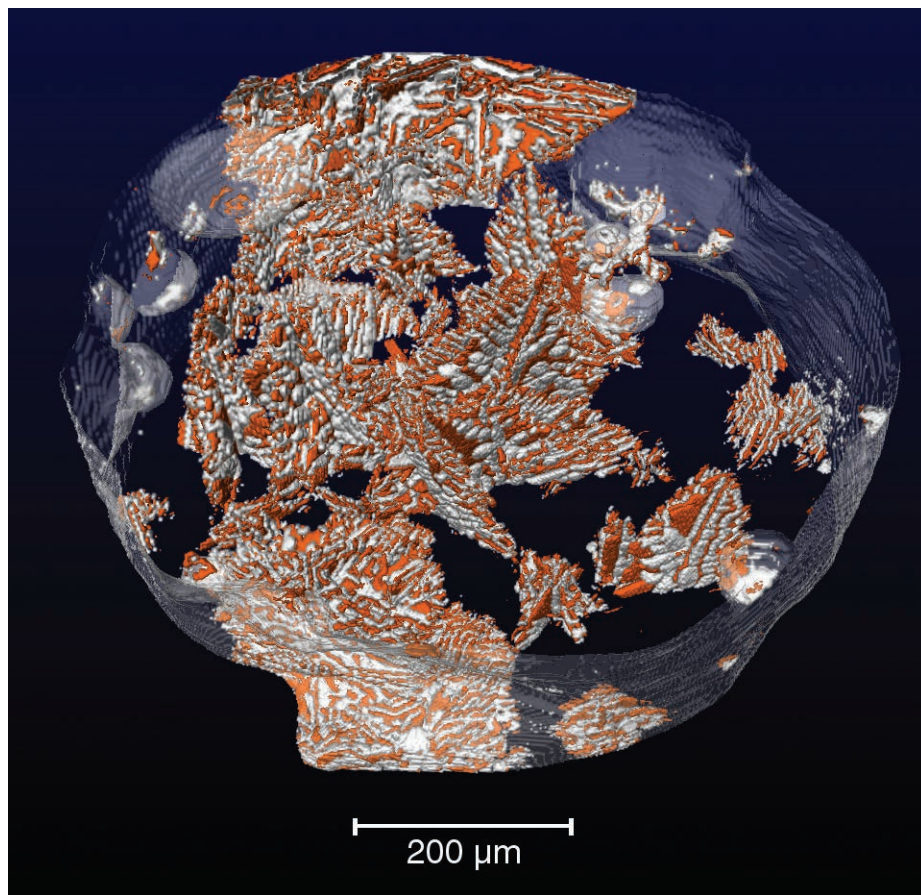


Fig. 1. Three-dimensional reconstruction of the region-of-interest based on the XRT data, some 3 min. into solidification of the sample. The yellow portions of the image indicate solid germanium, white is solid aluminum, and blue is the original liquid alloy that is not yet solidified. Length scale at bottom shows the mesoscale nature of the eutectic system. Covering a few tenths of a millimeter (several hundred micrometers), the overall structure is above the nanometer scale, but below the readily visible macroscopic scale.

In certain alloy systems, a liquid of fixed composition freezes to form a mixture of two different solid phases. This is known as the eutectic reaction. Oftentimes flakes, plates, or rods—generically referred to as lamellae—are formed. So-called “regular eutectic” materials feature lamellae which are more-or-less spaced in a repetitive, periodic fashion throughout the solid. In the case of irregular eutectics, this periodic spacing of the lamellae is usually absent. In practice, irregular eutectics often arise from liquids containing elements forming faceted phases in the material (e.g., silicon or germanium) along with non-facet-forming elements (aluminum or silver).

Models attempting to explain the growth of irregular eutectic patterns from liquids have been around for nearly 50 years. Experimental tests of these models sometimes involve quenching irregular eutectic alloys during growth, but quenching tends to distort the actual eutectic pattern. Another method uses optical micrographs of thin organic films. This method also has shortcomings, including the extrapolation of a two-dimensional pattern to a three-dimensional eutectic system. Moreover, organic compounds may not properly simulate the interfa-



cial dynamics that occur in real, metallic eutectics.

To more accurately test the existing models, the research team examined the solidification process of a eutectic alloy using x-ray microtomography (XRT). Performed at the XSD 2-BM-A,B beamline of the APS, the high-resolution XRT technique allowed for the reconstruction of three-dimensional images of a eutectic pattern as it grew over time. The eutectic alloy chosen was a roughly 50/50 mix (by weight) of faceted germanium and non-faceted aluminum, selected for two reasons. First, the large disparity in the atomic numbers of germanium and aluminum produces a stark contrast in x-ray attenuation, allowing the two elements to be easily distinguished. Secondly, germanium is a good proxy for similar faceted eutectic elements (e.g., silicon and gallium).

The germanium/aluminum alloy was formed as a 1-mm-diameter rod. Beginning as a liquid melt, the sample was cooled from just above the alloy's eutectic temperature of 420° C, to 3° C below. A three-dimensional reconstruction of the sample appears in Fig. 1, revealing the highly complex eutectic pattern that has emerged after 3 minutes into solidification. The orange-colored germanium appears as lamellae in the form of plates scattered throughout the image and the white aluminum appears as bulbous strips on the germanium plates. Figure 2 shows a close-up view of an individual plate.

The ability of the XRT technique to track the growth of the eutectic pattern in three dimensions has allowed new insights into the mechanisms responsible for such pattern formation, insights that cannot be obtained using other imaging methods. Several interesting conclusions were drawn from the XRT data. For instance, counter to the classical picture of a duplex solid-liquid growth front, it appears that instead the aluminum phases grow through holes within the germanium plates. Thus, defects within the faceted phase (in this case germanium) are critical to the growth process of the overall irregular eutectic system, and are largely responsible for the microstructural complexity that emerges during pattern formation.

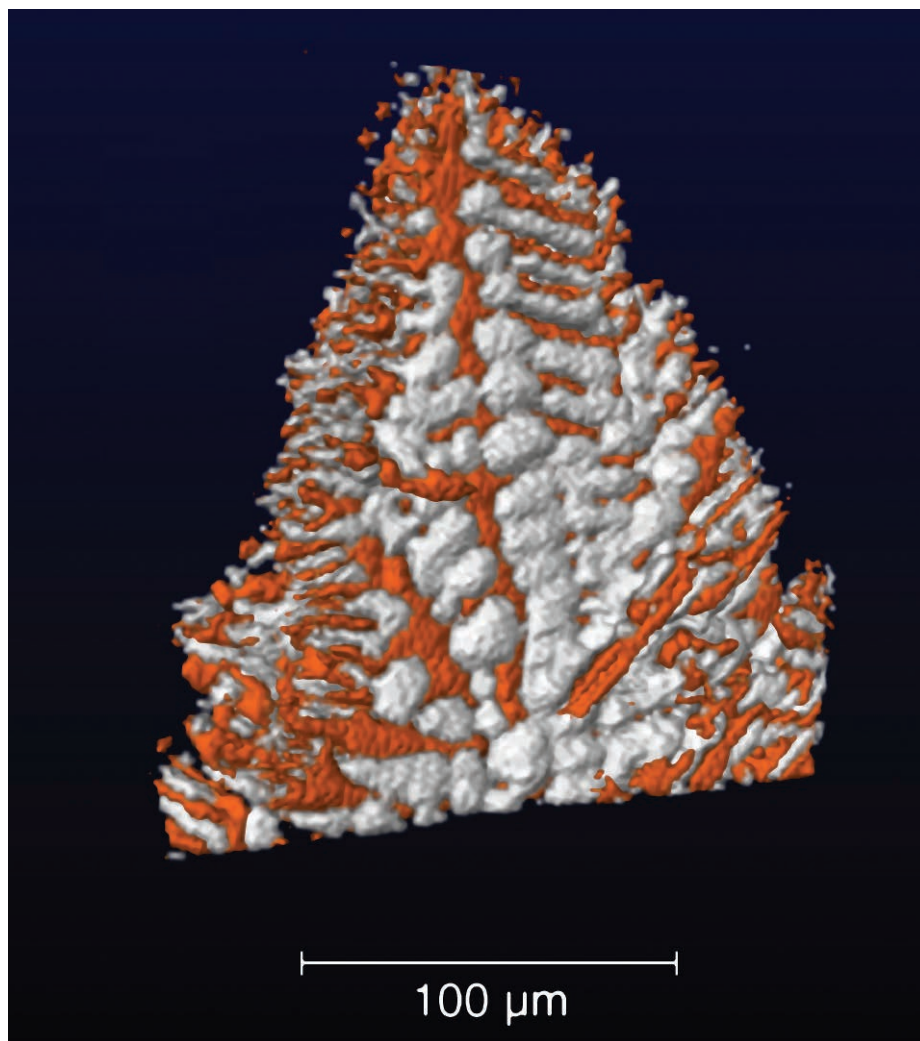


Fig. 2. Close-up view of one of the plates composing the eutectic system of Fig. 1. When a plate or other structure arises from a single nucleation site (i.e., a distinct site of solidification in the liquid) it is called 'colony'. The overall solid eutectic system of Fig. 1 is composed of many individual colonies, such as the plate shown here.

The results of this research, while confirming certain parts of previous models, reveal that none can fully explain all aspects of eutectic pattern formation. These insights will be utilized to improve the modeling and processing of irregular eutectic alloys.

— Philip Koth

**See:** Ashwin J. Shahani<sup>1†\*</sup>, Xianghui Xiao<sup>2</sup>, and Peter W. Voorhees<sup>1</sup>, "The mechanism of eutectic growth in highly anisotropic materials," *Nat. Commun.* 7, 12953 (2016).

DOI: 10.1038/ncomms12953

**Author affiliations:** <sup>1</sup>Northwestern University, <sup>2</sup>Argonne National Laboratory <sup>†</sup>Present address University of Michigan

**Correspondence:**

\* shahani@umich.edu

This work was supported by the Multidisciplinary University Research Initiative under award AFOSR FA9550-12-1-0458. Additional support was provided for A.J.S. by a National Science Foundation Graduate Research Fellowship under grant no. DGE-1324585. The sample preparation and data acquisition were supported by the DOE under contract no. DE-FG02-99ER45782. This research used resources of the Advanced Photon Source, a U.S. Department of Energy (DOE) Office of Science User Facility operated for the DOE Office of Science by Argonne National Laboratory under Contract No. DE-AC02-06CH11357.

2-BM-A,B • XSD • Physics, life sciences, geoscience, materials science • Tomography, phase contrast imaging • 10-170 keV, 11-35 keV • On-site • Accepting general users •



# A HIGH-PERFORMANCE, LOW-TEMPERATURE SOLID OXIDE FUEL CELL

Home remodeling companies sometimes use before and after pictures to visually dramatize the benefits of their services to consumers. Now, for the first time, researchers working at the U.S. Department of Energy's Advanced Photon Source (APS) have produced their own set of before-and-after images revealing the microscopic changes within a polycrystalline material subjected to high-speed impact. The research team used near-field high-energy diffraction microscopy (nf-HEDM), an x-ray imaging technique, to resolve the intricate, three-dimensional (3-D) effects of shock loading. These microscopic effects include both plastic deformation of crystalline grains and the formation of voids within the material. Conventional techniques either rely on surface measurements to infer the pre- and post-shocked structure of a material, or destructive methods that make it impossible to observe the same region before and after impact. In contrast, by combining the non-destructive nature of nf-HEDM with innovative experimental techniques, these researchers were able to image and compare pre- and post-shocked microstructure within a copper sample. The highly detailed 3-D imaging of microstructural changes obtained in this study will help improve predictive modeling of shock loading, leading to materials capable of better withstanding specific shock loading conditions.

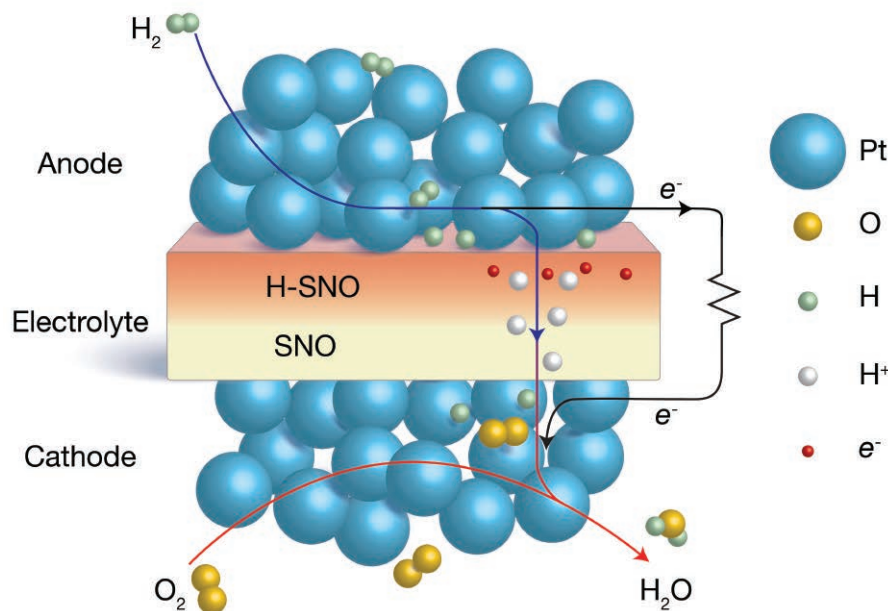


Fig. 1. A schematic of how the SNO-electrolyte fuel cell works. At the catalytic Pt anode, hydrogen molecules dissociate into protons and donate electrons to nickel in SNO. The electron doping process creates a Mott insulating state in the hydrogenated region, where electrons are localized. On the other hand, protons can still diffuse through the crystal. As a result, electrons are forced to pass through the external circuit and generate electrical power.

The researchers from Harvard University, Argonne, Rensselaer Polytechnic Institute, SiEnergy Systems, and Purdue University constructed nine free-standing micro-fabricated SOFCs using samarium nickelate ( $\text{SmNiO}_3$ ) (SNO) as the electrolyte (Fig. 2), even though it is a good conductor of electrons. SNO proved ideal because when hydrogen fuel is introduced at the anode of the fuel cells, hydrogen molecules dissociate into protons and electrons, creating a hydrogenated form of SNO (H-SNO) on the anode side that is electrically insulating. Once this insulating layer is formed, protons can continue to diffuse through the H-SNO electrolyte as long as hydrogen fuel continues to flow, with the electrons from the disassociated hydrogen molecules that are not involved in doping being forced to travel through the external electrical circuit powered by the SOFC. The H-SNO electrolyte not only showed extremely high ionic conductivity, its activation energy was very low, making it suitable for low-temperature fuel cell operation.

Several factors may collectively lead to the high ionic conductivity and low activation energy in SNO. The researchers theorized that when the hydrogen molecules dissociate, they dope  $\text{Ni}^{3+}$  ions in the SNO with some of their electrons, reducing them to  $\text{Ni}^{2+}$  ions, thereby forming insulating H-SNO on the anode side. To confirm the electron localization mechanism during fuel cell operation and to reveal the underlying reasons for the high ionic conductivity, both chemical and structural characterizations of the SNO hydrogenation process were performed. X-ray absorption near-edge spectroscopy (XANES) measurements of the nickel K-edge from pristine and hydrogenated SNO samples were conducted at XSD beamline 12-BM-B, at the APS, while x-ray diffraction measurements were made at XSD beamline 12-ID-C,D.

A substantial shift of the absorption edge to a lower energy was observed

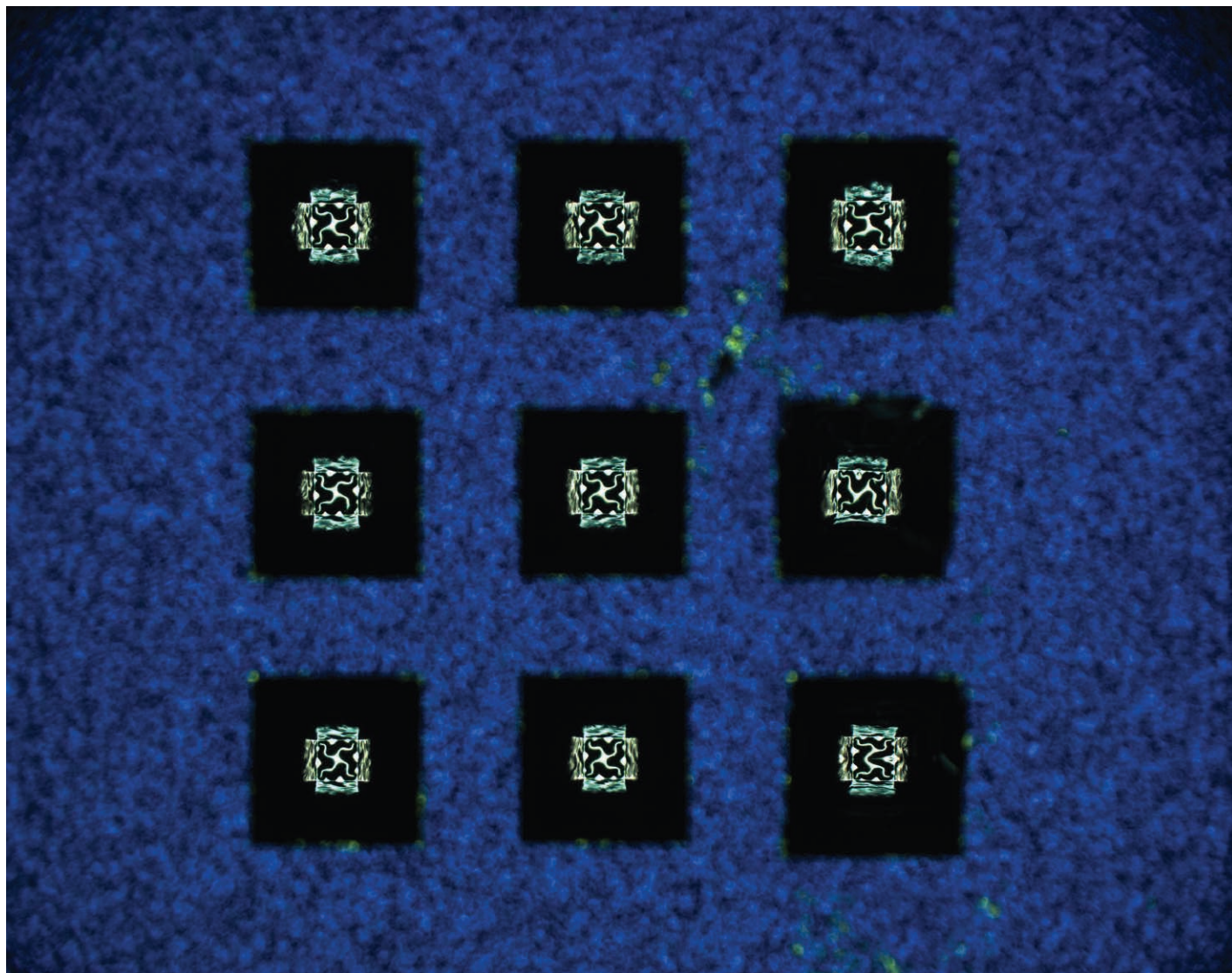


Fig. 2. An array of nine micro-fabricated fuel cells.

upon hydrogenation. The energies of the absorption edge and other features were consistent with a valence change to  $\text{Ni}^{2+}$  in SNO. The change of Ni valence state also verified that hydrogen exists as protons in H SNO. The angle-resolved XANES spectra additionally showed that proton incorporation not only happens at the surface but also throughout the H-SNO film. The synchrotron x-ray diffraction studies suggested that the SNO lattice expands during hydrogenation to accommodate proton transport.

The successful electron doping strategy establishes a new direction for the development of high-performance proton-conducting electrolytes for low-temperature SOFCs. — *Vic Comello*

*See:* You Zhou<sup>1\*\*</sup>, Xiaofei Guan<sup>1</sup>, Hua Zhou<sup>2</sup>, Koushik Ramadoss<sup>1</sup>, Suhare

Adam<sup>1</sup>, Huajun Liu<sup>2</sup>, Sungsik Lee<sup>2</sup>, Jian Shi<sup>1,3</sup>, Masaru Tsuchiya<sup>4</sup>, Dillon D. Fong<sup>2</sup>, and Shriram Ramanathan<sup>1,5\*</sup>, “Strongly correlated perovskite fuel cells,” *Nature* **534**, 231 (2016). DOI: 10.1038/nature17653

*Affiliations:* <sup>1</sup>Harvard University, <sup>2</sup>Argonne National Laboratory, <sup>3</sup>Rensselaer Polytechnic Institute, <sup>4</sup>SiEnergy Systems, <sup>5</sup>Purdue University

*Correspondence:*

\* shriram@purdue.edu

\*\* youzhou@fas.harvard.edu

Financial support was provided by the Army Research Office (grants W911NF-14-1-0348 and W911NF-14-1-0669), the Air Force Office of Scientific Research (grant FA9550-12-1-0189), the Advanced Research Projects Agency-Energy (ARPA-E), an IBM PhD Fellowship, and the National Academy of Sciences. Part of the work was performed at the Center for Nanoscale Systems at Harvard

University. D.D.F. was supported by the U.S. Department of Energy (DOE) Office of Science-Basic Energy Sciences, Materials Sciences and Engineering Division. This research used resources of the Advanced Photon Source, a U.S. DOE Office of Science User Facility operated for the DOE Office of Science by Argonne National Laboratory under contract no. DE-AC02-06CH11357.

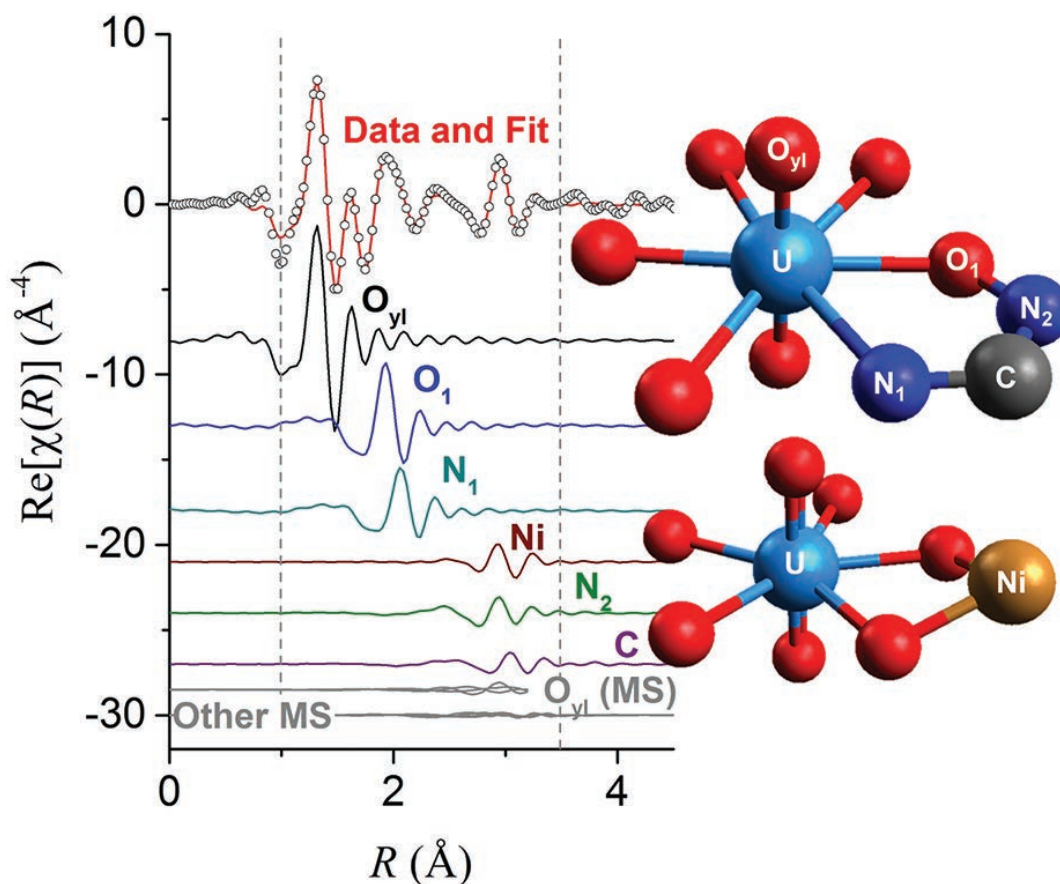
12-ID-C,D • XSD • Chemistry, physics, materials science • Small-angle x-ray scattering, grazing incidence small-angle scattering, wide-angle x-ray scattering, surface diffraction • 4.5-40 keV • On-site • Accepting general users •

12-BM-B • XSD • Materials science, polymer science, chemistry, physics, environmental science • X-ray absorption fine structure, general diffraction, x-ray reflectivity, fluorescence spectroscopy, small-angle x-ray scattering, wide-angle x-ray scattering • 4.5-26 keV, 10-30 keV • On-site • Accepting general users •



# IMPROVING THE BRAIDS THAT BIND URANIUM FROM SEAWATER

Nuclear power is one of the best ways currently available to supply clean, base-load electric power to the U.S. over the long term. But reserves of good uranium ore to fuel those plants are diminishing. By 2100 there will not be enough recoverable uranium left in terrestrial mines to meet the demands of existing power plants. However, if we cannot mine uranium on land, we may be able to sift it from the sea: The oceans contain huge reserves of uranium dissolved in seawater. State-of-the-art polymer fabrics soaked in seawater can recover 7 to 8 grams of uranium over a span of 30 days. Researchers trying to improve that fabric used the APS to inspect how uranium binds to the polymer at the molecular level. The results were surprisingly different than what scientists thought was going on, and open new possibilities for improving uranium recovery.





The polymer fabric's uranium catcher is a molecule called amidoxime. Amidoxime finds and binds uranium, sucking it out of seawater even at the extremely dilute concentration of 3.3 parts per billion that are normal in the open ocean. Researchers understood how amidoxime works when it is just a small molecule, but they did not know what happened when amidoxime molecules were integrated within a ropy, braided polymer fabric and exposed to ocean water. For example, other elements such as copper and vanadium may also be attracted by the binding sites. Unlike uranium, these other elements are important to ocean biology, and removing them from seawater could degrade the environment. In addition, they could occupy binding spots that would otherwise catch more uranium.

The team of researchers from The University of Chicago and Oak Ridge National Laboratory (ORNL) used x-ray absorption fine structure (XAFS) analysis at the Materials Research Collaborative Access Team 10-BM-A,B x-ray beamline at the APS, supplemented by pair distribution function (PDF) measurements obtained at XSD beamline 11-ID-B, also at the APS, to get a better picture of what was happening. The research group chose the APS for the quality of its high-energy x-rays, and the 10-BM and 11-ID beamlines because of their excellent beamline scientists. Not only do these personnel have experience working with radiological materials and can measure at the energies the experiment requires, but they always make sure the optics and detectors are well configured and able to collect high-quality data, according to the lead investigator.

XAFS reveals the oxidation state and local atomic environment of uranium (or any number of other metals)

< Fig. 1. The image shows the theoretical EXAFS paths that would fit the data gathered at beamline 10-BM, as well as the atomic arrangements of elements that would generate those paths.

by hitting the sample with x-rays that will only be absorbed by the element of interest. The x-rays excite the electrons closest to the nucleus to higher energies, and the electrons then scatter off of adjacent atoms before returning to fill their original place. This scattering subtly changes the amount of x-rays absorbed, creating a spectrum which hints as to what atoms surround the uranium. As each element absorbs x-rays of different energies, XAFS can infer how different metals are bound on the same sample. In contrast, PDF measurements investigate the distance between atoms by measuring the diffraction of the x-rays. While not capable of discriminating between different elements, it is particularly useful for non-crystalline samples, such as the adsorbents investigated in this study. The group was able to use XAFS to analyze uranium bound to both amidoxime polymers and in small molecule amidoxime crystals.

The results surprised them. Something significantly different was happening in the seawater-soaked polymer. The uranium bound to the amidoxime polymer in a distinctive way, not the way it bound to the small molecule amidoxime. In fact, it looked as if another atom such as vanadium, copper, or nickel might be bonding to the polymer in a manner that changed the atomic arrangement of the uranium binding site.

When the team compared their experimental results to computational models for different uranium-amidoxime bonding configurations, the closest match to the experimental XAFS spectrum was higher in energy (and therefore previously unexpected, Fig. 1). This led the scientists to propose that the structure of the polymer and its interaction with other metals in seawater dictates how the uranium is actually bound, rather than the chemical interactions that dominate with small molecules. This is a fundamental shift in how researchers conceptualize the way metals and polymers interact.

The researchers must do further

experiments to better understand how the polymer structure can be changed to enhance uranium binding. Their goal is to design a better polymer with more available spaces that are uniquely attractive to uranium, bringing uranium harvesting from the oceans closer to commercial reality. — *Kim Krieger*

**See:** C.W. Abney<sup>1,2\*\*</sup>, R.T. Mayes<sup>2</sup>, M. Piechowicz<sup>1</sup>, Z. Lin<sup>1</sup>, V.S. Bryantsev<sup>2</sup>, G.M. Veith<sup>2</sup>, S. Dai<sup>2</sup>, and W. Lin<sup>1\*</sup>, "XAFS investigation of polyamidoxime-bound uranyl contests the paradigm from small molecule studies," *Energ. Environ. Sci.* **9**, 448 (2016).

DOI: 10.1039/c5ee02913a

**Author affiliations:** <sup>1</sup>The University of Chicago, <sup>2</sup>Oak Ridge National Laboratory

**Correspondence:**

\* wenbinlin@uchicago.edu

\*\* abneycw@ornl.gov

Work at the University of Chicago was supported by the U.S. Department of Energy (DOE) Office of Nuclear Energy's Nuclear Energy University Program (Sub-Contract – 20 #120427, Project #3151). Work at ORNL was sponsored by the U.S. DOE Office of Nuclear Energy. Materials Research Collaborative Access Team operations are supported by the U.S. DOE and the Materials Research Collaborative Access Team member institutions. This research used resources of the National Energy Research Scientific Computing Centre, a DOE Office of Science user facility supported by the Office of Science of the U.S. DOE under Contract No. DE-AC02-05CH11231. This research used resources of the Advanced Photon Source, a U.S. DOE Office of Science User Facility operated for the DOE Office of Science by Argonne National Laboratory under Contract No. DE-AC02-06CH11357.

10-BM-A,B • MR-CAT • Materials science, chemistry, environmental science, physics • X-ray absorption fine structure • 4-32 keV • On-site • Accepting general users •

11-ID-B • XSD • Chemistry, environmental science, materials science • Pair distribution function, high-energy x-ray diffraction • 58.66 keV, 86.7 keV • On-site • Accepting general users •

# ELECTRODES DISTORT THE PROPERTIES OF QUANTUM WELLS

Today's most advanced microprocessors could be vastly outperformed in some important computational problems by quantum computers. Instead of switching current flow on and off to create the 1s and 0s of binary code, quantum computers rely on quantum mechanical properties of electrons, such as orbital state and spin. To make this happen, engineers have to develop quantum bits, or qubits, which they can reliably and predictably control; however, this has been a challenging task. Now, a team of researchers using the APS and the Center for Nanoscale Materials (CNM) at Argonne have revealed one issue that makes building such qubits so difficult. Armed with this information, the researchers hope engineers will be better able to predict the performance of their devices based on the stress from the electrodes, and perhaps alter their designs to compensate for it. It might even be possible to take advantage of the strain in designing the quantum dots, modifying it to change the electronic properties of the material. Gaining greater control over the electronic properties of the material may also allow researchers to create arrays of qubits with complicated structures to help them better understand the physics of confined electrons.

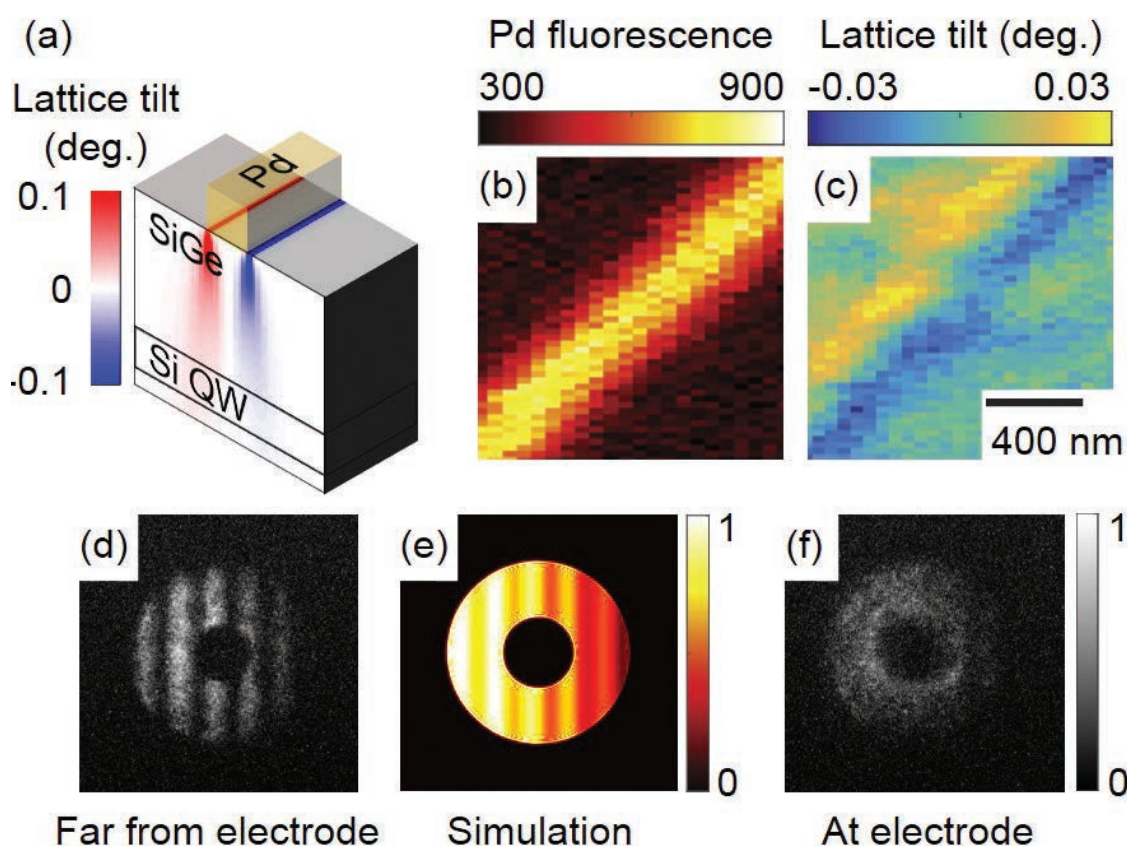


Fig. 1. The palladium electrode on top of a quantum well device causes the device's crystal lattice to tilt (a-c). Researchers compare experimental (d) and simulated (e) diffraction patterns from an un-tilted region far from the electrode with the diffraction pattern from a region near the electrode (f) to measure the distortion.

One method for making qubits involves creating quantum dots, which are tiny volumes of a semiconductor that can trap a single electron in a space known as a “quantum well.” Researchers create a device with a thin film of silicon, sandwiched between two thicker films of a silicon-germanium alloy. In the particular structure probed at the joint APS/CNM Hard X-Ray Nanoprobe at APS beamline 26-ID-C, these layers had thicknesses of 10, 91, and 300 nm. The researchers from the University of Wisconsin-Madison and Argonne capped the stack with a thin silicon layer and above it created a pattern of thin-film electrodes made of a metal such as palladium in order to set the location of the quantum well. The electric fields produced by the electrodes pushed electrons away, leaving only small spaces within the quantum well where the electrons could be confined—trapped at the interface between the silicon and the silicon-germanium. These locations are the quantum dots.

Working at such scales, tiny imperfections such as stresses induced by random variations in how the silicon-germanium crystal grows can throw off the properties of the device, making its performance difficult to predict. The variability produces mechanical strain in the devices, which changes how electrons move through the quantum wells. As a result, the engineers cannot tell what voltage will be needed to confine an electron in a given quantum dot, so they try out several until they hit the sweet spot. Not only is that an inefficient way to design a device, but the interactions among several electrodes may make it impossible to attain the right voltage for every qubit, rendering some of them useless. How much and how fast the strain changes across the device may also affect the quantum state of the confined electrons.

Engineers had not known much about the source of these distortions, magnitude, or impact of the distortions until these researchers used the Hard X-Ray Nanoprobe to measure them. The researchers developed a method using x-ray nanobeam diffraction to measure variations in strain over small areas in thin films. Applying it to the qubits, they discovered the major

source of mechanical distortion was the stress created by the metal electrode on top of the device. The effect was significant. The shift in the energy level caused by the stress from the electrode was about the same as the energy required to move the electron into or out of the quantum dot. That means not only would engineers need to compensate for the effect of the strain, they also couldn't know how to bias the electrode. — *Neil Savage*

**See:** J. Park<sup>1</sup>, Y. Ahn<sup>1</sup>, J.A. Tilka<sup>1</sup>, K.C. Sampson<sup>1</sup>, D.E. Savage<sup>1</sup>, J.R. Prance<sup>1</sup>, C.B. Simmons<sup>1</sup>, M.G. Lagally<sup>1</sup>, S.N. Coppersmith<sup>1</sup>, M.A. Eriksson<sup>1</sup>, M.V. Holt<sup>2</sup>, and P. G. Evans<sup>1\*</sup>, “Electrode-stress-induced nanoscale disorder in Si quantum electronic devices,” *APL. Mat.* **4**, 066102 (2016).

DOI: 10.1063/1.4954054

**Author affiliations:** <sup>1</sup>University of Wisconsin-Madison, <sup>2</sup>Argonne National Laboratory

**Correspondence:** \* pgevans@wisc.edu

J.P., Y.A., and P.G.E. acknowledge support from the U.S. Department of Energy (DOE)-Basic Energy Sciences, Materials Sciences and Engineering, under Contract No. DE-FG02-04ER46147 for the x-ray scattering studies and analysis. Development and maintenance of the growth facilities used for fabricating samples is supported by the U.S. DOE (Grant No. DE-FG02-03ER46028). The other authors acknowledge support from Army Research Office (Grant Nos. W911NF-08-1-0482 and W911NF-12-1-0607) and the NSF (Grant No. DMR-1206915). This research used shared facilities at the University of Wisconsin-Madison supported by the NSF MRSEC program under Grant No. DMR-1121288. J.A.T. acknowledges support from the NSF Graduate Research Fellowship Program under Grant No. DGE-1256259. Use of the Center for Nanoscale Materials and the Advanced Photon Source, both Office of Science user facilities, was supported by the U.S. DOE Office of Science-Basic Energy Sciences, under Contract No. DE-AC02-06CH11357.

26-ID-C • CNM/XSD • Physics, materials science • Nanodiffraction, nano-imaging, coherent x-ray scattering, synchrotron X-ray Scanning Tunneling Microscopy • 6-12 keV • On-site • Accepting general users •

## Defining the Quantum Computer

The Turing machine, developed by Alan Turing in the 1930s, is a theoretical device that consists of tape of unlimited length that is divided into little squares. Each square can either hold a symbol (1 or 0) or be left blank. A read-write device reads these symbols and blanks, which gives the machine its instructions to perform a certain program. In a quantum Turing machine, the difference is that the tape exists in a quantum state, as does the read-write head. This means that the symbols on the tape can be either 0 or 1 or a superposition of 0 and 1; in other words the symbols are both 0 and 1 (and all points in between) at the same time. While a normal Turing machine can only perform one calculation at a time, a quantum Turing machine can perform many calculations at once.

Today's computers, like a Turing machine, work by manipulating bits that exist in one of two states: a 0 or a 1. Quantum computers aren't limited to two states; they encode information as quantum bits, or qubits, which can exist in superposition. Qubits represent atoms, ions, photons or electrons and their respective control devices that are working together to act as computer memory and a processor. Because a quantum computer can contain these multiple states simultaneously, it has the potential to be millions of times more powerful than today's most powerful supercomputers.

This superposition of qubits is what gives quantum computers their inherent parallelism. According to physicist David Deutsch, this parallelism allows a quantum computer to work on a million computations at once, while a desktop PC works on one. A 30-qubit quantum computer would equal the processing power of a conventional computer that could run at 10 teraflops (trillions of floating-point operations per second). Today's typical desktop computers run at speeds measured in gigaflops (billions of floating-point operations per second).

Quantum computers also utilize another aspect of quantum mechanics known as entanglement. One problem with the idea of quantum computers is that if you try to look at the subatomic particles, you could bump them, and thereby change their value. If you look at a qubit in superposition to determine its value, the qubit will assume the value of either 0 or 1, but not both (effectively turning your spiffy quantum computer into a mundane digital computer). To make a practical quantum computer, scientists have to devise ways of making measurements indirectly to preserve the system's integrity. Entanglement provides a potential answer. In quantum physics, if you apply an outside force to two atoms, it can cause them to become entangled, and the second atom can take on the properties of the first atom. So if left alone, an atom will spin in all directions. The instant it is disturbed it chooses one spin, or one value; and at the same time, the second entangled atom will choose an opposite spin, or value. This allows scientists to know the value of the qubits without actually looking at them.

Source: Kevin Bonsor & Jonathan Strickland "How Quantum Computers Work" 8 December 2000. HowStuffWorks.com. <<http://computer.howstuffworks.com/quantum-computer.htm>> 25 January 2017



# AN ABUNDANT ALTERNATIVE TO LITHIUM-ION BATTERIES

Most of us walk around with a lithium-ion battery in our pocket, thanks to these battery's ubiquity in cell phones and other portable devices. But the lithium in these ubiquitous power sources is limited to that which can be extracted from the Earth's crust. The growing demand for lithium-ion batteries for electric vehicles and other portable devices may place a strain on global reserves in the coming decades. Sodium (Na) is abundant compared to lithium and shares the same charge, spurring research into the feasibility of sodium-ion batteries. Toward this goal, researchers interrogated the sodiation (addition of sodium) and (de)sodiation (removal of sodium) of  $\alpha$ -MnO<sub>2</sub> nanowires with experiments at the APS. Their insights into the differences between (de)sodiation and (de)lithiation of the nanowires may guide the development of better sodium batteries in the future.

The basic concept of lithium-ion batteries is that the lithium ion moves from the negative electrode to the positive electrode during discharge and back during charging. The concept would be similar for sodium-ion batteries, but the materials selected for the electrodes may need to be different to accommodate the larger size of the sodium ion compared to the lithium ion, among other considerations. In the current study, researchers from Michigan Technological University, Argonne, Shandong University (China), and the University of Illinois at Chicago evaluated sodium ion insertion in manganese oxide (MnO<sub>2</sub>) nanowires, which previous studies suggested could accommodate sodium's ions. However, those studies also found that, while the initial discharge capacity was as high as 350 mAh/g, over multiple charge-discharge cycles that capacity diminished substantially, to below 100 mAh/g at 100 cycles.

To better understand this loss in capacity, and develop approaches to maintain capacity over cycling, the researchers explored the character of the manganese oxide nanowire host material over (de)sodiation cycles using two complementary methods: transmission electron microscopy (TEM) and x-ray absorption spectroscopy (XAS). TEM allowed the researchers to structurally characterize the nanowires, while XAS

provides information on the valence state of manganese.

As a first step, the researchers took TEM images of the pristine manganese oxide nanowire. The wire had a roughly uniform 60-nm diameter, with a square-shaped cross section and a substructure consisting of a matrix of tunnels with manganese walls and potassium (K) ions dotted along each tunnel's central channel. During the formation of the tunnel structure, the K ions had been trapped inside.

Next, they added various concentrations of sodium to the nanowires to observe the effects of different degrees of sodiation on the nanowire structure. The tunnel lattice did become increasingly distorted with higher levels of sodiation and in the heavily sodiated nanowire, the tunneled structure became completely degraded. The researchers also observed what happened during sodiation/(de)sodiation cycling: Upon sodiation, the nanowire swelled radially, increasing in diameter by about 50%; upon (de)sodiation, the nanowire contracted by only about 15%, though in the following cycles the radial changes were limited to within 20%. After five cycles, no cracks or fractures in the nanowire were observed, suggesting good reversibility of the nanostructures.

To study the mechanism of cycling stability and the voltage profile for the

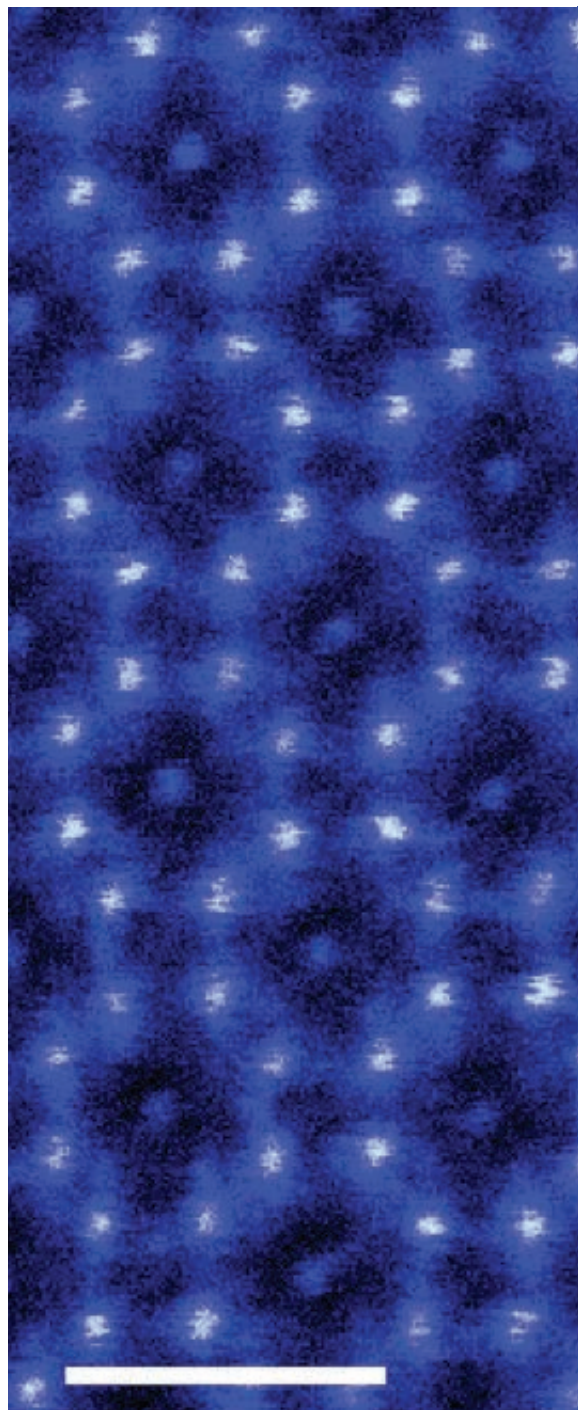
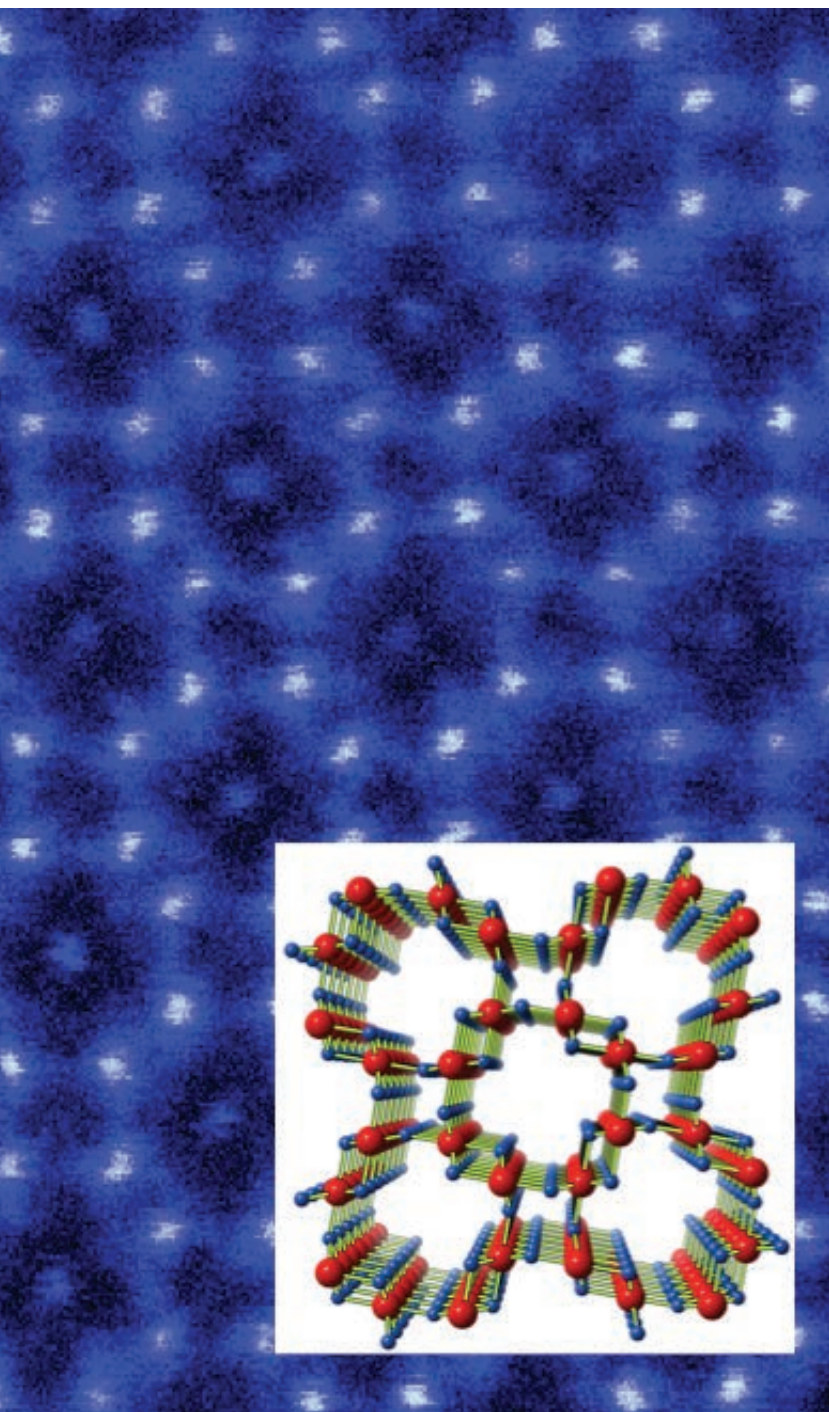


Fig. 1. TEM image showing atomic tunnel-based structure of  $\alpha$ -MnO<sub>2</sub> nanowire, featuring large 4.6X4.6 angstrom tunnels. The atomic model is given in the inset. Scale bar: 1 nm



9-BM-B,C • XSD • Materials science, chemistry, environmental science • X-ray absorption fine structure, x-ray absorption near-edge structure • 2.1-25.2 keV • On-site • Accepting general users •

(de) sodiation process of  $\text{MnO}_2$  nanowires, the researchers collected XAS data at the XSD 9-BM-B,C x-ray beamline at the APS during battery cycling. Initially, the battery boasted a discharge capacity of 300 mAh/g, which plummeted to 50 mAh/g after 50 cycles. As far as the valence state, the XAS spectra of pristine nanowires showed manganese largely in the 4+ state. After discharge, the manganese oxidation state drops to ~3+. Charging the nanowire again failed to get the manganese back up to 4+. This inability to recover manganese's pristine oxidation state may be one reason that the cycling is nonreversible and may be explained by the residual  $\text{Na}^+$  that remains in the nanowire despite full discharging, as suggested by the TEM data.

The fact that  $\text{MnO}_2$  tunnels cannot survive after the voltage drops below 1.5 V and Mn is reduced to below 3.5+ led the researchers to come up with a method to maintain the tunnel stability by controlling the cycling voltage window of a Na/ $\text{MnO}_2$  battery, which is actually to keep the Mn valence above 3.5+ with the tunnel-based  $\text{MnO}_2$  structure staying stable. Figure 1 shows the results of a Na/ $\text{MnO}_2$  battery being cycled between 4-0.5 V, 4-1.0 V, and 4-1.5 V. It apparently shows that the capacity retention is much better when the voltage is controlled at 4-1.5 V range, while the other two ranges make the battery degrade quickly during cycling.

As a final test, the researchers observed how lithium ions treated the manganese oxide nanowires over electrochemical cycling. Unlike the tunnel destruction observed with sodiation, lithiation caused little disruption in tunnel structure, likely owing to its smaller ionic size.

With additional structural engineering and chemical modification based on the findings in this study, the electrochemical performance of sodium batteries may be enhanced in future experiments. — *Erika Gebel Berg*

**See:** Yifei Yuan<sup>1</sup>, Lu Ma<sup>2</sup>, Kun He<sup>1,3</sup>, Wentao Yao<sup>1</sup>, Anmin Nie<sup>4</sup>, Xuanxuan Bi<sup>2</sup>, Khalil Amine<sup>2</sup>, Tianpin Wu<sup>2\*</sup>, Jun Lu<sup>2\*\*</sup>, and Reza Shahbazian-Yassar<sup>1,4\*\*\*</sup>, "Dynamic study of (De)sodiation in alpha- $\text{MnO}_2$  nanowires," *Nano Energy* **19**, 382 (2016).

DOI: 10.1016/j.nanoen.2015.11.028

**Author affiliations:** <sup>1</sup>Michigan Technological University, <sup>2</sup>Argonne National Laboratory, <sup>3</sup>Shandong University, <sup>4</sup>University of Illinois at Chicago

**Correspondence:** \* twu@aps.anl.gov \*\* junlu@anl.gov \*\*\*rsyassar@uic.edu

R. Shahbazian-Yassar acknowledges the financial support from the National Science Foundation (NSF) Award No. CMMI-1200383. Partial funding from Argonne National Laboratory under subcontract No.4F31422 is acknowledged. We also acknowledge support from the Center for Electrochemical Energy Science, an Energy Frontier Research Center funded by the U.S. Department of Energy (DOE) Office of Science-Basic Energy Sciences. The acquisition of the UIC-JEOLJEM- ARM200CF is supported by an MRI-R2 grant from the NSF (AwardNo.DMR-0959470). Support from the UIC Research Resources Center is also acknowledged. This research used resources of the Advanced Photon Source, a U.S. DOE Office of Science User Facility operated for the DOE Office of Science by Argonne National Laboratory under Contract No. DE-AC02-06CH11357.



# ELECTRODE OPTIONS FOR LITHIUM-ION BATTERIES

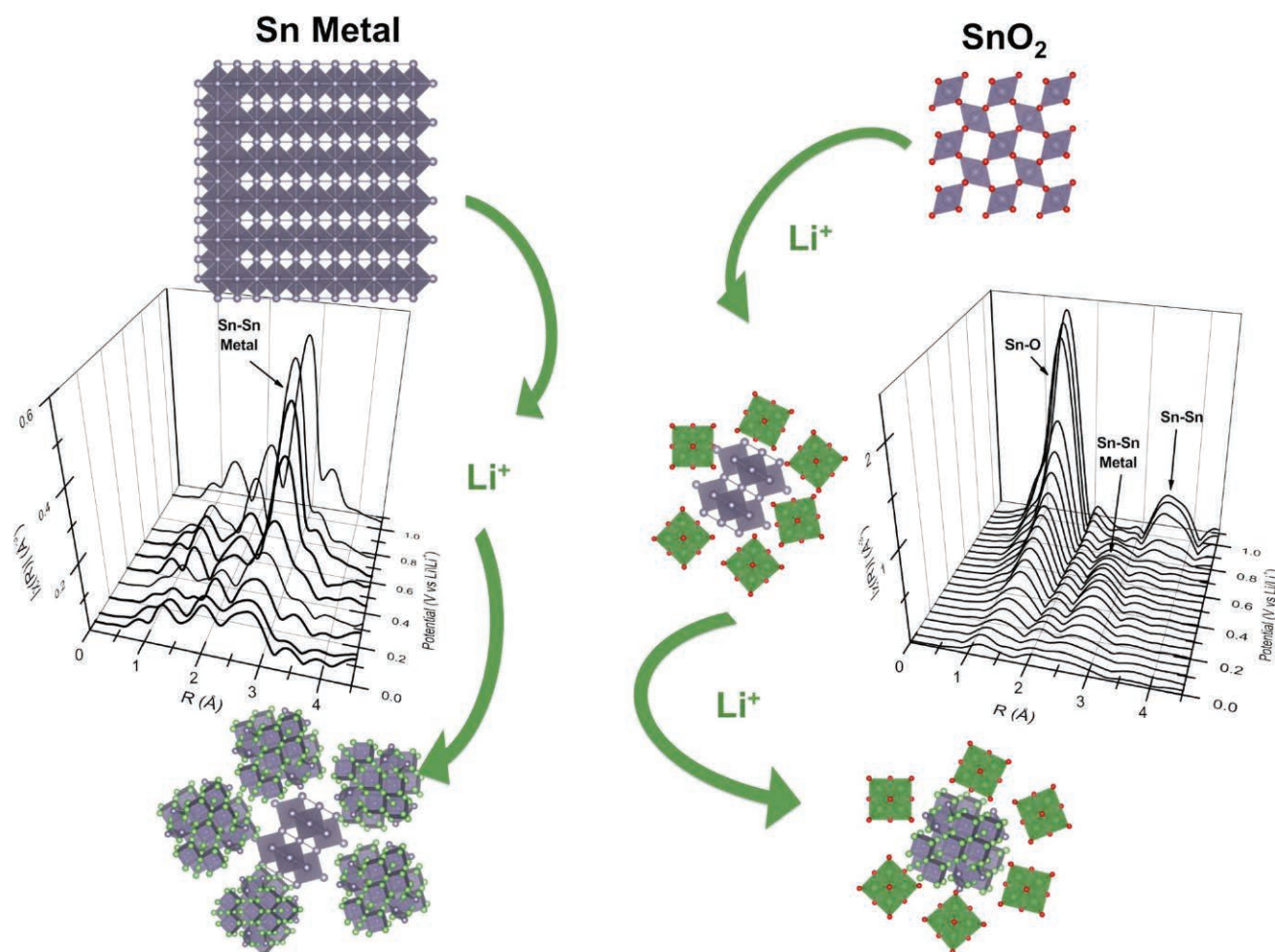


Fig. 1. Two types of battery anodes are compared. On the left, a pure tin anode is represented by a relatively large crystal nanoparticle (top). During the first lithiation, lithium ions (shown in green) begin to alloy with the tin atoms, as evidenced in the Sn-Sn metal peak in the x-ray absorption spectrum (middle). But the peaks do not completely disappear, implying that the lithium is unable to penetrate to the core of the nanoparticle (bottom). By contrast, the right side shows a tin oxide anode. In this case, the first lithiation converts tin oxide into small tin nanoparticles, surrounded by lithium oxide. The smaller size means lithium reaches nearly all the available tin atoms. The proof of this is the near disappearance of the Sn-Sn metal peak in the x-ray absorption spectrum. Image: Christopher Pelliccione



**L**ithium-ion batteries power many of the electronic devices that we've come to depend on. But these storage devices will need an upgrade for use in electric cars, where the battery's large weight undermines the energy efficiency. One place for improvement is in the anodes (or negative electrodes) that store lithium ions during charge up. Experiments performed at the APS have investigated high-capacity, tin-based anodes using x-ray absorption spectroscopy. The observations track structural changes within tin nanostructures, revealing why these anodes often fail after multiple uses. These results provide clues to engineers trying to design a battery that can drive us into the future.

The majority of lithium-ion batteries use carbon-based materials for their anode. In the case of a cell phone or laptop, carbon can store a sufficient amount of lithium ions, but increasing capacity will require new materials. One option has been tin, which can store three times more lithium charges per mass—thus reducing the overall weight of the battery. The typical design of a tin-based anode consists of a large number of tin nanoparticles embedded in a conductive support medium. As the battery is charged, lithium ions diffuse into the tin nanoparticles. Each tin atom can bind with as many as four lithium ions. But this high capacity poses a problem as the nanoparticles swell in size. The volume expansion can cause structural damage within the anode, eventually leading to broken electronic contacts and a dead battery.

One strategy for improving tin-based anodes is to use tin oxide ( $\text{SnO}_2$ ) rather than pure tin (Sn metal). Tests have shown that tin oxide anodes have greater longevity, but the key to this longer life is not completely understood. Researchers from the Illinois Institute of Technology and Argonne performed experiments on tin and tin-oxide anodes at the MR-CAT 10-ID-B beamline at the APS. This beamline provides high-energy x-rays (29.2 keV) capable of exciting the K-edge of tin.

The researchers collected spectra for both x-ray absorption near-edge structure (XANES) and x-ray absorption fine structure (EXAFS) studies. The XANES data reveal the electronic state of an absorbing tin atom, whereas the EXAFS observations provide information about the surrounding atomic

structure. The team applied models to their absorption spectra, which revealed whether the tin atoms were in a metallic state (Sn-Sn bonds), an oxide state (Sn-O bonds), or in a lithium alloy phase (Sn-Li bonds). The ability to observe lithium—through its bonding to tin—was a unique feature of this study, as normally lithium is too light to give an x-ray signal.

The team began with pristine (never-before-used) anodes and observed the structural changes during the initial lithiation, when lithium ions diffuse into the anode. For the pure tin case, they found that a fraction of the tin atoms remained in the metallic state, never alloying with lithium (Fig. 1). A possible explanation is that lithium atoms collect on the outer shell of tin nanoparticles, preventing other lithium ions from reaching the core. Volume expansion causes a break between the core and shell, which reduces the electrical conductivity within the anode. An indication of this structural damage was found in a reduction in the number of lithium neighbors after multiple charging-discharging cycles.

The situation was different for the tin-oxide anode. During the first lithiation, the tin oxide transforms into metallic tin surrounded by lithium oxide. The metallic tin collects into crystalline nanoparticles, but the lithium oxide acts as a structural buffer that prevents the nanoparticles from growing too large. The team estimated that the nanoparticles in a tin-oxide anode are only a few atoms in size, as compared to 100 nanometers across in the pure-tin anode. The smaller nanoparticle size and lithium oxide barrier help prevent struc-

tural damage and electrical disconnections. This explains why the tin oxide anode showed better reversibility after multiple charges.

However, the tin oxide anode is not without its own problems. Despite its benefit to structural stability, the lithium oxide envelope has the downside of decreasing the rate of lithium diffusion. This slow diffusion explains why the researchers only recorded 8 lithium neighbors for each tin atom, when the maximum number is 14. Further work with tin-based compounds will hopefully find a compromise that affords a structural stabilizing buffer without impeding lithium ion diffusion.

— Michael Schirber

**See:** Christopher J. Pelliccione<sup>1\*</sup>, Elena V. Timofeeva<sup>2</sup>, and Carlo U. Segre<sup>1\*\*</sup>, "Potential-Resolved *In Situ* X-ray Absorption Spectroscopy Study of Sn and  $\text{SnO}_2$  Nanomaterial Anodes for Lithium-Ion Batteries," *J. Phys. Chem. C* **120**, 5331 (2016).

DOI: 10.1021/acs.jpcc.5b12279

**Author affiliations:** <sup>1</sup>Illinois Institute of Technology, <sup>2</sup>Argonne National Laboratory

**Correspondence:**

\* cpellic1@hawk.iit.edu

\*\* segre@iit.edu

C.J.P. was supported by a U.S. Department of Education GAANN Fellowship, Award No. P200A090137. The project is supported by the U.S. Department of Energy (DOE) Office of Science-Basic Energy Science and the Advanced Research Project Agency-Energy under Award No. AR-000387. Materials Research Collaborative Access Team operations are supported by the U.S. DOE and the Materials Research Collaborative Access Team member institutions. This research used resources of the Advanced Photon Source, a U.S. DOE Office of Science User Facility operated for the DOE Office of Science by Argonne National Laboratory under Contract No. DE-AC02-06CH11357.

10-ID-B • MR-CAT • Materials science, environmental science, chemistry • X-ray absorption fine structure, time-resolved x-ray absorption fine structure, micro x-ray absorption fine structure, microfluorescence (hard x-ray) • 4.3-27 keV, 4.3-32 keV, 15-65 keV • On-site • Accepting general users •

# BUILDING BETTER BATTERIES WITH SELENIUM AND SULFUR

**L**ithium-ion batteries are ubiquitous, powering most smart phones, electric cars, and implantable medical devices. The batteries have their drawbacks though, such as high cost, limited energy storage capacity, and toxicity. To develop better batteries, researchers are looking into selenium (Se)-sulfur (S) batteries, which may someday offer a lower cost, higher energy density alternative to lithium ion batteries. Currently, selenium-based batteries still have a long way to go to match lithium-ion batteries as far as their ability to be charged and discharged over and over without losing their storage capacity. To figure out the capacity fading mechanism of selenium-based batteries over multiple charge/discharge cycles, researchers studied their properties utilizing the high-energy, highly penetrating x-ray beams from the APS. Their insights may help researchers design selenium-based batteries that can be endlessly recharged.

studying an amorphous substrate (Fig.1).

The x-ray absorption data set from the first redox cycle showed a symmetric shape, suggesting that the reaction proceeded reversibly. The Se K-edge XANES spectra for the  $\text{Se}_2\text{S}_5/\text{MPC}$  before charging matched the spectra of selenium powder, while the spectra after the first discharge matched that of  $\text{Li}_2\text{Se}$ , indicating that this product had formed. This finding was confirmed by *ex situ* high-energy x-ray diffraction experiments on this first discharged product, carried out on the XSD 11-ID-C

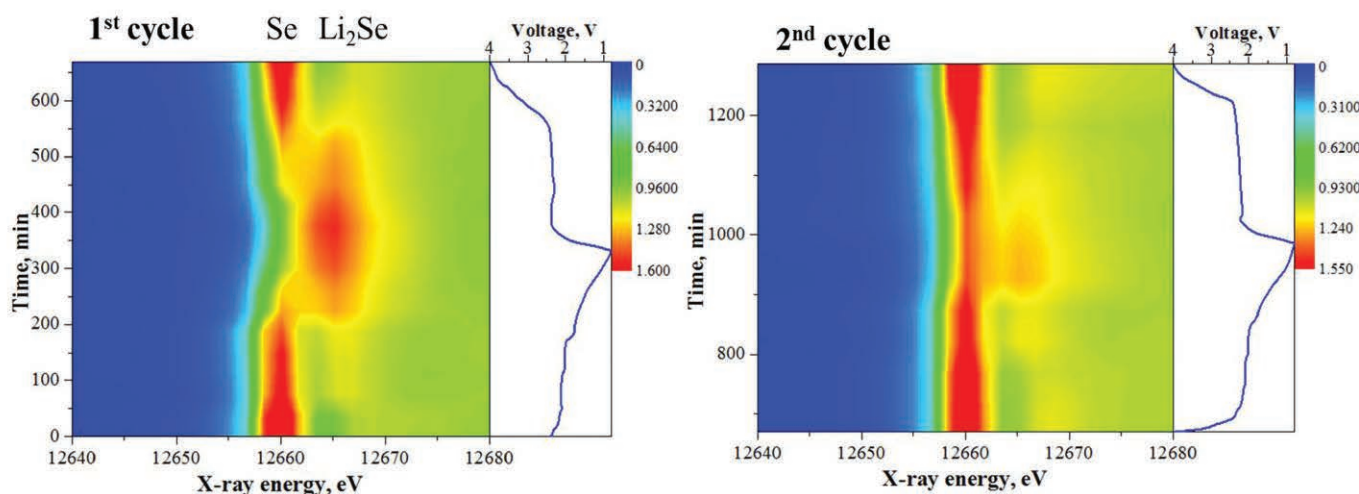


Fig. 1. Two-dimensional contour plots of *in situ* XANES data of  $\text{Se}_2\text{S}_5/\text{MPC}$  cathode at 0.2 C for the first electrochemical cycle (left) versus the second cycle (right), showing a distinctive change and loss of reversibility.

First, the researchers from Argonne National Laboratory, the University of Rochester, the University of Maryland, and Central Michigan University built a selenium/sulfur-based cathode. They embedded amorphous selenium-sulfur  $\text{Se}_2\text{S}_5$  in a micro/mesoporous carbon (MPC) matrix, as earlier work suggested that it was important to constrain the selenium-sulfur compounds to limit the dissolution of lithium polyselenides, leading to a continuous loss of the active material as well as the round trip energy efficiency. The  $\text{Se}_2\text{S}_5/\text{MPC}$  composite was prepared using modified va-

porization condensation, leaving the MPC with a 2-nm pore size to enhance confinement of polyselenides.

To gain insight into the electrochemical behavior of  $\text{Se}_2\text{S}_5/\text{MPC}$  in an ether-based electrolyte, which in prior experiments enhanced the redox reaction, the researchers brought the composite to the XSD 20-BM-B x-ray beamline at the APS. There, they carried out *in situ* x-ray absorption near edge spectroscopy selenium K-edge (XANES) using the transmission mode of the beamline. A cycling device was employed to charge and discharge the cell, using a constant rate of 0.2 C between 0.8 V and 4.0 V. Unlike x-ray crystallography, which relies on a regular crystalline structure, XANES reveals the average chemical environment of the material, regardless of phase, making it ideal for

beamline at the APS. (Small-angle x-ray scattering data were collected at XSD beamline 12-ID-B of the APS to further characterize the material.)

Next, the researchers performed a second cycle, again tracking the selenium spectrum with XANES. The second cycle spectra looked significantly different from that of the first cycle, indicating an incomplete reduction of the Se component to form  $\text{Li}_2\text{Se}$ . Even at the end of the second discharge, the Se K-edge for Se and  $\text{Li}_2\text{Se}$  can both be observed, indicating a decreased (de)lithiation reversibility. The data indicates that, while  $\text{Se}_2\text{S}_5$  remains confined to MPC, the reversibility of the reaction is compromised.

To further evaluate the electrochemical performance of  $\text{Se}_2\text{S}_5/\text{MPC}$ ,  
*"Selenium" cont'd. on page 66*

# GETTING THE MOST OUT OF MULTICRYSTALLINE SILICON

Solar cells are one of a broad range of energy sources that contribute to our nation's energy independence. They are an effective, scalable way to transform an abundant resource—sunlight—into electricity. But solar technologies, also known as photovoltaics, still have significant potential for improvement. For example, the multicrystalline silicon wafers used for photovoltaics are often contaminated with trace amounts of metals that clump together, interfering with the movement of electrons through the silicon crystal and reducing the amount of electricity the solar cell can produce from a given amount of sunlight. Gettering, a process that removes unwanted impurities by encouraging them to move to less disruptive locations, is known to dissolve clusters of metal atoms and move the resulting defects to less detrimental places in *p*-type multicrystalline silicon, the dominant technology in the solar marketplace. Researchers used the APS to show that gettinger works in the same way on *n*-type multicrystalline silicon. *N*-type materials are not commonly used right now, but theory suggests they should be less sensitive to some common trace impurities such as iron. Demonstrating that gettinger is an effective technique to further raise *n*-type microcrystalline silicon efficiencies may help deliver to the market the next generation of cost-effective and high-performing photovoltaic technology.

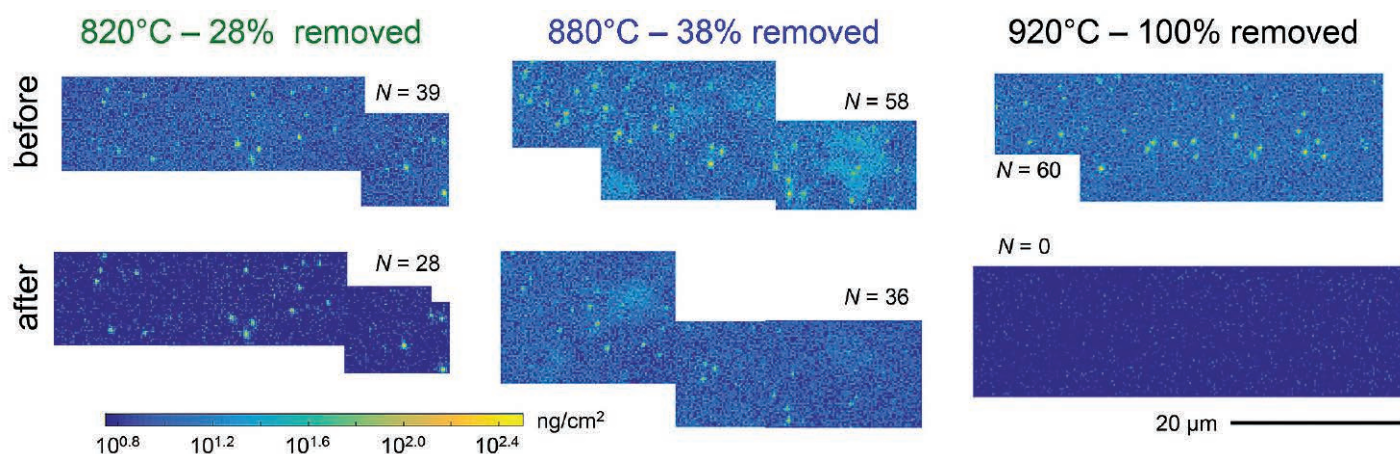


Fig. 1. Micro-XRF maps of iron clusters (yellow dots) in *n*-type microcrystalline silicon before (upper row) and after (lower row) gettinger to 820 (left), 880, or 920 (right) degrees Celsius. As the temperature increases, more iron dissolves, improving electrical efficiency. From A.E. Morishige et al., *Appl. Phys. Lett.* **108**, 202104 (2016). © 2017 AIP Publishing LLC

When sunlight hits a solar cell some of the light is absorbed by electrons in the material. The electrons get excited and abandon their atoms to travel through the solar cell and create an electrical current. The spots abandoned by the electrons are positively charged holes, which can also travel and create a current. Most photovoltaics used today are designed to have more holes than electrons. These

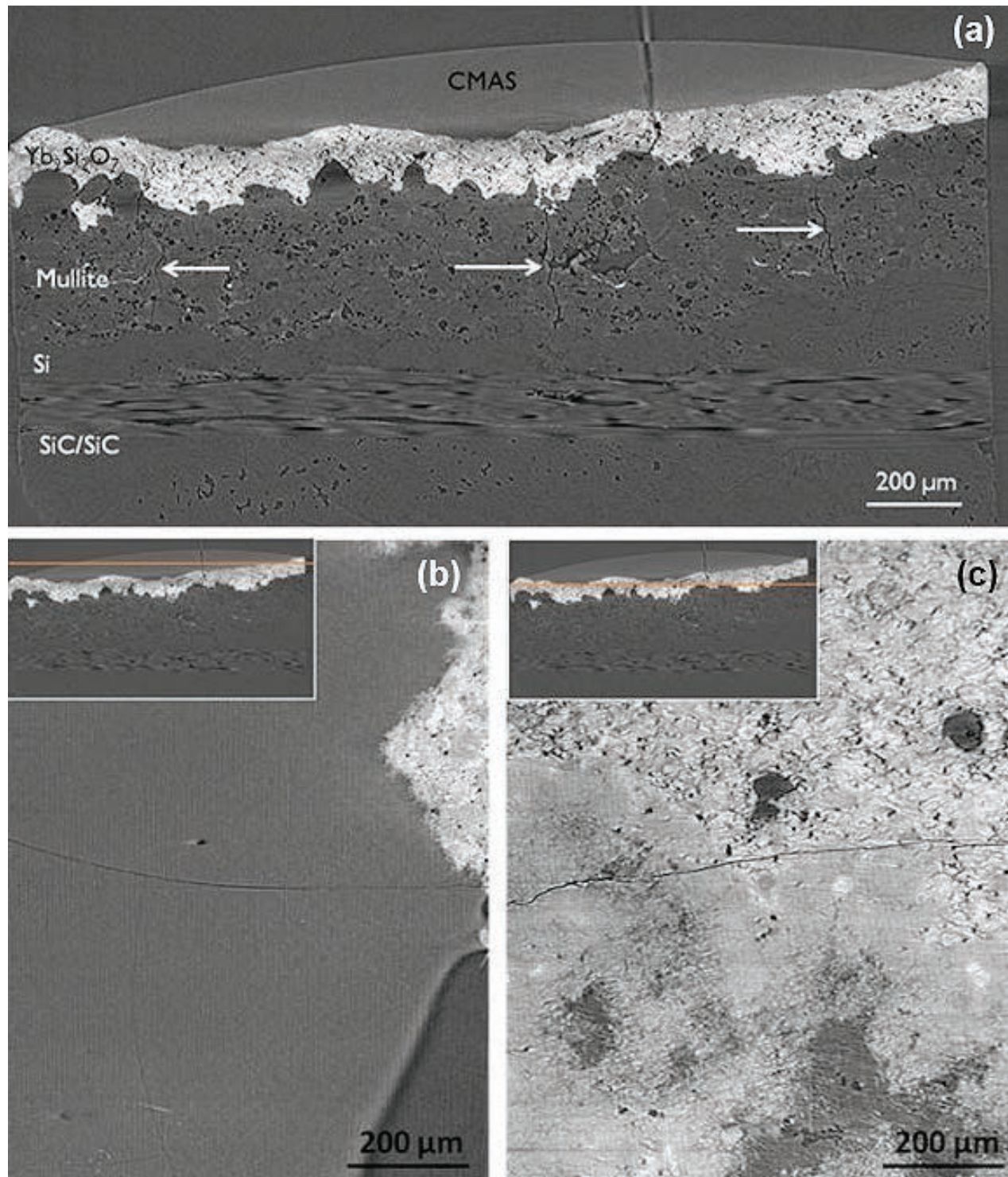
are the *p*-type materials. *N*-type materials, which have more electrons than holes, are less well understood but have the potential to be more efficient.

Researchers at MIT, Supreme, Inc., the University of California, San Diego, and Argonne used the APS to examine how detrimental trace metals are to *n*-type materials during the solar cell manufacturing process. They used micro-x-ray fluorescence spectroscopy

(micro-XRF) to map clumps of iron atoms in samples cut from *n*-type microcrystalline silicon wafers (Fig. 1). They also looked at how large the clumps were both before and after gettinger. In this case, gettinger involved heating the solar cells for 1 hour to 1 of 3 different temperatures, 820, 880, or 920° C. *"Silicon" cont'd. on page 66*



# PUTTING A COAT ON A HOT TURBINE



**G**as turbine engines get really, really hot. A typical gas turbine engine runs more than 10 times hotter than a normal car engine. Gas turbines need to run at these high temperatures though, because whether they're flying planes through the air or generating electricity on the ground, the hotter the engine runs, the more efficient it is. High operating temperatures introduce a unique set of challenges: Metals soften when they get too hot, weakening and deforming engine components; airborne particulate matter gets sucked into engines and melts and sticks to the turbine, causing damage that can lead to engine failure. In an electrical generator, failure can cause brownouts; in a plane, it can cost lives. So materials scientists search relentlessly for coatings that can better withstand the heat and airborne dust. Researchers used the APS to investigate exactly what happens to one of those potential coatings, yttrium disilicate, when in contact with airborne particulates at 1350° C. The structural changes illuminated by the APS were critical to evaluating the quality of the yttrium disilicate coating. While the material prevents damage to the underlying ceramic composite due to water vapor erosion, it would require additional barriers to protect it from particulate matter in turbine engines.

Most commercial gas turbines are currently made out of nickel-based superalloys. But these alloys are running into a wall; temperatures in the most efficient engines are getting high enough to soften even the best of them. The next generation of turbine components will likely be made of ceramic-matrix composites. Ceramics are very hard and heat resistant, but can react with combustion products, like water vapor, as well as molten particulate matter. To protect them, they can be coated with less reactive substances. Yttrium disilicate ( $\text{Yb}_2\text{Si}_2\text{O}_7$ ) is one possible coating. Initial tests showed that it stayed intact and relatively unscathed even in the presence of airborne dust at high temperatures.

< Fig. 1. X-ray computed tomography reconstructed images of a  $\text{Yb}_2\text{Si}_2\text{O}_7$ /mullite/ $\text{Si}/(\text{SiC}/\text{SiC})$  multilayer environmental barrier coating (EBC) after a 1-min heat treatment at 1300° C. (a) Cross-section of the multi-layer EBC sample; cracks in the mullite interlayer are highlighted by white arrows. (b) Reconstructed image parallel to the EBC surface through the calcium-magnesium-aluminosilicates glass. Inset is a cross-section highlighting the approximate y-position of the cut. (c) Reconstructed image parallel to the EBC surface through the  $\text{Yb}_2\text{Si}_2\text{O}_7$  topcoat. Inset is a cross-section highlighting the approximate y-position of the cut.

But scientists from Caltech, Northwestern University, and the Rolls-Royce Corporation wanted to know how yttrium disilicate would behave at the atomic level if exposed to dust during realistic operating conditions. First they took yttrium disilicate and repeatedly heated it to 1350° C and imaged it to establish a baseline. They then took particulate matter, similar to what might be in the air after a volcanic eruption or to sand on the ground, and put it onto the yttrium disilicate at 1350° C (Fig. 1). They then compared what had happened to the heated and particulate-coated yttrium disilicate to any changes on the baseline that had only been heated.

The researchers and colleagues from Argonne used three different techniques at XSD beamline 1-ID-B,C,E at the APS to image and analyze the material at atomic and nanometer scales. The beamline's extremely high x-ray energies allowed the researchers to send x-rays through a 1.5-mm-thick piece of material. There are very few places in the world besides the APS that can do that. Wide-angle scattering data showed how individual atoms were arranged in the yttrium disilicate. This revealed small displacements in the crystal structure, much smaller than the atoms themselves, indicating how the material is strained and where failures are likely to occur.

Small-angle scattering allowed the researchers to see structure at the nanometer scale, such as pores or the beginnings of cracks. And utilizing x-ray tomography, features at the micrometer scale, as small as 2.5- $\mu\text{m}$  wide could be visualized (Fig. 1). Using the three techniques at this single beamline, the researchers were able to examine how particulate material damaged the material, from subtle distortions of the crystal structure to serious cracking.

What the researchers found was that simple heating and cooling put only mild strain on yttrium disilicate. However, adding dust at high temperatures could seriously damage the coating. The particles appeared melted and filled pores in the yttrium disilicate coating, stressing it and producing cracks. The longer the amount of time the coating spent in contact with the molten particles, the worse the damage became. With extensive damage, the protective, but stressed coating can separate from the ceramic composite underneath, which may lead to catastrophic failure. — *Kim Krieger*

**See:** F. Stolzenburg<sup>1†</sup>, P. Kenesei<sup>2</sup>, J. Almer<sup>2</sup>, K.N. Lee<sup>3</sup>, M.T. Johnson<sup>4</sup>, K.T. Faber<sup>1,4\*</sup>, "The influence of calcium magnesium aluminosilicate deposits on internal stresses in  $\text{Yb}_2\text{Si}_2\text{O}_7$  multilayer environmental barrier coatings," *Acta Mater.* **105**, 189 (2016).

DOI: 10.1016/j.actamat.2015.12.016

**Author affiliations:** <sup>1</sup>Northwestern University, <sup>2</sup>Argonne National Laboratory, <sup>3</sup>Rolls-Royce Corporation, <sup>4</sup>California Institute of Technology <sup>†</sup>Present address: 3M

**Correspondence:** \* ktfaber@caltech.edu

A Northwestern University Terminal Year Fellowship provided partial support for F.S. This research used resources of the Advanced Photon Source, a U.S. Department of Energy (DOE) Office of Science User Facility operated for the DOE Office of Science by Argonne National Laboratory under Contract No. DE-AC02-06CH11357.



### *“Selenium” cont’d. from page 62*

the researchers charted the charge/discharge curves over 50 cycles. The initial charge capacity was found to be 1661.2 mA h g<sup>-1</sup>. By the 50th cycle, the discharge capacity was only 345.5 mA h g<sup>-1</sup>. The researchers attribute the poor performance over multiple cycles to the accumulation of highly soluble polyselenides, which can corrode the lithium anode as well as increase internal resistance.

Polyselenide only becomes problematic if it detaches from the carbon matrix, which was the researchers’ next subject of investigation. They performed ab initio calculations to understand how the polyselenide interacts with the carbon surface. They ran the simulation on different polyselenides—Li<sub>2</sub>Se, Li<sub>2</sub>Se<sub>4</sub>, and Li<sub>2</sub>Se<sub>6</sub>—to compare how tightly each species binds to the carbon surface. The longer the polyselenide chained, the more tightly it adhered to the carbon surface. The results suggest that cycling performance could be improved by altering the surface chemistry of the carbon to increase adherence of polyselenides. — *Erika Gebel Berg*

**See:** Gui-Liang Xu<sup>1</sup>, Tianyuan Ma<sup>1</sup>, Cheng-Jun Sun<sup>1</sup>, Chao Luo<sup>3</sup>, Lei Cheng<sup>1</sup>, Yang Ren<sup>1</sup>, Steve M. Heald<sup>1</sup>, Chunsheng Wang<sup>3</sup>, Larry Curtiss<sup>1</sup>, Jianguo Wen<sup>1</sup>, Dean J. Miller<sup>1</sup>, Tao Li<sup>1</sup>, Xiaobing Zuo<sup>1</sup>, Valeri Petkov<sup>4</sup>, Zonghai Chen<sup>1\*</sup>, and Khalil Amine<sup>1\*\*</sup>, “Insight into the Capacity Fading Mechanism of Amorphous Se<sub>2</sub>S<sub>5</sub> Confined in Micro/Mesoporous Carbon Matrix in Ether-Based Electrolytes,” *Nano Lett.* **16**, 2663 (2016).

DOI: 10.1021/acs.nanolett.6b00318

**Author affiliations:** <sup>1</sup>Argonne National Laboratory, <sup>2</sup>University of Rochester, <sup>3</sup>University of Maryland, <sup>4</sup>Central Michigan University

**Correspondence:** \*

zonghai.chen@anl.gov,

\*\*amine@anl.gov

Research at Argonne was funded by U.S. Department of Energy (DOE) Vehicle Technologies Office. Support from Tien Duong of the U.S. DOE’s Office of Vehicle Technologies Program is gratefully acknowledged. This work was partially supported by DOE-Basic Energy Sciences grant DE-SC0006877 (V.P.). APS Sector 20, which is managed by XSD in partnership with the

Canadian Light Source (CLS), is funded by the U.S. DOE Office of Science, and by the Natural Sciences and Engineering Research Council of Canada and the University of Washington via the CLS. This research used resources of the Advanced Photon Source, a U.S. DOE Office of Science User Facility operated for the DOE Office of Science by Argonne National Laboratory under Contract No. DE-AC02-06CH11357.

### *“Silicon” cont’d. from page 63*

X-rays from the XSD 2-ID-D beamline were shone onto the multicrystalline wafers both before and after gettering. The x-rays were energetic enough (10 keV) to excite electrons from the inner orbitals of the iron atom impurities. These electrons jumped out of their orbitals, and other electrons from the outer regions of the atoms fell into the vacated orbital spots. As they fell, the electrons gave off energy as fluorescent light. The spectrum of the fluorescence is characteristic of the energy differences of the orbitals between which the electron jumped. It reveals the type of atom it comes from, in this case transition metals including iron, nickel, cobalt, and copper. The researchers used the 2-ID-D beamline because it had x-rays of the right energies, a long length of focus so they could see into the depth of the wafer, and a smooth “on-the-fly” method of scanning, which made the experiment go much more quickly than typical step-by-step scanning.

The research team found that the lowest gettering temperature dissolved 28% of the clusters of iron impurities, and the 880° C fully dissolved 40% of the iron clusters. The highest temperature, 920° C, dissolved all of the clusters enough to make them undetectable.

The wafer-level results are promising, but more work needs to be done to economically manufacture *n*-type multicrystalline silicon solar cells. Rapid throughput is important in manufacturing, so shorter and lower-temperature processes may be economically favorable, but longer processing can significantly improve wafer performance if done properly. The gettering process is also known to decrease efficiency in *p*-type cells if done for too long or at too hot a temperature. It is unknown to what degree the same effect happens

in *n*-type materials. The researchers believe that manufacturing wafers with different processing times and temperatures and then measuring their efficiency in a full solar cell is an important next step. The only way to do this type of nanoscale-to-macroscale characterization is with synchrotrons such as APS. — *Kim Krieger*

**See:** Ashley E. Morishige<sup>1\*</sup>, Mallory A. Jensen<sup>1</sup>, Jasmin Hofstetter<sup>1</sup>, Patricia X.T. Yen<sup>1</sup>, Chenlei Wang<sup>2</sup>, Barry Lai<sup>3</sup>, David P. Fenning<sup>1,4</sup>, and Tonio Buonassisi<sup>1\*\*</sup>, “Synchrotron-based investigation of transition-metal getterability in *n*-type multicrystalline silicon,” *Appl. Phys. Lett.* **108**, 202104 (2016). DOI: 10.1063/1.4950765

**Author affiliations:** <sup>1</sup>Massachusetts Institute of Technology, <sup>2</sup>Supreme, Inc., <sup>3</sup>Argonne National Laboratory, <sup>4</sup>University of California, San Diego

**Correspondence:**

\* aemorish@alum.mit.edu

\*\* buonassisi@mit.edu

Funding provided by the National Science Foundation (NSF) and the U.S. Department of Energy (DOE) under NSF CA No. EEC-1041895. Portions of this research were carried out at the Center for Nanoscale Systems (CNS), a member of the National Nanotechnology Infrastructure Network, which is supported by NSF Award No. ECS-0335765. CNS is part of Harvard University. A.E.M. acknowledges the Department of Defense through the National Defense Science and Engineering Graduate Fellowship Program. M.A.J. and P.X.T.Y. acknowledge support by the NSF Graduate Research Fellowship under Grant No. 1122374. D.P.F. acknowledges support by the Martin Family Society of Fellows for Sustainability and the University of California, San Diego. This research used resources of the Advanced Photon Source, a U.S. DOE Office of Science User Facility operated for the DOE Office of Science by Argonne National Laboratory under Contract No. DE-AC02-06CH11357.

2-ID-D • XSD • Life sciences, materials science, environmental science, geoscience • Microfluorescence (hard x-ray), microdiffraction, micro x-ray absorption fine structure • 5-30 keV • On-site • Accepting general users



# IMPROVING THE DEVELOPMENT OF NEW MATERIALS FOR NUCLEAR ENERGY

The development and use of new materials have improved safety and affordability in the aerospace and automotive industries. Scientists are working to apply similar principles to the development of new materials for nuclear energy in order to extend reactor lifetimes and increase accident tolerance. Materials utilized within reactors face a variety of challenges, including the critical ability to withstand high radiation at high temperatures. A team of university and U.S. national laboratory researchers working at the APS and other DOE facilities at Argonne developed and demonstrated preliminary results for a new technique for evaluating fuel and reactor materials. This technique, which requires less time and expense than current techniques, involves irradiating potential materials with high-energy, atomic nucleus ions and then assessing the damage using synchrotron x-ray diffraction and electron microscopy.

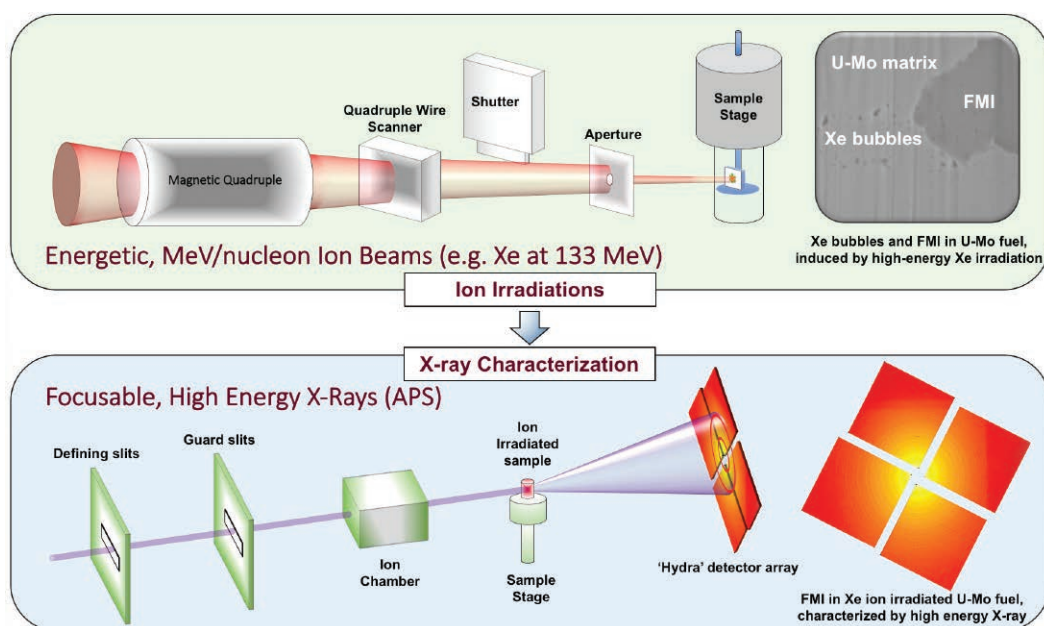


Fig. 1. The experimental setup for both steps of the new process to emulate and analyze the destructive effects occurring within nuclear reactors: on top, the nucleon ion beam that irradiates the sample and, below, the x-ray beam which characterizes the damage.

Unlike alternative energy sources such as wind and solar, nuclear energy is neither intermittent nor variable. To provide this consistent energy, nuclear reactors are utilized to power turbine generators with the heat produced by the nuclear reactions of the fuel. But the structural materials of the reactor and the fuel itself must be able to withstand the high-temperature and high-pressure environment that occurs during the radioactive decay or nuclear reaction of the fuel. Historically, testing new materials involves low irradiation dose rates over a long time and requires expensive precautions post-irradiation to handle the radioactive materials. To avoid these difficulties, the team from Argonne and Northwestern University pro-

posed a two-step technique. Figure 1 shows a cartoon diagram of the equipment used for irradiation and characterization, as well as a picture of an irradiated fuel sample. The irradiation was performed at Argonne's ATLAS accelerator to simulate damage from high-energy fission fragment ions, replicating the effects of years of reactor exposure in a matter of days at ATLAS.

The team assessed two types of materials with this technique. The first was two variants of uranium-molybdenum fuel: U-7Mo, which is 7% molybdenum by weight, and U-10Mo, which is 10% molybdenum by weight. Other researchers have investigated these fuels because they were developed to con-

*"Nuclear" cont'd. on page 69*

1-ID-B,C,E • XSD • Materials science, physics, chemistry • High-energy x-ray diffraction, tomography, small-angle x-ray scattering, fluorescence spectroscopy, pair distribution function, phase contrast imaging • 41-136 keV, 45-116 keV • On-site • Accepting general users •

34-ID-E • XSD • Materials science, physics, environmental science, geoscience • Microdiffraction, Laue crystallography, microbeam, microfluorescence (hard x-ray) • 7-30 keV • On-site • Accepting general users •

# THE WAY MAGNESIUM ALLOY STRESSES

**M**agnesium alloys are strong and light, but difficult to forge and shape at room temperature for use as structural components. To understand better how the lattice structure of these materials responds to deformation, researchers conducted real-time x-ray imaging and diffraction of samples of a commercial magnesium alloy. As in previous, non-x-ray work, they found significantly different responses when the alloy was stressed parallel or perpendicular to the extrusion axis, but the x-ray data collected at the APS enabled them to understand the lattice behavior responsible for the differences. These findings should help device designers make better use of such alloys.

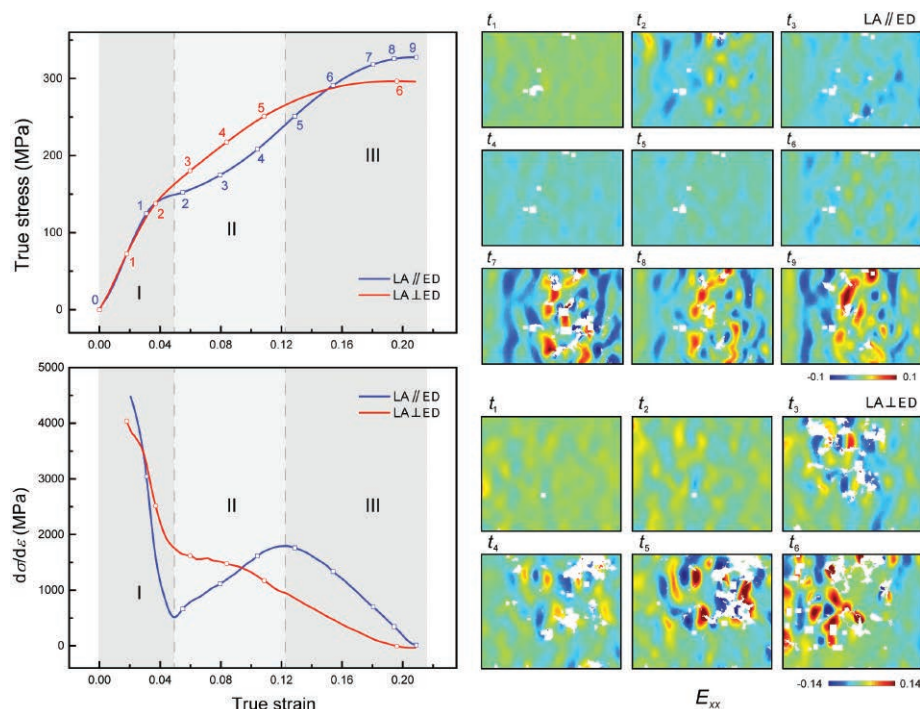


Fig.1. Left: Stress-strain curves (top) and strain-hardening rates (bottom) for magnesium alloy AZ31 under parallel (blue) and perpendicular (red) loading. Right: Strain fields in the normal direction inferred from phase-contrast x-ray imaging at the times marked on the stress-strain curves.

The widely used alloy AZ31 consists of magnesium with 3.1% aluminum, 0.9% zinc, and 0.4% manganese. Like pure magnesium, it has a hexagonal close-packed structure, and the extrusion method by which it is made causes most grains within the metal to have their c-axes perpendicular to the direction of extrusion. Previous research has established that the strain-hardening rate and other properties of AZ31 are anisotropic, the likely explanation being that dislocation motion and twinning behave differently depending on the direction of strain with respect to the lattice orientation. However, most studies of these effects have

involved analysis of samples only after they were subjected to strain.

A team of researchers from the University of Science and Technology of China, Southwest Jiaotong University, the Peac Institute of Multiscale Sciences in Chengdu, and Argonne National Laboratory performed a combination of diagnostic methods to understand the anisotropic deformation of AZ31 in real time. They cut small slabs, measuring 2.6 x 2.0 x 1.0 mm, from a large block of the alloy, with the longest direction parallel to the extrusion axis. The team built a miniature device to record the stress-strain response of these slabs as they were put

under increasing loads, either parallel or perpendicular to the extrusion axis, in the XSD beamline 32-ID-B. As the tests proceeded, they recorded phase-contrast imaging data and diffraction measurements.

As in earlier studies, the researchers found a three-regime stress-strain curve that differed between the parallel and perpendicular loading directions. In both cases, the strain-hardening rate (the slope of the stress-strain) curve, started out high and fell until the strain reached a value of about 0.04. For parallel loading, the strain-hardening rate then rose through the second regime, reached a maximum, then fell as the curve passed into the third regime. Under perpendicular loading, by contrast, the strain-hardening rate fell throughout the experiment, but with a sharp change of slope going from regime I to regime II.

X-ray imaging of the samples revealed changes in their grain structure as loading increased, from which the researchers inferred the changing strain field (Fig. 1). Under perpendicular stress, an initial elastic response was followed by continuous growth of local deformation, which steadily accumulated until the sample fractured. Under parallel stress, plastic deformation was seen in regime I of the response, but in regime II the strain field was seen to reorganize and become homogeneous, so that local concentrations of deformation eased. Localized deformation began to pile up again in regime III.

The diffraction gave insight into the lattice changes corresponding to the different deformation responses in the two stress direction. Samples under parallel loading showed clear indication of twinning in regime II, and the researchers found that once twin formation began, it establishes a front that moved quickly through a sample. The team also conducted experiments in which they stopped loading at a certain point and performed “post-mortem” electron backscatter diffraction studies, which confirmed the existence of twins.

Samples subjected to perpendicular loading, on the other hand, >>

<< showed very little evidence of twinning under stress.

The researchers conclude that the response to stress in AZ31 is controlled by a competition between twinning and the formation and motion of dislocations. Under parallel loading, twinning is the dominant process in regime II, and by allowing reorientation of the lattice serves to homogenize accumulated strain. This has the effect of increasing the strain-hardening rate, since it minimizes further changes to the alloy's structure as stress rises. In the case of perpendicular loading, twinning is much less common. The movement of dislocations, and their tendency to pile up at certain locations, makes the material more plastic and this decreases the strain-hardening rate. In regime III, dislocation motion dominates for both stress orientations, and the samples soften to the point of fracture.

Whether a high strain-hardening rate is good or bad depends on the use to which a material is being put. By explaining the lattice characteristics that define AZ31's macroscopic response, the new research should help engineers optimize their use of this alloy.

— David Lindley

**See:** L. Lu<sup>1,2,3</sup>, J.W. Huang<sup>3</sup>, D. Fan<sup>3</sup>, B.X. Bie<sup>3</sup>, T. Sun<sup>4</sup>, K. Fezzaa<sup>4</sup>, X.L. Gong<sup>1\*</sup>, and S.N. Luo<sup>2,3\*\*</sup>, "Anisotropic deformation of extruded magnesium alloy AZ31 under uniaxial compression: A study with simultaneous *in situ* synchrotron x-ray imaging and diffraction," *Acta Mater.* **120**, 86 (2016).

DOI: 10.1016/j.actamat.2016.08.029

**Author affiliations:** <sup>1</sup>University of Science and Technology of China, <sup>2</sup>Southwest Jiaotong University, <sup>3</sup>The Peac Institute of Multiscale Sciences, <sup>4</sup>Argonne National Laboratory

**Correspondence:**

\* gongxl@ustc.edu.cn

\*\* sluo@pims.ac.cn

This work was sponsored in part by the 973 project (No. 2014CB845904), and NSFC (No. 11472227) of China. This research used resources of the Advanced Photon Source, a U.S. Department of Energy (DOE) Office of Science User Facility operated for the DOE Office of Science by Argonne National Laboratory under Contract No. DE-AC02-06CH11357.

*"Nuclear" cont'd. from page 67*

vert high-performance research reactors to the use of low-enriched uranium, so these materials are of high interest to the research reactors community. The second material was HT9, a ferritic-martensitic steel to be used as fuel cladding material in advanced reactors. The U-7Mo was irradiated at ATLAS with 84-MeV Xe<sup>26+</sup> ions and the U-10Mo was irradiated with 105-MeV Xe<sup>26+</sup> ions. The HT9 samples were irradiated with 84-MeV Fe<sup>26+</sup> ions.

To assess the materials' response to the radiation, the samples were cut to reveal a cross section of the damage. Then the team used high-energy x-ray diffraction on the X-ray Science Division (XSD) 1-ID-B,C,E beamline and microbeam Laue diffraction at the XSD 34-ID-E beamline—both at the APS—to assess the damage. The APS and ATLAS are DOE Office of Science user facilities.

They found lattice strain to a depth of approximately 6  $\mu\text{m}$  in the U-10M fuel sample. Assessing the damage to a sample of U-7Mo fuel utilizing scanning electron microscopy and transmission electron microscopy at Northwestern and at the Argonne IVEM-Tandem Facility, a DOE Office of Nuclear Energy facility, the team also found build-up from the interaction between the fuel and its holding matrix, which is similar to what is found due to irradiation in a reactor and limits the performance of this type of fuel.

The team obtained only preliminary results for the HT9. Based on the synchrotron x-ray diffraction data, peak ion damage occurred approximately 4  $\mu\text{m}$  beneath the sample's surface. However, transmission electron microscopy results indicate the damage may have penetrated deeper. The lack of significant grain growth in the irradiated area indicates damage is mainly a function of an increase in crystallographic irregularities within the sample (an increase in dislocation density).

The team's results allow them to conclude that irradiation by energetic ions coupled with synchrotron x-ray diffraction analysis is indeed a useful technique for assessing the damage incurred by nuclear fuels and structural materials, and should be used during the future development of new reactor

materials. This new technique allows for spatially resolving the damage to reactor-related materials through use of an analogue for the conditions in the reactor environment, and should expedite the research and testing cycle of new materials for nuclear energy.

Additionally, this work provides the technical basis for the XMAT (eXtreme MATerials) beamline for the proposed Advanced Photon Source Upgrade. This beamline is aimed at developing new and more capable radiation tolerant materials for nuclear environments.

— Mary Alexandra Agner

**See:** M.J. Pellin<sup>1\*</sup>, Abdellatif M. Yacout<sup>1</sup>, Kun Mo<sup>1</sup>, Jonathan Almer<sup>1</sup>, S. Bhat-tacharya<sup>1,2</sup>, Walid Mohamed<sup>1</sup>, D. Seidman<sup>2</sup>, Bei Ye<sup>1</sup>, D. Yun<sup>1</sup>, Ruqing Xu<sup>1</sup>, and Shaofei Zhu<sup>1</sup>, "MeV per nucleon ion irradiation of nuclear materials with high energy synchrotron X-ray characterization," *J. Nucl. Mat.* **471**, 266 (2016).

DOI: 10.1016/j.jnucmat.2016.01.004

**Author affiliations:** <sup>1</sup>Argonne National Laboratory, <sup>2</sup>Northwestern University

**Correspondence:** \* Pellin@anl.gov

This work was supported in part by the U.S. Department of Energy (DOE) Office of Science-Basic Energy Sciences under Contract No. DE-AC02-06CH11357. This research used resources of the Argonne ATLAS facility, which is a DOE Office of Science User Facility, and the Argonne-Tandem Facility, a DOE Facility funded by the DOE Office of Nuclear Energy, operated under Contract No. DE-AC02-06CH11357 by UChicago Argonne, LLC. This work was supported by the U.S. DOE Office of Global Threat Reduction (NA-21), National Nuclear Security Administration, under Contract No. DE-AC-02-06CH11357 between UChicago Argonne, LLC, and the DOE and Argonne strategic Laboratory Directed Research and Development program. This work made use of the EPIC facility (NUANCE Center- Northwestern University), which has received support from the MRSEC program (NSF DMR-1121262) at the Materials Research Center; the Nanoscale Science and Engineering Center (NSF EEC-0647560) at the International Institute for Nanotechnology; and the State of Illinois, through the International Institute for Nanotechnology. This research used resources of the Advanced Photon Source, a U.S. DOE Office of Science User Facility operated for the DOE Office of Science by Argonne National Laboratory under Contract No. DE-AC02-06CH11357



# DESIGNING MORE-DURABLE MATERIALS WITH A 3-D-PRINTED TITANIUM ALLOY

Additive manufacturing (AM), commonly known as three-dimensional (3-D) printing, has shown great potential for use in biomedical and aerospace industries to produce custom designed parts. One titanium alloy, Ti-6Al-4V, used in additive manufacturing has attracted interest for its tensile properties but exhibits unreliable fatigue properties. Researchers propose that the alloy's poor durability comes from the material's porosity. Now, using synchrotron x-ray microtomography (XCT) at the APS, a team of scientists has been able to examine this feature with excellent resolution. Their findings reveal new details about how the gas pores form and may help manufacturers improve the materials' wear by adjusting their production processes.

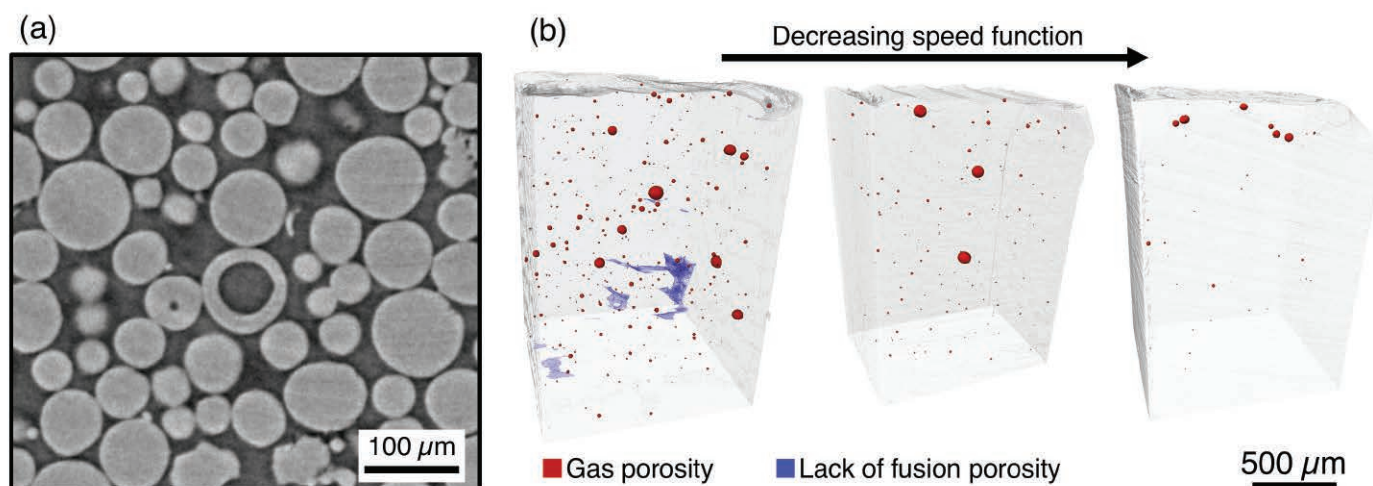


Fig. 1. (a) Reconstructed tomography slice showing large (50-μm diameter) internal porosity within the Ti-6Al-4V powder used to make the samples. (b) 3-D tomographic reconstructions displaying the effect of reducing speed function on the resulting porosity in the samples. Lower speed functions reduced both lack of fusion and gas porosity in the bulk but showed a concentration of gas porosity at the top surface at sufficiently low values.

Commercial 3-D printing technologies using computer-generated models to make materials layer by layer have become increasingly reliable over the last decade, but the products are still subject to occasional flaws and defects.

One such flaw is low fatigue resistance, or the ability to withstand repeated stress, which has been associated with the presence of gas pores in the material. Manufacturers have ad-

dressed this issue by applying a hot isostatic press treatment to the part, but this adds an extra step and has been known to decrease material strength, so materials engineers are interested in finding ways to reduce the formation of pores during manufacture.

In this work, researchers from Carnegie Mellon University investigated an additive manufacturing system called electron-beam melting, in which an electron beam selectively melts specific areas of an alloy powder bed and welds each successive layer together in a vacuum environment. Ti-6Al-4V is a popular material used for this method because of its strength, but suffers from variable fatigue properties due to the pores within the material.

Generally, pores may form be-

tween insufficiently melted layers or from the atomization process used to generate the alloy powder. While previous studies lacked the sensitivity to distinguish the type of porosity, the researchers were able to focus on the latter type, known as trapped gas pores, using XCT.

A total of 1500 radiographs were taken as a tiny sample rotated 180° and were then processed to generate a 3-D model of the material's structure. The method allowed the researchers to measure features within the material to a resolution of 1.5 μm. These experiments were performed at the XSD 2-BM-A,B beamline at the APS.

The team performed the x-ray microtomography experiments on five tita-

*"Titanium" cont'd. on page 72*

# SEEKING A LESS-EXPENSIVE, SAFER MEANS OF TRAPPING NOBLE GASES

Separating and trapping the noble gases xenon (Xe) and krypton (Kr) is of significant industrial and environmental interest. The common method for removing xenon and krypton from the air or recovering the gases from nuclear fuel involves cooling entire gas streams to a temperature close to that of liquid nitrogen. Such cryogenic separation is energy intensive and expensive. In an attempt to develop a less-expensive, more efficient alternative, an international group of researchers working at the APS explored separating Xe and Kr with a recently characterized class of porous materials called hybrid ultra-microporous materials (HUMs). The scientists focused their efforts on two specific HUMs, called CROFOUR-1-Ni and CROFOUR-2-Ni. The researchers discovered that these porous nets offer unprecedented selectivity towards Xe. Computer modeling indicates that the selectivity of these nets is tuned by synergy between the size of their pores and the strong electrostatic forces afforded by  $\text{CrO}_4^{2-}$  anions within the HUMs.

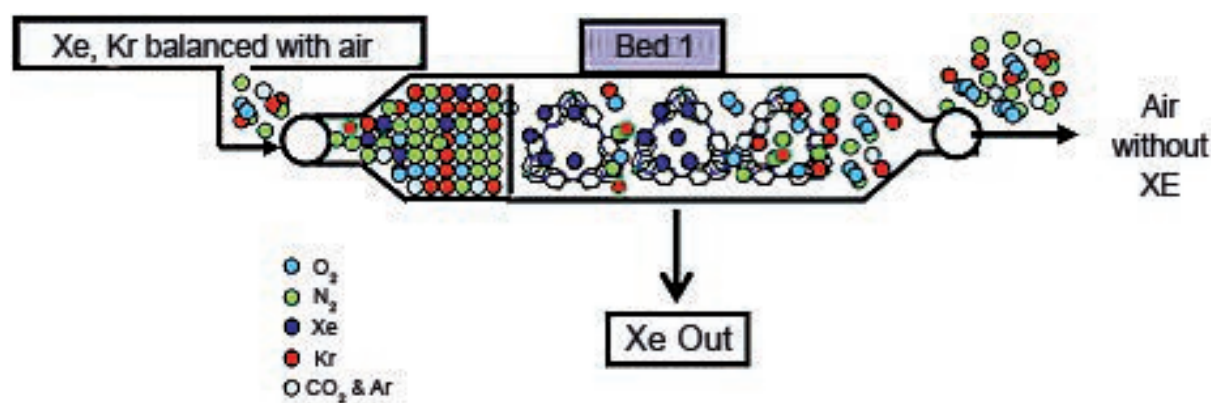


Fig 1. Column packed with hybrid ultra-microporous materials (HUMs) used for the selective removal of xenon from air. As air passes through the column, xenon (blue dots) gets trapped in the micropores of the HUM material, while the other species continue through to the other end.

17-BM-B • XSD • Chemistry, materials science  
• Powder diffraction, high-pressure diamond anvil cell • 27-51 keV • On-site • Accepting general users •

Xenon (Xe) and krypton (Kr) separation and adsorption—or binding—is of interest because these gases present either commercial value or an environmental threat. Xenon (Xe) gas is valuable owing to its application in commercial lighting, medical imaging and anesthesia. Also, radioactive Kr and Xe can be introduced to the atmosphere during the recycling of nuclear fuels such as uranium and plutonium. While radioactive isotopes of Xe quickly decay to very low concentrations, radioactive Kr has a half-life of more than 10 years and therefore must be captured and removed to prevent its uncontrolled release into the atmosphere. Currently, these gases are sequestered using a laborious process called cryogenic distillation, which requires the

temperature of whole streams of gas to be brought far below the point that water freezes.

A recent economic analysis of Xe/Kr separation by an international group of researchers from Pacific Northwest National Laboratory, Alexandria University (Egypt), the University of South Florida, Argonne, and the University of Limerick (Ireland) suggested that materials called metal-organic frameworks (MOF) can efficiently separate the gases at room temperature and could be more cost effective than cryogenic distillation in the context of nuclear fuel reprocessing plants. MOFs are customizable net-like materials with pores inside that are so small that often only a single molecule can fit inside.

*"Noble" cont'd. on page 72*

### *“Titanium” cont’d. from page 70*

nium alloy samples that were made with varying melt pool areas, which relates to the speed function of the system and can be compared to the manufacturers’ suggested settings. The researchers found that, on average, the trapped gas pores were less than 10  $\mu\text{m}$  in diameter and spherical in shape, which suggests that the gas was caught during solidification. Since the process is performed under a vacuum atmosphere, the gas is presumed to come from the metal alloy source. The pores were less prevalent as the manufacture speed function was decreased. Also, as the melt pool area was decreased below standard settings, the lack-of-fusion porosity (porosity caused by insufficient overlap of melt pools) increased dramatically.

The team also found that larger pores were concentrated at the surface of the increased melt pool area samples. The researchers suggest that remelting the material with each additional layer allows the gas to escape and explains the remaining pores at the surface.

Overall, these results show that reducing the speed function in electron beam melting can greatly reduce trapped gas porosity in the material. However, large pores gathered at the surface still represent a challenge to fatigue strength, so the team plans to further explore the other manufacturing parameters and their effect on the material’s properties. — *Tien Nguyen*

**See:** Ross Cunningham\*, Sneha P. Narra, Tugce Ozturk, Jack Beuth, and A.D. Rollett, “Evaluating the Effect of Processing Parameters on Porosity in Electron Beam Melted Ti-6Al-4V via Synchrotron X-ray Microtomography,” *JOM* **68**(3), 765 (2016).

DOI: 10.1007/s11837-015-1802-0

**Author affiliation:** Carnegie Mellon University

**Correspondence:**

\* rwcunnin@andrew.cmu.edu

The authors acknowledge America Makes for providing funding for this research under the project entitled “A Database Relating Powder Properties to Process Outcomes for Direct Metal AM,” Award Number FA8650-12-2-7230, and the National Science Foun-

dation for providing funding under Grant CMMI-1335298. They would also like to thank Xianghui Xiao and the rest of the 2-BM beamline staff at the APS for assisting in the acquisition of the synchrotron tomography data. This research used resources of the Advanced Photon Source, a U.S. Department of Energy (DOE) Office of Science User Facility operated for the DOE Office of Science by Argonne National Laboratory under Contract No. DE-AC02-06CH11357.

### *“Noble” cont’d. from page 71*

When one gas species has a higher affinity for the pore walls than other gas species, MOFs separate gaseous mixtures by selectively adsorbing that particular gas.

A new subclass of MOFs called hybrid ultra-microporous materials (HUMs) has demonstrated unparalleled ability to capture molecular species, such as  $\text{CO}_2$ , thanks to a combination of tunable pore size and strong electrostatic forces afforded by the material’s inorganic  $\text{CrO}_4^{2-}$  anions. The researchers performed column breakthrough experiments at room temperature to investigate the capacity of two HUM networks, CROFOUR-1-Ni and a new variant called CROFOUR-2-Ni, to separate and adsorb Xe. In these experiments, a mixture of gases is move down a column filled with either CROFOUR-1-Ni or CROFOUR-2-Ni, which selectively capture Xe (Fig. 1). The remaining gases, including Kr, Ar,  $\text{O}_2$ ,  $\text{N}_2$ , and  $\text{CO}_2$ , pass through the column and are measured at the other end by a mass spectrometer in real time. The team found that CROFOUR-1-Ni and CROFOUR-2-Ni had higher adsorption levels and greater Xe/Kr selectivity than a wide variety of existing porous materials including other MOFs and activated carbon.

The scientists then used x-ray power diffraction experiments, carried out at the XSD 17-BM-B beamline of the APS, to identify the binding sites of Xe and Kr adsorption in both HUMs. For these experiments, x-rays were directed at HUMs that had captured Xe or Kr. The patterns with which the x-rays bounced off the HUMs indicated exactly where Xe or Kr were bound. For both Xe and Kr, the binding site was located in the cage containing three  $\text{CrOCrO}_4^{2-}$

ions in proximity to each other. These measurements were in agreement with the group’s molecular simulations. Knowing the binding site can potentially help the researchers design even more effective adsorptive materials in the future.

In future experiments, the researchers plan to focus on systematic evaluation of the effect of pore size and functionality on the Xe/Kr adsorption performance of other microporous nets with the hope of discovering materials that can purify Xe even more efficiently and further drive down the cost of separating and adsorbing this gas industrially and environmentally relevant gas.

— *Chris Palmer*

**See:** Mona H. Mohamed<sup>1,2</sup>, Sameh K. Elsaidi<sup>1,2</sup>, Tony Pham<sup>3</sup>, Katherine A. Forrest<sup>3</sup>, Herbert T. Schaefer<sup>1</sup>, Adam Hogan<sup>3</sup>, Lukasz Wojtas<sup>3</sup>, Wenqian Xu<sup>4</sup>, Brian Space<sup>3</sup>, Michael J. Zaworotko<sup>5</sup>, and Praveen K. Thallapally<sup>1\*</sup>, “Hybrid Ultra-Microporous Materials for Selective Xenon Adsorption and Separation,” *Angew. Chem. Int. Ed.* **55**, 8285 (2016). DOI: 10.1002/anie.201602287

**Author affiliations:** <sup>1</sup>Pacific Northwest National Laboratory, <sup>2</sup>Alexandria University, <sup>3</sup>University of South Florida, <sup>4</sup>Argonne National Laboratory, <sup>5</sup>University of Limerick

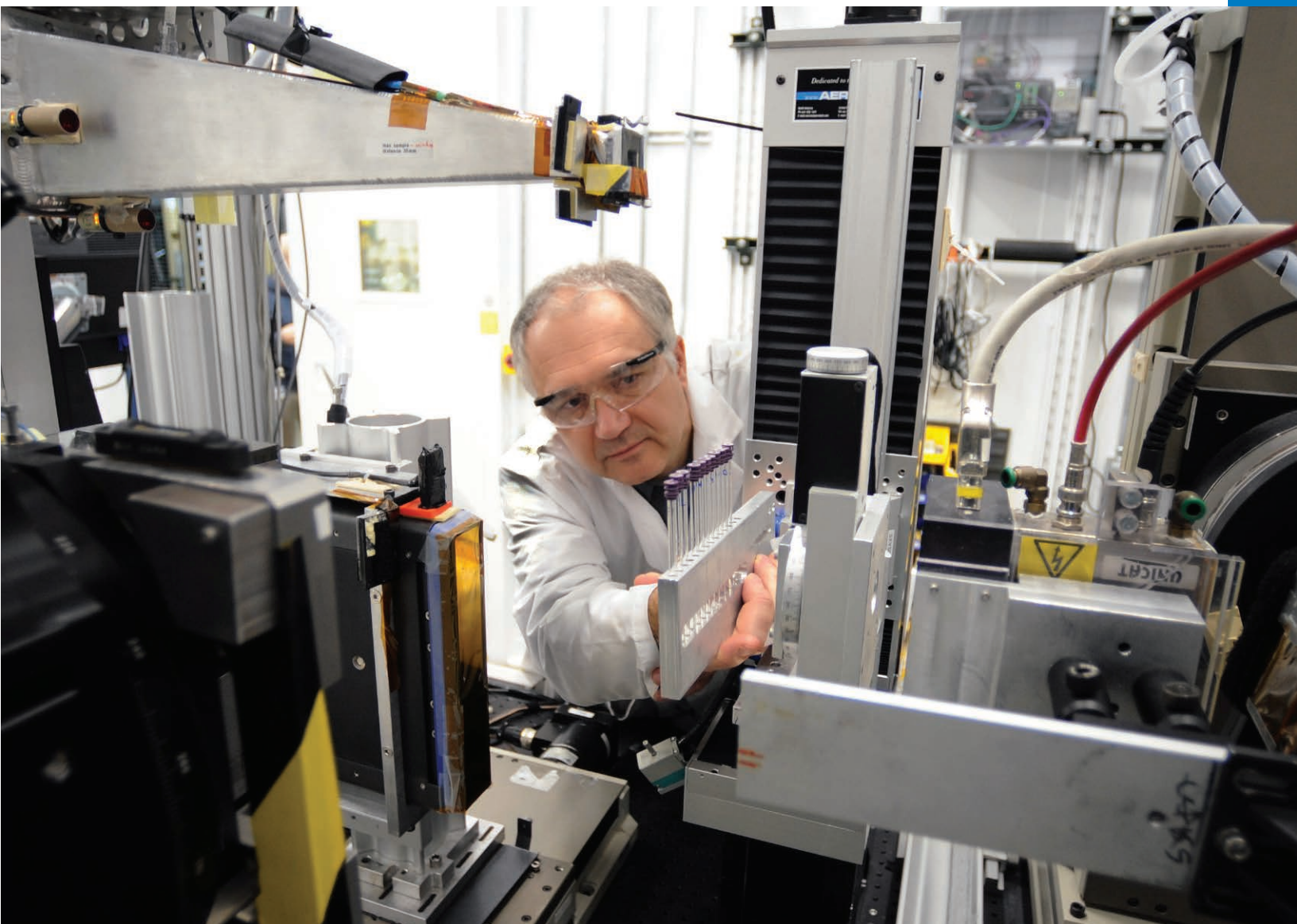
**Correspondence:**

\* praveen.thallapally@pnnl.gov

B.S. acknowledges the National Science Foundation (Award No. CHE-1152362), including support from the Major Research Instrumentation Program (Award No CHE-1531590), the computational resources that were made available by a XSEDE Grant (No. TG-DMR090028), and the use of the services provided by Research Computing at the University of South Florida. We (P.K.T) thank the U.S. Department of Energy (DOE) Office of Nuclear Energy for adsorption and breakthrough measurements. Pacific Northwest National Laboratory is a multi-program national laboratory operated for the U.S. DOE by Battelle Memorial Institute under Contract DE-AC05-76RL01830. M.J.Z. gratefully acknowledges Science Foundation Ireland (Award 13/RP/B2549) for support. This research used resources of the Advanced Photon Source, a U.S. DOE Office of Science User Facility operated for the DOE Office of Science by Argonne National Laboratory under Contract No. DE-AC02-06CH11357.



# SOFT MATERIALS & LIQUIDS



Argonne physicist and APS beamline scientist Jan Ilavsky of the XSD Chemical & Materials Science Group mounting a sample holder in the ultra-small-angle x-ray scattering (USAXS) instrument at XSD beamline 9-ID-C. The USAXS instrument can determine the size or structure of a sample's components across multiple length scales from angstroms ( $10^{-10}$  m) to about  $20\text{ }\mu\text{m}$  ( $10^{-6}$  m).



# IMAGING DRUG DISTRIBUTION FROM METERED-DOSE INHALERS

**M**any patients suffering from respiratory problems such as asthma experience quick and effective relief by inhaling medication present in a mist or spray. The most popular type of device for delivering a measured amount of aerosolized medication is the metered-dose inhaler (MDI). Although MDIs are compact, inexpensive, and generally effective for delivering inhaled medications, many patients receive less than the optimum drug dose. In order to improve device performance, optical imaging and other techniques have been used to characterize how the spray is distributed. However, these traditional techniques provide only limited information about medication dispersion within the quickly-evolving spray plume, and cannot directly visualize the concentration of the drug. Now these limitations have been overcome by subjecting MDI sprays to x-ray fluorescence spectroscopy (XFS), carried out at the XSD 7-BM-B beamline of the APS. In a series of experiments, the changing distribution of bromine (an element found in some common inhaler drugs) within MDI sprays was determined with millisecond precision. The team behind this research expects their experimental findings will lead to improvements in the drug-delivery performance of metered-dose inhalers.

Drug delivery from MDIs to the lungs can vary widely, from 40% to 10% of the medication present in each spray. Two factors are chiefly responsible for patients receiving low drug doses: incorrect operation of the device, and less-than-optimum performance of the MDI device itself. Device performance is directly related to how the drug is distributed within the spray; for instance, drug concentration may be higher in one region of the spray plume than another, potentially impeding drug delivery to the lungs. Understanding how the medication is precipitated, concentrated, and distributed within MDI

sprays is therefore essential to improving their performance.

Many techniques have been employed to characterize MDI sprays. High-speed optical imaging methods, e.g., Schlieren photography and shadowgraphs, measure the expansion of the spray plume and its rapidly-changing density variations. However, these methods cannot differentiate the medication from the spray's propellant. Although other diagnostic tools (e.g., particle filtration, various laser techniques) can determine medication distribution within the spray plume, their effectiveness is limited to areas far

downstream of the nozzle where the spray becomes diluted. In contrast, the dynamic phenomena of most interest, such as precipitation of medication from the vapor plume, occur largely in the "near-field" region extending from just inside the nozzle out to the first few millimeters.

Fortunately, synchrotron-based XFS is well suited for probing the near-field spray region. By causing the drug to fluoresce, its distribution and concentration throughout the evolving spray plume can be mapped with very high spatial (5  $\mu\text{m}$ ) and time (1 ms) resolutions. Moreover, XFS can measure the drug's concentration within the multitude of droplets that suddenly appear and grow throughout the spray.

Figure 1 depicts the basic experimental layout at 7-BM-B utilized by researchers from Argonne, Monash University (Australia), the University of Sydney (Australia), and Chiesi Limited (UK). The spray apparatus was constructed to mimic the spray from a real-world inhaler, including incorporating an actual MDI nozzle. The pressurized spray was composed of ipratropium bromide (the active drug) dissolved in ethanol and mixed with a standard hydrofluoroalkane (HFA) propellant. At spray initiation, focused synchrotron x-rays (the red line in Fig. 1) ejected the innermost (K level) electrons within the bromine atoms. Higher-level (L and M) electrons that replaced the missing core electrons caused the bromine



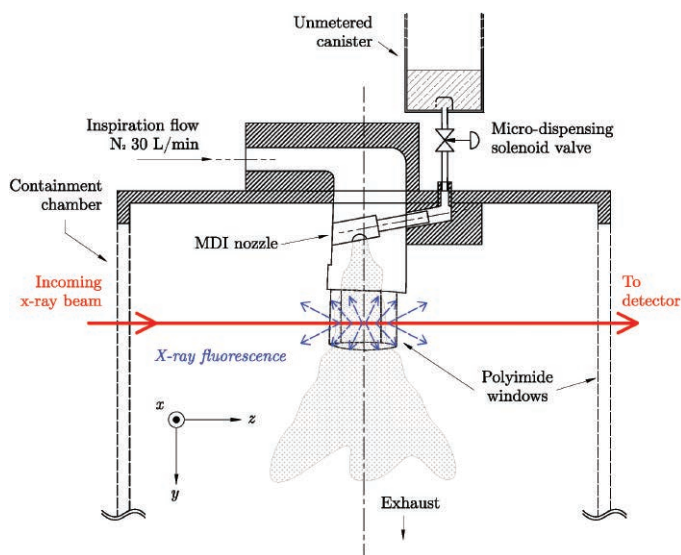


Fig. 1. Side view of the experimental spray chamber. The setup is designed to simulate key parameters of an actual inhaler, including use of a genuine MDI nozzle and a transparent polyimide 'mouthpiece' that mimics a genuine mouthpiece. The spray is controlled by a solenoid valve, while nitrogen ( $N_2$ ) flow simulates patient inhalation. The x-ray beam (red line) causes the ipratropium bromide in the spray to fluoresce, emitting x-rays represented by the blue lines.

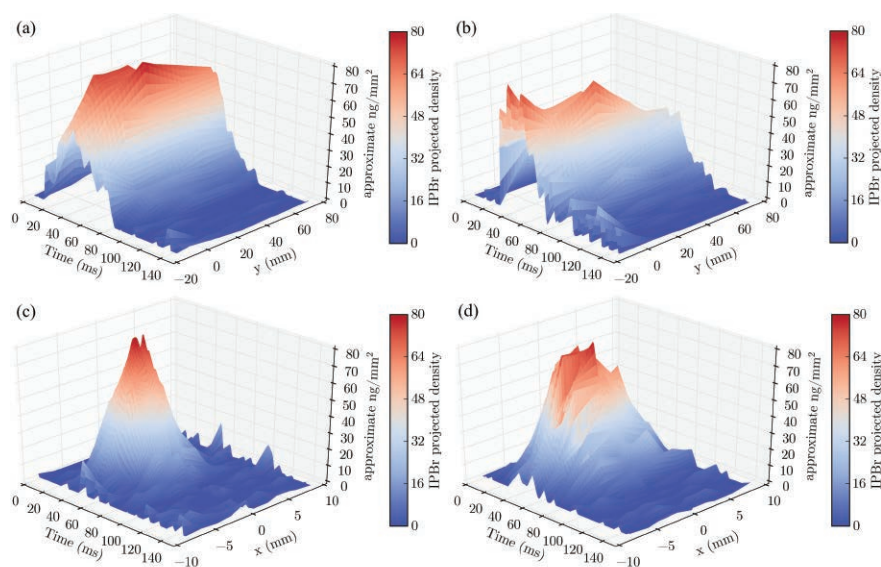


Fig. 2. Panels (a) and (b) show bromine concentrations measured along the centerline of the mouthpiece (dashed vertical line in Fig. 1). Vertical axes indicate drug concentration in nanograms (ng) per square millimeter. Both panels show that within 140 ms, the drug concentration rises sharply and peaks, then quickly dissipates. Note the difference in drug distribution with axial distance from the nozzle ( $y$ ) depending upon which propellant is used. Panels (c) and (d) are based on the same propellant (HFA-134a) and show how drug concentration falls away rapidly from the centerline of the mouthpiece in the transverse direction ( $x$ ). The effect is very pronounced close to the mouthpiece (5 mm), but less so further away (25 mm).

atoms to emit characteristic x-rays. By measuring the emitted x-ray fluorescence, bromine distribution and concentration were determined. The energy of the x-rays selected for the experiment (15 keV) is capable of exciting bromine, while the emitted fluorescence is only weakly absorbed by the spray's ethanol and propellant components.

Bromine concentration and distribution is depicted in the three-axis graphs of Fig. 2. Panels 2(a) and (b) show how bromine concentrations changed with distance using two different propellants (HFA-134a and HFA-227). Panels 2(c) and (d) reveal that drug concentration was highest around the centerline of the mouthpiece.

While bromine appears in many common inhaler medications, other inhaler drugs contain elements that also fluoresce for properly-tuned x-rays. Besides examining additional inhalant drugs, future experiments will measure how variations in nozzle design affect drug profiles in the critical near-field spray region. Moreover, combining XFS with laser excitation will aid in the measurement of drug precipitation and vaporization rates.

The ultimate aim of these experiments is improving MDI design to increase the fraction of medication consistently delivered to the lungs. — Philip Koth

**See:** Daniel J. Duke<sup>1\*</sup>, Alan L. Kastengren<sup>1</sup>, Nicholas Mason-Smith<sup>2</sup>, Yang Chen<sup>3</sup>, Paul M. Young<sup>3</sup>, Daniela Traini<sup>3</sup>, David Lewis<sup>4</sup>, Daniel Edgington-Mitchell<sup>2</sup>, and Damon Honnery<sup>3</sup>, "Temporally and Spatially Resolved x-ray Fluorescence Measurements of in-situ Drug Concentration in Metered-Dose Inhaler Sprays," *Pharm. Res.* **33**, 816 (2016).

DOI 10.1007/s11095-015-1828-6

**Author affiliations:** <sup>1</sup>Argonne National Laboratory, <sup>2</sup>Monash University, <sup>3</sup>University of Sydney, <sup>4</sup>Chiesi Limited

**Correspondence:** \* dduke@anl.gov

This research was supported by the Australian Research Council. This research used resources of the Advanced Photon Source, a U.S. Department of Energy (DOE) Office of Science User Facility operated for the DOE Office of Science by Argonne National Laboratory under contract no. DE-AC02-06CH11357.

Inhaler photo: [wikimedia.org/wiki/File:Metered-dose\\_Inhaler.JPG](https://commons.wikimedia.org/wiki/File:Metered-dose_Inhaler.JPG)

7-BM-B • XSD • Physics • Radiography, tomography, microfluorescence (hard x-ray) • 1-150 keV, 6-15 keV, 25-55 keV • On-site • Accepting general users •



# LOOKING AT THE LAG IN ROOM-TEMPERATURE IONIC LIQUIDS

Finding better energy storage technologies is a national priority that has led researchers to exotic substances such as room-temperature ionic liquids (RTILs). Such liquids consist of two molecules that have a positive and negative charge (as in table salt), but are unusual in that they remain liquid at room temperature. They have the potential to make excellent energy-dense batteries and supercapacitors, but their behavior at charged electrodes remains mysterious. For example, room-temperature ionic liquids are known to organize into separate layers of positive and negative charge where they touch a charged electrode, and these layers flip when the electrode's potential changes from positive to negative or vice-versa. But the layers take a mysteriously long time to do so — up to 10 sec — an extremely long time for a molecular process. This lag leads to hysteresis, which means that the structure of the liquid's surface at a certain electrical potential depends on how it got there; whether it started at a higher or lower potential as well as where it ended up. Researchers are using the APS to get a better look at what happens on the molecular level in room-temperature ionic liquids to make their lag last so long. A better understanding of the phenomena could lead to more efficient, low-hysteresis designer liquids and superior energy storage devices.

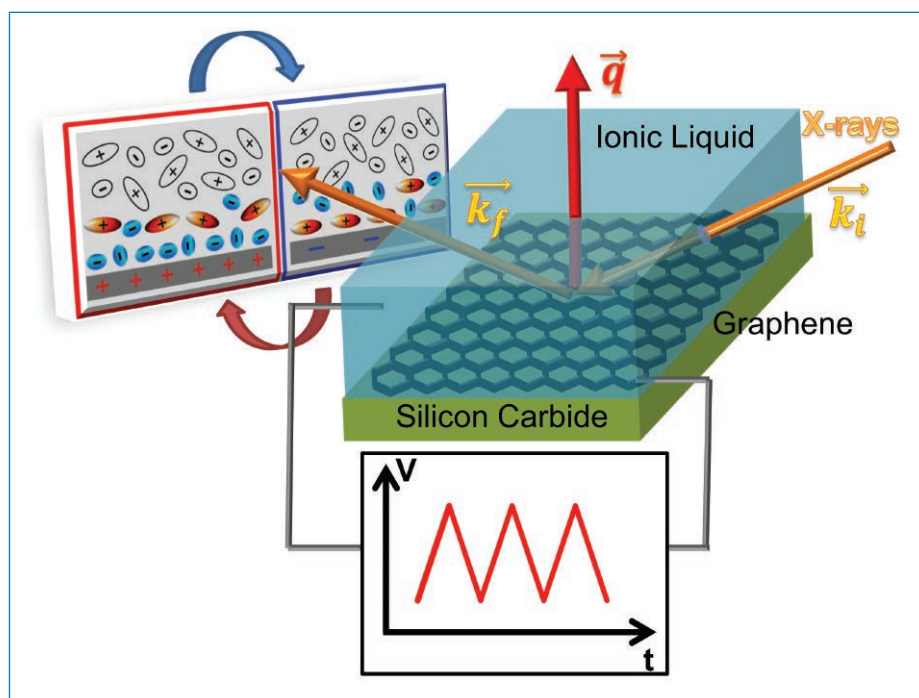


Fig.1. X-rays reflect off the interface between a room-temperature ionic liquid and a graphene electrode, revealing a layer of anions adsorbed onto the electrode. The layer flips charge when the electrode flips potential. Adapted from A. Uysal et al., *J. Phys. Condens. Matter* **27** 032101 (2015).

© 2015 IOP Publishing Ltd. All Rights Reserved

Room-temperature ionic liquids have been known about for a long time, but they weren't practical until the year 2000, when researchers discovered ones that were stable in air. Because every molecule in an RTIL can carry charge, such liquids could make energy storage devices that are much more energy dense than current technologies, in which most of the available space is taken up by the solvent the charge carriers flow through. Researchers have experimented with several different RTILs and electrode types and they always see the same thing. At the interface where the RTIL touches an electrode, the RTIL separates into layers of ions, with each layer either mostly positively or mostly negatively charged (Fig. 1). If the electrode has a positive potential, the RTIL will create a layer of mostly anions right against the electrode, with occasional patches of cations coexisting. If the potential of the electrode is then switched to negative, the ions will switch positions, with the ions adsorbed against the electrode gradually becoming mostly cations over a period of seconds.

Researchers from Vanderbilt University, Oak Ridge National Laboratory, Drexel University, and Argonne used the APS to get a more detailed understanding of how those layers of ions switch when the electrode potential changes. They used the XSD 6-ID-B,C,D, 12-ID-C,D, and 33-ID-D,E beamlines at the APS that use the high flux of high-energy x-ray photons to penetrate the RTIL and observe the evolution of the RTIL's layered structure under electrochemical control and in real-time.

The researchers used a graphene electrode because it is thin and flexible and shows promise for many different applications. They had the graphene touch the surface of the RTIL 1-methyl-3-nonylimidazolium bis-(trifluoromethanesulfonyl)imide.

The measurements taken at the  
*"Ionic" cont'd. on page 79*

# GROWING INORGANIC CRYSTALS ON ORGANIC SELF-ASSEMBLED MONOLAYERS

The ability to control crystal growth at interfaces is important to many significant processes including the scientific and technological development of thin films and sophisticated ferroelectric, semiconductor, and superconducting devices. Many of these applications rely on the formation of inorganic “heterostructures” in which inorganic crystals grow epitaxially on a crystalline inorganic substrate: the crystalline overlayer grows with a unique orientation on the underlying substrate. It is also known that inorganic crystals can grow epitaxially on soft/deformable organic substrates. This plays a major role in many biomineralization processes, such as those where organisms generate structures like shells and bones. However, much less is known about the mechanisms underlying this process. Researchers using high-brightness x-rays from the APS have now addressed this question by employing Bragg coherent diffraction imaging (BCDI) to analyze the epitaxial growth of calcite ( $\text{CaCO}_3$ ) crystals on organic self-assembled monolayers (SAMs). Their conclusions provide interesting (and in one case unexpected) insights into how organic SAMs control the growth of inorganic calcite crystals, which further enhances the advance of thin-film technologies.

Oriented  $\text{CaCO}_3$  crystals were precipitated on 11-mercaptopundecanoic acid SAMs on gold/silicon, and samples were isolated and analyzed at different times during crystal growth. Using a coherent x-ray beam from the XSD 34-ID-C beamline and BCDI, the researchers produced simultaneous images of the development of both the morphologies and the strain within the crystals over time. A series of two-dimensional x-ray diffraction patterns, collected around a selected Bragg reflection, were used to generate a three-dimensional pattern. After the application of a series of phase retrieval algorithms, these three-dimensional patterns allowed the researchers to detect small changes in the crystalline lattice of the imaged crystals. Figure 1 describes various experimental results during the development of dislocation loops as calcite crystals grow on SAMs.

The team's study yielded some surprising results and generated a new understanding of the mechanisms by which organic monolayers control the growth of and defect structures in inorganic crystals. They showed that although an organic monolayer is traditionally considered “soft” it can bring about a deformation within the lattice of the crystal. The lattice deformation lies primarily at the edges and corners of each crystal, while strain becomes increasingly concentrated at the corners as the crystal grows.

*“Monolayers” cont'd. on page 79*

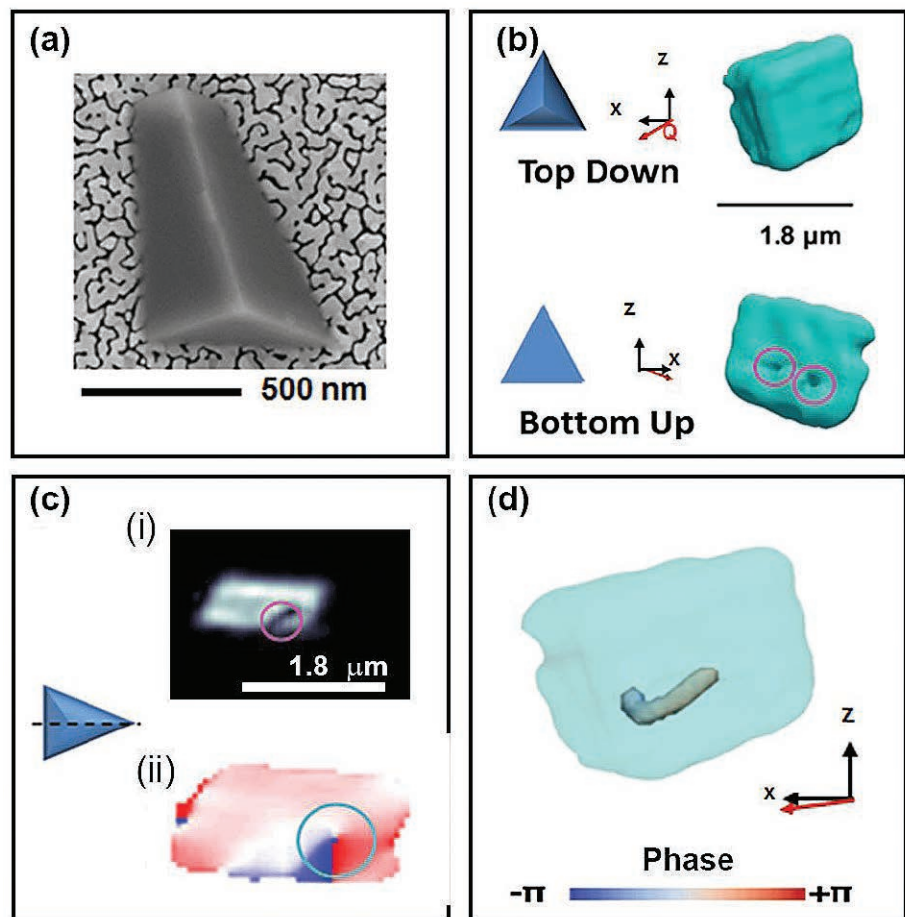


Fig. 1. Images describe: (a) morphological development of a calcite crystal on an organic SAM using a scanning electron microscope. (b) a reconstructed crystal shape nucleated on an organic SAM from BCDI amplitude measurements, as viewed from the indicated directions (blue triangles), with surface cusps circled on the base and Q the scattering vector. (c) (i) a section through an electron density map and (ii) a section cut through a displacement map, as made through the crystal's center, normal to the substrate. (d) a defect of a crystal with a low-density core surrounded by a spiral deformation field/phase, whose features identify a dislocation loop.

# TWO FOR ONE: SIMULTANEOUS X-RAY MEASUREMENTS OF DISSOLVED GAS AND CAVITATION BUBBLES

Understanding the dynamics of dissolved gases in fluids is essential to many scientific and engineering endeavors. Where large pressure changes exist, cavitation can also occur. Both phenomena cause bubbles to form in fluids, but the two are difficult to distinguish from one another when scientifically measured. This is particularly important when trying to understand the extent that a dissolved gas diffuses into cavitation bubbles in turbulent flows such as those found in high-pressure nozzles. In this study, researchers applied x-ray fluorescence (XRF) to determine both the density of a liquid flow and the concentration of noncondensable gas. Their experiment was performed at the APS with a submerged cylindrical nozzle under cavitating conditions. With complimentary results obtained earlier from other diagnostic techniques, their results further the understanding of gas diffusion into cavitation bubbles. Information gleaned from this study will improve methods of design and manufacture to reduce cavitation erosion, which causes extensive damage to machinery such as control valves, propellers, and pumps.

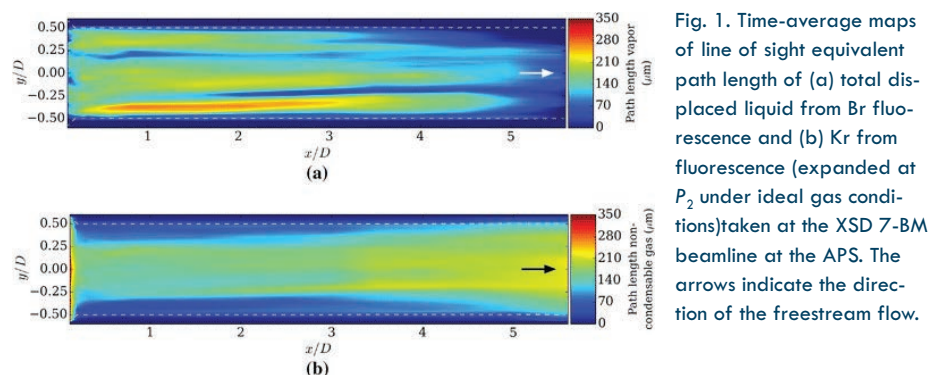


Fig. 1. Time-average maps of line of sight equivalent path length of (a) total displaced liquid from Br fluorescence and (b) Kr from fluorescence (expanded at  $P_2$  under ideal gas conditions) taken at the XSD 7-BM beamline at the APS. The arrows indicate the direction of the freestream flow.

At the center of their experiment is the study of the dynamics of dissolved gas (any gas that dissolves into another solute) and cavitation (the formation of vapor cavities in a fluid when subjected to tension, typically due to low pressure). The experimenters used a cylindrical test nozzle, with dimensions of 0.5-mm diameter and 3.05-mm length, manufactured from a thermoplastic polymer called polyether ether ketone (PEEK). The exit portion of the nozzle was submerged in liquid during the experiment, while maintained at a constant pressure.

The fluid used in the experiment, a gasoline surrogate, was doped with 400 ppm of a bromine (Br) additive called tetrabromomethane ( $\text{CBr}_4$ ; also known as carbon tetrabromide). The dissolved air in the fluid was removed by de-

gassing and replaced with krypton (Kr) gas. The procedure involved evacuating a storage tank, moving the contents into a piston accumulator, and pumping it through a brass orifice to assure the removal of excess air. The degassed fluid was then vacuum-stored for several hours. Krypton gas was bubbled through the fluid until an equilibrium pressure was reached.

Conducting the experiment at the XSD 7-BM-B beamline, the researchers from Argonne focused a 15-keV monochromatic x-ray beam using Kirkpatrick-Baez mirror optics. The beam simultaneously excited fluorescent emission from the Br and Kr components within the fluid. The emission from the K edges of Br and Kr were recorded using a silicon drift diode detector. The incoming beam intensity was normalized

using a diamond transmission photodiode. Total displacement of the liquid was measured from Br fluorescence, while the mass fraction of both the dissolved and nucleated gas was measured from Kr fluorescence (Fig. 1).

The team corrected for systematic errors in measurements due to reabsorption, intensity calibration, and detector dead-time. Various experimental uncertainties were also taken into account. Specifically, the researchers found uncertainties of 2.4% and 3.6% associated with projected densities of the liquid (Br) and gas (Kr) phases before reabsorption correction, and 4.3% and 6.4% after iterative reabsorption correction, respectively. The Kr/Br mass ratio was measured with an uncertainty of 8.3%. These analytic measurements were validated with independent diagnostic techniques, such as x-ray radiography.

Based on their experiments, the researchers concluded that many of the voids found exiting the nozzle are due not only to cavitation vapor. Instead, they discovered that these voids were also partially filled with nucleated gas. Ultimately, the expansion of dissolved gas into the voids formed by cavitation act to stabilize the bubbles and prevent them collapsing.

The information collected from this experiment will help in the many fields relevant to the fluid-flow dynamics of dissolved gas and cavitation. For instance, hydraulic oil can be adversely affected by the precipitation of gas bubbles, as can the presence of gas bubbles within nozzles used in high-pressure, direct fuel-injection systems found within internal combustion engines. In such cases, quantitative measurements, like the ones produced in this study with XRF, can help to minimize such serious problems.

— William Arthur Atkins

See: Daniel J. Duke\*, Alan L. Kastengren, Andrew B. Swantek, >>



<< Katarzyna E. Matusik, and Christopher F. Powell, "X-ray fluorescence measurements of dissolved gas and cavitation," *Exp. Fluids* **57**, 162 (2016). DOI 10.1007/s00348-016-2250-5  
*Author affiliation:* Argonne National Laboratory †Present address: Monash U.  
*Correspondence:*

\* daniel.duke@monash.edu

Argonne's fuel injection research is sponsored by the U.S. Department of Energy (DOE) Vehicle Technologies Program under the direction of Gurpreet Singh and Leo Breton. This research used resources of the Advanced Photon Source, a U.S. DOE Office of Science User Facility operated for the DOE Office of Science by Argonne National Laboratory under Contract No. DE-AC02-06CH11357.

#### *"Ionic" cont'd. from page 76*

APS suggest the RTIL's layered structure has two stable states—one when the electrode's potential is positive, the other when the electrode potential is negative. The results suggest that these two stable states are separated by an energy barrier, which has a size of approximately 0.15 eV. This energy barrier is sufficiently large that it takes time (and energy) for the ions to cross over it, leading to the observed hysteresis. The team also noted intermediate states — mixed patches of anion and cations— while the potential applied to the graphene surface changed. The team members from Vanderbilt created a computer model that successfully reproduced those intermediate states, confirming that the researchers understood mathematically what is going on.

The next step will be to figure out what is happening in various RTILs. Specifically, the researchers want to know how the physical structure of the molecules in the RTIL contributes to the hysteresis. If the researchers can understand that, they can design RTILs with molecular properties that cause as little hysteresis as possible.

— Kim Krieger

*See:* Ahmet Uysal<sup>1\*</sup>, Hua Zhou<sup>1</sup>, Guang Feng<sup>2\*\*</sup>, Sang Soo Lee<sup>1</sup>, Song Li<sup>2</sup>, Peter T. Cummings<sup>2</sup>, Pasquale F. Fulvio<sup>3†</sup>, Sheng Dai<sup>3</sup>, John K. McDonough<sup>4</sup>, Yury Gogotsi<sup>4</sup>, and Paul Fenter<sup>1\*\*\*</sup>, "Interfacial ionic 'liquids': connecting static and dynamic struc-

tures," *J. Phys. Condens. Matter* **27** 032101 (2015).

DOI: 10.1088/0953-8984/27/3/032101

*Author affiliations:* <sup>1</sup>Argonne National Laboratory, <sup>2</sup>Vanderbilt University, <sup>3</sup>Oak Ridge National Laboratory, <sup>4</sup>Drexel University †Present address: University of Puerto Rico

*Correspondence:* \* ahmet@anl.gov  
\*\* gfeng@hust.edu.cn  
\*\*\* pfenter@anl.gov

This work was supported as part of the Fluid Interface Reactions, Structures and Transport Center, an Energy Frontier Research Center funded by the U.S. Department of Energy (DOE) Office of Science-Basic Energy Sciences. This research used resources of the Advanced Photon Source, a U.S. DOE Office of Science User Facility operated for the U.S. DOE Office of Science by Argonne National Laboratory under Contract No. DE-AC02-06CH11357.

#### *"Monolayers" cont'd. from page 77*

The researchers from the University of Leeds (UK), SLAC National Accelerator Laboratory, DESY (Germany), University College London (UK), and Argonne also observed a most unexpected result. Each crystal contained a single dislocation loop that occupied exactly the same position within all of the sample crystals. The loop forms to relieve the stress field present at the crystal/substrate interface, where this strain increases as the crystal's volume increases. When stored elastic energy exceeds the energy needed to make a dislocation loop, then a dislocation grows to relieve the stress.

This dislocation loop has a different geometry from the "misfit dislocations" frequently observed in epitaxial inorganic heterostructures. In "classic" misfit dislocations, the apex of the loop is located at the interfaces between the substrate and overlayer. It has edge character parallel to the interface, which reduces the strain that occurs in the crystal overlayer because of the differences in lattice structure between the substrate and overgrowth crystal.

The dislocation loop formed in the studied organic/inorganic heterostructure system must therefore form by a different mechanism. The team contends that the loop arises from two effects: internal stress due to interfacial defects and the nanoscale roughness

of the substrate, where the nanoscale roughness of the substrate is the dominant factor.

This research provides new information about the factors that govern crystallization on organic substrates. It contributes important knowledge about stress relaxation and dislocation formation during epitaxial crystal growth, and demonstrates that the roughness of the substrate—whether organic or inorganic—should be considered when controlling defects and interfacial strain during epitaxial crystal growth.

— William Arthur Atkins

*See:* Johannes Ihli<sup>1†\*</sup>, Jesse N. Clark<sup>2,3</sup>, Alexander S. Côté<sup>4††</sup>, Yi-Yeoun Kim<sup>1</sup>, Anna S. Schenk<sup>1</sup>, Alexander N. Kulak<sup>1</sup>, Timothy P. Comyn<sup>1</sup>, Oliver Chammas<sup>1</sup>, Ross J. Harder<sup>5</sup>, Dorothy M. Duffy<sup>4</sup>, Ian K. Robinson<sup>4\*\*\*</sup>, and Fiona C. Meldrum<sup>1\*\*\*</sup>, "Strain-relief by single dislocation loops in calcite crystals grown on self-assembled monolayers," *Nat. Commun.* **7**, 11878 (15 June 2016). DOI: 10.1038/ncomms11878

*Author affiliations:* <sup>1</sup>University of Leeds, <sup>2</sup>SLAC National Accelerator Laboratory, <sup>3</sup>Deutsches Elektronensynchrotron (DESY), <sup>4</sup>University College London, <sup>5</sup>Argonne National Laboratory Present addresses: †Paul Scherrer Institute, ††University College London

*Correspondence:*

\* johannes.ihli@psi.ch

\*\* i.robinson@ucl.ac.uk

\*\*\* F.Meldrum@leeds.ac.uk

This work was supported by FP7-advanced grant from the European Research Council (J.N.C. and I.K.R.), by an Engineering and Physical Sciences Research Council Leadership Fellowship (F.C.M., J.I. and Y.Y.K.; EP/H005374/1) and EPSRC grant EP/K006304/1 (A.N.K.). F.C.M., A.S.S., D.M.D. and A.S.C. are also supported by an EPSRC Programme Grant (grant EP/I001514/1) that funds the Materials Interface with Biology (MIB) consortium. Beamline 34-ID-C was built with funds from the U.S. National Science Foundation under Grant DMR-9724294. This research used resources of the Advanced Light Source, a U.S. Department of Energy (DOE) Office of Science User Facility, under contract no. DE-AC02-05CH11231, and the Advanced Photon Source, a U.S. DOE Office of Science User Facility operated for the U.S. DOE Office of Science by Argonne under Contract No. DE-AC02-06CH11357.

# MEASURING THE MICROSTRUCTURE OF NATURAL GUMS

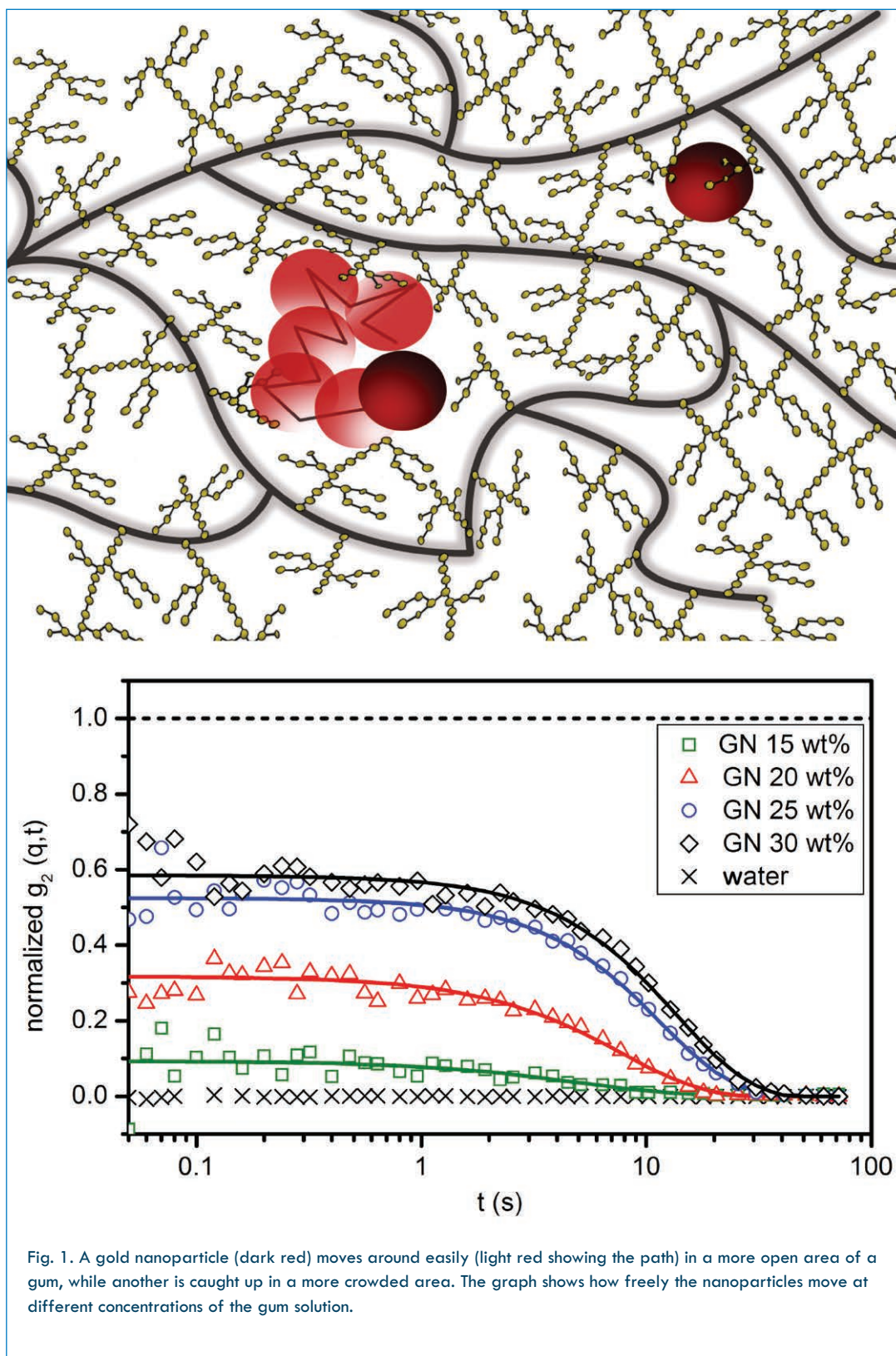


Fig. 1. A gold nanoparticle (dark red) moves around easily (light red showing the path) in a more open area of a gum, while another is caught up in a more crowded area. The graph shows how freely the nanoparticles move at different concentrations of the gum solution.

**A**ccacia gum is widely used in foods, pharmaceuticals, cosmetics, and inks as a stabilizer or thickening agent. Usually the gum, a natural polymer, is derived from two main species of acacia trees, *A. senegal* and *A. seyal*, but there are roughly 1200 species of acacia. People who harvest the trees commercially would like to know how the gums from different species, which have different chemical variations, compare, so they can predict their material properties and their usefulness in different applications. Now scientists working at the APS have shown they can use x-rays to characterize the structural properties of the gum and relate those to how the material behaves. Measurements of these and other gums may help commercial users of the material decide which type is best for a given application. Meanwhile, these researchers say their results demonstrate that x-ray photon correlation spectroscopy (XPCS) is a viable method for studying the structure and dynamics of natural polymers.

The researchers from Argonne, Universidade Federal do Paraná (Brazil), Instituto de Pesquisa Pelé Pequeno Príncipe (Brazil), and Johns Hopkins University studied gum derived from *A. mearnsii*, harvested from trees grown for tannin extraction in Brazil. The gum from that tree was known to have better emulsifying properties and different viscosities from the commercially available gum. The gum has three main components: the biopolymer arabinogalactan, an arabinogalactan-protein complex, and glycoprotein. Understanding the arrangement of these components and the spacing among them gives a hint to the macroscale rheological properties of the gum—how it stretches, recoils, or flows as forces are applied in a certain direction.

X-rays provide the nanometer-scale resolution necessary to measure the structure, but the gum, consisting mainly of carbon and nitrogen, does not scatter x-rays well, so investigators could not see the structure directly. To overcome this problem, they synthesized gold nanoparticles and mixed those into the polymer. By seeing how the nanoparticles moved, they could get an idea of how the average spacing in the gum structure changed as the gum concentration was varied.

The researchers first measured the macroscopic behavior of the gum, and used that to predict how much space would be available at the nanoscale to let the nanoparticles move freely. They then made x-ray measurements of both the commercial and the Brazilian gum, which turned out to agree with their predictions. Increasing the ratio of gum to

water in the solution thickens the gum and reduces nanoparticle movement, a result that is more evident in the Brazilian gum, suggesting the components are becoming more entangled and leaving less space (Fig. 1). That matches the behavior at the macroscale, in which the Brazilian gum becomes more viscous more quickly. Overall, the shear viscosity—a measure of how resistant a substance is to flow—is about 1000 times lower in the commercial gums than in the Brazilian gum.

To understand how the nanoparticles fit with the gum's molecules, researchers needed to know their size distribution. They performed small-angle x-ray scattering on the nanoparticle solution at the XSD 12-ID-C,D beamline to determine that the average nanoparticle diameter was  $4.8 \pm 0.8$  nm. That beamline has a large-area detector that can record the scattering from a wide range of nanoparticle sizes. The measurements were consistent with TEM images taken at the Argonne Center for Nanoscale Materials, which showed the gold nanoparticle's average diameter was  $5.0 \pm 1.2$  nm.

To characterize the gums, they performed XPCS at the XSD 8-ID-I beamline. That beamline uses a coherent x-ray beam sensitive to the arrangement of the particles and how that varies over time, allowing researchers to watch how the particles move. The instrument can look at changing speckled interference patterns from the material that are sensitive to motion at the nanoscale, providing the resolution necessary for the experiment. — *Neil Savage*

**See:** Aline Grein-Iankovski<sup>1,2</sup>, Izabel C. Riegel-Vidotti<sup>2</sup>, Fernanda F. Simas-Tosin<sup>2,3</sup>, Suresh Narayanan<sup>1</sup>, Robert L. Leheny<sup>4</sup>, and Alec R. Sandy<sup>1\*</sup>, “Exploring the relationship between nanoscale dynamics and macroscopic rheology in natural polymer gums,” *Soft Matter* **12**, 9321 (2016).

DOI: 10.1039/c6sm01492e

**Author affiliations:** <sup>1</sup>Argonne National Laboratory, <sup>2</sup>Universidade Federal do Paraná, <sup>3</sup>Instituto de Pesquisa Pelé Pequeno Príncipe, <sup>4</sup>Johns Hopkins University

**Correspondence:** \* asandy@anl.gov

Aline Grein-Iankovski acknowledges the scholarship from CAPES/PDSE (BEX 3193/14-4). The authors also acknowledge the Brazilian funding agency CNPq (Grant 477467/2010-5) and the U.S. National Science Foundation (NSF CBET-1336166). R.L.L. also thanks the Argonne National Laboratory X-ray Science Division Visiting Scientist Program for support. This research used resources of the Advanced Photon Source and the Center for Nanoscale Materials, U.S. Department of Energy (DOE) Office of Science User Facilities operated for the DOE Office of Science by Argonne National Laboratory under Contract No. DE-AC02-06CH11357.

8-ID-I • XSD • Polymer science, materials science, physics • X-ray photon correlation spectroscopy, intensity fluctuation spectroscopy, small-angle x-ray scattering • 6-12.5 keV, 7.35-7.35 keV, 7.35 keV • On-site • Accepting general users •

12-ID-C,D • XSD • Chemistry, physics, materials science • Small-angle x-ray scattering, grazing incidence small-angle scattering, wide-angle x-ray scattering, surface diffraction • 4.5-40 keV • On-site • Accepting general



# USING PRESSURE TO INTERROGATE THE BUNDLING BEHAVIOR OF AMPHIPHILES

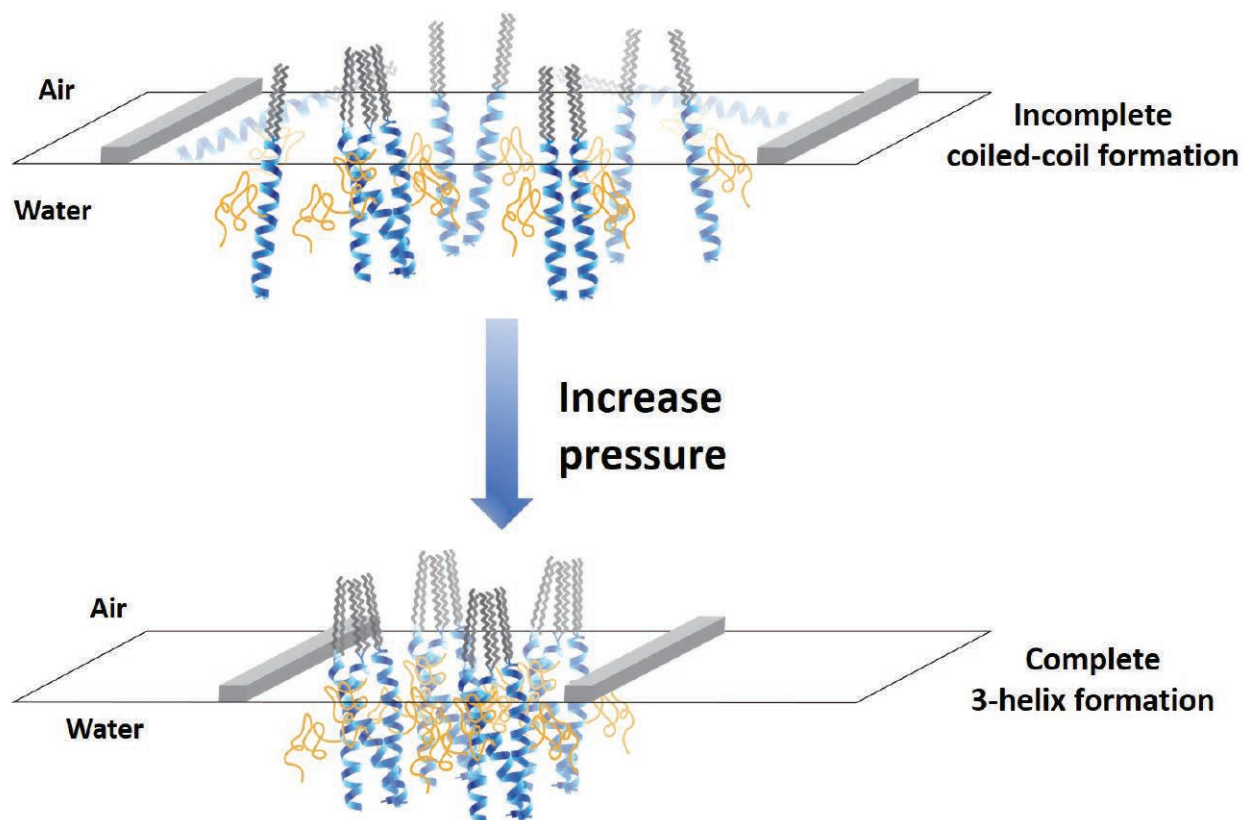


Fig. 1. The oligomeric state of PEGylated amphiphiles based on 3-helix bundle-forming peptide was found to be surface pressure dependent with mixture of dimers and trimers formed at intermediate surface pressure but transitioned completely into trimers upon increasing surface pressure.

Molecules in nature can enhance their binding to biological receptors by clustering to form more-complex structures. One class of biomaterials, called 3-helix peptide-polymer amphiphiles, adopt twisted “coiled-coils” and selectively accumulate in mouse tumors, which could be promising for drug delivery technologies. Amphiphiles are synthetic or natural long molecules that have a polar, hydrophilic (water-loving) head group and a hydrophobic (water-fearing) tail. They can self-assemble into a range of structures including micelles, vesicles, nanotubes, nanofibers, and lamellae. However, the assembly process for these amphiphiles is poorly understood and difficult to study in solution. In this work, scientists used x-ray techniques and pressure at the APS to investigate a monolayer of the self-assembled amphiphiles at the air-water interface, turning a difficult three-dimensional problem into a two-dimensional one. While these fundamental experiments provide crucial information that would be difficult to obtain via alternative routes, the researchers note that there are limits to extrapolating three-dimensional real world conclusions from two-dimensional data. Still, these coiled-coils peptide-polymer conjugates present a promising way to generate structured oligomeric states for future biological ligand-receptor applications.

Amphiphilic peptide-polymer conjugates’ unique assembly in solution stems from their component hydrophilic and hydrophobic parts. By understanding what impact each part has on the conjugates’ oligomeric assembly, researchers hope to influence their function and stability and direct them towards specific therapeutic targets in the body.

The researchers in this study, based at the Lawrence Berkeley National Lab and the University of California, Berkeley, probed how the assembly process was affected by two features: primary peptide structure and the presence of side-conjugated polyethylene glycol (PEG).

To that end, the team synthesized three types of compounds including non-PEGylated amphiphiles, PEGylated amphiphiles and PEGylated scrambled amphiphiles. The researchers deposited extremely small amounts of each type of amphiphile on a thin film of water and compressed the sample at 10 mm/min to form a layer of molecules pinned at the air-water interface. At one molecule in thickness, the monolayer effectively lets the research team analyze the assembly in two dimensions.

The monolayers were interrogated via two complementary x-ray tech-

niques that show how the molecules were packed on the surface. The team conducted these experiments at the 15-ID-B,C,D ChemMatCARS beamline at the APS.

The first technique, called x-ray reflectivity, gave out-of-plane information at the air-water interface, meaning it revealed whether the molecules are standing up or lying down. The second technique, grazing incidence x-ray diffraction, provided in-plane details on peptide bundling to form coiled-coil structures.

Though these x-ray techniques are well suited for studying very small samples, the collected signals were rather weak and required diligent analysis to ensure that the data is meaningful. To check their data, the researchers performed non-trivial data fitting and compared the results with the simulated profiles of possible oligomeric states.

With the combined power of these experimental strategies, the researchers found that the PEGylated scrambled amphiphiles did not form any recognizable oligomeric states, while the PEGylated and non-PEGylated amphiphiles formed well-defined layers that were slightly more pronounced in the latter. In other words, the results reveal that coiled-coil formation is highly dependent on peptide structure.

Under low pressure (10 mN/m), all three types of amphiphiles accumulated at the interface, with the peptide portion lying on the surface and the hydrophobic alkyl portions protruding into the air. At intermediate surface pressures (30 mN/m), the PEGylated amphiphiles formed mostly 2-helix dimers while non-PEGylated amphiphiles formed only 3-helix trimers. Upon increasing to higher pressures (40 mN/m), the researchers saw that both types of amphiphiles showed complete trimer formation (Fig.1). They hypothesized that this phenomenon arose from shorter inter-peptide distances at high pressure. Indeed, they observed a slight reduction in interhelical distance for the non-PEGylated variant while the PEGylated amphiphiles retained their interhelical distance. — *Tien Nguyen*

*See:* Reidar Lund<sup>1,2†</sup>, JooChuan Ang<sup>1</sup>, Jessica Y. Shu<sup>1</sup>, and Ting Xu<sup>1,2\*</sup>, “Understanding Peptide Oligomeric State in Langmuir Monolayers of Amphiphilic 3-Helix Bundle-Forming Peptide-PEG Conjugates,” *Biomacromolecules* **17**, 3964 (2016). DOI: 10.1021/acs.biomac.6b01356

*Author affiliations:* <sup>1</sup>University of California, Berkeley, <sup>2</sup>Lawrence Berkeley National Laboratory <sup>†</sup>Present address: University of Oslo

*Correspondence:* \* [tingxu@berkeley.edu](mailto:tingxu@berkeley.edu)

J.C.A., R.L., J.Y.S., and T.X. were supported by National Institutes of Health (Contract 5R21EB016947-02). We thank Binhua Lin and Mati Meron for technical support at beamline 15-ID-C of APS. ChemMatCARS is principally supported by the Divisions of Chemistry and Materials Research, National Science Foundation, under grant number NSF/CHE-1346572. This research used resources of the Advanced Photon Source, a U.S. Department of Energy (DOE) Office of Science User Facility operated for the DOE Office of Science by Argonne National Laboratory under Contract No. DE-AC02-06CH11357.

15-ID-B,C,D • ChemMatCARS • Materials science, chemistry • Anomalous and resonant scattering (hard x-ray), microdiffraction, high-pressure diamond anvil cell, single-crystal diffraction, liquid surface diffraction, x-ray reflectivity • 6-32 keV, 10-70 keV • On-site • Accepting general users •

# SQUISHY POLYMER BALLS DON'T ALWAYS CONFORM

**S**tuff a lot of billiard balls into a box, or marbles into a crate, or chromium atoms into a hunk of metal, and they will pack together in a familiar pattern. Billiards and marbles and chromium atoms bunch together as we expect hard spheres to bunch—in regular, symmetric, close-packed arrays. While polymers are neither hard nor spheres, some cluster into almost spherical balls that researchers expect to behave similarly. But it seems that sometimes they don't. Researchers used the APS to examine why and under what conditions polymer spheres do not conform into familiar patterns and explored the strange behavior of a simple block copolymer that was quickly cooled. Their results defy widely accepted ideas about how these materials behave. That such unexpected arrangements arise from simple copolymers shows that science still has much to learn about how these materials move and come together, and by doing so, scientists will learn much about the nature of aperiodic order in condensed matter of all kinds.

polymer particles reorganized into a fully periodic crystalline pattern with the particles arrayed with local tetrahedral packing. This behavior is similar to certain computer simulations of hard spheres in which a specific balance of repulsive and attractive forces suppress close-packed structures.

The researchers speculate that the fast temperature drop turns off molecular diffusion resulting in kinetic constraints that guide ordering of the material into a transient disordered state. This work begs the question: Were the ordered states that researchers have observed previously in particle-forming block polymers true equilibrium phases or just steps in a slow transition? There may be much more complexity to the movements and order of these materials than researchers have supposed.

Since the discovery of aperiodic order in metal alloys in the mid-1980s, researchers have observed quasi-crystalline arrangements in a growing variety of materials, which include nanoparticles, foams, and biological materials. But the underlying principles that dictate the formation of quasi-crystals in soft materials remain a mystery. The simple copolymer examined in this work serves as an ideal model to help researchers uncover these principles. The results demonstrate that at least some forms of order in this class of soft materials are non-equilibrium states—a pit-stop on the material's journey to something else. — *Jenny Morber*

**See:** Timothy M. Gillard<sup>1</sup>, Sangwoo Lee<sup>2</sup>, and Frank S. Bates<sup>1\*</sup>, "Dodecagonal quasicrystalline order in a diblock copolymer melt," *Proc. Nat. Acad. Sci.* **113**, 5167, (May 10, 2016).

DOI: 10.1073/pnas.1601692113

**Author affiliations:** <sup>1</sup>University of Minnesota, <sup>2</sup>Rensselaer Polytechnic Institute

**Correspondence:** \* bates001@umn.edu

This work was supported by the National Science Foundation under Award 1104368. DND-CAT is supported by Northwestern University, E.I. DuPont de Nemours & Co., and The Dow Chemical Company. This research used resources of the Advanced Photon Source, a U.S. Department of Energy (DOE) Office of Science User Facility operated for the DOE Office of Science by Argonne National Laboratory under Contract No. DE-AC02-06CH11357.

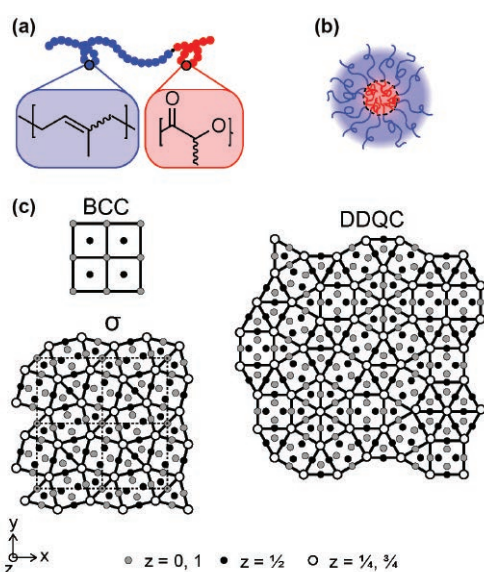


**Fig. 1** Schematic of the model asymmetric diblock copolymer and its states of order when cooled. (a) Chemical structures of IL diblock copolymers. Each "bead" is a specific repeat unit. (b) Red sequences cluster together to form nearly spherical particles. (c) Two-dimensional particle tiling patterns associated with the BCC,  $\sigma$ , and DDQC phases identified in the IL diblock copolymer viewed in the x-y plane. The BCC and  $\sigma$  phases were shown to be equilibrium states while the DDQC is a transient non-equilibrium phase.

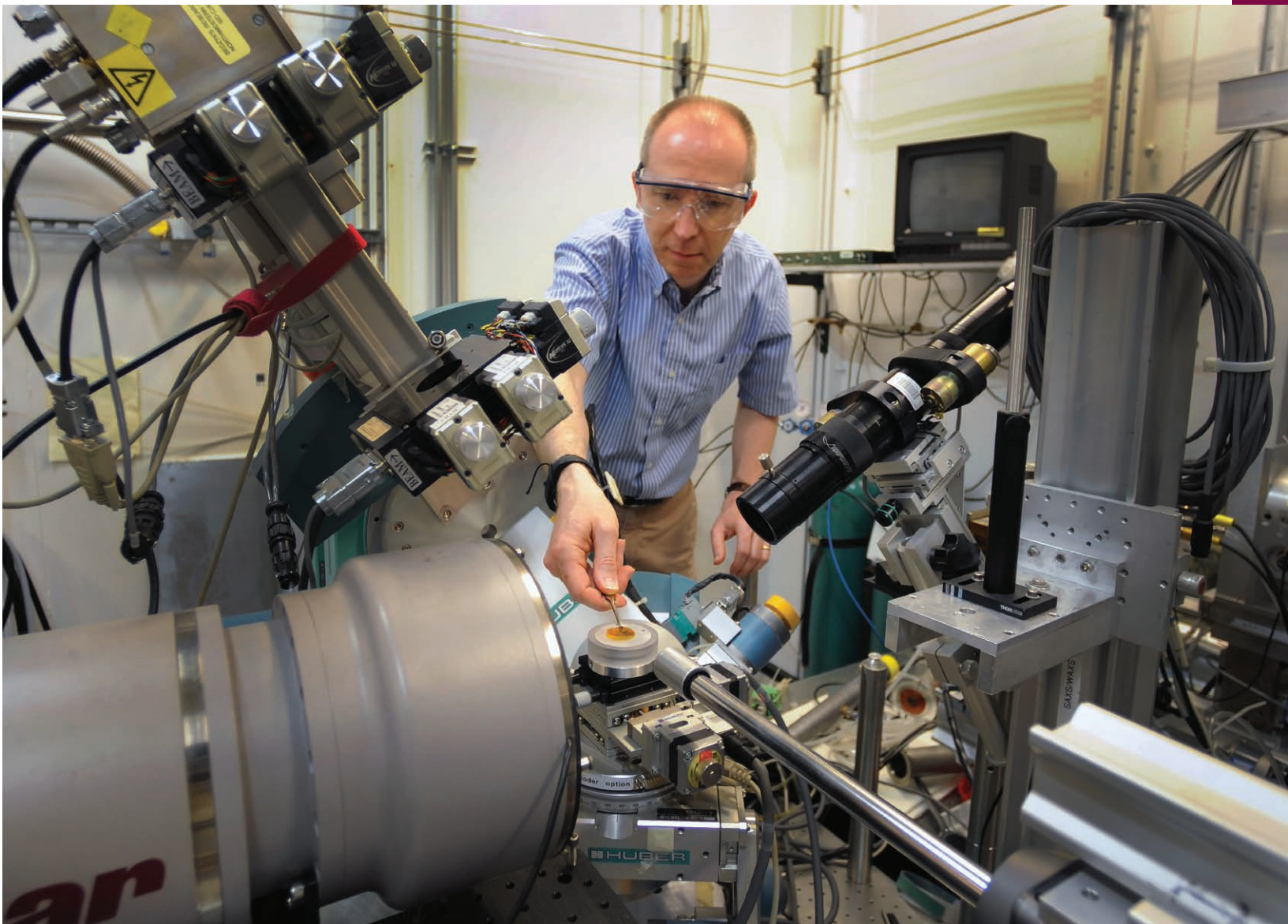
5-ID-B,C,D • DND-CAT • Materials science, polymer science • Powder diffraction, x-ray standing waves, x-ray optics development/techniques, small-angle x-ray scattering, surface diffraction, x-ray reflectivity, wide-angle x-ray scattering • 6-17.5 keV • On-site • Accepting general users •

A block copolymer is a little like a bead necklace, with each bead a molecular unit. These researchers, from the University of Minnesota and the Rensselaer Polytechnic Institute, used chains with two simple sequences of beads (Fig. 1). In this type of block copolymer, hundreds of individual molecular strings come together to form soft particles, like knots in the necklace. Usually, these particles cluster into close-packed arrangements when cooled below a certain temperature, squishing the necklace into the tightest possible wad. But when cooled far below this temperature, the close-packed arrangement sometimes does not appear. Researchers are unsure why.

The researchers mixed up some of this material, squeezed it into a thin quartz tube, cooled it very quickly, and then used small-angle x-ray scattering experiments performed on the DND-CAT 5-ID-B,C,D beamline at the APS to watch how the polymer necklaces arranged themselves over time.

The polymer formed soft particle-like regions as expected, but instead of bunching themselves into a periodic arrangement, the particles adopted a two-dimensional aperiodic pattern known as a quasicrystal. Over several hours to months, depending on the temperature, the





Denis Keane, Director of the DND-CAT x-ray facility at the APS, places a sample in the kappa geometry diffractometer at the DND-CAT 5-ID-C x-ray beamline. This instrument is used for measuring x-ray fluorescence, x-ray standing waves, and wide-angle x-ray scattering to determine the surface and bulk structure of thin films and other samples.

# NEON YIELDS SECRETS IN FIRST LOCK-UP

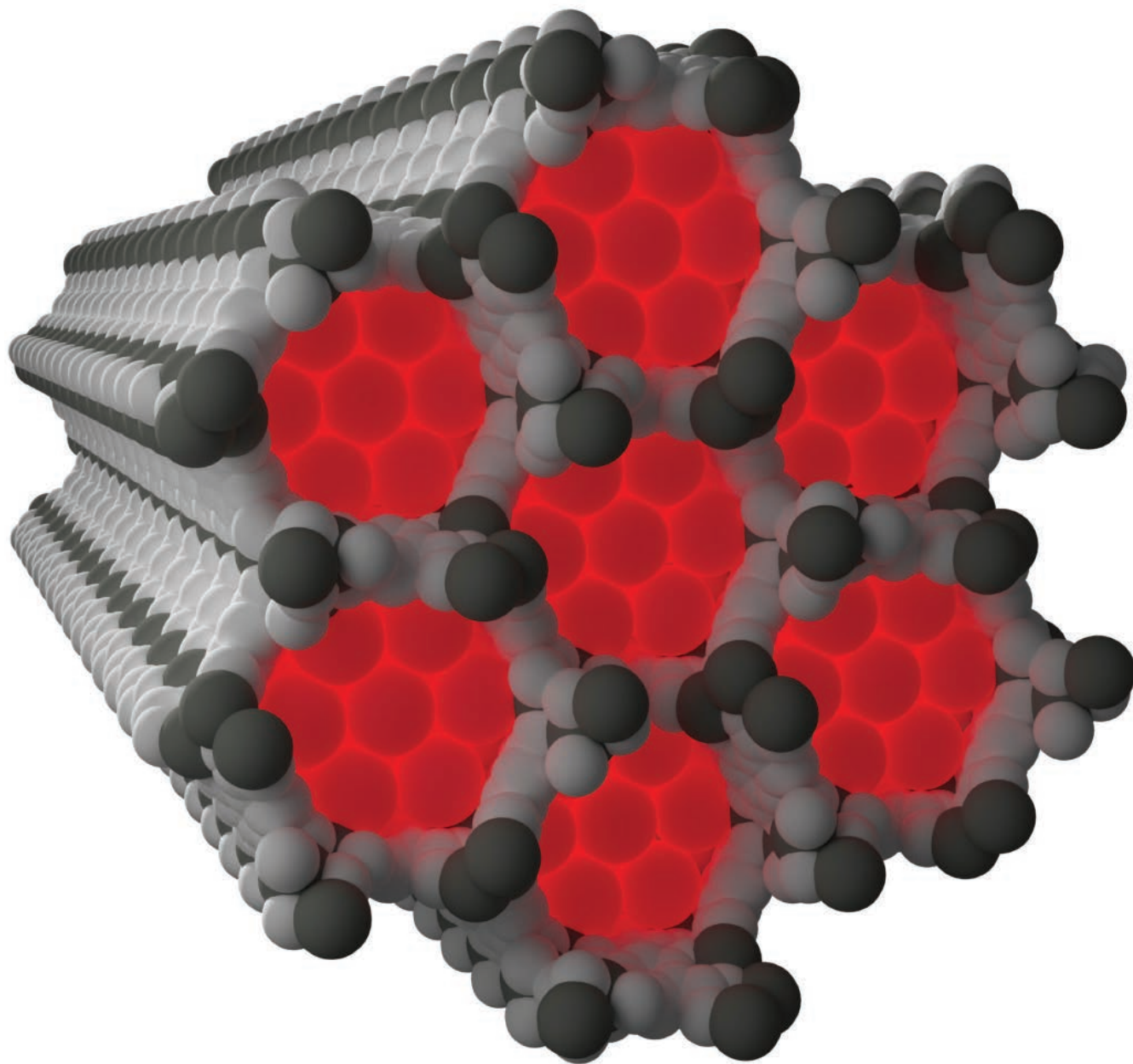


Fig. 1. Neon observed experimentally within the pores of NiMOF-74 at 100 K and 100 bar of neon gas pressure.



Neon is abundant in the Earth's atmosphere, but not on Earth itself. Neon does not bind with other compounds and is lighter than air, so it escapes into the atmosphere and out into space. What is left in Earth's air we extract to study, to light glowing signs, and make high-powered lasers. Since its discovery in 1898, neon has taught scientists much about the nature of stable atoms. But despite neon's importance to both science and industry, no one had previously reported capturing it in a molecular box in the way that nearly every other element has been studied. Organic and metal-organic crystal structures are critical in the study of materials, molecules, and gases, and with more than eight decades of scrutiny, researchers have reported experiments and results for over 850,000 crystal structures containing 94 different elements. But not neon. One of the most effective gas trapping boxes, called metal-organic-frameworks (MOFs), are composed of metal atoms or sheets connected by stretchy organic linking molecules. In this report, researchers working at the APS use MOFs to correct the surprising oversight and along the way reveal the first crystallographic observation of an interaction between neon and a transition metal—a result with tantalizing implications for neon capture.

Researchers exposed two well-studied MOFs to an atmosphere of neon under moderate pressure, lowered the temperature, and observed what happened. They tracked the movement of neon into the MOF's pores and how the atoms interacted with their environment through analysis of *in situ* x-ray powder diffraction data gathered on the XSD 17-BM-B beamline at the APS. This data allowed the researchers from the Cambridge Crystallographic Data Centre and Argonne to track the interactions of the neon atoms and how the structures responded to changes in temperature, pressure, or other conditions as the experiment progressed. The researchers were able to determine the percentage of neon that diffused into the MOFs or slipped back out, how the shape of the MOFs changed, and even how close the atoms snuggled up to each other as temperature varied and time passed.

One MOF was composed of thin and rigid copper sheets connected by flexible organic molecules. As expected, neon mimicked other gases previously studied with this MOF, and simply stacked into the elastic cylindrical channels. The atoms appeared to move into and out of the framework with similar ease, and the structure stretched to accommodate them. The

researchers found no evidence for strong guest-framework interactions, meaning that this structure would not work well to selectively grab neon from a mix of similar sized gases.

The second MOF contained nickel metal atoms and an organic molecule network that enclosed roughly hexagonal channels (Fig. 1). In this structure, the researchers noted that neon entered the pores more readily than it exited at similar pressure, which together with other evidence suggested an interaction between one of the neon atoms and the nickel in the framework. The transition metal-neon interaction hints that it could be possible to build an MOF capable of selectively capturing neon from a mix of gases.

It is now the 50th anniversary of the Cambridge Structural Database, "the world's repository for small-molecule organic and metal-organic crystal structures." Somehow neon had escaped the focus of decades of intense work to understand and refine crystal structures, but no longer.

This work is the first experimental report of neon captured in such an environment, and given the challenges involved in studying more unstable elements, may add the last new element to the crystal structure collection for quite some time. With noteworthy results, the interaction between neon

and a transition metal hints at exciting future possibilities for neon capture.

— Jenny Morber

**See:** Peter A. Wood<sup>1\*</sup>, Amy A. Sargeant<sup>2</sup>, Andrey A. Yakovenko<sup>3</sup>, Suzanna C. Ward<sup>1</sup>, and Colin R. Groom<sup>1</sup>, "Capturing neon – the first experimental structure of neon trapped within a metal-organic environment," *Chem. Commun.* **52**, 10048 (2016). DOI: 10.1039/c6cc04808k

**Author affiliations:** <sup>1</sup>Cambridge Crystallographic Data Centre (UK), <sup>2</sup>Cambridge Crystallographic Data Centre (Rutgers University), <sup>3</sup>Argonne National Laboratory

**Correspondence:**

\* wood@ccdc.cam.ac.uk

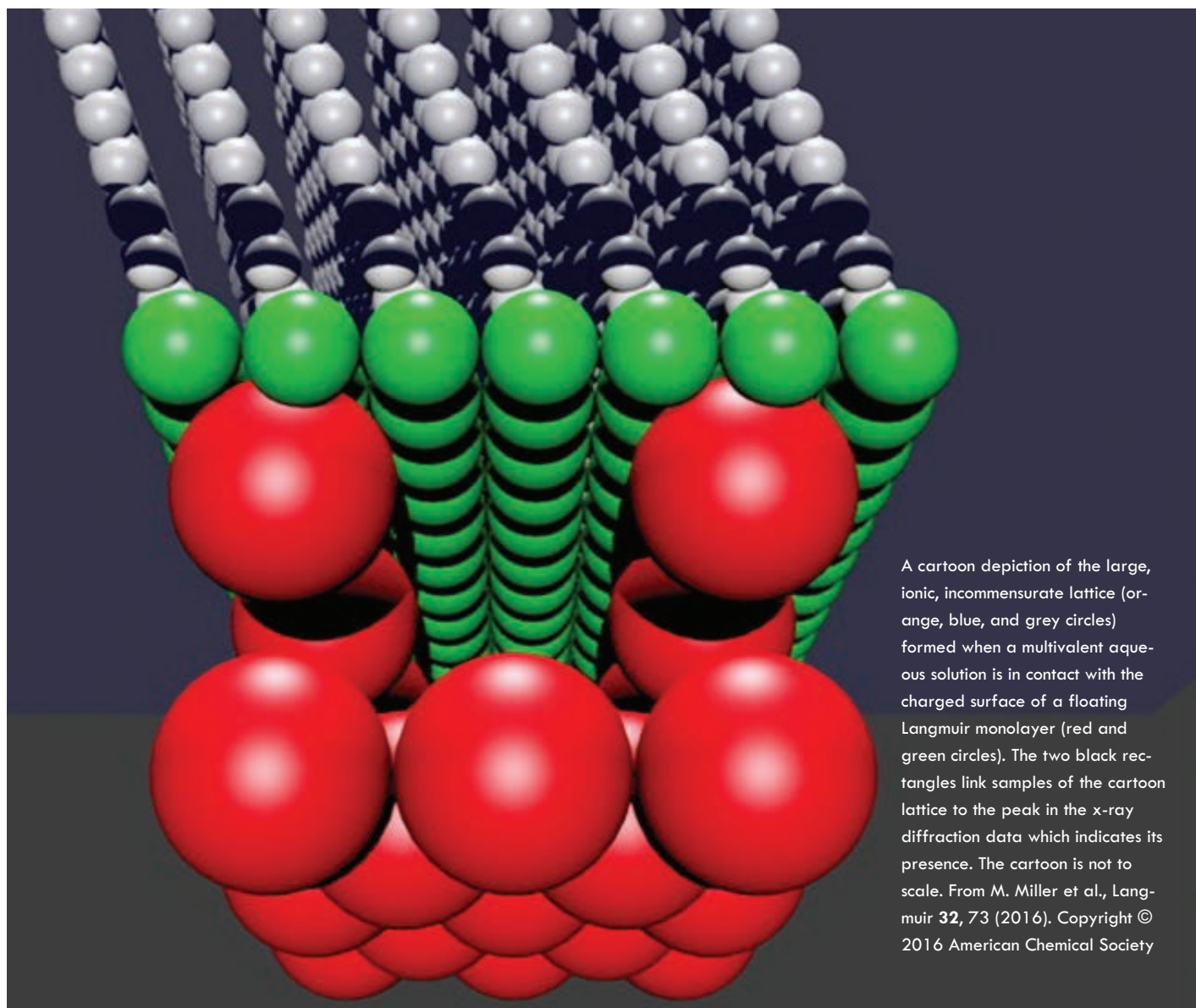
AAY thanks the Director's Postdoctoral Fellowship program at Argonne. Other costs were met from the Cambridge Crystallographic Data Centre scholarship and outreach fund. This research used resources of the Advanced Photon Source, a U.S. Department of Energy (DOE) Office of Science User Facility operated for the DOE Office of Science by Argonne National Laboratory under Contract No. DE-AC02-06CH11357.

17-BM-B • XSD • Chemistry, materials science • Powder diffraction, high-pressure diamond anvil cell • 27-51 keV • On-site • Accepting general users •



# WHEN YOUR LATTICES DON'T LINE UP: CHARGE INVERSION NEAR WET CHARGED SURFACES

**T**he combination of a charged surface or charged molecule adjacent to a room-temperature, aqueous solution occurs in many biological and colloidal applications, including protein folding and the interaction between viruses and their host cells. Previous work studying this situation has shown that charged colloidal particles can attract so many dissolved ions that the colloidal particles reverse their effective charge, which is impossible based on electrostatics alone. The mechanism for this charge inversion is an outstanding question. In new work, a research team with members from two Illinois universities used the APS to investigate the lattices formed in this type of environment and their possible role in this charge reversal. They found the first indication of ordered lattices composed of charged particles from the solution, whose incommensurate position with respect to the charged surface implies the lattice's formation is a product of ion-ion interactions rather than chemical attachment, as had been thought to be the case. In addition to addressing a topical electromagnetism question, these results can be applied to materials science as well as aspects of molecular biology that touch human life at a very basic level.



A simplified way to envision the aqueous solution in these systems is as a few large, charged colloidal particles or molecules surrounded by many smaller, multivalent ions. Charged colloidal particles or molecules will attract many of the smaller, oppositely-charged ions, called counterions. Explanations for the over-attraction of counterions fall into two categories: chemical mechanisms and physical mechanisms. The chemical mechanisms require chemical bonds between the counterion and charged surface; the physical mechanisms require the counterions to form a laterally ordered lattice. This lattice ordering can lower the free energy and create an environment in which it is favorable for the large colloidal particle or molecule to invert its charge by attracting too many dissolved ions.

To detect such a lattice, the team built systems composed of charged surfaces and aqueous solutions of multivalent ions. For the charged surfaces, they used amphiphilic monolayers consisting of carboxylic acid and phosphate head groups; these were selected because they form very dense ordered lattices. The team tested two aqueous solutions: erbium chloride or erbium nitrate.

The team of researchers from Northwestern University and The University of Chicago collected scattering intensity data both in-plane and normal to the plane using grazing-incidence synchrotron x-ray diffraction (GIXD) at the ChemMatCARS 15-ID-B,C,D x-ray beamline at the APS. The resulting diffraction peaks indicated the presence of three lattices: the charged surface, a lattice commensurate with the location of the head groups in the charged surface layer, and a hexagonal lattice incommensurate with the structure of the charged layer. The lower section of Fig. 1 depicts a cartoon of the charged surface and aqueous solution, with a large, dark rectangle indicating a portion of the incommensurate lattice; the smaller rectangle in the upper left calls out the x-ray data that indicates the presence of the incommensurate lattice.

The presence of the ordered lattice of counterions allowed the team to draw a number of conclusions.

This incommensurate layer gives physical evidence to support the mechanism

by which the counterions can invert the effective charge of the colloidal particle. This mechanism cannot be chemical, because the two lattices are not aligned, and so must be physical, based on the reduction in free energy produced by formation of an ordered lattice. The team's results also show that laterally ordered lattices can be made by counterions at temperatures near room temperature. Lastly, the correlation length of the incommensurate lattice is sufficiently large to rule out the presence of a condensed Wigner liquid phase, upsetting a popular candidate for explaining this charge inversion phenomenon.

With this recent work, the team has provided data that indicate a mechanism for charge inversion through the formation of ordered lattices in wet, room-temperature environments that include a charged surface.

— Mary Alexandra Agner

**See:** Mitchell Miller<sup>1</sup>, Miaoqi Chu<sup>1</sup>, Binhua Lin<sup>2</sup>, Mati Meron<sup>2</sup>, and Pulak Dutta<sup>1\*</sup>, "Observation of Ordered Structures in Counterion Layers near Wet Charged Surfaces: A Potential Mechanism for Charge Inversion," *Langmuir* **32**, 73 (2016).

DOI: 10.1021/acs.langmuir.5b04058

**Author affiliations:** <sup>1</sup>Northwestern University, <sup>2</sup>The University of Chicago

**Correspondence:**

\* pdutta@northwestern.edu

This research was supported by the U.S. National Science Foundation under Grant DMR-1309589. ChemMatCARS is principally supported by the Divisions of Chemistry and Materials Research, National Science Foundation, under grant number NSF/CHE-1346572. This research used resources of the Advanced Photon Source, a U.S. Depart-

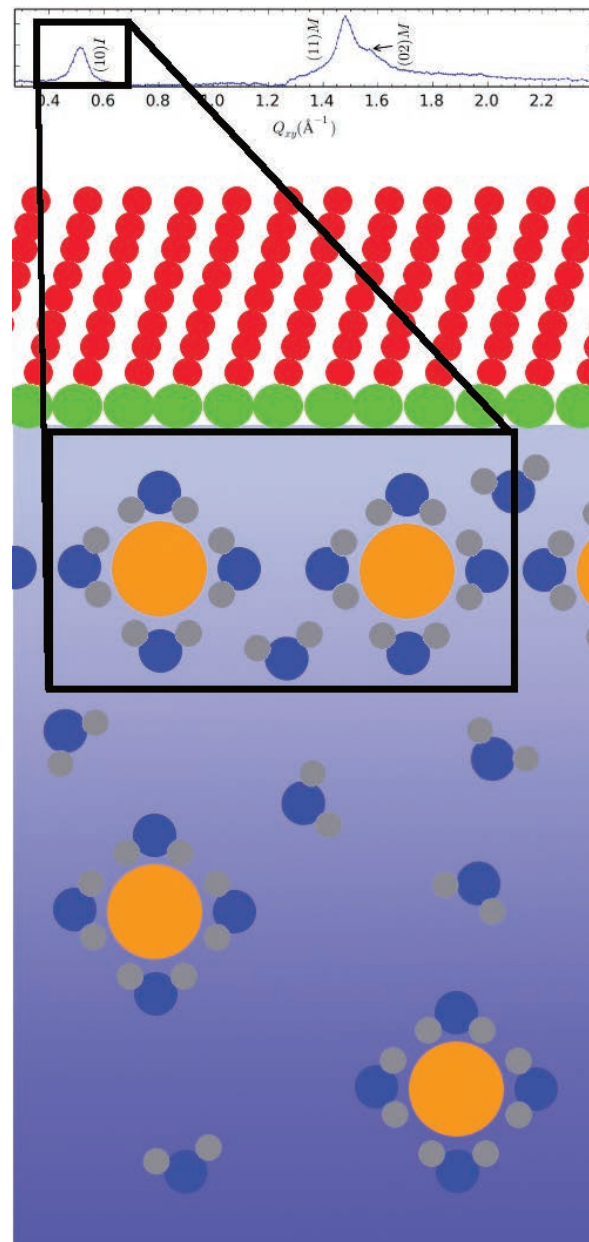


Fig. 1. Schematic diagram of the system studied. The negatively charged (green) head groups are in contact with the solution and attract positive (red) counterions.

ment of Energy (DOE) Office of Science User Facility operated for the U.S. DOE Office of Science by Argonne National Laboratory under Contract No. DE-AC02-06CH11357.

15-ID-B,C,D • ChemMatCARS • Materials science, chemistry • Anomalous and resonant scattering (hard x-ray), microdiffraction, high-pressure diamond anvil cell, single-crystal diffraction, liquid surface diffraction, x-ray reflectivity • 6-32 keV, 10-70 keV • On-site • Accepting general users •

# FAKING PHOTOSYNTHESIS TO MAKE HYDROGEN FUEL

**H**umans can learn a lot from plants. With energy from the sun, protein catalysts in plants efficiently split water to generate oxygen, storing the energy as carbohydrates. Scientists would like to perform a similar trick, using solar energy to split water and produce hydrogen fuel. Hydrogen fuel burns clean, producing only water as a byproduct, but splitting water is not an efficient task for humans. Researchers have taken baby steps toward artificial photosynthesis, building solar-powered water-splitting catalysts in the laboratory, but so far these catalysts remain far less efficient than their vegetal counterparts. One reason it's difficult to improve catalytic efficiency is that scientists don't fully understand the catalysts' water-splitting mechanism. To examine the reaction pathway of a cobalt-based catalyst in unprecedented detail, researchers collected x-ray absorption spectra at the APS. The data revealed electronic and structural features of the catalyst, offering clues for how the researchers can tweak the catalyst to run the reaction more efficiently. Such advances could bring down the cost of producing hydrogen fuel, making a hydrogen economy—a world run on water—a future possibility.

Photosynthetic water splitting is the breakdown of two water molecules into two H<sub>2</sub> molecules plus an O<sub>2</sub>. The reaction takes place in two steps: 1) water oxidation and 2) proton reduction. Chemically speaking, both steps are difficult, but for this study, the researchers focused only on speeding up the second step. The tough part of proton reduction involves forming a bond between two hydrogens to form H<sub>2</sub>, a process called hydrogen evolution, so that's where a catalyst can help. There are many hydrogen-evolving catalysts, but none rival biological enzymes, and most have additional drawbacks as well. Most existing catalysts aren't soluble in water, which is a problem since the end goal is to use the catalyst to turn water into fuel. Another factor is cost; many catalysts rely on the electron-moving properties of expensive metals, such as platinum or rhodium. In this study, the researchers examined the reaction pathways of a water-soluble hydrogen-evolving catalyst with a lower-cost cobalt center.

The catalyst's formula is [LCo<sup>III</sup>Cl<sub>2</sub>], with the cobalt stabilized by four nitro-

gen atoms embedded in a macrocycle ligand of ring moieties, represented as L in the formula. To figure out the exact steps the catalyst takes to form hydrogen-hydrogen bonds, a team of researchers from the Institute of Chemical Research of Catalonia (Spain), Southern Federal University (Russia), Universitat Autònoma de Barcelona (Spain), and Argonne used the XSD 20-BM-B and 11-ID-D x-ray beamlines at the APS to perform static and time-resolved x-ray absorption spectroscopy (tr-XAS).

The main advantages of time-resolved x-ray absorption spectroscopy over other methods is that it tracks the formation and decay of reaction intermediates, even those that disappear within picoseconds, as well as the kinetics of each reaction step. The team hoped to identify the reaction's rate-limiting step, as this is a key efficiency bottleneck and a target for optimization.

At the beamline, the researchers mixed the cobalt catalyst with a ruthenium-based photosensitizer. This photosensitizer is energized by light and can pass that energy to the catalyst to jumpstart the reaction. They also added

ascorbic acid to the mixture. The ascorbic acid acts as an electron donor, which provides a source of electrons for downstream reactions. The sample is flown into a free-flowing liquid jet sheet in the path of the x-ray beam and excited with an optical laser. The light sets the reaction in motion, with the photosensitizer funneling electrons from the donor to the catalyst. As the reaction progressed, the x-ray data showed that the structural environment around the cobalt metal center changes over the course of the reaction and also allowed the observation of the cobalt cycling through different oxidation states.

To better understand what was going on, the researchers compared the experimental data with numerical simulations of the reaction, which predicted the spectra from hypothetical intermediates. Together, the data and simulations allowed the researchers to map out the full mechanistic pathway of the reaction and determine the rate-limiting step (Fig. 1). The formation of the Co(I) occurred in a matter of nanoseconds, while the formation of the Co(III) hydride intermediate took microseconds to



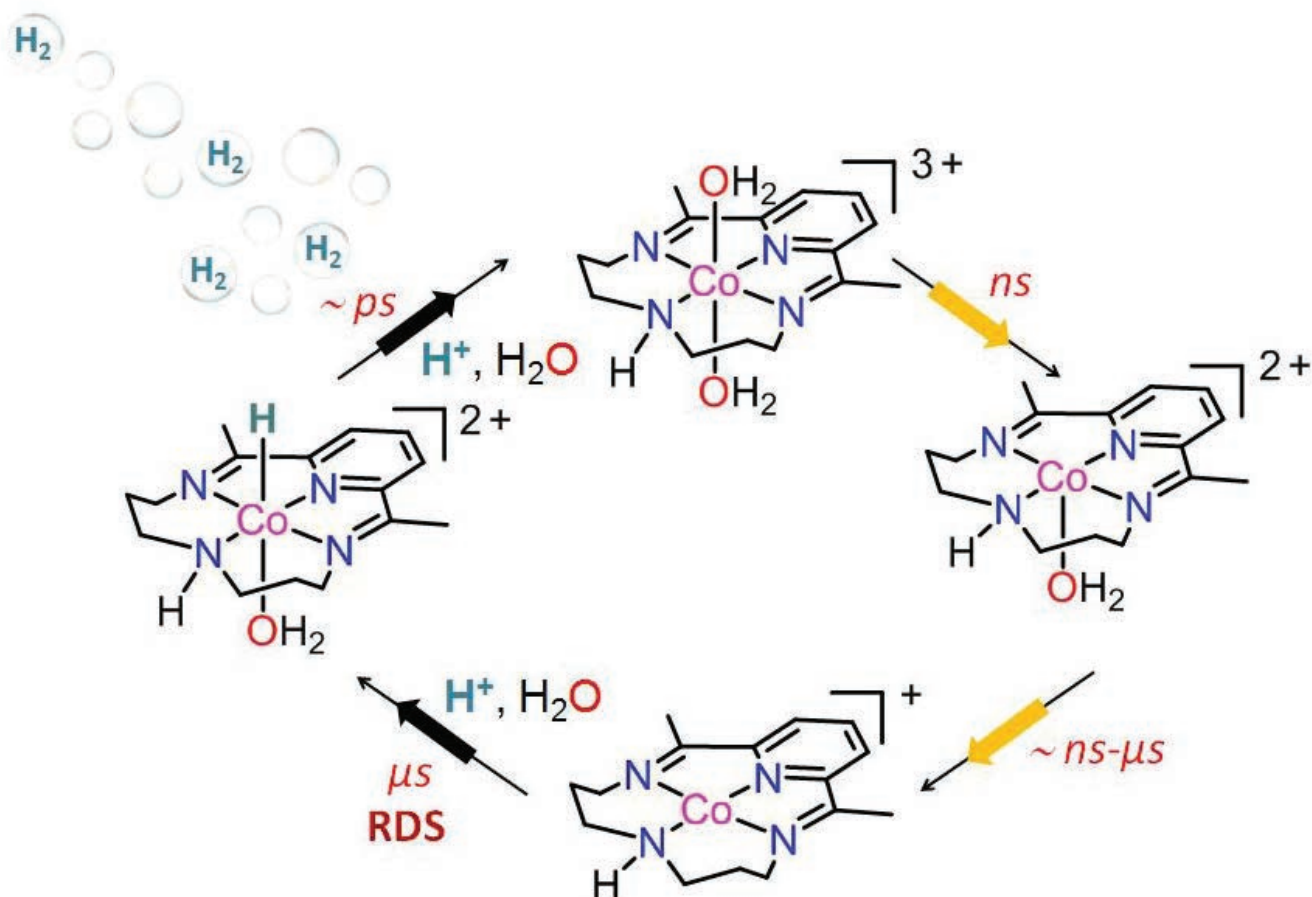


Fig. 1. The mechanistic pathway for the hydrogen evolution reaction, which produces  $H_2$  molecules, as catalyzed by a cobalt-based catalyst. The catalyst includes cobalt (pink), oxygen (red), and nitrogen (blue). The overall charge state of each intermediate along the catalytic cycle are shown (+3, +2, +1). Yellow arrows indicate steps that utilize energy from a light source. Kinetic timescales are also shown, with the rate-determining step (RDS) labeled.

form. The researchers concluded that the formation of the latter intermediate—the protonation of  $Co(I)$ —was therefore the rate-limiting step.

This discovery immediately suggests ways in which the researchers could adjust the structure of the macrocyclic ligand to speed up the reaction and improve the catalytic efficiency. The process is a bit of trial and error—make a tweak and see if the efficiency improves—but the researchers no longer have to make their tweaks in the dark.

— Erika Gebel Berg

**See:** Dooshaye Moonshiram<sup>1\*</sup>, Carolina Gimbert-Suriñach<sup>2\*</sup>, Alexander Guda<sup>3</sup>, Antonio Picon<sup>1</sup>, C. Stefan Lehmann<sup>1</sup>, Xiaoyi Zhang<sup>1</sup>, Gilles Doumy<sup>1</sup>, Anne Marie March<sup>1</sup>, Jordi Benet-Buchholz<sup>2</sup>, Alexander Soldatov<sup>3</sup>, Antoni Llobet<sup>2,4\*\*\*</sup>, and Stephen H. Southworth<sup>1</sup>, “Tracking the Structural and Electronic

Configurations of a Cobalt Proton Reduction Catalyst in Water,” *J. Am. Chem. Soc.* **138**, 10586 (2016). DOI: 10.1021/jacs.6b05680

**Author affiliations:** <sup>1</sup>Argonne National Laboratory, <sup>2</sup>Barcelona Institute of Science and Technology, <sup>3</sup>Southern Federal University, <sup>4</sup>Universitat Autònoma de Barcelona

**Correspondence:**

\* dmoonshi@gmail.com

\*\* cgimbert@icq.es \*\*\* allobet@icq.es

This work was supported by the U.S. Department of Energy (DOE) Office of Science—Basic Energy Sciences, Chemical Sciences, Geosciences, and Biosciences divisions under Contract no. DEAC02-06CH11357; We also acknowledge financial support from MINECO and the “Fondo Europeo de Desarrollo Regional” (FEDER) through grants CTQ-2013-49075-R, SEV-2013-0319, and CTQ-2014-52974-REDG; and from the EU COST actions CM1202 and CM1205. C.G.S.

is grateful to AGAUR and Generalitat de Catalunya for a “Beatriu de Pinós” postdoctoral grant. A.G. and A.S. thank the Russian Ministry of Education and Science for support (agreement no. 14.587.21.0002, unique identifier RFMEFI58714X0002). This research used resources of the Advanced Photon Source, a U.S. DOE Office of Science User Facility operated for the DOE Office of Science by Argonne National Laboratory under Contract no. DE-AC02-06CH11357.

11-ID-D • XSD • Chemistry, environmental science, materials science • Time-resolved x-ray absorption fine structure, time-resolved x-ray scattering, general diffraction • 6-25 keV • On-site • Accepting general users •

20-BM-B • XSD • Materials science, environmental science, chemistry • X-ray absorption fine structure, microfluorescence (hard x-ray), diffraction anomalous fine structure • 2.7-32 keV, 2.7-35 keV • On-site • Accepting general users •

# THE MODEL CATALYST

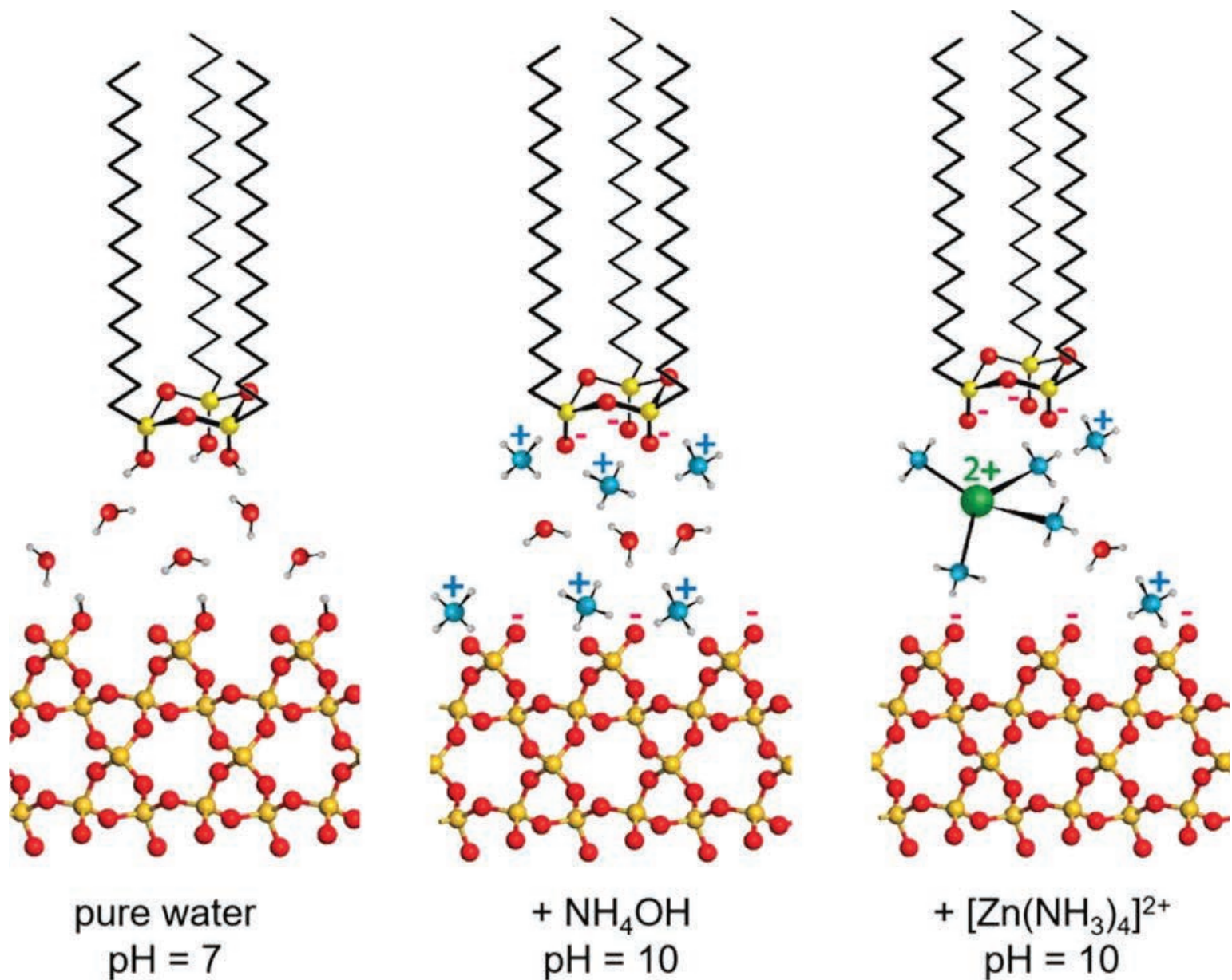


Fig. 1. Model mechanism of grafting of zinc ions under the OTOS film (top) and corresponding grafting mechanism of zinc ions at the silica interface (bottom). From M.W. Martynowycz et al., Am. Chem. Soc. **138**, 12432 (2016).

Scientists use catalysts to facilitate chemical reactions for making everything from pharmaceuticals and plastics to pesticides and food additives. Many catalysts are solids, and the reactions take place on their surfaces. Therefore, understanding the surface science is crucial to designing better catalysts. Researchers used the APS to investigate the surface of ultrathin films of siloxanes at the air-liquid interface, to which metal ions can be attached. This new structural analysis of the films, controversially very different from the former structural interpretations, provides a fresh insight into how these catalysts work and could lead to more efficient catalysts.

Designing new, efficient catalysts for speeding up a range of chemical reactions is a difficult task. Often times, new catalysts are discovered serendipitously. However, a better understanding of how the surfaces of solid catalysts interact with chemical reagents to make different products would be a much more effective approach for deliberate, as opposed to accidental design of catalysts with specificity for given reactions. Specificity means fewer side reactions and more product compound per unit of the reagent, or starting material, the chemist begins with.

Chemists have recently experimented with metal ions of cobalt, iron, and zinc bounded to a type of silicon dioxide known as amorphous silica, which make very stable catalysts. These materials have been shown to accelerate the conversion of propane by removal of some of its hydrogen atoms (dehydrogenation) to the more useful propene. Propene can be processed further into other chemically important compounds as well as being polymerized into polypropylene. Following the catalytic processes is difficult with conventional surface spectroscopic techniques. Unfortunately, these otherwise rather powerful techniques such as extended x-ray absorption fine structure and x-ray absorption near edge structure are not amenable to studying solid-liquid interfaces of the catalysts because of interference with the bulk solutions.

These limitations have almost put the study of this kind of catalyst off-limits. However, a new type of surface study using the ChemMatCARS 15-ID-B,C,D beamline at the APS has allowed researchers from the Illinois Institute of Technology, Argonne, and The University of Chicago to instead probe the

surface chemistry of monolayers of a silicon compound to which the catalytic metal ions can be attached. These ultrathin films, acting as a model for the amorphous silica catalysts, can then be studied with grazing incidence x-ray diffraction, x-ray reflectivity, and x-ray fluorescence spectroscopy.

Zinc ions can be bound to monolayer films of octadecyltriethoxysilane that are formed from octadecyltrimethoxysilane through the reactions of hydrolysis and condensation. Indeed, other researchers have tested these ultrathin films and suggested polymer formation based on x-ray and infrared surface studies. However, the new study on the ChemMatCARS beamline argues that the formation of polymers in this system is inconsistent with the experimental x-ray data (Fig. 1). These researchers explain that polymer formation is energetically unfavorable and is highly unlikely. Instead, based on their analysis, they have proposed formation of tiny rings of the siloxane molecules made of three units (trimers) rather than long, linear polymer chains.

Such cyclic trimers are entirely consistent with the new x-ray studies as well as with infrared data of the earlier research. According to the new data, positively charged zinc ions bind to the negatively charged oxygen atoms of the hydroxyl groups of the film. The cyclic trimers of the monolayer imitate the function of active sites of amorphous silica surface that are known to bind zinc ions at the solid-liquid interface. Moreover, the ratio of zinc ions to those hydroxyl groups is the same as is measured in zinc-on-silica catalysts, so it can be presumed that the nature of the active sites in the model material is the same as in the catalyst itself.

This new insight points the way to

a clearer understanding of metal-on-amorphous-silica catalysts and offers the possibility of new approaches to making these catalysts more effective and efficient for the production of fine chemicals. Additional studies must now be carried out to confirm definitively the one-to-one correspondence between their model and catalytic surface of amorphous silica. — *David Bradley*

**See:** Michael W. Martynowycz<sup>1,2</sup>, Bo Hu<sup>1‡</sup>, Ivan Kuzmenko<sup>2\*</sup>, Wei Bu<sup>3</sup>, Adam Hock<sup>1,2\*\*</sup>, and David Gidalevitz<sup>1\*\*\*</sup>, "Monomolecular Siloxane Film as a Model of Single Site Catalysts," *J. Am. Chem. Soc.* **138**, 12432 (2016). DOI: 10.1021/jacs.6b05711

**Author affiliations:** <sup>1</sup>Illinois Institute of Technology, <sup>2</sup>Argonne National Laboratory, <sup>3</sup>The University of Chicago <sup>‡</sup>Present address: Georgia Institute of Technology

**Correspondence:**

\* kuzmenko@aps.anl.gov

\*\* ahock@iit.edu \*\*\* gidalevitz@iit.edu

M.W.M is supported by the X-ray Science Division of Argonne as a Laboratory Graduate Fellow. ChemMatCARS Sector 15 is supported by the National Science Foundation under grant number NSF/CHE-1346572. This research used resources of the Advanced Photon Source, a U.S. Department of Energy (DOE) Office of Science User Facility operated for the DOE Office of Science by Argonne National Laboratory under Contract No. DE-AC02-06CH11357.

15-ID-B,C,D • ChemMatCARS • Materials science, chemistry • Anomalous and resonant scattering (hard x-ray), microdiffraction, high-pressure diamond anvil cell, single-crystal diffraction, liquid surface diffraction, x-ray reflectivity • 6-32 keV, 10-70 keV • On-site • Accepting general users •



# NATURAL BUILDING BLOCKS FOR NEW CATALYSTS

Taking a leaf out of nature's book has been a fruitful inspiration for scientists. Now, in a bid to make novel materials that might be useful for storing, separating, or reacting industrial and other gases, a way to make porous substances using a building block found in nature looks set to bear fruit. By using the porphyrin molecule at the heart of the respiration process in plants and animals, a new type of metal-organic framework (MOF) material can be constructed. The MOF is investigated by iron K-edge x-ray absorption and K-beta mainline emission spectroscopy measurements. Studies at the APS show the detailed structure of the pores in this solid, but sponge-like material and points to how it might be used to absorb other small molecules for catalytic conversions to make useful chemicals or even for solar energy conversion.

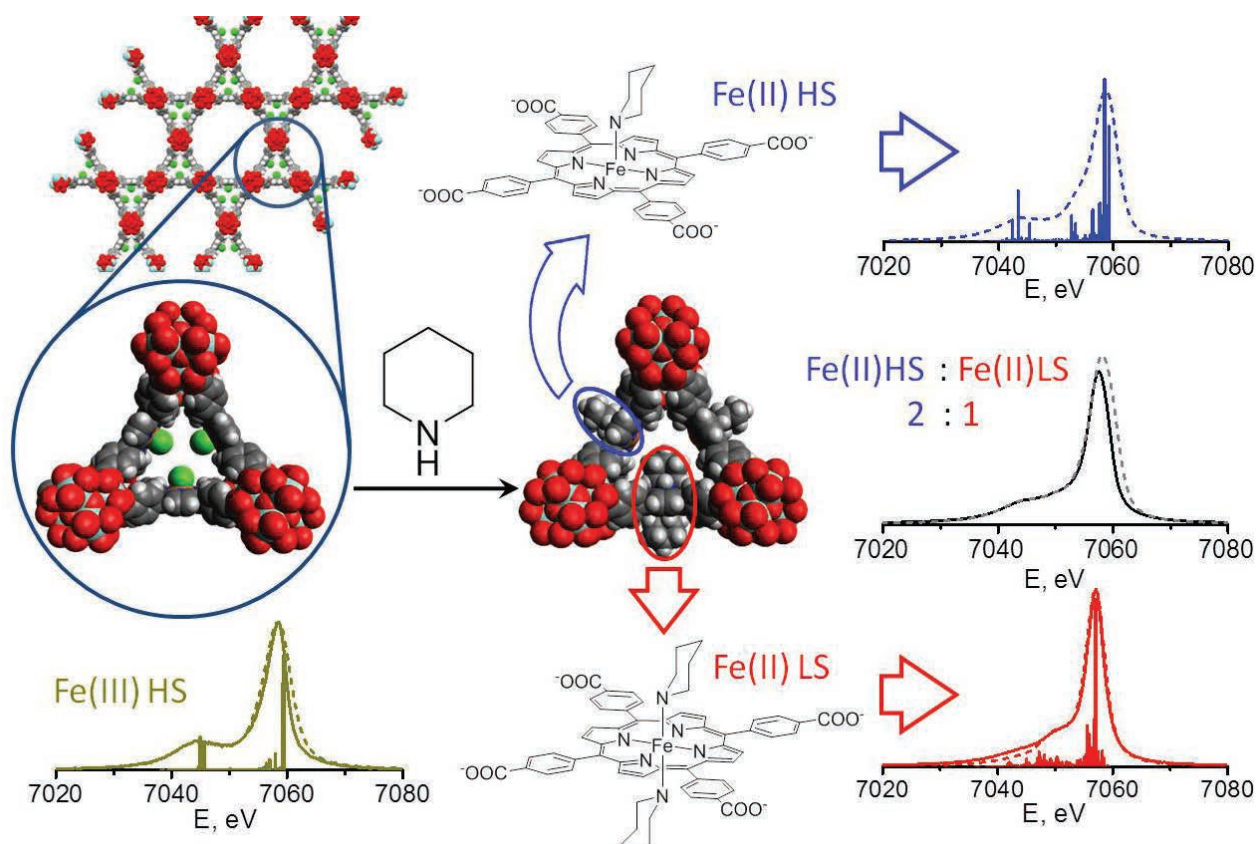


Fig. 1. Space-filling diagrams of the PCN-222(Fe) pores upon reduction with piperidine along with their K-beta x-ray emission spectra.

Metal-organic frameworks are a relatively recent discovery. They are three-dimensional (3-D) materials formed from a network of metal ions interlinked by any of various organic compound molecules. The organic groups act as spacers that keep the metal ions apart and open up a regular pattern of structures within the solid. In many cases, this lattice contains holes and channels that are big enough to absorb small molecules. As such, materials scientists have been searching for new MOFs by combining different metal ions with various classes of organic compound to create new types of catalysts for speeding up otherwise inefficient or energy-intensive manufacturing processes for the chemical, pharmaceutical, and agrochemicals industries. Other MOFs might selectively absorb one type of chemical and so could be used to separate different compounds from one another, acting as molecular sieves. Yet other types of MOF might be used to store explosive gases in a safe environment or even sequester carbon dioxide and other pollutants from exhausts to reduce greenhouse gas emissions.

Fundamentally, the porous nature of these 3-D lattices endows those MOFs with a vast internal surface area relative to their overall volume, which gives them a significant advantage over many other types of storage material. Metal-organic surface areas can range from 1000 to 5000 m<sup>2</sup>/gm of material. Unfortunately, many MOFs are too fragile for practical purposes and either break apart or collapse when heated or put under pressure or chemical stress. As such, scientists have endeavored to find alternative building blocks that can be used to construct robust and stable MOFs. One such building block using porphyrin molecules hooked to metal ions have recently been the focus of investigations. Natural magnesium porphyrins are essentially the active sites in the photosynthesis molecule chlorophyll, while iron porphyrin is the active site of hemoglobin, the protein in our red blood cells responsible for transporting oxygen in our bodies.

A MOF based on an iron-porphyrin building block and known as PCN-

222(Fe) has been built and modified using a reduction reaction with the organic compound piperidine (Fig. 1). This system served as a model for intermediate species along relevant potential catalytic pathways. X-ray studies at XSD beamline 20-ID-B,C at the APS and Beamline 2-2 at the Stanford Synchrotron Radiation Light Source, together with UV-visible diffuse reflectance, infrared, and resonance Raman spectroscopy, show details of the internal geometry of this MOF.

The studies notably reveal the influence of pore size restrictions on the reactive state of the iron atoms within its porous structure. Choosing a particular chemical structure for the metalloporphyrin building blocks used to construct a MOF should allow researchers to adjust the size and shape of the pores that are produced in that material. The insights from this work will help others to determine what porphyrin characteristics they should use to make a MOF for given application, whether storage, separation or catalysis.

Intriguingly, PNC-222(Fe) itself contains two different types of channels, or pores. This means there are two types of binding sites for gas and other molecules that might diffuse into the MOF and become chemically attached to the interior surface. The analytical methods tested with this particular example MOF will be applicable to other MOFs with and without guest molecules held within the pores.

— David Bradley

**See:** Pavel Kucheryavy<sup>1</sup>, Nicole Lahanas<sup>1</sup>, Ever Velasco<sup>1</sup>, Cheng-Jun Sun<sup>2</sup>, and Jenny V. Lockard<sup>1\*</sup>, "Probing Framework-Restricted Metal Axial Ligand and Spin State Patterns in a Post-Synthetically Reduced Iron-Porphyrin-Based Metal-Organic Framework," *J. Phys. Chem. Lett.* **7**, 1109 (2016). DOI: 10.1021/acs.jpcllett.6b00302

**Author affiliations:** <sup>1</sup>Rutgers University, <sup>2</sup>Argonne National Laboratory

**Correspondence:**

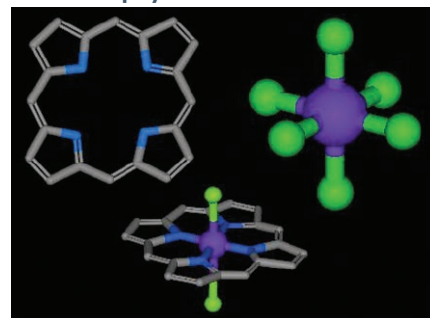
\* jlockard@rutgers.edu

J.V.L. would like to acknowledge support by the National Science Foundation under Grant No. DMR-1455127. Use of the Stan-

ford Synchrotron Radiation Lightsource, SLAC National Accelerator Laboratory, is supported by the U.S. Department of Energy (DOE) Office of Science-Basic Energy Sciences under Contract No. DE-AC02-76SF00515. This research used resources of the Advanced Photon Source, an Office of Science User Facility operated for the U.S. DOE Office of Science by Argonne National Laboratory, and was supported by the U.S. DOE under Contract No. DE-AC02-06CH11357, and the Canadian Light Source and its funding partners.

20-ID-B,C • XSD • Materials science, environmental science, chemistry • X-ray absorption fine structure, x-ray Raman scattering, micro x-ray absorption fine structure, microfluorescence (hard x-ray), time-resolved x-ray absorption fine structure, x-ray emission spectroscopy • 4.3-27 keV, 7-52 keV • On-site • Accepting general users •

### About Porphyrin



Nature impresses with the intricacy and precision in her designs, and teaches with the way she neatly applies a same basic concept to different situations. The molecule called **porphyrin** is one of those compounds with unique characteristics that are utilized cleverly at important points. A porphyrin is a rigid, square-planar molecule made of four pyrroles (a five-membered ring containing a nitrogen atom; image top left) connecting to form a larger ring. The molecule is stabilized by the aromatic character which extends over its entire structure. A porphyrin has four of its nitrogen atoms facing the center, which can capture a metal ion to form a very stable organometallic complex. It turns out that this property of the molecule is closely linked with the way it is used in living systems. When forming a complex, many metal ions accept six coordinating ligands to assume an octahedral (a shape made of two pyramids attached at the bases) configuration (image top right). The nitrogen atoms of a porphyrin occupy the four sites on the square plane of an octahedron, leaving two empty sites on the top and the bottom (bottom image). These two sites are then filled by the axial ligands, which are known to react in special ways. By using them, biological systems carry out a wide range of chemical reactions. Source: <http://www.org-chem.org/yuuki/porphyrin/porphyrin.html>



# PEPTIDE WRAPPING AIDS CATALYSIS

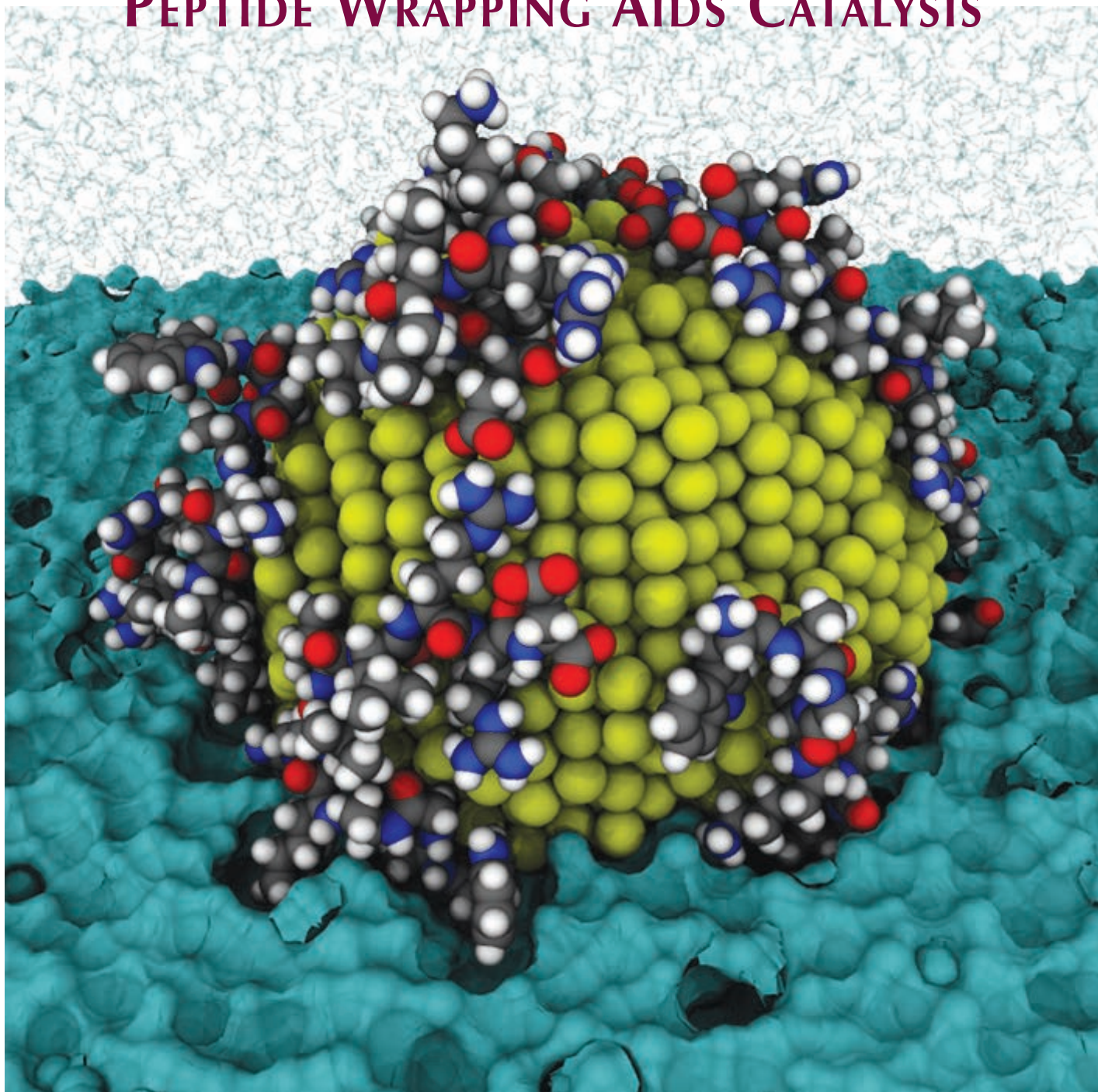


Fig. 1. Peptides wrap around a gold nanoparticle, controlling its growth. X-ray analysis has shown how different peptides affect the underlying nanoparticle structure. The information could help optimize the search for effective catalysts. Image: Zak Hughes

11-ID-C • XSD • Materials science, chemistry, physics • High-energy x-ray diffraction, diffuse x-ray scattering, pair distribution function • 105.1 keV • On-site • Accepting general users •



A peptide is a short chain of amino acids—a kind of “little cousin” to longer-chain proteins. In the body, peptides act as hormones and antibodies, and they are used by biologists to tag or identify proteins of interest. Perhaps surprisingly, they also find work in the field of nanofabrication. Certain peptides readily stick to metal nanoparticles, helping to control their growth. These peptide-wrapped nanoparticles have potential applications as catalysts for chemical reactions, but the factors that determine catalytic performance remain uncertain. An international team of researchers has now performed a detailed comparison of several catalyst candidates formed from different peptides attached to gold nanoparticles (Fig 1). Using atomic-scale structural data obtained at the APS, the researchers built three-dimensional models of the peptide-nanoparticle ensembles and found that those with looser peptide attachments performed better as catalysts. This knowledge could help optimize selection of peptides for particular catalysis applications.

In nanoparticle formation, peptides are added to a water-based solution containing metallic precursors. Reduction of the metallic precursor initiates nanoparticle nucleation and growth, where peptides serve the role of capping agents. That is, they attach to a single nanoparticle and prevent it from growing too large and precipitating out of solution. There are several advantages of using peptides in nanoparticle formation. The first is that the method works in water at room-temperature, as compared to other techniques that require heating and environmentally unfriendly organic solvents.

Another advantage of peptides is that they—and other biological molecules like DNA—offer a wide range of programmability. In trying to engineer a nanoparticle for a specific function, one can choose from a huge selection of peptides formed out of different combinations of the 20 commonly-used amino acids. As an example, a 10-amino-acid-long peptide can have over a trillion different sequences. Not all these peptide possibilities form attachments to nanoparticles, but researchers have identified large sets of peptides that work as capping agents for nanoparticles of different metals.

In regards to catalysis, different peptide-nanoparticle combinations are more effective than others, but the source of this variability is unknown. To investigate the properties that affect catalytic performance, the team selected 10 peptides that were previously studied for nanoparticle fabrication. Us-

ing standard procedures, the researchers grew gold nanoparticles with the different peptides. The resulting “PEPCANs” (peptide-promoted catalytic Au nanoparticles) were evaluated as catalysts in a common industrial reaction: 4-nitrophenol reduction. The different PEPCANs helped drive the reaction with varying success, with the most effective catalysts achieving a factor of two increase in performance.

The researchers then submitted each PEPCAN to a detailed structural analysis. Samples were exposed to 115-keV x-rays from the XSD 11-ID-C beamline at the APS and the diffraction patterns were recorded. The peaks in the data corresponded to the face-centered cubic structure that is common for gold crystals. However, the peaks were broadened, suggesting that some of the gold atoms were out of place. To resolve the internal structure, the team performed simulations that identified a model nanoparticle that reproduces the observed diffraction pattern. The results revealed that the peptide interaction produces disorder in the crystal structure at the surface of the nanoparticle. The model nanoparticle was subsequently used in a second round of simulations that determined the likely placement of peptides on the surface. This complete reconstruction was done for each of the PEPCANs.

The final step involved looking for correlations between the catalytic performance and different structural properties of the PEPCANs. The one property that showed the strongest

correlation was the so-called contact score, which is a measure of how long amino acids in a given peptide bind to the gold surface. The PEPCANs with the weakest contact score (least binding) were those that performed best as catalysts. Using this correlation, one could potentially find even better catalysts by searching through the vast peptide library and finding candidates that are predicted to have very weak contact scores. Such a search would be computationally intense, but it would be faster than the current method of trial and error. — *Michael Schirber*

**See:** Nicholas M. Bedford<sup>1,2,3\*</sup>, Zak E. Hughes<sup>4</sup>, Zhenghua Tang<sup>3,5</sup>, Yue Li<sup>6</sup>, Beverly D. Briggs<sup>3†</sup>, Yang Ren<sup>7</sup>, Mark T. Swihart<sup>6</sup>, Valeri G. Petkov<sup>8</sup>, Rajesh R. Naik<sup>2\*\*</sup>, Marc R. Knecht<sup>3\*\*\*</sup>, and Tiffany R. Walsh<sup>4\*\*\*\*</sup>, “Sequence-Dependent Structure/Function Relationships of Catalytic Peptide-Enabled Gold Nanoparticles Generated under Ambient Synthetic Conditions,” *J. Am. Chem. Soc.* **138**, 540 (2016). DOI: 10.1021/jacs.5b09529

**Author affiliations:** <sup>1</sup>National Institute of Standards and Technology, <sup>2</sup>Air Force Research Laboratory, <sup>3</sup>University of Miami, <sup>4</sup>Deakin University, <sup>5</sup>South China University of Technology, <sup>6</sup>State University of New York at Buffalo, <sup>7</sup>Argonne National Laboratory, <sup>8</sup>Central Michigan University

**Correspondence:**

\* nicholas.bedford@nist.gov

\*\* rajesh.naik@us.af.mil

\*\*\* knecht@miami.edu

\*\*\*\* tiffany.walsh@deakin.edu.au

This work was partially supported by the Air Force Office for Scientific Research (M.R.K. and T.R.W., Grant No. FA9550-12-1-0226; R.R.N., AFOSR LRIR) and U.S. Department of Energy (DOE)-Basic Energy Sciences grant DESC0006877 (V.G.P.). N.M.B. acknowledges fellowship support from the National Research Council Research Associateship award during the initial experiments of this study. T.R.W. thanks veski for an Innovation Fellowship. This research used resources of the Advanced Photon Source, a U.S. DOE Office of Science User Facility operated for the DOE Office of Science by Argonne National Laboratory under Contract No. DE-AC02-06CH11357

# TRACKING THE ACTIVE COPPER SITES IN A CATALYTIC MINERAL

When copper ions exchange into a zeolite, the mineral becomes catalytically active for the selective reduction of nitrogen oxides, which are harmful gaseous environmental pollutants found in engine exhaust, into benign nitrogen. Copper-loaded zeolite catalysts are currently in commercial use on diesel vehicles, but many questions remain about the interplay between the composition of the zeolite, the reaction conditions, the active sites, and the catalytic mechanism. To understand zeolite dynamics, researchers performed *operando* x-ray absorption spectroscopy (XAS) experiments on Cu-zeolites under reaction conditions at the MR-CAT insertion device and bending magnet beamlines at the APS and correlated the results with first-principles simulations. The findings reveal the importance of reaction conditions to the active site properties and structure, providing critical insight that is needed to tune catalytic activity.

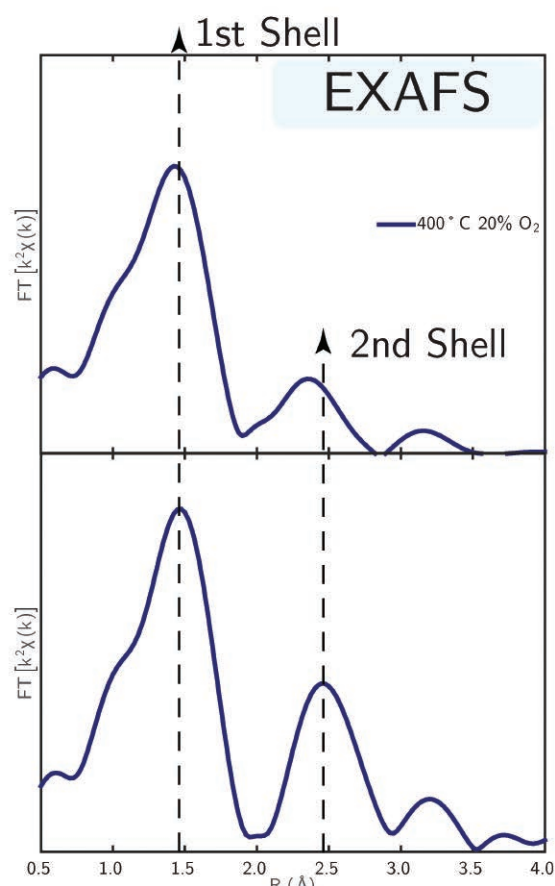


Fig. 1. EXAFS spectra and corresponding first-principles models distinguish two structural types of zeolite-supported Cu<sup>II</sup> ions.

The particular zeolite of interest is SSZ-13, a nanoporous aluminosilicate constructed of 4-, 6-, and 8-membered rings of silicon, aluminum, and oxygen atoms. Copper ions associate with the framework aluminum centers. The structure of Cu depends on the number and arrangement of aluminum within the lattice and the oxidation state of the copper ions, among other factors. To determine the relationship between composition, structure, and catalytic function, the researchers synthesized and characterized zeolites with a range of elemental composition. They used the XAS technique at the MR-CAT 10-ID-B and 10-BM-A,B beamlines to measure the oxidation state of the copper species and evaluate their local geometric and electronic structures, as a function of the zeolite compositions. Complementary x-ray absorption near edge absorption (XANES) data, also collected at the MR-CAT beamline, was used to assess the copper oxidation state. The researchers identified and enumerated two types of aluminum sites within the zeolite that determine the Cu active site structure: the 1Al site, a six-membered ring with one aluminum atom and five silicon atoms, and the 2Al site, a six-membered ring with two aluminum atoms and four silicon.

Next, the researchers loaded copper ions into the zeolites and, again with XAS and XANES, studied how these metal ions embedded themselves into the zeolite mineral. They found that the copper atoms preferred exchanging at the 2Al site, where they took the form of Cu<sup>II</sup> ions to exchanging at the 1Al site, where they exchanged in the Cu<sup>II</sup>OH state. To assess the effect of environmental conditions on the Cu oxidation state and coordination environment, the researchers ran a series of first-principles simulations at varying conditions, including temperature, pressure, and reactant chemical potential.

The researchers compared these data to those collected experimentally, and found quantitative agreement.

To assess zeolite behavior in a real-world scenario, the researchers next studied  
*"Copper" cont'd. on page 100*

# CARBON-ENCAPSULATED IRON PARTICLES FOR LESS EXPENSIVE, MORE EFFICIENT FUEL CELLS

Fuel cells are an important power source for an array of vehicles and other applications. However, the lack of cost-effective catalysts has prevented the use of fuel cells from spreading more widely. Iron-based non-precious metal catalysts have long been seen as an abundant, low-cost alternative to state-of-the-art platinum-based catalysts. Yet, such iron-based catalysts have remained out of reach due to challenges in identifying exactly which compound in the iron-containing, non-precious metal catalyst facilitates the oxygen reduction reaction. Researchers working at the APS used a sequential chlorine/hydrogen gas treatment to selectively remove all of the components of an iron-based catalyst that were not involved in oxygen reduction, leaving a single type of particle as the catalyst's active form: a carbon-encapsulated iron nanoparticle. This discovery may improve catalyst function and lower production costs, leading to more efficient, less expensive fuel cells that can be useful in vehicles and other power-hungry applications such as backup power generators and satellites.

Researchers from the University of Illinois at Urbana-Champaign, Knox College, Argonne, Yeshiva University, and Kyushu University (Japan) demonstrated that a high-temperature (900° C) gas-phase chlorine treatment deactivated non-precious metal catalysts, while a high-temperature (900° C) hydrogen treatment completely reactivated the catalysts (Fig. 1). They observed that iterative rounds of the treatments decreased the heterogeneity of the catalyst, which then allowed for the direct characterization of the species present in the deactivated and reactivated catalysts.

The team of researchers then used Mössbauer and x-ray absorption spectroscopy (XAS), carried out at the 9-BM-B,C beamline and MR-CAT

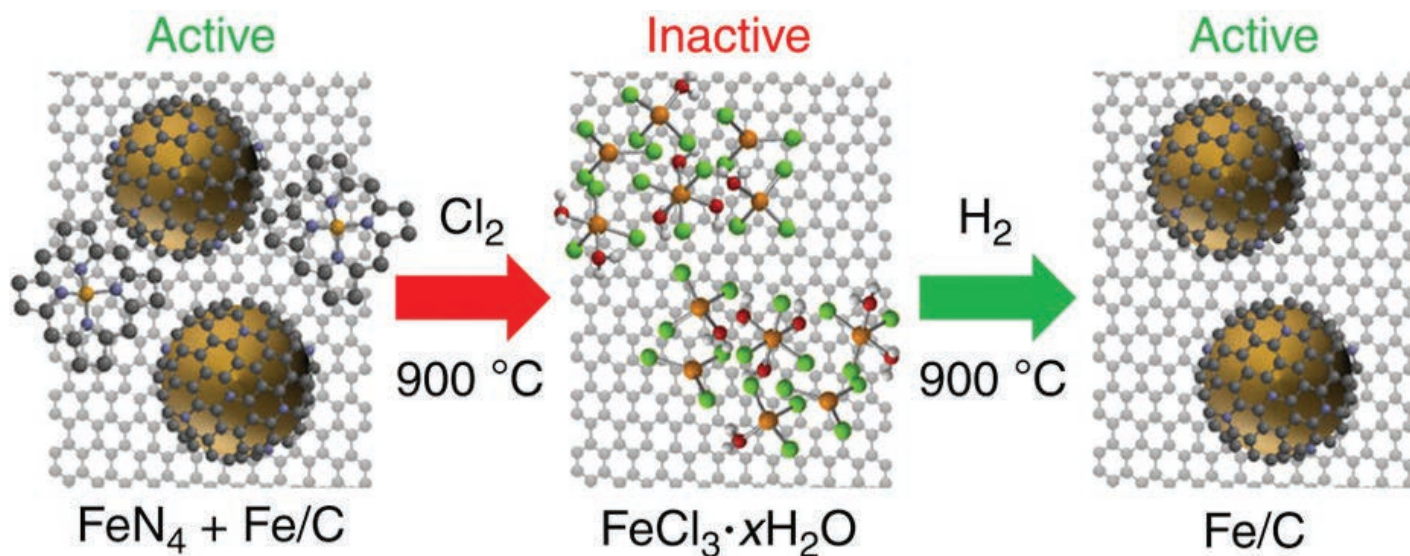


Fig. 1. Effect of a sequential high-temperature chlorine/hydrogen treatment on the activity of an iron-containing non-precious metal catalyst. Metallic Fe and  $\text{FeN}_4$  species are converted into dispersed  $\text{FeCl}_3 \cdot x\text{H}_2\text{O}$  that is then reformed into reduced Fe species by the  $\text{H}_2$  treatment. The absence of  $\text{FeN}_4$  sites in the  $\text{H}_2$ -treated catalyst indicates that these sites are not required for the observed oxygen reduction reaction activity.

beamline 10-BM-A,B at the APS, to identify the active species in the catalyst. The former technique was used to investigate nuclear structure using the absorption and re-emission of gamma rays, while the latter technique was used to deduce the local atomic environment of a compound by analyzing the way the compound absorbs a spectrum of x-rays.

The researchers observed that the untreated iron-based catalyst contained  
*"Fuel" cont'd. on page 100*



*“Copper” cont’d. from page 98*

copper speciation under the same working conditions used to catalyze the reduction of nitrogen oxide species. They used a custom-built reactor at the APS designed to collect XAS spectra under catalytic conditions, with the goal of determining the oxidation state of copper sites during the selective catalytic reaction of NO with ammonia to N<sub>2</sub>. Again, the researchers performed simulations under the same set of conditions for comparison. The structure and dynamics of the copper ions were found to depend strongly on the reaction environment. For example, Cu ions are solvated by water at ambient conditions, but the hydration is lost at higher temperatures. Cu ions are also solvated by NH<sub>3</sub> under NO reduction conditions, which importantly cause mobilization of copper ions within the zeolite framework.

Together, the experimental data and simulations were used to develop a self-consistent picture of the reaction mechanism on copper ions in different local zeolite environments. Overall turnover rates and activation energies of the NO reduction reactions were similar on isolated Cu ions, regardless of zeolite framework. These findings have implications for the other chemistries catalyzed by Cu ions exchanged in zeolites, including the partial oxidation of methane, a process that may someday be harnessed by scientists to generate chemicals and fuels from abundant raw materials. — *Erika Gebel Berg*

**See:** Christopher Paolucci<sup>1</sup>, Atish A. Parekh<sup>2</sup>, Ishant Khurana<sup>2</sup>, John R. Dilorio<sup>2</sup>, Hui Li<sup>1</sup>, Jonatan D. Albarracin Caballero<sup>2</sup>, Arthur J. Shih<sup>2</sup>, Trunojoyo Anggara<sup>1</sup>, W. Nicholas Delgass<sup>2</sup>, Jeffrey T. Miller<sup>2</sup>, Fabio H. Ribeiro<sup>2</sup>, Rajamani Gounder<sup>2</sup>, and William F. Schneider<sup>1\*</sup>, “Catalysis in a Cage: Condition-Dependent Speciation and Dynamics of Exchanged Cu Cations in SSZ-13 Zeolites,” *J. Am. Chem. Soc.* **138**, 6028 (2016).

DOI: 10.1021/jacs.6b02651

**Author affiliations:** <sup>1</sup>University of Notre Dame, <sup>2</sup>Purdue University

**Correspondence:** \* wschneider@nd.edu

Financial support was provided by the National Science Foundation GOALI program

under award number 1258715- CBET (Purdue) and 1258690-CBET (Notre Dame), and The Patrick and Jane Eilers Graduate Student Fellowship for Energy Related Research. We would like to thank Victor J. Cybulskis (Purdue) for his help in performing XAS experiments at the APS. We thank the Center for Research Computing at Notre Dame, and EMSL, a U.S. Department of Energy (DOE) Office of Science user facility sponsored by the Office of Biological and Environmental Research and located at Pacific Northwest National Laboratory, for support of computational resources. This research used resources of the Advanced Photon Source, an Office of Science User Facility operated for the U.S. DOE Office of Science by Argonne National Laboratory, and was supported by the U.S. DOE under Contract No. DE-AC02-06CH11357, and the Canadian Light Source and its funding partners.

10-BM-A,B • MR-CAT • Materials science, chemistry, environmental science, physics • x-ray absorption fine structure • 4-32 keV • On-site • Accepting general users •

10-ID-B • MR-CAT • Materials science, environmental science, chemistry • X-ray absorption fine structure, time-resolved x-ray absorption fine structure, microfluorescence (hard x-ray) • 4.3-27 keV, 4.8-32 keV, 15-65 keV • On-site • Accepting general users •

*“Fuel” cont’d. from page 99*

a combination of FeN<sub>4</sub> and reduced iron (Fe) species, making the direct characterization of the active species impossible, as expected. However, following the chlorine treatment, the Mössbauer and XAS analyses indicated that the metallic Fe and FeN<sub>4</sub> species were converted into dispersed FeCl<sub>3</sub>•xH<sub>2</sub>O, which is then reformed by the H<sub>2</sub> treatment into iron nanoparticles encapsulated by a carbon shell that helps stabilize the reactivated catalyst (Fig.1).

The researchers also used XAS, along with transmission electron microscopy, to measure the size of the nanoparticles. Their size indicates that the nanoscale features of the iron particles in the catalyst might contribute to their activity. Further experiments using x-ray photoelectron spectroscopy indicated that the surface of the carbon-encapsulated iron nanoparticles were doped with nitrogen, which the researchers speculated could also increase the oxygen reducing activity of the catalyst.

These findings may allow for the design and synthesis of purer forms of non-precious metal oxygen reduction catalysts with a higher loading of the active species. The research team will explore optimizing the catalyst nanoparticles by changing their size and increasing their abundance, using multi-component nanoparticles, and doping the surface of the catalyst with a variety of elements.

Catalyst enhancements derived from these experiments could possibly bring down the price of fuel cells, making them cost-effective for more types of applications, including powering automobiles. — *Chris Palmer*

**See:** Jason A. Varnell<sup>1</sup>, Edmund C.M. Tse<sup>1</sup>, Charles E. Schulz<sup>2</sup>, Tim T. Fister<sup>3</sup>, Richard T. Haasch<sup>1</sup>, Janis Timoshenko<sup>4</sup>, Anatoly I. Frenkel<sup>4</sup>, and Andrew A. Gewirth<sup>1,5\*</sup>, “Identification of carbon-encapsulated iron nanoparticles as active species in non-precious metal oxygen reduction catalysts,” *Nat. Commun.* **7**, 12582 (2016).

DOI: 10.1038/ncomms12582

**Author affiliations:** <sup>1</sup>University of Illinois at Urbana-Champaign, <sup>2</sup>Knox College, <sup>3</sup>Argonne National Laboratory, <sup>4</sup>Yeshiva University, <sup>5</sup>Kyushu University, **Correspondence:** \* agewirth@illinois.edu

J.A.V. acknowledges a Buhrke Fellowship from the Chemistry Department at the University of Illinois at Urbana-Champaign. E.C.M.T. acknowledges a Croucher Foundation Scholarship. The authors thank the U.S. National Science Foundation (NSF) (Grant CHE-1309731) for support of this research. A.I.F. and J.T. acknowledge support from the U.S. NSF Grant CHE-1534184. This work was carried out in part in the Frederick Seitz Materials Research Laboratory Central Facilities, which are partially supported by the U.S. Department of Energy (DOE) (DE-FG02-07ER46453 and DE-FG02-07ER46471). T.T.F. was supported by the Joint Center for Energy Storage Research, an Energy Innovation Hub funded by the U.S. DOE Office of Science. XAFS measurements at MR-CAT were supported by the Department of Energy and the MR-CAT member institutions. The authors thank Jing Liu for her help with XAS measurements at beamline 5-BM-D. This research used resources of the Advanced Photon Source, a U.S. DOE Office of Science User Facility operated for the DOE Office of Science by Argonne National Laboratory under contract no. DE-AC02-06CH11357.

# BUBBLES GET IN THE WAY OF ELECTROLYSIS

**E**lectrolysis of water into hydrogen and oxygen is a promising way to store the energy from sunlight as a fuel that can be used on demand to generate electricity or replace hydrocarbons in transportation. Small semiconductor-based devices that perform this conversion have shown great practical potential. By examining the real-time progress of electrolysis in a micron-scale system by means of high-speed x-ray imaging at the APS, researchers have found that the generation of hydrogen bubbles on catalytic surfaces can significantly inhibit further hydrogen evolution. The research indicates that the physical design of electrolytic devices is an essential factor in maximizing their efficiency.

A prototypical device to turn sunlight into hydrogen combines a p-type silicon wafer, which captures photons and generates charge carriers, with a platinum catalyst that speeds electrolysis. The device is immersed in a suitable solution, such as sulfuric acid. The catalyst is essential, as electrolysis would be unacceptably slow without it, but the placement of the platinum in relation to the silicon can inhibit photon capture. Moreover, generation of hydrogen bubbles creates a three-phase system, with solid, liquid, and gaseous components, and this complex environment strongly influences the kinetics of the reactions taking place within it.

A team of researchers from the University of Arkansas and Argonne set out to investigate how differences in the physical arrangement of the platinum affects the rate of hydrogen production. To isolate the effects of the semiconductor-metal surface on the gas-liquid-solid interface defining the bubble, they used a highly-doped silicon electrode to drive the reaction by simply cutting the silicon into small chips, 1.5 mm by 30 mm, and on them placed platinum in a variety of patterns, from a continuous layer to discrete squares from 3 to 30  $\mu\text{m}$  on a side. The chips were sealed into small vials filled with sulfuric acid and equipped with Kapton windows to allow passage of x-rays.

Working at XSD beamline 32-ID-C, the team used high-speed phase-contrast imaging, with micron-scale resolution and a rate of 10  $\mu\text{sec}$  per frame, to track the production and evolution of hydrogen at the surface of the catalyst.

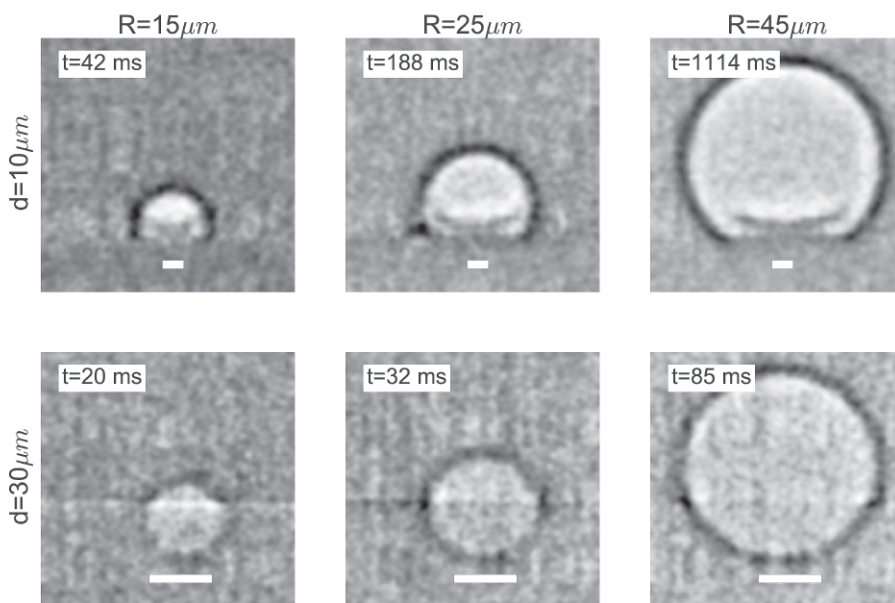


Fig. 1. Phase-contrast x-ray images show bubbles of hydrogen created by electrolysis forming on and clinging to small platinum squares measuring 10  $\mu\text{m}$  (upper sequence) and 30  $\mu\text{m}$  (lower sequence) on a side.

In experiments on silicon chips with a continuous platinum coating, they observed two modes of bubble production: nucleation and growth of a single bubble, which detached from the surface on reaching a certain size; and nucleation of small clusters of bubbles, which merged before detaching. In either case, the researchers inferred the hydrogen production rate from the sizes of the growing bubbles. The electrolysis rate followed Tafel kinetics, a standard formulation that quantifies the exponentially increasing electrolysis current with linear increases in electrochemical potential beyond the required thermodynamic potential (the overpotential).

The team then examined silicon

chips coated with small, discrete platinum squares. They developed software to recognize the edges of bubbles, infer their radius, and thus estimate hydrogen production as a function of time. In these experiments, the rate of hydrogen production was significantly less than predicted by Tafel kinetics. Rather than increasing exponentially with a linear increase in overpotential, the gas production rate plateaued, indicating that the process was limited by the bubble blocking reactant access to the catalyst. The smallest catalysts showed considerable irregularity around the plateau value, as individual bubbles detached and new ones began to grow.

*"Bubbles" cont'd. on page 103*

# A MATERIALS SOLUTION TO BREAKING THE OXYGEN-HYDROGEN BOND

**H**ydrogen has vast promise as an energy carrier. It can be burned for heat or react in a fuel cell to make electricity, with water as the only byproduct. But free hydrogen doesn't exist naturally. To make a hydrogen economy work, we need a way to produce the gas safely and affordably. Water, which is made of oxygen and hydrogen, would be an attractive hydrogen source if the oxygen-hydrogen bond could be easily broken. But splitting this bond, which is done electrochemically, takes a lot of energy. It quickly wears out the catalysts in the process and requires expensive noble metals such as gold or platinum. Less expensive metal compounds, such as cobalt and molybdenum sulfides, can also be used as catalysts, but the cobalt compounds tend to be unstable and the molybdenum compounds are not catalytically active enough to be economically attractive. Materials scientists used the Advanced Photon Source to probe the structure of various cobalt- and molybdenum-sulfur compounds, and found that an amorphous material called a chalcogel that combined all three elements overcame these limitations. The research could ultimately lead to better, less expensive catalysts that bring the hydrogen economy closer to reality.

Researchers from Argonne, Northwestern University and the University of Ljubljana (Slovenia) first took commercially available crystalline molybdenum sulfide and cobalt sulfide and compared them to the amorphous molybdenum- and cobalt sulfur chalcogels ( $\text{MoS}_x$ ,  $\text{CoS}_x$  and  $\text{CoMoS}_x$ , where  $x = 4$  to 6), using the APS to determine their structure and catalytic activity. Comparing the crystalline sulfides with the chalcogels revealed significant structural differences: the chalcogels had irregular numbers of sulfurs connected to each cobalt or molybdenum atom, and the distances between the sulfur and metal atoms varied quite a bit; in contrast, the crystalline sulfides had regular structures and molecular organization.

The team used XSD beamline 12-BM-B to perform extended x-ray absorption fine structure analysis on the chalcogels. And they used XSD beamline 11-ID-B to do rapid acquisition-pair distribution function analyses. The APS x-ray source produces a high density of very bright photons, making it easy to get good data for the measurements in just a few minutes of experimentation, and the beam lines are set up for just these types of experiments. In this case, the data showed that the  $\text{CoS}_x$  chalcogel was structured quite differently than the  $\text{CoMoS}_x$

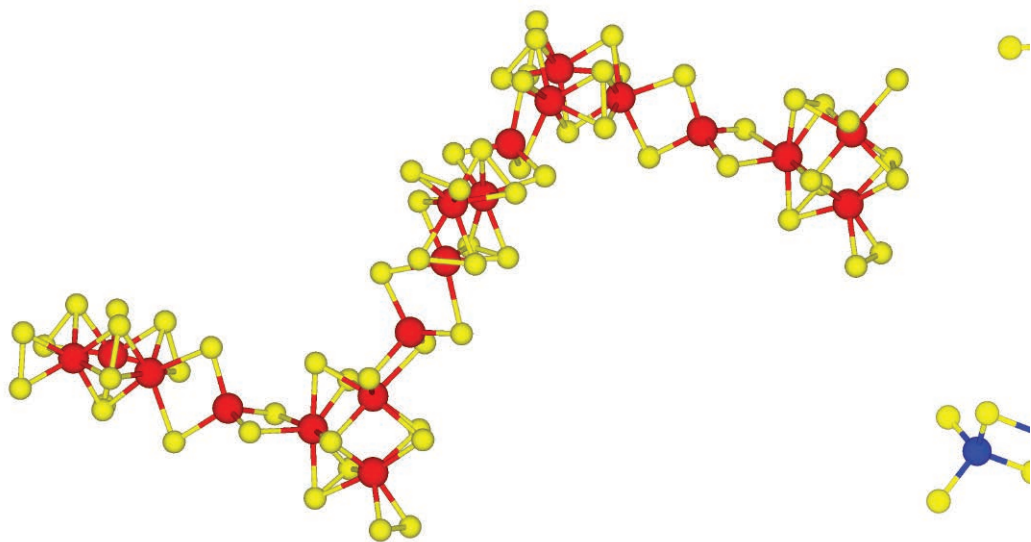


Fig. 1. The molybdenum chalcogel (a) is much more densely structured than the cobalt chalcogel (b), which has an open structure with an occasional cobalt-cobalt connection. The cobalt-molybdenum-sulfur chalcogel (c) consists of  $\text{Mo}_3\text{S}_{13}$  clusters connected by  $\text{CoS}_6$  octahedra in a moderately dense, compact arrangement.



chalcogel; both compounds tended to show the cobalt closely associated with six sulfurs, but the CoSx showed many cobalt-cobalt interactions as well. Those interactions were very unusual in the CoMoSx chalcogel (Fig. 1).

The overall structure of all the compounds was porous, with lots of surface area upon which catalytic splitting of water could take place.

Through other experiments, the team found that molybdenum sulfide is 35 to 40 times more stable than cobalt sulfide. But combining the molybdenum and cobalt together in the CoMoSx chalcogels increased cobalt-sulfur stability by five times without reducing the stability of the molybdenum sulfur clusters at all. This MoCoSx chalcogel was catalytically active in both acidic and alkaline environments. This is important because local acidity and alkalinity vary dramatically at the nanoscale whenever water molecules are split.

The work showed that a well-designed chalcogel that blends the highly

Nemanja Danilovic<sup>1</sup>, Subrahmanyam S. Kota<sup>2</sup>, Kee-Chul Chang<sup>1</sup>, Bostjan Genorio<sup>1,3</sup>, Dusan Strmcnik<sup>1</sup>, Vojislav R. Stamenkovic<sup>1</sup>, Mercurio G. Kanatzidis<sup>1,2\*</sup> and Nenad M. Markovic<sup>1\*\*</sup>, "Design of active and stable Co-Mo-Sx chalcogels as pH-universal catalysts for the hydrogen evolution reaction," *Nat. Mater.* **15**, 197 (February 2016).

DOI: 10.1038/NMAT4481

**Author affiliations:** <sup>1</sup>Argonne National Laboratory, <sup>2</sup>Northwestern University, <sup>3</sup>University of Ljubljana

**Correspondence:**

\* m-kanatzidis@northwestern.edu

\*\* nmmarkovic@anl.gov

This work was supported by the U.S. Department of Energy (DOE) Office of Science-Basic Energy Sciences, Division of Materials Sciences, under Contract No. DE-AC02-06CH11357. This research used resources of the Advanced Photon Source, a DOE Office of Science User Facility operated for the DOE Office of Science by Argonne National Laboratory under Contract No. DE-AC02-06CH11357.

*"Bubbles" cont'd. from page 101*

Close examination of x-ray images revealed that hydrogen bubbles grew considerably larger than the size of the catalyst squares, and clung on for an unexpectedly long time before detaching (Fig. 1). The researchers argue that in acidic conditions, the bubble surface adsorbs protons and acquires a net positive charge, creating an electrostatic attraction to the silicon cathode. Estimates of the molecular current density corresponding to hydrogen production were consistent with the idea that when a large bubble remains stuck to a small catalyst, the electrolysis reaction is mostly confined to the perimeter of the platinum square. In the interior, where only a thin liquid layer exists between the bubble and the electrode, hydrogen generation is largely suppressed.

The results of these studies thus lead to a cost-benefit problem. Covering an electrode with a patchwork of discrete catalyst sections leaves the rest of the silicon exposed for the task of capturing photons, but the formation and persistence of bubbles on the small catalyst areas inhibits electrolysis. The researchers conclude that the physical organization of materials can be as significant as the specific catalyst material for the efficient conversion of sunlight into hydrogen. — *David Lindley*

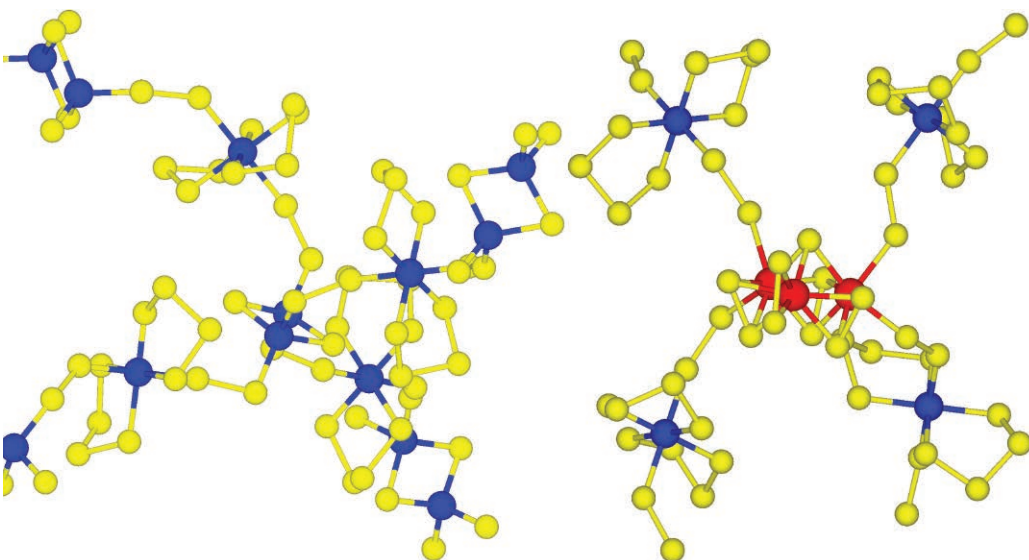
**See:** Robert H. Coridan<sup>1\*</sup>, Zebulun G. Schichtl<sup>1</sup>, Tao Sun<sup>2</sup>, and Kamel Fezzaa<sup>2</sup>, "Inhibition of Tafel Kinetics for Electrolytic Hydrogen Evolution on Isolated Micron Scale Electrocatalysts on Semiconductor Interfaces," *ACS Appl. Mater. Inter.* **8**, 24612 (2016).

DOI: 10.1021/acsami.6b07729

**Author affiliations:** <sup>1</sup>University of Arkansas, <sup>2</sup>Argonne National Laboratory

**Correspondence:** \* rcoridan@uark.edu

R.H.C. is supported in part by the University of Arkansas Office of Research and Economic Development. We thank Alex Deriy at the 32-ID-B beamline for his assistance in setting up the beamline experiment. This research used resources of the Advanced Photon Source, a U.S. Department of Energy (DOE) Office of Science User Facility operated for the DOE Office of Science by Argonne National Laboratory under Contract DE-AC02-06CH11357.



catalytic CoSx building blocks with the more stable MoSx units can create a low cost alternative to noble metal catalysts. This makes them promising candidates for hydrogen evolution reactions. The researchers next plan to try other, more common transition metals such as iron and nickel, in order to improve the reactivity and stability of the chalcogels. — *Kim Krieger*

**See:** Jakub Staszak-Jirkovský<sup>1</sup>, Christos D. Malliakas<sup>1,2</sup>, Pietro P. Lopes<sup>1</sup>,

111-ID-B • XSD • Chemistry, environmental science, materials science • Pair distribution function, high-energy x-ray diffraction • 58.66 keV, 86.7 keV • On-site • Accepting general users •

12-BM-B • XSD • Materials science, polymer science, chemistry, physics, environmental science • X-ray absorption fine structure, general diffraction, x-ray reflectivity, fluorescence spectroscopy, small-angle x-ray scattering, wide-angle x-ray scattering • 4.5-23 keV, 10-30 keV • On-site • Accepting general users •

(No Model.)

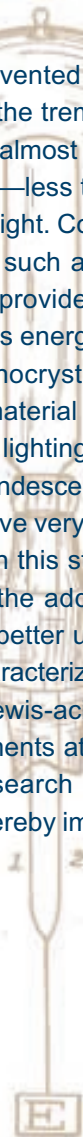
T. A. EDISON.  
INCANDESCENT LAMP.

No. 425,761.

Patented Apr. 15, 1890.

# TRANSFORMING HOW WE LIGHT THE WORLD

**I**n 1879, Thomas Edison invented a commercially practical incandescent lightbulb. Despite the tremendous success of Edison's invention and the passage of almost 150 years, modern incandescent lightbulbs are not energy efficient—less than 10% of the energy supplied to the bulb is converted to visible light. Compared with incandescent lighting, however, solid-state lighting such as the light-emitting diode (LED) lasts about 50 times longer and provides three or more times the luminous efficacy while using 80% less energy. For the solid-state lighting application, a semiconductor nanocrystal ("quantum dot") of indium phosphide (InP) is a promising material because its properties have the potential to give blue LED-based lighting the appropriate color rendering to compete aesthetically with incandescent lighting. However, current synthesis methods of this material have very poor photoluminescence yields, less than 1%. The researchers in this study report achieving yields with InP particles of 10% to 50% by the addition of a Lewis acid (cadmium oleate or zinc oleate). To form a better understanding of the mechanism behind this improvement, they characterized the structure and composition of both the core and surface of Lewis-acid-modified InP quantum dots by using x-ray absorption measurements at the APS, as well as other characterization techniques. This research could lead to more widespread adoption of solid-state lighting, thereby improving global energy efficiency.



WITNESSES:

*E. B. Rowland*  
*Edward. H. Pyall*

INVENTOR:

*Thomas A. Edison*  
*By Richard H. Dyer*  
*Atty*

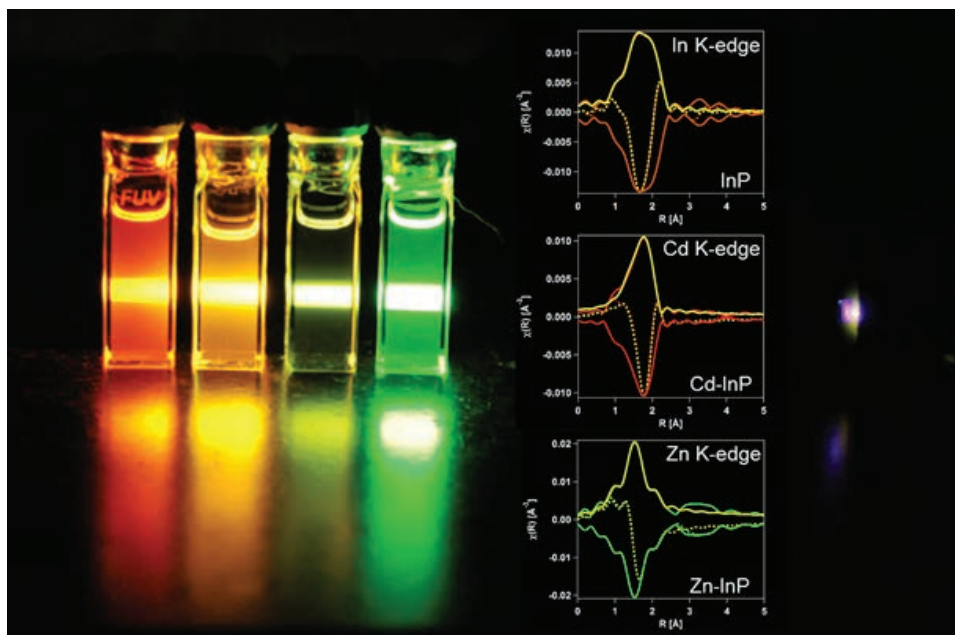


Fig. 1. Color tunability of modified InP quantum dots (left). The extended x-ray absorption fine structure spectra on the right show experimental and quantitative fits (yellow curves) of the first coordination shell. Spectra obtained at the APS.

For synthesis of the InP quantum dots,  $P(\text{SiMe}_3)_3$  is injected into a hot solution ( $315^\circ\text{C}$ ) of indium oleate. Particle nucleation and growth occurs rapidly, where the continuous size increase is monitored by ultraviolet-visible spectroscopy. The InP solution is post-synthetically modified through thermal treatment with metal carboxylates. Heating zinc or cadmium oleate with InP quantum dots at  $200^\circ\text{C}$  for several hours resulted in photoluminescence quantum yields of 10%-20% with zinc and 20%-50% with cadmium, significant improvements over that with current synthesis methods. Notably, in addition to photoluminescence turn-on, the authors found that the absorbance and emission maxima blue-shifted with zinc, and red-shifted with cadmium.

The possibility of cadmium/zinc alloying or shell growth were considered as explanations for the perceived optical shifts, but structural characterization indicated that particle sizes were conserved post-modification. Additionally, the InP lattice was retained as indicated by powder x-ray diffraction. Purification of these luminescent particles revealed the presence of  $\text{In}_2\text{O}_3$  by-products, indicating the likely displacement of surface indium carboxylates that could thermally decompose into  $\text{In}_2\text{O}_3$  nanoparticles. Thus, the authors investigated a mechanism in which exogenous metals

exchanged with surface indium.

Transmission and fluorescence x-ray absorption measurements of the samples were acquired at the MR-CAT 10-BM-A,B beamline at the APS. Figure 1 shows examples of extended x-ray absorption fine structure spectra collected for each metal species in the quantum dots. The orange, red, and green curves, which represent indium, cadmium, and zinc, respectively, show the distance to the nearest neighbor atoms (x-axis) with contributions to peak shape from coordination number. Quantitative fitting (yellow curves) required a combined environment of metal oxygen and metal phosphide in order to accurately represent the experimental data, verifying the authors' hypothesis that  $\text{Zn}^{2+}$  and  $\text{Cd}^{2+}$  were coordinated to the particle surfaces (Fig. 1). In addition, chemical etching experiments demonstrated that metal carboxylates could be stripped from the surface, and the photoluminescence would be effectively quenched. These analyses indicate that cadmium and zinc carboxylates predominantly displace native  $\text{In}^{3+}$  from the quantum dot surface to bind to phosphide, and that this effect is largely responsible for the observed photoluminescence boost.

A key finding was the ability to tune the absorbance and emission profiles of the quantum dots with no apparent

change in particle size. Importantly, the ability to color tune the luminescence of InP quantum dots without an associated change in particle size may offer a versatile strategy to access novel materials for solid-state lighting. Further examination of other metal ions than  $\text{Zn}^{2+}$  and  $\text{Cd}^{2+}$  is essential to formulate a complete picture regarding the mechanism and scope of the improved yield and tunability. — *Joseph E. Harmon*

**See:** Jennifer L. Stein<sup>1</sup>, Elizabeth A. Mader<sup>2</sup>, and Brandi M. Cossairt<sup>1\*</sup>, "Luminescent InP Quantum Dots with Tunable Emission by Post-Synthetic Modification with Lewis Acids," *J. Phys. Chem. Lett.* **7**, 1315 (2016).

DOI: 10.1021/acs.jpclett.6b00177

**Author affiliations:** <sup>1</sup>University of Washington, <sup>2</sup>Yale University,

**Correspondence:**

\* cossairt@chem.washington.edu

This research was supported by the 3M Non-Tenured Faculty Award and the National Science Foundation Grant CHE-1552164. MR-CAT operations are supported by the U.S. Department of Energy (DOE) and the MR-CAT member institutions. This research used resources of the Advanced Photon Source, a U.S. DOE Office of Science User Facility operated for the DOE Office of Science by Argonne National Laboratory under Contract No. DE-AC02-06CH11357.



# STRAINING IS BETTER FOR CATALYTIC REACTIONS

Catalysts speed chemical reactions without undergoing change themselves. Reactions that might have been too slow to be worthwhile on their own often become economically attractive once a catalyst is added; they're essential to the fast, efficient operations of oil refineries and industrial chemical manufacturing. Most catalysts work by providing a favorable spot for a reaction to take place. They may bring the two reactants closer together in the correct orientation, polarize a bond making it more likely to break, or form intermediate chemical species that would not otherwise form naturally. Catalysts often include precious metals such as gold and platinum. Because the activity of a catalyst depends on its surface area, industrial processes already maximize the surface area to reduce the amount of catalyst necessary to shepherd the reaction. To make the process any better, other methods will be needed. Using several techniques at the APS and the Argonne Center for Nanoscale Materials, researchers took an atomic-level look at how reactions strain the surface of gold nanoparticles acting as catalysts in the decomposition of ascorbic acid (Vitamin C). This is the first step in understanding how strain—deformation of the normal pattern of atoms—on the surface of a catalyst could make it better at facilitating chemical reactions.

Gold is a common catalyst, often used in catalytic combustion of fuels, removing noxious hydrogen sulfide and sulfur dioxide from more useful gases, and speeding oxidation in many different reactions. It also has properties similar to heavy metals that can poison biological systems by, for example, interfering with ascorbic acid, but is generally safe to work with. Gold is also very stable and electron-dense, so it reflects x-rays well and made a good system with which to study a new phenomenon.

The team of researchers from the University of California, San Diego, Argonne, the SLAC National Accelerator Laboratory, the Deutsches Elektronensynchrotron (Germany) and the University of Melbourne obtained three-dimensional (3-D) images of gold nanoparticles in the process of catalyzing ascorbic acid decomposition. They used Bragg coherent diffractive imaging at the XSD 34-ID-C x-ray beamline at the APS. The 34-ID-C beamline is the only one at APS specifically designed for Bragg coherent diffractive imaging. The x-ray source is tens of meters distant from the detector, and the line has very bright x-rays that are exactly in phase with each other (coherent). The researchers mixed gold nanoparticles with ascorbic acid and took measurements for more than an hour, starting before the reaction began and running until after it was over.

*"Straining" cont'd. on page 108*

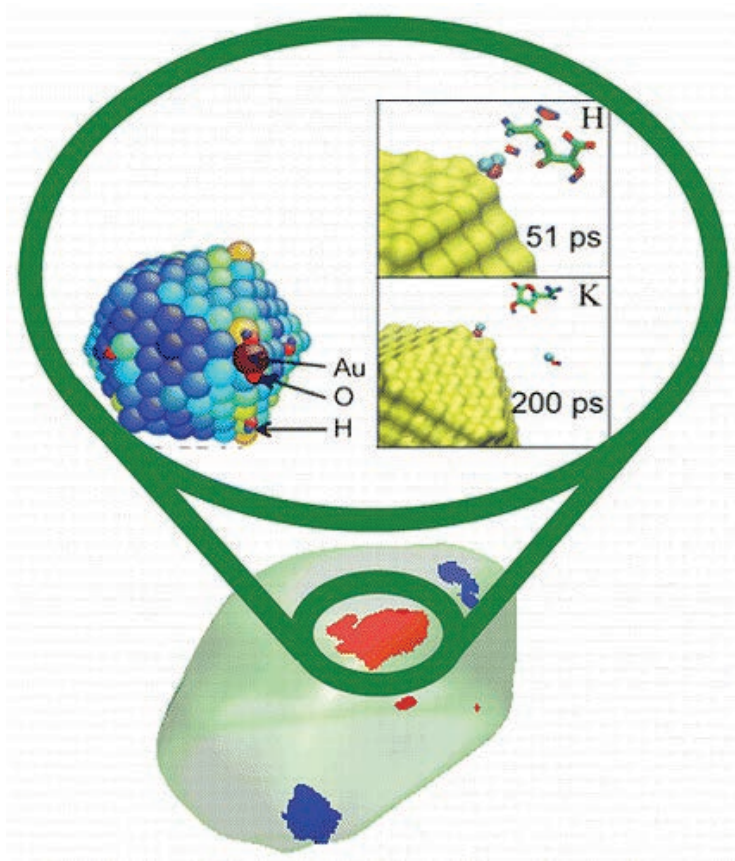


Fig.1. The expanded section of the image shows a strained section of the gold nanoparticle interacting with an ascorbic acid atom. Each shade of color indicates displacement of gold atoms, in 0.1 angstrom units; the dark blue atoms are not displaced at all, the light blue atoms are displaced 0.1A, the green atoms 0.2A, the yellow atoms 0.3A, the orange 0.4A and the maroon 0.6A. Image: A. Ulvestad et al. From *J. Phys. Chem. Lett.* **7**, 3008 (2016). © 2016 American Chemical Society

# WHAT MAKES A GIANT MOLECULE STABLE?

**P**olyoxometalates (POMs) are giant molecules, a few nanometers across, with various morphologies and compositions. Created in multi-hour chemical syntheses from small molecular reactants, they can have tunable redox and surface properties that make them useful as catalysts, as well as electric and magnetic properties with possible applications in nanomaterials. Until now, however, the formation mechanism of POMs has been poorly understood. By combining small-angle x-ray scattering at the APS and neutron scattering techniques, a team of researchers has now provided a clearer picture of the structure of these complex species and has also inferred a formation process that goes through three distinct stages, leading to crystallization. The findings should make it easier to devise synthesis routes for creating POMs with desirable customized characteristics.

The researchers chose to study a representative POM consisting of a silicon-molybdenum oxide core within an iron-molybdenum oxide shell (Fig. 1). The shell contained 72 molybdenum atoms and 30 iron atoms, and measured 2.5 nm in diameter. They used small-angle x-ray scattering (SAXS) at XSD x-ray beamlines 12-ID-B and 12-ID-C,D at the APS, along with elastic and inelastic neutron scattering conducted at the U.S. Department of Energy's (DOE's) Spallation Neutron Source at ORNL, to follow the synthe-

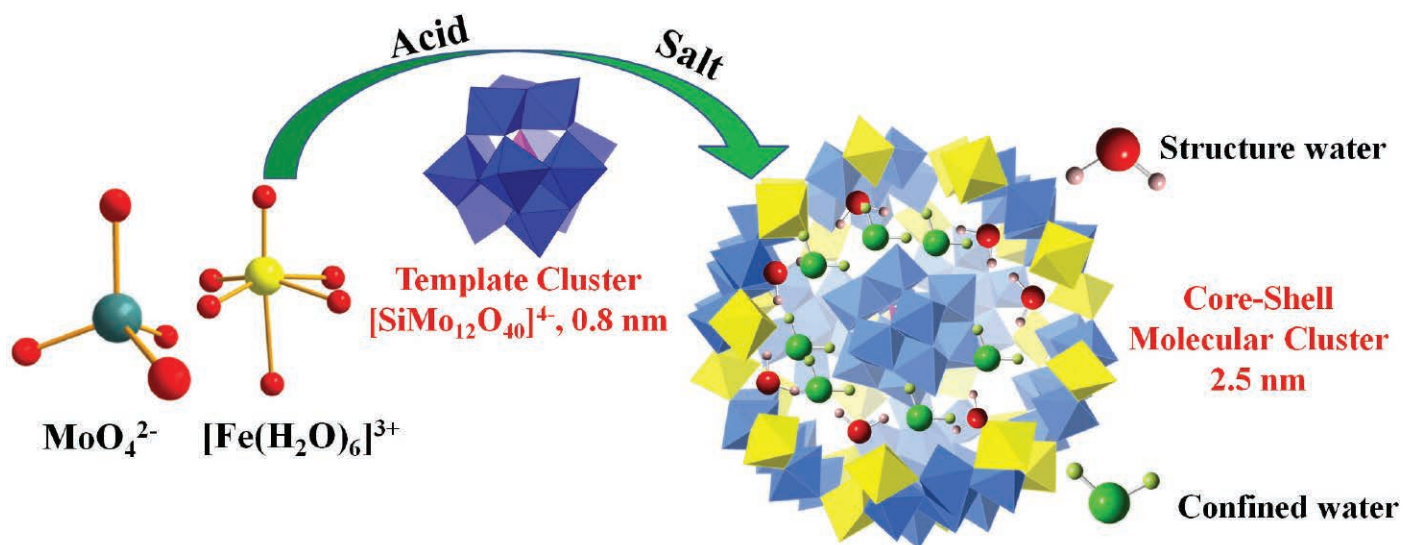


Fig. 1. Schematic of the reaction mechanism leading to the formation a giant polyoxometalate. The core component, a complex silicon-molybdenum oxide, reacts with molybdenum oxide and iron ion in acidic solution. Over the course of 24 hours or more, a shell forms around the core and the core-shell structure eventually crystallizes.

The researchers from Oak Ridge National Laboratory (ORNL), the University of Tennessee, and Argonne National Laboratory focused their attention on POMs with a core-shell structure. The shells of such POMs consist of transition metals linked into a framework connected together by oxo ligands. When such a shell encloses a core, typically also consisting of metal oxides, it results in what is known as a Keggin structure. Synthesis of POMs follows a standard route, in which the ionic core structure, al-

ready made, is placed in an acidic solution of transition metal oxides or ions. The core-shell structure precipitates out as a salt in a process that can occupy 24 hours. Mass spectrometry of samples from such reactions, taken at various times, have given some clues as to the nature of intermediate structures involved in the synthesis, but the sample extraction and preparation steps necessary for such studies cast doubt on whether the structures found are truly building blocks of the finished POM.

sis reaction *in situ*.

The SAXS measurements, on reactant solutions in quartz capillaries, provided a spatial resolution up to 40 nm and time resolution better than 0.1 s. First, the team studied POMs that had crystallized in their final state in order to determine the location of the core within the shell — not an easy task since the orientation of each core within its shell is random. By using an iterative modeling procedure that computed SAXS signals in which the cores had all possible alignments and were displaced by small distances from the centers of the shells, the researchers found a best fit to the result when the cores were strictly central in the structures.

*"Giant" cont'd. on page 108*

*“Straining” cont’d. from page 106*

From this data, they constructed the first detailed 3-D pictures of the strain a gold particle goes through during a chemical reaction on its surface.

But the researchers could only see the gold, not the ascorbic acid, using x-rays during the reaction. They needed another piece of data to understand what was actually happening to the ascorbic acid at the strained sites on the gold. So they compared their data with simulations run by researchers at the Center for Nanoscale Materials. The simulations let them identify exactly what the ascorbic acid was doing when the gold was strained in a specific configuration, down to 10-nm resolution. From that data, the researchers could start to guess which strains facilitated the decomposition reaction.

Because the strain corresponds to the position of atoms on the gold surface, and because gold catalyzes reactions by putting chemicals in a good position to react, it might be possible to enhance gold’s catalytic activity by changing how it is strained. That might increase the number of spots on the gold’s surface favorable to reactions, or even show chemists how to encourage certain reactions and discourage others.

The researchers say the next step would be to look at many different crystals, both of gold and other catalysts, to better understand how strain states affect catalysis. — *Kim Krieger*

**See:** Andrew Ulvestad<sup>1,2\*</sup>, Kiran Sasikumar<sup>2</sup>, Jong Woo Kim<sup>1,2</sup>, Ross Harder<sup>2</sup>, Evan Maxey<sup>2</sup>, Jesse N. Clark<sup>3,4</sup>, Badri Narayanan<sup>2</sup>, Sanket A. Deshmukh<sup>2</sup>, Nicola Ferrier<sup>2</sup>, Paul Mulvaney<sup>5</sup>, Subramanian K.R.S. Sankaranarayanan<sup>2</sup>, and Oleg G. Shpyrko<sup>1</sup>, “*In Situ* 3D Imaging of Catalysis Induced Strain in Gold Nanoparticles,” *J. Phys. Chem. Lett.* **7**, 3008 (2016).

DOI: 10.1021/acs.jpclett.6b01038

**Author affiliations:** <sup>1</sup>University of California, San Diego, <sup>2</sup>Argonne National Laboratory, <sup>3</sup>SLAC National Accelerator Laboratory, <sup>4</sup>Deutsches Elektronensynchrotron (DESY), <sup>5</sup>University of Melbourne

**Correspondence:** \* aulvestad@anl.gov

This work was supported by the U.S. Department of Energy (DOE) Office of Science-Basic Energy Sciences, under Contract DESC0001805. O.G.S. and A.U. are grateful to the UCSD Inamori Fellowship. J.N.C. gratefully acknowledges financial support from the Volkswagen Foundation. P.M. thanks the ARC for support through LF100100117. Use of the Center for Nanoscale Materials and Advanced Photon Source, both Office of Science user facilities, was supported by the U. S. DOE Office of Science-Basic Energy Sciences, under Contract No. DE-AC02-06CH11357.

34-ID-C • XSD • Materials science, physics • Coherent x-ray scattering • 5-15 keV • On-site • Accepting general users •

*“Giant” cont’d. from page 107*

Time-resolved SAXS studies made it possible to track the formation of the POMs over many hours. About 2.5 h after the reaction started, signs of shell formation began to appear. (When the reactants were mixed together without the cores, no shell structures appeared even after 24 h). The concentration of shells gradually increased, but at the 19-h mark, structure factor analysis indicated that they were systematically staying away from each other. Only after that time, when the shell concentration had increased to a presumably critical value, did the structures begin to collect together in crystalline form. Measurements of some samples about two weeks after synthesis showed the same structure, indicating the long-term stability of the POMs in aqueous solutions.

While the SAXS experiments revealed how the metal ions came together in the structures, the neutron scattering studies focused on the presence and location of water molecules. Two significant results emerged. Quasi-elastic scattering indicated the presence of water molecules that were mobile, but more sluggish than those in plain water. The researchers concluded that there are water molecules confined between the core and the shell, but able to move within this restricted space. In addition, inelastic peaks in the neutron scattering spectra pointed to the presence of fixed water molecules, which the team inferred are incorporated into molecular bridges that link core and shell. Both types of water molecule, they say, contribute to

the structural stability and longevity of the POMs.

This new insight into the mechanism by which POMs form should make it easier to devise structures with different compositions and symmetries, opening up possibilities for applications such as novel chemical catalysts or single-molecule magnets for digital memories. — *David Lindley*

**See:** Panchao Yin<sup>1\*</sup>, Bin Wu<sup>2</sup>, Eugene Mamontov<sup>1</sup>, Luke L. Daemen<sup>1</sup>, Yongqiang Cheng<sup>1</sup>, Tao Li<sup>3</sup>, Soenke Seifert<sup>3</sup>, Kunlun Hong<sup>1</sup>, Peter V. Bonnesen<sup>1</sup>, Jong Kahk Keum<sup>1</sup>, and Anibal J. Ramirez-Cuesta<sup>1</sup>, “X-ray and Neutron Scattering Study of the Formation of Core-Shell-Type Polyoxometalates,” *J. Am. Chem. Soc.* **138**, 2638 (2016). DOI: 10.1021/jacs.5b11465

**Author affiliations:** <sup>1</sup>Oak Ridge National Laboratory, <sup>2</sup>University of Tennessee, <sup>3</sup>Argonne National Laboratory

**Correspondence:** \* yinp@ornl.gov

P.Y. is grateful to the support of Clifford G. Shull Fellowship from the Neutron Sciences Directorate of ORNL. The research performed in BL-2 (BASIS) and BL-16B (VISION) at ORNL’s Spallation Neutron Source was sponsored by the Scientific User Facilities Division-Basic Energy Sciences, U.S. DOE. The sample preparation and initial SAXS study in the x-ray lab were conducted at the ORNL Center for Nanophase Materials Sciences, which is a DOE Office of Science User Facility. Oak Ridge National Laboratory is supported by the Office of Science of the U.S. DOE under Contract No. DE-AC05-00OR22725. This research used resources of the Advanced Photon Source, a U.S. DOE Office of Science User Facility operated for the DOE Office of Science by Argonne National Laboratory under Contract No. DE-AC02-06CH11357.

12-ID-B • XSD • Chemistry, materials science, life sciences, polymer science, physics • Small-angle x-ray scattering, grazing incidence small-angle scattering, wide-angle x-ray scattering, grazing incidence diffraction • 7.9-14 keV • On-site • Accepting general users •

12-ID-C,D • XSD • Chemistry, physics, materials science • Small-angle x-ray scattering, grazing incidence small-angle scattering, wide-angle x-ray scattering, surface diffraction • 4.5-40 keV • On-site • Accepting general



# IN THIS CONTAMINATION-RESISTANT CATALYST, EVERY PT ATOM IS AN ACTIVE SITE

Every material has a weakness; platinum (Pt) has at least two. It is expensive and it is easily contaminated by carbon monoxide (CO). Carbon monoxide poisoning has dogged the makers of fuel cells and hydrogen conversion devices for electric cars, emergency power generators, portable electronics, and more since the first prototypes appeared. Contamination in fuel cells can diminish performance via sluggish electrode kinetics, conductivity, and mass transfer, which results in a dramatic performance drop, particularly at low temperatures. With cost in mind, researchers have recently worked to define catalysts with the least possible concentration of Pt. It turns out that it doesn't take much Pt to make a Pt catalyst—just a few isolated atoms embedded in a sea of other materials. These catalysts are called “single-atom alloys,” or SAAs. Researchers used the APS to test SAAs of Pt embedded in copper, and found that the catalyst is not only low in Pt, but also addresses the problem of CO poisoning. Thanks to this new catalyst configuration, industrial processes that depend on Pt can run more efficiently and at lower cost. This work presents a solution to address CO contamination within a solution to address Pt concentration; it is a clever two-for-one.

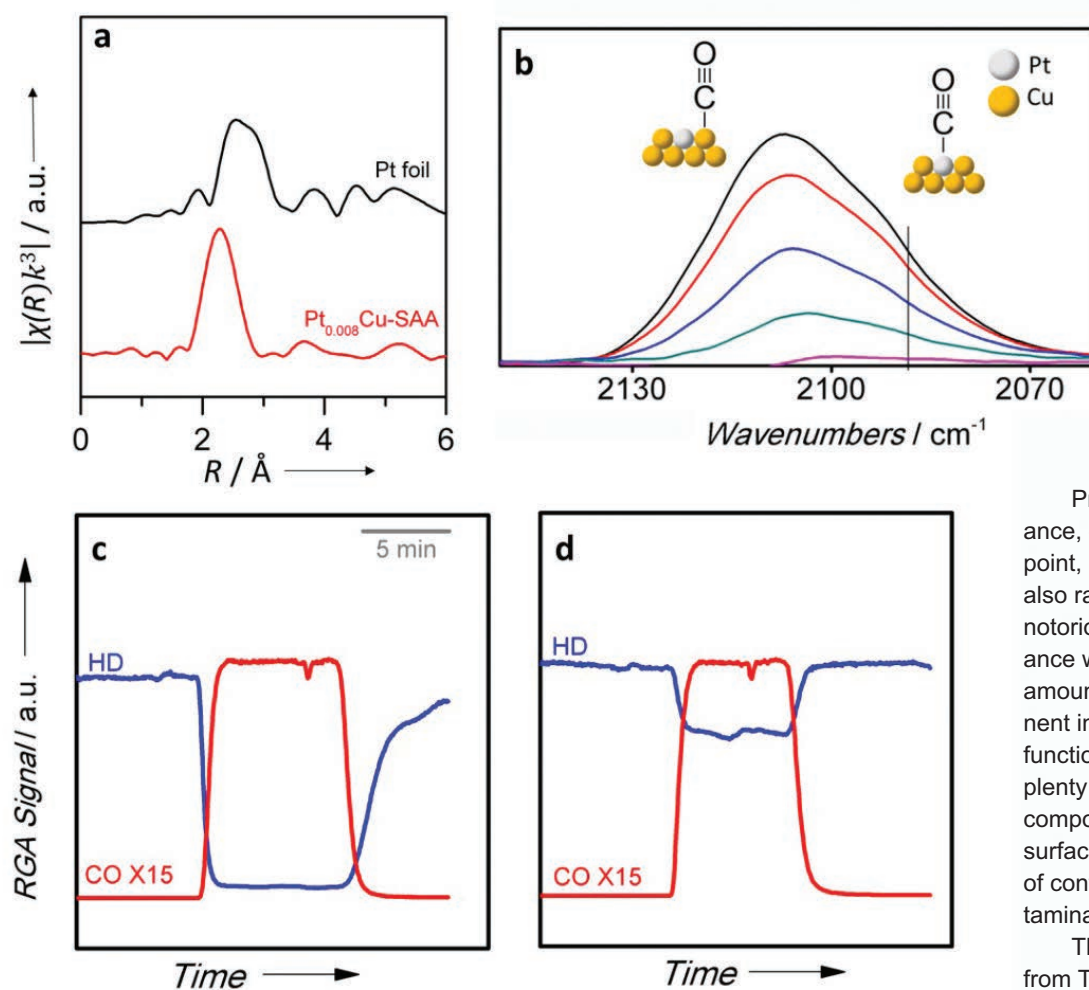


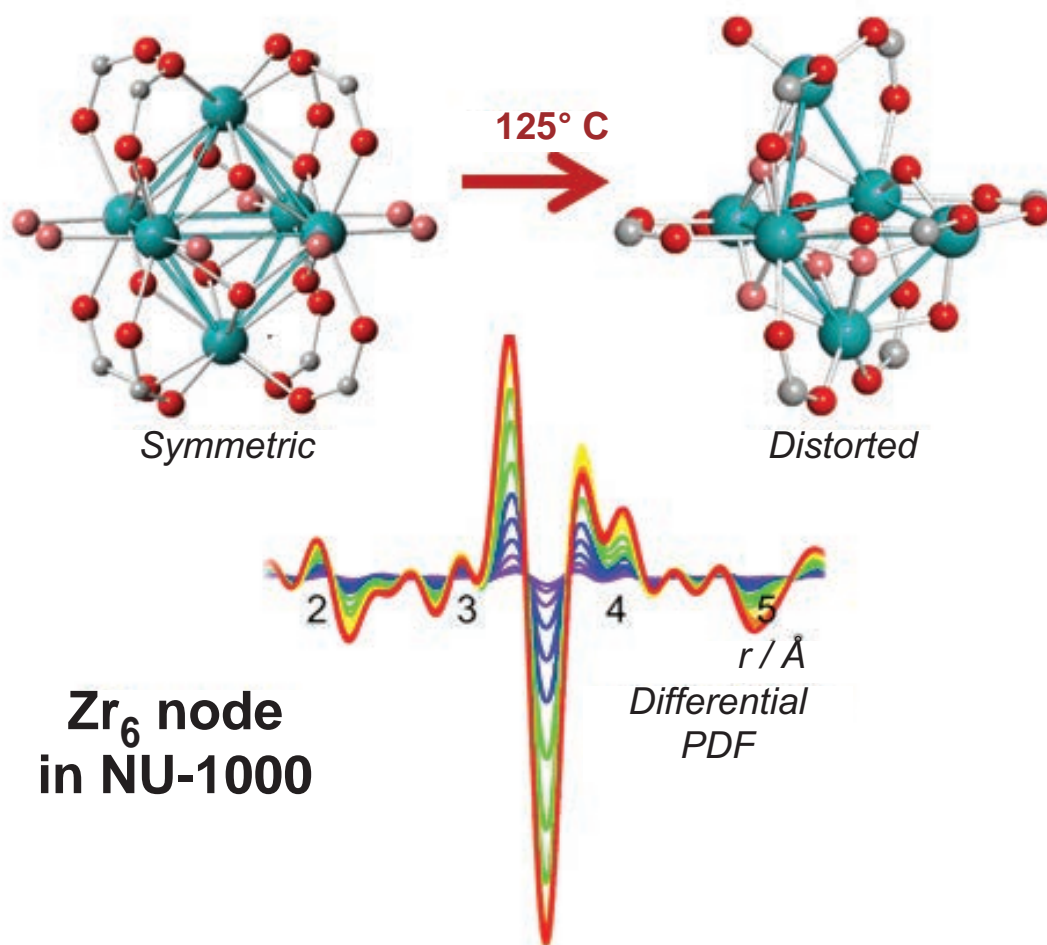
Fig. 1. a) Fourier transform of  $k^3$ -weighted Pt  $L_{III}$  EXAFS of Pt foil and  $Pt_{0.008}Cu$ -SAA in CO and  $H_2$  gases mixture plotted in R-space. b) IR spectra in the carbonyl range of pre-reduced  $Pt_{0.008}Cu$ -SAA. Real catalyst data for isothermal  $H_2$ - $D_2$  exchange over (c) Pt-NP and (d)  $Pt_{0.008}Cu$ -SAA at  $150^\circ\text{C}$ .

Prized for its corrosion resistance, density, ductility, high melting point, and chemical stability, Pt is also rare and difficult to mine. It is notorious for losing catalytic performance when exposed to even trace amounts of CO, a common component in hydrocarbon processing. To function well, a catalyst must provide plenty of surface sites for reaction components to interact, but a high surface material also provides plenty of contiguous sites for potential contamination.

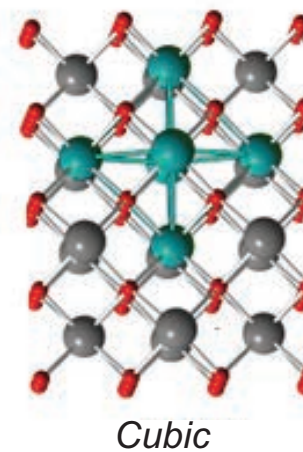
The researchers in this study, from Tufts University, Argonne, and the University of South Carolina, determined the binding strength of CO

*“Active” cont’d. on page 112*

# BETTER THAN PERFECT



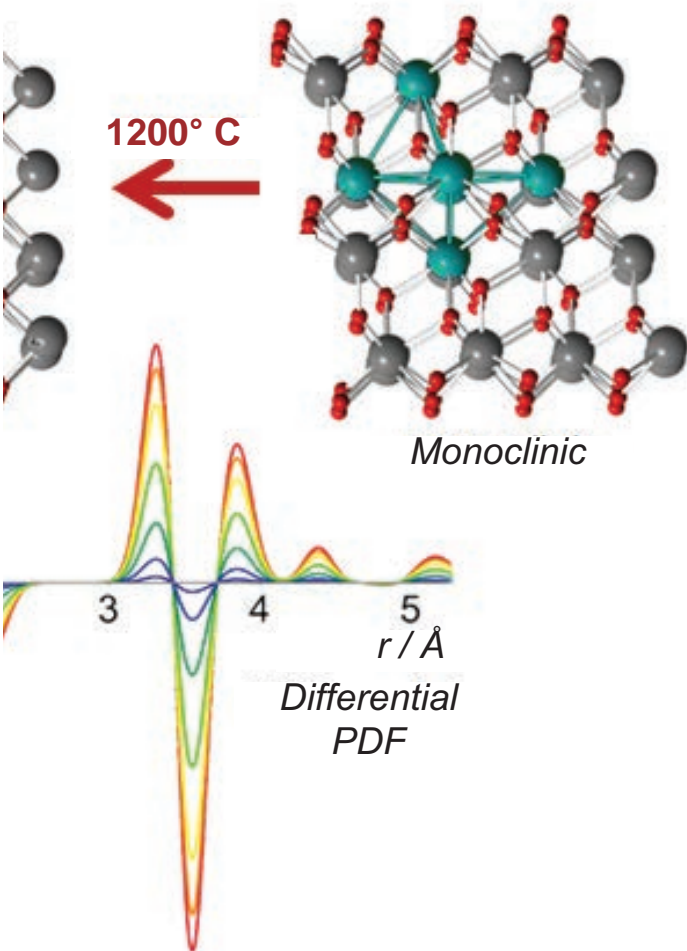
**$\text{Zr}_6$  node  
in NU-1000**



**Cubic**

**$\text{ZrO}_2$  Bulk**

Fig. 1. Beamline 11-ID-B data show “metal oxide” nodes present in UiO-66 and NU-1000. The distortions in their structures that appear as they are heated are similar to the well-known changes seen in the bulk mineral zirconia.



Understanding the parallels between how metal oxides behave as bulk compounds and how they behave as the few atom cluster components of important porous materials known as metal-organic frameworks (MOFs) could point to new ways to use these materials for gas storage, separation, and catalysis in the chemical industry, and even for destroying chemical weapons such as toxic nerve agents. Researchers working at the APS have recorded *in situ* -ray scattering data suitable for pair distribution function (PDF) and diffraction analyses and coupled this with density functional theory (DFT) computations to investigate the behavior of two related MOFs, UiO-66 and NU-1000. Both of these MOFs contain the same “metal oxide” clusters of six metal ions, that are connected in different ways by organic linker molecules. The metal can be zirconium (Zr) or hafnium (Hf). These experiments showed that the metal-oxide clusters distort when heated to temperatures at which these MOFs are often used. Having an atomic-scale picture for the mechanism by which these structural changes occur, and why, will be critical to applications of these and putatively other MOFs that contain these same metal-oxide clusters linked in a variety of ways. This research also underscores some fundamental aspects about the structural characteristics of the metal oxide units in MOFs.

Metal-organic frameworks are synthetic materials, solids in which individual metal ions or metal oxide clusters are connected together in a three-dimensional lattice linked by organic molecules. The specific metals, their characteristics, and the size and shape of the organic linkers endow different MOFs with different properties. The long linkers can leave hollows, pores, and channels within the MOFs that, like their natural mineral counterparts the zeolites, can absorb, or more technically adsorb, small molecules that diffuse into the channels and stick to the surface inside.

This adsorption has led to research focusing on potential applications of MOFs including safe storage of hazardous gases such as hydrogen. The specific chemistry of a given MOF makes it selective for the adsorption of some chemicals and not others, such that some MOFs can be used as molecular-scale sieves to separate one gas from another, oxygen from air for instance. The reactivity of the MOF components can also make their internal

*“Perfect” cont’d. on page 112*



*“Active” cont’d. from page 109*

to isolated Pt atoms, and Pt atoms in clumps, surrounded by copper (Cu) metal. They reacted these configurations with small amounts of CO in real time at elevated temperatures and observed how the materials changed and at what temperatures the CO desorbed, using a variety of infrared, electron, and x-ray techniques (Fig. 1), including x-ray absorption spectroscopy (XAS) performed at XSD beamline 12-BM-B at the APS. As expected, CO adsorbed more weakly to Pt-Cu SAAs than Pt-Cu alloys that contained Pt clusters.

In traditional Pt catalysts, CO readily attaches to Pt atoms, blocking sites needed for hydrogen activation. But groups of metal atoms function differently from single atom sites. Larger CO molecules trying to squeeze onto a single Pt atom is rather like a large pickup negotiating a parking space meant for compacts—it doesn’t happen easily. And with fewer Pt atoms blocked by CO molecules, more are available to facilitate reactions.

These results suggested that Pt SAAs should work more efficiently in hydrogen activation and oxidation reactions than other Pt catalyst configurations. The researchers then performed tests to determine if what was suggested would actually work, and they were rewarded with a positive result. With the same CO concentration in the gas phase, the Pt-Cu SAA yielded 12 times more hydrogen than Pt nanoparticle catalysts. — *Jenny Morber*

**See:** Jilei Liu<sup>1</sup>, Felicia R. Lucci<sup>1</sup>, Ming Yang<sup>1</sup>, Sungsik Lee<sup>2</sup>, Matthew D. Marcinkowski<sup>1</sup>, Andrew J. Therrien<sup>1</sup>, Christopher T. Williams<sup>3</sup>, E. Charles H. Sykes<sup>1\*\*</sup>, and Maria Flytzani-Stephanopoulos<sup>1\*</sup>, “Tackling CO Poisoning with Single-Atom Alloy Catalysts,” *J. Am. Chem. Soc.* **138**, 6396 (2016).

DOI: 10.1021/jacs.6b03339

**Author affiliations:** <sup>1</sup>Tufts University, <sup>2</sup>Argonne National Laboratory, <sup>3</sup>University of South Carolina

**Correspondence:** \* maria.flytzani-stephanopoulos@tufts.edu  
\*\* charles.sykes@tufts.edu

This work supported by the National Science Foundation (CBET-1159882 to J.L.), and the U.S. Department of Energy (DOE, DE-

FG02-05ER15730 to A.J.T. and M.F.-S. and DE-FG02-10ER16170 to F.R.L. and E.C.H.S.). M.D.M. thanks the Tufts University Department of Chemistry for an Illumina Fellowship. This research used resources of the Advanced Photon Source, a U.S. DOE Office of Science User Facility operated for the DOE Office of Science by Argonne National Laboratory under Contract No. DE-AC02-06CH11357.

*“Perfect” cont’d. from page 111*

surface area a reaction bed for catalytic reactions where two molecules may be adsorbed and react, or a single molecule, such as a toxic nerve agent, might be adsorbed and find itself converted into harmless decomposition products when heated inside the MOF.

Critically, data obtained at the APS on XSD beamline 11-ID-B by researchers from the Inorganometallic Catalyst Design Center, a DOE Energy Frontier Research Center, show that for the particular “metal oxide” nodes present in UiO-66 and NU-1000 prepared by researchers at Northwestern University, the distortions in their structures that appear as they are heated are similar to the well-known changes seen in the bulk mineral zirconia, zirconium dioxide. Indeed, the distortions can be mapped to the different crystalline, polymorphic forms of zirconia. However, the data show that these distortions occur in the MOF framework at much lower temperatures than occur in the bulk mineral. This difference can be explained as being due to the nanoscopic nature of MOF nodes as opposed to what is essentially an infinite, three-dimensional lattice within the bulk zirconia crystals. Complementary computational studies by researchers at the University of Minnesota further illuminated this behavior

Given that it is the strength and stability of the chemical bond between zirconium and oxygen atoms that inspired the use of the “zirconium oxide” cluster to make more stable MOFs, it is surprising that the cluster distorts at such mild temperatures and without obvious change to the three-dimensional MOF structure. This finding could be critical to the ongoing use of these MOFs in catalysis and other applications. The distortion of the structure of the nodes within a MOF from their regular, symmetric octahedral arrangement is intriguing and does not lead to the

collapse of the structure, rather the opposite. Thermal treatment of NU-1000 distorts the nodes, which changes the chemistry of the surface available for catalytic reactions, leading to a twenty-fold increase in activity of this material for the hydrolytic degradation of chemical warfare agents, including G-type nerve agents.

It is likely that the cluster nodes of other MOFs may well undergo distortions on heating to quite mild temperatures. Some of those distortions may hold the key to new useful properties as seen here for the NU-1000 distortion. What is emphasized from the perspective of fundamental science is that the metal oxide units in MOFs are not the rigid, rock-solid structural units they had been assumed to be. — *David Bradley*

**See:** Ana E. Platero-Prats<sup>1</sup>, Andreas Mavrandonakis<sup>2</sup>, Leighanne C. Gallington<sup>1</sup>, Yangyang Liu<sup>3</sup>, Joseph T. Hupp<sup>3</sup>, Omar K. Farha<sup>3,4</sup>, Christopher J. Cramer<sup>2</sup>, and Karena W. Chapman<sup>1\*</sup>, “Structural Transitions of the Metal-Oxide Nodes within Metal-Organic Frameworks: On the Local Structures of NU-1000 and UiO-66,” *J. Am. Chem. Soc.* **138**, 4178 (2016).

DOI: 10.1021/jacs.6b00069

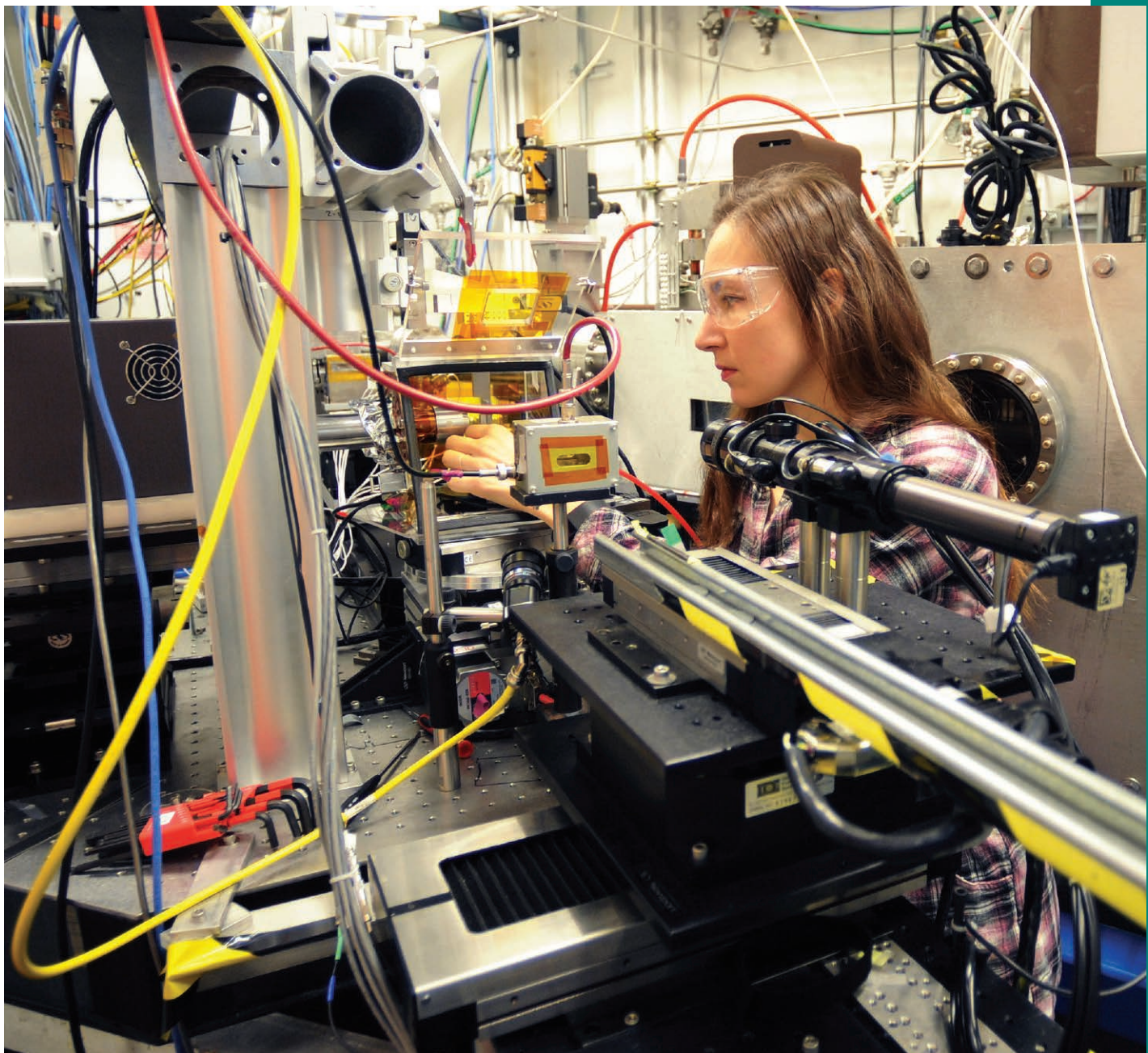
**Author affiliations:** <sup>1</sup>Argonne National Laboratory, <sup>2</sup>University of Minnesota, Twin Cities, <sup>3</sup>Northwestern University, <sup>4</sup>King Abdulaziz University

**Correspondence:**

\* chapmank@aps.anl.gov

This work was supported as part of the Inorganometallic Catalysis Design Center, an Energy Frontier Research Center funded by the U.S. Department of Energy (DOE) Office of Science-Basic Energy Sciences under Award No. DE-SC0012702. A.E.P.P. acknowledges a Beatriz de Pinós fellowship (BP-DGR 2014) from the Ministry of Economy and Knowledge from the Catalan Government. This research used resources of the Advanced Photon Source, a U.S. DOE Office of Science User Facility operated for the DOE Office of Science by Argonne National Laboratory under Contract No. DE-AC02-06CH11357.

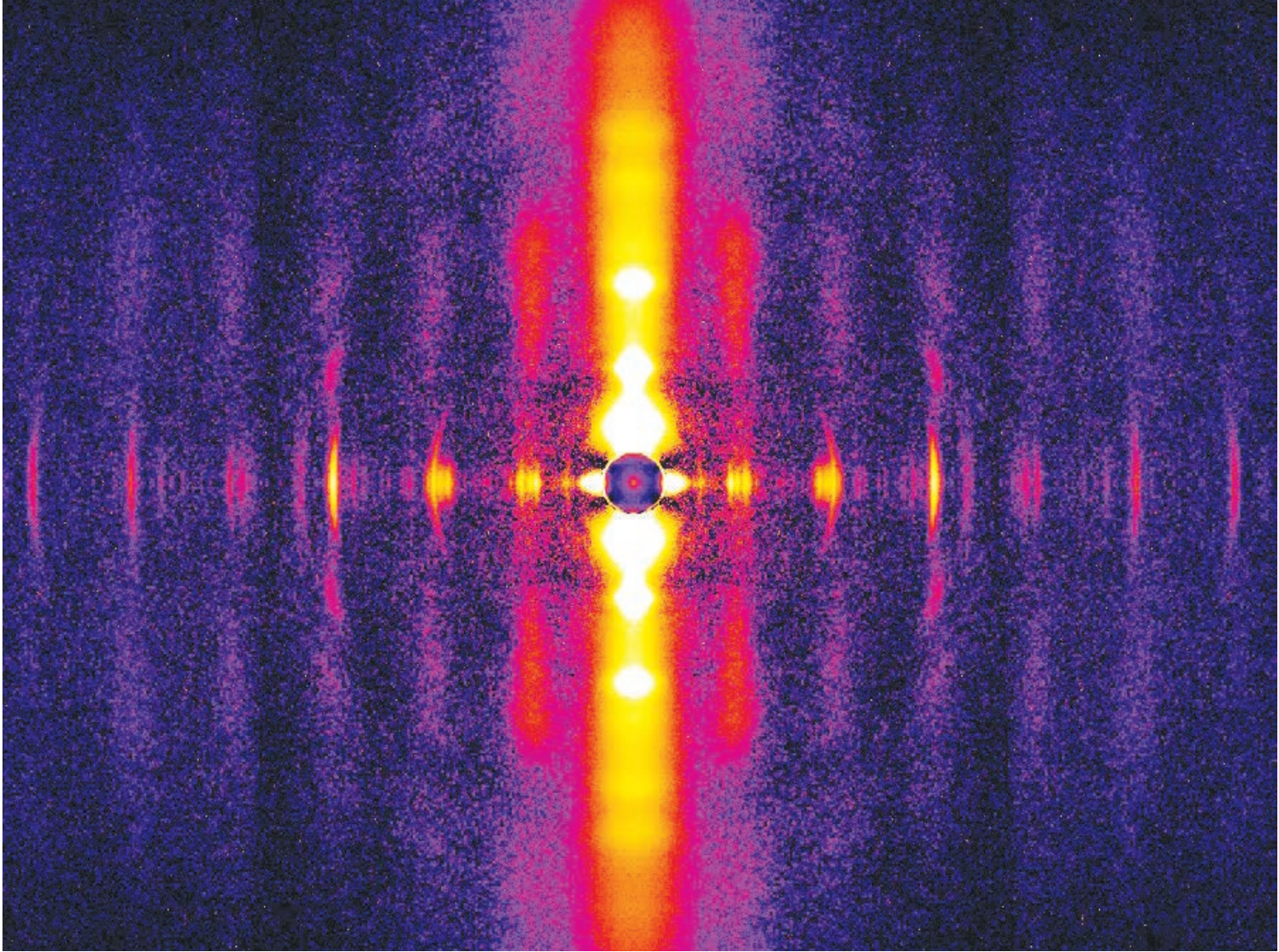
11-ID-B • XSD • Chemistry, environmental science, materials science • Pair distribution function, high-energy x-ray diffraction • 58.66 keV, 86.7 keV • On-site • Accepting general users •



Olga Antipova, assistant physicist and beamline scientist with the XSD Microscopy Group at the APS, places a sample in the x-ray fluorescent microprobe at the XSD 2-ID-E beamline. This instrument is used for imaging and quantification of various elements in biological and other samples, which is critical for understanding numerous normal and pathological processes.



# UNEARTHING THE MECHANISM OF THE FRANK-STARLING LAW, A CENTRAL REGULATOR OF HEART FUNCTION





The Frank-Starling law of the heart is a basic physiological principle first observed more than 100 years ago. It describes how the heart is able to move blood through the body in a regulated way by pumping out as much blood as it receives. To understand the nature of the molecular mechanism underlying this important regulatory process, researchers from Loyola University together with colleagues from the Illinois Institute of Technology and the University of Wisconsin–Madison conducted x-ray diffraction experiments at the APS to examine myocardial muscles of rats deficient in length-dependent activation (LDA) of muscle fibers in the heart. Their work shows that the protein titin is critically important for transmitting the stretch-induced signals within the heart's muscles known to impact the strength with which the heart contracts. This work not only solves a piece of the mystery of how the Frank-Starling law determines cardiac function, but provides an avenue for targeted development of drugs to treat heart failure.

The Frank-Starling law states that the extent to which the heart's ventricles (and resident muscle fibers) are stretched when filled with blood during the diastolic phase of the cardiac cycle is directly related to the force with which the heart is able to pump blood into the aorta during systole (contraction). This balance is critical for heart function, and is disrupted in patients with heart failure. In these patients, the heart is not able to move the blood that fills the ventricles during diastole through the heart so that it can be sufficiently oxygenated.

Within the walls of the ventricles, muscle fibers are comprised of striated muscle tissue called sarcomeres. Each sarcomere houses contractile proteins arranged into bundles of thin and thick filaments made primarily from proteins myosin and actin, respectively. When these filaments interact, the muscle contracts, generating force. Previous research showed LDA of sarcomeres results from an enhanced response of the contractile proteins to the local concentration of calcium, and that the protein titin, which helps muscles spring

back after stretching or contracting, is important for mediating this effect. In fact, mutations in titin are known to disrupt the Frank-Starling Mechanism. The nature of titin's involvement, however, and the reason why muscles, given the same amount of calcium, exert more force when stretched farther, remained unclear.

In this study, the researchers used high-brightness x-rays and the x-ray diffraction technique at the Bio-CAT x-ray beamline 18-ID-D at the APS to observe sarcomere-length induced changes in muscle filaments that harbored either normal (WT) or mutant (HM) titin (Fig. 1).

Their results revealed that the length-dependent changes observed in the x-ray diffraction reflections were present only in the normal, WT, muscle. This means that transmission of the "length signal" in the sarcomeres that occurs during filling of the ventricles, depends upon titin to induce the structural alterations in the thick and thin filaments that drive the force of the contraction. Further, these rearrangements correlate with the degree of titin strain, supporting the central role of this protein in the Frank-Starling law.

These findings represent a significant advancement in our understanding of cardiac function and pave the way for future work that may lead to targeted development of therapies for patients with heart failure.

— Emma Nichols

**See:** Younss Ait-Mou<sup>1‡</sup>, Karen Hsu<sup>1‡‡</sup>, Gerrie P. Farman<sup>1‡‡‡</sup>, Mohit Kumar<sup>1</sup>, Marion L. Greaser<sup>3</sup>, Thomas C. Irving<sup>2</sup>, and Pieter P. de Tombe<sup>1\*</sup>, "Titin strain contributes to the Frank-Starling law of the heart by structural rearrangements of both thin- and thick-filament proteins," *Proc. Natl. Acad. Sci. USA* **113**(8), 2306 (February 23, 2016).

DOI: 10.1073/pnas.1516732113

**Author affiliations:** <sup>1</sup>Loyola University Chicago, <sup>2</sup>Illinois Institute of Technology, <sup>3</sup>University of Wisconsin–Madison Present addresses: <sup>‡</sup>Sidra Medical and Research Center, <sup>‡‡</sup>San Diego State University, <sup>‡‡‡</sup>University of Massachusetts at Lowell

**Correspondence:** \* pdetombe@luc.edu

This work was supported, in part, by National Institutes of Health (NIH) Grants HL075494 and GM103622. Bio-CAT is supported by Grant 9 P41 GM103622 from the National Institute of General Medical Sciences of the NIH. This research used resources of the Advanced Photon Source, a U.S. Department of Energy (DOE) Office of Science User Facility operated for the DOE Office of Science by Argonne National Laboratory under Contract No. DE-AC02-06CH11357.

18-ID-D • Bio-CAT • Life sciences • Fiber diffraction, microdiffraction, small-angle x-ray scattering, time-resolved x-ray scattering • 3.5-35 keV • On-site • Accepting general users •

**Fig. 1.** A typical two-dimensional x-ray diffraction pattern of heart muscle, obtained at the Biophysics Collaborative Access team beamline at the APS. Meridional reflections (horizontal, yellow) arise from thin and thick filament proteins. Stretching of these fibers can change the spacing and/or intensity of these reflection, allowing researchers to observe changes within the heart's muscle on a nanometer scale.

# HUNTING FOR TRACE ELEMENTS IN THE ZEBRAFISH EMBRYO

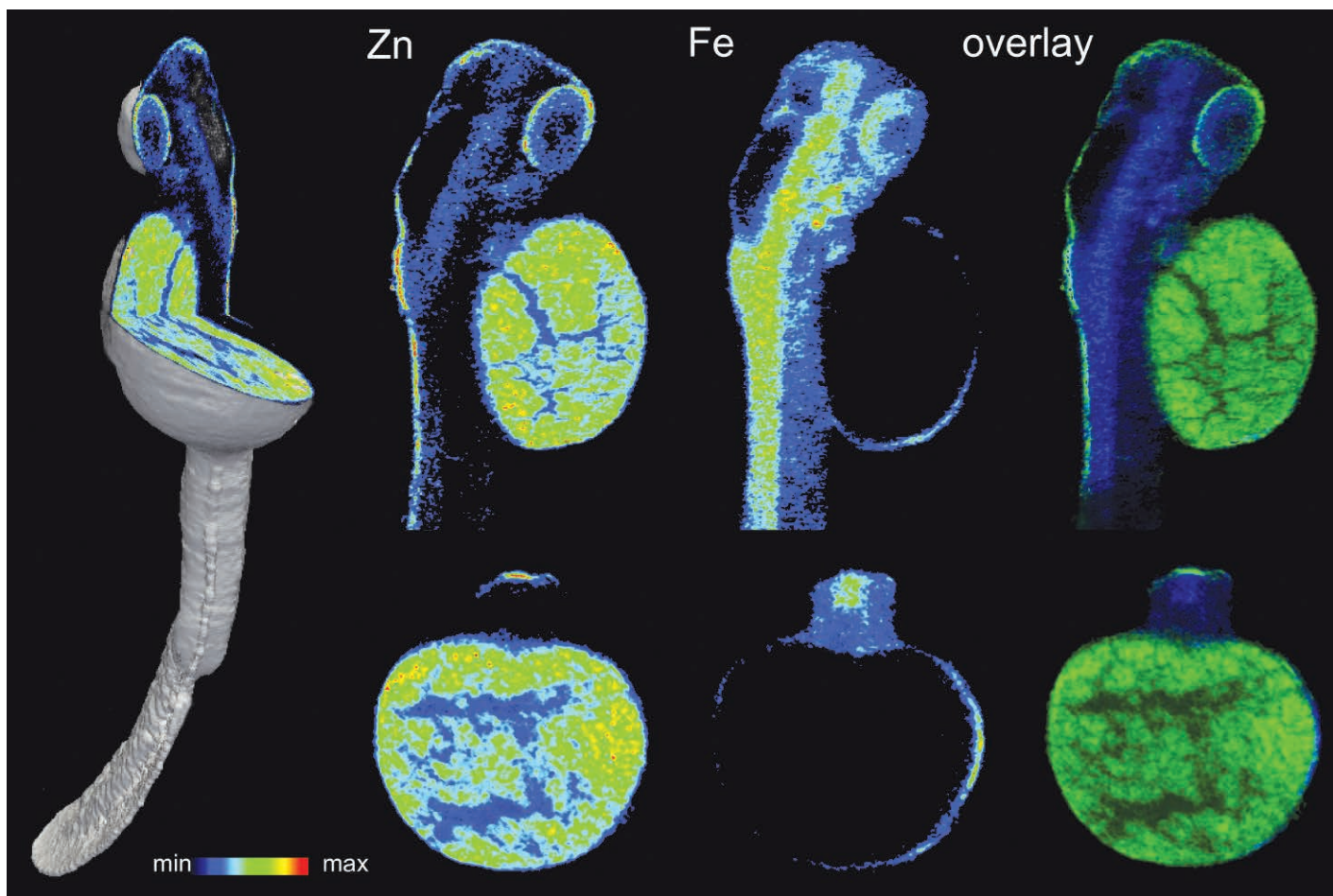


Fig 1. Three-dimensional visualization of the zinc and iron distribution in a zebrafish embryo by x-ray fluorescence tomography at the 2-ID-E beamline at APS 48 h after fertilization. Left: Three-dimensional rendering of the embryo revealing the inside of the embryo across two virtual slices. Middle: Zinc and iron distribution across each of the two slices shown in the rendering on the left. Right: Overlay of the zinc (green) and iron (blue) distribution indicating mostly mutually exclusion of locations with high concentrations.

One lingering question in the field of developmental biology is exactly how trace metals, such as zinc and iron, are used by a growing embryo. It is well known that these nutrients are key components of many enzymes and proteins that play critical roles in cellular proliferation, differentiation, and embryonic development. Zinc and iron are important for the healthy function of all cells, but some organs and tissues have increased demands for these metals to perform their specialized roles. At present, it remains unclear how these trace nutrients are redistributed to reach their target sites during early development. To investigate this question, a team of researchers used data gathered from the APS to visualize zinc and iron in zebrafish embryos at the onset of the hatching period, a critical period for development of many organs including the heart, liver, and eye. Their findings provide new insights into this early time in development and could eventually provide crucial information into why development might go awry.

In the past several years, zebrafish (*Danio rerio*)—a popular freshwater home aquarium species—has also gained popularity as a laboratory model to study basic biology and genetics. Despite the obvious differences between humans and zebrafish, the two species have much in common: About 70% of human genes have homologs in the zebrafish. These animals also display a similar pattern of early embryonic development, going through many of the same distinct stages as humans while they mature.

Taking advantage of this homology, the research team from the Georgia Institute of Technology used micro x-ray fluorescence tomography to identify the locations of the highest concentrations of zinc and iron during the hatching period. Two days after fertilization, at the onset of the hatching period, the researchers embedded zebrafish embryos in resin, and excised the specimen with a laser beam to limit attenuation of the high-intensity x-rays used in tomographic imaging. Then, with Argonne scientists and x-rays from the XSD 2-ID-E beamline, the researchers scanned the embryos to reveal unique three-dimensional “fingerprints” of the trace elements present (Fig. 1).

Their analysis showed that the locations with the highest zinc and iron concentrations were mostly mutually exclusive. Zinc concentrations were greatest in the yolk sac and yolk exten-

sion, the structures that feed the zebrafish embryo until it is ready for other food after hatching. About 83% of the total zinc content of each embryo was contained in these structures. Conversely, iron concentrations were highest in the myotome, the part of the embryo that will eventually develop into skeletal muscles, and portions of the brain. The liver was another iron-rich organ, while the tip of the tail and the single atrium of the embryonic heart were distinctly rich in zinc.

The basis for many of these findings can be explained from prior research, the researchers note. For example, it makes sense to find iron in the liver since this organ is well known as a major storage site for ferritin, the primary protein responsible for intracellular iron storage and release. However, the reasons behind other findings are less clear and will require further study.

The scientists add that they recently performed a similar study that investigated the concentrations of these trace elements 24 h after fertilization. They plan to continue studying other key points in development using similar methodology to reveal how zinc, iron, and other trace elements redistribute during embryogenesis.

Understanding which organs are using these elements, and in what concentrations, could shed light on the role of trace metals in healthy development. These findings could also eventually help researchers to understand what

happens when there is an insufficient supply of these nutrients or redistribution doesn't properly occur.

— Christen Brownlee

**See:** Daisy Bourassa<sup>1</sup>, Sophie-Charlotte Gleber<sup>2</sup>, Stefan Vogt<sup>2</sup>, Chong Hyun Shin<sup>1</sup>, and Christoph J. Fahrni<sup>1\*</sup>, “MicroXRF tomographic visualization of zinc and iron in the zebrafish embryo at the onset of the hatching period,” *Metalomics* **8**, 1122 (2016).

DOI: 10.1039/c6mt00073h

**Author affiliations:** <sup>1</sup>Georgia Institute of Technology, <sup>2</sup>Argonne National Laboratory

**Correspondence:**

\* fahrni@chemistry.gatech.edu

Financial support by the National Science Foundation (CHE- 1306943) is gratefully acknowledged. The study was also supported in part by the Robert P. Apkarian Integrated Electron Microscopy Core (RPAIEMC), which is subsidized by the Emory College of Arts and Sciences and the Emory University School of Medicine and is one of the Emory Integrated Core Facilities. This research used resources of the Advanced Photon Source, a U.S. Department of Energy (DOE) Office of Science User Facility operated for the DOE Office of Science by Argonne National Laboratory under Contract No. DE-AC02-06CH11357.

2-ID-E • XSD • Life sciences, environmental science, materials science • Microfluorescence (hard x-ray), tomography • 7-10.5 keV, 11-17 keV • On-site • Accepting general users •



# SILICON BIOMIMICRY



Fig. 1. Transmission x-ray microscopy three-dimensional data set of a representative region of mesostructured silicon (left). A thin slice of the data set (green lines) highlights the presence of both intra- and inter-granular voids (right). Representing silicon as a semi-transparent matrix allows clearer visualization of the voids (upper right). Magenta, silicon; blue, intra-granular voids; open regions in the whole volume or thin slice, inter-granular voids.

**B**esides its incredible number of uses in computers and electronics, silicon (Si) has many biomedical applications. Silicon is biocompatible, biodegradable, and has important electrical, optical, mechanical, and thermal properties. By creating tinier silicon nanowire assemblies full of nano-scale voids, researchers constructed a device that could attach to the plasma membrane of a cell and generate a current to stimulate that cell, and then characterized the structure of the device using the APS. This work could one day lead to the creation of an artificial human tissue or even a functioning organ.

Researchers are working to engineer Si-based forms that behave like natural biomaterials for subcellular interfaces and biophysical modulation. For example, a Si-based medical device injected or implanted into human tissue could stimulate nerve cells or manipulate the behavior of muscles and organs. To achieve such amazing functionality, the device must be capable of interacting with the tissue, be no more than a few microns in diameter, and be soft. For it to be medically useful, the device must disperse in saline so that it is injectable. The device must also be light-activated and must degrade on a convenient time scale so that it does not have to be surgically removed. All of that put together is a pretty tall order, but the potential rewards are very high.

To meet the challenges of creating these materials, researchers from The University of Chicago designed a chemical vapor deposition apparatus that creates a device composed of two types of silicon, oxidized silicon and pure silicon. They first created a  $\text{SiO}_2$  mold composed of submicroscopic channels that were connected by even tinier micro-bridges. When silane ( $\text{SiH}_4$ ) gas is injected into the nano-scale voids in the mold, the gas decomposes into pure silicon. The scientists then dissolve the mold, which leaves behind a web of silicon nanowires that are connected by oxidized silicon micro-bridges. The material has a structure full of nano-scale voids, so that it is squishy like a sponge. The oxidized silicon absorbs water, which decreases its rigidity. The

material's rigidity compares with the collagen fibers that make up tissues, tendons, ligaments, cartilage and bone; by contrast, the silicon materials used in transistors are up to 100 times more rigid. Also important, is that the pure silicon in the device can absorb light. To characterize the structure of the device, small-angle x-ray scattering measurements were conducted at the XSD 12-ID-B beamline at the APS. Transmission x-ray microscopy nano-computed tomography was performed on the new transmission x-ray microscope at XSD beamline 32-ID-B,C (Fig. 1).

When the researchers injected the particles into a neuron culture it attached to the cell's plasma membrane. By shining light on a particle, its transient heating generated enough capacitive current in the membrane to stimulate the neuron and change the cell activity. Researchers will next attempt to stimulate nerves in living animals. They will go for nerves in the peripheral nervous system that connect to organs. These nerves are fairly close to the body surface so they can be stimulated by near-infra-red wavelength light that can penetrate the skin.

In the future, light activated devices could be engineered to replace human tissue or entire organs. To make a functioning organ, a tightly focused beam of light would need to manipulate each individual cell in the engineered tissue. An advantage to this type of therapy is that it does not require a change in the genetics of an organism. — *Dana Desonie*

**See:** Yuanwen Jiang<sup>1</sup>, João L. Carvalho-de-Souza<sup>1</sup>, Raymond C.S.Wong<sup>1</sup>, Zhiqiang Luo<sup>1</sup>, Dieter Isheim<sup>2</sup>, Xiaobing Zuo<sup>3</sup>, Alan W. Nicholls<sup>4</sup>, Il Woong Jung<sup>3</sup>, Jiping Yue<sup>1</sup>, Di-Jia Liu<sup>3</sup>, Yucai Wang<sup>1</sup>, Vincent De Andrade<sup>3</sup>, Xianghui Xiao<sup>3</sup>, Luizetta Navrazhnykh<sup>1</sup>, Dara E.Weiss<sup>1</sup>, Xiaoyang Wu<sup>1</sup>, David N. Seidman<sup>2</sup>, Francisco Bezanilla<sup>1\*</sup> and Bozhi Tian<sup>1\*\*</sup>, "Heterogeneous silicon mesostructures for lipid-supported bioelectric interfaces," *Nat. Mater.* **15**, 1023 (September 2016). DOI: 10.1038/NMAT4673  
**Author affiliations:** <sup>1</sup>The University of Chicago, <sup>2</sup>Northwestern University, <sup>3</sup>Argonne National Laboratory, <sup>4</sup>University of Illinois at Chicago

**Correspondence:**

\* fbezanilla@uchicago.edu

\*\* btian@uchicago.edu

This work is supported by the Air Force Office of Scientific Research (AFOSR FA9550-14-1-0175, FA9550-15-1-0285), the National Science Foundation (NSF CAREER, DMR-1254637; NSF MRSEC, DMR 1420709), the Searle Scholars Foundation, the National Institutes of Health (NIH GM030376), and The University of Chicago Start-up Fund. A portion of this work was performed at the Center for Nanoscale Materials, a U.S. Department of Energy (DOE) Office of Science-Basic Energy Sciences user facility under Contract No. DE-AC02-06CH11357. This research used resources of the Advanced Photon Source, a U.S. DOE Office of Science user facility operated for the DOE Office of Science by Argonne National Laboratory under Contract No. DE-AC02-06CH11357.

12-ID-B • XSD • Chemistry, materials science, life sciences, polymer science, physics • Small-angle x-ray scattering, grazing incidence small-angle scattering, wide-angle x-ray scattering, grazing incidence diffraction • 7.9-14 keV • On-site • Accepting general users •

32-ID-B,C • Materials science, life sciences, geoscience • Phase contrast imaging, radiography, transmission x-ray microscopy, tomography • 7-40 keV • On-site • Accepting general users •

# TAPBPR: A NOVEL PROTEIN CHAPERONE WITH A ROLE IN PEPTIDE EDITING IN IMMUNE RECOGNITION

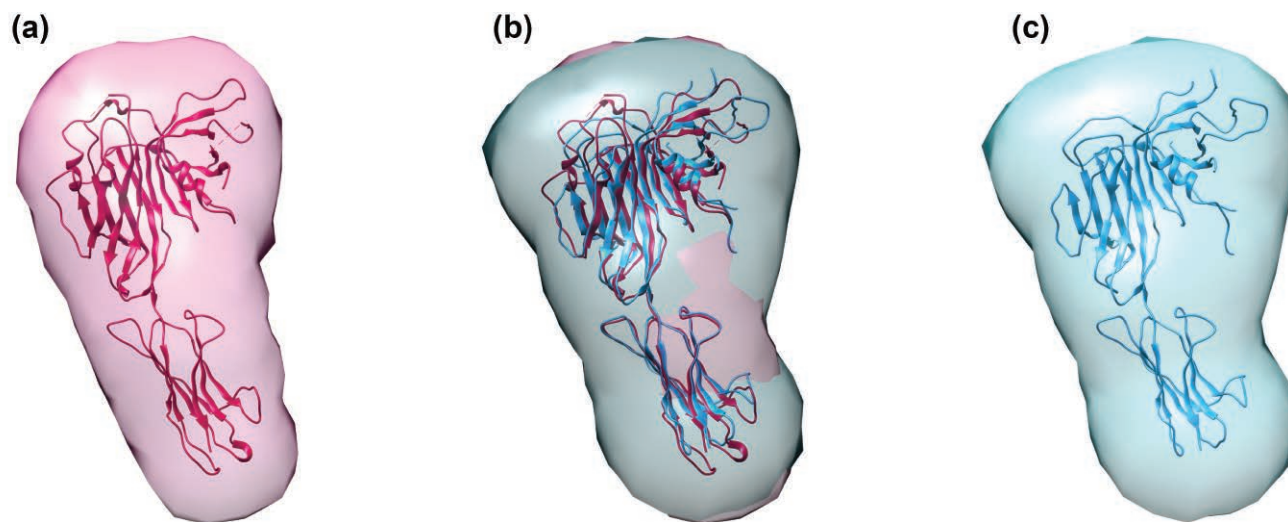


Fig. 1. Calculated SAXS envelopes for tapasin (a) and TAPBPR (c), as well as both envelopes superimposed (b). A ribbon diagram of the high-resolution x-ray structure of Tapasin, or of a molecular homology model of TAPBPR, is also superposed on the SAXS envelopes.

18-ID-D • Bio-CAT • Life sciences • Fiber diffraction, microdiffraction, small-angle x-ray scattering, time-resolved x-ray scattering • 3.5-35 keV • On-site • Accepting general users •



**T**AP binding protein, related (TAPBPR), a novel protein chaperone, plays a role in loading peptides onto major histocompatibility class I (MHC I) molecules during the process of immune surveillance. However, until now, how TAPBPR functions in antigen presentation has been unknown. Researchers investigated the biochemical function of TAPBPR, comparing it with tapasin, another chaperone with a similar protein sequence. Using direct binding studies, they demonstrated that TAPBPR functions as a peptide editor, and binds MHC I molecules that are either peptide-free or complexed with low affinity peptides. Because macromolecular crystallography has so far proven unsuccessful for obtaining high-resolution structural information on TAPBPR, the researchers instead collected small-angle x-ray scattering (SAXS) data at the APS. This allowed them to confirm the structural similarities between TAPBPR and tapasin. The results of this study could lead to ways to modulate peptide loading in vaccine design, improving T-cell recognition.

TAPBPR is involved in the intracellular loading of peptides onto MHC I molecules. MHC I molecules are important components of the immune system and are expressed on the surface of most cells in all species of jawed vertebrates. Many variants of MHC I molecules exist within a population, and they bind and display peptides on their surface: in healthy cells, they display peptide fragments derived from biosynthetic pathways—typically from the cell's own “housekeeping” proteins—which do not stimulate an immune response. However, if a cell is infected by a microorganism, or if a cell is a dysregulated tumor cell, MHC I molecules bind and display peptide fragments of the microbe or the tumor. These MHC I–antigen complexes serve as flags on the cell surface that are recognized by T cell receptors on cytotoxic T lymphocytes.

TAPBPR shares approximately 20% of its protein sequence with tapasin, another well-studied chaperone. Tapasin is part of a complex protein machine called the “peptide loading complex,” which is the major loader of peptides onto MHC I molecules. However, how TAPBPR functions in peptide loading has been unclear.

The researchers in this study, from the National Institutes of Health, the U.S. Food and Drug Administration, and the University of Oklahoma Health Sciences Center conducted studies to characterize the biochemical function of TAPBPR. They wanted to better understand how TAPBPR interacts with MHC I molecules to facilitate peptide loading.

They also wanted to determine the structure of TAPBPR, and to compare it with the structure of tapasin, which is already known.

The researchers engineered recombinant TAPBPR for expression in an insect cell system. They investigated the interaction of TAPBPR with MHC I molecules, by using direct binding studies including analytical ultracentrifugation, surface plasmon resonance, and fluorescence polarization assays. These studies showed that TAPBPR functions as a peptide editor and binds MHC I molecules that are either complexed with low affinity peptides or emptied of photolabile peptides by exposure to ultraviolet light. As noted, researchers have so far been unsuccessful in using crystallography to obtain high-resolution structural information on TAPBPR. Instead of using crystallography, the researchers in this study took a different approach to determining and comparing the structural shapes of purified TAPBPR molecules and the related tapasin molecule. By collecting SAXS data at the Bio-CAT 18-ID-D x-ray beamline at the APS, they were able to calculate a low-resolution envelope for both tapasin (Fig. 1a) and TAPBPR (Fig. 1c). They were also able to fit the x-ray structures of tapasin and a molecular model of TAPBPR into their respective SAXS-determined low-resolution envelopes (Fig. 1).

In this way, the researchers identified the similarities between the two molecules that provide the foundation for investigating the steps of peptide loading. The results of this research

therefore have potential to guide future studies to modulate peptide loading for T-cell recognition, as well as in designing peptide-based vaccines.

— Nicola Parry

**See:** Giora I. Morozov<sup>1</sup>, Huaying Zhao<sup>1</sup>, Michael G. Mage<sup>1</sup>, Lisa F. Boyd<sup>1</sup>, Jian-sheng Jiang<sup>1</sup>, Michael A. Dolan<sup>1</sup>, Ramesh Venna<sup>2</sup>, Michael A. Norcross<sup>2</sup>, Curtis P. McMurtrey<sup>3</sup>, William Hildebrand<sup>3</sup>, Peter Schuck<sup>1</sup>, Kannan Nataraajan<sup>1</sup>, and David H. Margulies<sup>1\*</sup>, “Interaction of TAPBPR, a tapasin homolog, with MHC-I molecules promotes peptide editing,” *Proc. Nat. Acad. Sci. USA* **113**(8), E1006 (February 23, 2016). DOI: 10.1073/pnas.1519894113.

**Author affiliations:** <sup>1</sup>National Institutes of Health, <sup>2</sup>U.S. Food and Drug Administration, <sup>3</sup>University of Oklahoma Health Sciences Center

**Correspondence:** \* dhm@nih.gov

SAXS research was supported by Grant 9 P41 GM103622 from the National Institute of General Medical Sciences of the National Institutes of Health. The research was supported by the intramural research programs of the National Institute of Allergy and Infectious Diseases (Project AI0000394) and National Institute of Biomedical Imaging and Bioengineering (Project EB000008)/National Institutes of Health and the Center for Drug Evaluation and Research/Federal Drug Administration (Project 1617). This research used resources of the Advanced Photon Source, a U.S. Department of Energy (DOE) Office of Science User Facility operated for the DOE Office of Science by Argonne National Laboratory under contract no. DE-AC02-06CH11357.

# AN UNUSUAL SHAPE CHANGE TO DELIVER SELENOCYSTEINE TO PROTEINS

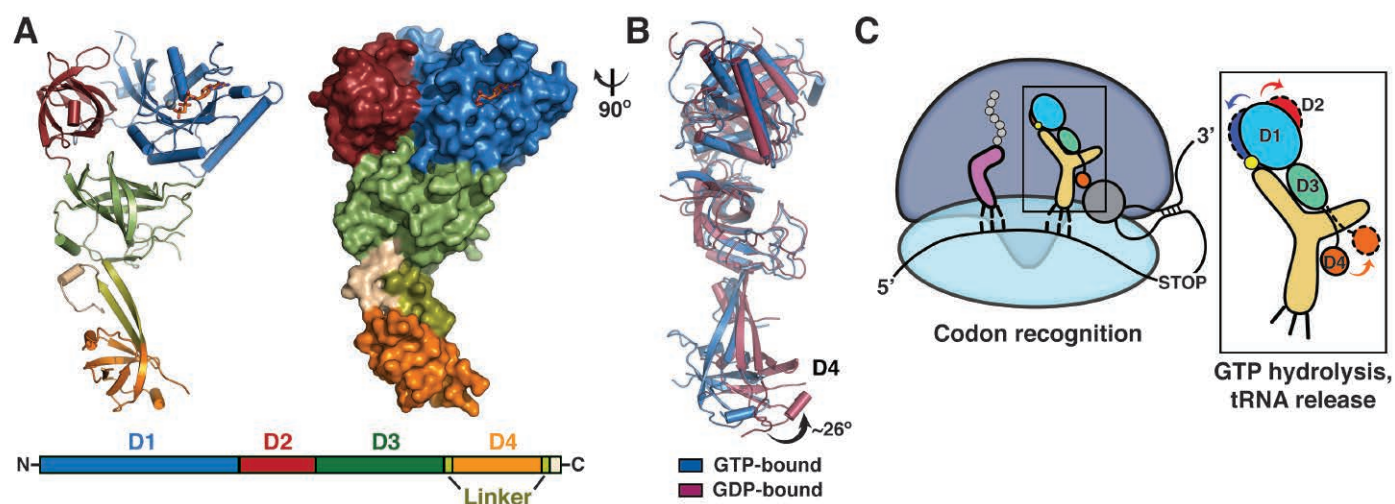


Fig. 1. (A) Cartoon (left) and surface diagram (right) of the overall structure and domain organization of human eEFSec. The color-coding is according to the scheme shown below. (B) The GTP-to-GDP exchange on human eEFSec induces an unexpected conformational change in D4, but not in D1. A comparison of the GTP- (light blue) and GDP-bound states (light red) reveals a lack of the canonical conformational change in the EF-Tu-like domain (D1-3). Instead, D4 swings  $\sim 26^\circ$  towards the dorsal face of the molecule and away from the tRNA-binding site. The view is rotated  $\sim 90^\circ$  clockwise relative to that in (A).

18-ID-D • Bio-CAT • Life sciences • Fiber diffraction, microdiffraction, small-angle x-ray scattering, time-resolved x-ray scattering • 3.5-35 keV • On-site • Accepting general users •

19-ID-D • SBC-CAT • Life sciences • Macromolecular crystallography, multi-wavelength anomalous dispersion, subatomic ( $<0.85 \text{ \AA}$ ) resolution, microbeam, ultra-low-temperature (15K), large unit cell crystallography, single-wavelength anomalous dispersion • 6.5-19.5 keV • On-site, remote, mail-in • Accepting general users •

**T**he element selenium is incorporated into proteins through the 21st amino acid selenocysteine (Sec). Such selenoproteins are critically important to all types of life, suggesting that being able to accurately decode the Sec codon and correctly placing this amino acid in proteins is biologically fundamental. However, little is known about biosynthesis of selenoproteins in eukaryotic cells. To better understand this process, a team of researchers used data gathered at two APS sectors to determine the crystal structure of the human translational elongation factor responsible for recognizing and delivering the transfer RNA (tRNA) carrying Sec to the ribosome. They produced some surprising findings, which suggest that the mechanism for elongation factor to incorporate selenium into growing protein chains is different from that of elongation factors associated with every other type of amino acid.

Standard amino acids rely on the elongation factors eEF1A and EF-Tu. EF-Tu in particular is made of three sections, known as domains 1, 2, and 3. To perform its job, EF-Tu utilizes a molecule called guanosine triphosphate. Previous research has shown that during the process of delivering an amino acid-carrying (or aminoacyl) tRNA into a lengthening protein, one of the phosphates on the GTP molecule EF-Tu carries is cleaved off, or hydrolyzed, which turns it into guanosine diphosphate (GDP). This triggers a major conformational change: domain 1 rotates about 90 degrees away from domains 2 and 3, which helps the tRNA release EF-Tu and subsequent positioning at the appropriate site on the ribosome.

However, the tRNA associated with Sec requires a different elongation factor. In prokaryotic cells, that factor is SelB, and in eukaryotes, it's eEFSec. Both of these elongation factors are made of four domains. Some studies have shown that SelB doesn't undergo a conformational change after the GTP-to-GDP exchange, but little was known about the behavior of eEFSec.

To learn more about this process, investigators from the University of Illinois at Chicago, the Rutgers-Robert Wood Johnson Medical School, the University of Texas Southwestern Medical Center, the Illinois Institute of Technology, and Yale University used the Bio-CAT 18-ID-D, SBC-CAT 19-ID-D, and LS-CAT 21-ID beamlines at the APS to determine the crystal structure of eEFSec while it's complexed with

non-hydrolyzable analogs of GTP, as well as GDP.

Their findings show that eEFSec has a structure shaped like a chalice: domains 1, 2, and 3 represent the cup, a linker region represents the stem, and domain 4 represents the base (Fig. 1). Further investigation showed the presence of a hydrogen bond between amino acid residues in domain 3 and the linker that seemed to act like a hinge—a clue that something unusual might take place at this region during hydrolysis.

Sure enough, when the researchers determined the crystal structure of eEFSec complexed with GDP, they found that domain 4 swung 26 degrees away from the other three domains. Domains 1 and 2 also underwent small shifts, with domain 1 moving slightly toward the predicted tRNA binding face and domain 2 toward the opposite direction.

Although the movement of domains 1 and 2 seem to tighten the Sec-binding pocket, which could help lower the binding affinity of the Sec tRNA, the movement of domain 4 is more mysterious. The authors speculate that the swing of domain 4 might help eject the tRNA and dissociate eEFSec from the ribosome.

More research will be necessary to better define the reasons behind this conformational change, the researchers say. Either way, it differs significantly from the mechanisms that eEF1A and EF-Tu use to deliver their aminoacyl-tRNAs to growing protein chains. The authors note that another research team recently revealed that some microor-

ganisms use different codons to encode Sec, suggesting that more surprises about this amino acid are in store.

— Christen Brownlee

**See:** Malgorzata Dobosz-Bartoszek<sup>1</sup>, Mark H. Pinkerton<sup>2</sup>, Zbyszek Otwinowski<sup>3</sup>, Srinivas Chakravarthy<sup>4</sup>, Dieter Söll<sup>5</sup>, Paul R. Copeland<sup>2</sup>, and Miljan Simonovic<sup>1\*</sup>, "Crystal structures of the human elongation factor eEFSec suggest a non-canonical mechanism for selenocysteine incorporation," *Nat. Commun.* **7**, 12941 (2016).

DOI: 10.1038/ncomms12941

**Author affiliations:** <sup>1</sup>University of Illinois at Chicago, <sup>2</sup>Rutgers-Robert Wood Johnson Medical School, <sup>3</sup>University of Texas Southwestern Medical Center, <sup>4</sup>Illinois Institute of Technology, <sup>5</sup>Yale University

**Correspondence:** \* msimon5@uic.edu

We thank the staff of LS-CAT and SBC-CAT beamlines at the APS and organizers of the 7th Annual CCP4 USA Crystallography School for their help during x-ray data collection and processing, the staff at the Advanced Protein Characterization Facility (SBC-CAT, APS) for access to Mosquito crystallization robots, and the staff of Bio-CAT beamline for help during small-angle x-ray scattering data collection. The initial part of the study was supported by the University of Illinois at Chicago startup fund and a grant from the American Cancer Society, Illinois Division (225752 to M.S.). The subsequent studies were supported by grants from the National Institute of General Medical Sciences (GM097042 to M.S., GM070773 to P.R.C. and GM22854 to D.S.). Use of LS-CAT was supported by the Michigan Economic Development Corporation and the Michigan Technology Tri-Corridor (grant 085P1000817). SBC-CAT is operated by UChicago Argonne, LLC, for the U.S. Department of Energy (DOE) Office of Biological and Environmental Research under Contract No. DE-AC02-6CH11357. Bio-CAT is supported by a grant from the National Institute of General Medical Sciences of the National Institutes of Health (P41 GM103622). Use of the Pilatus 3 1M detector was provided by grant 1S10D018090-01 from the National Institute of General Medical Sciences. This research used resources of the Advanced Photon Source, a U.S. DOE Office of Science User Facility operated for the DOE Office of Science by ANL under contract no. DE-AC02-06CH11357.



# CANCER RISK OF CHROMIUM SUPPLEMENTS FOR DIABETES

Chromium (Cr), in the form of organic complexes, is very widely consumed in some food supplements for bodybuilders and dieters, in many multi-vitamin supplements, as well as in antidiabetic chromium supplements. It has been shown to undergo a chemical change —oxidation— in living cells, thanks to researchers using the APS to carry out new x-ray studies on chromium(III). This natural oxidation process converts chromium(III) into cancer-causing chromium(VI). The findings also suggest that commonly consumed antidiabetic chromium supplements may have their biological efficacy via the chromium(VI) state, since chromium(VI) but not chromium(III) inhibits phosphatase enzymes, enhancing and mimicking insulin activity. However, the carcinogenicity of chromium(VI) is cause for concern for those using the supplements under medical advice, as well others who use chromium supplements.

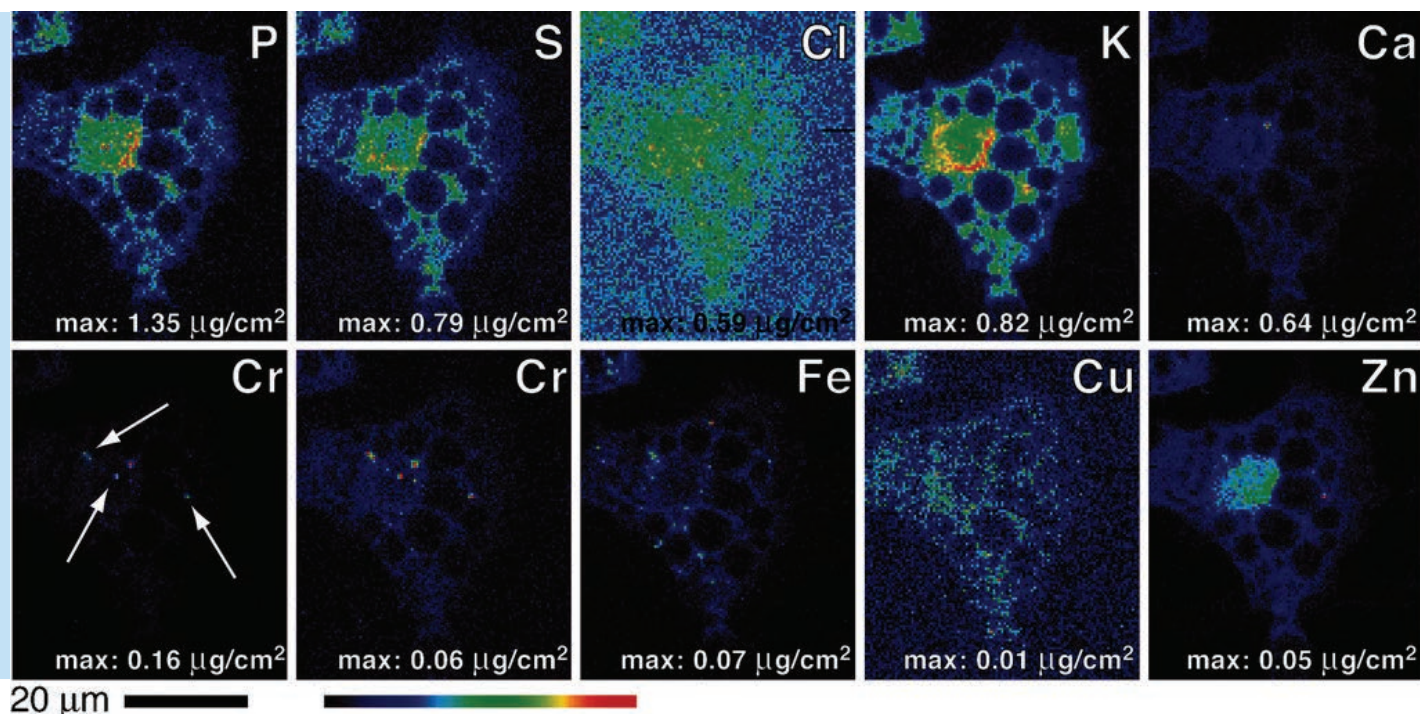


Fig. 1. X-ray fluorescence microscopy elemental maps of a  $\text{Cr}^{\text{III}}$ -treated (100  $\mu\text{m}$ , 20 h at 310 K) adipocyte with Cr punctate structures (arrows) of unknown identity. A second Cr map is shown, with the maximum scaled to 40% to show low-concentration features. The "holes" are x-ray-transparent fat globules that were observed under a microscope. From L.E. Wu et al., *Angew. Chem. Int. Ed.* **55**, 1742 (2016). © 2016 Wiley-VCH Verlag GmbH & Co. KGaA, Weinheim

It has been some 30 years since research first hinted that supplements containing organic complexes of chromium metal, such as chromium picolinate, might be able to improve the health of people with insulin resistance or type 2 diabetes. There was also some suggestion that the same compounds might help with weight loss, given that obesity is closely linked to insulin's ability to control blood sugar levels. Since that time, research and development has worked toward developing safe chromium compounds as pharmaceuticals for treating diabetes and obesity. In parallel, there has been a surge in marketing of chromium compounds as dietary supplements for the self-treatment of diabetes and obesity.

One compound being investigated as a new agent for treating diabetes is  $[\text{Cr}_3\text{O}(\text{OCOEt})_6(\text{OH}_2)_3]$ . This chromium compound is one of the most active of the chromium supplements and was first proposed as a molecular model for the postulated active peptide chromodulin. This is purported to transport chromium around the body and interact with insulin receptors in the pancreas, the organ responsible for controlling blood sugar, but mounting evidence has disputed this postulate.

It turns out that the model compound  $[\text{Cr}_3\text{O}(\text{OCOEt})_6(\text{OH}_2)_3]$  does indeed undergo oxidation triggered by hydrogen peroxide to form the reactive chromium(VI) and chromium(V) forms. Researchers from The University of Sydney (Australia), the Garvan Institute of Medical Research (Australia), and Argonne, utilizing x-ray fluorescence microscopy and x-ray absorption near-edge structure at XSD beamline 2-ID-D of the APS, found that these carcinogenic forms of the metal are also generated in fat cells, or adipocytes, which are essential in the control and pathogenesis of type 2 diabetes. The supplement is absorbed by adipocytes where it concentrates in "chromium hotspots," which contain concentrations of derivatives of the original chromium(III) compound in higher oxidation states (Fig. 1).

The main substance present in these hotspots is a compound in which the metal ion is attached to a sulfur-containing chemical group, chromium(VI) thiolate. While chromium(VI) in the body is troublesome, the formation of a thiolate under physiological conditions might explain how these drugs could work, because thiolate is chemically similar to the sulfur-containing amino acid cysteine, which is present in many proteins and in the catalytic proteins known as enzymes.

In vitro studies show that the chromium(VI) and chromium(V) ions can bind to the cysteine residues present at the active sites to inhibit enzymes known as tyrosine phosphatases (PTPs). Inhibition of these enzymes promotes the cascade of biochemical reactions involved in insulin signaling. A chromium compound that binds to such an enzyme has also been shown to modulate the activity of those enzymes in cells and so control the cascade, mimicking and enhancing the activity of the body's natural sugar control hormone, insulin.

The carcinogenicity of chromium(VI) and chromium(V) are now well established and this new research points to possible serious problems with chromium(III), too. Indeed, the new research shows how chromium(III) could be readily converted to the harmful forms of the metal ion in the body and this is likely to be borne out by long-term epidemiological studies. Of course, latency time for chromium-induced cancers is 10 to 40 years and the longest human clinical trials are a mere 2 years, which is completely irrelevant to carcinogenic risk.

The human and animal studies by other groups on the accumulation of chromium(III) in the kidneys, liver, and reproductive organs indicate that accumulation will take 10 or more years to reach potentially highly toxic equilibrium levels with regular dosing. Hence short-term human clinical trials and animal models are completely irrelevant to this

long-term toxic potential, a point that is especially relevant to young athletes and people taking chromium supplements unwittingly for body-building and weight loss, respectively, even though there is no good evidence for any benefit of doing so. Indeed, companies have had to stop advertising this in many jurisdictions because of lack of solid evidence for efficacy. — *David Bradley*

*See:* Lindsay E. Wu<sup>1,2,‡</sup>, Aviva Levina<sup>1</sup>, Hugh H. Harris<sup>1,‡</sup>, Zhonghou Cai<sup>3</sup>, Barry Lai<sup>3</sup>, Stefan Vogt<sup>3</sup>, David E. James<sup>2,‡,‡</sup>, and Peter A. Lay<sup>1\*</sup>, "Carcinogenic Chromium(VI) Compounds Formed by Intracellular Oxidation of Chromium(III) Dietary Supplements by Adipocytes," *Angew. Chem. Int. Ed.* **55**, 1742 (2016).

DOI: 10.1002/anie.201509065

*Author affiliations:* <sup>1</sup>The University of Sydney, <sup>2</sup>Garvan Institute of Medical Research, <sup>3</sup>Argonne National Laboratory <sup>‡</sup>Present addresses: University of New South Wales, <sup>‡‡</sup>The University of Adelaide, <sup>‡‡‡</sup>The University of Sydney

*Correspondence:*

\* peter.lay@sydney.edu.au

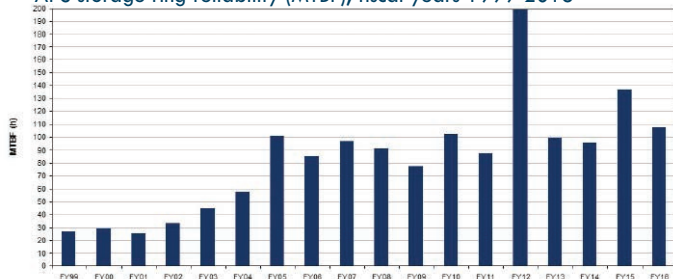
Financial support for this work was provided to P.A.L. by the Australian Research Council and the Australian Synchrotron Research Program (ASRP). The researchers thank the ASRP for an ASRP Research Fellowship (H.H.H.) and for access to APS and ANBF facilities (Photon Factory, Tsukuba, Japan). The ASRP is funded by the Commonwealth of Australia under the Major National Research Facilities Program. L.E.W. is a Cancer Institute NSW Early Career Fellow. This research used resources of the Advanced Photon Source, a U.S. Department of Energy (DOE) Office of Science User Facility operated for the DOE Office of Science by Argonne National Laboratory (DE-AC02-06CH11357).

2-ID-D • XSD • Life sciences, materials science, environmental science • Microfluorescence (hard x-ray), micro x-ray absorption fine structure, nano-imaging • 5-30 keV • On-site • Accepting general users

## X-RAY AVAILABILITY AND RELIABILITY

In fiscal year 2016\*, the APS x-ray source continued to function as a highly reliable delivery system for synchrotron x-ray beams for research. Several factors support the overall growth in both the APS user community and the number of experiments carried out by that community. But there is a direct correlation between the number of x-ray hours available to users; the success of the APS experiment program; and the physicists, engineers, and technicians responsible for achieving and maintaining optimum x-ray source performance. Below are definitions of important measures for the delivery of x-ray beam to users (latest data shown graphically).

### APS storage ring reliability (MTBF), fiscal years 1999-2016

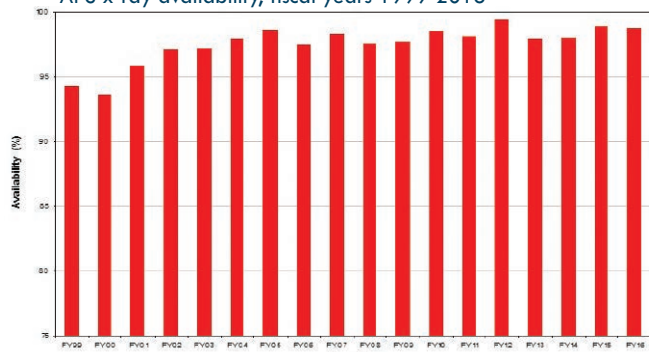


**Storage Ring Reliability:** A measure of the mean time between beam losses (faults), or MTBF, calculated by taking the delivered beam and dividing by the total number of faults. The APS targets, and routinely exceeds, 70 h MTBF. A fault is defined as complete unavailability of beam either via beam loss or removal of shutter permit not related to weather. A fault also occurs when beam has decayed to the point where stability and orbit can no longer be considered reliable. At the APS, this threshold is 50 mA.

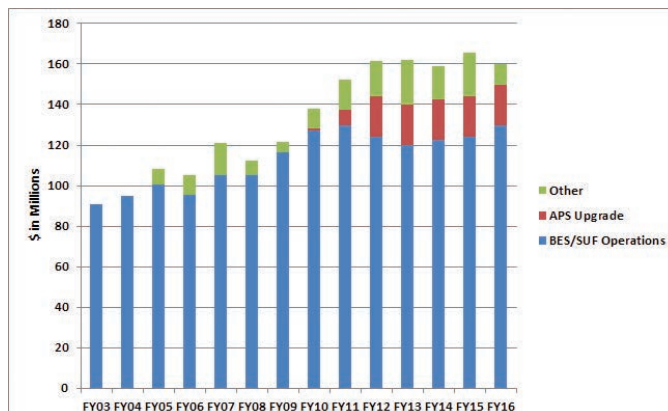
**X-ray Availability:** The number of hours that the beam is available to the users divided by the number of hours of scheduled beam delivery prior to the beginning of a run. The specific definition of available beam is that the APS main control room has granted permission to the users to open their shutters, *and* there is more than 50-mA stored beam in the storage ring.

\* While the highlights in, and title of, this report cover calendar year 2016, data on accelerator performance and user statistics are measured on the basis of fiscal years.

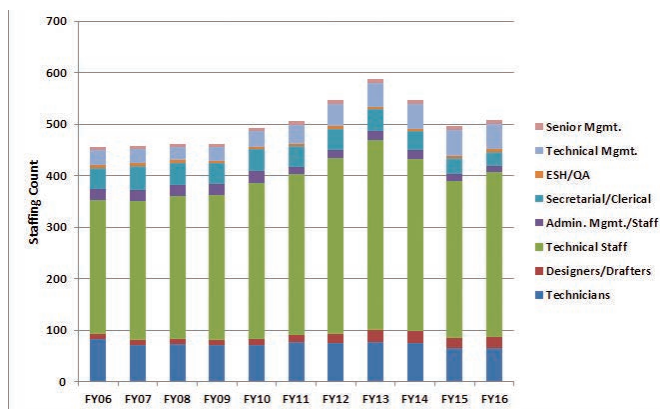
### APS x-ray availability, fiscal years 1999-2016



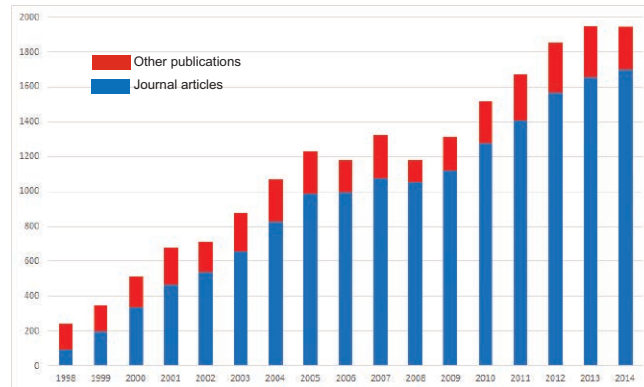
## APS funding levels, fiscal years 2003-2016



## APS staffing levels, fiscal years 2006-2016

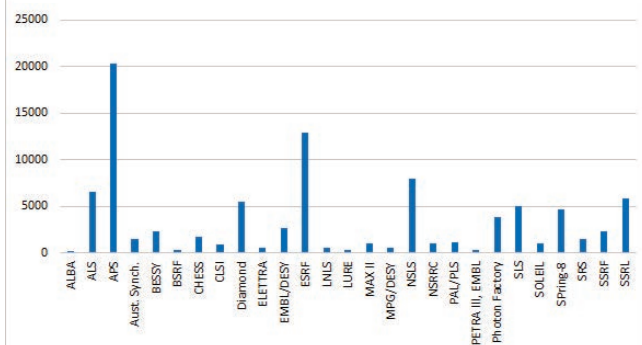


## Number of APS publications, calendar years 1998-2014, recorded as of 5.16



For lists of APS publications see <http://www.aps.anl.gov/Science/Publications/>

## Deposits in Protein Data Bank from research at major synchrotron light sources, calendar years 1998-2017 (of 17.6.26)





# STRUCTURAL BIOLOGY



Norma Duke, beamline scientist and user support macromolecular crystallographer with SBC-CAT, in the 19-ID-D research station at the APS. The majority of protein crystallography data collection operations at the APS are conducted remotely, requiring staff to simply load user's samples into a nitrogen filled dewar for remote mounting. Pictured is the installation of a V1 Universal puck (uni-puck) into a Rigaku Americas' Actor Robot multi-puck dewar. The robot arm is in the parked position awaiting instructions for mounting after all samples are loaded.

# IS THE GATE LOCKED OR JUST SHUT?

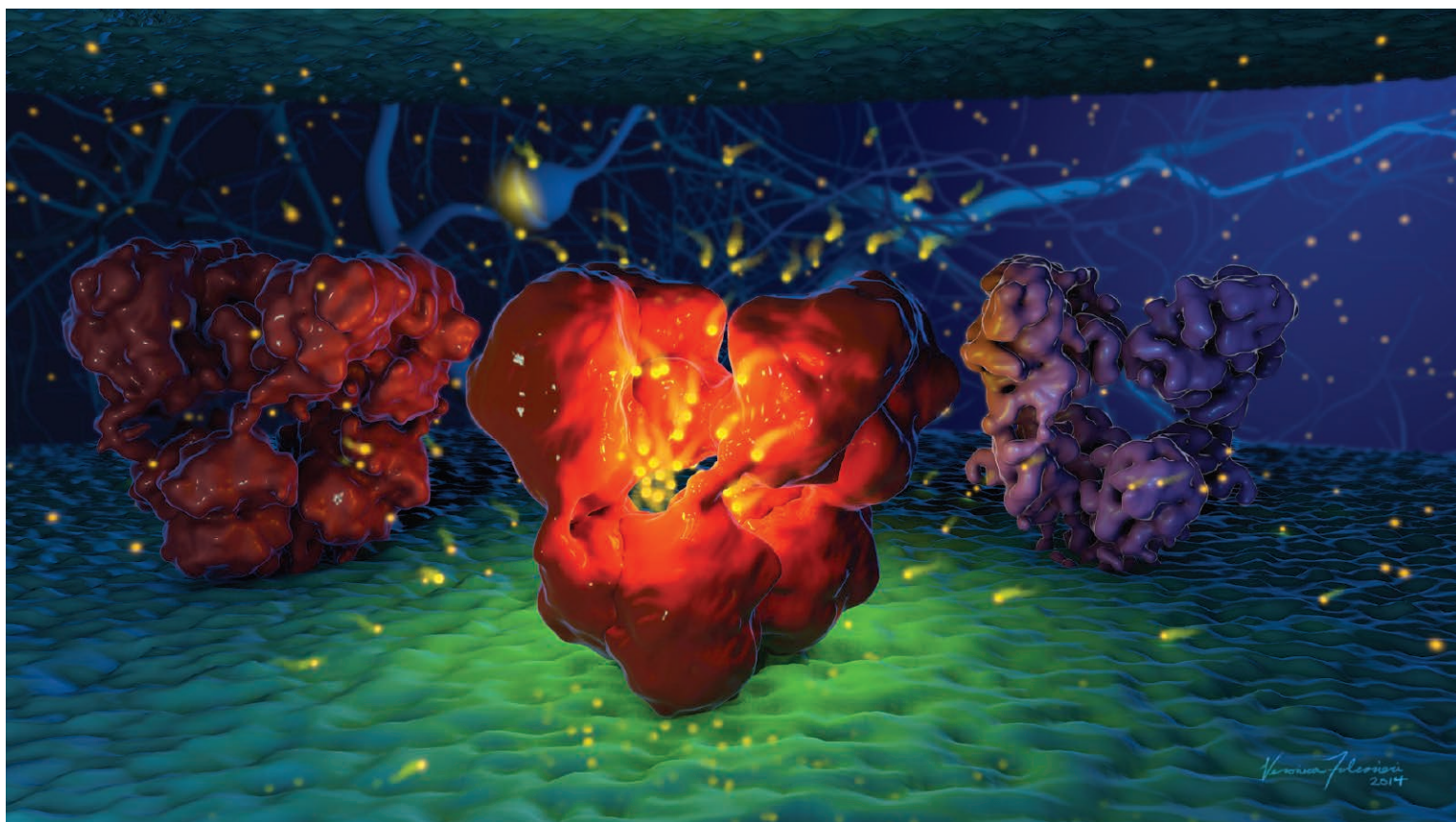


Fig. 1. Artistic representation of glutamate receptors (orange/red) in a cellular membrane (green). Ions (bright yellow spots) can be seen moving within and between cells and through the channel.  
Image: Veronica Falconieri/Subramaniam Lab/CCR/NCI/NIH

22-ID-D • SER-CAT • Life sciences • Macromolecular crystallography, multi-wavelength anomalous dispersion, single-wavelength anomalous dispersion, microbeam • 6-20 keV  
• On-site, remote • Accepting general users •



**G**lutamate is a neurotransmitter used by the central nervous system to transmit excitatory and inhibitory signals that regulate various aspects of human cognition, memory, and learning. These signals are mediated by glutamate receptors on the surface of neuronal cells that regulate the flow of ions through a transmembrane channel to propagate the signal (Fig. 1). The strength of the response depends on the strength of the signal, the type of receptor, its location, and the state of receptor. As one might imagine for such a critical neuronal component, dysfunction of glutamate receptors has been implicated in a variety of diseases including multiple sclerosis, Parkinson's disease, schizophrenia, and seizures. Understanding how glutamate receptors work is obviously of great interest to both medicine and psychology, and researchers have already solved the three-dimensional structures of a number of glutamate receptors in the "bound" state (ion channel open) and in the "resting" state (ion channel closed). However, the structure of a third state, in which the receptor is temporarily desensitized and the ion channel is held closed, has been elusive. Now, in work conducted in part at the APS, elucidation of the structure of a desensitized glutamate receptor has closed this important gap in our understanding of the receptor's activation-deactivation cycle. The work promises to impact treatment for diseases affected by glutamate receptor dysregulation and to provide important information for understanding basic neuronal functions involved in cognition.

In order to determine the structure of the desensitized glutamate receptor, the research team from the National Institutes of Health (NIH) captured the desensitized state with a high-affinity agonist that promotes deep desensitization and used cryo-electron microscopy (cryo-EM) to accomplish the structure determination without the need for crystallization. The cryo-EM was carried out at the NIH and crystallographic analyses of some fragments of the receptor were carried out at the SER-CAT 22-ID-D beamline at the APS to provide supporting structural information. The cryo-EM structure of the receptor (Fig. 1) shows that the structure looks a little like a bouquet of flowers with their stems stuck into the membrane. That is, the receptor displays a large amino-terminal domain (ATD) on the outside of the membrane that is made up of four subunits arrayed in two-fold symmetry. Below the ATD, closer to the membrane and connected to the ATD by slender linkers, is a smaller set of four subunits, the ligand binding domain (LBD), arrayed in a pinwheel formation. Finally, the transmembrane helices, which form the ion

channel, adopt a four-fold symmetry and alignment consistent with a closed ion channel state, as expected.

A central question of the work was how does the desensitized receptor apparently maintain a different ligand-binding domain structure from the resting state of the receptor while both maintain the same closed channel? Based on the structures, the outer domain, the ATD, is similar in both the desensitized state and the resting state but the LBD is markedly different. In the desensitized state, the LBD splays downward tugging on the ATD from below. This action causes the ATD to be much closer to the LBD in the desensitized state, causing much more interaction between the domains and causing the linkers between them to adopt a helical structure and pack against the LBD. In the resting state, the ATD and LBD domains don't interact and are separated by about 15 Å of space.

The structure for the desensitized LBD shows that this domain is tilted in the desensitized state compared to the resting state and this causes the formation of a ring-like structure the researchers call the "desensitization ring".

They hypothesized that this ring could contribute to the stability of the desensitized state of the receptor and slow the return to the resting state. Mutational analysis of amino acids in the ring showed that it is important for the stability of the desensitization state and the recovery of the resting state but not the depth of the desensitization well. Further modeling of the ion channel, which is similar in resting and desensitized states, suggests that ion channel closure and the depth of desensitization are mediated by interactions between the LBD and the transmembrane domains of the channel. Understanding this important step in the activation-deactivation cycle of glutamate receptors will certainly help to guide future research and medicine development in this area. — *Sandy Field*

**See:** Joel R. Meyerson<sup>\*\*\*†</sup>, Sagar Chitatori, Alan Merk, Prashant Rao, Tae Hee Han, Mihaela Serpe, Mark L. Mayer<sup>\*\*</sup>, and Sriram Subramaniam<sup>\*</sup>, "Structural basis of kainate subtype glutamate receptor desensitization," *Nature* **537**, 567 (2 September 2016).

DOI: 10.1038/nature19352

**Author affiliation:** National Institutes of Health <sup>†</sup>Present address: Brandeis University

**Correspondence:** \* ss1@nih.gov

\*\* mayerm@mail.nih.gov

\*\*\* jmeyerson@brandeis.edu

This research was supported by the intramural programs of the National Cancer Institute, and the Eunice Kennedy Shriver National Institute of Child Health and Human Development, National Institutes of Health (NIH), the Intramural AIDS Targeted Antiviral Program at NIH, and the NIH-FEI Living Laboratory for Structural Biology. SER-CAT supporting institutions may be found at [www.ser-cat.org/members.html](http://www.ser-cat.org/members.html). The cryo-EM work was done in the Subramaniam laboratory at NIH (<http://electron.nci.nih.gov>). This research used resources of the Advanced Photon Source, a U.S. Department of Energy (DOE) Office of Science User Facility operated for the DOE Office of Science by Argonne National Laboratory under Contract No. DE-AC02-06CH11357.



# NEW INSIGHTS INTO THE MECHANISMS UNDERLYING LYSOSOMAL DISEASE AND EBOLA INFECTION

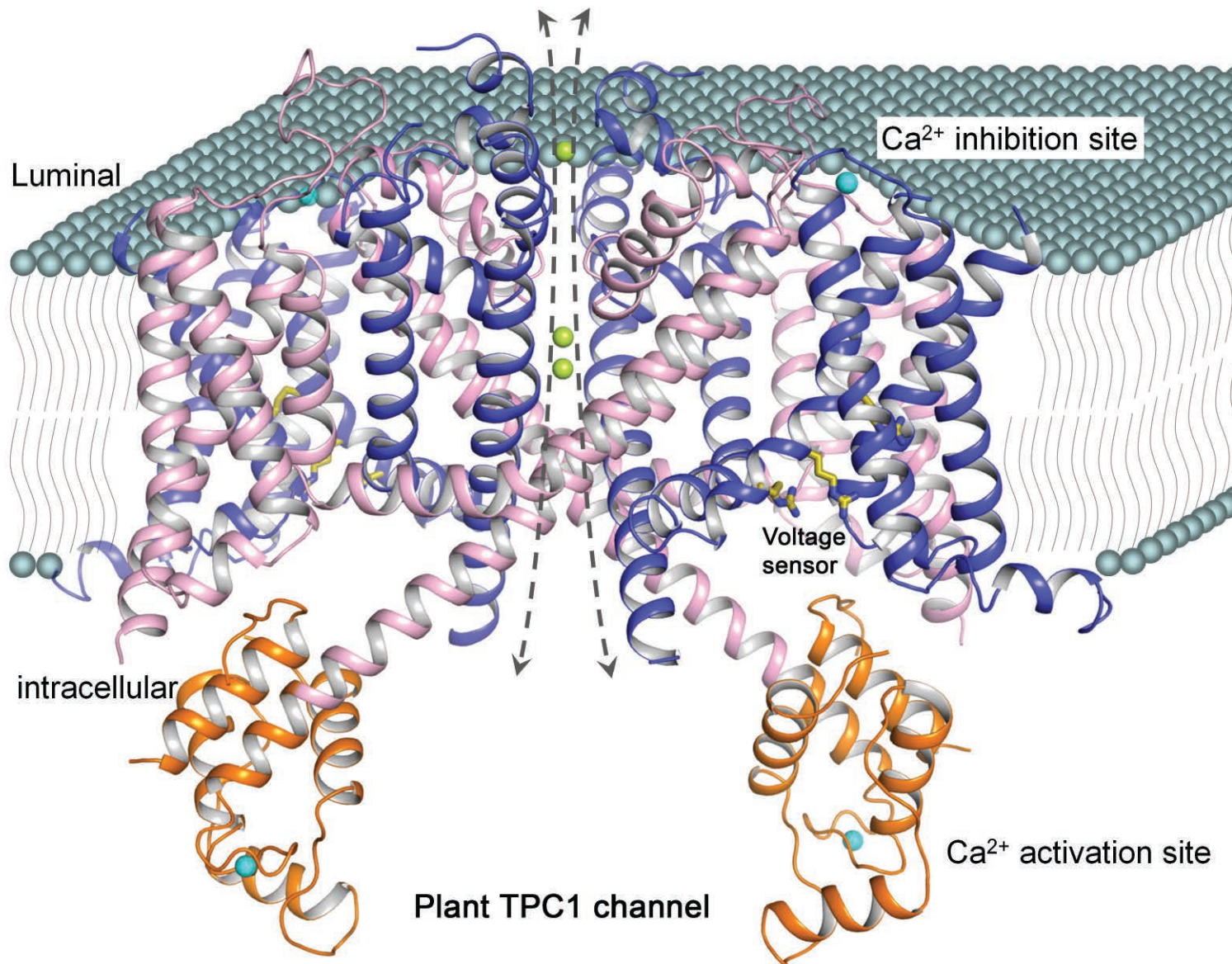


Fig. 1. Side view of the AtTPC1 channel dimer. The six-transmembrane domains (blue and pink) pass through the vacuolar membrane (teal spheres) where they form a channel that permits the passage of Na<sup>+</sup>, K<sup>+</sup> and Ca<sup>2+</sup>. The intracellular EF hands (orange) contain the Ca<sup>2+</sup> activation site (cyan), and Ca<sup>2+</sup> inhibition site is indicated on the luminal side of the membrane.

**T**wo-pore channels (TPCs) are voltage-gated ion channel proteins that detect, generate, and propagate electrical signals by opening and closing ion pathways across a cell membrane. These electrical pulses drive a fascinating range of physiological activities ranging from the coordinated beating of the heart to processing of sensations and emotions. Building on a longstanding interest in studying how these channels detect membrane potential and control the state of the ion pathway, researchers used x-ray diffraction experiments at the APS and at the Advanced Light Source (ALS) at the Lawrence Berkeley National Laboratory to build the first three-dimensional structure of the two-pore channel TCP1 in a closed conformation at a resolution of  $\sim 3.3$  Å. This work expands a fundamental understanding of TPCs and provides an avenue for treatments that target TCP1 in lysosomal diseases and Ebola.

Electrical impulses are an important mode of communication between cells in the human body. Initiation and propagation of these messages by a specialized group of proteins, voltage-gated ion channels, occurs through changes in membrane potential via the flow of  $\text{Na}^+$  or  $\text{K}^+$  ions across cell membranes. Voltage-gated ion channels sense membrane potential and act to control voltage changes by rapidly switching the ion pathway on and off. The resultant pulse-like electrical signals generate impulses that drive a many functions in body organs, including neurological function and the maintenance of blood pressure.

Though much of the research in this field has focused upon channels localized to the cell plasma membrane, more recent work has shown that TPCs reside within the membranes of organelles in plant and animal cells. In humans, TPCs regulate the ionic homeostasis and pH within lysosomes, organelles with low internal pH involved in cellular metabolism and catabolite export and trafficking. TPCs also determine lysosomal membrane potential and excitability and may regulate lysosomal  $\text{Ca}^{2+}$  release. These functions tie TPCs to both lysosomal storage diseases ( $\sim 50$  rare inherited diseases for which treatment is limited) as well as to the release of Ebola virus from lysosomes into the host cell. These roles make TPCs potential targets for the treatment of both rare diseases as well as Ebola infection.

In this study, the researchers from the University of Texas Southwestern Medical Center and the University of

Pennsylvania utilized the SBC 19-ID-D and XSD GM/CA-XSD 23-ID-B and 23-ID-D x-ray beamlines at the APS, as well as the BL8.2.1 and BL8.2.2 beamlines at the ALS, to obtain a high-resolution x-ray structure of a plant TPC channel from *Arabidopsis thaliana* (AtTPC1) with a comprehensive characterization of channel activity (Fig. 1).

The AtTPC1 structure provides an excellent model system to further investigate the TPC channel family. The structure also provides a long-awaited view of a channel voltage sensor in the closed resting state, a significant finding given that all other known voltage-gated channel structures are in the open activated state.

These findings initiate a paradigm shift in our understanding of how voltage-gated channels switch on and off in response to membrane potential changes. This knowledge can be used to address lysosomal diseases and viral infections in which  $\text{Ca}^{2+}$  release in lysosomes is a central part of the infectious process. — *Emma Nichols*

**See:** Jiangtao Guo<sup>1</sup>, Weizhong Zeng<sup>1</sup>, Qingfeng Chen<sup>1</sup>, Changkeun Lee<sup>1</sup>, Liping Chen<sup>1</sup>, Yi Yang<sup>1</sup>, Chunlei Cang<sup>2</sup>, Dejian Ren<sup>2</sup>, and Youxing Jiang<sup>1\*</sup>, "Structure of the voltage-gated two-pore channel TPC1 from *Arabidopsis thaliana*," *Nature* **531**, 196 (10 March 2016). DOI: 10.1038/nature16446

**Author affiliations:** <sup>1</sup>University of Texas Southwestern Medical Center, <sup>2</sup>University of Pennsylvania

**Correspondence:**

\* youxing.jiang@utsouthwestern.edu

This work was supported in part by the Howard Hughes Medical Institute and by grants from the National Institutes of Health (GM079179 to Y.J.; NS055293 and NS074257 to D.R.) and the Welch Foundation (Grant I-1578 to Y.J.). The Advanced Light Source is supported by the Director, Office of Science-Basic Energy Sciences, of the U.S. Department of Energy (DOE) under contract no. DE-AC02-05CH11231. SBC-CAT is operated by UChicago Argonne, LLC, for the U.S. DOE Office of Biological and Environmental Research under Contract No. DE-AC02-06CH11357. GM/CA-XSD has been funded in whole or in part with Federal funds from the National Cancer Institute (ACB-12002) and the National Institute of General Medical Sciences (AGM-12006). This research used resources of the Advanced Photon Source, a U.S. DOE Office of Science User Facility operated for the DOE Office of Science by Argonne National Laboratory under Contract No. DE-AC02-06CH11357.

**19-ID-D • SBC-CAT • Life sciences • Macromolecular crystallography, multi-wavelength anomalous dispersion, subatomic ( $<0.85$  Å) resolution, microbeam, ultra-low-temperature (15K), large unit cell crystallography, single-wavelength anomalous dispersion • 6.5-19.5 keV • On-site, remote, mail-in • Accepting general users •**

**23-ID-B • GM/CA-XSD • Life sciences • Macromolecular crystallography, microbeam, large unit cell crystallography, subatomic ( $<0.85$  Å) resolution, multi-wavelength anomalous dispersion, single-wavelength anomalous dispersion • 3.5-20 keV • On-site, remote • Accepting general users •**

**23-ID-D • GM/CA-XSD • Life sciences • Macromolecular crystallography, microbeam, large unit cell crystallography, subatomic ( $<0.85$  Å) resolution, multi-wavelength anomalous dispersion, single-wavelength anomalous dispersion • 5-20 keV • On-site, remote • Accepting general users •**



# FIGHTING EBOLA WITH AN ANTIBODY COCKTAIL

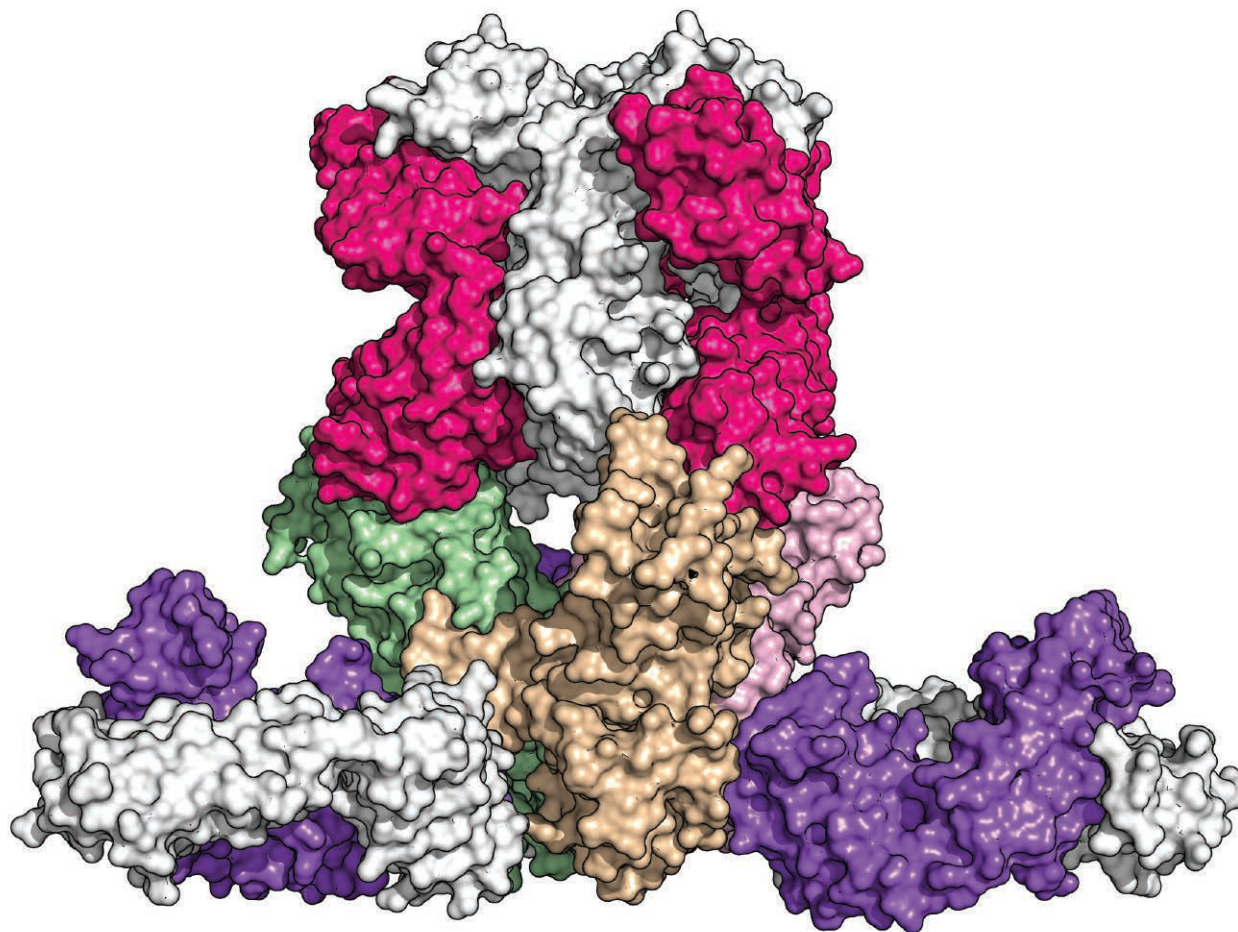


Fig. 1. Molecular surface representation of Ebola glycoprotein (tan, green, pink) bound at the top by Fab114 (magenta, white) and at the side by Fab100 (purple, white). Credit: Morgan Gilman

19-ID-D • SBC-CAT • Life sciences • Macromolecular crystallography, multi-wavelength anomalous dispersion, subatomic ( $<0.85$  Å) resolution, microbeam, ultra-low-temperature (15K), large unit cell crystallography, single-wavelength anomalous dispersion • 6.5-19.5 keV • On-site, remote, mail-in • Accepting general users •



**D**uring the Ebola outbreak that began in 2014, more than 11,000 people are reported to have died from the disease. While that epidemic was eventually contained, the threat of the Ebola virus remains and, to date, there is no approved therapy. Two monoclonal antibodies, mAb100 and mAb114, originally isolated from a human Ebola survivor appear to block all signs of the virus when administered to monkeys. To figure out how the antibodies neutralize the Ebola virus, researchers solved the structures of the antibody pieces that bind the virus (antigen-binding fragment or Fab) alone and in complex with the part of the Ebola virus to which the Fab binds using diffraction data collected at the APS. The structures, in conjunction with other data, reveal the antibodies' strategies for undermining Ebola, providing critical information to facilitate the development of a treatment or vaccine for Ebola.

When a virus attacks the body, the immune system produces antibodies that recognize a particular antigen on the virus and trigger the body's defenses. In 1995, an Ebola epidemic ravaged Kikwik, a city in the Democratic Republic of Congo. In a previous study, the researchers isolated two monoclonal antibodies from the blood samples taken from one of the survivors of the Kikwik outbreak. These antibodies, working together, may be special, neutralizing in the test tube multiple strains of the Ebola virus collected over 40 years. Plus, the antibody cocktail saved rhesus monkeys infected with Ebola virus as many as five days prior to receiving the treatment. Despite these promising findings, important questions remained, particularly the questions of how the antibodies recognize and work together to block the Ebola virus.

To find the Ebola antigen, the researchers in this study, from the National Institutes of Health, the Geisel School of Medicine at Dartmouth, the Frederick National Laboratory for Cancer Research, Tsinghua University (China), the Brigham and Women's Hospital, Università della Svizzera Italiana (Switzerland), National Laboratory of Public Health (Democratic Republic of the Congo), Boston Children's Hospital, and ETH Zurich (Switzerland) first crystallized and solved the structures of Fab100 and Fab114 to high resolution, 2.0 Å, at SBC-CAT beamline 19-ID-D at the APS (Fig. 1). Next, the researchers identified, roughly, the part of the Ebola virus to which both antibodies bind: the Ebola virus glycoprotein, a chalice-shaped trimer involved in viral entry

into host cells. The glycoprotein structure, minus one segment not involved in antibody binding, had been solved previously. The researchers co-crystallized the Fab fragments with the Ebola glycoprotein segment to form a ternary protein complex. Using molecular replacement information from the unbound protein structures, they solved the complex ternary structure to a resolution of 6.7 Å.

The structure yielded many insights into the structural and molecular basis for Ebola virus neutralization by mAb100 and mAb114. The researchers found that mAb100 recognizes the base of the Ebola virus glycoprotein trimer, blocking access to the cathepsin-cleavage loop. For the virus to gain entry into the host cell, endosomal cathepsin catalyzes the proteolytic cleavage of the glycoprotein, a process that mAb100 would appear to shut down. Meanwhile, mAb114 provides a complementary interference with viral invasion by interacting with the glycan cap and inner chalice of the glycoprotein. Another critical step in viral entry into the cell is the binding of the cleaved glycoprotein by a particular cellular receptor, a pathway that is blocked by mAb114.

These discoveries may help develop a treatment or vaccine for Ebola, as well as other members of the *Filoviridae* family of viruses that use the same strategy to gain entry into host cells. For example, mAb100 and mAb114 may be used directly in the treatment of Ebola. Alternately, researchers may use the structural information in the rational design of new antibody variants with improved potency

and/or breadth against related filoviruses. — *Erika Gebel Berg*

**See:** John Misasi<sup>1,5,8</sup>, Morgan S.A. Gilman<sup>2</sup>, Masaru Kanekiyo<sup>1</sup>, Miao Gui<sup>4</sup>, Alberto Cagigi<sup>1</sup>, Sabue Mulangu<sup>1</sup>, Davide Corti<sup>6</sup>, Julie E. Ledgerwood<sup>1</sup>, Antonio Lanzavecchia<sup>6,9</sup>, James Cunningham<sup>5</sup>, Jean Jacques Muyembe-Tamfun<sup>7</sup>, Ulrich Baxa<sup>3</sup>, Barney S. Graham<sup>1</sup>, Ye Xiang<sup>4\*\*</sup>, Nancy J. Sullivan<sup>1\*</sup>, and Jason S. McLellan<sup>2</sup>, "Structural and molecular basis for Ebola virus neutralization by protective human antibodies," *Science* **351**(6279), 1343 (18 March 2016).

DOI: 10.1126/science.aad6117

**Author affiliations:** <sup>1</sup>National Institutes of Health, <sup>2</sup>Geisel School of Medicine at Dartmouth, <sup>3</sup>Frederick National Laboratory for Cancer Research, <sup>4</sup>Tsinghua University, <sup>5</sup>Brigham and Women's Hospital, <sup>6</sup>Università della Svizzera Italiana, <sup>7</sup>National Laboratory of Public Health, Democratic Republic of the Congo, <sup>8</sup>Boston Children's Hospital, <sup>9</sup>ETH Zurich

**Correspondence:** \* njsull@mail.nih.gov  
\*\* yxiang@mail.tsinghua.edu.cn

This work was supported by the Intramural Research Program of the Vaccine Research Center, the National Institute of Allergy and Infectious Diseases, and the National Institutes of Health (NIH). J.M. received grant support from NIH-5K08AI079381 and a Boston Children's Hospital Faculty Development award. M.S.A.G. was supported by the National Institute of General Medical Sciences, NIH, under award T32GM008704. Y.X. received grant support from the 973 program (2015CB14010102), the National Natural Science Foundation of China (81550001 and 31470721), and the Junior Thousand Talents Program of China (20131770418). This work was funded in part with federal funds from the Frederick National Laboratory for Cancer Research, NIH, under contract HHSN261200800001E. SBC-CAT is operated by UChicago Argonne, LLC, for the U.S. Department of Energy (DOE), Office of Biological and Environmental Research under contract DE-AC02-06CH11357. This research used resources of the Advanced Photon Source, a U.S. DOE Office of Science User Facility operated for the DOE Office of Science by Argonne National Laboratory under Contract No. DE-AC02-06CH11357.

# HOW A ZIKA PROTEIN COULD GUIDE VACCINE DEVELOPMENT

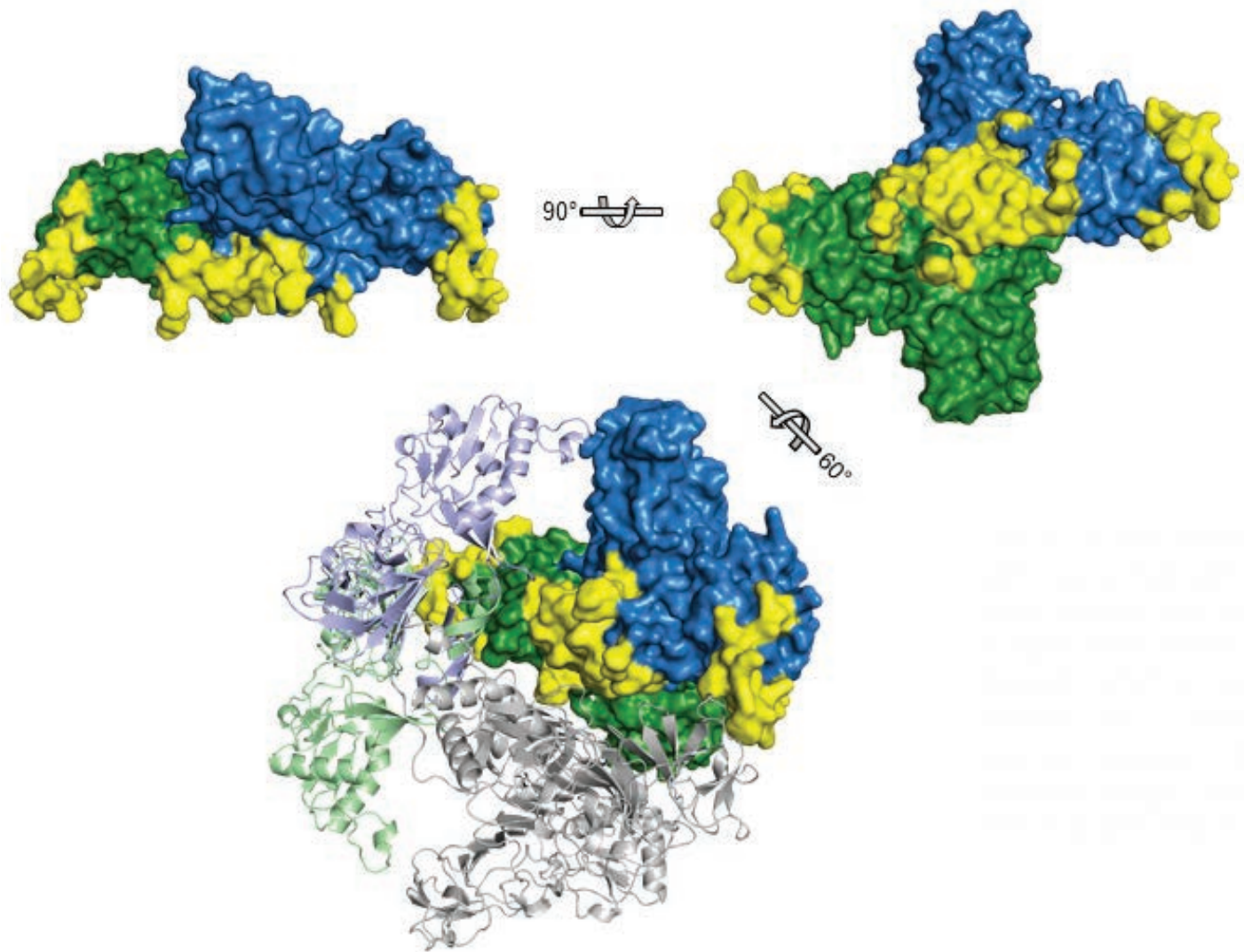


Fig. 1. Zika virus NS1 dimer side (top left) and inner face (top right) views highlight hydrophobic regions (yellow), which interact with membranes on cell surfaces. Three NS1 dimers assemble into a soluble hexamer (bottom) which circulates in the bloodstream of infected patients. NS1 in the absence of the virus is sufficient to cause vascular leakage in biological model systems. In the hexamer image, one dimer is shown as a solid surface, one as a gray ribbon and the third as a colored ribbon.

23-ID-D • GM/CA-XSD • Life sciences •  
 Macromolecular crystallography, microbeam,  
 large unit cell crystallography, subatomic  
 (<0.85 Å) resolution, multi-wavelength anomalous  
 dispersion, single-wavelength anomalous  
 dispersion • 5-20 keV • On-site, remote  
 • Accepting general users •

**B**ecause of its critical roles in viral replication and disease pathogenesis, the flavivirus nonstructural protein 1 (NS1) is an attractive target for design of vaccines and drugs that could protect against diseases such as Zika, West Nile, and dengue that are caused by flaviviruses. Despite advances in understanding of the structure of NS1, some important features remained unknown. Researchers therefore set out to further investigate its molecular structure. They used data for Zika NS1 collected at the APS to determine how NS1 interacts with cell membranes. They also found that the outer surface of the Zika NS1 has electrical charge properties that differ from those of NS1 proteins from other flaviviruses. The results of this study could help scientists better understand how Zika virus affects the immune system, and could also help with development of vaccines and antiviral drugs to help control Zika disease.

Flaviviruses such as Zika, dengue, and West Nile viruses are arthropod-borne pathogens that present significant public health threats worldwide. In particular, Zika virus recently became an international health emergency, not only because of its rapid spread throughout Central and South America, but also because of its association with severe birth defects and with Guillain-Barré syndrome.

NS1 is a highly-conserved protein among flaviviruses and plays key roles in viral infections. When the virus infects a host, NS1 is involved in viral replication and packaging, allowing the virus to continue infecting more cells in the host. Some NS1 is also secreted as hexamers (Fig. 1) into the bloodstream of infected individuals, and higher NS1 levels have been found to correlate with more severe illness. Even in the absence of virus, studies have shown that NS1 alone is sufficient to cause vascular leakage in biological model systems.

Researchers from the University of Michigan had previously solved structures for the NS1 protein from dengue virus serotype 2 and from West Nile virus (also using data collected at the GM/CA-XSD beamline at the APS). So, when Zika virus infection was linked with an increased incidence of microcephaly and Guillain-Barré syndrome, they realized they could also contribute to understanding this new viral threat.

In collaboration with researchers from Purdue University, they conducted studies to determine the structure of Zika virus NS1. Although their previous work with the NS1 protein had estab-

lished its basic structure, several features were not resolved. Using data collected at GM/CA-XSD beamline 23-ID-D at the APS, the researchers were able to determine more detailed information about the Zika virus NS1 protein, which helped to fill in these gaps.

For example, they found that Zika virus NS1 has electrostatic charge properties that differ from those of NS1 proteins in other flaviviruses. They also identified a part of the protein that was not visible in the earlier NS1 structures—an additional hydrophobic surface for membrane association (Fig. 1) during viral replication. Elucidating the Zika virus NS1 structure helped the researchers to understand how NS1 circulates in the bloodstream of infected patients as a protein-lipid particle.

According to the researchers, this new information about the Zika virus NS1 structure adds important details of the molecular framework for understanding how NS1 accomplishes its functions in the infection cycle. Scientists can compare the structural features of the NS1 proteins of different viruses to gain insights into the divergent activities among these proteins, and how this affects the characteristics of the diseases these different viruses cause.

Because no vaccine or treatment currently exists for Zika virus infection, the results of this research therefore have potential to help scientists design vaccines and antiviral drugs against Zika virus.

The researchers are currently also working to understand how NS1 proteins influence the immune system and

stimulate vascular leakage. In addition, they are collaborating with other laboratories to better understand how NS1 contributes to the disease states in a viral infection.

Understanding of the NS1 domain structure is guiding current research into dissecting the regions responsible for immune system modulation, virus replication and packaging, and stimulation of vascular leakage. Hopefully, these insights will guide new therapeutics and vaccine development.

— Nicola Parry

**See:** W. Clay Brown<sup>1</sup>, David L. Akey<sup>1</sup>, Jamie R. Konwerski<sup>1</sup>, Jeffrey T. Tarasch<sup>1</sup>, Georgios Skiniotis<sup>1</sup>, Richard J. Kuhn<sup>3</sup>, and Janet L. Smith<sup>1\*</sup>, “Extended surface for membrane association in Zika virus NS1 structure,” *Nat. Struct. Mol. Biol.* **23**(9), 865 (September 2016). DOI: 10.1038/nsmb.3268

**Author affiliations:** <sup>1</sup>University of Michigan, <sup>2</sup>Purdue University

**Correspondence:**

\* janetsmith@umich.edu

This work was supported by a Margaret J. Hunter Collegiate Professorship in the Life Sciences to J.L.S. and by the University of Michigan Life Sciences Institute. GM/CA-XSD is supported by the National Institutes of Health National Institute of General Medical Sciences (AGM-12006) and the National Cancer Institute (ACB-12002). This research used resources of the Advanced Photon Source, a U.S. Department of Energy (DOE) Office of Science User Facility operated for the DOE Office of Science by Argonne National Laboratory under Contract No. DE-AC02-06CH11357.



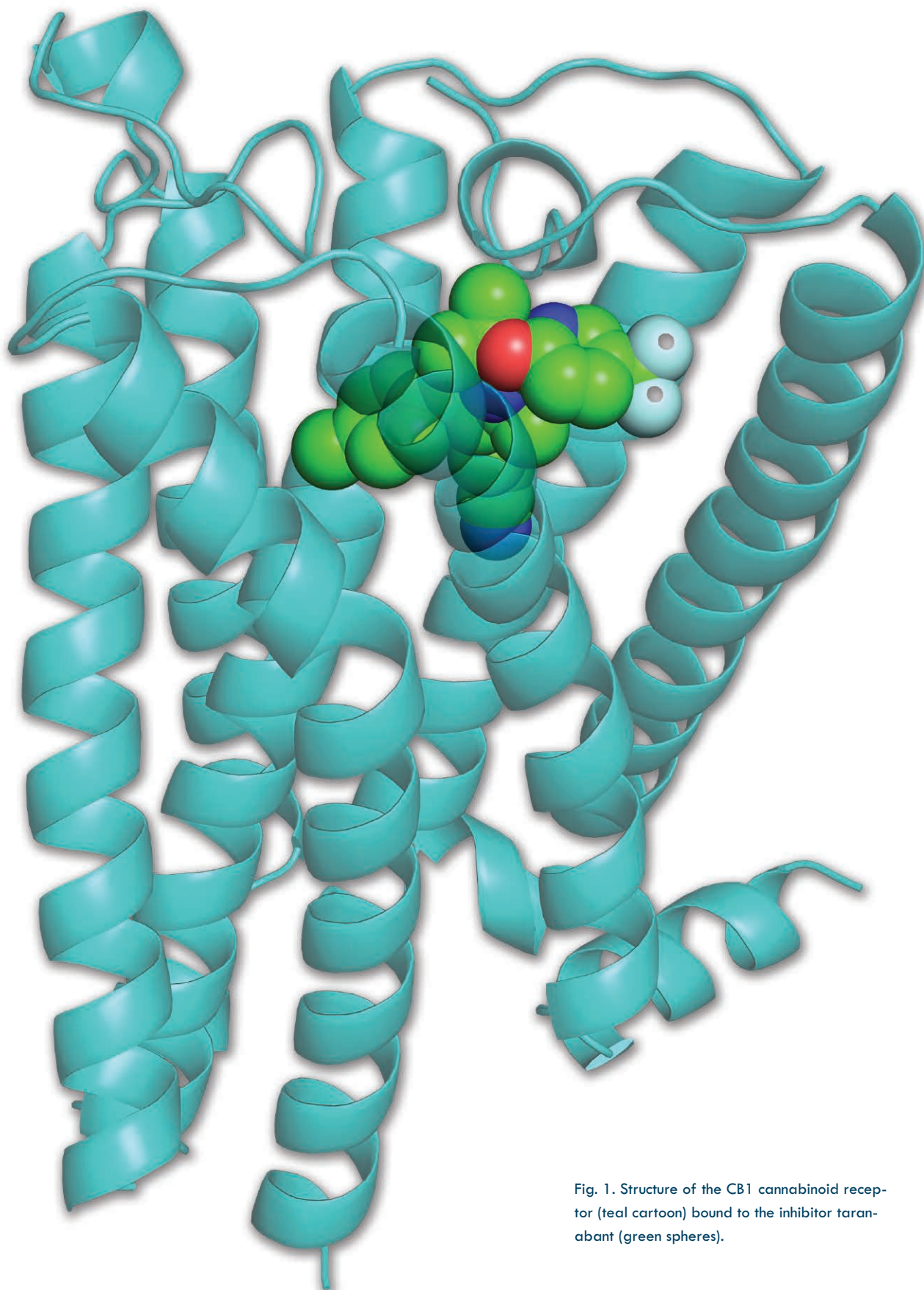


Fig. 1. Structure of the CB1 cannabinoid receptor (teal cartoon) bound to the inhibitor taranabant (green spheres).

# STRUCTURAL INSIGHTS INTO CANNABIS RECEPTORS COULD LEAD TO NEW THERAPIES

**T**he cannabinoid CB1 receptor forms part of the mammalian endocannabinoid system, which plays important roles in many aspects of physiology and pathology. Although scientific advances have led to discovery of numerous compounds that target this receptor and have the potential to treat various conditions, knowledge of its detailed structure has so far been lacking. To increase understanding of the receptor's mechanism and function, researchers set out to determine the crystal structure of CB1 at high resolution. Using x-ray diffraction data collected at the APS, they characterized the structure of the receptor's pocket where compounds such as  $\Delta^9$ -tetrahydrocannabinol (THC), as well as cannabinoid inhibitor drugs, bind to CB1. The results of this study could help scientists better understand how cannabinoids affect the brain, and could also help with discovery of new therapies that target the CB1 receptor to treat conditions such as epilepsy or marijuana addiction.

The cannabinoid receptors (CB1 and CB2) are major players in the human endocannabinoid system, which is involved in regulating various physiological processes, including appetite and pain-sensation. CB1 is predominantly found in the nervous system, while CB2 is mostly located in the immune system. These G protein-coupled receptors (GPCRs) are activated by the endocannabinoids anandamide and 2-arachidonoyl-glycerol (2-AG), which are made in the body, as well as the cannabinoid THC, which is the main psychoactive component of marijuana.

Cannabinoid receptors therefore represent a potential target for the design and development of new therapeutic drugs. CB1, for example, is the most abundant GPCR in the human brain, has multiple physiological functions in the central nervous system (CNS), and is an important target for design of cannabinoid inhibitor drugs to treat conditions such as obesity, neuropathic pain, and epilepsy.

X-ray diffraction data collected at the GM/CA-XSD beamline 23-ID-B at the APS helped the researchers from The University of Texas Southwestern Medical Center elucidate the CB1 receptor at high resolution (Fig. 1). This allowed them to unambiguously characterize the structure of its ligand binding pocket. This pocket in the receptor is where modulators such as cannabi-

noids made in the body, THC, and cannabinoid inhibitor drugs work to influence the receptor. As such, this pocket is an important focus for scientists involved in development of cannabinoid inhibitor drugs.

In their study, the researchers identified the mode of binding for a clinically tested cannabinoid receptor antagonist, taranabant (Fig. 1), and gained insights into how modulators enter the CB1 receptor.

By characterizing the extracellular loops of the CB1 receptor, they showed that these regions are structurally different than they are in other lipid-activated GPCRs in the same family, such as the sphingosine phosphate receptor, which is found throughout the body and regulates important physiological actions, including vascular development and cardiac function. When they used the clinical antagonist, the researchers also showed that it binds at a different position in the CB1 receptor than it does in other GPCRs from the same family.

Cannabinoid inhibitor drugs are becoming increasingly important, both for their potential medical uses and for their societal impacts in situations such as drug abuse and addiction. Because determining the CB1 receptor structure helps to improve understanding of how these drugs bind to the receptor, the results of this research therefore have potential to allow future rational drug de-

sign and optimization. The researchers are currently also working on crystallization of the activated CB1 receptor, and hope to obtain structures of CB1 bound to an agonist. — *Nicola Parry*

**See:** Zhenhua Shao<sup>1</sup>, Jie Yin<sup>1</sup>, Karen Chapman<sup>1</sup>, Magdalena Grzemska<sup>1</sup>, Lindsay Clark<sup>1</sup>, Junmei Wang<sup>2</sup>, and Daniel M. Rosenbaum<sup>1\*</sup>, "High-resolution crystal structure of the human CB1 cannabinoid receptor," *Nature* **540**(22), 602 (29 December 2016).

DOI: 10.1038/nature20613

**Author affiliation:** The University of Texas Southwestern Medical Center

**Correspondence:**

\* dan.rosenbaum@utsouthwestern.edu

We thank the staff of the GM/CA-XSD beamline 23-ID-B at the APS for support during data collection. This project was supported by a Welch Foundation grant (I-1770 to D.M.R.) and a Packard Foundation Fellowship (D.M.R.). This research used resources of the Advanced Photon Source, a U.S. Department of Energy (DOE) Office of Science User Facility operated for the DOE Office of Science by Argonne National Laboratory under Contract No. DE-AC02-06CH11357.

23-ID-B • GM/CA-XSD • Life sciences • Macromolecular crystallography, microbeam, large unit cell crystallography, subatomic (<0.85 Å) resolution, multi-wavelength anomalous dispersion, single-wavelength anomalous dispersion • 3.5-20 keV • On-site, remote • Accepting general users •

# FROM TRASH TAG TO MAJOR CELLULAR MEDIATOR: THE EMERGING ROLE OF THE UBIQUITIN SYSTEM

Ubiquitin is a protein that earned its name from the fact that it is ubiquitous; it is found in almost all cells of eukaryotic organisms. The addition of ubiquitin to cellular proteins has been identified as an important mechanism for tagging proteins for disposal by the cellular degradation system, the proteasome. More recently, proteins of the ubiquitin system have been implicated as key players in such diverse cellular activities as apoptosis, immune regulation, host-pathogen interactions, and cellular aging, and in diseases such as cancer, autism, and muscular dystrophies. So, understanding the details of the system is of importance to many different areas of research and medicine. In this research study, carried out at the APS, the goal is to elucidate the interactions of enzymes that are central to ubiquitination, the addition of ubiquitin to a substrate target protein. Understanding these interactions is critical to understanding how the complex ubiquitin system works and to the rational design of drugs that target an ever-widening array of ubiquitin-system-related diseases.

Ubiquitination is accomplished by the action of enzymes that work in sequence, E1, E2, and E3, to add ubiquitin to a target protein. The human genome codes for 2 E1s, ~40 E2s, and over 600 E3s, suggesting that E3 is where the system's target specificity and heterogeneity resides. E3 enzymes work in complex with an assembly of other proteins that guide E3-target interactions. One of these E3 enzymes, Cullin3, interacts with members of a large family of BTB proteins that act as target adaptors. Structures from one subfamily of BTB proteins in complex with Cullin3 have been solved. However, another subfamily, the KCTD subgroup, does not share the same Cullin3 interaction sites.

In order to learn more about how KCTD

proteins interact with the Cullin3 E3 enzyme, a team of investigators from the University of Toronto, the Princess Margaret Cancer Centre, and the Hospital for Sick Children Research Institute in Toronto (all in Canada) used a variety of structural, biophysical, and biochemical methods to probe the interactions between Cullin3 and six KCTD adaptor proteins, KCTDs 1, 5, 6, 9, 16, and 17.

The first step for the team was to solve the crystal structures for KCTD1 and KCTD9. Data obtained from studies at the IMCA-CAT 17-ID-B beamline of the APS showed that these proteins form pentameric structures that contain five molecules of KCTD. KCTD9 exhibits a single rigid structure while KCTD1 exhibits three different pentameric forms,

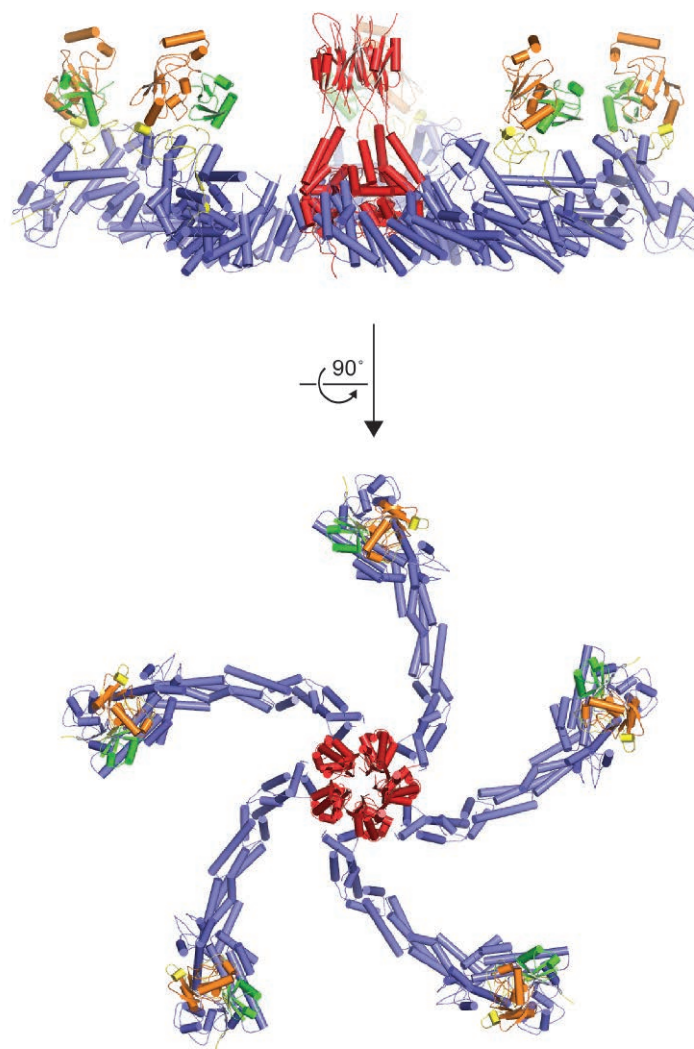


Fig. 1. Model of a pentameric KCTD/Cullin3 E3 ligase complex. The 5-fold symmetric KCTD protein (red) assembles 5 individual Cullin3/Rbx1/E2~Ubiquitin subcomplexes (blue, yellow, orange and green, respectively) into a “pinwheel” structure. All five Cullin3 chains curve up toward the C-terminal domain face of the KCTD pentamer and position the E2~ubiquitin chains in the proximity of the presumed substrate binding site.



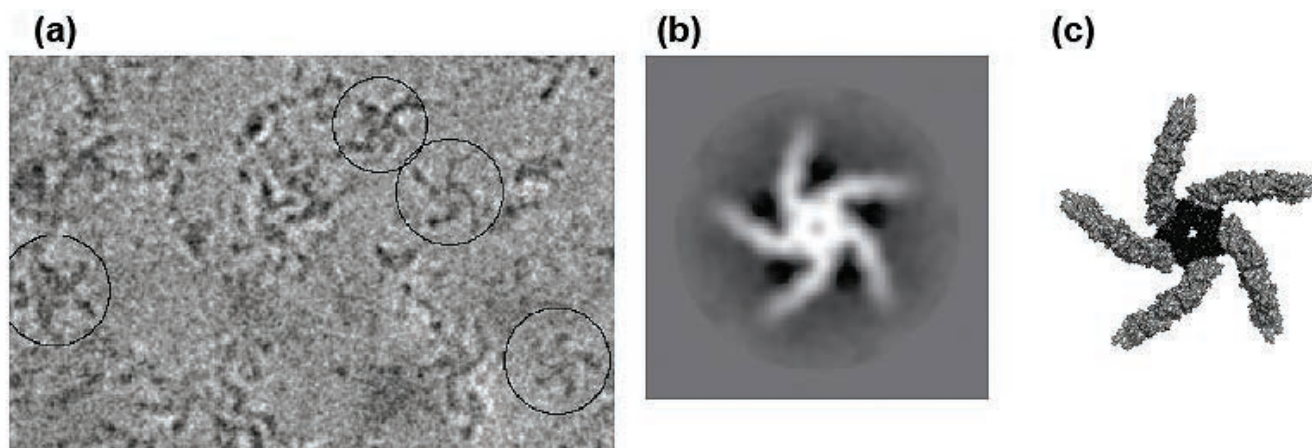


Fig. 2. The KCTD9/Cul3 complex as visualized by cryo electron-microscopy. (a) Micrograph of individual complexes (circled). (b) 5-fold averaged complex. (c). Molecular model with the KCTD9 pentamer (black) and the associated Cul3 arms (grey).

suggesting a more dynamic structure. The research team provided additional support for these pentameric structures by analyzing the size of the KCTD proteins in solution by analytical size exclusion chromatography (SEC). SEC experiments showed that all of the KCTDs tested exhibited sizes in solution that were consistent with adoption of pentameric structures.

Their next question concerned the interaction of the KCTD pentamers with Cullin3. SEC and isothermal titration calorimetry (ITC) were used to investigate the interactions of the KCTD proteins with Cullin3 in solution and the strength of those interactions. Mixtures of the KCTD proteins with Cullin3 exhibited sizes and dissociation constants consistent with a 5:5 complex of Cullin3 with KCTDs 5, 6, 9, and 17 but no Cullin3 binding to KCTD1 or KCTD 16. These data were supported by experiments conducted with mutated forms of KCTD5 and KCTD9 that showed that changes in amino acids thought to be involved in Cullin3 interactions disrupted binding.

In order to understand more about the 5:5 stoichiometry of the KCTD proteins with Cullin3 suggested by the crystal structures and biophysical tests, the team used a previous Cullin3/adaptor complex structure to model interac-

tions with their own KCTD9 structure. Modeling suggested a pinwheel-shaped structure with the KCTD9 pentamer at the center and five Cullin3 proteins as the arms of the wheel (Figure 1). To test this experimentally, the team made complexes of Cullin3 plus KCTD9 and analyzed them by cryo-electron microscopy. The images obtained from the cryo-EM were a match for those from the model (Figure 2). Further modeling allowed them to look more closely at how Cullin3 interacts with the KCTD pentamer. Their model predicts that Cullin3 interacts with two adjacent KCTDs in the pentamer.

This may explain why KCTD1, with its more dynamic pentameric structure, does not bind to Cullin3. However, with so many E3s and so many adaptors, the details of this interaction and of how these proteins impact cellular processes and disease states provide plenty of topics for future study.

— Sandy Field

**See:** Alan X. Ji<sup>1</sup>, Anh Chu<sup>1</sup>, Tine Kragh Nielsen<sup>2</sup>, Samir Benlekbi<sup>3</sup>, John L. Rubinstein<sup>1,3</sup>, and Gilbert G. Privé<sup>1,2\*</sup>, "Structural Insights into KCTD Protein Assembly and Cullin3 Recognition," *J. Mol. Biol.* **428**, 92 (2016).

DOI: 10.1016/j.jmb.2015.08.019

**Author affiliations:** <sup>1</sup>University of

Toronto, <sup>2</sup>Princess Margaret Cancer Centre, <sup>3</sup>The Hospital for Sick Children Research Institute

**Correspondence:**

\* [prive@uhnres.utoronto.ca](mailto:prive@uhnres.utoronto.ca)

This work was supported by grants to G.G.P. from the Canadian Cancer Society Research Institute, Cancer Research Society and Canadian Institutes of Health Research. J.L.R. was supported by Canadian Institutes of Health Research grant MOP 81294 and the Canada Research Chairs program. This research was funded in part by the Ontario Ministry of Health and Long-Term Care. The IMCA-CAT beamline is supported by the companies of the Industrial Macromolecular Crystallography Association through a contract with Hauptman-Woodward Medical Research Institute. This research used resources of the Advanced Photon Source, a U.S. Department of Energy (DOE) Office of Science User Facility operated for the DOE Office of Science by Argonne National Laboratory under Contract No. DE-AC02-06CH11357.

17-ID-B • IMCA-CAT • Life sciences • Macromolecular crystallography, multi-wavelength anomalous dispersion, microbeam, single-wavelength anomalous dispersion, large unit cell crystallography • Subatomic (<0.85 Å) resolution • 6-20 keV • On-site, remote • Accepting general users •

# A PROMISING NEW TOOL FOR DRUG DESIGN

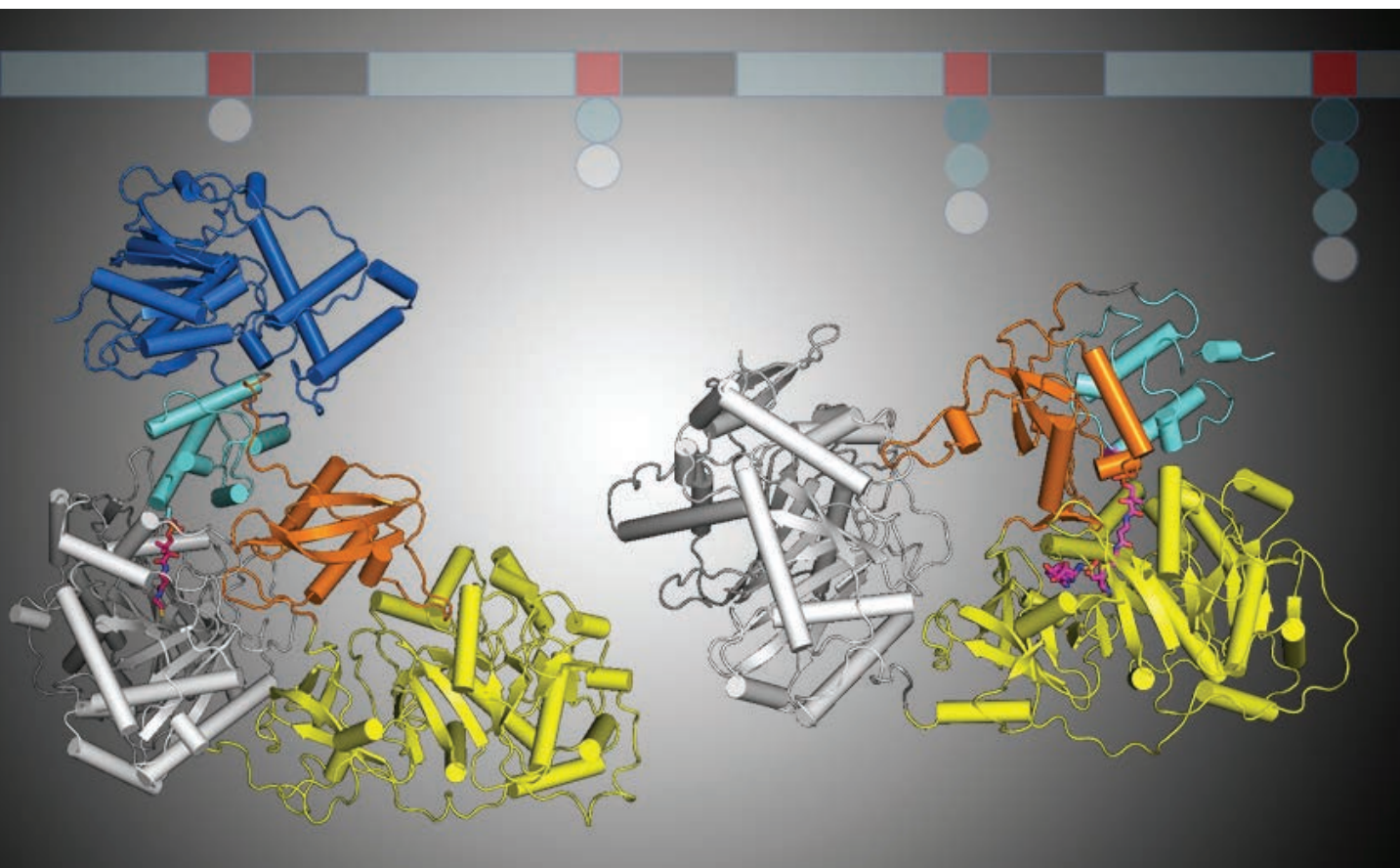


Fig. 1. Two multi-domain NRPS proteins. Left panel shows PCP (cyan) bound within the condensation domain (white). Rotation of the small adenylation C-terminal subdomain (orange) transports the PCP to the adenylation domain active site in the structure on the right.

Bacteria and fungi are skilled biochemists that can make an unusual variety of natural peptides, some of which have immunosuppressant, antibiotic, or cytotoxic effects that make them useful medicines. These peptides are made utilizing the 20 common amino acids we all use, plus variations of these, such as D-amino acids and cyclic forms, that provide them with their unique properties. These peptides are not built by the normal ribosomal machinery that translates messenger RNA (mRNA) into protein but by non-ribosomal peptide synthetases (NRPSs) that work without ribosomes or mRNA to guide them. NRPSs are multi-domain modular cellular machines that work in a kind of assembly line to catalyze each reaction in the generation of these unusual peptides. Researchers are interested in how NRPSs work in order to understand the chemistry underlying how these unique natural products are made and in the exciting prospect that the amazing chemical diversity generated by NRPSs can be re-engineered to make novel drugs and antibiotics. For both of these goals, detailed structural knowledge of NRPSs is needed. Work by a team of scientists using the APS has provided important insights into how bacterial NRPSs catalyze some of the key steps of peptide synthesis and how the domains of these modular cellular machines interact. This more detailed understanding of the elegantly coordinated movements of the domains of the NRPS, as well as a view of ligands bound within the condensation domain will assist researchers in finding ways to engineer these interactions to create new and potentially valuable peptide natural products.

NRPSs catalyze the formation of a peptide natural product. The product is built while attached to peptidyl carrier proteins (PCPs) that orchestrate the process by delivering the intermediates to adjacent catalytic domains. The basic steps of this process include activation of the new amino acid and transfer to the PCP by the adenylation domain, creation of the peptide bond between the newly activated amino acid and the growing peptide on the adjacent module by the condensation domain, and release of the product by a thioesterase or reductase domain. Additional tailoring domains may be associated with the NRPS to accomplish unique chemical modifications as they are needed.

A key question in the field of NRPS research has centered on how the PCP migrates between the different catalytic domain active sites. That is, do the PCP and the domains float around randomly until they make a productive interaction or are their interactions more organized? In order to get at an answer to this question, these investigators from the Hauptman-Woodward Medical Research Institute, the University at Buffalo, the University of Minnesota, and the University of Michigan sought to

capture some of these catalytic reactions "in the act" by crystalizing NRPS proteins trapped at various stages of the peptide building process.

In work conducted at the GM/CA-XSD beamline 23-ID-B at the APS, they were able to solve the structures of three NRPSs captured at three different stages of catalysis. One was without ligand, the second used an inhibitor to illustrate delivery of the PCP to the adenylation domain, and the third showed the delivery of the PCP to the condensation domain. These snapshots of catalysis provided insights into how the PCP moves between two of the three NRPS domains.

The results provide new information about the conformations of the adenylation and condensation domains while they interact with the PCP to load the activated amino acid onto the PCP and then shift the loaded PCP over to the condensation domain for peptide bond formation. The adenylation domain structure shows that, rather than a random process, the adenylation domain first catalyzes the activation of the amino acid then rotates a small C-terminal subdomain to deliver the PCP to the adenylation domain to be loaded with

the amino acid substrate (Figure 1). The other crystal structure then picks up the story to reveal that once the PCP is loaded, a reversal of this conformational change transports the PCP back to the condensation domain while the adenylation domain activates a second amino acid to prepare for the next cycle.

The research team is continuing their studies to look at additional multidomain NRPS enzymes bound with informative ligands that will give insight into the ability of the NRPS domains to catalyze peptide natural product biosynthesis. — *Sandy Field*

**See:** Eric J. Drake<sup>1,2</sup>, Bradley R. Miller<sup>1,2</sup>, Ce Shi<sup>3</sup>, Jeffrey T. Tarrasch<sup>4</sup>, Jesse A. Sundlov<sup>1,2</sup>, C. Leigh Allen<sup>1</sup>, Georgios Skiniotis<sup>4</sup>, Courtney C. Aldrich<sup>3</sup>, and Andrew M. Gulick<sup>1,2\*</sup>, "Structures of two distinct conformations of holo-non-ribosomal peptide synthetases," *Nature* **235**, 529 (15 January 2016). DOI: 10.1038/nature16163  
**Author affiliations:** <sup>1</sup>Hauptman-Woodward Medical Research Institute, <sup>2</sup>University at Buffalo, <sup>3</sup>University of Minnesota, <sup>4</sup>University of Michigan

**Correspondence:**

\* gulick@hwi.buffalo.edu

This work was funded in part by National Institutes of Health GM-068440 (to A.M.G.) and GM-115601 (to G.S.), and Award W81XWH-11-2-0218 from the Telemedicine and Advanced Technology Research Center of the U.S. Army Medical Research and Materiel Command (A.M.G.). A Stafford Fellowship (to B.R.M.) and support from the Hauptman-Woodward Institute is acknowledged. GM/CA-XSD has been funded in whole or in part with Federal funds from the National Cancer Institute (ACB-12002) and the National Institute of General Medical Sciences (AGM-12006). This research used resources of the Advanced Photon Source, a U.S. Department of Energy (DOE) Office of Science User Facility operated for the DOE Office of Science by Argonne National Laboratory under Contract No. DE-AC02-06CH11357.

23-ID-B • GM/CA-XSD • Life sciences • Macromolecular crystallography, microbeam, large unit cell crystallography, subatomic (<0.85 Å) resolution, multi-wavelength anomalous dispersion, single-wavelength anomalous dispersion • 3.5-20 keV • On-site, remote • Accepting general users •



# STRUCTURE OF THE HUMAN SEROTONIN TRANSPORTER ELUCIDATES AN ANTIDEPRESSANT MECHANISM

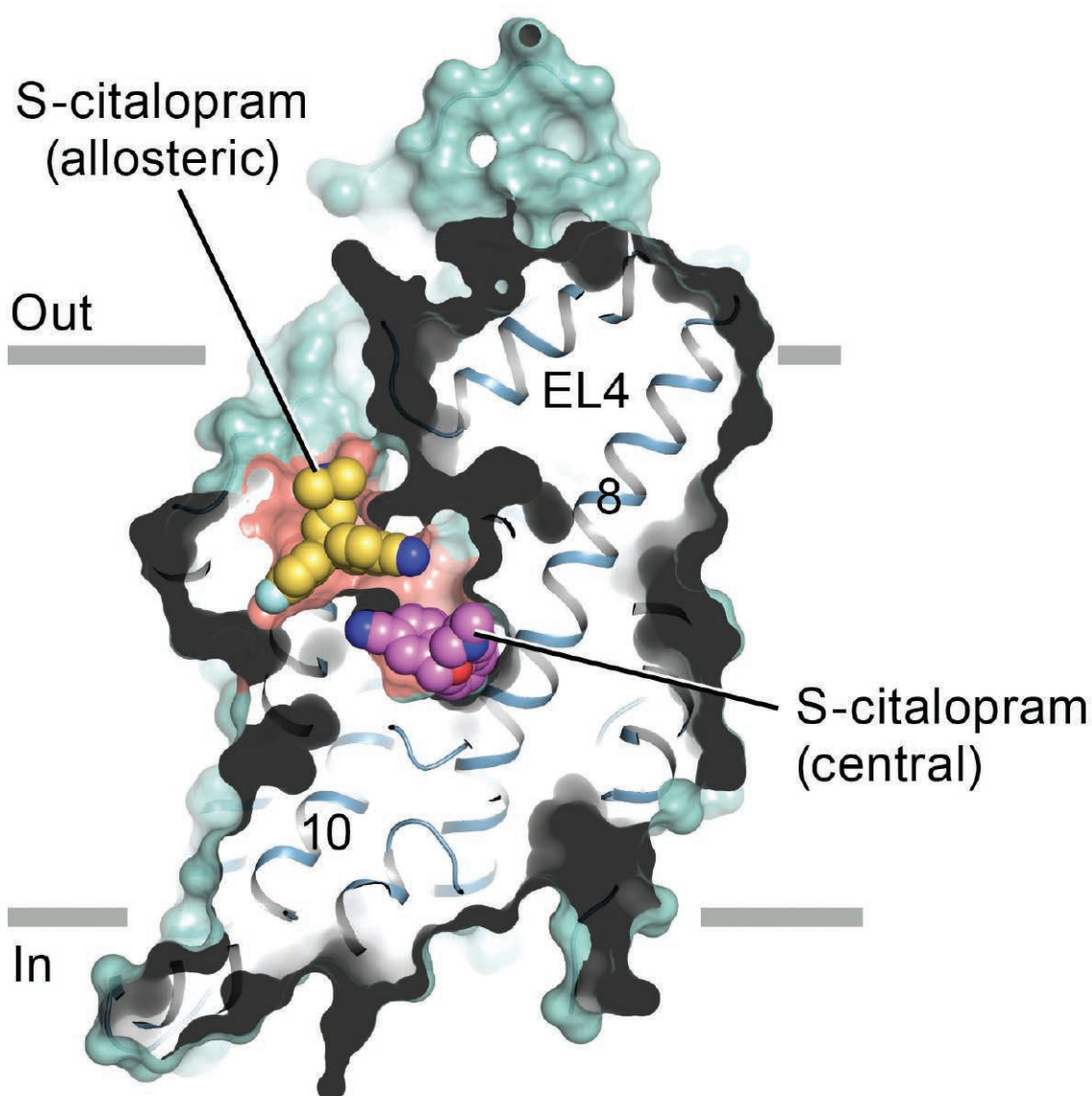


Fig. 1. The image depicts a slice through a surface representation of the serotonin transporter bound the antidepressant S-citalopram. S-citalopram molecules bound to the allosteric (yellow) and central (magenta) sites are shown as spheres.

**S**erotonin is an important neuronal modulator that is essential for the functioning of the central nervous system, cardiovascular system, digestion, body temperature, endocrine system, and reproduction. Serotonin acts through membrane receptors in neurons to regulate the production of a wide range of neurotransmitters and hormones. This signaling is terminated through reuptake of serotonin by the serotonin transporter (SERT) that removes serotonin from the surrounding space between neurons. Antidepressant drugs such as the serotonin-specific reuptake inhibitors (SSRIs), like Prozac, work by inhibiting reuptake, keeping serotonin signaling active. In addition to depression, dysregulation of transporters in the neurotransmitter transporter family has been identified as important in diseases such as anxiety disorder, attention-deficit hyperactivity disorder, epilepsy, and Parkinson's disease. However, although the structures of homologous bacterial and fruit fly transporters have provided insight into the pharmacology of this important class of transport proteins, the structural details of human SERT have yet to be uncovered. Now, in work by a team that utilized high-brightness x-ray beams from the U.S. Department of Energy's Advanced Photon Source (APS) at Argonne National Laboratory, the structure of human SERT in complex with two SSRIs has been solved. The structures provide important new information about how antidepressants block serotonin binding and transporter activity, the possible role of known disease mutations, and allosteric regulation of the transporter. These discoveries will aid in the design of small molecules capable of more-precise activity against a variety of neurological disorders.

The first step in crystallization of a large and unstable transporter like SERT is to find the correct conditions for protein production. The team found that wild type SERT was not amenable to crystallization in detergent micelles, but they were able to find several mutations that stabilized the protein and preserved antidepressant binding. Using this stable human SERT variant and by adding a stabilizing antibody, they were able to get crystals for human SERT in complex with each of two SSRI pharmaceuticals, citalopram (Celexa) and paroxetine (Paxil).

The structures, solved from x-ray diffraction data sets collected at the Northeastern Collaborative Access Team (NE-CAT) x-ray beamlines 24-ID-C and 24-ID-E at the APS and the Advanced Light Source (ALS) beamline 5.02 at the Lawrence Berkeley National Laboratory, showed that SERT adopts an outward-open conformation when bound to the inhibitors. (Both the APS and ALS are Office of Science user facilities.) The antidepressant binds to a central site between transmembrane helices 1, 3, 6, 8, and 10 about halfway into the membrane (Fig. 1). Citalopram,

which is known to have allosteric binding activity, also binds to another site adjacent to the central site in a vestibule that directly blocks the first inhibitor from leaving the central site. This observation explains the mechanism for how the allosteric site slows the off-rate of inhibitors by blocking exit from the central site.

The structure shows details for the locations of amino acid changes that are known to vary among the human population and mutations that are known to be involved in various psychiatric disorders. The locations of these amino acids show that they are poised to enhance serotonin transport, destabilize the transporter, or render the transporter insensitive to regulation, and thus provide a host of new targets for more specific intervention in neurotransmitter transporter-related diseases.

The transport activity of SERT is dependent on sodium and chloride ions. Sodium was found to bind to transmembrane domains 1, 6, and 7, while chloride ions are bound by transmembrane domains 2, 6, and 7. The outward open conformation of SERT provides a pathway from the extracellu-

lar space to the central binding site that allows these ions, as well as substrate and inhibitors, access into the membrane.

Overall, the structure of human SERT provides many insights into how these important transporters function and how SSRIs interact with them. This work promises to lead to the development of new strategies and drugs for the management of a wide array of neurological disorders. — *Sandy Field*

*See:* Jonathan A. Coleman, Evan M. Green<sup>‡</sup>, and Eric Gouaux\*, "X-ray structures and mechanism of the human serotonin transporter," *Nature* **532**, 334 (21 April 2016).

DOI: 10.1038/nature17629

*Author affiliation:* Oregon Health & Science University <sup>‡</sup>Present address: University of California, San Francisco

*Correspondence:* \* gouauxe@ohsu.edu

J.A.C. has support from a Banting postdoctoral fellowship from the Canadian Institutes of Health Research. We are particularly grateful to Bernie and Jennifer LaCroute for their generous support, as well as for funding from the National Institutes of Health (NIH) (5R37MH070039). E.G. is an Investigator with the Howard Hughes Medical Institute. The Advanced Light Source is a U.S. Department of Energy (DOE) Scientific User Facility supported by the Director, Office of Science, Office of Basic Energy Sciences and operated for the DOE Office of Science by Lawrence Berkeley National Laboratory. The Northeastern Collaborative Access Team beamlines, which are funded by the National Institute of General Medical Sciences from the National Institutes of Health (P41 GM103403). The Pilatus 6M detector on 24-ID-C beam line is funded by a NIH-ORIP HEI grant (S10 RR029205). This research used resources of the Advanced Photon Source, a U.S. DOE Office of Science User Facility operated for the DOE Office of Science by Argonne National Laboratory under Contract No. DE-AC02-06CH11357.

24-ID-C • NE-CAT • Life sciences • Macromolecular crystallography, microdiffraction, single-wavelength anomalous dispersion, single-crystal diffraction, microbeam, multi-wavelength anomalous dispersion, subatomic (<0.85 Å) resolution • 6.5-23 keV • On-site, remote • Accepting general users •

24-ID-E • NE-CAT • Life sciences • Macromolecular crystallography, microbeam, microdiffraction, single-wavelength anomalous dispersion, single-crystal diffraction • 12.68 keV • On-site, remote • Accepting general users •

# THE STRUCTURE OF A PROTEIN THAT FACILITATES CANCER SPREAD

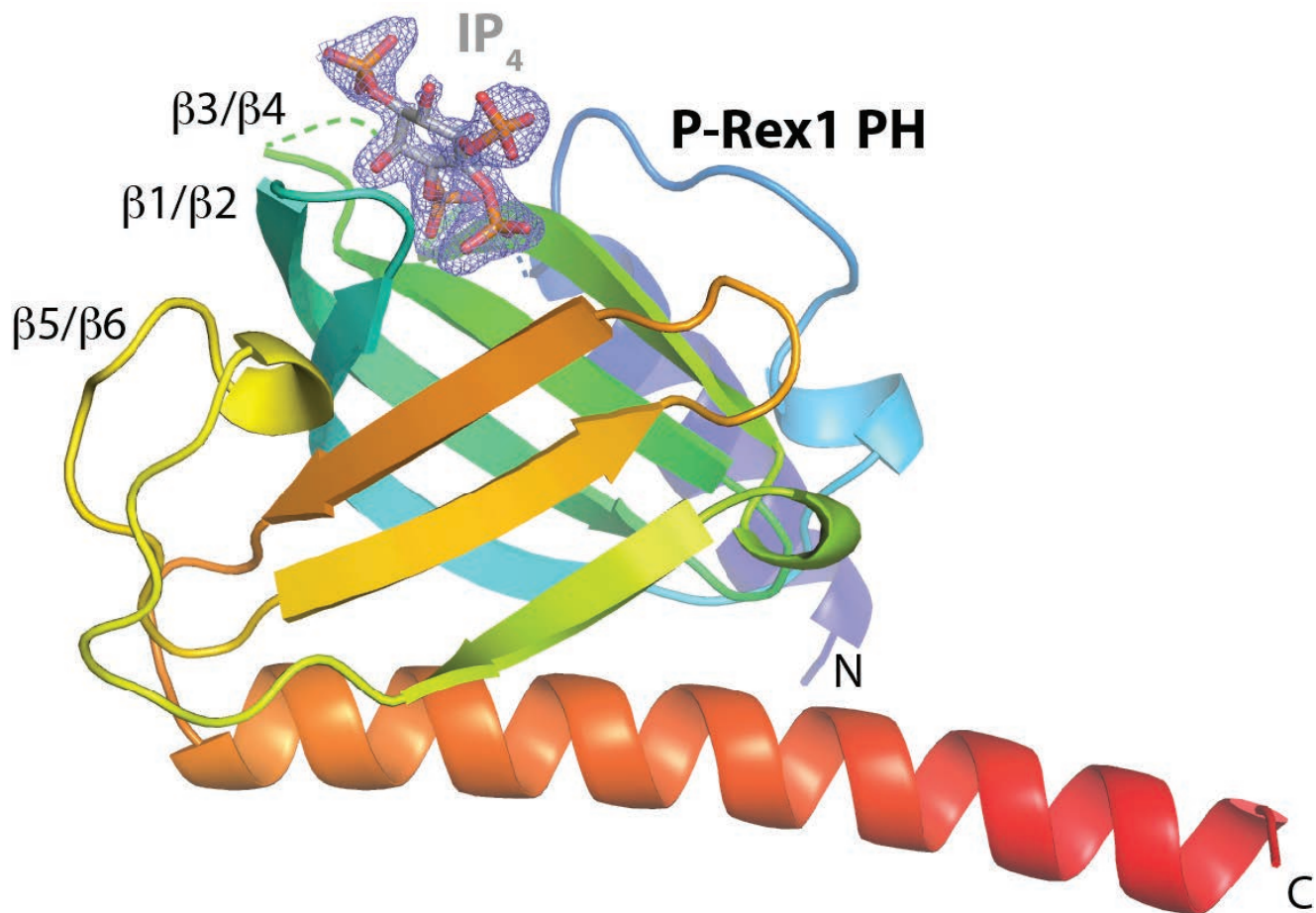


Fig. 1. Ins(1,3,4,5)P4 ( $IP_4$ ), a soluble analog of  $PIP_3$ , bound in a pocket formed at one end of the P-Rex1 PH domain. The electron density map of  $IP_4$  is shown as a blue wire mesh overlaying a ball and stick model of the molecule.



**M**etastasis is the spread of cancer from its original location to different parts of the body. It can occur when cancer cells invade nearby tissues or when the cells migrate through the body via the lymphatic and circulatory systems. Patients diagnosed with metastatic cancer, also known as stage IV cancer, have significantly lower survival rates than those whose cancer does not metastasize. A key strategy that scientists are exploring for undermining metastasis is inhibiting or disabling proteins that allow cells to become mobile. One such protein, called P-Rex1, has been found to play an important role in metastasis, making it an attractive therapeutic target. In order for P-Rex1 to facilitate the spread of cancer cells, it needs to be turned on by two other molecules, one of which is PIP<sub>3</sub>, a phospholipid embedded in the surface membrane of cells. Currently, science does not understand how PIP<sub>3</sub> activates P-Rex1. In a new study, researchers used x-ray crystallography at the APS to take molecular snapshots of P-Rex1 bound to PIP<sub>3</sub>. They not only pinpointed the location of the binding site, they also determined that this interaction is required to switch P-Rex1 on. In addition, they found the interaction was not necessary for mobilizing P-Rex1 to the cell membrane. These findings provide important insights into P-Rex1 regulation and present potential tools for targeting the PIP<sub>3</sub>-binding pocket of P-Rex1 with a new generation of cancer chemotherapeutic agents.

Metastasis is the ability of cancer cells to become mobile and form tumors at distant sites within the body and is responsible for the majority of cancer deaths. However, most current anti-cancer agents only suppress tumor growth. Therefore, small molecules that can inhibit proteins responsible for cell migration represent an intriguing new direction for cancer chemotherapy.

Experiments in a number of cell lines in the lab have shown that the P-Rex1 (phosphatidylinositol 3,4,5-trisphosphate (PIP<sub>3</sub>)-dependent Rac exchanger 1) molecule plays a role in the metastasis of breast cancer, prostate cancer and melanoma. Specifically, P-Rex1 enables cells to become mobile, possibly by eliciting changes to a structural component within cells called the actin cytoskeleton. Rearrangement of the cytoskeleton, which gives cells their strength and shape, can be accompanied by cell migration.

To better understand the molecular basis for P-Rex1 regulation by two cell-membrane-bound molecules, PIP<sub>3</sub> and Gβγ, researchers from the University of Michigan used x-ray diffraction data collected at the LS-CAT 21-ID-D at the APS to determine the high-reso-

lution structures of P-Rex1 in complex with a soluble analog of PIP<sub>3</sub> called IP4 (Fig. 1).

The research team used their molecular snapshots to define which residues within the PIP<sub>3</sub>-binding site are important for interaction with P-Rex1 and for increasing its activity within cells. The team also determined that mutating these residues does not interfere with the ability of P-Rex1 to associate with the cell membrane. Therefore, simple localization of P-Rex1 to the membrane, where its substrates are located, is not sufficient to elicit its activity. Furthermore, additional molecular structures elucidated by the team showed that P-Rex1 exhibits inherent flexibility, which may have important implications toward how it is regulated within the body.

P-Rex1 continues to be an attractive target for therapeutics that suppress cancer metastasis. The new structural and functional data captured in this study have now confirmed the location of the regulatory PIP<sub>3</sub>-binding site within P-Rex1, which will greatly assist in the identification or rational design of small molecules that target its mechanism of activation.

— Chris Palmer

**See:** Jennifer N. Cash, Ellen M. Davis, and John J.G. Tesmer\*, "Structural and Biochemical Characterization of the Catalytic Core of the Metastatic Factor P-Rex1 and Its Regulation by PtdIns(3,4,5)P<sub>3</sub>," *Structure* **24**, 730 (May 3, 2016).

DOI: 10.1016/j.str.2016.02.022

**Author affiliation:** University of Michigan

**Correspondence:** \* tesmerjj@umich.edu

This work was supported in part by National Institutes of Health grants HL086865 and HL122416 to J.T., an American Cancer Society-Michigan Cancer Research Fund Postdoctoral Fellowship (PF-14-224-01-DMC) to J.C., and an American Heart Association Undergraduate Student Research Program Award (14UFEL20510027) to E.D. Use of LS-CAT was supported by the Michigan Economic Development Corporation and the Michigan Technology Tri-Corridor (Grant 085P1000817). This research used resources of the Advanced Photon Source, a U.S. Department of Energy (DOE) Office of Science User Facility operated for the DOE Office of Science by Argonne National Laboratory under Contract No. DE-AC02-06CH11357.

21-ID-D • LS-CAT • Life sciences • Macromolecular crystallography • 6.5-20 keV • On-site, remote, mail-in • Accepting general users •

# AN INSIDE LOOK AT A NOTORIOUS HOSPITAL-ACQUIRED INFECTION

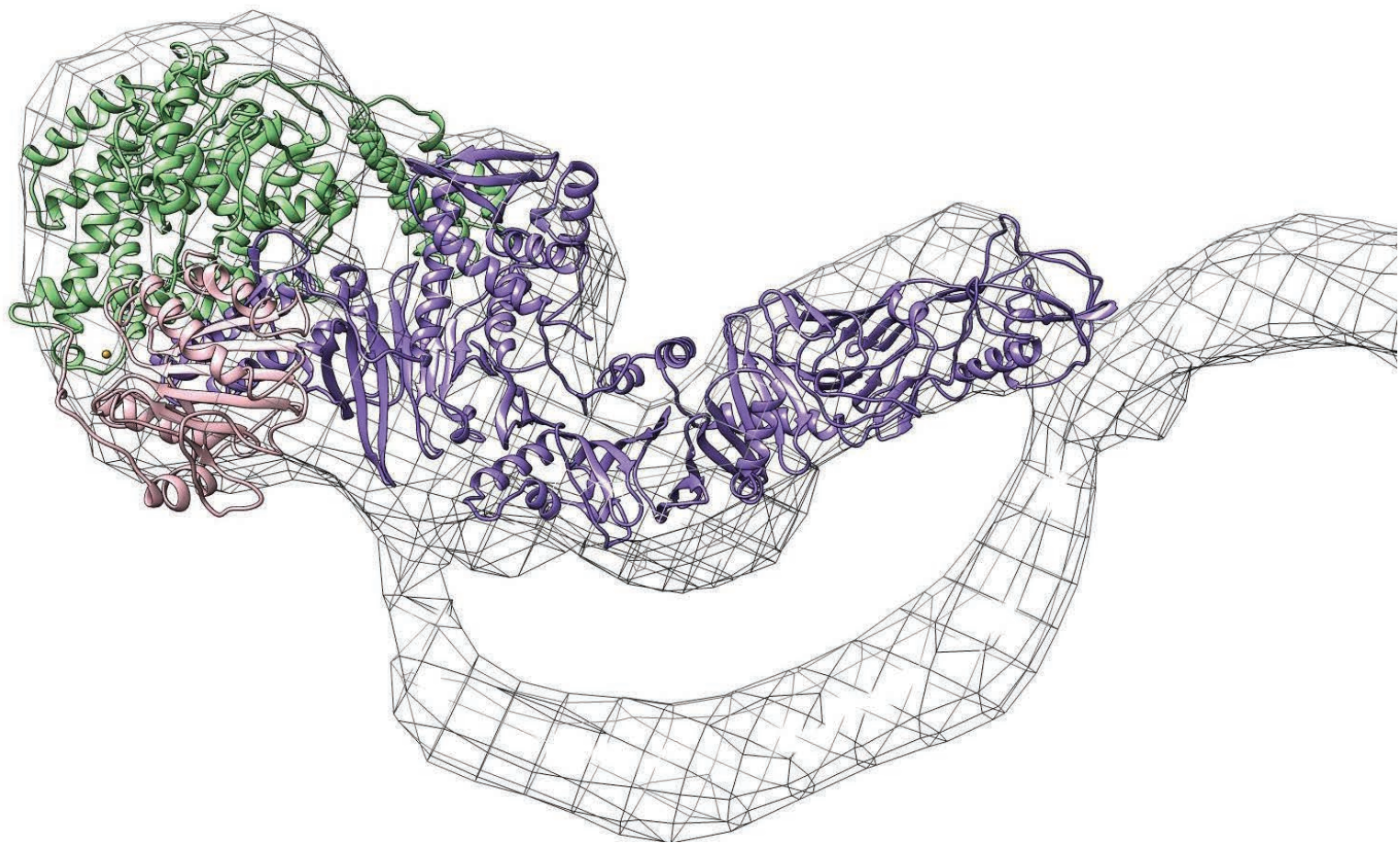
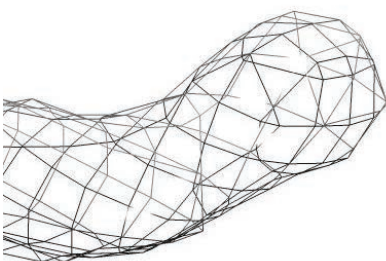


Fig. 1. The crystal structure of the 1832 amino acid TcdA fragment placed in a 20-Å structure obtained by electron microscopy with the glucosyltransferase domain in green, the autoprocessing domain and zinc atom shown in pink, and the pore-forming delivery domain shown in purple.

**C***lostridium difficile* causes many infections in the U.S. health care system. While antibiotics can be effective against the pathogen, the bacterium was linked to the deaths of 29,000 people in the United States in 2011. The devastating effects of *Clostridium difficile* are mediated by two homologous bacterial toxins, toxin A and toxin B, that are believed to be primarily responsible for the disease symptoms, including diarrhea, inflammation, and necrosis in the colon. Researchers from the Vanderbilt University School of Medicine, the University of Toronto and the Molecular Structure & Function Research Institute at The Hospital for Sick Children, Indiana University, Case Western Reserve University Center for Synchrotron Biosciences, and the Veterans Affairs Tennessee Valley Healthcare System crystallized and solved the structure of *Clostridium difficile* toxin A using data collected at the APS, garnering insights that may aid in the development of treatments and vaccines that target the toxins in the future.



To gain access into human cells, toxin A binds the cell surface, and then, using receptor-mediated endocytosis, the endosome enters the cytosol, carrying the toxin inside. The toxin's glucosyltransferase domain escapes the endosome when the toxin forms a pore in the endosome's membrane and the toxin cleaves itself in two via autopro-cessing, allowing the catalytic domain to enter the cytosol, where it does its damage. There, the glucosyltransferase targets small GTPases, glucosylating and thus deactivating the enzymes.

Due in part to their large molecular weights, efforts to crystallize toxin A and solve a high-resolution structure have been unsuccessful. Evidence from low-resolution structural approaches, electron microscopy and small-angle x-ray scattering, suggested that a particular piece of the toxin could adopt multiple conformations relative to the rest of the protein, suggesting that it may be interfering with crystallization attempts. So, the researchers lopped off that region, leaving a 1,832 amino-acid fragment of toxin A, which crystallized well. They took crystals to the LS-CAT beamline 21-ID-D, and solved a 3.25-Å-resolution structure (Fig. 1).

The structure of toxin A revealed a number of surprises and insights. For

example, the researchers observed an anomalous signal in their diffraction data and discovered a zinc atom hiding in the structure that hadn't been anticipated. They performed x-ray absorption spectroscopy at the National Synchrotron Light Source beamline X3B to confirm that toxin A indeed bound zinc in solution. When the researchers removed zinc from the toxin via chelation, the enzyme's ability to cleave itself proteolytically was eliminated. Reintroducing zinc to the toxin restored the activity, leading the researchers to conclude that zinc is required for the toxin to autopro-cess and release its glucosyltransferase domain into the cytosol.

The researchers also characterized a domain that facilitates the delivery of the toxin into the cytosol ("the delivery domain"). This domain appeared to act as a scaffold for the pH-dependent formation of the endosomal pore, consisting of hydrophobic alpha helices.

Perhaps of greatest interest was the identification of a surface loop in a portion of the toxin's delivery domain. This sequence of the toxin is conserved widely among clostridial toxins. Making even a small mutation in this region impaired the toxin's ability to kill cells. Further experiments suggested that mutations in this loop impair pore formation, offering an appealing target for future therapeutic design.

— Erika Gebel Berg

**See:** Nicole M. Chumbler<sup>1</sup>, Stacey A. Rutherford<sup>1</sup>, Zhifen Zhang<sup>2</sup>, Melissa A. Farrow<sup>1</sup>, John P. Lisher<sup>3</sup>, Erik Farquhar<sup>4</sup>, David P. Giedroc<sup>3</sup>, Benjamin W. Spiller<sup>1</sup>, Roman A. Melnyk<sup>2</sup>, and D. Bor-

den Lacy<sup>1,5\*</sup>, "Crystal structure of *Clostridium difficile* toxin A," *Nat. Microbio.* **1**, 15002 (2016).

DOI: 10.1038/nmicrobiol.2015.2

**Author affiliations:** <sup>1</sup>Vanderbilt University School of Medicine, <sup>2</sup>University of Toronto and the Molecular Structure & Function Research Institute at The Hospital for Sick Children, <sup>3</sup>Indiana University, <sup>4</sup>Case Western Reserve University Center for Synchrotron Biosciences, <sup>5</sup>Veterans Affairs Tennessee Valley Healthcare System

**Correspondence:**

\* borden.lacy@vanderbilt.edu

This research was supported by the National Institute of Allergy and Infectious Diseases of the National Institutes of Health (award no. R01AI095755 to D.B.L.) and the National Institute of General Medical Sciences (award no. R01GM042569 to D.P.G.). Use of LS-CAT was supported by the Michigan Economic Development Corporation and the Michigan Technology Tri-Corridor (grant no. 085P1000817). Use of the National Synchrotron Light Source (NSLS), Brookhaven National Laboratory, was supported by the U.S. Department of Energy (DOE) Office of Science-Basic Energy Sciences (contract no. DE-AC02-98CH10886). Operations at the NSLS beamline X3B were supported by NIH P30-EB009998. This research used resources of the Advanced Photon Source, a U.S. DOE Office of Science User Facility operated for the DOE Office of Science by Argonne National Laboratory under Contract No. DE-AC02-06CH11357.

21-ID-D • LS-CAT • Life sciences • Macromolecular crystallography • 6.5-20 keV • On-site, remote, mail-in • Accepting general users •



# HOW BACTERIA GET THEIR SUGAR FIX

**L**ike the majority of plants and animals, bacteria power themselves with sugars such as glucose. However, bacteria have a unique process for slurping up sugars from their environment. At the heart of bacteria's sugar uptake machinery is the energy-dependent phosphoenolpyruvate:carbohydrate phosphotransferase system (PTS). Little is known about how the PTS membrane-embedded components, part of the glucose superfamily of EIIC transporters, selectively mediate the passage of carbohydrates across the bacterial membrane. To learn more about one of these components, a team of researchers used x-ray crystallography at the APS to functionally characterize the structure of one of the EIIC components, a maltose transporter called bcMalT. They found that bcMalT crystallized in an outward-facing occluded conformation, in contrast to the structure of another EIIC transporter, bcChbC, which the research team had previously crystallized in an inward-facing occluded conformation. The two EIICs were found to differ in the position of a structurally conserved substrate-binding domain. After comparing the two structures, the team hypothesized that sugar is shuttled into the cell via an "elevator car"-type transport mechanism. These findings offer an explanation for how bacterial glucose superfamily EIIC transporters first recognize, then consume sugars. This knowledge can assist researchers in devising novel antibacterial agents that interfere with the microbes' sugar transport system.

The PTS is responsible for carrying out the energy-dependent transport of carbohydrates as well as a variety of regulatory functions in bacteria. Active sugar uptake is driven by modification of the translocated sugar with a phosphate group that derives from phosphoenol pyruvate. This phosphate is transferred to the sugar through a series of proteins that include, in order of phosphorylation, enzyme I (EI), histidine-containing phosphocarrier protein (HPr), enzyme IIA (EIIA), and enzyme IIB (EIIB). The protein that transports the sugar across the membrane and also catalyzes the transfer of the phosphate group from EIIB is the integral membrane protein enzyme IIC (EIIC).

The EIIC components of the PTS are grouped in four different superfamilies, the largest of which is the glucose superfamily. The PTS has been the subject of extensive study for nearly half a century, but understanding of the system has remained incomplete due to the lack of any structures for the integral membrane component EIICs responsible for the transport of the sugar across the inner bacterial membrane. These researchers had previously crys-

tallized the structure of one of the components of the glucose superfamily EIIC from *Bacillus cereus*, called bcChbC, in an inward-facing occluded conformation, in which the sugar is located close to the intracellular side of the plasma membrane.

EIICs, like other membrane embedded transporters, transport sugar molecules across the plasma membrane by alternating between the inward and outward facing conformations. In order to understand both the mechanism of transport within EIIC proteins and identify residues that confer selectivity to the glucose superfamily PTS EIIC transporters, the team solved the x-ray structure of bcMalT, an outward-facing EIIC transporter, using the IMCA-CAT 17-ID-B and NE-CAT 24-ID-C x-ray beamlines at the APS; and beamlines 8.2.2 and 5.0.2 at the Berkeley Center for Structural Biology at the Advanced Light Source, Lawrence Berkeley National Laboratory, .

The team observed that the structure of bcMalT possesses the same overall fold as the previously described bcChbC structure, but the location of the substrate-binding domain differs by

a displacement of roughly 20 angstroms (Fig. 1).

Comparison of bcChbC and bcMalT inspired the team to propose the elevator car-type transport mechanism in which a large motion of the substrate-binding domain moves the substrate from one side of the bilayer membrane to the other. The transport cycle begins with an outward-facing open state in which the substrate-binding cavity is accessible to the sugar from the periplasmic side. A rotation of a transmembrane segment (TM7) closes off the cavity to create the substrate-bound, outward-facing occluded state, represented by the recently reported bcMalT crystal structure. The substrate-binding domain, comprising 5 transmembrane helices (TM6-10) and 2 loops (HP1 and HP2), moves as a single unit toward the cytoplasm to form the inward-occluded state, similar to the previously reported bcChbC crystal structure. Finally, movement of a loop between TM4 and TM5 allows docking of EIIB and thus phosphorylation of the sugar, which causes the sugar to be released into the cytoplasm.

Characterizing the crystal structure

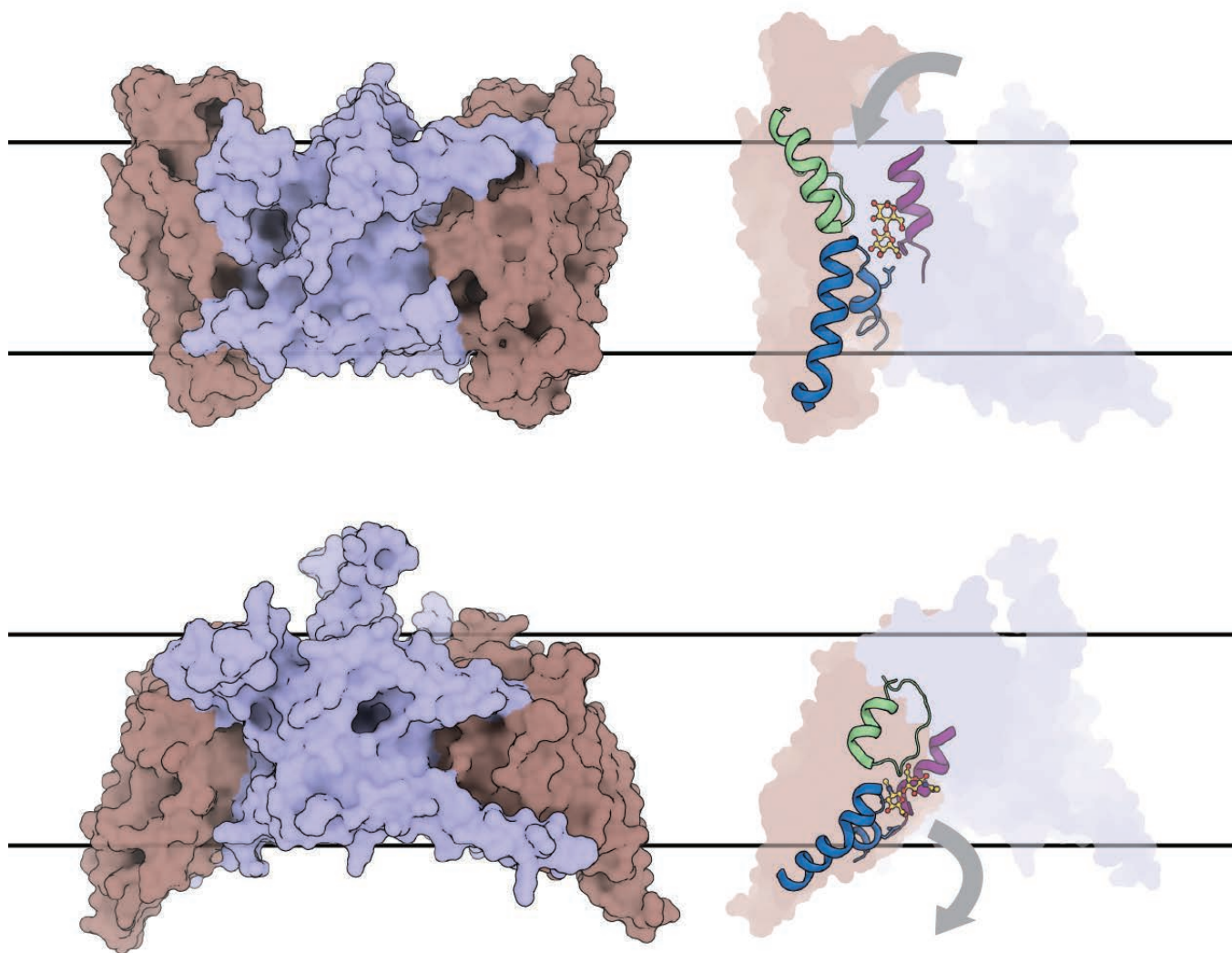


Fig. 1. Diagram showing a potential model for the glucose superfamily EIIC transport cycle in bacteria. The dimeric sugar transporter bcMalT (top left) and bcChbC (bottom left) share the same overall fold, but in recent crystal structures their C-terminal substrate binding domains differ in position relative to the lipid bilayer (black lines). This difference suggests a conformational change that renders the substrate binding accessible alternately to the periplasmic (top right) or cytoplasmic (bottom right) side of the membrane, facilitating sugar transport.

of bcMalT has enabled better understanding of how the EIIC glucose transport system works in bacteria, which ultimately can aid in the development of a new class of antibiotics that targets this group of transporters. — *Chris Palmer*

**See:** Jason G. McCoy<sup>1†</sup>, Zhenning Ren<sup>1</sup>, Vitali Stanevich<sup>1</sup>, Jumin Lee<sup>2</sup>, Sharmistha Mitra<sup>1</sup>, Elena J. Levin<sup>1</sup>, Sebastien Poget<sup>3</sup>, Matthias Quick<sup>4</sup>, Wonpil Im<sup>2</sup>, and Ming Zhou<sup>1\*</sup>, “The Structure of a Sugar Transporter of the Glucose EIIC Superfamily Provides Insight into the Elevator Mechanism of Membrane Transport,” *Structure* **24**, 956 (June 7, 2016). DOI: 10.1016/j.str.2016.04.003  
**Author affiliations:** <sup>1</sup>Baylor College of

Medicine, <sup>2</sup>The University of Kansas, <sup>3</sup>College of Staten Island, <sup>4</sup>New York State Psychiatric Institute <sup>†</sup>Present address: Broad Institute  
**Correspondence:** \* mzhou@bcm.edu

This work was supported by the National Institutes of Health (R01GM098878, R01HL086392, R01DK088057, U54GM095315, and U54GM087519); the American Heart Association (12EIA88 50017); and the Cancer Prevention and Research Institute of Texas (R1223). IMCA-CAT is supported by the companies of the Industrial Macromolecular Crystallography Association through a contract with Hauptman-Woodward Medical Research Institute; NE-CAT is supported by P41 GM103403 from the National Institute of General Medical Sciences; the Advanced Light Source is

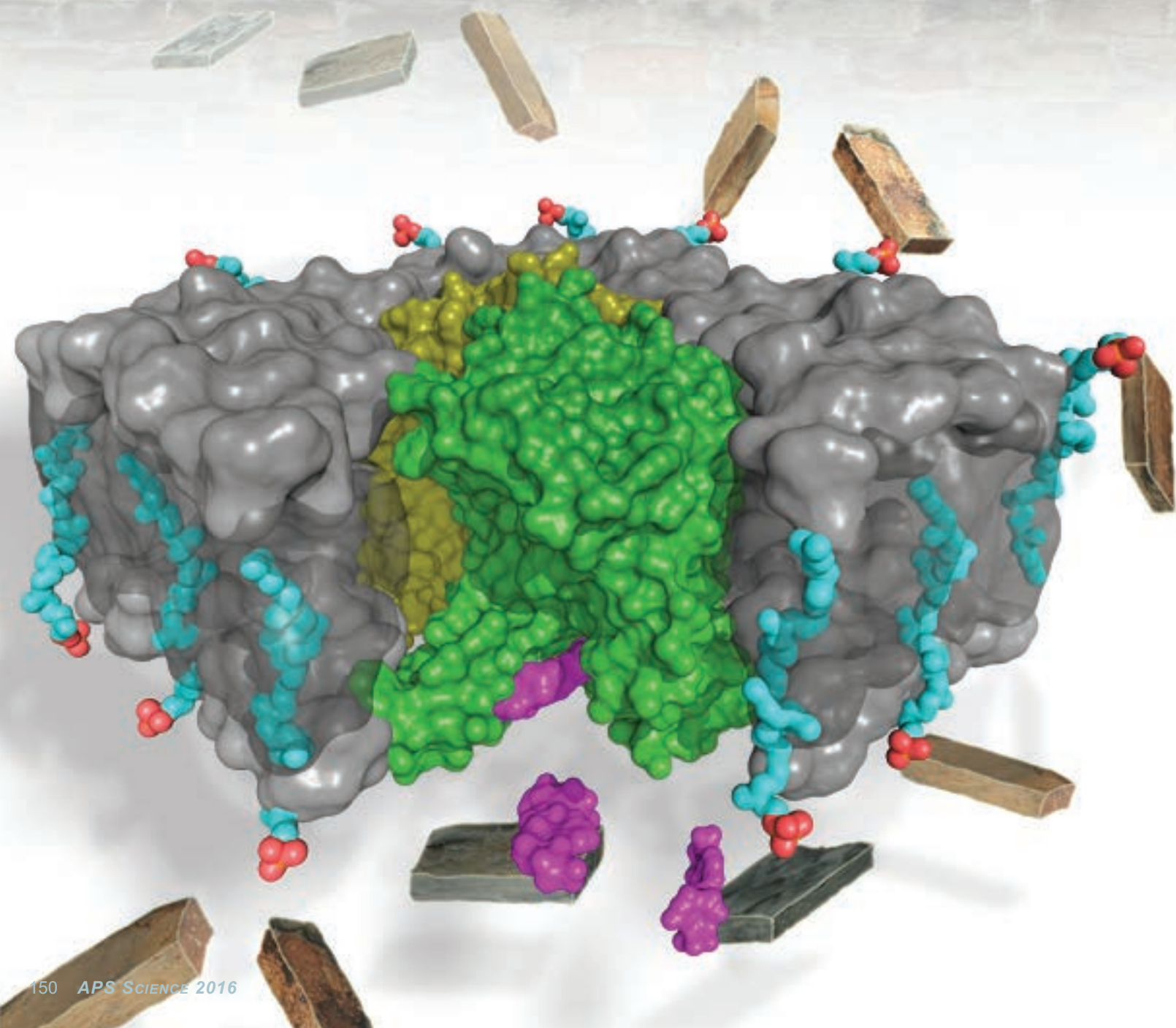
a U.S. Department of Energy (DOE) Scientific User Facility supported by the Director, Office of Science, Office of Basic Energy Sciences and operated for the DOE Office of Science by Lawrence Berkeley National Laboratory. This research used resources of the Advanced Photon Source, a U.S. DOE Office of Science User Facility operated for the DOE Office of Science by Argonne National Laboratory under Contract No. DE-AC02-06CH11357.

**17-ID-B • IMCA-CAT • Life sciences • Macromolecular crystallography, multi-wavelength anomalous dispersion, microbeam, single-wavelength anomalous dispersion, large unit cell crystallography • Subatomic (<0.85 Å) resolution • 6-20 keV • On-site, remote • Accepting general users •**

**24-ID-C • NE-CAT • Life sciences • Macromolecular crystallography, microdiffraction, single-wavelength anomalous dispersion, single-crystal diffraction, microbeam, multi-wavelength anomalous dispersion, subatomic (<0.85 Å) resolution • 6.5-23 keV • On-site, remote • Accepting general users •**



# OUTSMARTING ANTIBIOTIC-RESISTANT BACTERIA





**A**ntibiotics have saved millions of lives but have also been the cause of their own undoing. From the moment penicillin first started being used as an antibiotic in 1942, bacteria have been busily developing resistance to this life-saving drug and the others that have followed it. As we develop and use new antibiotics, bacteria develop resistance to them and we are forced into an arms race in which we must constantly develop new ways to battle these clever microscopic warriors. Penicillin was developed from a natural product that inhibits cell wall synthesis in bacteria. Although bacteria have found ways to circumvent the specific action of penicillin, the existence of other natural antibiotics that work by different but related mechanisms provides evidence that cell wall synthesis is still a good target for antibiotics. Now, results from the APS have helped a team of researchers take an important step toward development of a new antibiotic that can block bacterial cell wall synthesis.

The focus of the team's effort is the *MraY* enzyme, an integral membrane protein that catalyzes the first step in peptidoglycan biosynthesis. Peptidoglycan is an essential component of the bacterial cell wall and is important for cell division – the process that bacteria use to multiply. The researchers, from the Duke University Medical Center, Hokkaido University (Japan), and Duke University, solved the crystal structure of *MraY* in complex with a natural inhibitor, *muraymycinD2* (MD2), that has shown the ability—in animal models and in the lab—to kill some of the most lethal antibiotic resistant bacteria, including methicillin-resistant *Staphylococcus aureus* (MRSA), vancomycin-resistant *Enterococcus* (VRE), and *Mycobacterium tuberculosis*. Understanding how MD2 inhibits the *MraY* enzyme is crucial for developing a similar compound for clinical use in people.

The structure, from x-ray data collected at the SER-CAT 22-ID-D and NE-CAT 24-ID-C beamlines at the APS, shows that *MraY* has 10 transmembrane helices (TMs) with 5 cytoplasmic loops. Most of the protein is in the membrane (Fig. 1). The catalytic site is a cleft framed by TM domains 3,

4, 5, 8, and 9, and loops B, C, D, and E. Three critical amino acids that are known to be important for catalysis and are conserved in this family of enzymes are located in the catalytic cleft.

One of the interesting questions about the MD2 inhibitor is how it can bind *MraY* even though it does not look anything like the natural substrate of the enzyme. Specifically, MD2 is a competitive inhibitor of *MraY* but does not have the sugar and pyrophosphate groups that are required for the natural substrate of *MraY*. The structure shows that MD2 inserts between loops C and D and interacts with TM9, but does not interact with the three critical catalytic amino acids. Instead, it causes a large conformational change in *MraY* in which TM9 rotates away from the active site and loop E rearranges. These changes reshape the active site and are accompanied by further rearrangements in loops A and D and in TM domains 1 and 5, and the unwinding of loop C. MD2 interacts with the new active site created by the movements of TM9 and loop E and with the new rearrangements of TM5 and loops C and D.

All of this moving also creates substantial changes in the nature of the charges that are present in the active site, a potential factor in binding of the inhibitor. Mutational analysis shows that the MD2 inhibitor does not interact with the same area of the active site as the part of the substrate it was previously thought to mimic, the pyrophosphate group, and *in vitro* experiments show that magnesium ( $Mg^{2+}$ ), which is

critical for the enzymatic activity, is not important for MD2 binding.

The structure of *MraY* with its natural inhibitor, MD2, explains why MD2 does not need the same groups as the natural substrate in order to bind to the *MraY* active site and provides crucial information needed for designing drugs to inhibit this essential bacterial enzyme.

— Sandy Field

**See:** Ben C. Chung<sup>1</sup>, Ellene H. Mashalidis<sup>1</sup>, Tetsuya Tanino<sup>2</sup>, Mijung Kim<sup>3</sup>, Akira Matsuda<sup>2</sup>, Jiyong Hong<sup>3</sup>, Satoshi Ichikawa<sup>2</sup>, and Seok-Yong Lee<sup>1\*</sup>, “Structural insights into inhibition of lipid I production in bacterial cell wall synthesis,” *Nature* **533**, 557 (26 May 2016). DOI: 10.1038/nature17636

**Author affiliations:** <sup>1</sup>Duke University Medical Center, <sup>2</sup>Hokkaido University, <sup>3</sup>Duke University

**Correspondence:**

\* seok-yong.lee@duke.edu

This work was supported by NIH R01 GM100984 (S.-Y.L.) and Duke startup funds (S.-Y.L.). This work was also supported by the JSPS Grant-in-Aid for Scientific Research on Innovative Areas “Chemical Biology of Natural Products” (S.I., grant number 24102502) and Scientific Research (B) (S.I., grant number 25293026). This research used resources of the Advanced Photon Source, a U.S. Department of Energy (DOE) Office of Science User Facility operated for the DOE Office of Science by Argonne National Laboratory under Contract No. DE-AC02-06CH11357.

< Fig. 1. A schematic portraying the structure of *MraY* (in green and brown), an essential enzyme in bacterial cell wall synthesis. The enzyme is bound to the antibiotic *muraymycin* (magenta), which is overlaid on an image of a brick wall that symbolizes the bacterial cell wall. Drugs that bind *MraY* can inhibit bacterial cell wall synthesis. Image credit: Ben Chung

# BATTLING BACTERIAL RESISTANCE

**P**olymyxin antibiotics are one of our last lines of defense against multi-drug-resistant bacteria. They are made by certain Gram positive bacteria to selectively kill Gram negative bacteria by disrupting their outer membranes through interactions with specific lipopolysaccharides (LPS). However, in an escalation of this conflict and in response to our use of polymyxins as antibiotics, some Gram negative bacteria have developed resistance to polymyxins. This is predominantly accomplished by an enzyme, aminoarabinose transferase (ArnT), that can modify the LPS so that polymyxins cannot use it to bind to the membrane anymore. Drugs that inhibit ArnT could overcome this resistance and improve the efficacy of this critical class of antibiotics. In an important first step toward developing such inhibitors, a research team utilized high-brightness x-ray beams from the APS to solve the structure of ArnT with and without one of its lipid substrates. The work reveals how substrates bind to the enzyme and identifies amino acids that are critical for its catalytic activity, important information for drug design.

Polymyxins bind to LPS on the bacterial outer membrane through electrostatic interactions with negatively charged groups on the LPS. The enzyme ArnT modifies LPS and confers resistance to polymyxins by catalyzing a reaction that “caps” LPS with the positively charged sugar L-Ara4N. The sugar is added to a part of LPS called lipid A specifically at the negatively charged groups that interact with polymyxins. L-Ara4N is transported to the reaction by undecaprenyl phosphate (UndP), a lipid carrier. This means that ArnT must bring two lipid substrates, lipid A and the UndP-L-Ara4N, together to the active site for catalysis to occur.

The team, led by Columbia University scientists, working together with colleagues from the University of Georgia, the Medical College of Wisconsin, Cornell University, the New York Structural Biology Center, and the Technische Universität München (Germany) solved the crystal structures of ArnT and ArnT plus UndP at the NE-CAT beamlines 24-ID-C and 24-ID-E at the APS. The structures revealed that ArnT is a monomeric protein with 13 trans-membrane domains that span the bacterial inner membrane, 3 juxtamem-

brane helices, and a soluble domain that is oriented toward the periplasmic space between the two Gram negative bacterial membranes (Fig. 1). They also showed that there are three cavities in the structure that are spacious enough to accommodate the substrates.

Cavity one is the largest and is hypothesized to bind to lipid A due to its size and the configuration of hydrophobic and hydrophilic regions in the space. It is part way in the membrane and part way out of the membrane and the hydrophobic area is oriented in such a way that it is potentially accessible from the outer leaflet of the inner bacterial membrane. However, in the ArnT structure, the opening for cavity one appears to be partially blocked by a periplasmic loop between transmembrane domains 7 and 8. Interestingly, in the ArnT plus UndP structure, binding of the UndP substrate causes a conformational shift involving a rearrangement of the loop and may thus allow lipid A to bind. This suggests that the lipid A and UndP substrates bind in sequence, with UndP binding first.

Cavity two is smaller than cavity one and is mostly hydrophilic and within the membrane region. It has a small

passage that connects it to cavity one. The ArnT plus UndP structure shows that the charged end of the UndP binds to cavity two while the hydrophobic end of the UndP binds to cavity three. Cavity three is close to the cytoplasmic (interior of the cell) side of the membrane and is hydrophobic in nature. The UndP structure shows the interactions of conserved amino acids in cavity two that appear to be essential for binding the hydrophilic end of UndP.

Finally, the structure pinpoints the location of a zinc ion that is coordinated by amino acids that are important for ArnT function. This zinc ion is located above cavity two and mutations that disrupt zinc binding also block resistance to polymyxins. The team hopes to use the valuable information they have discovered about ArnT to design drugs that can reverse polymyxin resistance, adding their own new weapons to the antibiotic resistance arms race.

— *Sandy Field*

**See:** Vasileios I. Petrou<sup>1</sup>, Carmen M. Herrera<sup>2</sup>, Kathryn M. Schultz<sup>3</sup>, Oliver B. Clarke<sup>1</sup>, Jérémie Vendome<sup>1</sup>, David Tomasek<sup>1</sup>, Surajit Banerjee<sup>4</sup>, Kana-galaghatta R. Rajashankar<sup>4</sup>, Meagan Belcher Dufrisne<sup>1</sup>, Brian Kloss<sup>5</sup>, Edda

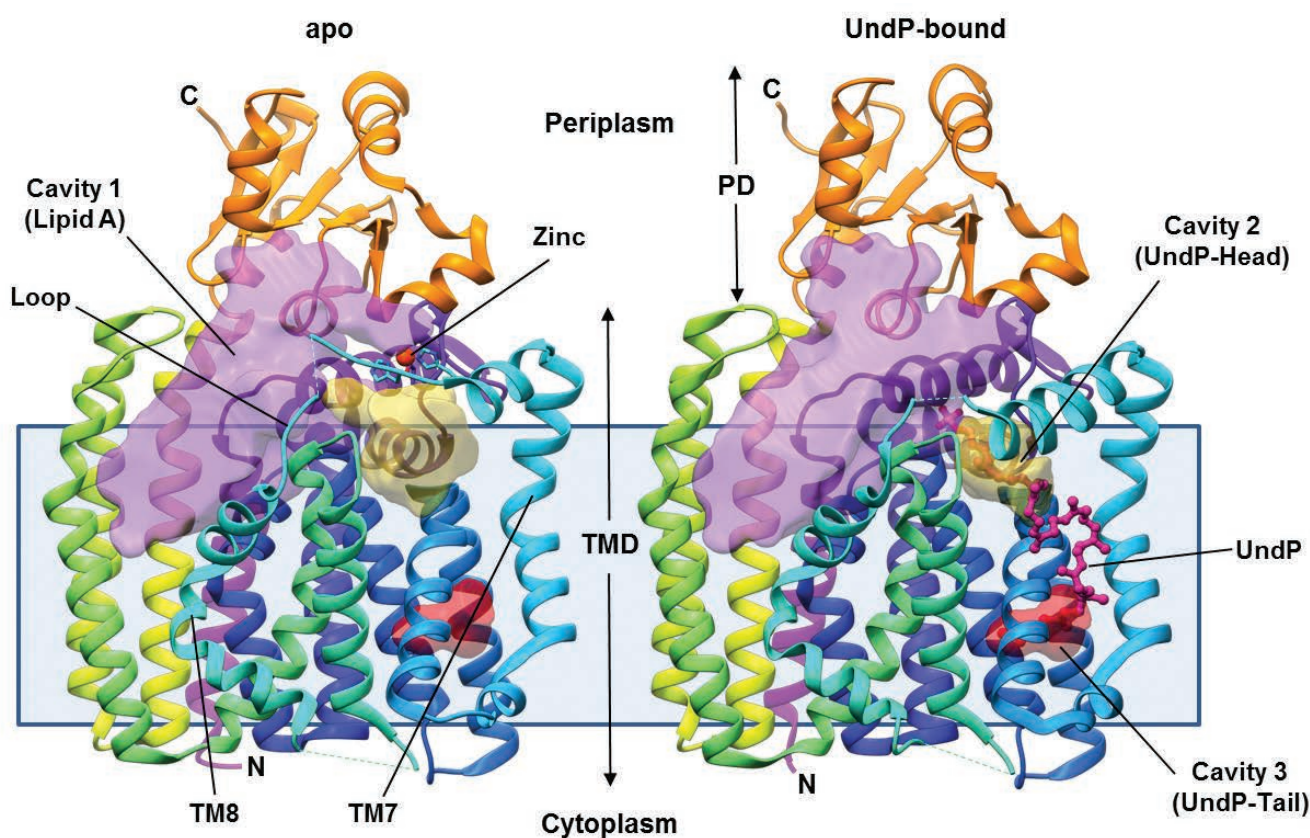


Fig. 1. Structures of aminoarabinose transferase ArnT from *Cupriavidus metallidurans* in the apo and UndP-bound conformations. The transmembrane domain (TMD) is shown in spectral (rainbow) coloring spanning purple (N-term.) to yellow (C-term.). The periplasmic domain (PD) is shown in orange. N- and C-termini of the protein are labeled (N,C). Zinc bound to the apo structure is shown in dark orange. Notable features of the structures (zinc, cavities, TM7 and TM8, flexible loop) are annotated on the structure(s). The undecaprenyl phosphate molecule in the UndP-bound structure is shown in ball and stick representation in magenta color. The coloring for cavities is identical between the apo and UndP-bound structure. (PDB codes: apo; 5EZM, UndP-bound; 5F15).

Kloppmann<sup>6</sup>, Burkhard Rost<sup>6</sup>, Candice S. Klug<sup>3</sup>, M. Stephen Trent<sup>2</sup>, Lawrence Shapiro<sup>1</sup>, Filippo Mancia<sup>1\*</sup>, "Structures of aminoarabinose transferase ArnT suggest a molecular basis for lipid A glycosylation," *Science* **351**(6273), 608 (5 February 2016).

DOI: 10.1126/science.aad1172

**Author affiliations:** <sup>1</sup>Columbia University, <sup>2</sup>University of Georgia, <sup>3</sup>Medical College of Wisconsin, <sup>4</sup>Cornell University, <sup>5</sup>New York Structural Biology Center, <sup>6</sup>Technische Universität München

**Correspondence:**

\* fm123@cumc.columbia.edu

This work was supported by a National Institute of General Medical Sciences (NIGMS) initiative to the New York Consortium on Membrane Protein Structure (NYCOMPS;

U54 GM095315) and by NIGMS grant R01 GM111980 (F.M.). Also acknowledged are National Institutes of Health grants AI064184 and AI076322 (M.S.T.), and grant W911NF-12-1-0390 from the Army Research Office (M.S.T.). O.B.C. was supported by a Charles H. Revson Senior Fellowship. The Northeastern Collaborative Access Team beamlines are funded by NIGMS from the National Institutes of Health (NIH, P41 GM103403). The Pilatus 6M detector on 24-ID-C beam line is funded by a NIH-ORIP HEI grant (S10 RR029205). This research used resources of the Advanced Photon Source, a U.S. Department of Energy (DOE) Office of Science User Facility operated for the DOE Office of Science by Argonne National Laboratory under Contract No. DE-AC02-06CH11357.

24-ID-C • NE-CAT • Life sciences • Macromolecular crystallography, microdiffraction, single-wavelength anomalous dispersion, single-crystal diffraction, microbeam, multi-wavelength anomalous dispersion, subatomic (<0.85 Å) resolution • 6.5-23 keV • On-site, remote • Accepting general users •

24-ID-E • NE-CAT • Life sciences • Macromolecular crystallography, microbeam, microdiffraction, single-wavelength anomalous dispersion, single-crystal diffraction • 12.68 keV • On-site, remote • Accepting general users •



# WATCHING THE COMPLETE CYCLE OF CELLULOSE BIOSYNTHESIS

Cellulose is a linear polymer made from single glucose molecules that are joined together by their C1 and C4 carbons. The most abundant polymer on Earth, cellulose is a structural molecule produced primarily by vascular plants (plants that have lignified tissues for conducting water and minerals throughout the plant), but also by some bacteria and even animals. An understanding of the molecular mechanism underlying production of this molecule holds tremendous potential for applications ranging from bioenergy to development of agents to treat complex biofilm infections. Using the APS, researchers were able to take snapshots of the cellulose synthase BcsA-BcsB at intermediate stages of cellulose biosynthesis. By observing these states within the context of an ordered protein crystal, or *in crystallo*, the high-resolution diffraction pattern obtained provided unprecedented insights into the biosynthesis mechanism.

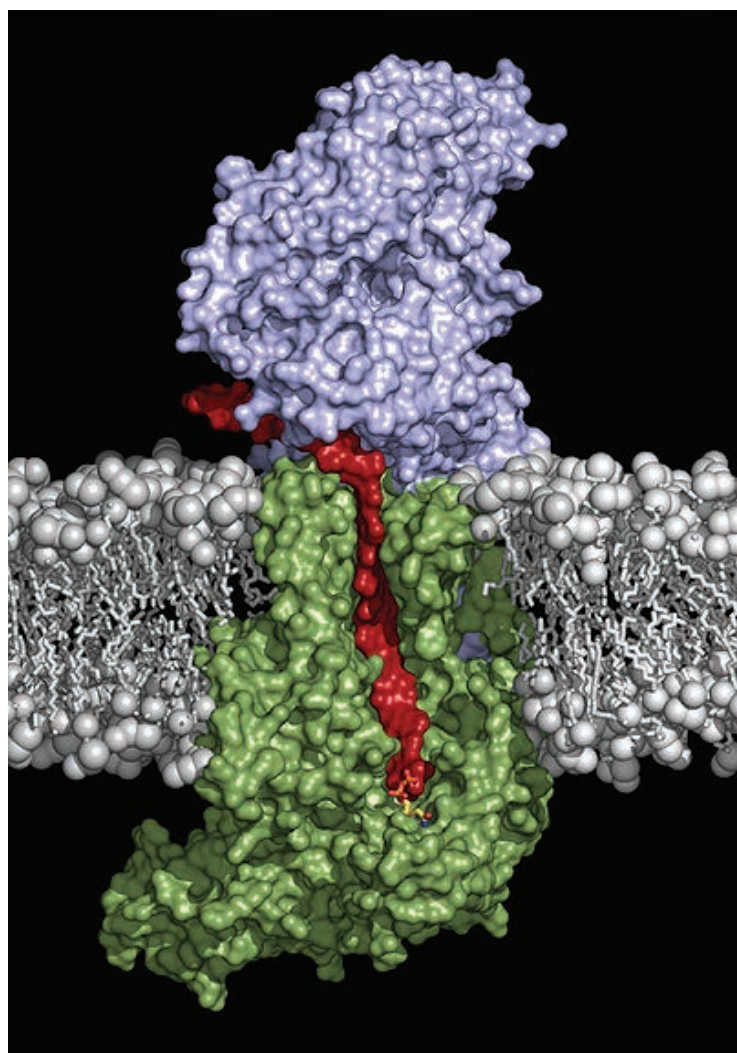


Fig. 1. A surface-model depiction of the bacterial cellulose synthase BcsA-BcsB complex. The complex is embedded in the cell membrane, and BcsA (green) and BcsB (lilac) subunits are sufficient to synthesize and translocate the cellulose polymer (red) in a processive manner.

In order to serve its biological function, cellulose must be synthesized and secreted from the cell by a membrane-embedded protein complex. As a processive and membrane-embedded glycosyltransferase, cellulose synthase is able to build long linear cellulose chains from glucose building blocks and pass these chains through a membrane channel formed by the same enzyme in a process called translocation.

In this work, researchers from the University of Virginia School of Medicine and the University of British Columbia (Canada) were able to detail, for the first time, each of the steps in a complete cycle of cellulose synthesis thanks to high-resolution “snapshots” of the BcsA-BcsB complex in various stages of cellulose synthesis (Fig. 1) obtained using high-brightness x-rays at the SER-CAT 22-ID-D, GM/CA-XSD 23-ID-B and 23-ID-D, and NE-CAT 24-ID-C beamlines of the APS. This complex method, called *in crystallo* enzymology, examines the changing structure of the complex as it moves through each of the steps of synthesis and translocation by collecting diffraction patterns of the complex at each stage of the process. Complementary biochemical experiments confirm the importance of the observed conformational changes of the protein and provide functional support for the model.

Together, the results of this study illustrate the mechanism by which the BcsA-BcsB complex synthesizes and transports cellulose across the plasma membrane. In order to synthesize cellulose, BcsA must first recognize the UDP-activated glucose (UDP-Glc) that serves as a substrate for the elongation reaction. After the glucose is transferred from UDP-Glc to the elongating cellulose chain, UDP must be replaced with a new substrate molecule. This is accomplished by a series of conformational changes in the protein. These include both the retraction of a catalytic site “gating loop” from the active site,

such that UDP can leave and a new UDP-Glc molecule can bind to the catalytic pocket and the movement of a “finger helix,” a short alpha-helix that contacts the last glucose unit of the cellulose chain, from the “up” position to the “down” position. Upon binding of a new UDP-Glc molecule, the finger helix returns to the “up” position and pushes the elongated cellulose chain into the transmembrane channel, thereby beginning the cycle again. This ratcheting movement pushes the cellulose through the transmembrane channel of BcsA after each elongation cycle, one glucose unit at a time.

Cellulose is an important polymer for production of biofuels, is a major component of plant fibers (e.g., cotton and wood) and is central to the formation of bacterial biofilms.

With the structure of the BcsA-BcsB complex as a springboard, future work will include comparative studies that assess the differences and similarities between the *Rhodobacter* BcsA-BcsB complex presented here and complexes present in plants. In addition, future mechanistic studies that address how cellulose is transported across a second outer membrane present in gram-negative bacteria may pave the way for development of anti-microbial agents for difficult-to-treat biofilm infections. — *Emma Nichols*

**See:** Jacob L. W. Morgan<sup>1</sup>, Joshua T. McNamara<sup>1\*</sup>, Michael Fischer<sup>2‡</sup>, Jamie Rich<sup>2‡‡</sup>, Hong-Ming Chen<sup>2</sup>, Stephen G. Withers<sup>2</sup>, and Jochen Zimmer<sup>1\*</sup>, “Observing cellulose biosynthesis and membrane translocation *in crystallo*,” *Nature* **531**(32), 329 (17 March 2016). DOI: 10.1038/nature16966

**Author affiliations:** <sup>1</sup>University of Virginia School of Medicine, <sup>2</sup>University of British Columbia Present Addresses:

<sup>‡</sup>Sandoz GmbH, <sup>‡‡</sup>Kairos Therapeutics

**Correspondence:**

\* jochen\_zimmer@virginia.edu

SER-CAT supporting institutions may be found at [www.ser-cat.org/members.html](http://www.ser-cat.org/members.html). GM/CA-XSD has been funded in whole or in part with Federal funds from the National Cancer Institute (ACB-12002) and the National Institute of General Medical Sciences (AGM-12006). NE-CAT beamlines are funded by the National Institute of General Medical Sciences from the National Institutes of Health (P41 GM103403). The Pilatus 6M detector on the 24-ID-C beamline is funded by a NIH-ORIP HEI grant (S10 RR029205). J.L.W.M. is supported by a National Science Foundation Graduate Research Fellowship, Grant No. DGE-1315231. M.F. thanks the Austrian Science Fund (FWF) (J3293-B21) for an Erwin Schrödinger postdoctoral fellowship. This research was primarily supported by the National Institutes of Health, Grant 1R01GM101001, awarded to J.Z.; S.G.W. thanks the Natural Sciences and Engineering Research Council of Canada for financial support. This research used resources of the Advanced Photon Source, a U.S. Department of Energy (DOE) Office of Science User Facility operated for the DOE Office of Science by Argonne National Laboratory under Contract No. DE-AC02-06CH11357.

22-ID-D • SER-CAT • Life sciences • Macromolecular crystallography, multi-wavelength anomalous dispersion, single-wavelength anomalous dispersion, microbeam • 6-20 keV • On-site, remote • Accepting general users •

23-ID-B • GM/CA-XSD • Life sciences • Macromolecular crystallography, microbeam, large unit cell crystallography, subatomic (<0.85 Å) resolution, multi-wavelength anomalous dispersion, single-wavelength anomalous dispersion • 3.5-20 keV • On-site, remote • Accepting general users •

23-ID-D • GM/CA-XSD • Life sciences • Macromolecular crystallography, microbeam, large unit cell crystallography, subatomic (<0.85 Å) resolution, multi-wavelength anomalous dispersion, single-wavelength anomalous dispersion • 5-20 keV • On-site, remote • Accepting general users •

24-ID-C • NE-CAT • Life sciences • Macromolecular crystallography, microdiffraction, single-wavelength anomalous dispersion, single-crystal diffraction, microbeam, multi-wavelength anomalous dispersion, subatomic (<0.85 Å) resolution • 6.5-23 keV • On-site, remote • Accepting general users •

# BEGINNING TO SEE THE LIGHT

**S**unlight powers nearly all life on Earth. In order to make the most efficient use of this life-giving energy source, photosynthetic organisms including plants, fungi, and bacteria have developed complex molecular machinery for detecting and orienting towards light. A key piece of this machinery is a class of proteins called phytochromes. Embedded in the heart of phytochromes are light-sensitive molecules called chromophores, which, upon absorbing light, deform in a stereotyped manner. These atomic-level structural changes are amplified to produce nanoscale changes to the structure of the surrounding phytochrome. Such changes ultimately lead to changes in gene expression that drive movement of the organism towards the light source, but the structure of photoactivated phytochrome and the nature of the conformational changes it experiences were not known. Previously, a team of researchers used an x-ray scattering method to examine the detailed molecular structure of an incomplete version of a phytochrome protein from the extremophile bacteria species *Deinococcus radiodurans*. In a new study, the same research team was able to study the entire intact protein. Comparisons of the resting and active states of the intact phytochrome with time-resolved x-ray scattering carried out at the APS revealed that light absorption induces a fluid corkscrew motion within the phytochrome structure, in contrast with the simpler trap-door motion that was observed in the earlier study of the partial phytochrome. These findings fill in critical gaps in the knowledge of the structural changes that phytochromes undergo during the detection of light. Modifications to these important proteins could lead to advances in medicine and agriculture.

Phytochromes are composed of evolutionarily conserved domains. The Per/Arndt/Sim (PAS) and phosphodiesterase/adenyl cyclase/FhlA GAF domains assume a tightly packed, globular structure stabilized by a figure-eight-like knot formed by the backbone. The PHY domain is connected to the GAF domain through a long helical spine. Embedded in the PAS or GAF domains are light-absorbing chromophore molecules. The so-called PHY “tongue” makes contact with the chromophore and is folded over in the phytochrome’s resting state and flipped upwards in the active state. Finally, upon conformational changes within the phytochrome, histidine kinase output domains initiate the expression of specific sets of genes, which regulate the organism’s response to the presence of light.

When light excites the chromophore, an internal rotation is caused

when a bond between neighboring carbon atoms within the molecule breaks (Fig. 1). Little is known about how this structural change is coupled to the remainder of the protein. Two years ago, using time-resolved x-ray scattering, this team of researchers observed a large-scale change from the resting to active stages of a truncated, mutant version of phytochrome from *Deinococcus radiodurans* that was lacking the histidine kinase output domains. The researchers concluded that the primary structural change within the photoactivated phytochrome was the refolding of the PHY tongue, like a flap closing down over a hole.

More recently, the same team of researchers from the University of Gothenburg (Sweden), the University of Jyväskylä (Finland), The University of Chicago, Tampere University of Technology (Finland), the Paul Scherrer Institut (Switzerland), and the European

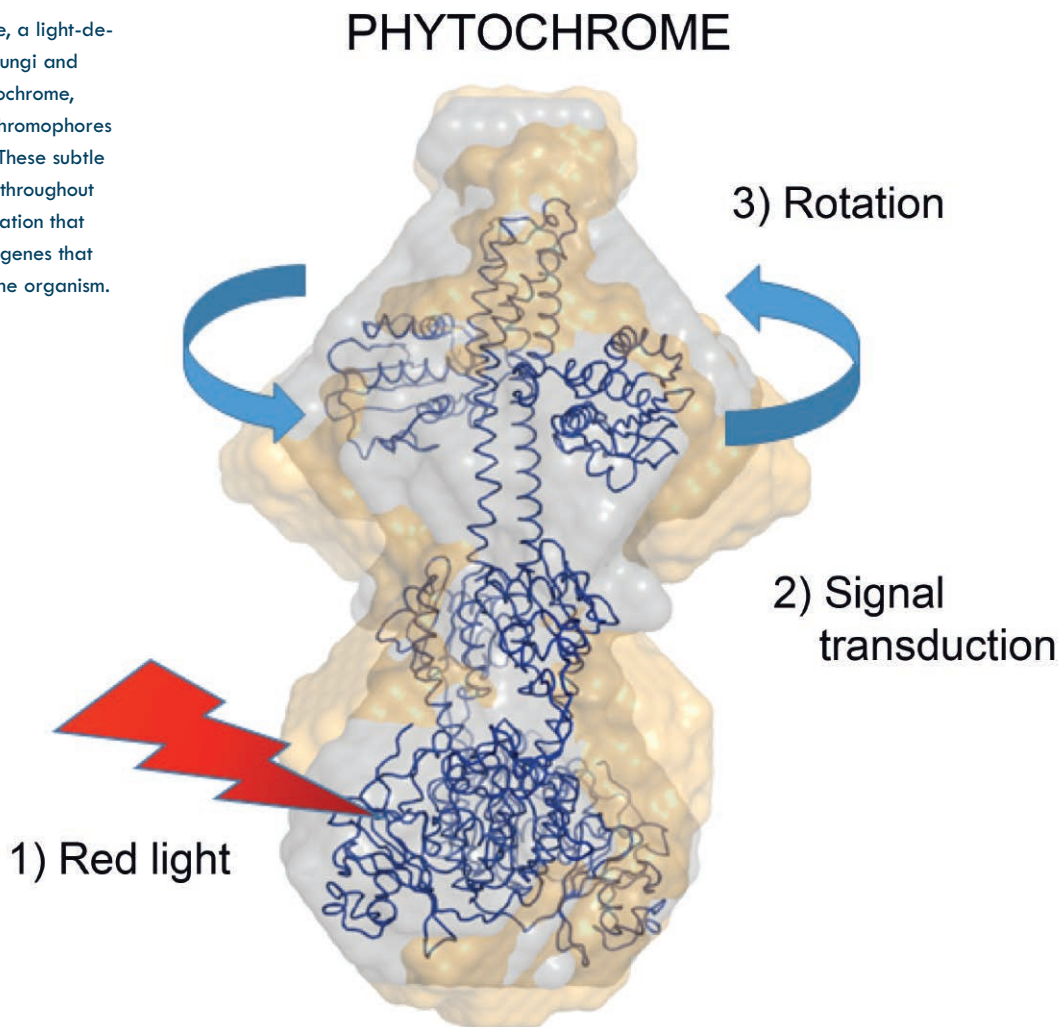
Synchrotron Radiation Facility (ESRF, France) employed time-resolved x-ray scattering at the BioCARS beamline 14-ID-B of the APS, and at beamline ID09B of the ESRF, to characterize the full-length phytochrome from *Deinococcus radiodurans* with the histidine kinase output domains intact.

The time-resolved x-ray scattering technique utilizes an optical laser pulse to initiate the photoreactions of a phytochrome protein and an x-ray probe to monitor the ensuing structural changes. Because x-rays scatter off all atomic pairs in the protein, an x-ray scattering pattern provides real-time information on structural dynamics.

This new set of experiments revealed that a twist of the histidine kinase output domains with respect to the chromophore-binding domains represents the dominant change between the photoactivated and resting states. The time-resolved data further show



Fig. 1. Activation of a phytochrome, a light-detecting protein found in bacteria, fungi and plants. When light strikes the phytochrome, light-absorbing molecules called chromophores undergo conformational changes. These subtle structural changes are transduced throughout the protein, causing an internal rotation that triggers the expression of specific genes that indicates the presence of light to the organism.



that the small, localized structural changes in the chromophore-binding domains occur on the microsecond time scales. The global structural change propagates outwards to the entire phytochrome structure within a few milliseconds.

This new knowledge regarding the structural changes that the phytochrome undergoes upon activation by light may be used by scientists to direct the manipulation of the protein in the name of making advances in numerous fields, including medicine and agriculture. — *Chris Palmer*

**See:** Alexander Björling<sup>1</sup>, Oskar Berntsson<sup>1</sup>, Heli Lehtivuori<sup>2</sup>, Heikki Takala<sup>1,2</sup>, Ashley J. Hughes<sup>1</sup>, Matthijs Panman<sup>1</sup>, Maria Hoernke<sup>1</sup>, Stephan Niebling<sup>1</sup>, Léocadie Henry<sup>1</sup>, Robert Henning<sup>3</sup>, Irina Kosheleva<sup>3</sup>, Vladimir Chukharev<sup>4</sup>, Nikolai V. Tkachenko<sup>4</sup>, Andreas Menzel<sup>5</sup>, Gemma Newby<sup>6</sup>, Dmitry

Khakhulin<sup>6</sup>, Michael Wulff<sup>6</sup>, Janne A. Ihalainen<sup>2\*</sup>, and Sebastian Westenhoff<sup>1\*\*</sup>, “Structural photoactivation of a full-length bacterial phytochrome,” *Sci. Adv.* **2**, e1600920 (12 August 2016). DOI: 10.1126/sciadv.1600920

**Author affiliations:** <sup>1</sup>University of Gothenburg, <sup>2</sup>University of Jyväskylä, <sup>3</sup>The University of Chicago, <sup>4</sup>Tampere University of Technology, <sup>5</sup>Paul Scherrer Institut, <sup>6</sup>European Synchrotron Radiation Facility

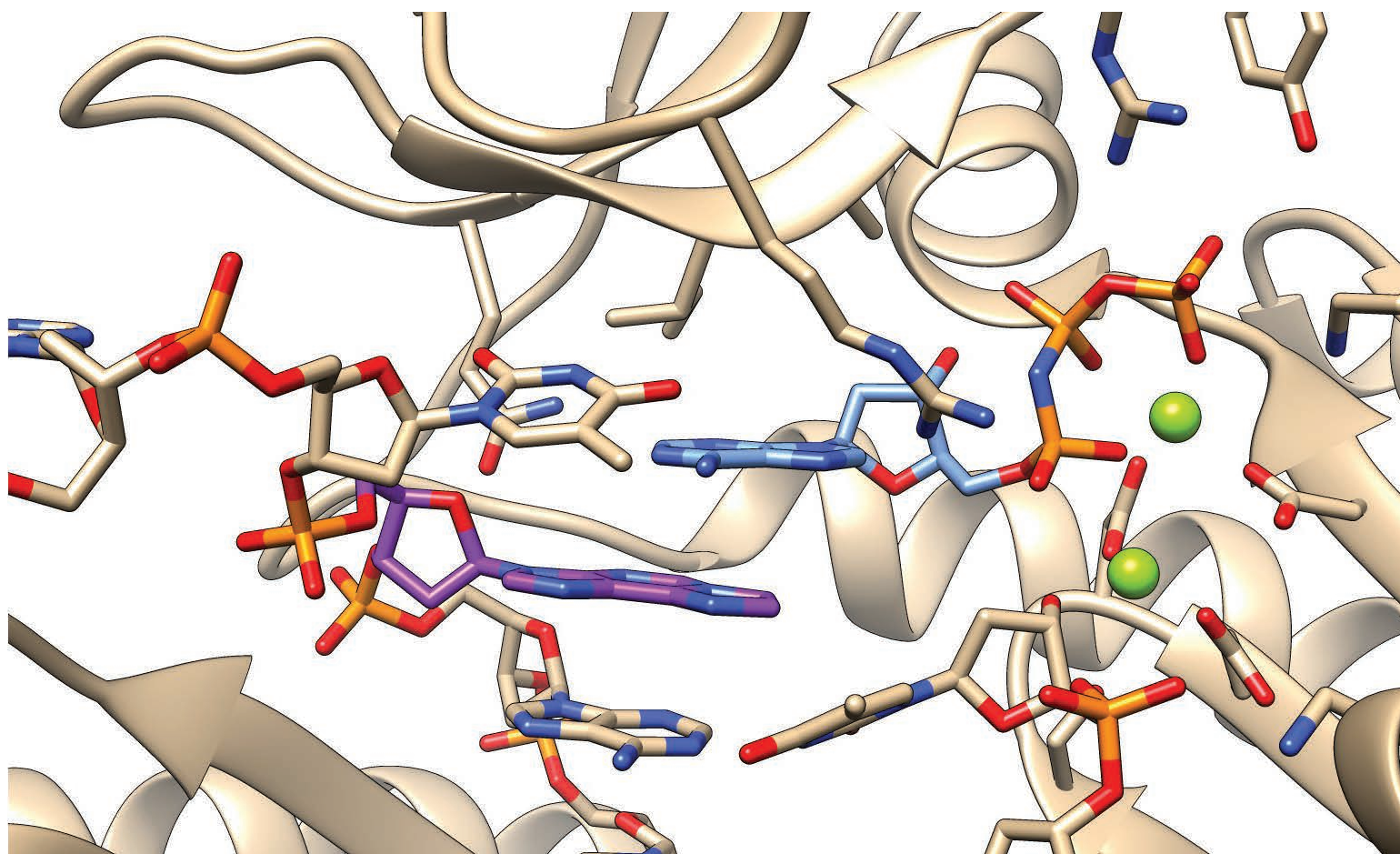
**Correspondence:**

\* janne.ihalainen@jyu.fi,  
\*\* westenho@chem.gu.se

The authors acknowledge funding from The Swedish Foundation for International Cooperation in Research and Higher Education. S.W. acknowledges funding from the European Research Council and the Foundation of Strategic Research, Sweden. J.A.I., H.T., and H.L. acknowledge funding from the Academy of Finland and Finnish Cultural Foundation. M.H. was funded by Marie Curie

grant IEF-GA-2013-CHE-624864 ANISO-PROTEINXRAY. Beamline access at ID09b and BM29 of the ESRF is acknowledged. use of BioCARS was also supported by National Institutes of Health (NIH) National Institute of General Medical Sciences grant 1R24GM111072. The time-resolved setup at BioCARS was funded in part through a collaboration with P. Anfinrud (NIH/National Institute of Diabetes and Digestive and Kidney Diseases). This research used resources of the Advanced Photon Source, a U.S. Department of Energy (DOE) Office of Science User Facility operated for the DOE Office of Science by Argonne National Laboratory under Contract No. DE-AC02-06CH11357.

14-ID-B • BioCARS • Life sciences, materials science, physics, chemistry • Time-resolved crystallography, time-resolved x-ray scattering, Laue crystallography, wide-angle x-ray scattering, biohazards at the BSL2/3 level, macromolecular crystallography • 7-19 keV • On site • Accepting general users •



# LESSONS FROM IMPERFECT ATTEMPTS TO REPLICATE DAMAGED DNA

Cancer, aging, and a host of other diseases are linked to damage or “lesions” in DNA, the molecular blueprint for a cell. The body has developed a sophisticated machinery to deal with DNA damage. For example, human translesion polymerase  $\eta$  can bypass DNA damage caused by UV radiation. Unfortunately, the polymerase can also bypass intentional damage inflicted by the anticancer drug cisplatin, leading to chemoresistance. Sometimes, though, the polymerase can get it wrong, leading to errors in the replicated DNA. Damage that takes the form of a segment of DNA bound to the cancer-causing chemical 1, $N^6$ -ethenodeoxyadenosine (“etheno”) triggers error-prone bypass by polymerase  $\eta$ . To figure out why the polymerase makes miscoded DNA in this case, researchers solved the structure of polymerase  $\eta$  in complex with etheno-damaged DNA using x-ray diffraction data collected at the APS. Insights from structural studies into how polymerases bypass DNA damage may pave the way to the discovery of inhibitors of translesion synthesis, helping chemotherapeutics such as cisplatin remain effective.

The source of DNA damage can come from outside the body, such as with environmental pollutants, or inside the body, as with free radicals. Etheno lesions are known to stem from exposure to vinyl chloride, an industrial chemical used in the production of PVC. Scientists have also observed that rats that hadn't encountered vinyl chloride can also develop etheno lesions, which were eventually attributed to lipid peroxidation. The etheno lesion in both cases consists of two extra carbon atoms attached to a DNA base in an exocyclic arrangement.

To explore the structure and kinetics of the replication of DNA strands

with etheno lesions by human translesion DNA polymerase  $\eta$ , researchers from Vanderbilt University School of Medicine performed a series of kinetic experiments. They discovered that the polymerase prefers to incorporate dATP or dGTP, compared to dTTP, across from the etheno lesion. Additional analysis using mass spectrometry revealed the same preference for purines, while also showing that the polymerase tends to not only create a point mutation, but in some cases a complete frameshift, suggesting “slippage” of the polymerase around the lesion.

As a next step, the researchers wanted to get a close look at what was going on, so they generated five different crystals of the polymerase in complex with a DNA construct containing an etheno lesion. Three of those crystals captured the polymerase at the stage of replication known as “insertion,” while the other two crystals were in the “extension” phase. All five crystal structures were solved to high-resolution using data from the LS-CAT 21-ID-F and 21-ID-G beamlines at the APS.

From two of the insertion structures, the team was able to figure out why the polymerase tends to produce frameshift misincorporations. Non-hydrolyzable dATP or dGTP analogs in the complex were found not to pair with

the etheno lesion, but instead to form a staggered configuration that would lead the polymerase to omit a base pair at that site. Another insertion site structure showed the dTTP positioned opposite to the lesion, forming two hydrogen bonds with the etheno adduct, though in an energetically unfavorable conformation. The extension site complexes provided insights into why dTTP isn't the preferred nucleoside for the polymerase to place opposite of the etheno adduct, based on an observation of disorder in a portion of the DNA primer.

— Erika Gebel Berg

**See:** Amritraj Patra, Yan Su, Qianqian Zhang<sup>‡</sup>, Kevin M. Johnson, F. Peter Guengerich\*, and Martin Egli\*\*, “Structural and Kinetic Analysis of Miscoding Opposite the DNA Adduct 1, $N^6$ -Ethenodeoxyadenosine by Human Translesion DNA Polymerase  $\eta$ ” *J. Biol. Chem.* **29**(27), 14134 (July 1, 2016). DOI 10.1074/jbc.M116.732487

**Author affiliation:** Vanderbilt University School of Medicine <sup>‡</sup>Present address: Shanghai CP Guojian Pharmaceutical Co.

**Correspondence:**

\* f.guengerich@vanderbilt.edu

\*\* martin.egli@vanderbilt.edu

Work supported by National Institutes of Health Grants R01 ES010375 (to F. P. G. and M. E.), P01 CA160032 (to M. E.), R01 ES010546 (to F. P. G.), T32 CA009582 (to K. M. J.), and P30 ES000267 (to F. P. G. and M. E.). Vanderbilt Univ. is a member institution of LS-CAT. LS-CAT is supported by the Michigan Economic Development Corporation and the Michigan Technology Tri-Corridor (Grant 085P1000817). This research used resources of the Advanced Photon Source, a U.S. DOE Office of Science User Facility operated for the DOE Office of Science by Argonne National Laboratory under Contract No. DE-AC02-06CH11357.

21-ID-F/21-ID-G • LS-CAT • Life sciences • Macromolecular crystallography • 12.7 keV • On-site, remote, mail-in • Accepting general users •

< Fig. 1. Structural basis of error-prone bypass of the etheno-dA DNA adduct by human polymerase  $\eta$  revealed by the crystal structure of the ternary polymerase•DNA•dNTP complex trapped at the insertion stage. The illustration depicts the staggered arrangement between the incoming non-hydrolyzable dATP analog and etheno-dA from the DNA template strand at the polymerase active site that is consistent with frameshifting. The template strand is on the left and the primer strand is on the right, carbon atoms of etheno adduct and dATP analog are colored in magenta and blue, respectively, Mg<sup>2+</sup> ions are light green spheres, and side chains of selected amino acids are shown and are colored by atom.



## EGF Repeat

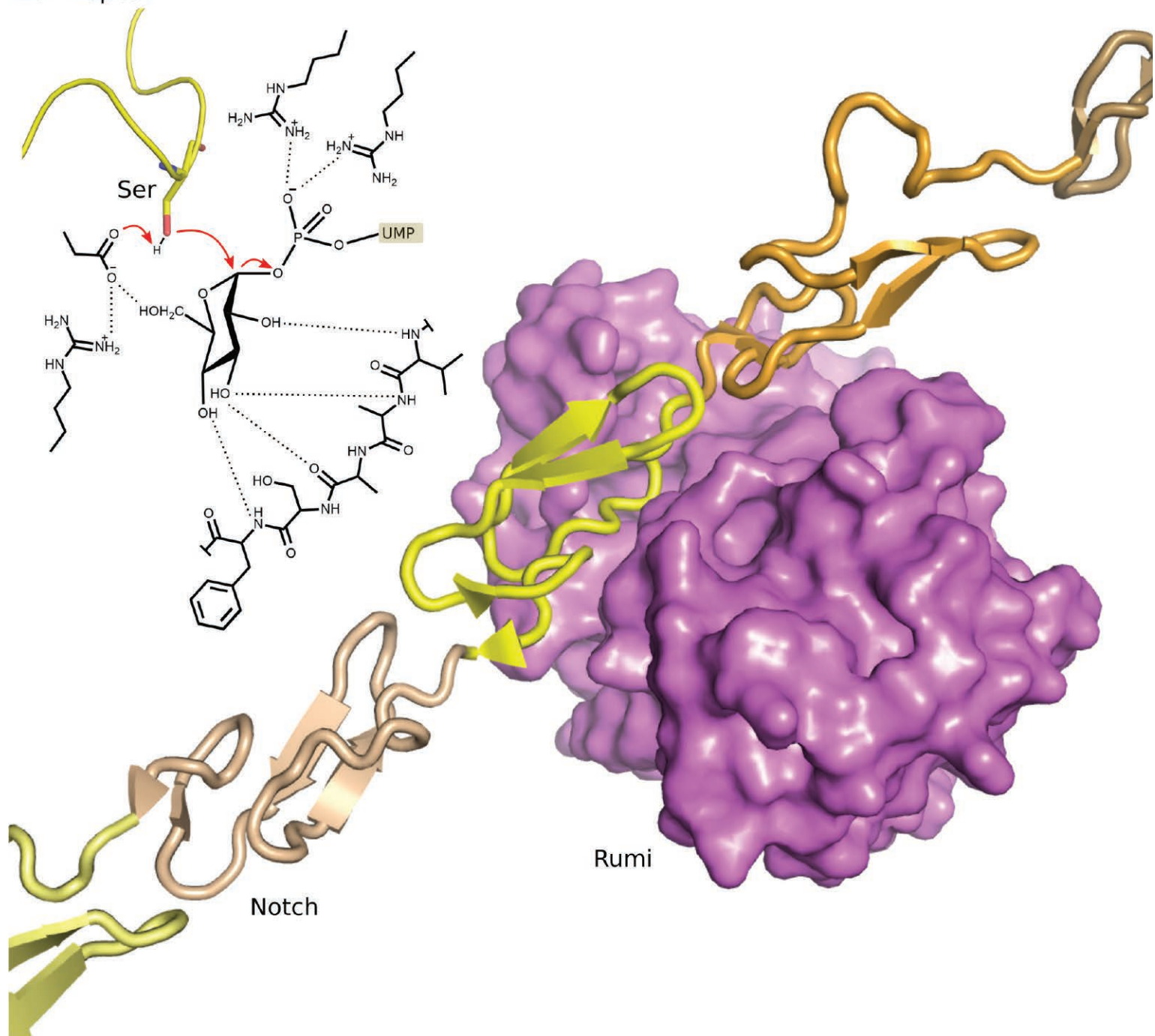


Fig. 1. Schematic of Rumi in complex with Notch. Right: A model based on the Rumi-EGF crystal structure shows how Rumi recognizes one Notch EGF repeat (in yellow) among others. Left: Schematics showing the chemical mechanism for how Rumi modifies the serine (Ser) in an EGF repeat by adding glucose.

31-ID-D • LRL-CAT • Life sciences • Macromolecular crystallography, single-wavelength anomalous dispersion • 9-13.5 keV • Mail-in • Accepting general users •

# MODULATING A MAJOR DRIVER OF DEVELOPMENT

**D**uring development of multicellular organisms, a major signaling protein called Notch controls the expression of genes to help determine which cells should develop into specific cell types, like skin, heart, or neurons. Defects in Notch function can cause birth defects. Notch has also been shown to have tumor promoting activity and can lead to various cancers, especially leukemias. In the normal course of development, the function of Notch can be modified by a number of other proteins. One such protein, Rumi, modifies Notch by adding glucose molecules to the protein. Mutations in Rumi are linked to a number of diseases including a skin disorder called Dowling-Degos disease and a form of muscular dystrophy. Researchers working at the APS have created the first atomic-level structural models of Rumi in complex with Notch and glucose. These models reveal the details of Rumi's interactions with Notch, paving the way for potential anti-cancer medications that target Rumi.

While the genomes of multicellular organisms contain many thousands of genes, it is the complex patterns in the way these genes get expressed during the various stages of early life that guide organisms' development. Gene expression is systematically controlled by signaling proteins that tell neighboring cells in the developing organism what cell type to become and when. One important signaling protein, called Notch, is a complex protein chain that spans the cell membrane with 36 repeating folds, called EGF repeats, in its extracellular portion that can each be modified by enzymes in different ways to control the protein's overall function.

Many of the enzymes that can modify Notch have been identified, as have the resulting changes to Notch's function. The protein Rumi—associated with a variety of diseases, including a form of skin hyperpigmentation called Dowling-Degos disease and a form of muscular dystrophy—is the only protein that has been found to modify Notch, as well as other signaling molecules, by adding glucose molecules to the protein. Indeed, this process, called glycosylation, is essential for Notch to fold itself into its final complex form and, therefore, to function normally.

In addition to its role in development, mutated forms of Notch can function as oncogenes, driving tumor formation especially in leukemias. Rumi itself

is also known to be overexpressed in some leukemias. Therefore, Rumi may be an important target of anti-cancer medications. However, to accurately target Rumi, it would be important to understand with precise detail the way in which it adds glucose to Notch. Yet, this mechanism has been elusive for a variety of reasons including the difficulty in generating sufficient amounts of Rumi protein. Large amounts of proteins are required to generate the structural models necessary to determine these mechanisms.

Researchers at Brookhaven National Laboratory, the University of Georgia, and Stony Brook University overcame the challenges in generating samples of Rumi. Historically, large amounts of proteins have been generated using bacteria, but enzymes like Rumi do not fold properly when expressed in bacteria. Recent improvements in use of human cells to generate large amounts of enzymes like Rumi allowed these researchers to produce sufficient properly folded protein to perform structural studies. They also took advantage of a fruit-fly-derived version of Rumi and a human protein that offers a reasonable facsimile of Notch to generate co-crystals. The scientists then used extremely bright x-rays at the LRL-CAT 31-ID-D beamline at the APS and National Synchrotron Light Source (NSLS) beamlines X25, X29, and X4A

at Brookhaven National Laboratory to probe the crystal structures of Rumi bound to Notch and reconstructed three-dimensional images of the structures.

The research team's detailed three-dimensional molecular structures revealed that Rumi recognizes a six-amino-acid sequence—C-X-S-X-(P/A)-C—on many of the EGF repeats of Notch (Fig. 1). When Rumi binds, the section of Notch that accepts glucose molecules fits very precisely into the active site on Rumi.

The team subsequently found that five Rumi mutations identified in cancers and Dowling-Degos disease are clustered around an active site that facilitates glycosylation and that these mutations adversely affect Rumi's activity. The researchers conclude that disruption to Rumi activity may partially underlie these diseases, and that the mechanistic insights gained in this study may facilitate the development of new cancer therapeutics that target Rumi's modulation of Notch signaling.

— Chris Palmer

**See:** Hongjun Yu<sup>1</sup>, Hideyuki Takeuchi<sup>2</sup>, Megumi Takeuchi<sup>2</sup>, Qun Liu<sup>1</sup>, Joshua Kantharia<sup>3</sup>, Robert S Haltiwanger<sup>2\*</sup>, and Huilin Li<sup>1,3\*\*</sup>, "Structural analysis of Notch-regulating Rumi reveals basis for pathogenic mutations," *Nat. Chem. Biol.* **12**, 735 (September 2016). DOI: 10.1038/nchembio.2135

**Author affiliations:** <sup>1</sup>Brookhaven National Laboratory, <sup>2</sup>University of Georgia, <sup>3</sup>Stony Brook University

**Correspondence:**

\* rhalti@uga.edu \*\* hli@bnl.gov

This work was supported by the National Institutes of Health (grants GM061126 (to R.S.H.) and AG029979 (to H.L.) and SBU-BNL (seed grant to R.S.H. and H.L.)). We thank the staff at the APS and NSLS beamlines. The NSLS and the APS are supported by the U.S. Department of Energy Office of Science-Basic Energy Sciences under Contracts No. DE-AC02-98CH10886 and DE-AC02-06CH11357, respectively. Use of the LRL-CAT beamline at Sector 31 of the APS was provided by Eli Lilly Company, which operates the facility.

# A NOVEL ROUTE TO A RNA CAP

The transcription of DNA into RNA is a universal aspect of life, and the integrity of the process is essential for an organism's health. Putting a chemical “cap”—7-methylguanylate—on the end of a eukaryotic mRNA is one way a cell ensures that the mRNA is stable, efficiently translated, and shipped to the right location within the cell. Recent evidence suggests that capping may also occur in prokaryotes, but, instead of 7-methylguanylate, the bacterial caps contain nicotinamide adenine dinucleotide (NAD<sup>+</sup>/NADH) or 3'-desphospho-coenzyme A (dpCoA). Eukaryotic capping with 7-methylguanylate occurs after the initiation of transcription, as a chemical reaction that adds 7-methylguanylate to a pre-formed RNA 5' end. Researchers initially suspected the process would be similar in bacteria, but turns out, they were wrong. In this study, relying partially on evidence gathered at two U.S. Department of Energy Office of Science user facilities, the APS and the National Synchrotron Light Source II (NSLS-II), researchers found a completely different capping mechanism, one that may also occur in eukaryotes. This novel insight into the fundamental process of transcription is a game changer, generating a new paradigm for how cells process genetic information.

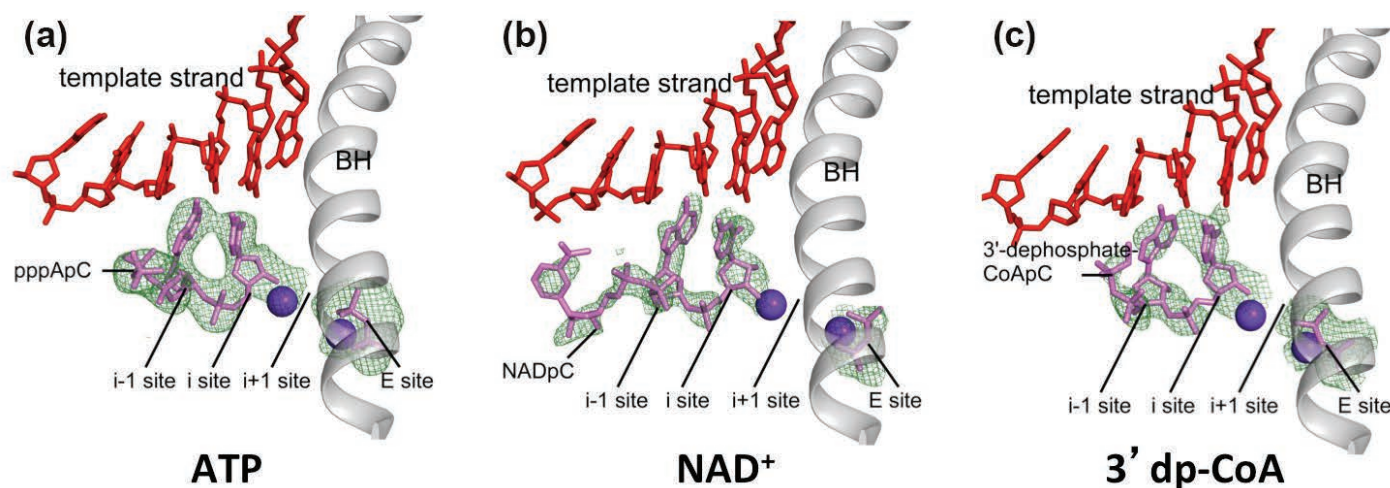


Fig. 1. A side-by-side comparison of the initial product complexes of transcription using different initiating nucleotides: ATP (A), NAD<sup>+</sup> (B), and 3' dpCoA (C). The DNA template strand is shown in red, the initial RNA transcription product is shown in pink, the violet sphere is the RNAP active-center catalytic Mg<sup>2+</sup> ion, and BH is the RNAP active-center bridge helix ( $\alpha$ -helix that forms wall of RNAP active center).



In canonical transcription initiation, RNA polymerase (RNAP) starts a new strand of RNA with an ATP as the first (initiating) nucleotide at the 5' end. The researchers hypothesized that, since NAD<sup>+</sup>, NADH, and dpCoA share an adenosine diphosphate substructure with ATP, these nucleotides potentially also could serve as initiating nucleotides. If true, NAD<sup>+</sup>, NADH, or dpCoA, which the researchers in this study collectively referred to as "non-canonical initiating nucleotides" (NCIN), would become the 5' end of the RNA, capping the end *ab initio*, as transcription begins.

To assess the hypothesis that NCIN-mediated initiation caps RNA, the researchers, from Rutgers University, the Czech Academy of Science, Charles University in Prague (Czech Republic), and Texas A&M University, performed *in vitro* transcription experiments with *Escherichia coli* RNAP plus a genes for RNAs previously identified as likely to have NAD<sup>+</sup> caps *in vivo*. When ATP was added as the initiating entity, the RNAs were uncapped and were sensitive to digestion by RppH, an enzyme that selectively digests uncapped RNAs and insensitive to digestion by NudC, an enzyme that selectively digests capped RNAs. In contrast, when NAD<sup>+</sup>, NADH, or dpCoA was added as the initiating entity, the RNAs were capped, as demonstrated by insensitivity to RppH and sensitivity to NudC, and also, directly, by mass spectrometry.

The researchers confirmed these results *in vivo* as well, and then demonstrated that NCIN capping has functional consequences in bacterial cells. They assessed the stabilities of NCIN-capped RNAs, comparing them to uncapped RNAs, by tracking how long they remained in the cell after the addition of an RNA-synthesis inhibitor rifampin. The NCIN-capped RNAs had

longer half-lives than the uncapped RNAs, corresponding to a three- to four-fold increase in stability with capping. Furthermore, NCIN capping appeared to relate to the bacterial growth-phase, with two-fold higher capping in the stationary phase versus the exponential phase.

While capping with NAD<sup>+</sup>, NADH, and dpCoA had only been observed in bacteria, the researchers wondered if it also may occur, and may have the same mechanism, in eukaryotes. To begin to answer that question, the researchers performed analogous *in vitro* experiments with a eukaryotic version of RNAP, years RNAP II. The eukaryotic RNAP appeared to have no problem using NAD<sup>+</sup> or NADH as an initiating nucleotide, forming products that were sensitive to NudC and insensitive to RppH. The researchers concluded that eukaryotic RNAP was capable of using NCIN and that the resulting RNA products were capped at the 5' end, and one subsequently published paper and another in-press, soon-to-be-published paper have confirmed that this type of capping occurs in eukaryotic cells.

Finally, the researchers examined the structural basis for transcription initiation by solving three crystal structures (using data gathered, in part, at the SBC-CAT beamline 19-ID-D at the APS and beamline X29A at the Brookhaven National Laboratory NSLS-II) of RNAP-promoter complexes in the presence of ATP, NAD<sup>+</sup>, or dpCoA as the initiating nucleotide and CTP as an extending nucleotide. In each case, the structure revealed that RNAP could indeed use the given nucleotide to initiate transcription, and was captured at a stage of the transcription reaction that had never before been observed, at the threshold of RNA extension. For the ATP case, the crystal structure is the first to show an initial product complex for a cellular RNAP. — *Erika Gebel Berg*

**See:** Jeremy G. Bird<sup>1</sup>, Yu Zhang<sup>1</sup>, Yuan Tian<sup>1</sup>, Natalya Panova<sup>2</sup>, Ivan Barvik<sup>3</sup>, Landon Greene<sup>4</sup>, Min Liu<sup>1</sup>, Brian Buckley<sup>1</sup>, Libor Krásný<sup>2</sup>, Jeehiun K. Lee<sup>1</sup>, Craig D. Kaplan<sup>5</sup>, Richard H. Ebright<sup>1\*\*</sup>, and Bryce E. Nickels<sup>1\*</sup>, "The mechanism of RNA 5' capping with NAD<sup>+</sup>, NADH and desphospho-CoA," *Nature* **535**, 444 (2 July 2016).

DOI: 10.1038/nature18622

**Author affiliations:** <sup>1</sup>Rutgers University, <sup>2</sup>Czech Academy of Sciences, <sup>3</sup>Charles University in Prague, <sup>4</sup>Bristol-Myers Squibb Company, <sup>5</sup>Texas A&M University

**Correspondence:**

\* bnickels@waksman.rutgers.edu

\*\* ebright@waksman.rutgers.edu

This work was supported by National Science Foundation grant CHE-1361462 (J.K.L.), Welch Foundation Grant A-1763 (C.D.K.), Czech Science Foundation 15-05228S (L.K., N.P.), and National Institutes of Health (NIH) grants NIEHS P30 ES005022, GM097260 (C.D.K.), GM041376 (R.H.E.), GM088343 (B.E.N.), GM096454 (B.E.N.), and GM115910 (B.E.N.). SBC-CAT is operated by UChicago Argonne, LLC, for the U.S. Department of Energy (DOE) Office of Biological and Environmental Research under contract DE-AC02-06CH11357. The National Synchrotron Light Source II is a U.S. DOE Office of Science User Facility operated for the DOE Office of Science by Brookhaven National Laboratory under Contract No. DE-SC0012704. This research used resources of the Advanced Photon Source, a U.S. DOE Office of Science User Facility operated for the DOE Office of Science by Argonne National Laboratory under contract no. DE-AC02-06CH11357.

19-ID-D • SBC-CAT • Life sciences • Macromolecular crystallography, multi-wavelength anomalous dispersion, subatomic (<0.85 Å) resolution, microbeam, ultra-low-temperature (15K), large unit cell crystallography, single-wavelength anomalous dispersion • 6.5-19.5 keV • On-site, remote, mail-in • Accepting general users •

# HOW CELLS DISTRIBUTE GENETIC MATERIAL DURING CELL DIVISION

The yeast MIND complex is critical for ensuring that a dividing cell's duplicated genetic material, packaged as chromosomes, is shared appropriately by the daughter cells. This process is complex and often dysregulated in pathologies such as cancer and birth defects. In order to develop an atomic model to help explain the most interesting regulatory properties of the MIND complex, researchers used the APS to determine its structure. In conjunction with complementary biochemical data, the structure showed specific ways in which molecular signals govern the assembly and disassembly of the proteins that drive chromosome "segregation" into daughter cells.

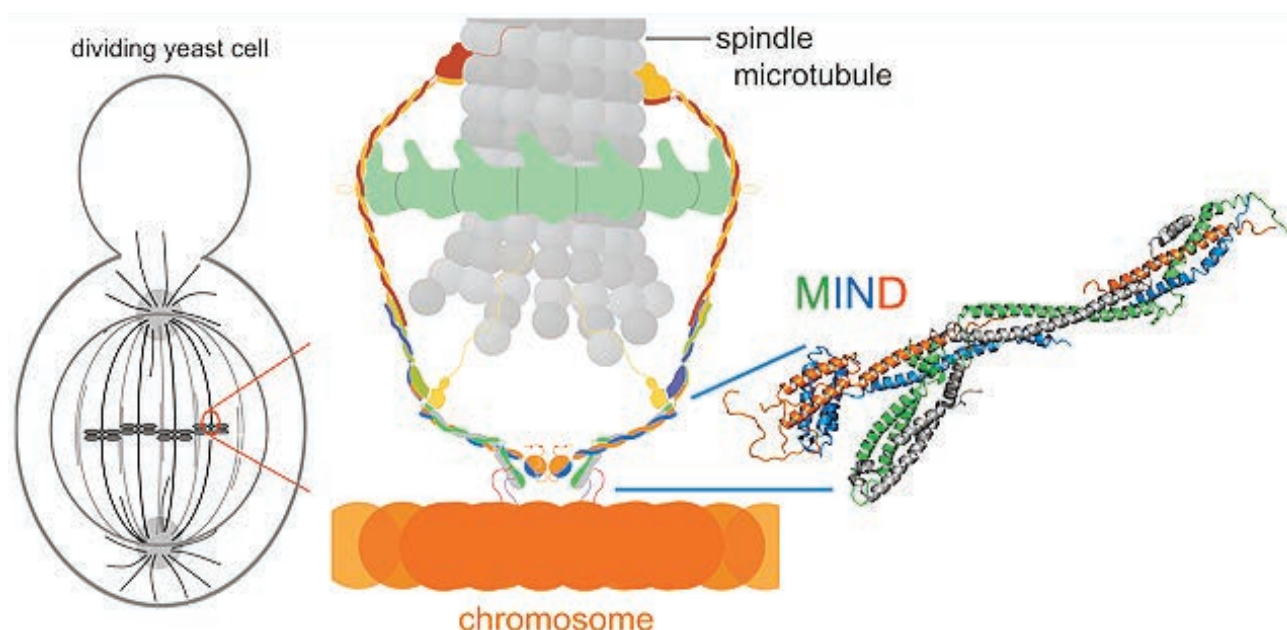


Fig. 1. The mitotic spindle separating chromosomes in a budding yeast cell (left), requires attachment of spindle microtubule (grey) to the chromosome (orange) via a kinetochore (center). The MIND complex (structure shown far right) is critical for kinetochore assembly.

Within animal cells, DNA is organized into distinct chromosomes. During cell replication, or mitosis, cells replicate and divide their genetic material into two daughter cells. As a part of this complex and elegant process, thread like structures, called microtubules, attach to each of the cell's duplicated chromosomes at a structure called a kinetochore. The chromosomes are then evenly separated into the daughter cells as the mitotic spindle pulls the chromosomes apart to opposite poles of the dividing cell (Fig. 1). To ensure fidelity, the process is tightly controlled, and the proteins involved must be active at the right location at the appropriate

time. Cells that mistakenly inherit multiple copies of a chromosome, or are missing a chromosome, cannot function: dysregulation of chromosome segregation during development can cause birth defects, and is a molecular hallmark of many types of cancer.

The kinetochore is an assembly of proteins that connects the chromosome to the microtubules of the mitotic spindle. The MIND assembly has an especially important role in regulating kinetochore assembly early in cell division as well as disassembly once cell division is complete. To develop an atomic model of the MIND complex proteins,

*"Genetic" cont'd. on page 166*

# LEARNING THE TRICKS OF A DOUBLE-TIMING ENZYME

Most enzymes have one job, with structures that are honed by evolution for a single specific purpose. However, a few special enzymes do double duty, targeting two different substrates. Such enigmatic catalysts beg the question of how one enzyme, with a single structure, recognizes two substrates with different structures. To answer that question, a team of researchers used the APS to solve the structure of a dual-specificity enzyme in the act of catalysis. The researchers focused on RlmN, an RNA methylase that targets both ribosomal RNA (rRNA) as well as transfer RNA (tRNA). These methylation reactions are critical for integrity during translation of genetic information. While the rRNA and tRNA substrates share little sequence similarity, the findings reveal that at the level of three-dimensional structure, they may not be so different after all. The study also highlights a potentially ancient evolutionary connection between rRNA and tRNA.



Fig. 1. Cartoon diagram of RNA-modifying enzyme RlmN (blue) bound to transfer RNA (gray).

RlmN is known best for its ability to methylate C2 of adenosine A2503 of the 23S rRNA subunit. The C2 of adenosine is relatively inert, requiring some extra effort on RlmN's part for methylation. RlmN uses an iron-sulfur cluster to coordinate the cofactor S-adenosylmethionine (SAM), which supplies the methyl group for the reaction. Unlike most SAM methyltransferases, RlmN employs a second equivalent of SAM that is used to overcome the inertness of the C2 of adenosine. This activity places RlmN in another group of enzymes termed radical SAM enzymes. These catalysts share a basic reaction scheme that involves cleaving SAM reductively to produce a radical intermediate, facilitating abstraction of a hydrogen atom from substrate to jumpstart complex multi-step radical reactions.

RlmN's large nucleic acid substrate presents challenges for structural study. To better understand its ability to modify RNA, the research team from Pennsylvania State University took advantage of knowledge about the role of two of RlmN's cysteine residues, C118 and C355. These amino acids orchestrate the methylation reaction chemistry. The researchers generated a C118A RlmN variant known to become cross-linked to RNA during the reaction, stopping the cycle at an intermediate step. C118A even becomes crosslinked to unknown RNAs during protein production in *Escherichia coli* and this mystery complex was the first target for crystallographic analysis at the GM/CA-XSD 23-ID-B x-ray beamline at the APS. The structure revealed that RlmN was bound to a tRNA, specifically tRNA<sup>Glu</sup> (RlmN C118A-tRNA<sup>Glu</sup>), at A37. The result is consistent with a report in the literature of this second methylation activity. Another version of RlmN C118A-tRNA<sup>Glu</sup> was produced, crystallized with *in vitro* transcribed RNA, and the

*"Enzyme" cont'd. on page 166*



*“Genetic” cont’d. from page 164*

researchers from the Harvard Medical School and the Howard Hughes Medical Institute crystallized the MIND complex and collected numerous diffraction patterns to build a molecular snapshot, utilizing the NE-CAT 24-ID-C and 24-ID-E beamlines at the APS. The microfocus and adjustable wavelength capabilities of the 24-ID-C beamline, along with the pixel-array detector, were central to collection of over 400 promising data sets used to build the final structure. Because the MIND complex is inherently flexible, and the crystals formed were small and irregular, use of the APS was an essential component of success, according to the researchers.

The researchers’ model included potential sites at which a type of cell-cycle dependent chemical modification, called phosphorylation, would allow for regulation of kinetochore assembly and disassembly. Subsequent biochemical analysis confirmed that MIND does indeed integrate phospho-regulatory inputs in order to drive kinetochore assembly and disassembly. In addition, the structure offered insight into how the interactions between the protein members of the MIND assembly can withstand the physical forces associated with pulling chromosomes apart.

The findings add to the developing molecular description of how cells replicate their genomes and distribute the two copies correctly during mitosis. The molecular interactions revealed by the MIND structure are a valuable contribution to this larger picture.

— Emma Nichols

**See:** Yoana N. Dimitrova<sup>1</sup>, Simon Jenni<sup>1</sup>, Roberto Valverde<sup>1</sup>, Yadana Khin<sup>1</sup>, and Stephen C. Harrison<sup>1,2\*</sup>, “Structure of the MIND Complex Defines a Regulatory Focus for Yeast Kinetochore Assembly,” *Cell* **167**, 1014 (November 3, 2016).

DOI: 10.1016/j.cell.2016.10.011

**Author affiliations:** <sup>1</sup>Harvard Medical School, <sup>2</sup>Howard Hughes Medical Inst.

**Correspondence:**

\* harrison@crystal.harvard.edu

The research was supported by the Howard Hughes Medical Institute and by National Institutes of Health (NIH) grant GM62580 (S.C.H.). We thank the NE-CAT staff at the APS for advice and assistance in data col-

lection. NE-CAT is funded by NIH grant P41 GM103403 and the Pilatus 6M detector on 24-ID-C by NIH-ORIP HEI grant S10-RR029205. This research used resources of the Advanced Photon Source, a U.S. Department of Energy (DOE) Office of Science User Facility operated for the DOE Office of Science by Argonne National Laboratory under Contract No. DE-AC02-06CH11357.

24-ID-C • NE-CAT • Life sciences • Macromolecular crystallography, microdiffraction, single-wavelength anomalous dispersion, single-crystal diffraction, microbeam, multi-wavelength anomalous dispersion, subatomic (<0.85 Å) resolution • 6.5-23 keV • On-site, remote • Accepting general users •

24-ID-E • NE-CAT • Life sciences, macromolecular crystallography • Microbeam, microdiffraction, single-wavelength anomalous dispersion, single-crystal diffraction • 12.68 keV • On-site • Remote • Accepting general users •

*“Enzyme” cont’d. from page 165*

structure was solved using data collected at the LS-CAT beamline at the APS. The in vivo and in vitro constructs sported similar structures and provided, for the first time, atomic-level insight into the catalytic mechanism behind the methylation of RNA by RlmN.

The crystal structures provided a detailed look at the relationship between various parts of the enzyme active site and the tRNA, allowing the researchers to flesh out a detailed reaction scheme. RlmN uses C355 as a methyl carrier, activating it to a methylene radical that can attack adenosine C2. C118 is required for product release, explaining why C118A RlmN is stalled at the cross-link stage. Remarkably, the crystal structure shows the cleavage products of SAM--5'-deoxyadenosine and methionine--lingering in the active site, suggesting that they remain there until the methylated RNA is released.

One of the more surprising revelations from the crystal structures was the orientation of the tRNA. In isolation, tRNA forms a distinct compact three-dimensional structure. In the construct, it appears as though the enzyme has essentially pulled the tRNA apart. The enzyme interacts with the tRNA backbone and side chains at dozens of points along the nucleic acid's length, including the 3' end region, the D-stem region and especially the anticodon stem-loop region. The enzyme accesses the A37 site through an induced-fit strategy that

completely unfolds the stem-loop region. The researchers suspect that the enzyme's capacity to unwind the nucleic acid is critical for the recognition of both tRNA as well as its target rRNA.

RlmN is one of only two RNA modification enzymes with dual specificity. The other, RluA, also targets an rRNA and tRNA, but, as this study reveals, through an entirely distinct mechanism. While RluA recognition relies on sequence elements that are conserved between rRNA and tRNA, RlmN appears to be able to target two substrates with little sequence similarity based on similarities in their tertiary structures. The findings point to an intriguing evolutionary link between the core of the ribosome and tRNA, suggesting they may have originated from the same ancestral RNA.

— Erika Gebel Berg

**See:** Erica L. Schwalm, Tyler L. Grove, Squire J. Booker\*, and Amie K. Boal\*\*, “Crystallographic capture of a radical S-adenosylmethionine enzyme in the act of modifying tRNA,” *Science* **352**(6283), 309 (15 April 2016).

DOI: 10.1126/science.aad5367

**Author affiliation:** Pennsylvania State University

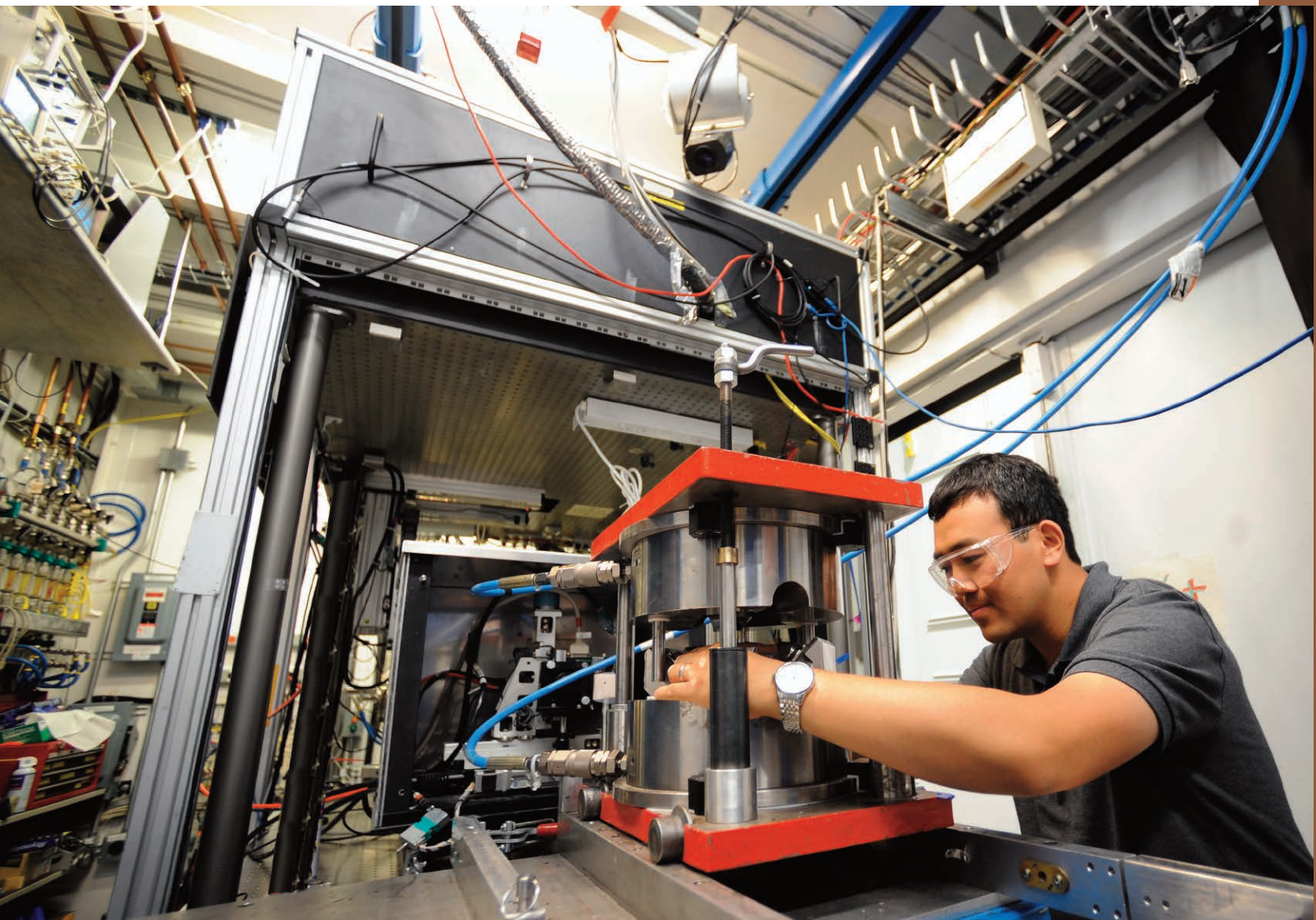
**Correspondence:** \* squire@psu.edu

\*\* akb20@psu.edu

This work has been supported by NIH grants GM100011 (A.K.B.) and GM101957 (S.J.B.), the Searle Scholars Program (A.K.B.), and Tobacco Settlement Funds (TSF13/14 SAP\_4100062216) to S.J.B. Use of the LS-CAT Sector 21 was supported by the Michigan Economic Development Corporation and the Michigan Technology Tri-Corridor (grant 085P1000817). GM/CA-XSD has been funded in whole or in part with federal funds from the National Cancer Institute (Y1-CO-1020) and the National Institute of General Medical Science (Y1-GM-1104). This research used resources of the Advanced Photon Source, a U.S. Department of Energy (DOE) Office of Science User Facility operated for the DOE Office of Science by Argonne National Laboratory under Contract No. DE-AC02-06CH11357.

23-ID-B • GM/CA-XSD • Life sciences • Macromolecular crystallography, microbeam, large unit cell crystallography, subatomic (<0.85 Å) resolution, multi-wavelength anomalous dispersion, single-wavelength anomalous dispersion • 3.5-20 keV • On-site, remote • Accepting general users •

# ENVIRONMENTAL, GEOLOGICAL & PLANETARY SCIENCE



Feng Shi, a postdoctoral researcher with GSECARS at Sector 13 of the APS, is setting up a sample for acoustic emission (AE) experiment in the deformation DIA (D-DIA) apparatus in the beamline 13-BM-D station. The combination of D-DIA, which allows controlled deformation under high pressure and temperature, and *in situ* AE monitoring allows users to conduct laboratory simulations on deep earthquakes to understand physical mechanisms of rock failures in the Earth's deep interior. GSECARS is the only synchrotron facility in the world with this unique combination of techniques.



# DISCOVERY OF A NEW MANTLE IRON OXIDE

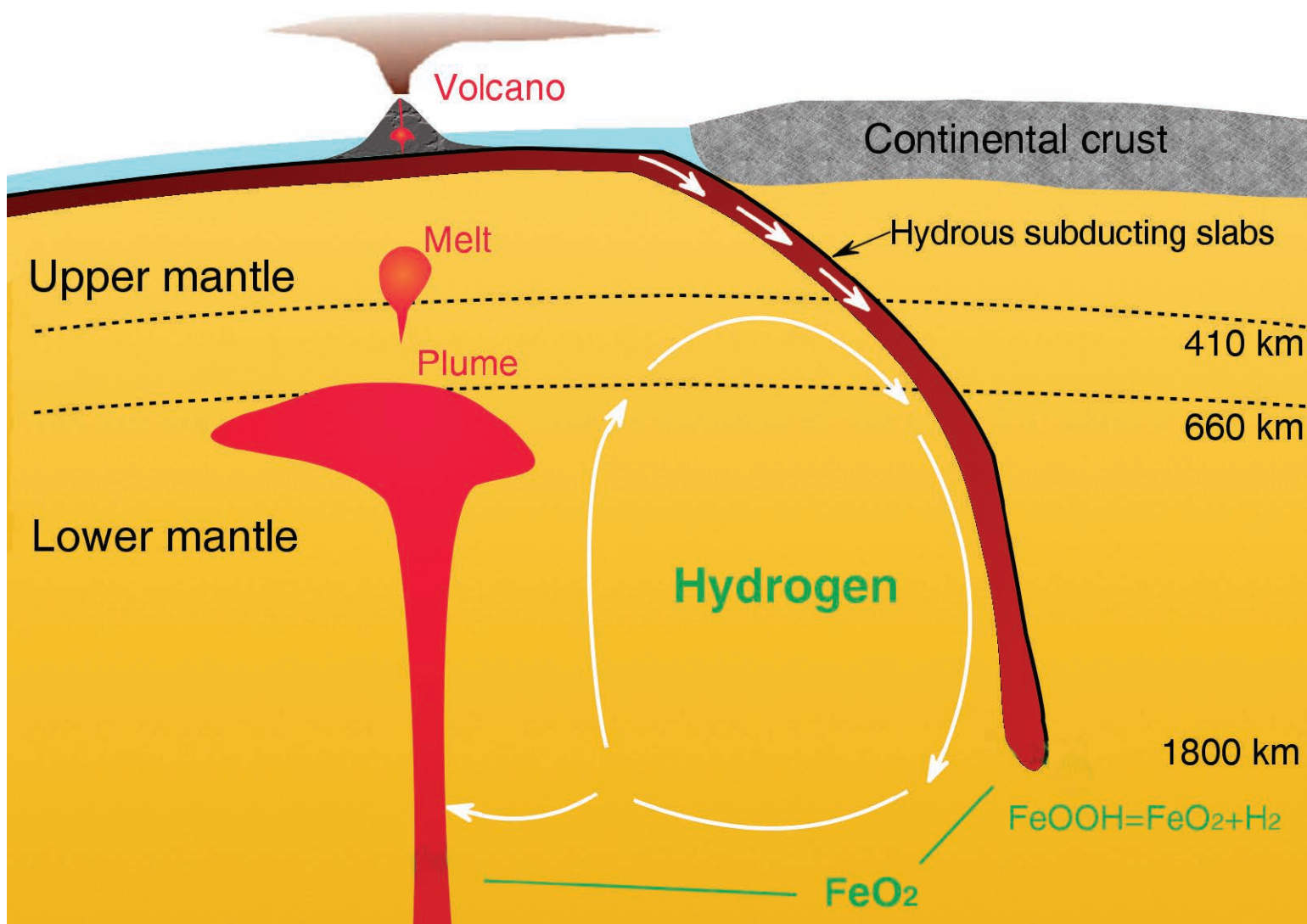


Fig. 1. A cross-section diagram of the Earth's interior depicting the process that generates  $\text{FeO}_2$ : the subduction of hydrous slabs containing rust ( $\text{FeOOH}$ ) which, on reaching 1800-km depth, undergo a change producing  $\text{FeO}_2$  and  $\text{H}_2$ . The  $\text{FeO}_2$  can be raised again toward the surface as part of a mantle plume.



The theory of plate tectonics relates the chemistry and physics of the human-accessible crust and upper oceans with that of Earth's mantle and core. Scientists must know the minerals involved in plate tectonic processes—especially those in the oxygen-iron system which are not present at the Earth's surface—in order to accurately interpret the available seismic, thermal, and geochemical data. Now, computational modeling and high-pressure synchrotron x-ray experiments at the APS have provided evidence for the existence of a new iron oxide—FeO<sub>2</sub>—whose presence and chemical interactions could give previously-unavailable insight into a number of seismic and geochemical anomalies in the deep mantle.

Plate tectonics processes such as mantle convection, crustal subduction, and sea-floor spreading are all affected by the compounds participating in them. Historical events, such as core-mantle separation and atmospheric evolution, were also affected by the composition and behavior of the minerals involved. So it's important for scientists to know and characterize deep Earth compounds to successfully interpret measurements of Earth's interior. New work by a team composed of researchers from the Center for High Pressure Science and Technology Advanced Research (China) and the Carnegie Institute for Science Geophysical Laboratory focused on this issue. They began with a computational analysis searching for possible iron-oxygen compounds at pressures from 100 to 300 GPa. Their models indicated that FeO<sub>2</sub> would be stable and was energetically favorable at all the pressures included in the models.

To physically create FeO<sub>2</sub>, the team put hematite powder (Fe<sub>2</sub>O<sub>3</sub>) loaded in cryogenically condensed liquid O<sub>2</sub> into a diamond anvil cell and raised the pressure to 78 GPa. They interrogated the sample by angular dispersive x-ray diffraction, only to find little change in the sample. However, when they heated the sample to 1800 K at a high pressure, the sample turned semi-transparent. X-ray diffraction results showed a set of peaks that did not correspond to Fe<sub>2</sub>O<sub>3</sub> or O<sub>2</sub> phases and are described by a simple cubic structure with space group  $P\bar{a}3_1$ . The team utilized x-ray diffraction at the HP-CAT 16-BM-B and 16-ID-B and GSECARS 13-BM-C x-ray beamlines at the APS and at the BL15U1 station at the Shanghai Synchrotron Radiation Facility to confirm the space group of

the iron oxide compound.

This new iron oxide, FeO<sub>2</sub>, is highly stable, with a structure similar to pyrite. The iron in FeO<sub>2</sub>, like pyrite, is considered ferrous (having a +2 oxidation state). Further exploration of the chemical bonds allowed the team to conclude that the way to understand FeO<sub>2</sub> is as wüstite (FeO) holding extra O<sub>2</sub>.

But what mechanism creates the new iron oxide? The team showed that subjecting FeOOH — more commonly known as rust — to the pressures and temperatures of the deep mantle causes FeO<sub>2</sub> to form. Figure 1 illustrates the mantle processes involving FeO<sub>2</sub>. The team postulates that the FeO<sub>2</sub> would accumulate in the deep lower mantle, and thus could be a source of the seismic anomalies there. Upwelling mantle plumes could raise the FeO<sub>2</sub> to the middle lower mantle where it would decompose to provide a source of O<sub>2</sub>, potentially changing the composition of nearby minerals. This implies that every slab of surface material sinking as part of plate tectonics has most likely contributed to the generation of FeO<sub>2</sub>, creating reservoirs of the extra O<sub>2</sub> in the mantle.

The team further hypothesizes that these processes could have provided a source of surface O<sub>2</sub> and thus played a part in the Great Oxidation Event (GOE), which occurred approximately 2 billion years ago. Current theories posit a primarily biological cause for the increase of O<sub>2</sub> in Earth's atmosphere during the GOE.

This new evidence for the existence of FeO<sub>2</sub> opens up possibilities for explaining many of the currently unanswered questions about the deep mantle. But this is only the beginning of this effort, as each of those answers begins

with a more comprehensive understanding of FeO<sub>2</sub> and its behavior.

— Mary Alexandra Agner

**See:** Qingyang Hu<sup>1,2</sup>, Duck Young Kim<sup>1,2</sup>, Wenge Yang<sup>1,2</sup>, Liuxiang Yang<sup>1,2</sup>, Yue Meng<sup>2</sup>, Li Zhang<sup>1,2</sup>, and Ho-Kwang Mao<sup>1,2\*</sup>, "FeO<sub>2</sub> and FeOOH under deep lower-mantle conditions and Earth's oxygen-hydrogen cycles," *Nature* **534**, 241 (2016).

DOI: 10.1038/nature18018

**Author affiliations:** <sup>1</sup>Center for High Pressure Science and Technology Advanced Research, <sup>2</sup>Carnegie Institution for Science

**Correspondence:** \* hmao@gl.ciw.edu

Q.H. and H.-K.M. were supported by National Science Foundation (NSF) grants EAR-1345112 and EAR-1447438. L.Z. was supported by the Foundation of President of China Academy of Engineering Physics (grant no. 201402032) and the National Natural Science Foundation of China (grant no. 41574080). This work was also supported in part by the National Natural Science Foundation of China (grant number U1530402). High Pressure Collaborative Access Team operations are supported by the U.S. Department of Energy (DOE)-National Nuclear Security Administration under award number DE-NA0001974 and by the DOE-Office of Science-Basic Energy Sciences under award number DE-FG02-99ER45775, with partial instrumentation funding by the NSF. 13-BM-C operation is supported by COM-PRES through the Partnership for Extreme Crystallography (PX2) project, under NSF Cooperative Agreement EAR 11-57758. GeoSoilEnviroCARS is supported by the NSF-Earth Sciences (EAR-1128799) and U.S. DOE-GeoSciences (DE-FG02-94ER14466). This research used resources of the Advanced Photon Source, a U.S. DOE Office of Science User Facility operated for the DOE Office of Science by Argonne National Laboratory under Contract No. DE-AC02-06CH11357.

# REDUCING THE UNDERGROUND MIGRATION OF URANIUM

Although uranium (U) has been widely used for over 70 years in a variety of military and commercial roles, the safe disposal and remediation of this toxic, radioactive element remains a challenge. Waste uranium comes from multiple sources, including tailings from mining operations, the spent fuel rods of fission power plants, and decommissioned nuclear weapons. Regardless of the source, waste uranium often ends up below ground where it can contaminate groundwater, so scientists continue to search for strategies to slow the underground migration of this toxic, radioactive hazard. One strategy involves introducing substances below ground that retard the formation of highly-soluble uranium compounds. In this study, scientists exposed uranium oxides to calcium and phosphate as a means of keeping the uranium in a low-solubility mineral form. The researchers tracked the chemical changes associated with this process using several techniques, including x-ray spectral measurements performed at the APS). Their observations confirmed that calcium and phosphate slow the transition from less-soluble uranium compounds to more-soluble ones. While the protective effects of the chemical treatment eventually faded under real-world oxidizing conditions, the processes employed and the data gathered will substantially contribute toward the goal of reducing subsurface uranium hazards.

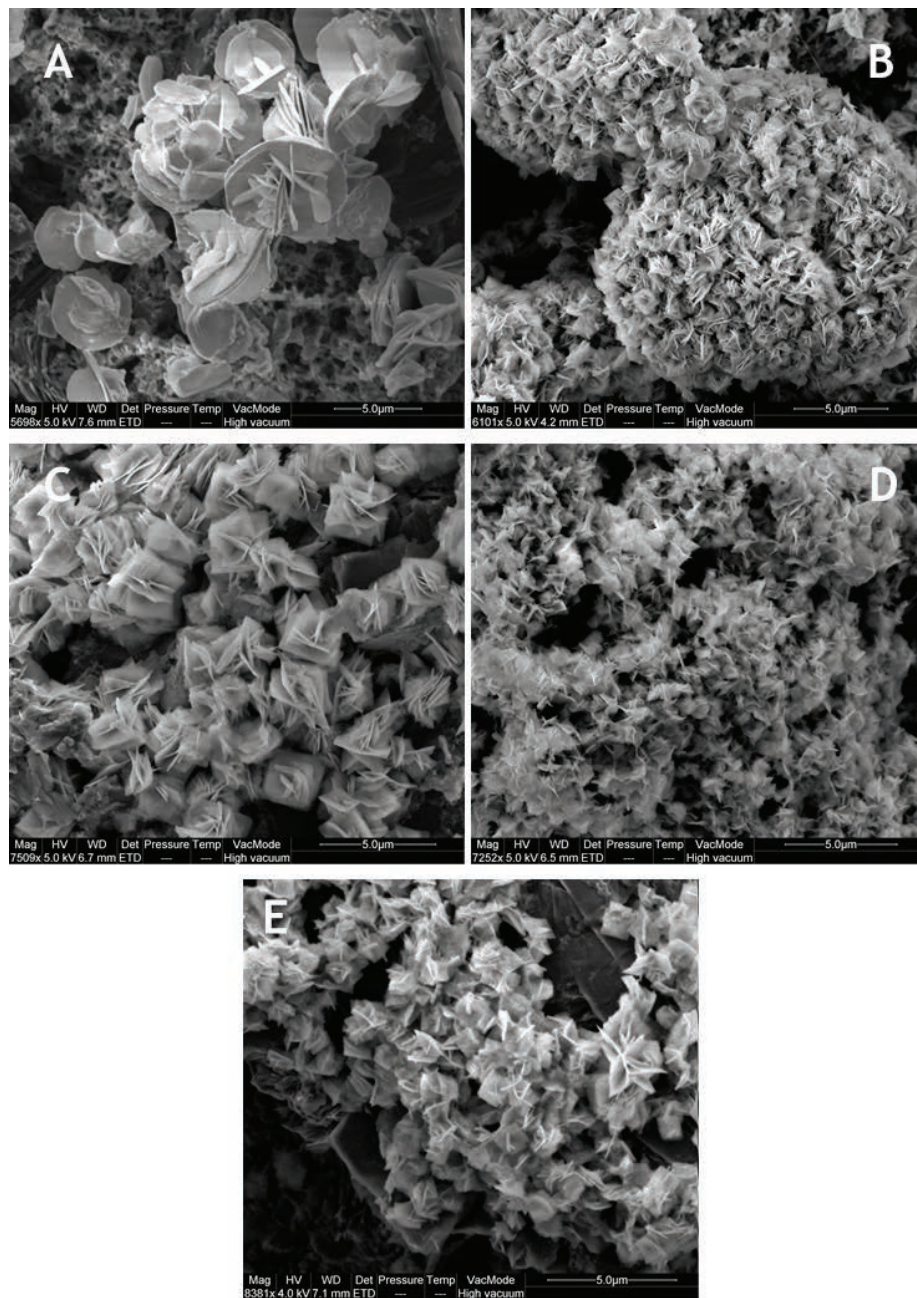


Fig. 1. Micrographs obtained with a scanning electron microscope (SEM). The images show the results of  $U^{IV}$  solids oxidized over three days (72 hours). The top two panels compare oxidized  $UO_2$  with (a) no added Ca or  $PO_4$ , to (b) 400 micromoles/L (400  $\mu M$ ) of added Ca and  $PO_4$ . The middle and bottom panels compare oxidized  $U^{IV}-PO_4$  that had (c) no added Ca or  $PO_4$ , to (d) 100  $\mu M$  of added Ca and  $PO_4$ , and (e) 400  $\mu M$  of added Ca and  $PO_4$ . (5- $\mu m$  scale bars are located at bottom right of each micrograph; other data at bottom of each picture displays SEM magnification, etc.)



Uranium is naturally present at low concentrations in soil and rocks, where its inherent radioactivity contributes to normal background radiation levels. However, ground contaminated with higher-than-normal concentrations can pose serious environmental and health-safety risks. When removal of subsurface uranium is impractical, scientists attempt to restrict its underground movement. The chief culprit in uranium migration is groundwater: this heavy metal readily forms compounds that can dissolve in water. By inducing uranium to form compounds with low solubility, its migration can be considerably reduced.

The researchers in this study, from Argonne, the Illinois Institute of Technology, and the Bulgarian Academy of Sciences, tracked the chemical evolution of two important uranium compounds. The first was uranium dioxide,  $\text{UO}_2$ , a major constituent of uranium ore. The second was a more complex uranium/phosphate compound produced naturally by subsurface bacteria, denoted  $\text{U-PO}_4$ . (In both cases, the oxidation state of the uranium was +4, so that these compounds are more precisely labeled as  $\text{U}^{\text{IV}}\text{O}_2$  and  $\text{U}^{\text{IV}}\text{-PO}_4$ .) The  $\text{U}^{\text{IV}}\text{O}_2$  formed nanoparticles, while the  $\text{U}^{\text{IV}}\text{-PO}_4$  exhibited an amorphous (non-crystalline) structure. In soil, both compounds will combine with subsurface oxygen to form new compounds. These chemical reactions can change the original oxidation state of the uranium, from +4 to +6 (denoted  $\text{U}^{\text{VI}}$  and  $\text{U}^{\text{VI}}$ , respectively). This change in oxidation number is important since compounds containing  $\text{U}^{\text{IV}}$  are generally less water soluble than  $\text{U}^{\text{VI}}$  compounds.

Initially,  $\text{U}^{\text{IV}}\text{-PO}_4$  and nanoparticulate  $\text{U}^{\text{IV}}\text{O}_2$  were placed in neutral water solutions (pH 7.0) containing dissolved oxygen and carbon dioxide. Experiments were performed with and without the addition of calcium (Ca) and phosphate ( $\text{PO}_4$ ) to the solutions. Adding calcium and phosphate significantly altered the ensuing chemical reactions. This difference can be seen in the micrographs of Fig. 1, which compare the uranium compounds after three days in their oxygenated solutions, both with and without exposure to  $\text{Ca/PO}_4$ . The morphological differences between the oxidized uranium solids are dramatic.

The chemical species present in the solutions (some with  $\text{Ca/PO}_4$ , others without) were tracked with several distinct measurement techniques, including x-ray absorption near-edge spectroscopy (XANES), performed at the MR-CAT 10-BM-A,B x-ray beamline at the APS. XANES was used to observe the oxidation states of the uranium compounds present in each of the solutions.

Figure 2 is a plot based on the XANES data showing that the addition of calcium and phosphate reduced the oxidation rates of the  $\text{U}^{\text{IV}}\text{O}_2$  and  $\text{U}^{\text{IV}}\text{-PO}_4$  compounds, thereby slowing the conversion from the less-soluble  $\text{U}^{\text{IV}}$  state to the more-soluble  $\text{U}^{\text{VI}}$  state. While the addition of calcium and phosphate lowered the oxidation rate 10-fold, the two compounds eventually oxidized completely. Nevertheless, this finding indicates that subsurface uranium exposed to sufficient calcium/phosphate levels, whether naturally from the surrounding environment or artificially by injection into the waste site, is one possible strategy for slowing uranium migration.

Another important observation was an observed build-up of a  $\text{Ca-U}^{\text{VI}}\text{-PO}_4$  coating on the  $\text{U}^{\text{IV}}\text{O}_2$  nanoparticle surfaces, which served to limit further oxidation. Additionally, the researchers expect that the chemical reaction rates determined from these experiments will be used to improve the numerical modeling of actual subsurface uranium migration. — Philip Koth

See: Drew E. Latta<sup>1\*</sup>, Kenneth M. Kemner<sup>1</sup>, Bhoopesh Mishra<sup>1,2</sup>, and Maxim I. Boyanov<sup>1,3</sup>, "Effects of calcium and phosphate on uranium(IV) oxidation: Comparison between nanoparticulate uraninite and amorphous  $\text{U}^{\text{IV}}\text{-phosphate}$ ," *Geochim. Cosmochim. Acta* **174**, 122 (2016).

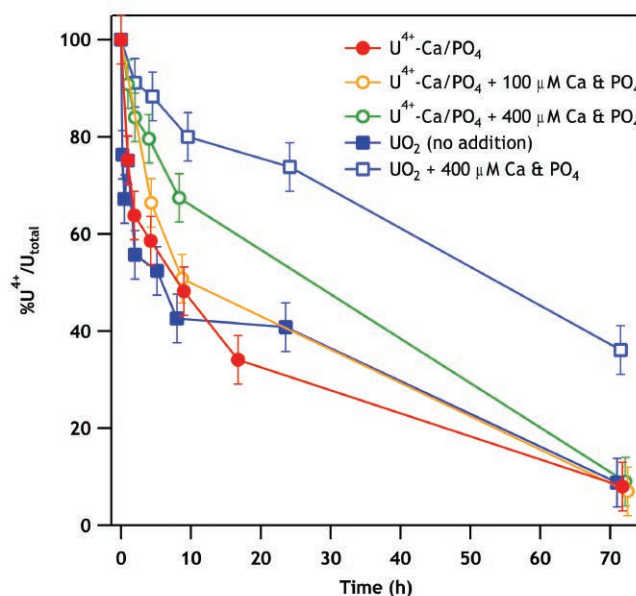


Fig. 2. Plot of oxidation rates of uranium compounds  $\text{U}^{\text{IV}}\text{-phosphate}$  and uranium dioxide,  $\text{UO}_2$ . Data derived from XANES x-ray spectroscopy. Squares represent oxidation data for  $\text{UO}_2$ , while circles are oxidation data for  $\text{U}^{\text{IV}}\text{-phosphate}$ . Legend at top-right indicates whether or not calcium/phosphate was added to solution. Note how adding 400 micromoles ( $\mu\text{M}$ ) of calcium and phosphate significantly slows oxidation of both  $\text{UO}_2$  and  $\text{U}^{\text{IV}}\text{-phosphate}$ . (" $\text{U}^{4+}$ " and " $\text{U}^{\text{IV}}$ " both indicate uranium possessing an oxidation state of +4.)

DOI: 10.1016/j.gca.2015.11.010

Author affiliations: <sup>1</sup>Argonne National Laboratory, <sup>2</sup>Illinois Institute of Technology, <sup>3</sup>Bulgarian Academy of Sciences  
Correspondence:

\* drew-latta@uiowa.edu

This research is part of the Subsurface Science Scientific Focus Area at Argonne National Laboratory, which is supported by the U.S. Department of Energy (DOE) Subsurface Biogeochemical Research Program, Office of Biological and Environmental Research, Office of Science. Use of the Electron Microscopy Center at Argonne and the Advanced Photon Source was supported by the U.S. DOE Office of Science-Basic Energy Sciences. Materials Research Collaborative Access Team operations are supported by the DOE and the Materials Research Collaborative Access Team member institutions. All work at Argonne was carried out under Contract No. DE-AC02-06CH11357.

10-BM-A,B • MR-CAT • Materials science, chemistry, environmental science, physics • X-ray absorption fine structure, x-ray lithography, tomography • 3-200 keV, 4-32 keV • On-site • Accepting general users •



# ENHANCING OUR UNDERSTANDING OF MANTLE MELT FRACTION

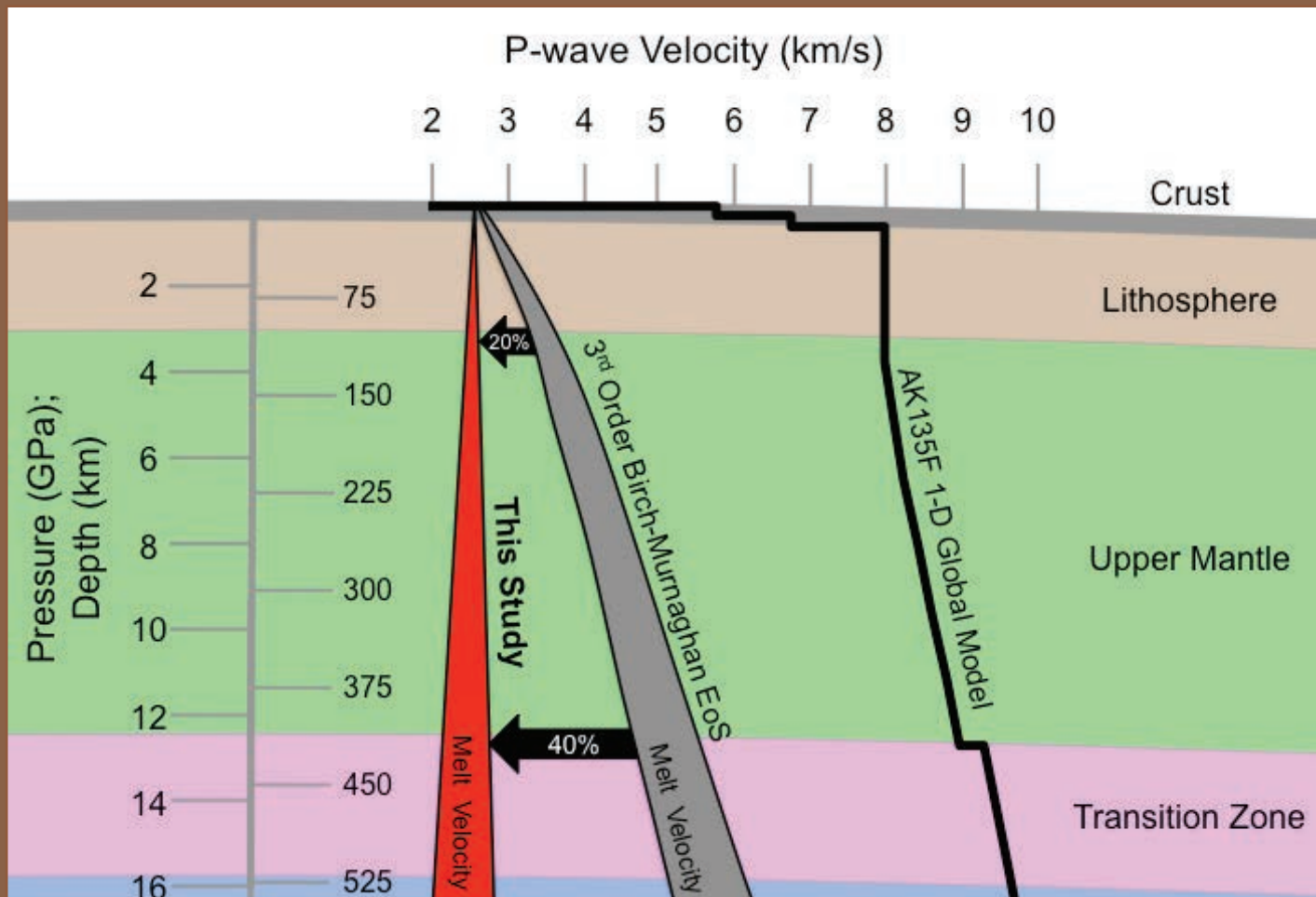


Fig. 1. *P* wave velocity as a function of depth for this new data, compared with two preexisting velocity-pressure relationships: a global Earth computational model and the extrapolation of Birch's Law (labeled 3rd Order Birch-Murnaghan Equations of State). The new results give considerably lower velocities than the other models due to the amorphous structure of glass.

Scientists study how seismic waves change while traveling through rocks in order to determine the composition and physical state of the materials that comprise Earth's interior. The current theory relating seismic wave velocities and the materials in the mantle relies on results from challenging-to-conduct laboratory experiments manipulating crystalline solids; consequently, most scientists utilize extrapolations of these existing measurements for other physical states such as glasses and melts. In research APS, an international team discovered that melts do not exhibit the behavior predicted by these extrapolations. They further found that existing extrapolative relationships might overestimate the amount of melt in the Earth's upper mantle. This overestimation impacts our current understanding of key concepts in plate tectonics, such as the amount of coupling between the plates and the mantle.

In this new work, a team of researchers from the University of California, Davis, Aarhus University (Denmark), Northwestern University, and The University of Chicago found that melts do not follow the relationship prescribed by Birch's Law: that the velocity of pressure waves, also called *P* waves, increases in denser rocks. Instead, melts slow down the seismic waves at depths corresponding to the Earth's crust and upper mantle. To reach this conclusion, the team combined ultrasonic and tomographic data from basalt glass to determine the relationship between the elasticity and density of the glass.

The team used United States Geological Survey standard basalt glass from the Columbia River flood basalt province as their experimental sample. They began by taking volumetric measurements of the basalt glass using high-pressure x-ray microtomography (HPXMT) at the GSECARS beamline 13-BM-D at the APS. From this, they determined the density of the glass as a function of pressure.

Next, they measured acoustic wave travel times using gigahertz-ultrasonic interferometry at Northwestern University. By combining the tomographic and ultrasonic results, the team determined how *P* wave velocity, adiabatic bulk modulus, and shear modulus vary as a function of pressure.

The values determined for these pressure-dependent characteristics were unexpected. Unlike a highly structured silicate network in a mineral, which repeats periodically over a mineral's volume, a glass has a more flexible structure because it consists of disordered regions: differently sized rings

and randomly oriented chains of silica polyhedra. The team concluded that the amorphous structure of the silicate rings and chains in the basalt glass were what produced the unexpected values for these characteristics: the rings and chains bend, twist, and buckle when compressed, unlike the shortening of interatomic bonds, which occurs during compression of highly ordered silicate minerals.

Another of the team's conclusions was that seismic waves move more slowly through melts than previously thought; seismic wave velocities decrease in basalt glass even in increasing pressure. Figure 1 shows *P* wave velocity as a function of depth for three sets of data, allowing for a visual comparison of how this new data yields much lower velocities than those calculated by previous studies.

The implications of this conclusion are that most models overestimate the amount of melt associated with the low seismic velocity zone near the boundary between the plastically deforming portion of the mantle and the rigid shell above it, which is comprised of both crust and mantle. This overestimate impacts many existing theories, including plate tectonics, which assumes a high volume of silicate melts that allow the rigid plates to slide without friction over the malleable mantle, with little coupling. A smaller amount of melt would require the theory to include friction between the plates and the mantle. This requirement would increase the complexity of the theory, but also empower it to better account for plate subduction since friction between the plates would induce coupling and help explain the downward forces acting on the plates.

Seismic wave velocities and plate coupling are only two examples of large-scale events affected by the small-scale amorphous structure of basalt glasses. These new results show that the behavior of basalt glass under pressure offers an updated picture of Earth's interior and ongoing geophysical processes.

— Mary Alexandra Agner

**See:** Alisha N. Clark<sup>1\*†</sup>, Charles E. Leshner<sup>1,2</sup>, Steven D. Jacobsen<sup>3</sup>, and Yanbin Wang<sup>4</sup>, "Anomalous density and elastic properties of basalt at high pressure: Reevaluating of the effect of melt fraction on seismic velocity in the Earth's crust and upper mantle," *J. Geophys. Res. Solid Earth* **121**, 4232 (2016). DOI: 10.1002/2016JB012973.

**Author affiliations:** <sup>1</sup>University of California, Davis, <sup>2</sup>Aarhus University, <sup>3</sup>Northwestern University, <sup>4</sup>The University of Chicago <sup>†</sup>Present address: Université Pierre-et-Marie-Curie

**Correspondence:**

\* [anclark@ucdavis.edu](mailto:anclark@ucdavis.edu)

\* [alisha.clark@impmc.upmc.fr](mailto:alisha.clark@impmc.upmc.fr)

This research was supported in part by U.S. National Science Foundation (NSF) grants EAR-1215714 to C.E.L. EAR-1452344 to S.D.J., and EAR-1214376 to Y.W.; and a grant from the UC Lab Fees Research Program (12-LR-237546) to C.E.L. C.E.L. also acknowledges support from the Danish National Research Foundation for the Niels Bohr Professorship at Aarhus University, and S.D.J. acknowledges support from the Carnegie/Department of Energy (DOE) Alliance Center, the David and Lucile Packard Foundation, and the Alexander von Humboldt Foundation. GSECARS is supported by the NSF-Earth Sciences (EAR-1128799) and U.S. DOE-GeoSciences (DE-FG02-94ER14466). This research used resources of the Advanced Photon Source, a U.S. DOE Office of Science User Facility operated for the DOE Office of Science by Argonne National Laboratory under Contract No. DE-AC02-06CH11357.

13-BM-D • GSECARS • Geoscience, environmental science • Tomography, high-pressure diamond anvil cell, high-pressure multi-anvil press, x-ray absorption fine structure • 4.5-80 keV • On-site • Accepting general users •



# ICE WITH HYDROGEN STUFFING

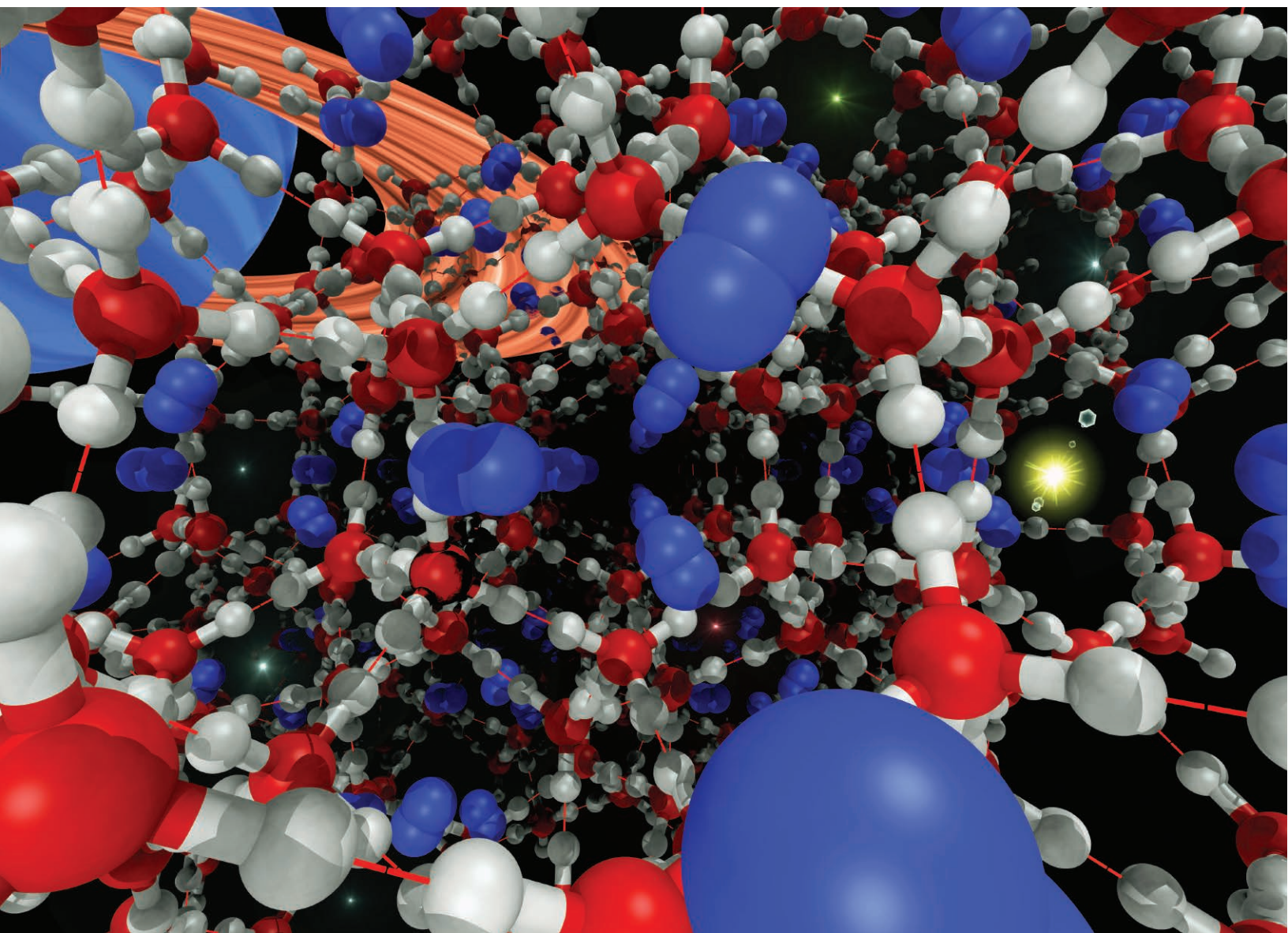


Fig. 1. This artist's illustration depicts the crystal structure of a form of hydrogen-filled ice called  $C_0$ . As determined from x-ray diffraction data collected at APS, hydrogen molecules (shown in blue) are held within spiral-shaped channels of water molecules (shown in red and gray). This phase of ice may be an important constituent on icy worlds in the outer solar system.

16-ID-B • HP-CAT • Materials science, geoscience, chemistry, physics • Microdiffraction, single-crystal diffraction, high-pressure diamond anvil cell • 18-60 keV • On-site • Accepting general users •



Normal ice, as found in a freezer, has a crystal structure with water molecules arranged in a hexagonal pattern. However, that's just one of the many forms of ice. If one lowered the freezer temperature below  $-100^{\circ}\text{C}$  or increased the pressure by a factor of a 1000, it would make ice in an entirely different arrangement. Likewise, introducing hydrogen gas would result in other crystal structures with hydrogen molecules filling in spaces between water molecules. A recently discovered hydrogen-stuffed ice, called  $\text{C}_0$ , has now been characterized for the first time. Researchers performed x-ray diffraction at the APS on single crystals of  $\text{C}_0$  and found that its structure is similar to that of the mineral quartz. Due to its stability at low temperature and high pressure, this quartz-like ice might potentially be a major "mineral" in the crust of ice-covered planetary bodies in the outer solar system.

Pure ice comes in (at least) 17 different crystalline structures. In addition, there are currently four known hydrogen-stuffed ices, but researchers have just started to explore this class of materials. Up until now, only three of the four  $\text{H}_2+\text{H}_2\text{O}$  systems have been fully characterized. The first, referred to as structure two (sII), was found to have polyhedral water cages that trap  $\text{H}_2$  molecules. The second and third, called clathrate one ( $\text{C}_1$ ) and clathrate two ( $\text{C}_2$ ), have structures that resemble known forms of ice, but with hydrogen gas slipping into gaps between water molecules. The fourth member—and most recent addition—to this class is  $\text{C}_0$ . It was given this name because it forms at lower pressure than  $\text{C}_1$  and  $\text{C}_2$ , but higher pressure than sII. Early evidence for the existence of  $\text{C}_0$  appeared in 2011, but preliminary experiments on powder samples were not able to definitely identify the structure because the crystal grains were too small.

Growing large single crystals of  $\text{C}_0$  is tricky. This phase of ice only forms at pressures of around 4000 ATM (400 MPa) and temperatures below  $7^{\circ}\text{C}$  (280 K). Using a diamond anvil cell and a cryostat, researchers from the Carnegie Institution of Washington, the University of Hawaii, George Washington University, and Lawrence Livermore National Laboratory managed to keep a mixture of  $\text{H}_2$  and  $\text{H}_2\text{O}$  stabilized at the  $\text{C}_0$  freezing point. Under these conditions, the team grew single crystals of  $\text{C}_0$  that were hundreds of microns across.

The researchers analyzed their crystal samples with two complemen-

tary measurement techniques—Raman spectroscopy and x-ray diffraction (XRD). The Raman spectroscopy, in which laser radiation probes molecular rotations and vibrations, provided information on the hydrogen atoms. The spectra showed a large range of rotational excitations, indicating that the  $\text{H}_2$  molecules are free to rotate inside  $\text{C}_0$ . To determine the positions of the water molecules in the crystal, the team performed single-crystal XRD measurements at the HP-CAT 16-ID-B beamline, which is well-equipped to handle highly-pressurized samples. In the experiments, incoming x-rays with wavelength of  $0.37\text{ \AA}$  scattered primarily off of oxygen atoms, producing a diffraction pattern consistent with a hexagonal structure.

By incorporating the XRD and Raman information together, the team was able to build a three-dimensional model of the  $\text{C}_0$  structure. They found that the hydrogen-bonded water molecules form a network of spiral-shaped channels, and the  $\text{H}_2$  molecules reside inside these channels. The fact that hydrogen gas makes up 5.3% of the weight of this ice structure could prove useful for renewable energy applications. Although many engineering hurdles stand in the way, one can imagine storing hydrogen with a  $\text{C}_0$ -based tank for use in a non-polluting hydrogen car.

The spiral structure of water molecules in  $\text{C}_0$  bears a resemblance to the atomic arrangement in quartz, which is one form of silicate ( $\text{SiO}_2$ ). This analogy is interesting as scientists have often looked for parallels between  $\text{SiO}_2$  and  $\text{H}_2\text{O}$ , since they both form tetrahedral configurations between their atoms.

And just as quartz is commonly found on Earth,  $\text{C}_0$  ice might be fairly abundant in the outer solar system. The presence of  $\text{C}_0$  in the icy crust of a frozen world, such as Saturn's moon Enceladus, could affect the temperature of the interior, as hydrogen-stuffed ice is a poorer conductor of heat than pure ice. — *Michael Schirber*

**See:** Timothy A. Strobel<sup>1</sup>, Maddury Somayazulu<sup>1</sup>, Stanislav V. Sinogeikin<sup>1</sup>, Przemyslaw Dera<sup>2</sup>, and Russell J. Hemley<sup>3,4</sup>, "Hydrogen-Stuffed, Quartz-like Water Ice," *J. Am. Chem. Soc.* **138**, 13786 (2016).

DOI: 10.1021/jacs.6b06986

**Author affiliations:** <sup>1</sup>Carnegie Institution of Washington, <sup>2</sup>University of Hawaii at Manoa, <sup>3</sup>George Washington University, <sup>4</sup>Lawrence Livermore National Laboratory

**Correspondence:** \* tstrobel@ciw.edu

This work was supported by EFree, an Energy Frontier Research Center funded by the U.S. Department of Energy (DOE) Office of Science-Basic Energy Sciences (BES), under grant no. DE-SC0001057. HP-CAT operations are supported by DOE-National Nuclear Security Administration under award no. DENA0001974 and DOE-BES under award no. DE-FG02-99ER45775, with partial instrumentation funding by the National Science Foundation. Work at Lawrence Livermore National Laboratory was performed under the auspices of the U.S. DOE under contract no. DE-AC52-07NA27344. This research used resources of the Advanced Photon Source, a U.S. DOE Office of Science User Facility operated for the DOE Office of Science by Argonne National Laboratory under Contract No. DE-AC02-06CH11357.

# OXYGEN FUGACITY IN CHROMITE: UNDERSTANDING THE SOLAR SYSTEM



Fig. 1. The black grains in this Martian meteorite — ALH 84001 — are chromite crystals, which were utilized to determine the oxygen fugacity of the sample.

Oxygen fugacity (an equivalent of the partial pressure of oxygen in a particular environment, e.g., atmosphere, rocks, etc., corrected for the nonideal character of the gas) affects all of Earth's environments, from the deepest core to the atmosphere, and even to life itself. Meteorites are gifts from beyond Earth that offer scientists the chance to understand the makeup of extraterrestrial bodies, how the early solar system formed, and the processes that created the nearby planets and our Moon. Researchers at the APS employed a new analytical technique for measuring oxygen fugacity on samples that previously could not be measured, expanding our knowledge of our solar system.

The effects of oxygen fugacity ( $fO_2$ ) in different Earth environments vary widely. In the Earth's core, silicon is present as an alloyed element in low  $fO_2$ , while higher  $fO_2$  favors oxygen (O) or sulphur (S). In the Earth's interior (core and mantle),  $fO_2$  determines the composition of the metal phase and whether the silicate minerals are more magnesium- or iron-rich. The abundance of oxygen and water drives igneous processes, like magma generation, fractionation, and low-pressure differentiation and the secondary processes of thermal metamorphism and aqueous alteration. In crustal rocks,  $fO_2$  determines oxidation state—for example, whether iron is present as native iron, ferrous iron ( $Fe^{2+}$ ), or ferric iron ( $Fe^{3+}$ ). High  $fO_2$  in Earth's atmosphere creates a pleasant mix of carbon dioxide and water, but low  $fO_2$  leads to a deadly concoction of methane and carbon monoxide. Since complex molecules are sensitive to oxidation state, life as we know it could only begin in the right  $fO_2$  environment.

Earth exhibits a higher range of oxidation values than other planets and astromaterials due to the presence of an O-rich atmosphere, liquid water, and hydrated interior from the long-term recycling provided by plate tectonics. Using Earth samples as their models, scientists measure the  $fO_2$  of extraterrestrial materials to understand their sources; e.g., whether a meteorite came from a nearby planet or from an asteroid. Chondritic and achondritic meteorites, solar gas, Ca-Al-rich inclusions, zoned metal grains, cometary grains, and cosmic dust and asteroid particles all record effects of variable  $fO_2$ , and thus reveal a great deal about the formation of the early solar system. On the other hand, the  $fO_2$  of meteorites plucked from the surface of larger bodies with high-pressure interiors such

as Mars and Earth's Moon show a history of degassing, volatile solubility, fractionation, assimilation, and ascent across a wide range of pressures.

Many igneous and metamorphic rocks contain oxybarometers, mineral assemblages that allow researchers to measure or at least constrain  $fO_2$ , but some do not. In this research, a team from NASA-JSC, The University of Chicago, and Jacobs Engineering describe a new technique for analyzing  $fO_2$  in samples that do not contain traditional multi-phase oxybarometers, but do contain large and accessible spinel-structured chromite. Vanadium (V) pre-edge peak intensity and energy in chromite varies with  $fO_2$ , so the researchers measured the valence of vanadium in near-edge structures in chromite. These measurements were made using synchrotron micro-x-ray absorption near-edge structure (XANES) spectroscopy (SmX) at the GSECARS 13-ID-E x-ray beamline at the APS. Oxidation state and coordination affect the fluorescent x-ray intensity and energy features in the XANES spectrum. The XANES derived  $fO_2$  was determined from measurements of experimentally produced spinels of known  $fO_2$ .

The researchers measured V  $fO_2$  in samples from achondritic meteorites, oxidized chondritic meteorites, and terrestrial basalts from the Mexican Volcanic Belt. They reviewed known  $fO_2$  values for primitive materials such as achondrites and chondrites for comparison. Chondritic meteorite samples with aqueous alteration had slightly higher  $fO_2$  values. The numbers were also high in regions where fluids move through rock, such as the mantle wedge between the surface lithosphere and the subducting lithospheric slab in a subduction zone, or in the crust. These examples again suggest an important link between water and oxidation. Earth

and Mars samples have higher values of  $fO_2$  due to the role of pressure in dissolving volatiles into magmas. Researchers have lots of information on  $fO_2$  in Earth's upper mantle, but not from other planets since we do not have mantle samples from elsewhere.

By using this new analytical technique, known as "V XANES," scientists will better be able to understand the oxygen fugacity variation of the inner solar system. The technique can be applied to a wider range of samples than previously possible, leading to a better-constrained history for the origin and evolution of our solar system.

— Dana Desonie

**See:** Kevin Righter<sup>1\*</sup>, Steve R. Sutton<sup>2</sup>, Lisa Danielson<sup>3</sup>, Kellye Pando<sup>3</sup>, and Matt Newville<sup>2</sup>, "Redox variations in the inner solar system with new constraints from vanadium XANES in spinels," *Am. Mineral.* **101**, 1928 (2016).

DOI: 10.2138/am-2016-5638

**Author affiliations:** <sup>1</sup>NASA-JSC, <sup>2</sup>The University of Chicago, <sup>3</sup>Jacobs Engineering

**Correspondence:**

\* kevin.righter-1@nasa.gov

This work was supported by an RTOP from the NASA Cosmochemistry/Emerging Worlds programs. Geo-SoilEnviroCARS is supported by the National Science Foundation, Earth Sciences (EAR-1128799) and the U.S. Department of Energy (DOE)-Geo-Sciences (DE-FG02-94ER14466). This research used resources of the Advanced Photon Source, a U.S. DOE Office of Science User Facility operated for the DOE Office of Science by Argonne National Laboratory under Contract No. DE-AC02-06CH11357.

**GSECARS • 13-ID-E • Geoscience, environmental science • Microfluorescence (hard x-ray), micro x-ray absorption fine structure, microdiffraction, fluorescence spectroscopy • 2.4-28 keV, 5.4-28 keV • On-site • Accepting general users •**



# THE RELATIONSHIP OF METAL IONS TO MANGANESE DEPOSITS IN WATER PIPES

**M**anganese (Mn) is found in surface and ground waters utilized as sources for drinking water, typically at low concentrations. Human actions, such as fertilizer use, soil disturbances, and mining, increase Mn in the environment. Protecting the public water supply requires understanding the physicochemical characteristics of Mn deposits in different types of water distribution pipes. To provide drinking water, public utilities transport water in metal pipes and treat it chemically with disinfectants such as free chlorine or chloramine. Chloramine is less reactive than chlorine so it is not as effective as a disinfectant, but it lasts longer in water and so has longer exposure to the pipes. In this study, researchers analyzed Mn deposits in lead and brass pipes from two different utilities, one that disinfects with chlorine and the other with chloramine. They mapped the distribution of a wide range of metal ions in the Mn deposits utilizing high-brightness x-rays from the APS. The same metal ions were present in all Mn deposits independent of pipe composition. This study shows that the alloying elements in the pipes and the disinfectants did not influence the mineralogy of Mn deposits, and that toxic metal ions may be more likely to end up in consumer taps as Mn deposits are destabilized.

relative concentrations of Cr, Cu, Fe, Mn, Pb, and Sr were recorded. Their results show that lead pipes contained roughly an order of magnitude more Mn, but similar metal ion concentrations. Mn deposits in the brass pipes had greater variability in metal ion concentrations, even within the same utility. The differences in metal ion concentrations may result from the differing ratios of birnessite, hollandite and braunite and how well each adsorbed or incorporated metal ions, although this cannot account for the trace metal concentration differences in the two pipe types.

The EPA regulates Mn in water for esthetic as well as for health effects. Drinking water with Mn concentrations of greater than 0.05 mg/L is referred to as “black water” for its unpleasant color, odor and taste. Negative health effects are not a concern until concentrations are an order of magnitude higher. These values are consistent with the World Health Organization guide for Mn in drinking water.

The researchers note that this study demonstrates the need for access to facilities like APS, in particular Sector 20 and their staff, to collect the type of data required to more comprehensively understand mineral and metal ion distribution in deposits associated with drinking water pipes.

— Dana Desonie

**See:** Tammie L. Gerke<sup>1\*</sup>, Brenda J. Little<sup>2</sup>, J. Barry Maynard<sup>2</sup>, “Manganese deposition in drinking water distribution systems,” *Sci. Total Environ.* **541**, 184 (2016).

**Author affiliations:** <sup>1</sup>University of Cincinnati, <sup>2</sup>Naval Research Laboratory

**Correspondence:**

\* gerketl@miamioh.edu

This research used resources of the Advanced Photon Source, an Office of Science User Facility operated for the U.S. Department of Energy (DOE) Office of Science by Argonne National Laboratory, and was supported by the U.S. DOE under Contract No. DE-AC02-06CH11357, and the Canadian Light Source and its funding partners.

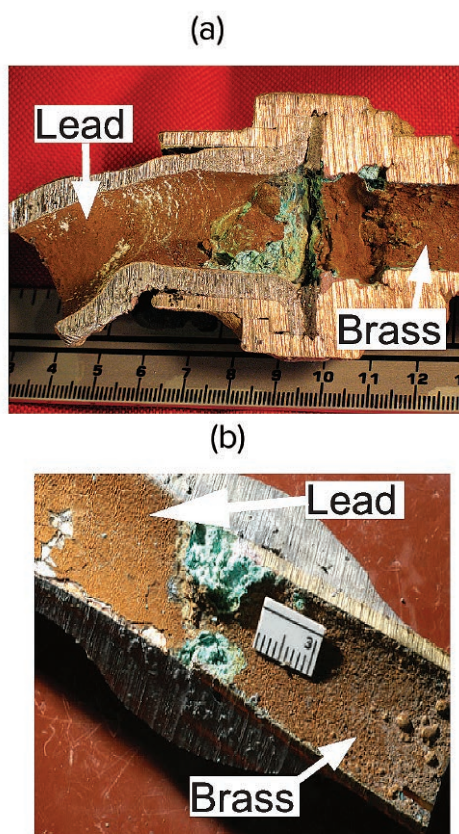
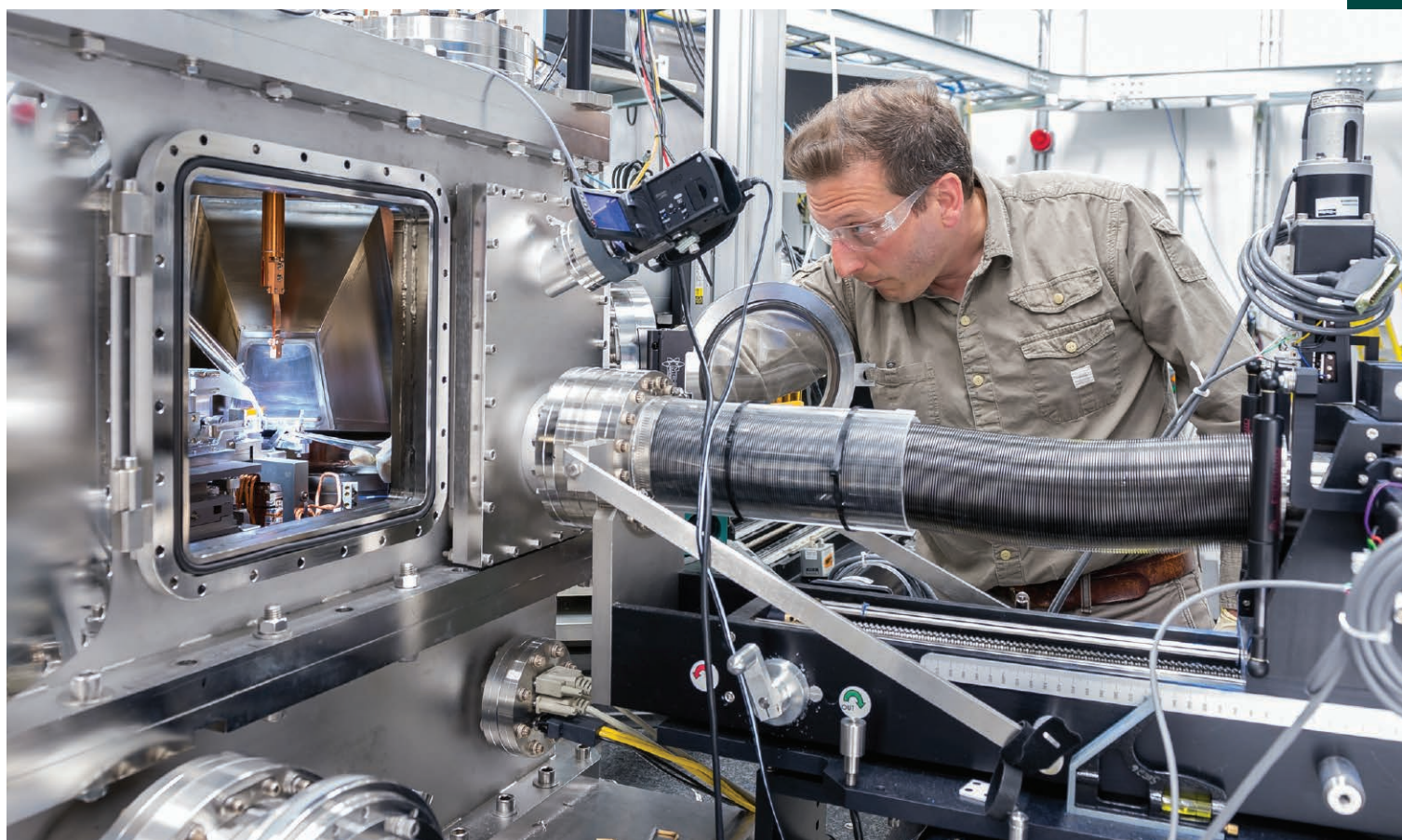


Fig. 1. Images of lead water service line with brass connector from (a) Utility A and (b) Utility B. The scale for both images is in centimeters.

Oxidizing disinfectants and some bacteria can oxidize soluble  $Mn^{2+}$  to insoluble  $Mn^{3+}$  and  $Mn^{4+}$ , which can be deposited on internal pipe surfaces as oxides or oxyhydroxides (birnessite and hollandite). In addition, a Mn silicate phase (braunite) was identified. Chains of  $MnO_6$  octahedra readily incorporate metal ions, e.g., chromium (Cr), copper (Cu), iron (Fe), lead (Pb) and strontium (Sr). Adsorbed metal ions can then be oxidized from less to more toxic forms; for example,  $Cr^{3+}$  to  $Cr^{6+}$ . All of these metals, except Fe, potentially cause health problems and are of concern to the U.S. Environmental Protection Agency (EPA). Mn-minerals deposited in drinking water distribution pipes or the metals adsorbed on their surfaces can be resuspended by physical processes or changes in water chemistry, typically due to switches in source water or disinfection strategy. The dissolution or resuspension of metals can then reach consumers taps.

The researchers, from the University of Cincinnati and the Naval Research Laboratory employed x-ray  $\mu$ -beam studies at XSD beamline 20-BM-B at the APS;  $\mu$ -x-ray fluorescence maps (also from 20-BM-B) of the



Martin Holt, scientist at the Argonne Center for Nanoscale Materials (CNM), places a sample in the Hard X-ray Nanoprobe operated by the CNM and XSD at Sector 26 of the APS. This instrument is used for imaging strain fields near defects and interfaces to understand structural correlations with chemical activity and dynamics in quantum and nanoscale materials for energy.



# BUILDING WITH DNA TINKER TOYS

**D**NA encodes the genetic information of life and thus plays a major role in biology. But it also moonlights as a mechanical building block in nanotechnology. Researchers have developed ways of using it as a programmable bond to assemble nanoparticle building blocks into a wide-range of crystalline structures. However, these DNA-interconnected nanoparticle superlattices are susceptible to thermal degradation, limiting their use in certain practical applications. One solution is to add molecules that slip—or intercalate—between the DNA base pairs to make the DNA “bonds” stronger. A new study of this intercalation technique used x-rays from the APS to monitor the structural changes that occur during this process. The researchers identified an intercalator that significantly strengthens DNA bonds and used it to construct a complex, hierarchical superlattice architecture, comprised of gold nanoparticles in its core and quantum dots in its shell, opening possibilities for the fabrication of new, technologically important materials.

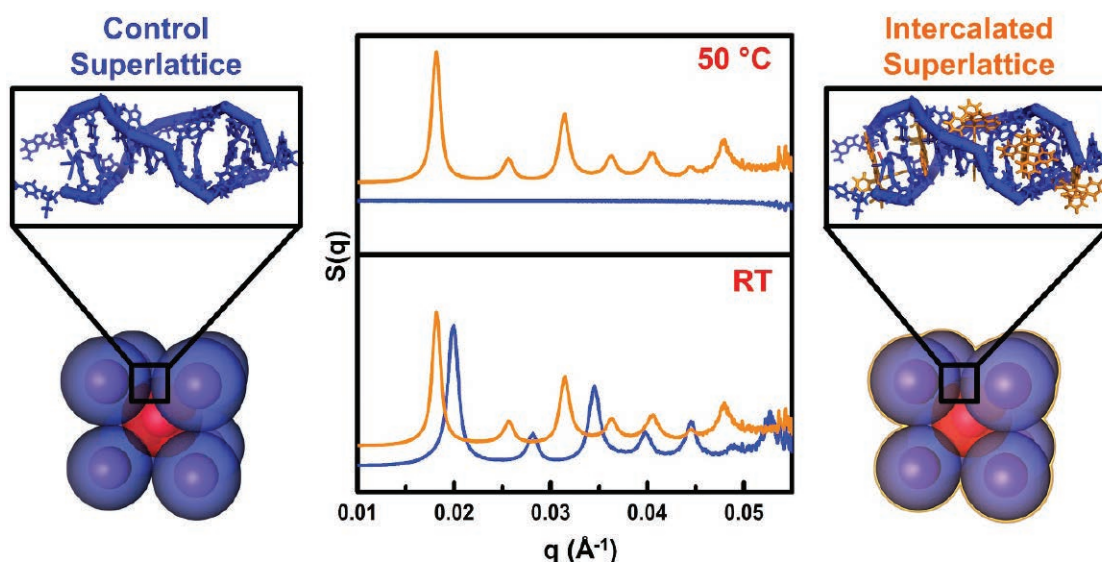


Fig. 1. Nanoparticles superlattices are linked together with duplexed DNA strands (shown in blue on the left). To strengthen these so-called DNA “bonds”, researchers can add intercalators (shown in orange on the right). The middle graphs show X-ray diffraction patterns for both the control superlattice (blue) and the intercalated superlattice (orange). At room temperature (RT), one sees crystal diffraction peaks for both samples. However, when the solution is heated to 50° Celsius, the control superlattice disintegrates and the peaks are not seen. The intercalated superlattice, by contrast, maintains its structure, which is evidenced by sharp diffraction peaks. Image: Soyoung E. Seo and Mary X. Wang



DNA-directed nanoparticle assembly is in some ways a materials scientist's dream. DNA coding allows one to pre-program a set of nanoparticles so that they assemble with nanometer-scale precision into a three-dimensional lattice having practically any desired crystal symmetry.

The first step is to chemically attach DNA strands to the surfaces of a set of nanoparticles. Then, one adds DNA linkers that hybridize (or bond) with the strands anchored to the particles. These linkers have short single-stranded regions—called “sticky ends”—that dangle off the nanoparticles. If their codes (written in the nucleobases) match up, the sticky end of one nanoparticle can bond to the sticky end of another nanoparticle. By carefully arranging these “DNA duplex interconnects,” one can build superlattice architectures with, for example, a body-centered cubic symmetry.

Although this methodology has been utilized to couple nanoparticle building blocks of different compositions together to create complex materials, these architectures can disassemble when heated above the melting temperatures of the DNA interconnects. Researchers have strengthened the bonds by incorporating different types of nucleic acids or changing sequences. However, if the bonds are too strong, the desired versatility and dynamic nature of the assembled structures are reduced. One solution is to build nanostructures using the DNA-directed assembly technique and then post-synthetically add small-molecule intercalators that can bind to the DNA interconnects. These intercalators can insert between the DNA bases without disturbing the original structures, locking them into place at higher temperatures.

A research team from Northwestern University investigated a variety of ruthenium-based DNA intercalators (molecules with a ruthenium core, one inserting ligand, and two ancillary ligands). The researchers modified the binding affinities of these molecules to

DNA duplexes by altering the sterics (atomic arrangement) and charge of the ancillary ligands.

In order to study the effect that the intercalators had on the bond strength, the team incubated the different intercalators in solutions with gold nanoparticle-based superlattices. They then heated each sample and monitored the response of the superlattice structures with small-angle x-ray scattering (SAXS) at the DND-CAT 5-ID-B,C,D beamline at APS. The superlattice structures were detected through specific x-ray diffraction peaks. These peaks disappeared above the melting temperature of the superlattice (Fig. 1).

By comparing the intercalated samples with a control superlattice, the team showed that the intercalators raised the melting temperatures—proof that their presence strengthened the binding of the DNA strands. The intercalator producing the largest effect (called “complex 1”) increased the melting temperature of the superlattices by 15° C above that of the non-intercalated sample. The SAXS data agreed with other measurements of the melting temperature taken with UV-vis spectroscopy.

To demonstrate the power of this technique, the researchers constructed a hierarchical structure made with two types of nanoparticles. They synthesized DNA-nanoparticle superlattices composed of gold nanoparticles and then added complex 1. After the intercalation, the superlattices became “fixed seeds” for further nanoparticle assembly. The team showed this by adding DNA-modified semiconductor quantum dots to their seed solution. The sample was heated and then slowly cooled to allow the DNA-functionalized quantum dots to assemble around the DNA-functionalized gold nanoparticle-based crystal seeds. The seed superlattices withstood the higher temperatures thanks to the intercalators. The resulting core-shell structure, which exhibits unique optical properties, had never been realized before.

The ability to significantly raise the

superlattice melting temperature post-synthetically using intercalators opens new possibilities in materials fabrication. — *Michael Schirber*

**See:** Soyoung E. Seo, Mary X. Wang, Chad M. Shade, Jessica L. Rouge, Keith A. Brown, and Chad A. Mirkin\*, “Modulating the Bond Strength of DNA-Nanoparticle Superlattices,” *ACS Nano* **10**, 1771 (2016). DOI: 10.1021/acsnano.5b07103

**Author affiliation:**

Northwestern University

**Correspondence:**

\* chadnano@northwestern.edu

This material is based upon work supported by Air Force Office of Scientific Research Award FA9550-11-1-0275, and the Centers of Cancer Nanotechnology Excellence (CCNE) initiative of the National Institutes of Health (NIH) under Award U54 CA151880. This work made use of the EPIC facility (NUANCE Center-Northwestern University), which has received support from the MRSEC program (NSF DMR-1121262) at the Materials Research Center; the International Institute for Nanotechnology (IIN); and the State of Illinois, through the IIN. M. Wang gratefully acknowledges a Graduate Research Fellowship from the National Science Foundation (NSFGRFP) and a Northwestern University Ryan Fellowship. J. Rouge acknowledges a postdoctoral fellowship from the PhRMA foundation. K. Brown gratefully acknowledges support from Northwestern University's International Institute for Nanotechnology. The DuPont-Northwestern-Dow Collaborative Access Team is supported by Northwestern University, E.I. DuPont de Nemours & Co., and The Dow Chemical Company. This research used resources of the Advanced Photon Source, a U.S. Department of Energy (DOE) Office of Science User Facility operated for the DOE Office of Science by Argonne National Laboratory under Contract No. DE-AC02-06CH11357.

5-ID-B,C,D • DND-CAT • Materials science, polymer science, chemistry • Powder diffraction, x-ray standing waves, x-ray optics development/techniques, small-angle x-ray scattering, surface diffraction, x-ray reflectivity, wide-angle x-ray scattering • 6-17.5 keV • On-site • Accepting general users •



# CREATING BONDS FOR PROGRAMMABLE ATOMS

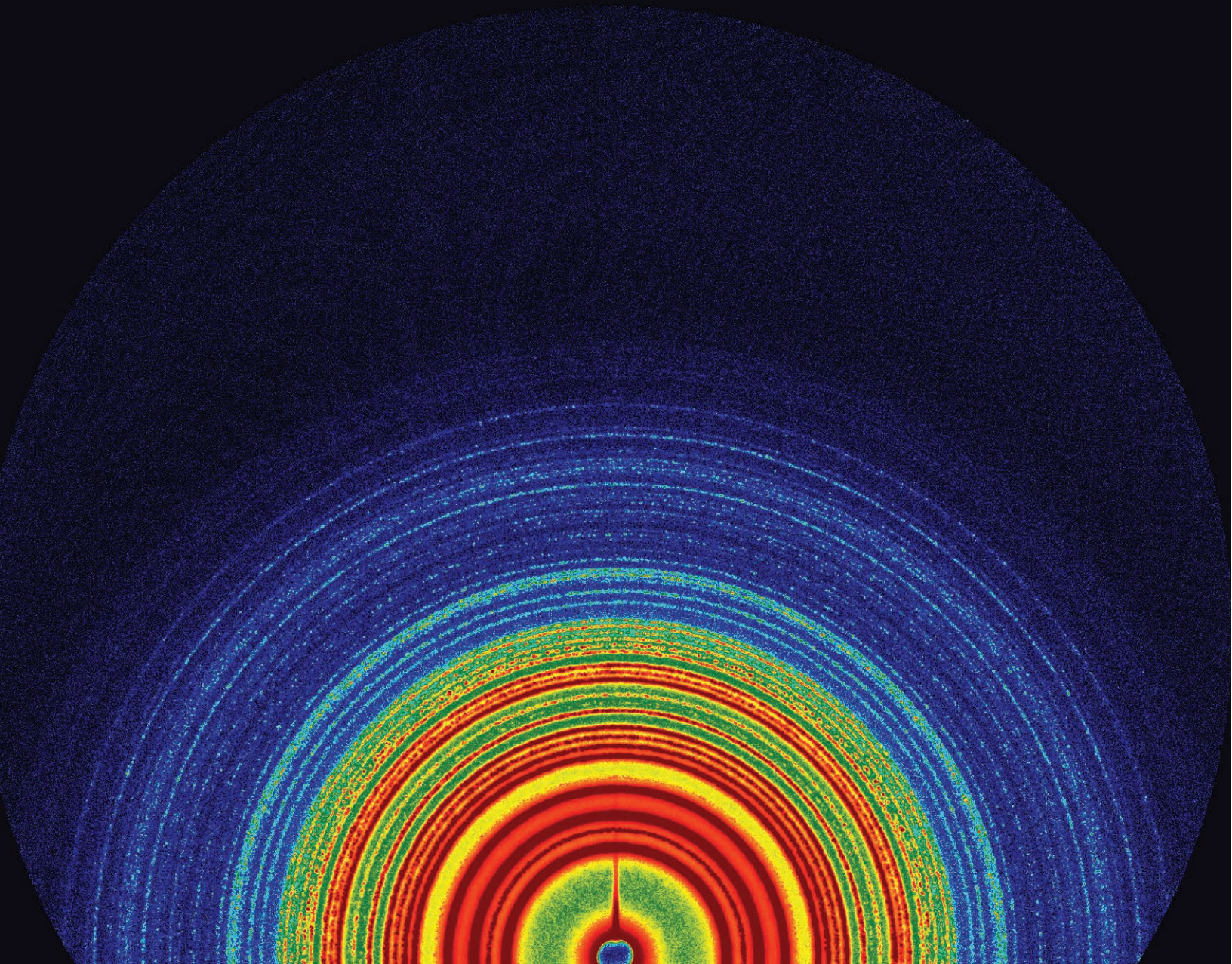


Fig. 1. SAXS shows a characteristic scattering pattern for a tripple-linker programmable atom.



**B**uilding devices at the nanoscale can lead to all sorts of new creations, from molecular diagnostic tests to tiny lenses for manipulating light, but constructing them requires a new set of tools. One approach taken is to synthesize strands of DNA, which link to other strands depending on the sequence of nucleic acids with which they are designed, acting as a sort of programmable glue. Attaching those strands to metal or organic nanoparticles gives researchers a set of building blocks that they can arrange and rearrange to make a broad range of functional devices. Now scientists using the APS have shown they can greatly increase the versatility of those building blocks using DNA-strand topologies that mimics multiple bonds between atoms.

The scientists, from Northwestern University, had demonstrated 20 years ago that they could make DNA-functionalized gold nanoparticles and assemble them into crystalline structures. They have also used a rigid organic molecule as the core of the nanoparticle, replacing the gold. They have employed the building blocks, which they term “programmable atom equivalents,” (PAEs) to create molecular diagnostic tests that take advantage of how the structures interact with light.

The PAEs consist of a nanoparticle core coated with DNA. A shell of DNA “linkers” are added; one end binds to the DNA on the nanoparticle, the other end remains loose, available to bind to complementary linkers on other PAEs. The resulting DNA-based “bonds” can also be broken by controlled heating at a temperature that depends on the specific sequence of the DNA linkers.

In this study, the scientists wanted to compare their standard linear linker design to those that had two or three linkers branching out from the end of the DNA strands. Starting with gold nanoparticles, they added DNA conjugated with a non-binding poly(ethylene glycol) moiety and a thiol group. The “poly(ethylene glycol),” to which they hybridized the complementary linkers. Heating their samples to between approximately 38° C and 49° C, they found that the melting temperature was higher for the double-linker particles than for the single-linker versions, and even higher for those with three linkers.

They also found that the version with the double and triple linkers

showed less strain on the crystals (Fig. 2). The single-stranded versions have to bend and stretch more to find a complementary strand on a nearby nanoparticle to link to, but those with more branches are able to contact a neighboring strand more easily. Strain can change the properties of a crystal, for good or ill, so controlling both strain and melting temperature gives the researchers flexibility in tuning the properties of the PAEs.

The study, carried out with colleagues from Argonne, was carried out using small-angle x-ray scattering (SAXS) at the DND-CAT 5-ID-B,C,D beamline at APS, which is equipped to provide the resolution needed to see spacings of 10s to 100s of nanometers between the particles, revealing their arrangement. The DND-CAT beamline also has a heated stage that allows researchers to watch the crystallization process in action. Of course, DNA is easily damaged by x-rays, so the researchers limited the exposure time to approximately 0.1 sec and moved the position where the beam hit the sample to avoid destroying the DNA.

Future studies could involve examining PAEs made from other types of nanoparticles. That could include other metals, such as silver, iron oxide, and platinum, as well as protein nanoparticles. The latter could be created with a surface chemistry that allows shapes beyond the spheres of the gold nanoparticles, such as rods with the DNA only attached at the ends, in order to create a chain of molecules.

— Neil Savage

**See:** Ryan V. Thaner<sup>1</sup>, Ibrahim Eryazici<sup>1</sup>, Robert J. Macfarlane<sup>1</sup>, Keith A. Brown<sup>1</sup>, Byeongdu Lee<sup>2†</sup> SonBinh T. Nguyen<sup>1\*\*</sup>, and Chad A. Mirkin<sup>1\*</sup>, “The Significance of Multivalent Bonding Motifs and “Bond Order” in DNA-Directed Nanoparticle Crystallization,” *J. Am. Chem. Soc.* **138**, 6119 (2016). DOI: 10.1021/jacs.6b02479

**Author affiliations:** <sup>1</sup>Northwestern University, <sup>2</sup>Argonne National Laboratory

**Correspondence:**

\* chadnano@northwestern.edu

\*\* stn@northwestern.edu

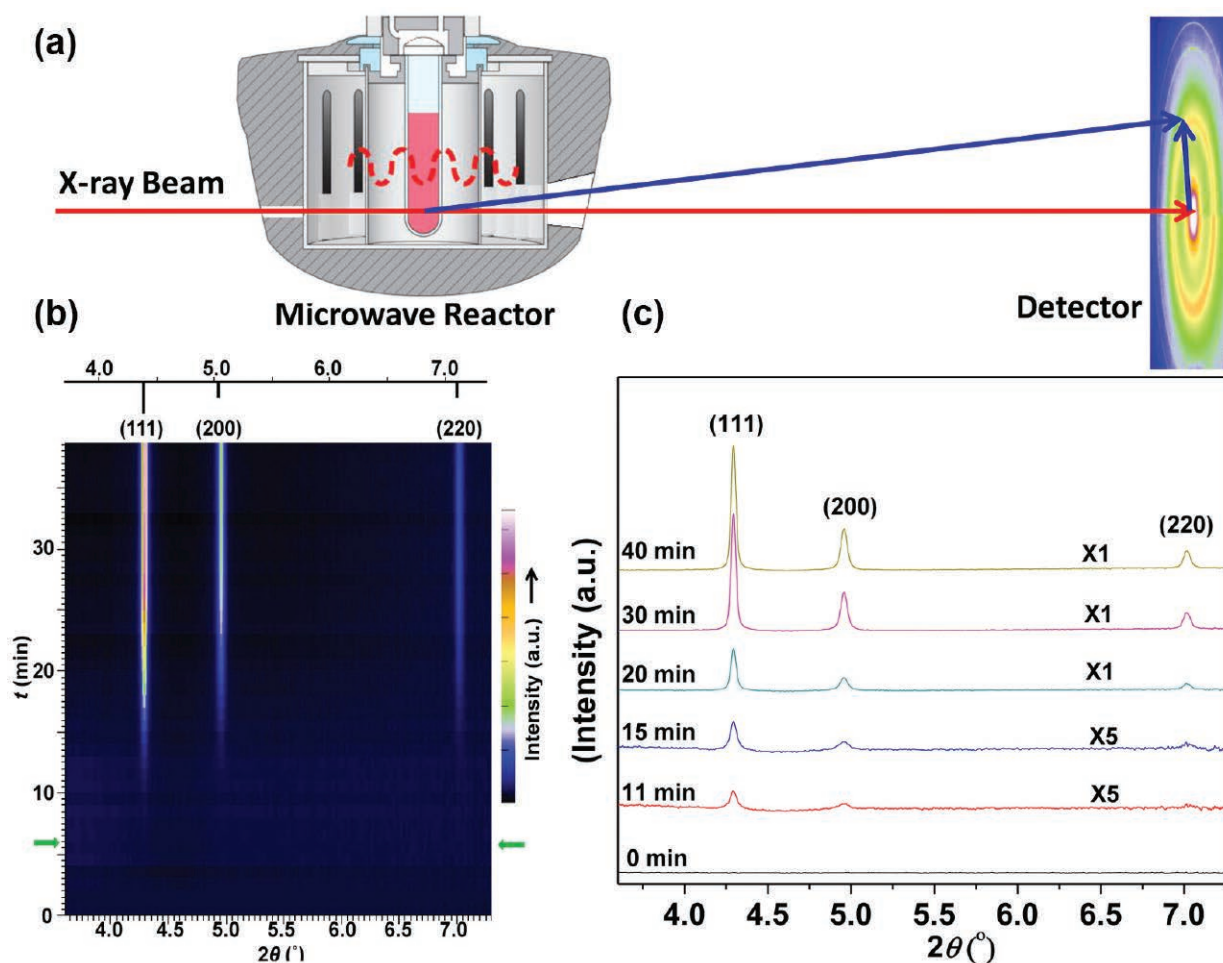
This material is based upon work supported by the following awards: Air Force Office of Scientific Research FA9550-11-1-0275 and FA9550-12-1-0280; the Center for Cancer Nanotechnology Excellence initiative of the National Institutes of Health U54CA151880 and U54CA199091. R.V.T. gratefully acknowledges a National Science Foundation Graduate Research Fellowship. DND-CAT is supported by The Dow Chemical Company, E.I. DuPont de Nemours & Co., and Northwestern University. This research used resources of the Advanced Photon Source, a U.S. Department of Energy (DOE) Office of Science User Facility operated for the DOE Office of Science by Argonne National Laboratory under contract no. DE-AC02-06CH11357.

5-ID-B,C,D • DND-CAT • Materials science, polymer science, chemistry • Powder diffraction, x-ray standing waves, x-ray optics development/ techniques, small-angle x-ray scattering, surface diffraction, x-ray reflectivity, wide-angle x-ray scattering • 6-17.5 keV • On-site • Accepting general users •



# PEEKING INTO A MICROWAVE REACTOR

Heating is often a necessary ingredient in chemical reactions, and like home cooks, chemists can save time by heating with microwaves. Microwave reactors offer a direct and efficient way of heating reactants for organic synthesis and other industrial processes. Over the last decade, researchers have begun producing nanomaterials inside these types of reactors. One problem, though, is that the microwave radiation can interfere with instruments that would normally track the progress of the chemical reactions. To get around this, researchers have utilized a synchrotron beam at the APS to probe the interior of a working microwave reactor. The x-ray scattering measurements gave a real-time view of the formation of silver nanocrystals. The resulting data revealed directionally-dependent growth rates, which could be used to control the final shape of the nanoparticles that have potential for use in a range of applications.



In demonstrations, microwave reactors have been used to fabricate a wide range of nanomaterials, including metal nanoparticles, metal-oxide nanostructures and nanoscale biomaterials. Compared to conventional methods in which heat is diffused from the heating apparatus and applied to an entire solution bath, microwaves deliver heat directly to the reactants, so less energy is wasted. This selective heating synthesizes products faster than conventional methods, and it opens up different reaction pathways involving short-lived metastable states.

To optimize the output from microwave nanochemistry, researchers need a way to peer inside the reactors and observe the structural evolution of nanomaterial products. High-energy x-rays have the ability to penetrate the reactor vessel, as well as the reaction solvent, and retrieve information about the state of the nanomaterials.

To explore this potential, researchers Argonne installed a working reactor in the XSD high-energy 1-ID-B,C,E beamline at the APS. The setup allows samples containing several milliliters of solution to be analyzed in real-time using time-resolved high-energy x-ray diffraction (HEXRD).

The reaction that the researchers chose to investigate was the nucleation and growth of silver nanoparticles.

< Fig. 1. Time-resolved HEXRD patterns recorded in the course of microwave synthesis of Ag nanoparticles at 140 °C. (a) Scheme illustration of the *in situ* HEXRD experiment setup. (b) Contour plot of the HEXRD patterns at different reaction times. The green arrows highlight the time when the temperature ramp ended and the temperature reached 140 °C. The standard XRD pattern of Ag (ICDD PDF 04-001-3180) was plotted as a reference (top sticks). (c) HEXRD patterns at a number of key times. The wavelength of the high-energy x-ray was 0.1771 Å. From Q. Liu et al., *Nano Lett.* **16**, 715 (2016). © 2015 American Chemical Society

These tiny clusters of silver atoms have applications in conductive inks, photovoltaic devices, and anti-bacterial coatings. For their “recipe,” the researchers combined silver nitrate with a reducing agent (ethylene glycol) and a surfactant (polyvinylpyrrolidone) to help stabilize the nanoparticles. By heating the solution to 140° C inside the microwave reactor, the researchers could drive the reduction reaction that converts silver ions into silver atoms. These atoms combine to form small crystal seeds that eventually grow into nano-sized particles.

The team followed the reaction’s progress by taking an x-ray diffraction snapshot every minute or so (Fig. 1). The first diffraction peaks for silver crystals appeared about 5 minutes after the temperature reached 140° Celsius. As time continued, these peaks became stronger, indicating that the small crystal seeds were growing larger. The shape of the growth curve indicated that the seed formation was a typical first-order reaction. But within a few minutes, the growth accelerated, signaling a shift in the reaction dynamics toward a self-catalytic reaction. In this case, the seeds act as catalysts by providing a stable surface on which atoms can bind. The reaction rate only slowed down when the system ran out of silver atoms, which was about 35 min after the start of the experiment.

When compared to conventional heating methods, the microwave-based generation of silver nanoparticles showed less sensitivity to both the initial concentration of silver nitrate and the amount of surfactant. The real-time analysis also revealed a time-dependent anisotropy in the crystal growth. Specifically, the team measured two separate diffraction peaks: one peak for the Ag(111) crystal plane and the other for the Ag(200) plane. In the beginning, the Ag(111) peak was relatively larger than the Ag(200) peak, implying the growth preferentially enlarged the

Ag(111) plane. This trend was reversed in the later stages of the reaction, with the nanoparticles growing primarily along the Ag(200) plane.

The observed crystal anisotropy could prove useful for controlling the size and shape of a nanomaterial. For example, an engineer wanting silver nanorods of a particular aspect ratio could stop the reaction at a particular time. Being able to select the geometry of a nanoparticle is important for determining its catalytic properties. Moreover, the shape of a nanoparticle decides which wavelengths of light it will absorb. As such, controlling growth dynamics in a microwave reactor could let researchers tune the color of a nanomaterial. — *Michael Schirber*

**See:** Qi Liu, Min-Rui Gao, Yuzi Liu, John S. Okasinski, Yang Ren, and Yugang Sun\*, “Quantifying the Nucleation and Growth Kinetics of Microwave Nanochemistry Enabled by *in situ* High-Energy X-ray Scattering,” *Nano Lett.* **16**, 715 (2016).

DOI: 10.1021/acs.nanolett.5b04541

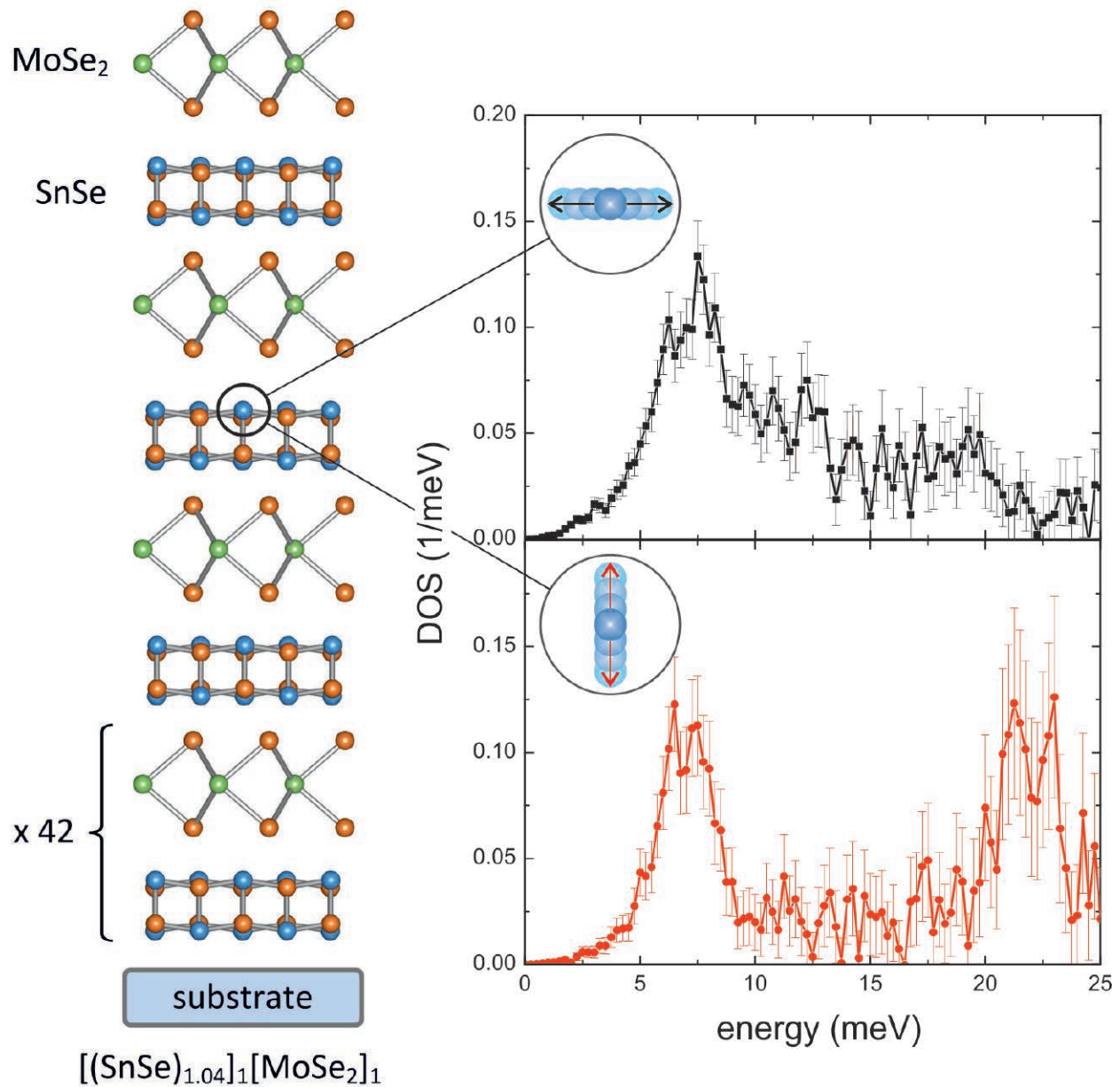
**Author affiliation:** Argonne National Laboratory

**Correspondence:** \* ygsun@temple.edu

Use of the Center for Nanoscale Materials, an Office of Science user facility, was supported by the U.S. Department of Energy (DOE) Office of Science, Office of Basic Energy Sciences, under Contract No. DE-AC02-06CH11357. This research used resources of the Advanced Photon Source, a U.S. DOE Office of Science User Facility operated for the DOE Office of Science by Argonne National Laboratory under Contract No. DE-AC02-06CH11357.

1-ID-B,C,E • XSD • Materials science, physics, chemistry • High-energy x-ray diffraction, tomography, small-angle x-ray scattering, fluorescence spectroscopy, pair distribution function, phase contrast imaging • 41-136 keV, 45-116 keV • On-site • Accepting general users •

# SOUNDING OUT THERMAL CONDUCTORS





**F**erecrystals are unusual materials. They consist of extremely thin layers, in which each individual layer is well ordered, but the layers are stacked in a random orientation, so that the lattice of one layer does not necessarily match with the lattice of the next. This endows the ferecrystals with some interesting properties, including low thermal conductivity, which researchers are trying to understand. If they can, the material might someday be used to make miniature thermoelectric converters, which could power tiny sensors or other nanoscale devices. One research group, using the APS, looked at a particular type of ferecrystal and found surprising results that have the potential for application in thermoelectrics.

Thermoelectric energy generators depend on materials with low thermal conductivity. If heat moves too easily through a material it will dissipate before being converted into electricity. To study the thermal conductivity of a ferecrystal, the researchers from Forschungszentrum Jülich GmbH (Germany), the Oregon Institute of Technology, the University of Oregon, and Oak Ridge National Laboratory, together with colleagues from Argonne, made measurements of the phonons that exist within it. Phonons are vibrations in the material that carry energy; having many phonons in lower energy states means that the material can dissipate heat too readily. Higher-energy phonons carry heat much less effectively, meaning the material has lower thermal conductivity.

Conventional methods of measuring phonons, particularly the low-energy ones, do not work on these materials because they are so small, with only a few layers, each with thicknesses measured in nanometers. So the researchers turned to nuclear inelastic scattering (NIS), which depends on the presence of tin in the ferecrystals. The researchers struck the nucleus of a specific tin isotope with an x-ray, causing it to ring like a tiny bell and producing a vibration that they could then measure as it moved through the structure, a technique that relies on the Mössbauer effect.

The materials they examined were a pair of thin films, approximately 50-

nm thick, consisting of alternating layers of tin selenide and molybdenum diselenide. To produce the 23.88-keV resonances required for ringing the tin bell, they performed the NIS at the XSD 3-ID-B,C,D beamline of APS. A monochromator with an energy resolution of 1.2 meV allowed them to measure the phonons moving both parallel and perpendicular to the layers (Fig. 1).

While a higher percentage of parallel phonons had energies below 10 meV, the researchers say they were astonished to find that in the perpendicular direction, the ferecrystals also had a high percentage of phonons in the higher energy region, between 20 meV and 25 meV. In most materials at nanoscales, phonons tend to cluster at lower energies (Fig. 1). The researchers do not understand the phenomenon they witnessed, but say it is promising for thermoelectrical generation, because the more phonons that exist at higher energies, the fewer low-energy phonons there are to dissipate heat.

The team also measured the speed of sound in the material, which is determined by the lower-energy phonons, also known as acoustic phonons. That result matched well with general findings of decelerated phonons in nanoscale systems.

The next step in this research will be to apply the same techniques to other material systems, to see if they produce similar spreads of phonons. One material the team may try would be tin selenide/titanium telluride systems, because the Mössbauer effect and NIS also work with tellurium.

Researchers are still trying to gain a fundamental understanding of ferecrystals, but if they can figure out why the phonon energies are distributed as

they are, they might then find a way to encourage more of the high-energy states, which would allow them to make better materials for a future generation of thermoelectric generators.

— Neil Savage

**See:** Benedikt Klobes<sup>1\*</sup>, Michael Y. Hu<sup>2</sup>, Matt Beekman<sup>3</sup>, David C. Johnson<sup>4</sup>, and Raphaël P. Hermann<sup>1,5</sup>, "Confined lattice dynamics of single and quadruple SnSe bilayers in  $[(\text{SnSe})_{1.04}]_m[\text{MoSe}_2]_n$  ferecrystals," *Nanoscale* **8**, 856 (2016).

DOI: 10.1039/c5nr06138e

**Author affiliations:** <sup>1</sup>Forschungszentrum Jülich GmbH, <sup>2</sup>Argonne National Laboratory, <sup>3</sup>Oregon Institute of Technology, <sup>4</sup>University of Oregon, <sup>5</sup>Oak Ridge National Laboratory

**Correspondence:**

\* bklobes@hs-bremerhaven.de

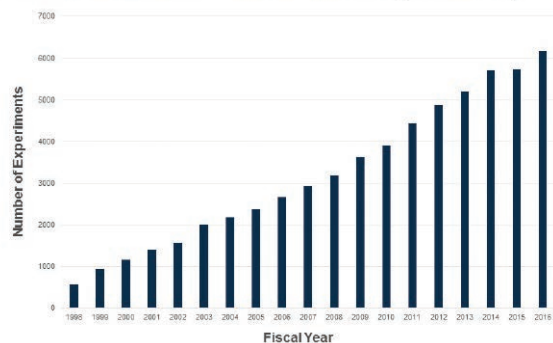
Financial support by the German Research Society (DFG) within the framework of priority program SPP 1386 is acknowledged. M.B. and D.C.J. acknowledge support from the National Science Foundation under grant DMR-1266217. R.P.H. acknowledges support from the Helmholtz Society for grant VH-NG407 and support from the U.S. Department of Energy (DOE) Office of Science-Basic Energy Sciences, Materials Sciences and Engineering Division. Jiyong Zhao and Bogdan Leu (both XSD) are acknowledged for help with the experiment. This research used resources of the Advanced Photon Source, a U.S. DOE Office of Science User Facility operated for the DOE Office of Science by Argonne National Laboratory under Contract No. DE-AC02-06CH11357.

3-ID-B,C,D • XSD • Physics, geoscience, life sciences, chemistry, materials science • Nuclear resonant scattering, inelastic x-ray scattering, high-pressure diamond anvil cell • 7-27 keV, 14.41-14.42 keV • On-site • Accepting general users •

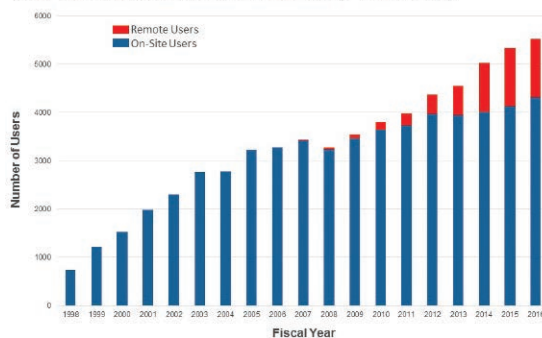
< Fig. 1. Ferecrystals consisting of alternating layers of tin selenide and molybdenum diselenide were studied with nuclear inelastic scattering. The resulting phonons that moved parallel to the layers had more energy states below 10 meV, but a large percent of perpendicular vibrations were at higher energy levels.

## DATA

NUMBER OF EXPERIMENTS AT THE APS (FY98-FY16)

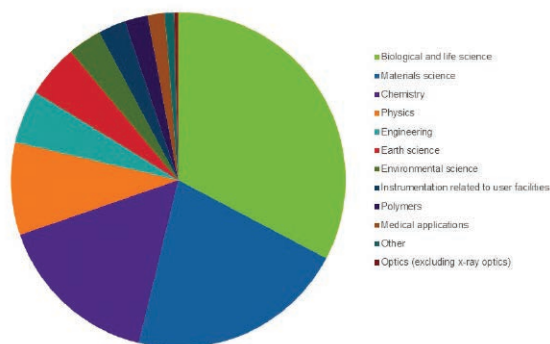


**APS ON-SITE AND REMOTE USERS (FY98-FY16\*)**

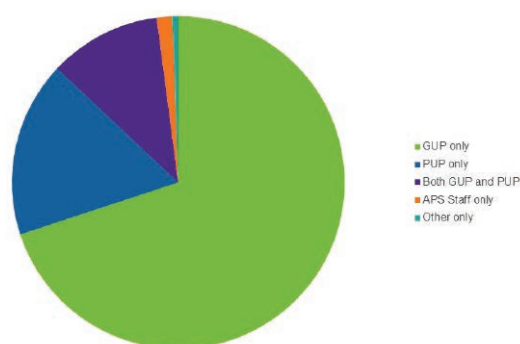


\*Prior to FY14, mail-in users were not included in the Remote category.

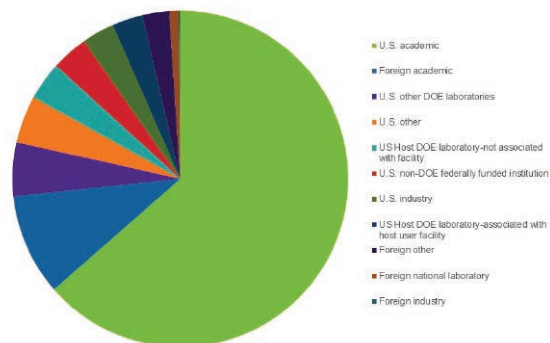
### APS USERS BY EXPERIMENT SUBJECT (FY16)



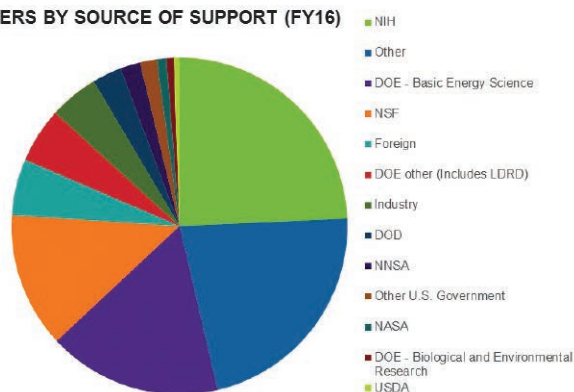
### APS USERS BY USER TYPE (FY16)



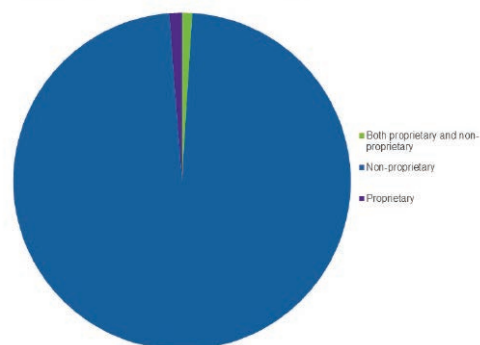
### APS USERS BY EMPLOYER (FY16)



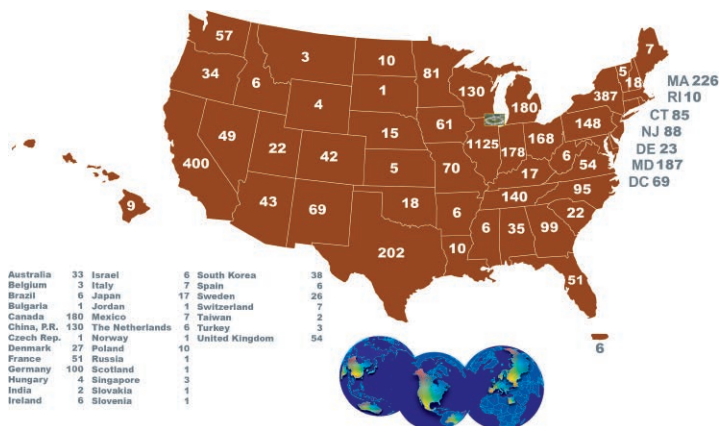
**APS USERS BY SOURCE OF SUPPORT (FY16)**



**APS USERS BY PROPRIETARY TYPE (FY16)**

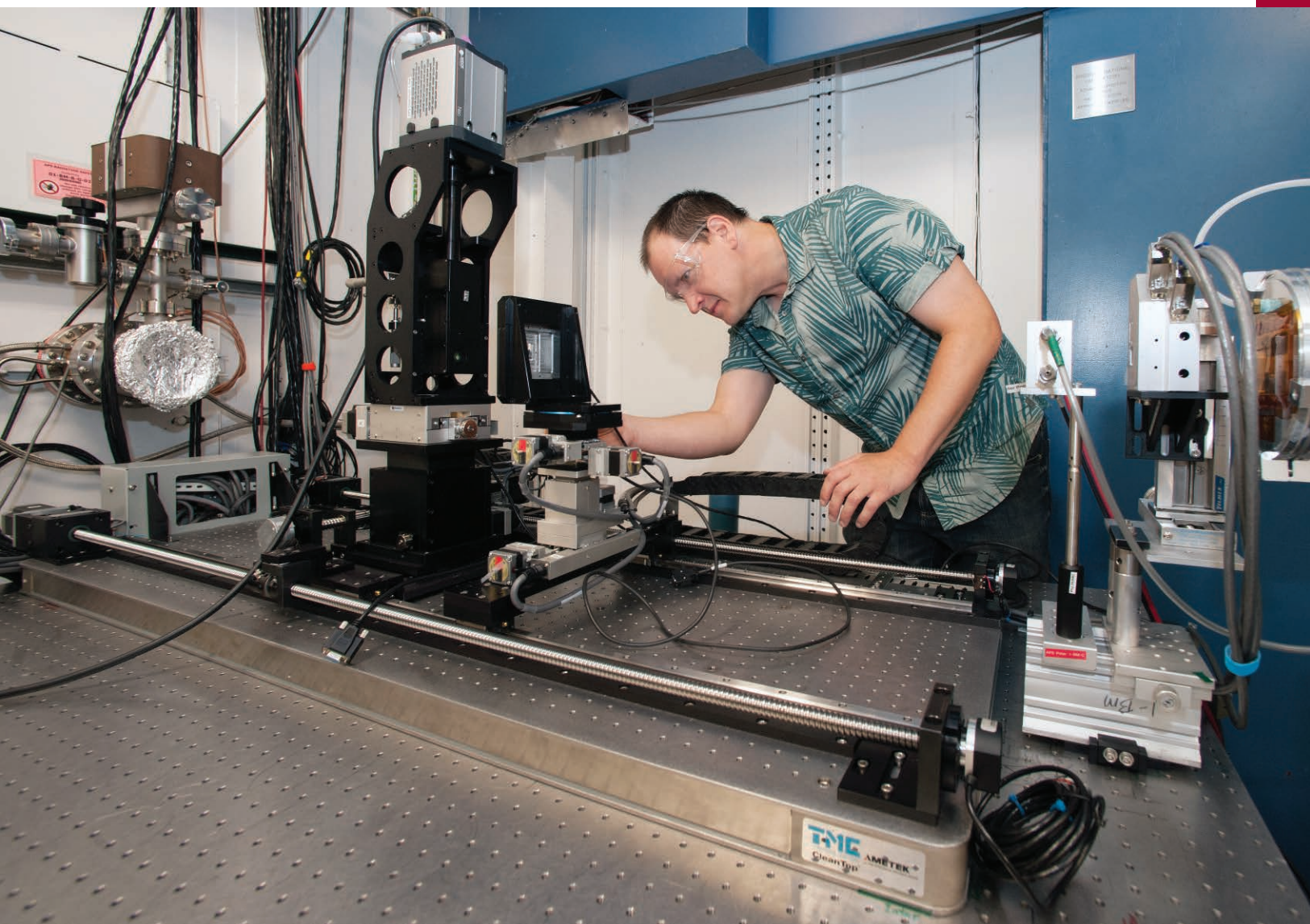


### APS users by institutional geographic distribution (FY 2016)





# NOVEL ACCELERATOR & X-RAY TECHNIQUES & INSTRUMENTATION



Argonne physicist and beamline scientist Stanislav Stoupin formerly of the XSD Optics Group working on the portable grating x-ray interferometer. This instrument is part of the optics & detector testing beamline 1-BM-B,C at the APS.



# SUCCESSFUL INSTALLATION AND OPERATION OF SCU 18-2 AT APS SECTOR 6

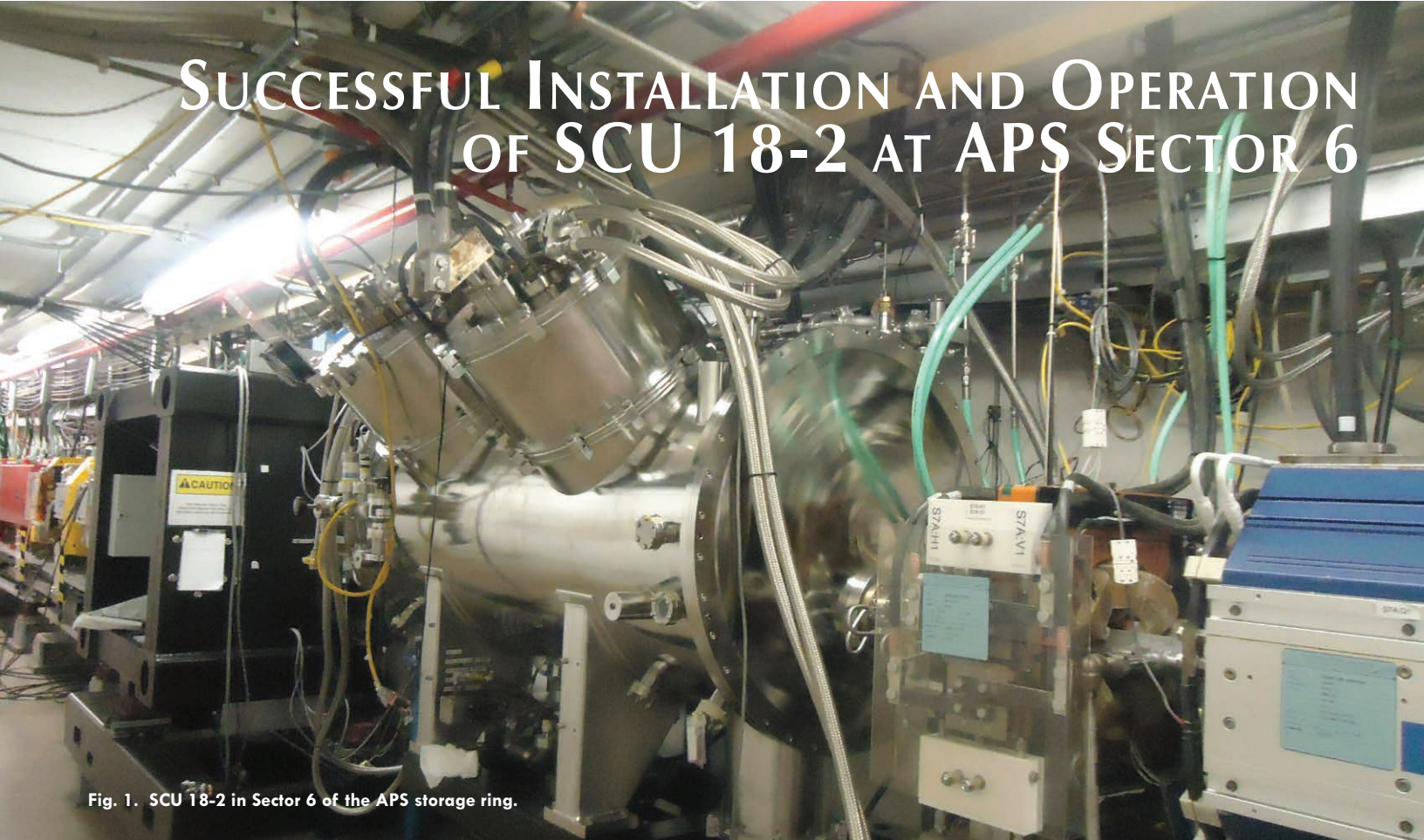


Fig. 1. SCU 18-2 in Sector 6 of the APS storage ring.

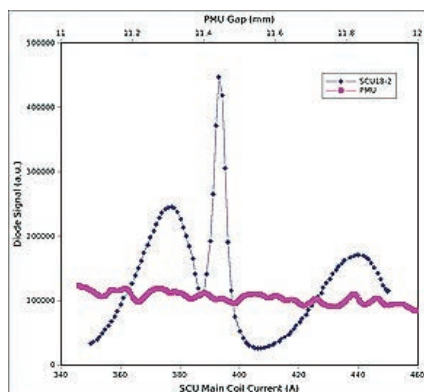


Fig. 2. Measured flux versus current and gap for SCU 18-2 and Undulator A.

Development of superconducting undulator (SCU) technology continues at the APS. The experience of building and successfully operating the first short-length, 16-mm-period-length superconducting undulator, SCU0, paved the way for a 1.1-m-long, 18-mm-period device, SCU18-1, which has been in operation in Sector 1 at the APS since May 2015.

The SCU team has recently completed one more 1.1-m-long, 18-mm-period-length undulator, SCU 18-2, which replaced SCU0 in Sector 6 in September 2016 (Fig.1).

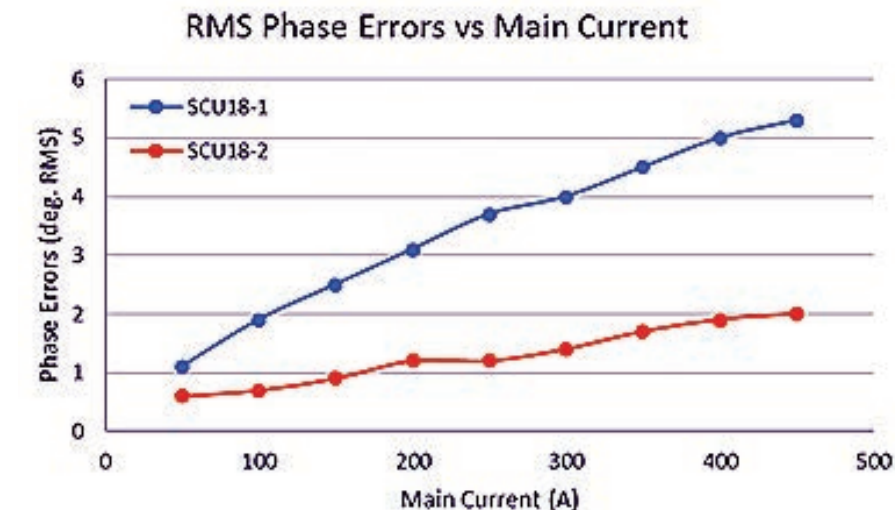


Fig. 3. Measured phase errors for superconducting undulator SCU18-2 equipped with the novel gap tuning system, in comparison with undulator SCU18-1 which does not have such a system.

During its first operating cycle, 12 different user groups have benefited from flux increases of a factor of 4 to 6 from SCU18-2 over SCU0, depending on monochromator energy setting and harmonic choice. The plot in Fig. 2 shows the measured SCU18-2 flux at 85 keV in comparison with that of Undulator A.

A novel magnetic gap tuning system was implemented in undulator SCU 18-2. It is based on a set of mechanical

clamps and highly precise gap spacers, and allows for reduction of the maximum variation in the magnetic gap over the length of the SCU magnet to below 25  $\mu\text{m}$ . Correspondingly, the phase errors do not exceed 2 deg. RMS, as shown in Fig. 3.

The second superconducting undulator, SCU 18-2, is in continuous user operation at APS Sector 6.

Contact: Yury Ivanyushenkov,  
yury@aps.anl.gov

# FIRST TEST OF THE APS UPGRADE PROTOTYPE FEEDBACK CONTROLLER

The ASD Diagnostics and Power Supplies Groups, together with the AES Controls Group and members of the APS Upgrade Project (APS-U) completed initial testing of the APS-U feedback controller (FBC) in the spring and summer of 2016. Figure 1 shows the layout of the “4x4” test hardware located in sectors 27 and 28 of the APS storage ring. In green are shown the new orbit feedback hardware including the FBC at the heart of the test. Four insertion device A:P0 and B:P0 beam position monitors (bpm) are connected to commercial Libera Brilliance+ bpm electronics from Instrumentation Technologies Solkan, Slovenia, to obtain beam position for processing in the FBC.

The feedback controller receives the turn-by-turn (TBT) or 271-kHz beam position data, decimates it by 12 kHz to 22.6 kHz and processes it to obtain corrector set-points. The corrector set-points are then applied using a special test interface between the feedback controller and the existing fast corrector power supplies. The fast correctors used are the A:H3's and B:H4s in sectors 27 and 28.

In addition, the FBC is able to send its bpm and corrector data to a data acquisition system (DAQ), which allows the data to be captured and includes a convenient interface to perform various measurements.

The main objective in this test was to stabilize the beam at the Sector 27 insertion device (ID) A:P0 and B:P0 bpm's using the four fast correctors in a 4-bump configuration.

In addition to beam stabilization, additional goals for the test included demonstrating that all hardware functions properly together, increasing the sampling rate by a factor of 15 over the existing APS storage ring real-time feedback (RTFB) system to 22.6 kHz. Key measurements performed with the system were closed loop bandwidth and total rms motion over the closed-loop bandwidth. The top plot of Fig. 2

shows that at the (horizontal plane) Sector 27 upstream B:P0 bpm,  $f_c=464$  Hz closed loop bandwidth was achieved, which is the point at which the orbit position at the bpm shows no attenuation (unity attenuation ratio) due to feedback compared to the open-loop or feedback-off case. The same result was obtained at the downstream A:P0 bpm. This is about a factor of 5 above that of the existing APS storage ring RTFB system. The bottom plot of Fig. 2 shows the open- and closed-loop integrated rms motion showing a closed-loop rms motion of  $1.85\text{ }\mu\text{m}$  from  $\sim 0.3$  Hz to 464 Hz. This is about a factor of 3 smaller over the same band compared to the open-loop case as shown in the figure. The closed-loop bandwidth and rms motion achieved in the test is a dramatic improvement over that of the operational RTFB system, which has a closed-loop bandwidth of  $\sim 0.1$  Hz to 80 Hz, with rms motion of  $4\text{ }\mu\text{m}$ .

APS-U prototype feedback system testing will be extended in FY 2017 to nearly a full complement of APS-U feedback hardware including 16 bpm's, and 4 fast and 4 slow correctors. Additional mechanical motion detectors at the BPMs and next-generation x-ray bpm's will be incorporated into the system. Latency or time-delays through the system will also be greatly reduced, which is expected to increase the closed-loop bandwidth toward 1000 Hz.

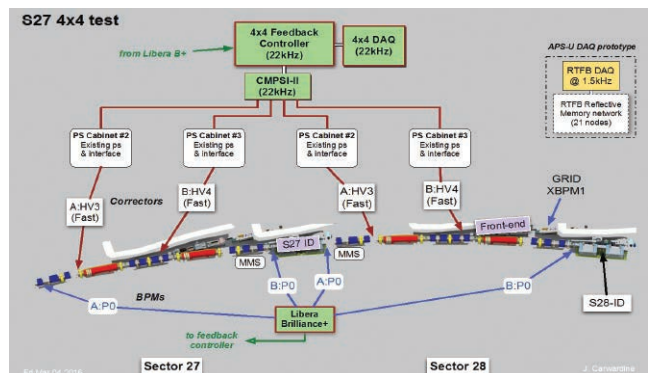


Fig. 1. Layout of the “4x4” test in sectors 27 and 28 of the storage ring. Shown in green is the new prototype orbit feedback hardware used to perform the test.

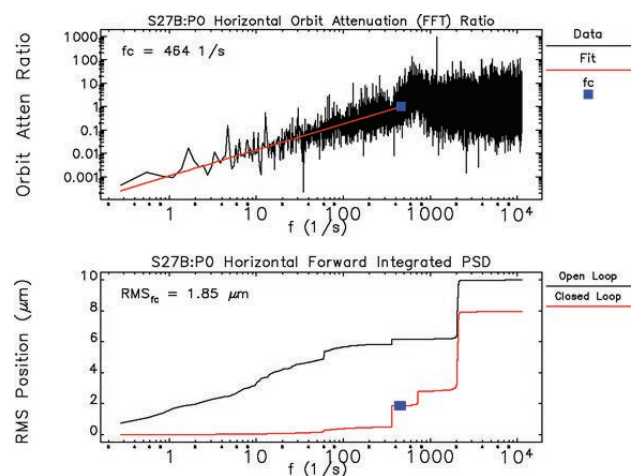


Fig. 2. Orbit attenuation and closed-loop bandwidth plot for S27B:P0 (upstream ID P0 bpm). Top plot: Orbit attenuation showing closed-loop bandwidth cutoff frequency ( $f_c$ ) point from a fit ( $f_c=464$  Hz and orbit attenuation at the blue square). Bottom plot: Open- and closed-loop forward integrated power spectral density function indicating  $1.85\text{-mm}$  rms motion closed loop from 0.3 Hz to the 464 Hz cutoff frequency.

A main objective of the extended testing will be to demonstrate how close the feedback system can meet the demanding long term and AC stability specifications for APS-U ( $1\text{ }\mu\text{m}$  rms over 7 days and  $1.7\text{-}\mu\text{m}$  and  $0.4\text{-}\mu\text{m}$  horizontal and vertical rms motion in the band 0.01 to 1000 Hz in the present APS storage ring.

Contact: Nicholas Sereno,  
sereno@anl.gov



# A FAST-CORRECTOR POWER SUPPLY AND CONTROLLER FOR APS-U

A new fast-orbit feedback system is being developed for the proposed APS-U that will have a correction bandwidth more than 10x the existing real-time feedback (RTFB) system. Achieving this wide bandwidth requires fast responses from the storage ring corrector magnets and associated power supplies, which must have at least 10-kHz bandwidth while also supplying the necessary DC current for steering. The members of the Power Supply Working Team of the APS-U successfully developed a fast corrector power supply along with a power supply controller through the APS-U R&D programs. The design is a DC-to-DC converter based on a standard H-bridge switching-mode circuit with four MOSFET devices as the switches to provide a bipolar output current of  $\pm 15$  A.

The control of the MOSFET devices uses a pulse-width modulation method with a frequency of 250 kHz for each MOSFET. The four switches are interleaved in phase to produce a combined switching frequency of 500 kHz at the output of the power supply. The high switching frequency provides a fast response to changes in the current command. The feedback control loop of the power supply employs a phase-lead compensator in addition to a standard proportional-and-integral controller to minimize the phase delay in the output current at high frequencies. With the high switching frequency and the phase-lead compensation, the power supply has achieved a small-signal (0.5% of the full current range) bandwidth greater than 10 kHz with a 40-V DC input from the APS storage ring DC distribution system.

Each fast corrector power supply receives its set point for the output current from the RTFB system via a power supply controller. The controller has to minimize the communication time delay between the RTFB system and the power supplies. The design of the controller uses a system-on-chip (SoC) field programmable gate array

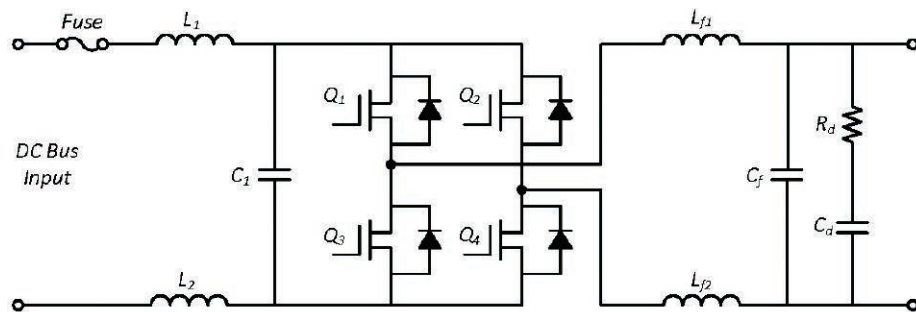


Fig. 1. An H-bridge switching-mode circuit for the APS-U fast corrector power supplies.



Fig. 2. A bipolar power supply controller and two fast corrector power supplies installed in Sector 27 for APS-U integrated beam stability R&D.

(FPGA) that combines an FPGA fabric with an embedded microprocessor system. The communication interface of the controller incorporates a high-speed gigabit Ethernet FPGA logic developed by Lawrence Berkeley National Laboratory. This high-speed communication interface achieved the time delay of less than 10  $\mu$ s required by the APS-U. Each controller can control up to eight power supplies with set points from either the RTFB sys-

tems or through the regular control networks, and has digital and analog I/O to provide full power supply control and monitoring capabilities.

Four power supply controllers and eight power supplies have been installed in APS Sector 27 and Sector 28 to facilitate the APS-U integrated beam stability R&D.

Contact: Ju Wang, [juw@anl.gov](mailto:juw@anl.gov)



# SOLID-STATE RF AMPLIFIER R&D AT THE ADVANCED PHOTON SOURCE

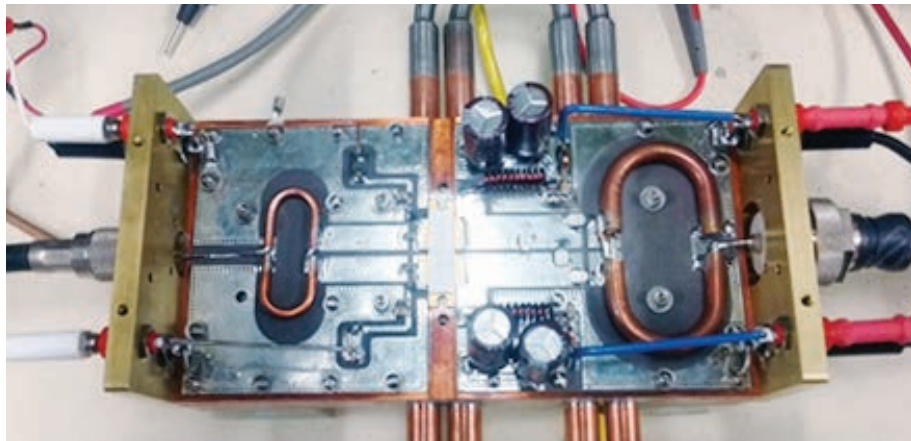


Fig. 1. First prototype 352-MHz, 2-kW, single-device, solid-state amplifier.

Due to recent advances in semiconductor and transistor technology, particle accelerator radio-frequency (rf) systems have begun to adopt solid-state rf power technology to replace traditional vacuum tube amplifier systems. Solid-state rf amplifiers and related modular topologies offer major advantages over the traditional vacuum-tube designs, including operation, low voltage and high efficiency, longer device lifetime, redundant power capability, and reduced maintenance requirements over time. These advantages have made solid-state rf systems an attractive alternative to vacuum tube designs, particularly since availability of the vacuum tubes have become major issues in recent years.

The development of laterally diffused metal oxide semiconductor (LDMOS) field-effect transistor devices capable of 1250 W continuous wave output power per device has further propelled the advance of solid-state technology in new and existing accelerator rf systems. The higher power output per device reduces combining system complexity and associated losses to improve efficiency, and helps to keep the overall size of solid-state rf systems reasonable.

The Radio Frequency Group of ASD has initiated R&D on a solid-state rf system. The goals of the R&D effort include achieving high-efficiency, 2-kW, continuous-wave (cw) output

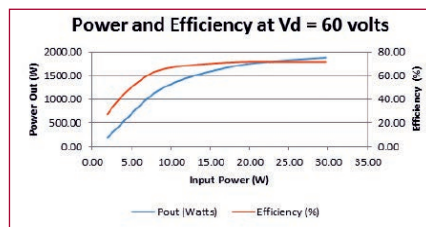


Fig. 2. Performance data on first prototype 352-MHz, 2-kW, single-device, solid-state amplifier.

power at 352 MHz using a single push-pull LDMOS device, and demonstrating a multi-input, power-combining resonant rf cavity. Advances in these areas will make it possible to construct a compact and modular 200-kW rf system that will provide higher efficiency performance and better reliability over the existing vacuum tube-based rf system.

Demonstrated so far is achieving a 2-kW cw at 75.4% efficiency utilizing in-house designed enhanced cooling techniques (Figs. 1 and 2). Production of six complete 2-kW amplifiers is presently under way, along with six driver stages.

Design of an output-combining rf cavity was completed utilizing electromagnetic simulation tools (Fig. 3). Assembly of the combining cavity is under way (Fig. 4) with the goal of demonstrating 12-kW cw output by combining the output of six, 2-kW amplifier modules.

Contact: Ali. Nassiri, [nassiri@anl.gov](mailto:nassiri@anl.gov)

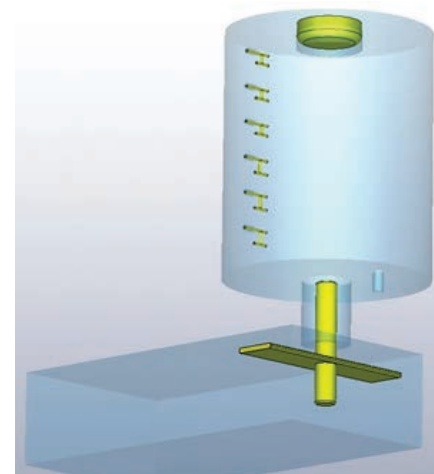


Fig. 4. Rf simulation rendering of the output combining cavity fitted with six input coupling loops to achieve 12-kW total output power.



Fig. 3. Rf power meter indication from first operation at design goal of 2-kW cw rf output.



Fig. 5: Assembly of 12-kW demonstration system, showing the base of the output-combining cavity assembled to the waveguide line and terminating load.



# NANODIAMOND BALLS GENERATE UNPRECEDENTED TERAPASCAL STATIC PRESSURE

A team of scientists has fashioned complement anvils for a diamond anvil cell that can create record-breaking static pressures (Fig. 1). These anvils are fabricated from microballs made of nanocrystalline diamond with a unique microstructure, and achieved pressures above 1 TPa, or about three times the pressure at the Earth's core. The behavior of materials at such conditions had only been studied theoretically. Utilizing the APS, the European Synchrotron Radiation Facility (ESRF) in France, and the Bavarian Geoinstitute for Experimental Geochemistry and Geophysics (BGI) in Germany, the team found that the nanocrystalline microballs exhibited extraordinary mechanical and optical properties and examined the microstructures that gave them their strength. Using the microballs to generate extreme pressures may allow researchers to take compression experiments—which can induce changes in a material's properties, form new “super” materials, or simulate exotic environments such as the interior of massive planets—to new heights.

Bulk nanocrystalline and nanopolycrystalline diamond are two of the strongest known materials. Nanocrystalline diamond comprises only crystals smaller than 50 nm in size whereas nanopolycrystalline includes submicrometer-sized grains as well. Nanocrystalline diamond was used for creating extreme pressures inside a laboratory apparatus known as a diamond anvil cell, in which materials are squished between two opposing diamonds at high temperature and pressures. Scientists have put sample materials under extreme stress on using diamond anvil cells to produce many interesting structural, magnetic and elec-

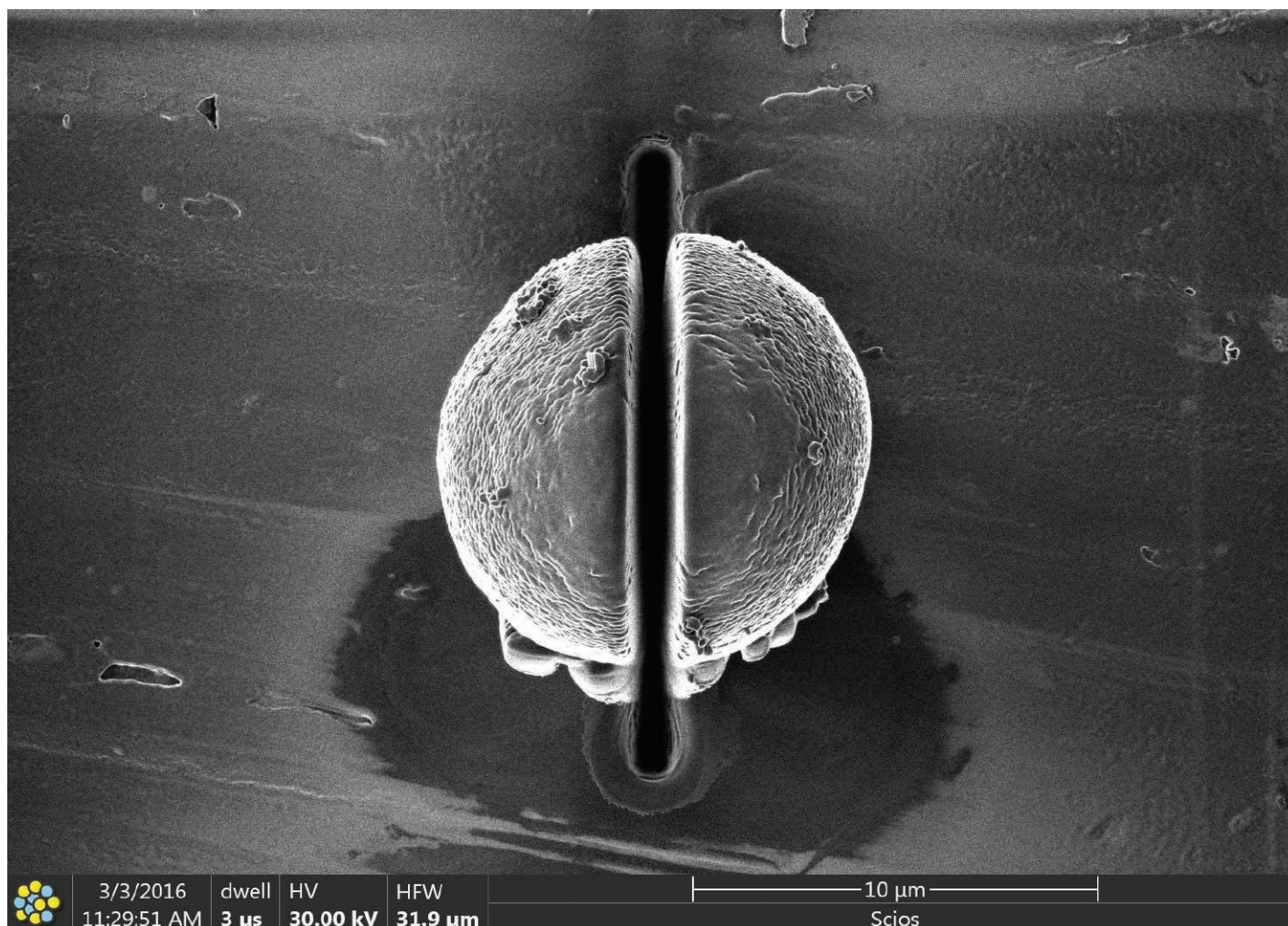


Fig. 1. Two complement anvils for a diamond anvil cell are prepared from a single microball made of nanocrystalline diamond.



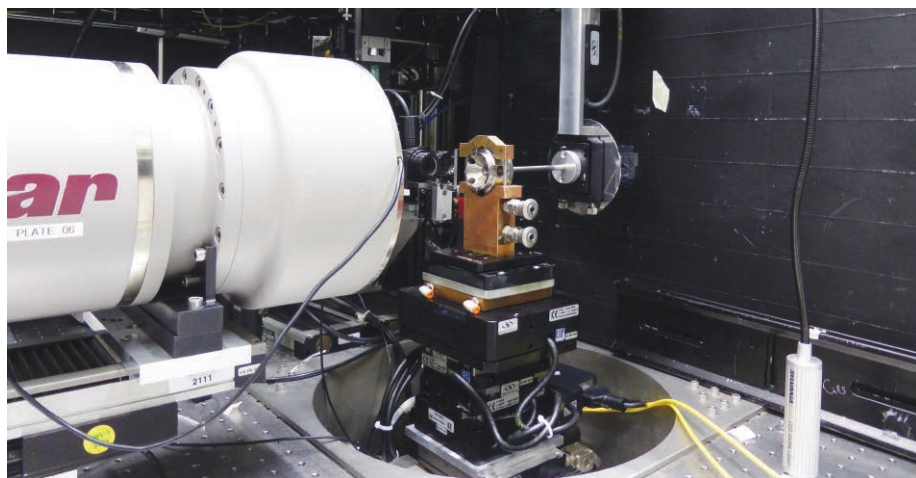


Fig. 2. A double-stage dsDAC (with implemented secondary nanocrystalline diamond anvils) mounted at the GSECARS 13-ID-C,D beamline) at the APS. Image credit: Natalia Dubrovinskaia

tronic changes within the material. In a recent experiment, osmium was compressed to more than 770 GPa and exhibited a new kind of electronic transition, suggesting that other discoveries may yet be uncovered at even higher pressures.

Now, this team of researchers has demonstrated that nanocrystalline diamond microballs integrated into a diamond anvil cell can create unprecedented terapascal pressures.

The team made the nanocrystalline microballs by subjecting glassy carbon to 18 GPa of pressure in a multianvil apparatus at 2000° C. The researchers used x-ray diffraction and Raman spectroscopy techniques to measure the microballs compressibility and observed an exceptional yield strength of about 460 GPa, which is at least three times that of single-crystal diamonds. The high-pressure x-ray diffraction experiments were conducted at the GSECARS 13-ID-C,D beamline at the APS (Fig. 2), the BGI, and beamline ID09 at the ESRF.

The researchers found that the nanocrystalline microballs dented the nanopolycrystalline diamond anvil surface at pressures above 150 GPa, revealing the new material's superior hardness, which is impossible to quantify using the current hardness scale which can't account for materials harder than bulk diamond.

To understand the microballs' exceptional properties, the researchers probed their microstructure and composition using aberration-corrected transmission electron microscopy and spa-

tially resolved electron energy loss spectroscopy. These investigations showed that nanocrystalline diamond had very small nanograin sizes of about 3-9 nm. The grain boundaries appeared incoherent and similar in thickness to a single layer of graphene. The researchers suggest this unique microstructure gives rise to the notable mechanical properties of the nanocrystalline diamond.

Then the team tested the nanocrystalline microballs' incorporation into a diamond anvil cell. The microballs were milled in two to produce half-spheres that were placed on opposing diamonds to act as second-stage anvils. A gold foil sample 1-μm thick was steadily compressed between the microballs while x-ray diffraction experiments measured the reflections of gold. Using the Birch-Murnaghan equation of state for gold, which correlates observed lattice parameters to pressure, researchers found that static pressures reached almost 1.1 TPa.

Even at the highest pressures in the experiment, the nanocrystalline diamond stayed optically transparent, meaning that the material does not produce additional spectral features to the diamond anvils, which is attractive for ultrahigh-pressure infrared spectroscopy studies.

In the form of diamond spheres, the microballs are also valuable as x-ray divergent negative lenses. The researchers lined up nine nanocrystalline microballs in front of the x-ray beam and demonstrated that the microballs can cause light to diverge, which could

be useful for developing new x-ray microscopy techniques. — *Tien Nguyen*

**See:** Natalia Dubrovinskaia<sup>1\*</sup>, Leonid Dubrovinsky<sup>1</sup>, Natalia A. Solopova<sup>1</sup>, Artem Abakumov<sup>2†</sup>, Stuart Turner<sup>2</sup>, Michael Hanfland<sup>3</sup>, Elena Bykova<sup>1</sup>, Maxim Bykov<sup>1</sup>, Clemens Prescher<sup>4</sup>, Vitali B. Prakapenka<sup>4</sup>, Sylvain Petitgirard<sup>1</sup>, Irina Chuvashova<sup>1</sup>, Biliana Gasharova<sup>5</sup>, Yves-Laurent Mathis<sup>5</sup>, Petr Ershov<sup>6</sup>, Irina Snigireva<sup>3</sup>, Anatoly Snigirev<sup>3,6</sup>, "Terapascal static pressure generation with ultrahigh yield strength nanodiamond," *Sci. Adv.* **2**, e1600341 (20 July 2016).

DOI: 10.1126/sciadv.1600341

**Author affiliations:** <sup>1</sup>University of Bayreuth, <sup>2</sup>University of Antwerp, <sup>3</sup>European Synchrotron Radiation Facility, <sup>4</sup>The University of Chicago, <sup>5</sup>Karlsruhe Institute of Technology, <sup>6</sup>Immanuel Kant Baltic Federal University <sup>†</sup>Present address: Skolkovo Institute of Science and Technology

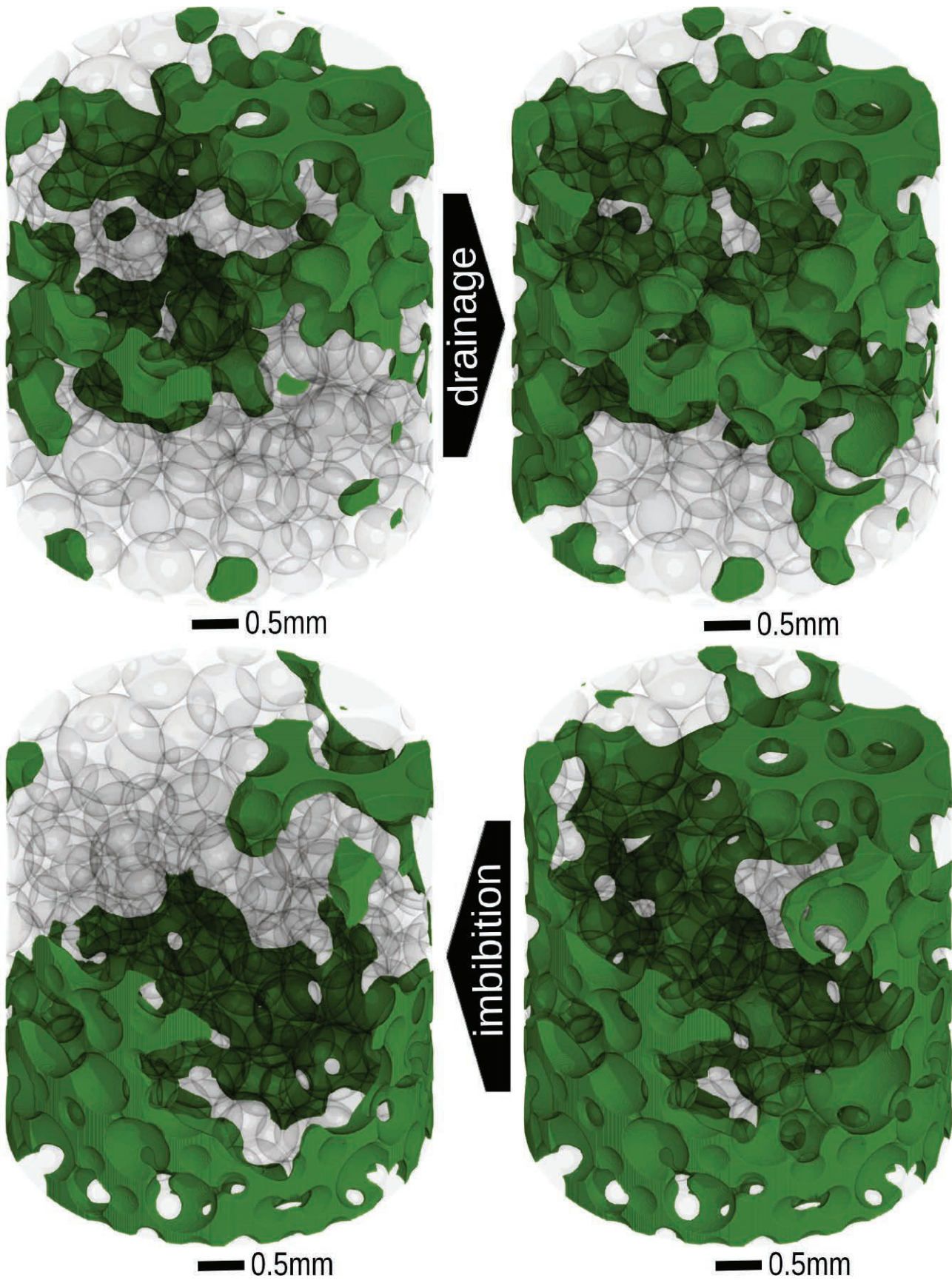
**Correspondence:** \* natalia.dubrovinskaia@uni-bayreuth.de

N.D. thanks the German Research Foundation [Deutsche Forschungsgemeinschaft (DFG)] and the Federal Ministry of Education and Research (BMBF; Germany) for financial support through the DFG Heisenberg Programme (projects no. DU 954-6/1 and DU 954-6/2) and project no. DU 954-8/1 and the BMBF grant no. 5K13WC3 (Verbundprojekt O5K2013, Teilprojekt 2, PT-DESY). L.D. thanks the DFG and the BMBF (Germany) for financial support. A.S. thanks the Ministry of Science and Education of Russian Federation through grant no. 14.Y26.31.0002 for financial support. GSECARS is supported by the National Science Foundation-Earth Sciences (EAR-1634415) and the U.S. Department of Energy (DOE)-GeoSciences (DE-FG02-94ER14466). This research used resources of the Advanced Photon Source, a U.S. DOE Office of Science user facility operated for the DOE Office of Science by Argonne National Laboratory under Contract No. DE-AC02-06CH11357.

13-ID-C,D • GSECARS • Geoscience, environmental science • Surface diffraction, x-ray standing waves, microdiffraction, x-ray absorption fine structure, resonant inelastic x-ray scattering, high-pressure diamond anvil cell, high-pressure multi-anvil press, x-ray emission spectroscopy • 4.9-45 keV, 10-75 keV • On-site • Accepting general users •



# FLUID TOPOLOGY IN REAL TIME



**T**he ability of researchers to understand fluid topology (the study of properties of space that are preserved under continuous deformation in porous media) has recently advanced in part due to the maturation of fast x-ray tomography performed in real time. The resultant knowledge has many applications. For example, for carbon sequestration it is important to know the trapping efficiency of a medium for carbon dioxide. In oil production, pore-scale displacement mechanisms during water flooding affect the continuity of oil clusters with direct consequences for production efficiency. An international team of researchers used these novel measures at the APS to further our understanding of fluid topology and to advance the field.

Immiscible, two-phase flow is ubiquitous both in nature and industrial applications involving porous media. The phase distribution of the flowing fluids is determined by pore space structure, solid phase wettability, and external hydraulic forcing. The complicated spatial arrangement of fluids needs to be described by a simple set of measurable state variables to build useful models for practical applications. These state variables have traditionally been the fluid saturation and macroscopic pressure difference between fluids. However, these models do not account for fluid topology, which in this case represents the connectivity of the fluids. This oversimplification causes difficulties in describing the hysteretic behavior of two-phase flow at the pore scale, among other things. Hysteresis represents the fact that the same fluid saturation can be reached at different pressure differences, depending on whether the sample is drained or imbibed. In a field scale scenario, this would be the difference between a rise or a lowering of the groundwater table in response to rain or prolonged dry spells.

Advances in fast x-ray tomography have increased the ability of researchers to track moving fluid interfaces during immiscible flow in porous media. This technique is restricted to small porous samples of a few mm in diameter because the field of view is

constrained by the cross-sectional area of the beam. Here, the researchers monitored fluid distributions with fast synchrotron-based x-ray tomography at the GSECARS 13-BM-D beamline at the APS. Fluid was pumped continuously during image acquisition and data was collected in real-time. The researchers produced high-quality datasets showing the phase distribution of a wetting (water) and nonwetting (oil) fluid during a complete drainage and imbibition cycle in a coarse-grained material (Fig.1).

The researchers discovered a previously unrecognized source of hysteresis: the shape of the displacement front. This front features different patterns like capillary fingering, flat frontal displacement, or cluster growth, and can be described by topological measures. At the same saturation, fluids might be fully connected or very fragmented depending on this underlying pore-scale displacement mechanism. Understanding these features is extremely important because fluid topology directly influence effective process behavior, such as carbon dioxide trapping efficiency or oil production during water flooding. A topological invariant, the Euler characteristic of the nonwetting phase, describes this local fluid connectedness through a simple, dimensionless number. A comparison with various other drainage and imbibition experiments in similar porous media has shown that the way this Euler characteristic changes with saturation is very characteristic for specific displacement processes, expressed by a single scaling exponent, and less dependent on other factors like the rock geometry. This topological characterization may therefore be the optimal choice to im-

prove macroscopic formulations of two-phase immiscible displacement in porous rock.

The researchers showed that fluid topology reveals the underlying fluid displacement pattern and helps to explain hysteresis effects. As fast x-ray tomography continues to develop, high-quality measurements of fluid topology in real time will become standard. The validity of this work will be checked in experiments on complex natural rocks, like sandstone and limestone, under different flow regimes. — *Dana Desonie*

**See:** S. Schlüter<sup>1,2\*</sup>, S. Berg<sup>3</sup>, M. Rücker<sup>3,4</sup>, R.T. Armstrong<sup>5</sup>, H.-J. Vogel<sup>1,6</sup>, R. Hilfer<sup>7</sup>, and D. Wildenschild<sup>2</sup>, "Pore-scale displacement mechanisms as a source of hysteresis for two-phase flow in porous media," *Water Resour. Res.* **52**(3), 2194 (24 March 2016). DOI: 10.1002/2015WR018254.

**Author affiliations:** <sup>1</sup>Helmholtz-Centre for Environmental Research–UFZ <sup>2</sup>Oregon State University, <sup>3</sup>Shell Global Solutions International B.V., <sup>4</sup>Imperial College London, <sup>5</sup>University of New South Wales, <sup>6</sup>Martin-Luther-Universität Halle-Wittenberg, <sup>7</sup>Universität Stuttgart

**Correspondence:**

\* steffen.schluter@ufz.de

This research was supported by the U.S. National Science Foundation award no. EAR-1344877. We thank Mark Rivers at the Advanced Photon Source for assistance at the GSECARS beamline. The first author is grateful to the Alexander-von-Humboldt Foundation for granting a Feodor-von-Lynen scholarship. Rudolf Hilfer thanks the Deutsche Forschungsgemeinschaft for financial support. GSECARS is supported by the National Science Foundation-Earth Sciences (EAR-1634415) and the U.S. Department of Energy (DOE)-GeoSciences (DE-FG02-94ER14466). This research used resources of the Advanced Photon Source, a U.S. DOE Office of Science user facility operated for the DOE Office of Science by Argonne National Laboratory under Contract No. DE-AC02-06CH11357.

13-BM-D • GSECARS • Geoscience, environmental science • Tomography, high-pressure diamond anvil cell, high-pressure multi-anvil press • 4.5-80 keV • On-site • Accepting general users •

< Fig. 1. Fluid distribution during drainage (top) and imbibition (bottom) at different fluid saturation in a sandy material. During drainage the non-wetting phase (dodecane oil, green) displaces the wetting phase (salty brine, transparent) and vice versa. The different flow directions lead to different displacement patterns.



# A NEW X-RAY BRAGG COHERENT DIFFRACTION 3-D IMAGING METHOD

The nanoscale strain distributions and lattice distortions in crystals dictate many crystal properties, but are often difficult to measure under realistic working conditions. Increasingly, Bragg coherent x-ray diffraction imaging (BCDI) is being used at synchrotron sources to address this challenge by nondestructively imaging nanoscale strain fields in crystalline materials in three dimensions (3-D) using penetrating hard x-rays. While these studies have proved valuable, the breadth of feasible 3D BCDI measurements could expand substantially if current experimental requirements, such as repeated sample rotations, could be eliminated without sacrificing imaging capabilities. To extend the BCDI technique and enable new strain imaging studies of materials in environments where sample manipulation is difficult and details of nanoscale strain distribution and evolution remain elusive, an international team of researchers has developed a new BCDI technique that does not require sample manipulation. Included in the method is a new 3-D Fourier transform that enables reconstruction of 3-D images from this type of data. The researchers demonstrated the new approach by performing measurements on a sub-micron-sized gold nanocrystal using a mirror-focused coherent x-ray beam at the XSD 34-ID-C beamline at the APS.

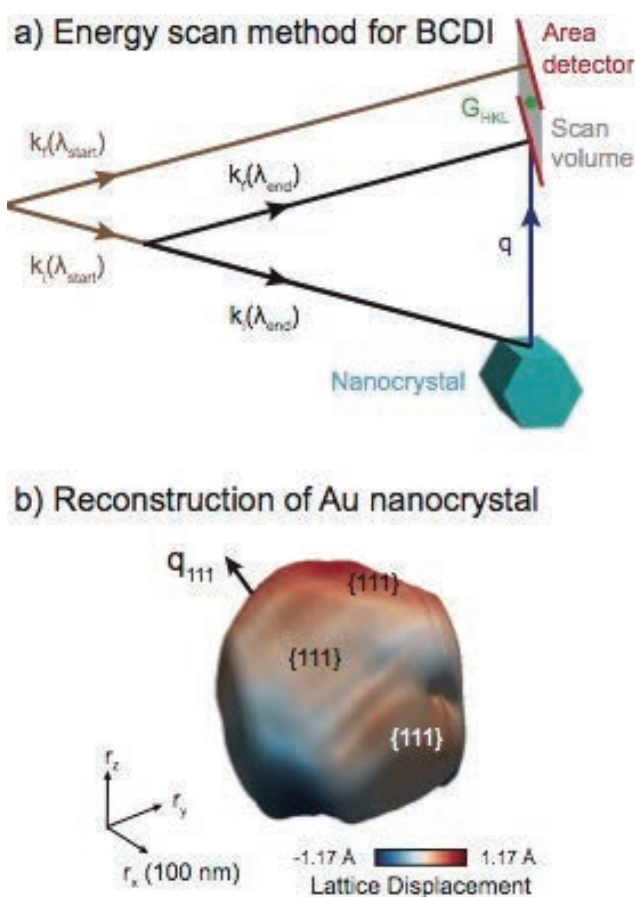


Fig. 1. (a) Bragg coherent diffraction imaging data can be measured by scanning the x-ray energy without sample motion, and inverted (b) using the new vwBCDI phase-retrieval algorithm.

In the standard BCDI technique, an isolated nanocrystal is illuminated by a coherent x-ray beam, producing an array of diffraction pattern amplitudes on a two-dimensional (2-D) detector. A 3-D reciprocal space map of lattice distortions within the crystal is constructed from a series of such 2-D slices taken at different angular positions in the vicinity of the Bragg angle (rocking curves). To reconstruct the 3-D density and strain distribution in the crystalline sample, however, it is necessary to know both the amplitudes and the phases of the 3-D Fourier transform of the diffracting nanocrystal. Over the years, phase-retrieval algorithms have been developed to calculate suitable phases relatively easily.

In the new variable-wavelength BCDI (vwBCDI) technique, the reciprocal space volume about a Bragg peak is measured by finely scanning the wavelength of the incident x-ray beam, thus eliminating the need to rotate the sample. To reconstruct 3-D images from this type of data, the researchers developed a new phase-retrieval method designed to handle x-ray wavelength variability in BCDI (Fig. 1). In arriving at the new method, the researchers leveraged the properties of the Fourier slice projection theorem and the relationship between spatial sampling and array size in a 2-D discrete Fourier transform to define a slice-by-slice 3-D Fourier transform appropriate for the vwBCDI approach.

The researchers then performed BCDI and vwBCDI measurements on the gold nanocrystal and compared the results. Both approaches produced comparable lattice distortion data. The good agreement between the two reconstruction methods

*"Bragg" cont'd. on page 200*



# STUDYING ULTRAFAST PHOTO-INDUCED MESOSCOPIC PHASE TRANSITIONS

Phenomena such as insulator-to-metal phase transitions (IMTs), colossal magnetoresistance, and high-temperature superconductivity often involve the spontaneous appearance of spatially separated regions having distinct structural, magnetic, and electronic properties. The IMT of vanadium dioxide ( $\text{VO}_2$ ) is of particular interest, as the correlated-electron material exhibits an orders-of-magnitude change in electrical conductivity across the transition, in addition to a change in lattice symmetry. This close-to-room-temperature transition can be triggered by optical excitation on ultrafast time scales, and so promises important applications in low-power ultrafast electronics. The ultrafast nature of the transition is also of fundamental interest because this seemingly simple binary oxide compound may serve as a model system that provides new insights into high-temperature superconductivity, charge stripes, quantized spin and charge fluctuations, and ferroelectricity. Dynamic solid-solid phase transitions involving spatially separated regions that span length scales from nanometers to micrometers are very difficult to characterize because critical information underlying the phase transitions, such as localized phase competition, cannot be resolved by measurements that are spatially averaged over many phase-separated regions. An international team of researchers working at the APS developed a state-of-the-art laser-pumped x-ray diffraction imaging technique for just such applications.

The time-resolved x-ray diffraction microscopy technique, which has 350-nm spatial resolution and 100-ps temporal resolution (Fig. 1a), was applied to quantitatively studying structural phase propagation during a photo-induced phase transition in a  $\text{VO}_2$  thin film. The experiment, which was conducted at the XSD 7-ID-B,C,D beam-line of the APS, represents the first hard x-ray measurement with sub-nanosecond and sub-micrometer resolutions that directly captures a mesoscopic structural phase transformation in a correlated material. The sub-micrometer length and sub-nanosecond time resolutions allowed the scientists from Argonne, the University of Wisconsin-Madison, the IBM Almaden Research Center, and the Max Planck Institute for Microstructure Physics (Germany) to follow the structural phase progression

*"Mesoscopic" cont'd. on page 200*

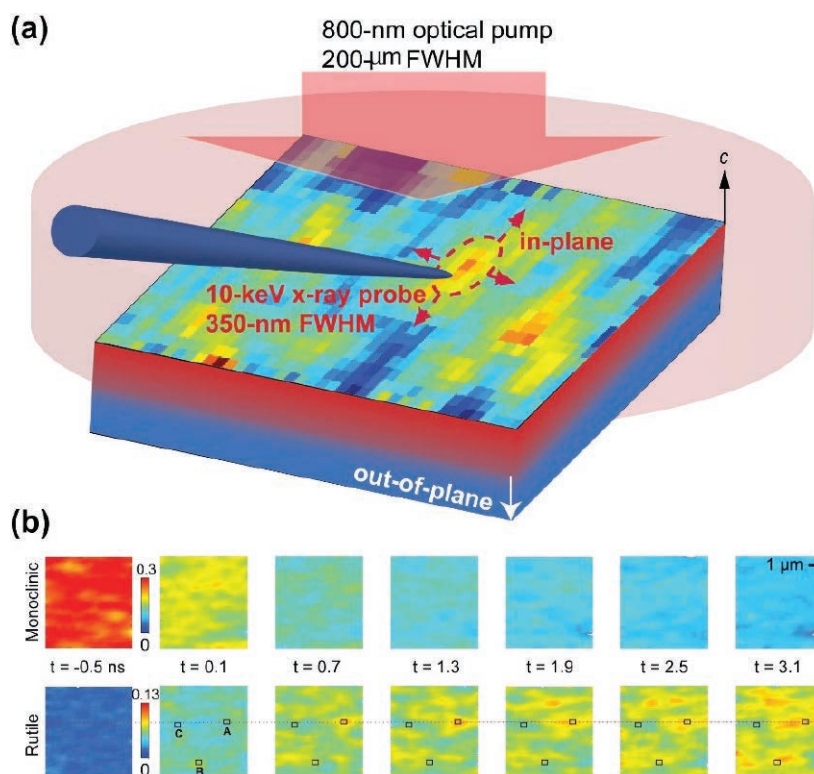


Fig. 1. (a) Experimental setup of the laser pump/hard x-ray diffraction microscopy probe technique. The structural phase progression of a  $\text{VO}_2$  film along in-plane and out-of-plane directions, indicated by red and white arrows, respectively, is probed by synchrotron-based focused x-ray pulses upon homogenous optical excitation along the in-plane direction. The blue and red regions represent monoclinic (M) and rutile (R) phases respectively. (b) The intensity maps of the M and R phases measured at a sequence of time delays excited by an optical pulse with a fluence of  $1.4 \text{ mJ}/\text{cm}^2$ . The x-ray diffraction intensity from the M phase regions decreases after laser excitation, while the R phase regions emerge at discrete sites (e.g., site A) and spread out in the thin film. The color bars show the normalized diffraction intensity.

*“Bragg” cont’d. from page 198*

demonstrates that vwBCDI preserves the strain-sensitive 3-D imaging capability of current rocking-curve-based BCDI methods without requiring any sample motion. This capability will greatly simplify certain *in situ* strain measurements in environments in which it is difficult to accurately rotate the sample about a precise center of rotation or is otherwise cumbersome. Currently the new method does not incorporate the energy dependence of the scattering factor. Thus, vwBCDI scans should be performed far away from absorption edges of the elements in the sample. However, enabling element-sensitive vwBCDI may be feasible with near-edge energy scanning, if additional resonant scattering effects are incorporated into the phase-retrieval algorithm. — *Vic Comello*

**See:** W. Cha<sup>1</sup>, A. Ulvestad<sup>1</sup>, M. Allain<sup>2</sup>, V. Chamard<sup>2</sup>, R. Harder<sup>1</sup>, S.J. Leake<sup>3</sup>, J. Maser<sup>1</sup>, P.H. Fuoss<sup>1</sup>, and S.O. Hruszkewycz<sup>1\*</sup>, “Three Dimensional Variable-Wavelength X-Ray Bragg Coherent Diffraction Imaging,” *Phys. Rev. Lett.* **117**, 225501 (2016).

DOI: 10.1103/PhysRevLett.117.225501

**Author affiliations:** <sup>1</sup>Argonne National Laboratory, <sup>2</sup>Aix-Marseille University, CNRS, <sup>3</sup>The European Synchrotron Radiation Facility

**Correspondence:** \* shrus@anl.gov

Development of variable x-ray wavelength transforms was supported by the U.S. Department of Energy (DOE) Office of Science-Basic Energy Sciences, Materials Sciences and Engineering Division. Creation of back-projection operators for Bragg diffraction was partially funded by the French Agence Nationale de la Recherche under Project No. ANR- 11-BS10-0005. Sample preparation was supported by Engineering and Physical Sciences Research Council Grant No. EP/D052939/1. The authors gratefully acknowledge the Advanced Photon Source X-ray Science Division Optics Group for help with sample preparation. This research used resources of the Advanced Photon Source, a U.S. DOE Office of Science User Facility operated for the DOE Office of Science by Argonne National Laboratory under Contract No. DE-AC02-06CH11357.

34-ID-C • XSD • Materials science, physics • Coherent x-ray scattering • 5-15 keV • On-site • Accepting general users •

*“Mesoscopic” cont’d. from page 199*

during the photo-induced phase transition.

Time-resolved mapping of the real-space structural transformation was achieved by tracking the Bragg diffraction signatures of the structural phases. The first stage in the phase transition is a symmetry change from the monoclinic (M) state to the rutile (R) state at isolated nucleation sites on the unit-cell level, which occurs on a femtosecond time scale following optical excitation (Fig. 1b). These nucleation sites possibly relate to both local strain states that favor the stabilization of the high-temperature R phase and variations in grain size, since smaller single crystalline particles require less activation energy for the phase transition.

At this point, the optical excitation has created an unstable high-energy M state in which the energy to supply the latent heat for the transition to the R state has already been stored at the electronic level. The second stage occurs when the lattice is superheated above the transition temperature a few picoseconds later, as a result of electron-phonon coupling during which the absorbed radiation energy is transferred to the lattice. At this stage, the M state film has sufficiently high energy for the structural phase transition, but a lattice symmetry change has not yet occurred. The third stage is a domino-like lattice transformation propagating from the nucleation sites into the excited but not yet transformed M state film. This process is a displacive lattice transformation, in which the lattice symmetry change results from straightening V–V atom pairs without diffusive heat transport. The displacive lattice transformation occurs at a speed that is faster than in-plane thermal diffusion but slower than the sound speed in VO<sub>2</sub>.

The visualization of phase transformations by means of the time-resolved x-ray imaging technique opens new opportunities for studying ultrafast nanoscale phase transitions and separations in correlated materials. Further studies using the same technique on different VO<sub>2</sub> thin films will reveal, for example, the dependence of phase progression speed on grain size and crystalline orientations. These insights are important not only for understand-

ing mesoscale phase transformations but also for designing ultrafast optoelectronic devices using VO<sub>2</sub>. For example, faster structural phase transformations as a whole may occur in VO<sub>2</sub> with more nucleation sites, while a faster phase front progression that approaches the sound speed may occur in ultrathin VO<sub>2</sub> films that contain fewer grain boundaries. — *Vic Comello*

**See:** Yi Zhu<sup>1</sup>, Zhonghou Cai<sup>1</sup>, Pice Chen<sup>2†</sup>, Qingteng Zhang<sup>2††</sup>, Matthew J. Highland<sup>1</sup>, Il Woong Jung<sup>1</sup>, Donald A. Walko<sup>1</sup>, Eric M. Dufresne<sup>1</sup>, Jaewoo Jeong<sup>3</sup>, Mahesh G. Samant<sup>3</sup>, Stuart S.P. Parkin<sup>3,4</sup>, John W. Freeland<sup>1</sup>, Paul G. Evans<sup>2</sup>, and Haidan Wen<sup>1\*</sup>, “Mesoscopic structural phase progression in photo-excited VO<sub>2</sub> revealed by time-resolved x-ray diffraction microscopy,” *Sci. Rep.* **6**, 21999 (2016).

DOI: 10.1038/srep21999

**Author affiliations:** <sup>1</sup>Argonne National Laboratory, <sup>2</sup>University of Wisconsin-Madison, <sup>3</sup>IBM Almaden Research Center, <sup>4</sup>Max Planck Institute for Microstructure Physics Present addresses: <sup>†</sup>Northwestern University, <sup>††</sup>Argonne

**Correspondence:** \* wen@aps.anl.gov

Work at Argonne was supported by the U.S. Department of Energy (DOE), Office of Science, Office of Basic Energy Sciences, under Contract No. DE-AC02-06CH11357. H.W. and J.F. acknowledge the support for the data analysis from the DOE, Office of Science, Office of Basic Energy Sciences, under Contract No. DE-SC0012375. Work at the University of Wisconsin was supported by the DOE, Office of Basic Energy Sciences, Division of Materials Sciences and Engineering, through Grant No. DEFG02-10ER46147. This research used resources of the Advanced Photon Source, a U.S. DOE Office of Science User Facility operated for the DOE Office of Science by Argonne National Laboratory under Contract No. DE-AC02-06CH11357.

7-ID-B,C,D • XSD • Materials science, atomic physics, chemistry • Time-resolved x-ray scattering, time-resolved x-ray absorption fine structure, phase contrast imaging • 6-21 keV • On-site • Accepting general users •

# PROBING THE MECHANICS OF PROTEIN FUNCTION

Proteins are complex biological machines that we are just beginning to understand. They perform almost all of the activities of the cell from DNA replication to cellular motility. However, while the chemistry of many protein interactions has yielded to investigation, the physics has been harder to access experimentally. Just as it is important to understand the internal mechanics of larger machines in order to understand how they function, understanding the mechanics underlying different protein conformational states is key to understanding the relationships between protein structure and function. Unlike macroscopic machines, the mechanics that govern protein conformational changes are mediated through a collection of weak, heterogeneous interactions that are hard to capture both spatially and temporally. Work at the APS has made an important first step to answering these fundamental questions by developing a model system in which they can stimulate and record the movements of atoms within proteins in a crystal. These findings lay the groundwork for developing tools that will provide a deeper understanding of the mechanics of protein structural changes and their relationship to biological functions. This work has the potential to impact a diverse range of fields where understanding and manipulating protein function may have important applications such as in the design of new medicines and in biomechanical engineering.

The technique is called electric field-stimulated x-ray crystallography (EF-X) and involves applying an electric field to a protein crystal while simultaneously collecting x-ray data using fast x-ray pulses. The electric field pulses drive motions within the protein crystal which can then be recorded in sub-microsecond time frames. The theory is based on the idea that charged groups and atoms with dipoles will be affected by the electric field and will move in response to the field. However, the question is, will these movements be biologically relevant? That is, will the atoms move to conformations that are adopted by the protein during its normal functions?

The team of researchers from UT Southwestern Medical Center and The University of Chicago had two concerns regarding the set-up of the experiment.

*"Function" cont'd. on page 203*

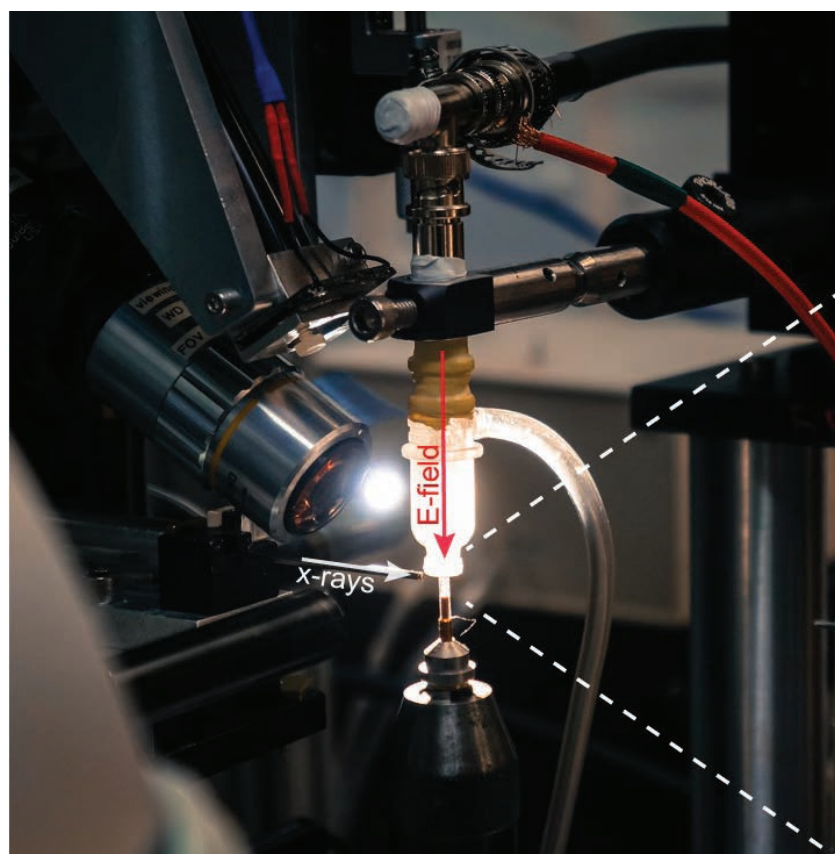
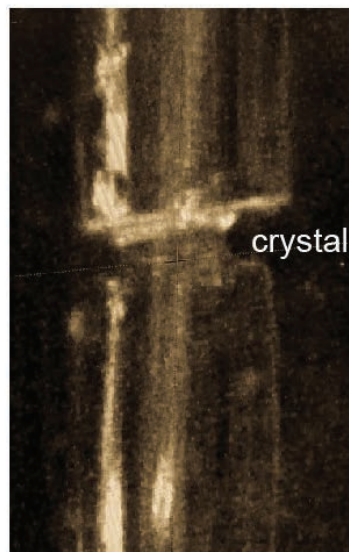


Fig. 1. Image of the custom-made EF-X crystallography set-up. The left panel shows how the apparatus that holds the crystal and applies the electric field pulse (red arrow) is positioned relative to the x-ray beam (white arrow). The right panel shows a close-up of the protein crystal held between two glass capillaries that serve as electrodes. The crystal is glued to the bottom electrode while the electric field pulse is transmitted through the top electrode.





# AN X-RAY VISION OF A METAL 3-D PRINTING PROCESS

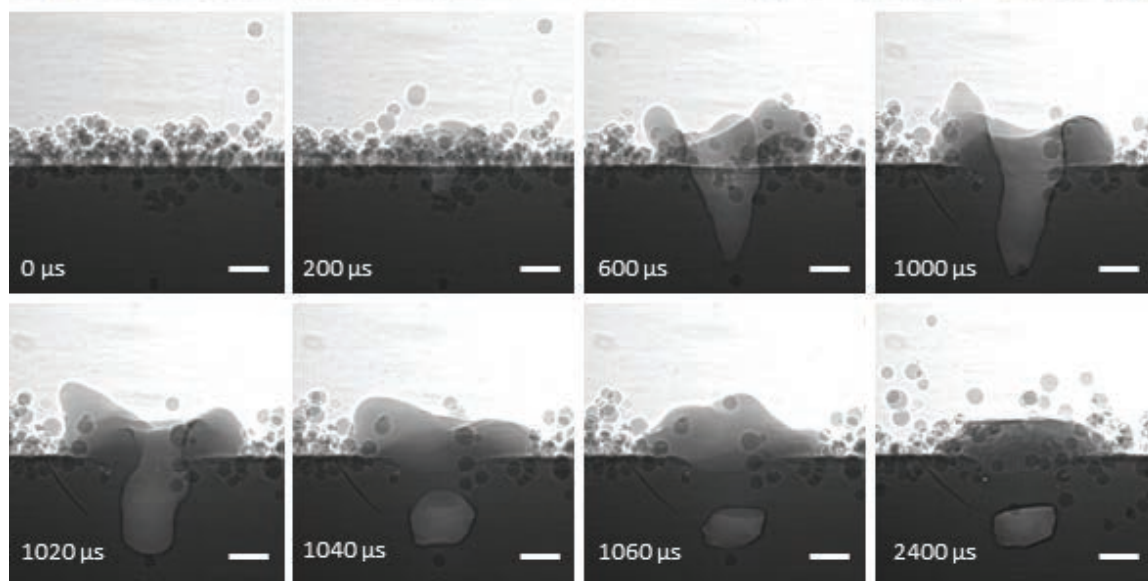
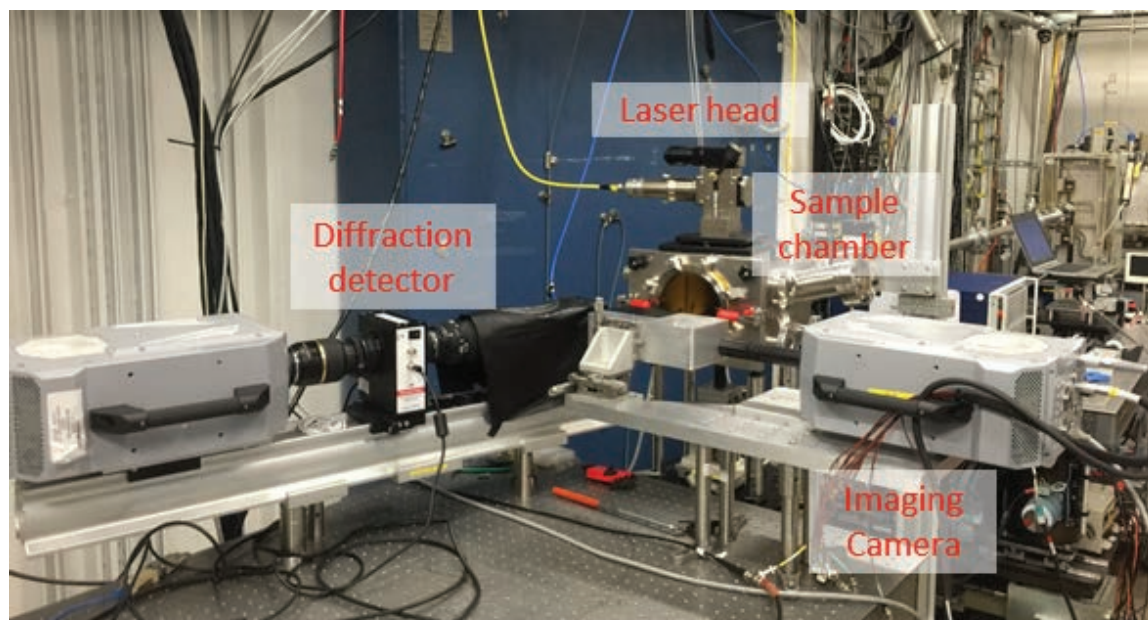


Fig. 1. (a) Setup of the high-speed x-ray experiment on laser powder bed fusion process at beamline 32-ID-B. (b) High-speed x-ray images of laser powder-bed fusion, showing a keyhole mode melting process. The scale bar is 100  $\mu\text{m}$ .

Additive manufacturing (AM), aka, three-dimensional (3-D) printing of metallic materials, has advanced rapidly over the past three decades. The worldwide research efforts in recent years have largely transformed the metal AM from means for rapid prototyping to full production mode, particularly in medical, aerospace, automobile, and de-

fense industries. AM exhibits unique advantages over traditional cutting and milling techniques, including more efficient use of raw materials, less generation of hazard waste, less consumption of energy, shorter supply chain, reduced time to market, and most importantly, the fabrication of products with extreme complexities.

Laser powder bed fusion (LPBF) is a widely used AM technique for building metal parts, in which a laser is scanned across a thin layer of metallic powders, and locally melts the powders to the bottom layer. There are many phenomena involved in the LPBF process, including but not limited to, melting and partial vaporization >>

<< of metallic powders, flow of the molten metals, powder spatter ejection, rapid solidification, non-equilibrium phase transition, etc. These physical processes are highly dynamic and transient due to the extremely high heating and cooling rates in LPBF. Oftentimes, their complex interplays result in a product with rough surface, large porosity and residual stress, and/or unfavorable phase and grain structures. These structure defects largely degrade the performance of the manufactured parts.

In order to understand the mechanisms responsible for the formation of various structure defects in additively manufactured parts, it is essential to develop and apply *in situ* characterization techniques to monitor the dynamic microstructural evolution in real time. However, due to the highly transient nature of the laser-metal interaction, experimentally characterizing the dynamics of the LPBF process has been challenging.

A team of researchers from the XSD Imaging Group, with collaborators from Argonne, Carnegie Mellon University, and Missouri University of Science and Technology addressed this issue by applying high-speed synchrotron x-ray imaging and diffraction techniques. The team demonstrated that quantitative structural information on melt pool size/shape, powder ejection, solidification, and phase transformation can be obtained from high resolution, time-resolved x-ray images and diffraction patterns.

The experiment platform and the data analysis algorithms they developed will help researchers not only understand the physics underpinning the formation of different defects, but also build high-fidelity models to guide the process optimization for manufacturing parts with different geometries and dimensions.

Contact [taosun@aps.anl.gov](mailto:taosun@aps.anl.gov)

C. Zhao, K. Fezzaa, R. Cunningham, H. Wen, F. De Carlo, L. Chen, A. Rollett, and T. Sun, "Real-time monitoring of laser powder bed fusion process using high-speed x-ray imaging and diffraction," submitted.

#### "Function" cont'd. from page 201

First, what electric field strength would be appropriate to use, and, second, what protein could they use that undergoes known interactions that are representative of a typical protein so they can apply the technique to other crystals? For the first question, they calculated that an electric field strength of 1,000,000 V/cm (1 MV/cm) would drive the atomic motions they wanted to look at. This sounds dangerously large but is actually close to what has been calculated for physiological voltages across cellular membranes at 0.125 MV/cm (100 mV) and, therefore, is a biologically relevant voltage. Happily, the team was able to apply this electric field to protein crystals without overheating and blowing them up, a critical part of the experiment.

The next challenge was to define the model protein. They chose a protein domain called PDZ that undergoes known changes when it binds to its ligand and also exhibits structural movements away from the site of binding that are translated throughout the protein. This gave the team the opportunity to observe structural changes that are typical of many proteins.

The experiment was conducted by building a custom set-up for x-ray diffraction (Fig. 1). The whole apparatus was then placed into the x-ray facility at the BioCARS 14-ID-B beamline at the APS for data collection. Some high-resolution data was also collected at the Stanford Synchrotron Radiation Lightsource beamline 11-1.

The results of the experiment were exactly what the team had hoped for. The crystals were able to tolerate 100-500-ns pulses of 1-MV/cm and the x-ray data showed that amino acid side chains, solvent atoms, and backbone atoms move in response to the field. Interestingly, PDZ forms crystals with four differently-oriented monomers in each crystal unit and these monomers break symmetry under the influence of the electric field. This causes the atoms of two of the monomers to move one way in the field and the atoms of the other two to move the other way, providing an internal control for distinguishing real motions from those that are caused by overheating or crystal damage. More importantly, however, the team was

able to correlate the motions observed in the electric field-stimulated crystal with known conformations of PDZ, indicating that the changes they see are likely to be biologically relevant. This finding paves the way to the study of other proteins and their mechanics.

— Sandy Field

See: Doeke R. Hekstra<sup>1†</sup>, K. Ian White<sup>1</sup>, Michael A. Socolich<sup>1</sup>, Robert W. Henning<sup>2</sup>, Vukica Šrajer<sup>2</sup>, and Rama Ranganathan<sup>1\*</sup>, "Electric-field-stimulated protein mechanics," *Nature* **540**, 400 (15 December 2016).

DOI: 10.1038/nature20571

Author affiliations: <sup>1</sup>UT Southwestern Medical Center, <sup>2</sup>The University of Chicago <sup>†</sup>Present address: Department of Molecular and Cellular Biology and School of Engineering and Applied Sciences, Harvard University

Correspondence:

\* [rama.ranganathan@utsouthwestern.edu](mailto:rama.ranganathan@utsouthwestern.edu)

We thank the staff at BioCARS, the Stanford Synchrotron Radiation Lightsource, and the UT Southwestern Medical Center Structural Biology Laboratory for technical support.

R.R. acknowledges support from National Institutes of Health (NIH) grant R01GM123456, the Robert A. Welch Foundation (I-1366), the Lyda Hill Endowment for Systems Biology, and the Green Center for Systems Biology. BioCARS is supported by NIH grant R24GM111072 and through a collaboration with P. Anfinrud (NIH/ National Institute of Diabetes and Digestive and Kidney Diseases). The Stanford Synchrotron Radiation Lightsource is supported by the U.S. Department of Energy (DOE) Contract No. DE-AC02-76SF00515) and by the NIH (P41GM103393). This research used resources of the Advanced Photon Source, a U.S. DOE Office of Science User Facility operated for the DOE Office of Science by Argonne National Laboratory under Contract No. DE-AC02-06CH11357.

14-ID-B • BioCARS • Life sciences, materials science, physics, chemistry • Time-resolved crystallography, time-resolved x-ray scattering, Laue crystallography, wide-angle x-ray scattering, biohazards at the BSL2/3 level, macromolecular crystallography • 7-19 keV • On site • Accepting general users •



# A GRAPHENE WINDOW TO BETTER MICROFLUIDICS

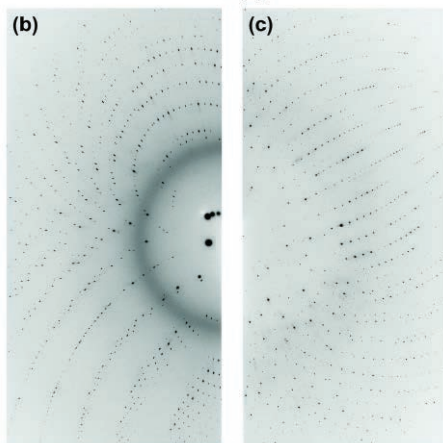
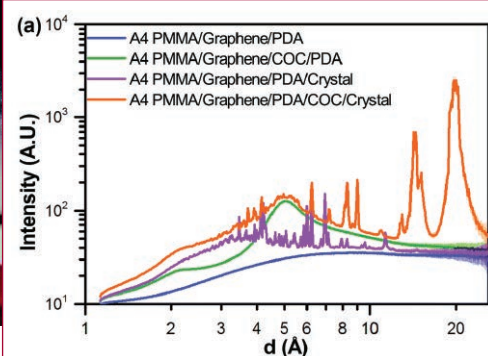
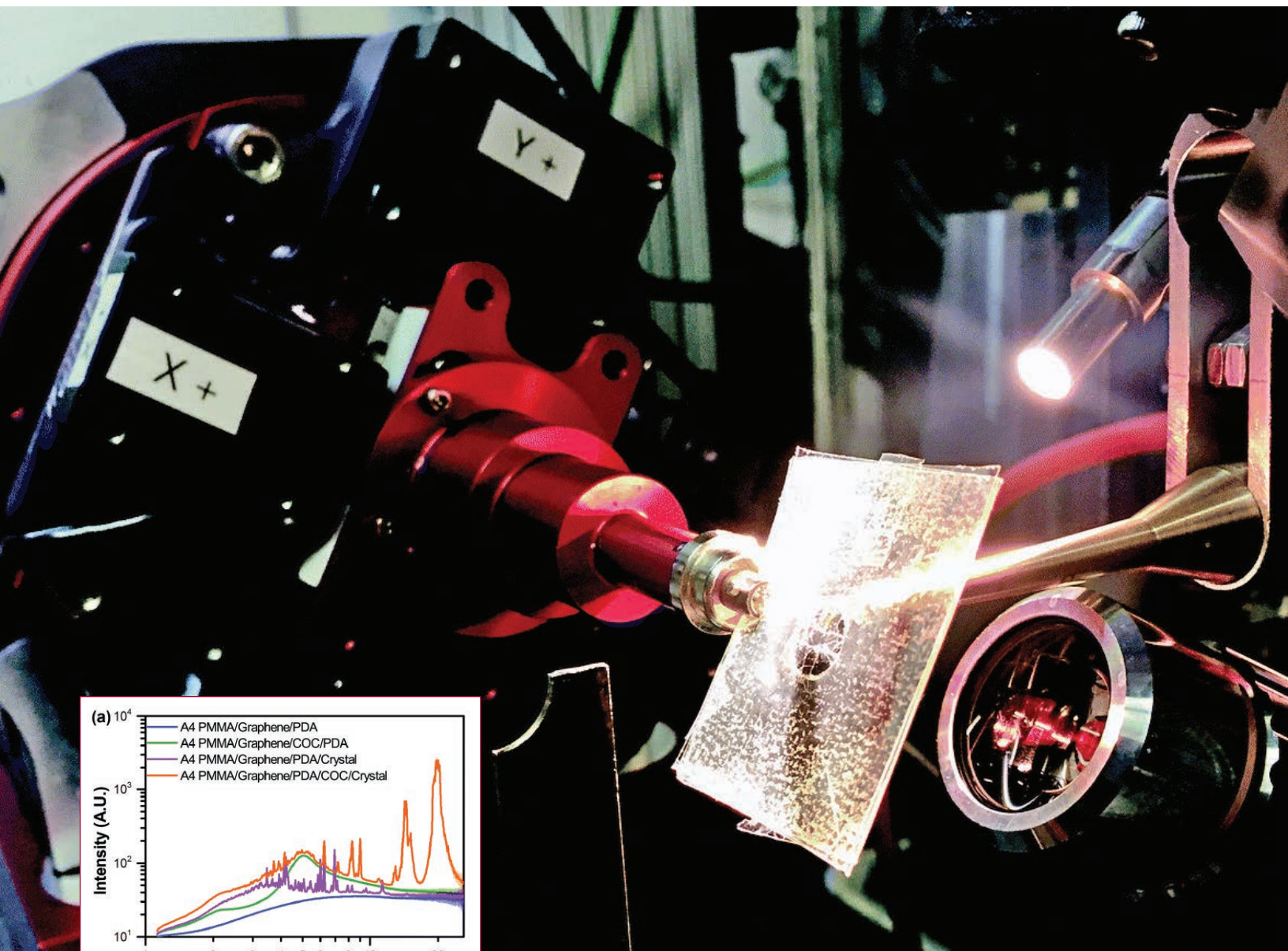


Fig. 1 (above). A microbatch-style graphene-based microfluidic chip mounted at the 14-ID-B station at the APS.

Fig. 2 (left). (a) One-dimensional integrated x-ray intensity profiles showing the relative strength of the observed diffraction signal from a HEWL crystal compared to the noise resulting from background scattering due to the presence of device materials as a function of resolution. The corresponding two-dimensional diffraction images for the (b) A4 PMMA/graphene/PDA/COC/crystal dataset (orange), and the (c) A4 PMMA/graphene/PDA/crystal dataset (magenta) shown in (a). Both figures: S. Sui et al., *Lab Chip* **16**, 3082 (2016). © The Royal Society of Chemistry 2016

14-ID-B • BioCARS • Life sciences, materials science, physics, chemistry • Time-resolved crystallography, time-resolved x-ray scattering, Laue crystallography, wide-angle x-ray scattering, biohazards at the BSL2/3 level, macromolecular crystallography • 7-19 keV • On site • Accepting general users •



Working with protein microcrystals can be an enormously challenging endeavor. Aside from their extremely small size, microcrystals can be delicate, difficult to handle, and susceptible to radiation damage from x-ray diffraction studies. Microfluidic “lab-on-a-chip” technologies offer some highly promising ways to circumvent these difficulties, but can bring with them new problems to overcome. A team of experimenters from the University of Massachusetts Amherst and The University of Chicago utilized high-brightness x-rays from the APS as they developed a new strategy to combat these limitations by combining microfluidics with another cutting-edge technology, single-layer graphene, for serial protein crystallography in an ultrathin microfluidic chip.

In serial crystallography, protein crystals are characterized by combining data from many smaller crystals to provide a complete dataset. Microfluidic devices can make this process much easier and more efficient than bulk crystallization techniques, providing an environment in which hundreds or even thousands of microcrystals can be grown under precisely controlled conditions and preserved for long periods.

But there are nagging problems with this process, among them the inevitable attenuation of the x-ray beam as it passes through the microfluidic device, which is generally made of glass, plastic, or PDMS (poly(dimethylsiloxane)) material. Creating thinner devices that are more amenable to x-ray transmission is technically difficult and can allow the loss of water with subsequent sample dehydration.

These are the issues that the research team sought to overcome.

Inspired by recent work in which a graphene layer wrapping protected protein crystals from dehydration with only limited beam attenuation, the team fashioned a thin film of graphene and a support layer of PMMA (poly(methylmethacrylate)) for use as a diffusion barrier in a microfluidic chip. Including this combined ~1- $\mu$ m-thick PMMA/graphene window, the chip comprised five layers, with microfluidic channels cut into a ~100- $\mu$ m-thick COC (cyclic olefin copolymer) film. The team examined the composition and quality of the device using Raman spectroscopy, permeability measurements, and atomic force microscopy, all of which confirmed the microchip structure.

As a practical demonstration of the advantages of graphene-based mi-

crofluidics, the researchers used their device to determine the crystal structure of hen egg white lysozyme (HEWL). They conducted x-ray diffraction studies at the BioCARS 14-ID-B beamline at the APS, collecting multiple data frames at different beam angles using a polychromatic, 12-keV x-ray beam (Fig. 1).

With the graphene layer doing double duty as both an x-ray window with low beam attenuation and high signal-to-noise, and also as a diffusion barrier to prevent evaporation, the research team performed microbatch and counter-diffusion crystallization trials with the HEWL model system. Crystals formed easily and quickly inside the device and remained stable for days to weeks afterward, remaining undisturbed even after they were shipped from the lab to the APS facility for study.

Observations of background scattering and signal-to-noise (Fig. 2) showed that both were excellent, particularly in comparison to previous mounting strategies for serial crystallography, which were approximated for these experiments by collecting data on crystals through a ~100- $\mu$ m-thick COC layer. The high quality of data was maintained even when considering variations in the incidence angle of the x-ray beam resulting from variations in sample orientation. The experimenters' device displayed a signal transmission of 99.9% even up to a  $\pm 55^\circ$  rotation, compared to previously reported PDMS/COC-based chips where a maximum of 77% transmission could only be achieved in the absence of rotation. High-quality, high-resolution images and diffraction data were obtained in various configurations compared to mi-

crofluidic devices constructed of more traditional materials.

The investigators plan to expand on this work with further experiments to enable structure determination of novel protein targets and ultimately time-resolved structural studies of protein dynamics. Although this research concentrates on protein crystallography, the strategies for microfluidic device fabrication could have broad applications across many disciplines, including DNA analysis and microarrays, pathology and medical diagnostics, nanotechnology, biophysics—essentially every field that makes use of microfluidics and lab-on-a-chip technologies.

— Mark Wolverton

**See:** Shuo Sui<sup>1</sup>, Yuxi Wang<sup>1</sup>, Kristopher W. Kolewe<sup>1</sup>, Vukica Srajer<sup>2</sup>, Robert Henning<sup>2</sup>, Jessica D. Schiffman<sup>1</sup>, Christos Dimitrakopoulos<sup>1</sup>, and Sarah L. Perry<sup>1\*</sup>, “Graphene-based microfluidics for serial crystallography,” *Lab Chip* **16**, 3082 (2016).

DOI: 10.1039/C6LC00451B

**Author affiliations:** <sup>1</sup>The University of Massachusetts Amherst, <sup>2</sup>The University of Chicago

**Correspondence:**

\* perrys@engin.umass.edu

K.W. K. was supported by National Research Service Award T32 GM008515 from the National Institutes of Health (NIH). Use of BioCARS was supported by the National Institute of General Medical Sciences of the NIH under grant number R24GM111072. This research used resources of the Advanced Photon Source, a U.S. Department of Energy (DOE) Office of Science User Facility operated for the DOE Office of Science by Argonne National Laboratory under Contract No. DE-AC02-06CH11357.

# FAST FIND FOR POLYMER GRATING ROUGH EDGES

Gratings are used to filter particles with dimensions from millimeters to micrometers; they are also used to split and diffract light in scientific instruments and security "holograms" on credit cards and products. Gratings are even used to lay out the basic nanoscale patterns for making the integrated circuits at the heart of every modern electrical device, from smart phone to smart refrigerator. Fitting more circuits in these devices requires high-fidelity gratings with smaller separations, even below 10 nanometers. A new approach to studying the imperfections in such gratings could be used to make the smoother and better at their job. That is the goal of new research carried out at the APS. The results point to a tried-and-true synchrotron x-ray research technique as a potentially effective tool for examining the surfaces and internal structures of gratings down to the nanoscale level.

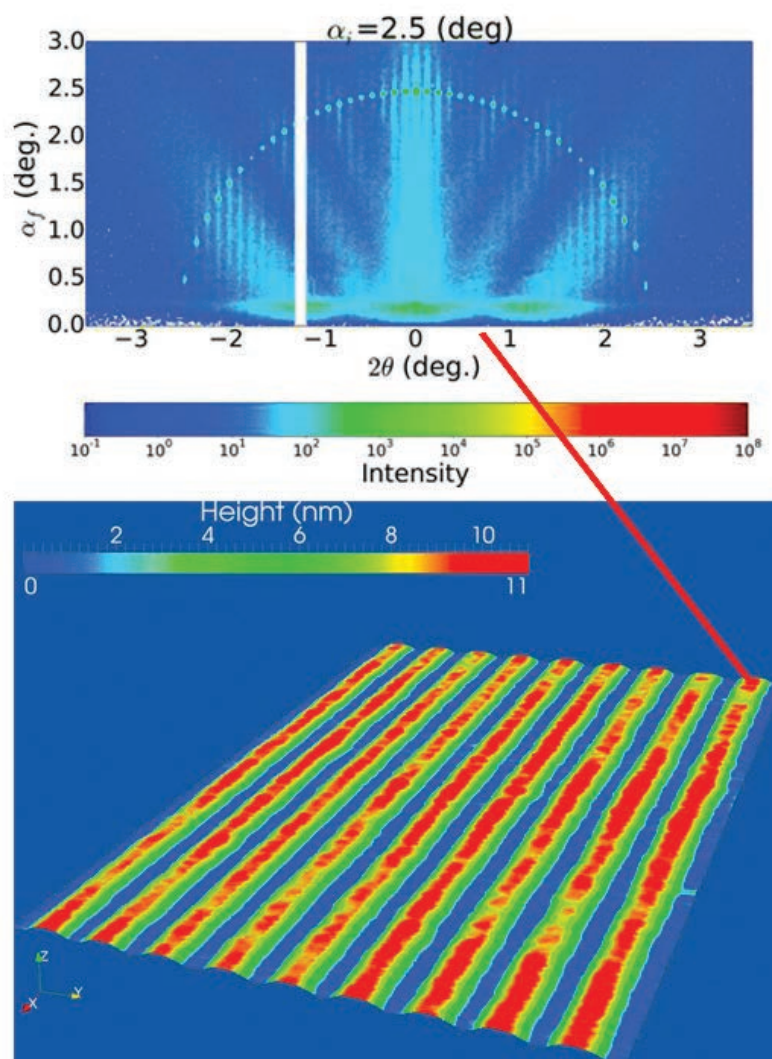
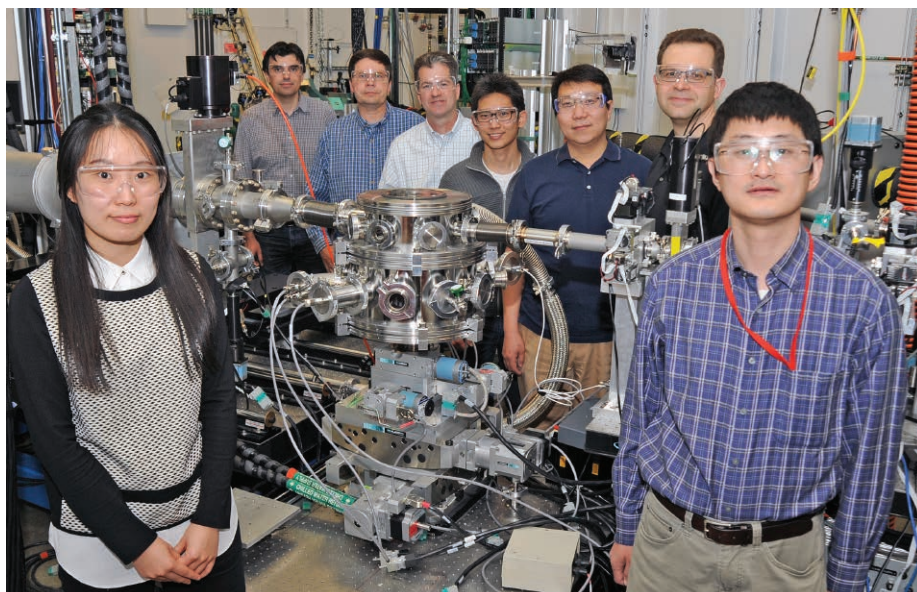


Fig. 1. GISAXS measurements probe quantitatively the fidelity of nanometer-sized polystyrene gratings. From H. S. Suh et al., *J. Appl. Cryst.* 49, 823 (2016). © International Union of Crystallography

Characterizing imperfections at very small length scales in gratings used in a wide variety of technological applications is a challenging problem and one that is absolutely critical to many areas of science. Modern research in filtering processes, scientific measurements, and chip manufacturing could all be improved by a clearer understanding of gratings. Researchers from The University of Chicago and Argonne used grazing-incidence small-angle x-ray scattering (GISAXS) to examine polymer gratings manufactured by IMEC (Belgium). The researchers found that GISAXS can reveal flaws efficiently and even more accurately than state-of-the-art atomic force microscopy and so allow manufacturers to implement new schemes for quality control, and design new and improved products.

Polymer gratings used in a wide range of applications consist of regularly spaced arrays of shapes arranged in parallel. These patterns can have functional detail at a wide range of lengths, from visible spacing to microscopic and then nanoscale features. Checking that they are made with precision and suitable for a given job can be done with a microscope. Specifically, for the fine gratings used in scientific instrumentation, scanning electron microscopy, transmission electron microscopy, atomic force microscopy, and variations and combinations of those techniques can be used. These sophisticated techniques are costly to employ as well as suffering from a frustrating drawback: They can only examine a tiny area of any given grating at a time (Fig. 1). This limitation of microscopy means that the time required to check a complete grating can be prohibitive. In contrast, there are several x-ray techniques—such as x-ray scattering—that can probe with nanoscopic detail a large surface area very quickly at high resolution. Indeed, various x-ray scattering techniques have been used over the last decade or more to examine gratings. However, even these techniques have limitations.

But the reflection-mode technique GISAXS involves exposing the surface of the sample to a focused synchrotron x-ray beam at a grazing incidence angle rather than perpendicular. The large area of a sample in this setup dramati-



Several of the study's co-authors shown in the beamline 8-ID-E research station with the sample environment that was developed for this project under a partner-user proposal led by Paul Nealey and Wei Chen. From left to right: Xuanxuan Chen, Manolis Doxastakis, Mike Fisher (XSD, the sample chamber designer), Paul Nealey, Hyo Seon Suh, Wei Chen, Joseph Strzalka, and Zhang Jiang. Not pictured are co-authors Paulina A. Rincon-Delgadillo, Jin Wang, Roel Gronheid, Juan J. de Pablo, and Nicola Ferrier. This multi-sample vacuum environment has streamlined operations and is now used practically daily, by at least 75% of the 8-ID-E grazing-incidence scattering users.

cally enhances the intensity of the signal produced, which means measurements can be obtained very quickly compared to all other approaches. The technique also has the major benefit of extracting complete three-dimensional (3-D) information from the sample in a single step and requires none of the post-processing needed by other techniques to reconstruct the surface details in 3-D from what is essentially a two-dimensional scan.

A systematic study of GISAXS data acquired for polymer grating structures using different grazing angles at XSD beamline 8-ID-E at the APS shows just how well this technique works on a cross-linked polystyrene (xPS) nanoscale grating. Comparison with the much slower atomic force microscopy images from the same grating are coincident in the details they reveal, for instance showing the rough edges. This, the researchers suggest, points to GISAXS being a potentially useful technique for examining surface details of polymer gratings and even the internal structure of the components of the grating, which are all extracted in 3-D by the technique. — David Bradley

See: Hyo Seon Suh<sup>1,2</sup>, Xuanxuan

Chen<sup>1</sup>, Paulina A. Rincon-Delgadillo<sup>3</sup>, Zhang Jiang<sup>2</sup>, Joseph Strzalka<sup>2</sup>, Jin Wang<sup>2</sup>, Wei Chen<sup>1,2</sup>, Roel Gronheid<sup>3</sup>, Juan J. de Pablo<sup>1,2</sup>, Nicola Ferrier<sup>1,2</sup>, Manolis Doxastakis<sup>2\*</sup>, and Paul F. Nealey<sup>1,2\*\*</sup>, "Characterization of the shape and line-edge roughness of polymer gratings with grazing incidence small-angle X-ray scattering and atomic force microscopy," *J. Appl. Cryst.* **49**, 823 (2016).

DOI: 10.1107/S1600576716004453

**Author affiliations:** <sup>1</sup>The University of Chicago, <sup>2</sup>Argonne National Laboratory, <sup>3</sup>IMEC

**Correspondence:** \* edoxasta@utk.edu  
\*\* nealey@uchicago.edu

This research used resources of the Advanced Photon Source and the Center for Nanoscale Materials, which are U.S. Department of Energy (DOE) Office of Science user facilities operated for the DOE Office of Science by Argonne National Laboratory under contract No. DE-AC02-06CH11357.

8-ID-E • XSD • Materials science, polymer science, physics • Grazing incidence small-angle scattering, x-ray photon correlation spectroscopy • 7.35-7.35 keV, 11-11 keV • On-site • Accepting general users •



# ADDING WHITE X-RAYS FOR IMPROVED BRAGG COHERENT DIFFRACTION IMAGING

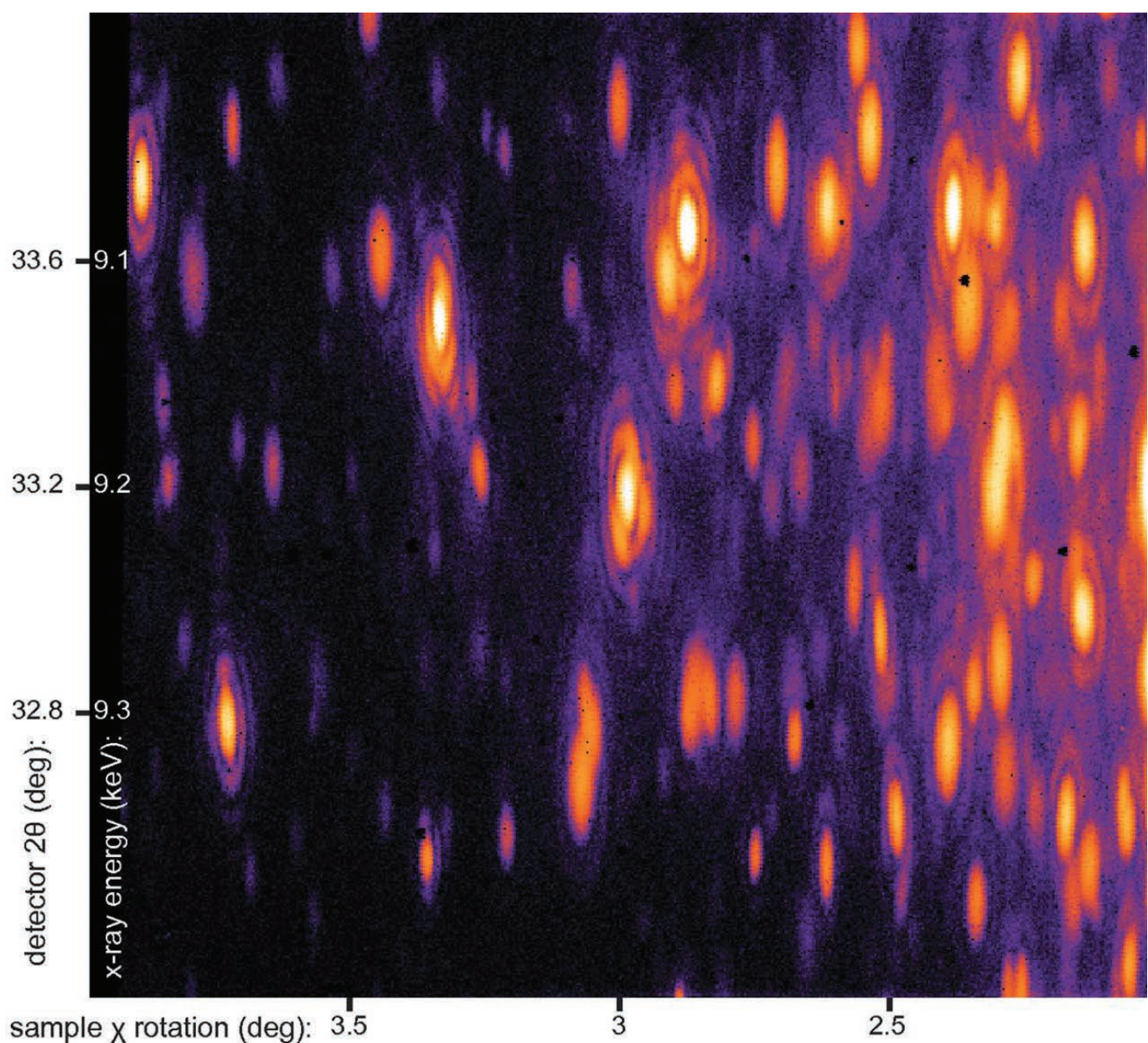


Fig. 1. Diffraction pattern derived from a beam of coherent white (polychromatic) x-rays, showing the Bragg peaks from gold nanoparticles situated on a silicon substrate. The white x-rays allow capture of the Bragg peaks from all the nanoparticles, even though they possess slightly different crystalline orientations. Due to a slight tilt of the silicon substrate, the majority of Bragg peaks are concentrated in the right half of the image.

The synchrotron x-ray research technique Bragg coherent diffraction imaging (BCDI) is especially useful for imaging crystalline nanoparticles. The APS produces the highly-intense, coherent (in-phase), and monochromatic (single-wavelength) x-rays required for high-resolution BCDI imaging. Although this technique is in some ways simpler than other imaging methods (e.g., no lenses are needed to image the sample), it nonetheless requires equipment and procedures that tend to complicate and constrain the imaging process. For one thing, samples must be rotated to achieve three-dimensional (3-D) images. Moreover, only samples with a specific crystallographic orientation can be imaged during an experiment. Researchers from Argonne have now circumvented these limitations by adding coherent white (polychromatic) x-rays to the BCDI protocol. In a demonstration experiment, white x-rays were used to scan a relatively large volume of gold nanoparticles (Fig. 1), each with its own crystalline orientation; 3-D imaging of individual nanocrystals was then achieved using monochromatic x-rays, without the need for sample rotation. This new BCDI technique is expected to allow scientists to select and three-dimensionally image individual nanocrystals within a large ensemble of crystallites, under a variety of strain and other conditions.

The “lensless” imaging technique, as coherent diffraction imaging (CDI) is sometimes called, was introduced in the late 1990s. CDI foregoes the use of image-forming lenses, instead relying upon a coherent beam of monochromatic radiation diffracted from a sample. An image is then extracted from the diffraction pattern using algorithm-based computer processing. Tomographic 3-D images can be obtained by rotating the sample through the beam. By using coherent monochromatic radiation of sufficiently small wavelength (namely x-rays or electron beams), CDI can produce high-resolution images of protein molecules, nanotubes, and other nanoscale particles (generally 400 nanometers or less). When applied to nanocrystals, the technique is more aptly called Bragg coherent diffraction imaging (BCDI), providing 3-D nanoscale imaging capabilities that are sensitive to strain within the nanocrystal being studied.

One drawback of present BCDI techniques is the difficulty imaging differently-oriented crystals within a volume. It would be beneficial to simultaneously examine all the constitutive nanoparticles and grains of a material, in spite of the wide range of crystalline orientations present, in order to form a comprehensive strain-sensitive image of the sample. Another difficulty of current BCDI techniques relates to sample rotation: the need to precisely rotate the

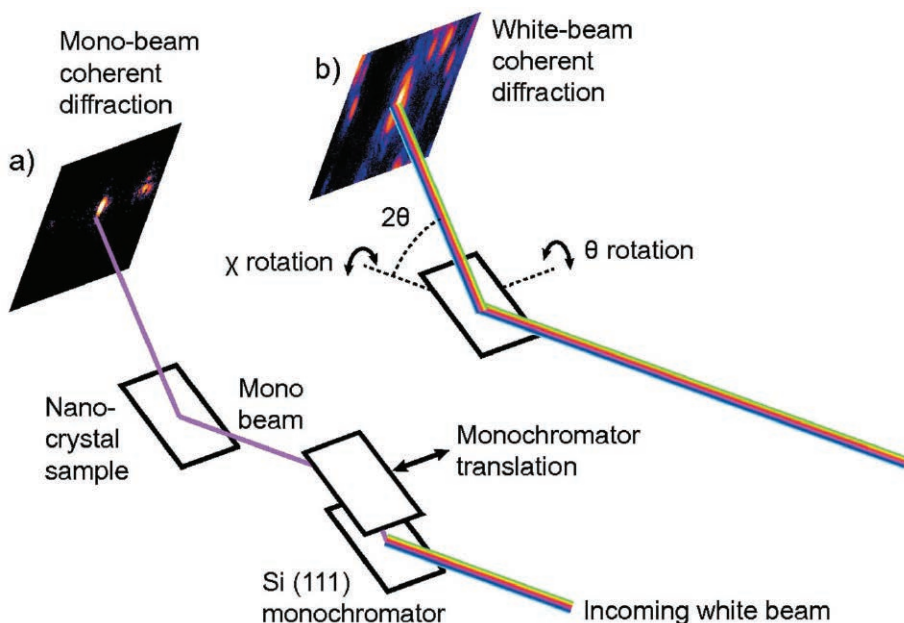


Fig. 2. The two basic configurations of the experiment. In both the lower (a) and upper (b) panels, a beam of coherent white x-rays comes from the right. In lower panel (a) an adjustable monochromator intercepts the white beam thereby delivering coherent monochromatic x-rays to the sample, which produces a typical coherent diffraction pattern from those few gold nanoparticles which meet the Bragg condition. Upper panel (b) shows the x-ray diffraction pattern with the monochromator absent. The beam of coherent white x-rays (embodying multiple wavelengths) reveals the orientation and size of numerous nanocrystals possessing a variety of crystalline orientations.

sample in tiny increments for 3-D imaging can limit the design of new experiments.

The two-stage BCDI process demonstrated in this study overcomes these limitations by first probing a complex crystalline sample with coherent white x-rays, followed by a series of coherent monochromatic x-rays of slightly

differing energies. The complex crystalline material investigated here consisted of gold nanoparticles on a silicon substrate, probed with x-rays derived from the XSD beamline 34-ID-E at the APS.

The basic experimental setup is depicted in Fig. 2. The upper portion of *“Imaging” cont’d. on page 211*



# PRECISELY MEASURING SMALL STRAINS IN TINY VOLUMES

Engineers designing integrated circuits often intentionally create small distortions of the structure as one way of enhancing the performance of semiconductor devices. Introducing this strain can change the semiconductor's electronic properties and affect parameters such as the current that can be driven through a field-effect transistor. Having a way to understand and control strain on very tiny scales could help in designing new generations of devices, from better fuel cells to circuits for quantum computers. Sorting out the effects of strains in an region 100 nm or less across, when the structure is expanding or shrinking by only one 100th of 1%, has been extremely challenging. Now a group of researchers has developed techniques that used a tightly focused x-ray beam at the APS to measure strain in small volumes. The method can be easily adapted to other material systems where there is a need to understand complex diffraction patterns. It could be applied to other semiconductor materials, as well as to complex oxide materials used in building fuel cells, in which strain can affect the catalytic activity of the oxide. >>

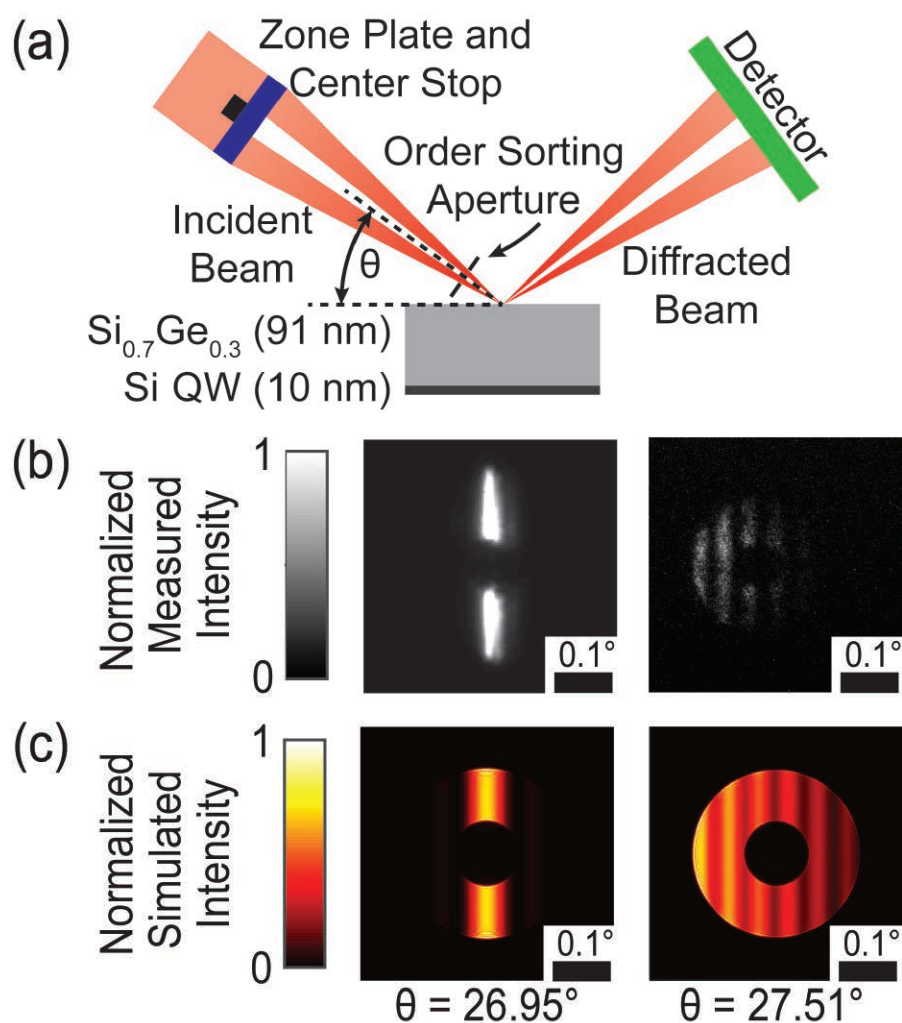


Fig. 1. In the experimental setup (a) a Fresnel zone plate focuses the x-ray beam onto a thin-film consisting of silicon and silicon-germanium layers. A detector measures the diffracted beam, revealing the intensity distribution (b). Researchers compare the intensity they measure to the intensity predicted by the simulation (c), allowing them to see small strains.

26-ID-C • CNM/XSD • Physics, materials sci  
• Nanodiffraction, nano-imaging, coherent x-ray scattering, synchrotron x-ray scanning tunneling microscopy • 6-12 keV • On-site • Accepting general users •



<< Researchers from the University of Wisconsin-Madison and Argonne studied the x-ray nanobeam diffraction patterns from a semiconductor structure that consisted of a 91-nm-thick layer of silicon-germanium and a 10-nm-thick film of silicon. In x-ray diffraction, an x-ray beam strikes a crystalline structure and produces a pattern, with varying x-ray intensity that depends on the arrangement of atoms within the structure and on the angle at which the beam hits the crystal. Such patterns reveal structural information about the portion of the sample with which the x-rays have interacted. One key advantage of the technique is that the x-rays can measure small strains without preparations that destroy the sample, so the subtle mechanical effects producing the strain are preserved.

The technique gets tricky when it's applied to strain in a small volume, however. In order to make the measurements on such tiny scales, the beam has to be focused to a very small spot. In this case, the researchers used a Fresnel zone plate to focus the beam to spot sizes approximately 30 to 50 nm across, producing an angular divergence on the order of 100ths of degrees. The Hard X-Ray Nanoprobe at APS beamline 26-ID-C, operated jointly by the APS and the Center for Nanoscale Materials (CNM) both of which are Office of Science user facilities, provided a narrow beam with a short x-ray wavelength to produce diffraction patterns from the crystal.

Though scientists have developed methods to interpret diffraction patterns, the addition of the focusing optics makes the pattern much more complex. To sort out this problem, the researchers calculated the diffraction patterns that should be produced by layered semiconductor structures. The method involves calculating the wave field of the focused x-ray beam, and of the beam after it is scattered by the sample. Propagating this scattered beam to the location of the detector produces an accurate simulation of the diffraction pattern and the variation of its intensity at different locations on the sample. Features such as interference fringes depend on the angle between the incoming x-ray beam and the sample, and provide information about the

mechanical distortion of the lattice. By comparing the simulated diffraction patterns with those produced by their experiment, the researchers could measure these quantities precisely in any spot on the sample and find the mechanical deformation caused by the stress. — *Neil Savage*

**See:** J.A. Tilka<sup>1</sup>, J. Park<sup>1</sup>, Y. Ahn<sup>1</sup>, A. Pateras<sup>1</sup>, K.C. Sampson<sup>1</sup>, D.E. Savage<sup>1</sup>, J.R. Prance<sup>1</sup>, C.B. Simmons<sup>1</sup>, S.N. Coppersmith<sup>1</sup>, M.A. Eriksson<sup>1</sup>, M.G. Lagally<sup>1</sup>, M.V. Holt<sup>2</sup>, and P.G. Evans<sup>1\*</sup>, "Combining experiment and optical simulation in coherent X-ray nanobeam characterization of Si/SiGe semiconductor heterostructures," *J. Appl. Phys.* **120**, 015304 (2016). DOI: 10.1063/1.4955043

**Author affiliations:** <sup>1</sup>University of Wisconsin-Madison, <sup>2</sup>Argonne National Laboratory

**Correspondence:** \* pgevans@wisc.edu

J.P., Y.A., A.P., and P.G.E. were supported by the U.S. Department of Energy (DOE) Office of Science-Basic Energy Sciences, Materials Sciences and Engineering, under Contract No. DE-FG02-04ER46147 for the x-ray scattering studies and analysis. J.A.T. acknowledges support from the National Science Foundation (NSF) Graduate Research Fellowship Program under Grant No. DGE-1256259. Development and maintenance of the growth facilities used for fabricating samples are supported by the U.S. DOE (DEFG02-03ER46028). The other authors acknowledge support from the Army Research Office (W911NF-08-1-0482, W911NF-12-1-0607) and NSF (DMR-1206915). This research used NSF-supported shared facilities supported by the University of Wisconsin Materials Research Science and Engineering Center (DMR-1121288). Use of the Center for Nanoscale Materials and the Advanced Photon Source, both Office of Science user facilities, was supported by the U.S. DOE Office of Science-Basic Energy Sciences, under Contract No. DE-AC02-06CH11357.

---

#### *"Imaging" cont'd. from page 209*

the schematic shows a beam of coherent white x-rays diffracting from the sample. An actual diffraction pattern produced with white x-rays is shown in Fig. 1. Each bright spot is caused by x-rays diffracting from an individual gold nanoparticle.

The simultaneous capture of the diffraction peaks from all the gold

nanoparticles is only possible due to the use of coherent white x-rays: because the gold nanoparticles are oriented in different directions, x-rays of different wavelengths are required to meet the many Bragg conditions present. (A Bragg condition occurs when x-rays diffracting from a single gold nanocrystal constructively interfere, yielding a bright x-ray "Bragg peak" that reveals its structure and orientation.)

The lower portion of Fig. 2 shows monochromatic x-rays being filtered from the white beam by an adjustable monochromator, which allows a range of single-wavelength x-rays to be selected. From the wide-area diffraction pattern of Fig. 1, the researchers chose a single nanoparticle for 3-D imaging. By using a series of monochromatic x-rays of slightly different wavelengths (~1 electron-volt increments), a data set suitable for 3-D imaging was obtained.

This step-wise procedure was carried out for the gold nanoparticle whose Bragg peak is located at the center of Fig. 1. The resulting 3-D data set revealed a faceted and circular (though somewhat flattened) gold nanoparticle, about 150 nanometers thick with a 360-nm maximum diameter. The researchers intend to use this data set to construct a 3-D image of the nanoparticle using a new variable-wavelength BCDI algorithm they recently developed. — *Philip Koth*

**See:** Wonsuk Cha, Wenjun Liu, Ross Harder, Ruqing Xu, Paul H. Fuoss, and Stephan O. Hruszkewycz\*, "Utilizing broadband X-rays in a Bragg coherent X-ray diffraction imaging experiment," *J. Synchrotron Rad.* **23**, 1241 (2016). DOI: 10.1107/S1600577516010523

**Author affiliation:**

Argonne National Laboratory

**Correspondence:** \* shrus@anl.gov

This work, including use of the Advanced Photon Source, was supported by the U.S. Department of Energy (DOE) Office of Science-Basic Energy Sciences, under Contract No. DEAC02-06CH11357. P.H.F. and S.O.H. were supported by the U.S. DOE-Basic Energy Sciences, Materials Sciences and Engineering Division.

34-ID-E • XSD • Materials science, physics, environmental science, geoscience • Microdiffraction, Laue crystallography, microbeam • 7-30 keV • On-site • Accepting general users •

# MAKING MORE-PERFECT THIN FILMS

**X**-rays reveal the structure of things we cannot otherwise see, like leg bones, and even tiny objects, like DNA chains, viruses, and individual atoms. As the size of the material being x-rayed shrinks, the individual objects that it comprises become more difficult to distinguish. X-ray images of extremely tiny materials are best when the materials are composed of identical objects arranged in a precise order, like a perfect crystal. These images can also be used to calculate statistical averages of disorder, but not to locate individual disorders. Researchers working at the APS have developed a new way of using coherent x-rays, specifically heterodyne mode x-ray photon correlation spectroscopy (XPCS), to study surfaces, interfaces, and bulk defects in thin films as the films are being grown. Mixed bulk and surface x-rays can pick out the speeds of small groups of atoms, providing a measure of the velocity of surface and subsurface features, such as voids and other defects. Once they are found, improved industrial techniques can be developed to create thin films with fewer imperfections.

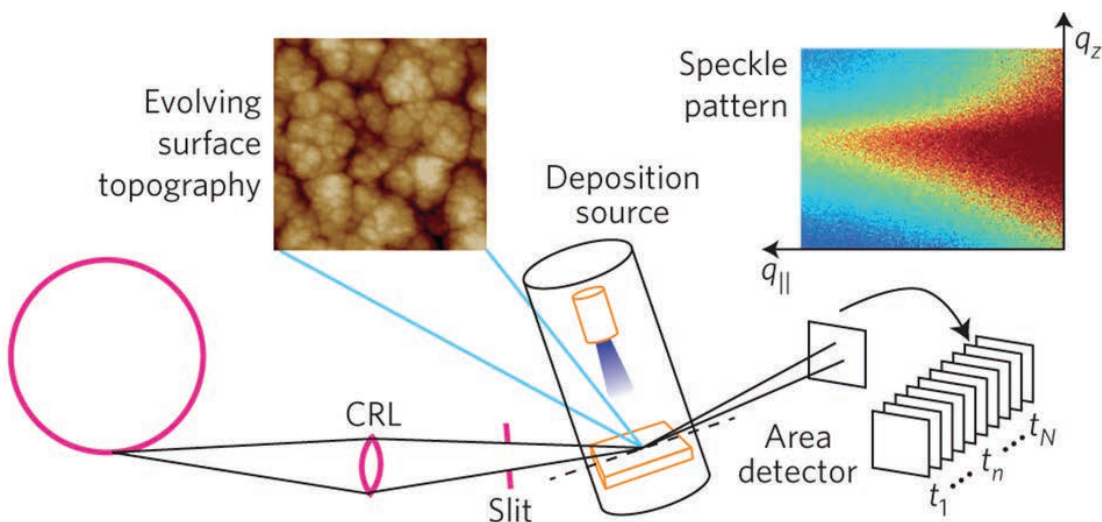


Fig. 1. X-rays from the APS are focused by a compound refractive lens (CRL) and a collimating slit system into an ultrahigh-vacuum sample enclosure. An amorphous thin film is deposited, which causes the surface to advance at the growth velocity and also induces random fluctuations in the surface roughness. Scattered coherent x-rays form a speckle pattern that corresponds to the detailed configuration of the surface, which is recorded versus time by a high-resolution photon-sensitive x-ray area detector. From J.G. Ulbrandt et al. *Nat. Phys.* **12**, 794 (AUGUST 2016). © 2016 Macmillan Publishers Limited, part of Springer Nature. All rights reserved.

Thin films are layers of materials that may be only fractions of nanometers in thickness, grown by deposition in a vacuum chamber. In one common technique for creating thin films, known as “sputtering,” a plasma knocks material from target atoms and onto the film surface. Thus far, researchers have been unable to monitor the deposition of atoms on the film during deposition because the atoms are too small to be imaged, but it is important to understand the interactions of surface and buried defects in thin films so that better ones can be created. X-rays have the potential to probe both surface and interior defects since they are highly penetrating and sensitive to features measuring mere nanometers. How-

ever, thus far x-ray patterns of thin films have been blurry because the arrangement of their atoms is complex and disordered, and subsurface study is extremely difficult, especially in real time as the films are being grown.

The researchers in this study, from the University of Vermont, Boston University, and Argonne, employed XPCS at XSD beamline 8-ID-I of the APS. Their approach improves x-ray scattering techniques by imposing order on the x-rays so that they can detect disorder in the material. Two types of defects are common in thin films:

nanocolumns that grow with the film surface as the layers are being deposited, and voids that form at the surface and are trapped. In XPCS, a scattered x-ray wave bounces off the surface of the thin film in response to nanocolumns. These waves mix with scattered waves of x-rays bouncing off the disordered defects, which are voids at and beneath the surface. The mixed x-rays indicate the motion of the voids and nanocolumns. Waves that bounce off the surface determine speed, because the rate at which the film

was deposited is known. Waves that bounce off interior defects in the subsurface develop oscillations because the irregularities cause the atoms to go different speeds. Once the defects are observed, they can be left to grow into the film or be eliminated. Even more important is that the XPCS technique can be used to monitor atoms in motion, even if they are moving independently and erratically, while the thin film is being made.

This new technique can lead to the creation of thin films that are smoother with fewer defects and voids. Increasing the quality of thin films improves their usefulness in a range of industrial, medical, and consumer

*“Films” cont’d. on page 213*

# A NEW IMAGING MODE USING A GERMANIUM ENERGY-DISPERSIVE STRIP DETECTOR

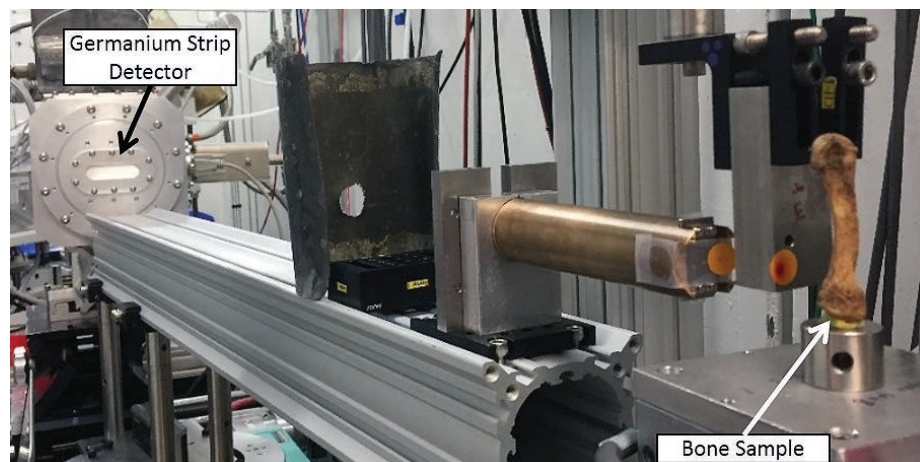


Fig. 1. The new Germanium Strip Detector at 6-BM-A,B is located at the far left in the photograph. A human second metacarpal bone from the Roman-era cemetery in the UK is at near right of the photo.

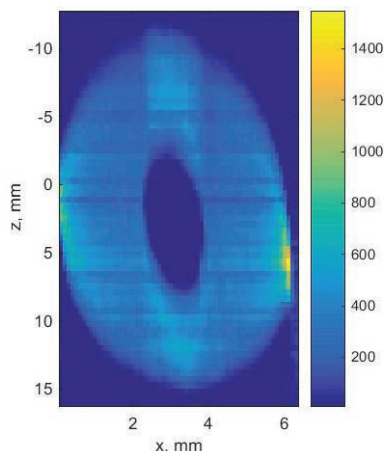


Fig. 2. The energy dispersive real space reconstruction of a hydroxyapatite (hAp) bone phantom is shown to the left. Several diffraction peaks were reconstructed and peak intensity from one is shown here (hAp 004 reflection). The shape including empty central region is correctly reconstructed.

X-ray diffraction provides a wealth of information including crystallographic phases comprising a material along with the strain and texture states of those phases. There is great interest in measuring these properties in a spatially-resolved fashion, within a sample cross-section. Several monochromatic x-ray techniques have been developed recently at the APS, using area detectors and a sample rotation.

A team of detector developers from the APS and from the National Synchrotron Light Source-II (NSLS-II) at

Brookhaven National Laboratory (BNL) together with scientists from the APS and Northwestern University have developed a new and complementary imaging technique using white-beam radiation and a Germanium Strip Detector. The use of high-energy x-rays from an APS bending magnet allows measurements on up to centimeter-sized specimens. It also does not require sample rotations to extract cross-sectional information, so it can be used to image a wider array of geometries than with standard tomography techniques (namely high-aspect-ratio samples) with target areas including batteries, bone implants, and aerospace components.

The heart of the technique is the germanium detector developed by the APS and NSLS-II detector groups, which combines low-noise readout electronics with a high-quality germanium sensor to provide position and energy resolution. The first-generation detector (Fig. 1) consists of a 3-mm-thick germanium sensor with 64 strips on a 0.5-mm pitch. An energy spectrum is measured from each strip simultaneously; the energy resolution is 400-500 eV. Currently, the maximum energy is limited to 50 keV. Further detector developments will enable energies to ~100 keV to be imaged, allowing thicker and/or higher-z materials to be investigated.

The new imaging mode was accomplished with a slit and single trans-

lation across the sample, and applied to a three-dimensional printed bone "phantom" to confirm accuracy. Several diffraction peaks were reconstructed; peak intensity from one is shown in Fig. 2. The peak centers from each phase present can also be reconstructed to yield strain information.

Contact: Jonathan Almer,  
almer@aps.anl.gov  
Antonino Miceli, amiceli@anl.gov

This effort is the work of detector developers from APS (Jonathan Baldwin, Antonino Miceli, Orlando Quaranta, Russell Woods) and NSLS-II (Anthony Kuczewski, Joseph Mead, Abdul Rumaiz, Peter Siddons) as well as scientists from the APS (Jonathan Almer, John Okasinski) and Northwestern University (Stuart Stock).

## "Films" cont'd. from page 212

products, such as cell phone screens, thin-film solar cells, drug delivery systems, and even potato chip bags.

— Dana Desonie

See: Jeffrey G. Ulbrandt<sup>1</sup>, Meliha G. Rainville<sup>2</sup>, Christa Wagenbach<sup>2</sup>, Suresh Narayanan<sup>3</sup>, Alec R. Sandy<sup>3</sup>, Hua Zhou<sup>3</sup>, Karl F. Ludwig, Jr.<sup>2</sup>, and Randall L. Headrick<sup>1\*</sup>, "Direct measurement of the propagation velocity of defects using coherent X-rays," *Nat. Phys.* **12**, 794 (AUGUST 2016).

DOI: 10.1038/NPHYS3708

Author affiliations: <sup>1</sup>University of Vermont, Burlington, <sup>2</sup>Boston University, <sup>3</sup>Argonne National Laboratory

Correspondence: \* rheadrick@uvm.edu

R.L.H. and J.G.U. were supported by the U.S. Department of Energy (DOE) Office of Science-Basic Energy Sciences (BES) under DE-FG02-07ER46380; C.W., K.F.L., and M.G.R. were supported by DOE-BES grant DE-FG02-03ER46037. This research used resources of the Advanced Photon Source, a U.S. DOE Office of Science User Facility operated for the DOE Office of Science by Argonne National Laboratory under Contract No. DE-AC02-06CH11357.



# QUICK-SCANNING XAFS AT APS BEAMLINE 9-BM

A new quick-scanning double crystal monochromator (DCM), which allows collection of a full extended x-ray absorption fine structure (EXAFS) spectrum in as little as five seconds, has been added to X-ray Science Division (XSD) beamline 9-BM-B,C at the U.S. Department of Energy's Advanced Photon Source (APS) at Argonne National Laboratory. This ability is now available to APS users for the study of chemical reactions and material transformations on short time scales, while maintaining the important capability of reaching the low-energy phosphorous and sulfur K-edges.

The new DCM was engineered by Instrument Design Technologies, and includes a frictionless air-bearing rotary stage with a direct drive motor that enables quick scanning of the DCM crystal angle and, thereby, x-ray beam energy. The frictionless motion allows for excellent beam stability to be maintained while rapidly changing energy over hundreds of electron volts.

The crystals are directly water cooled for excellent temperature and energy stability. Furthermore, high-resolution encoders track the DCM crystal angle, providing excellent reproducibility of the beam energy. Both Si (111) and (220) crystals are available, and the beamline provides access to energies from 2.1 to 25 keV.

In combination with the existing 9-BM gas handling systems and low-energy capabilities, the quick-scanning DCM makes 9-BM an ideal location for *in situ* catalysis and environmental research.

Contact: Dale L. Brewé,  
[brewel@aps.anl.gov](mailto:brewel@aps.anl.gov); Steve M. Heald,  
[heald@aps.anl.gov](mailto:heald@aps.anl.gov);  
George Sterbinsky,  
[sterbinsky@anl.gov](mailto:sterbinsky@anl.gov);  
Tianpin Wu [twu@anl.gov](mailto:twu@anl.gov)

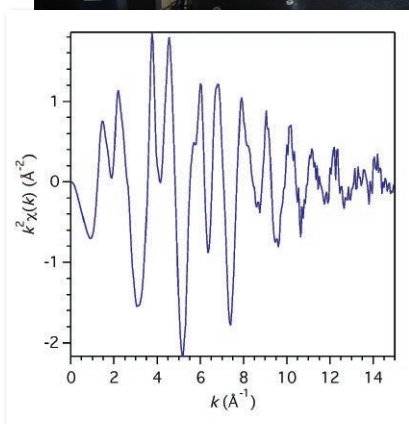
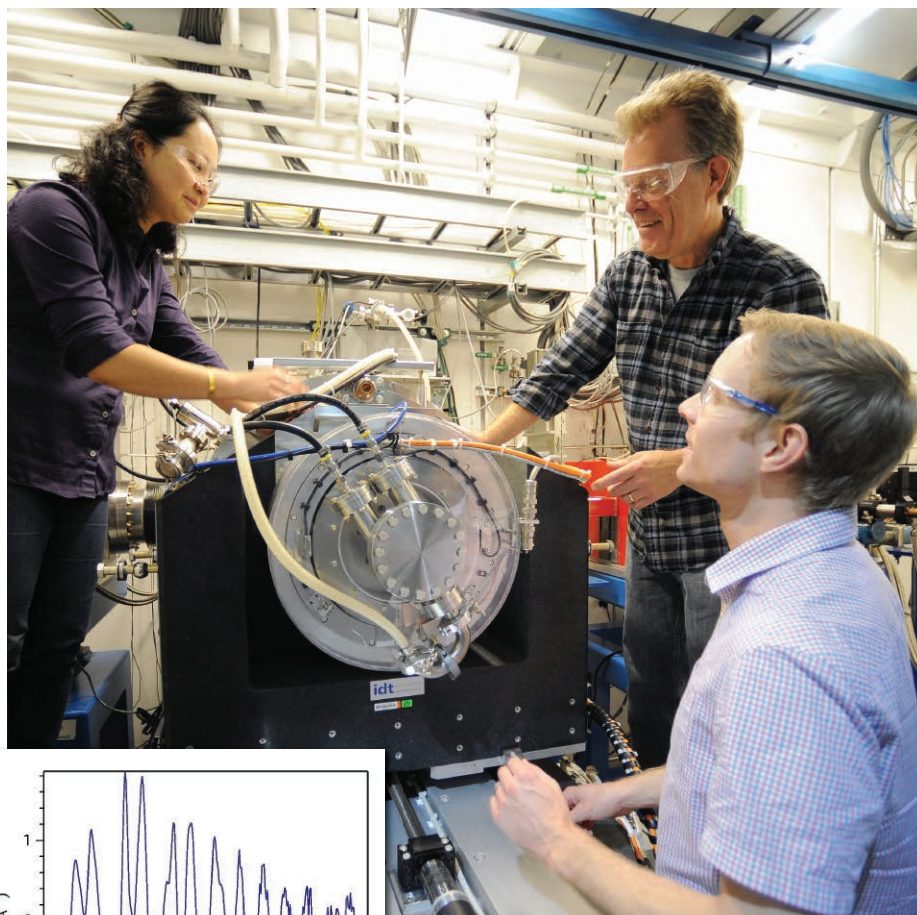


Photo: Tianpin Wu (left), Dale Brewé (right), and George Sterbinsky (foreground), all XSD-SPC, with the quick-scanning XAFS instrument at APS beamline station 9-BM-B. Inset: An EXAFS spectrum collected in 5.5 sec from a ZnO pellet using quick-scanning XAFS at APS beamline 9-BM.

Partial funding for the monochromator came from ExxonMobil Corporation. This research used resources of the Advanced Photon Source, a U.S. DOE Office of Science User Facility operated for the DOE Office of Science by Argonne National Laboratory under Contract No. DE-AC02-06CH11357.

9-BM-B,C • XSD • Materials science, chemistry, environmental science • X-ray absorption fine structure, x-ray absorption near-edge structure • 2.1-25 keV • On-site • Accepting general users •

# NANO-CALORIMETRY FOR THE CONCURRENT DETERMINATION OF THERMODYNAMIC STATES OF X-RAY PROBED VOLUMES

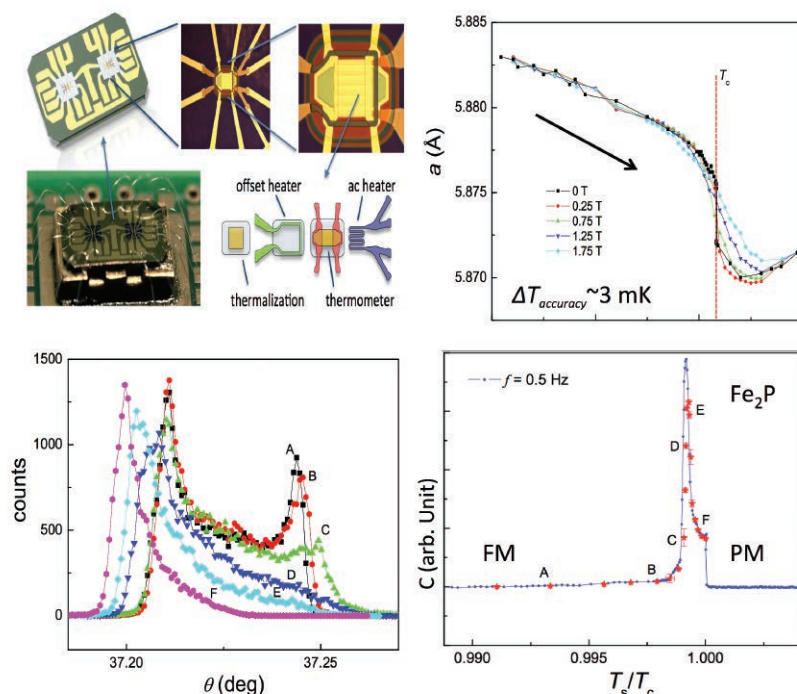


Fig. 1. Top Left: The various layers contained in the membrane based nano-calorimeter. Heaters are patterned from Ti, the thermometer is a sputtered AuGe film, contact pads are Au. The various layers are separated by  $\text{SiO}_2$  insulation layers. The  $\text{Si}_3\text{N}_4$ -windows are  $1 \times 1 \text{ nm}^2$ , and the active area in the center is  $80 \times 80 \text{ nm}^2$ . Upper Right: Lattice parameter vs temperature through the ferromagnetic transition at various magnetic fields. Lower Left: Transverse scans of the (4,2,0) Bragg peak of  $\text{Fe}_2\text{P}$  at various temperatures labeled by letters. Right below the transition, the peak splits, possibly a signature of a magnetism-induced structural transition, such as twinning. Lower right: Temperature dependence of the specific heat of  $\text{Fe}_2\text{P}$  in the vicinity of the transition. The letters identify the temperatures of the x-ray scans.

In materials research, calorimetry, that is, measurements of the specific heat and/or of the latent heat, provides one of the basic thermodynamic characterizations. It directly probes the energy contained in the various degrees of freedom in the material under study as function-of-state variables such as temperature, applied magnetic field, or strain. Specific heat measurements are highly sensitive to phase transitions, giving information on the order of the transition, the effect of fluctuations, and the universality class.

In highly correlated electron systems, interesting and unexpected behaviors can arise due to the coexistence, the competition, and/or intertwining of several order parameters such as superconductivity, nematic or-

der, magnetism, or structural distortions. In such cases, in addition to calorimetry, complementary transport, magnetic, or structural measurements are usually required to obtain a complete picture of the physics. Ideally, these measurements should be performed simultaneously on the same sample in a multi-modal fashion in order to avoid spurious effects due to features such as sample inhomogeneity, variations in doping level, or uncontrolled actual sample temperature.

Recent advances in electronics and nano-fabrication have enabled chip-based calorimetry, opening the door to performance of diffraction experiments with simultaneous thermodynamic information from the bulk, including structural, electronic, orbital, and

magnetic phase transitions, in particular, in applied magnetic fields and at low temperatures.

A team of researchers from Argonne and Stockholm University has combined a chip-based nano-calorimeter and a magnet variable-temperature insert to directly measure specific heat concurrently with x-ray scattering. An intrinsic high resolution and an excellent absolute accuracy of measured temperature and specific heat using tiny samples (e.g., 100 ng) are the hallmark of nano-calorimetry. This calorimeter is millimeters in dimension and can easily be incorporated into virtually any cryostat being used at user facilities.

The active part of the calorimeter consists of a stack of thermalization layer, thermometer, and heaters separated by insulation layers (Fig. 1, upper left). During measurements, an AC heater gives rise to a small temperature oscillation, which is measured with a custom-designed field-programmable gate-array-based lock-in system, which also measures and independently controls the local sample temperature, keeping the cryostat cold finger at the lowest desired temperature.

For initial proof-of-principle investigations, di-iron phosphide ( $\text{Fe}_2\text{P}$ ) showing magneto-caloric effect (MCE) and a cuprate ( $\text{Y}_2\text{Ba}_3\text{Cu}_3\text{O}_{6.92}$ , YBCO) superconductor were chosen.  $\text{Fe}_2\text{P}$  has a hexagonal structure, which undergoes a first-order paramagnetic-to-ferromagnetic phase transition at  $T_c \cong 217 \text{ K}$ . It is a model system for first-order magnetic phase transitions with a strong magneto-crystalline anisotropy controlling its MCE. Thermodynamic studies indicated that the onset of spontaneous magnetization along the c-axis for perpendicular fields is associated with a magneto-elastic (ME) transition. Indeed concurrent x-ray and calorimetry measurements (Fig. 1) unambiguously showed ME; a large change in lattice parameter through  $T_c$  was observed, consistent

*"States" cont'd on page 218*



# A NEW BENT BRAGG-LAUE MONOCHROMATOR AT APS BEAMLINE 17-BM-B

A new high-energy Bragg-Laue monochromator was built, installed, commissioned, and introduced in operation at XSD beamline 17-BM-B in 2016. The monochromator adopts a novel design composed of a meridionally bent Bragg silicon (311) crystal and a sagittally bent Laue crystal. The bent Bragg crystal increases the angular acceptance and focuses the beam in the vertical direction, and the bent Laue crystal focuses the monochromatic beam horizontally. This configuration enables the monochromator to provide a focused beam of less than  $500\text{ }\mu\text{m}$  (H)  $\times$   $500\text{ }\mu\text{m}$  (V) in the experimental station with decent photon flux ( $1 \times 10^{11}$  ph/s at 40 keV) and energy resolution ( $2 \times 10^{-4}$   $\Delta E/E$  at 40 keV). The new setup does not require any additional optical components (e.g., mirrors) to perform such focusing. The new monochromator has a tunable energy between 27 keV and 51 keV, an optimal energy range for material research using a two-dimensional diffraction technique in transmission geometry. The two beam energies are primarily used; 27 keV is selected when the 2 $\theta$  resolution is the preference, while 51 keV is used for collecting data to high Q space ( $Q_{\text{max}} = 19\text{ }\text{\AA}^{-1}$ ) for pair distribution function (PDF) analysis.

Beamline 17-BM-B is a rapid-acquisition powder diffraction beamline equipped with a PerkinElmer a-Si flat panel detector. Previously, 17-BM-A,B operated at 12 keV to 18 keV with the former monochromator, which was installed by the Industrial Macromolecular Crystallography Association Center for Advancing Therapeutics and utilized for the study of pharmaceutical samples. When 17-BM-A,B was incorporated into the XSD Structural Science (SRS) Group in 2013, the user program was switched and expanded to broad areas of materials science and inorganic chemistry, including electrochemistry, catalysis, gas storage materials, functional nanomaterials, high-pressure research, etc. Many

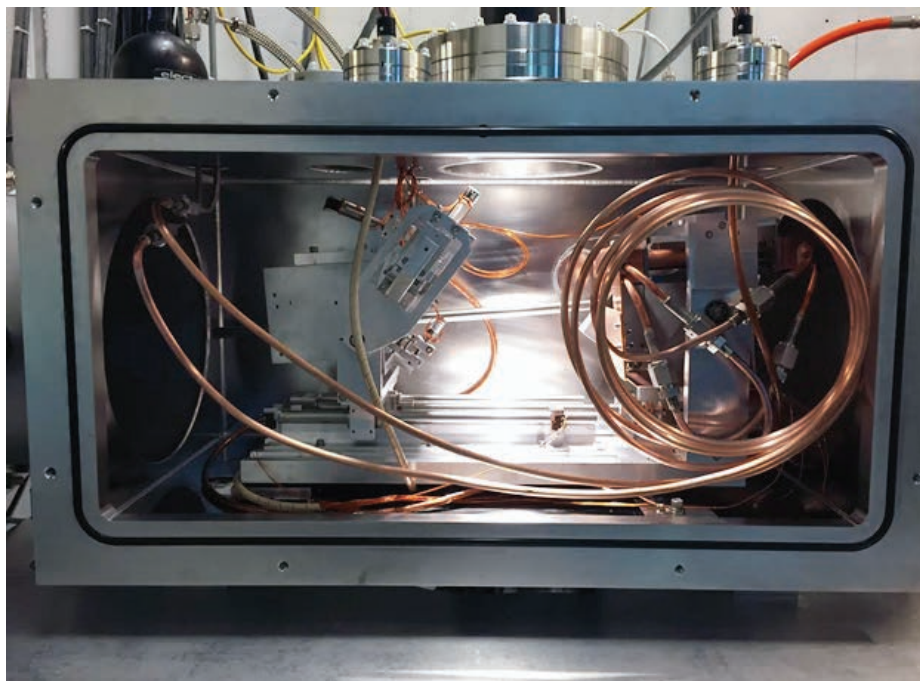


Fig. 1. The new Bragg-Laue monochromator installed at 17-BM.

samples as well as *in situ* sample cells present strong x-ray absorption at 18 keV that significantly reduced the intensity of the diffracted beams transmitting through the samples and the cells. Increasing the monochromatic beam energy leads to more intense diffractions and shorter data collection time needed to obtain a decent x-ray diffraction pattern, which is essential to a beamline focusing on *in situ* and *operando* studies. Besides, a higher energy would be able to compress enough high Q diffraction cones forward onto the area detector for complete structural characterization with the Rietveld method.

Considering these factors among others, 30 keV to 50 keV is the optimal range for diffraction and scattering studies at 17-BM-A,B, and was targeted when designing the new monochromator. This medium- to high-energy range, currently under-represented at APS and other light sources in the U.S., complements other beamlines managed by the SRS Group; 11-ID-B and 11-ID-C primarily for PDF studies and high-energy dif-

fraction ( $>60$  keV), and 11-ID-D for time-resolved spectroscopy and scattering studies (6 keV to 28 keV).

An advanced feature of the new monochromator is the meridionally bendable first crystal. The crystal is U-shaped with its bottom surface (150 mm  $\times$  60 mm) receiving the white beam at an angle of  $3^\circ$  to  $8^\circ$  between the surface and the white beam. A piezo placed within and pushing against the two legs of the crystal is able to bend the bottom surface to a radius of 220 m to maximize the angular acceptance and focus the beam in the vertical direction. Compared to a conventional double-Laue monochromator where both Laue crystals are sagittally bent without vertical focusing capability, the new Bragg-Laue monochromator can increase the flux through a  $300\text{-}\mu\text{m}$  pinhole aperture at the experimental hutch by 3 to 5 times.

The monochromator was installed and commissioned at the beginning of the 2016-3 APS user run. Also installed was a white-beam filter set composed of graphite and silicon carbide sheets

*"Bent" cont'd on page 218*



# THREE DIMENSIONAL, VARIABLE-WAVELENGTH, X-RAY BRAGG COHERENT DIFFRACTIVE IMAGING

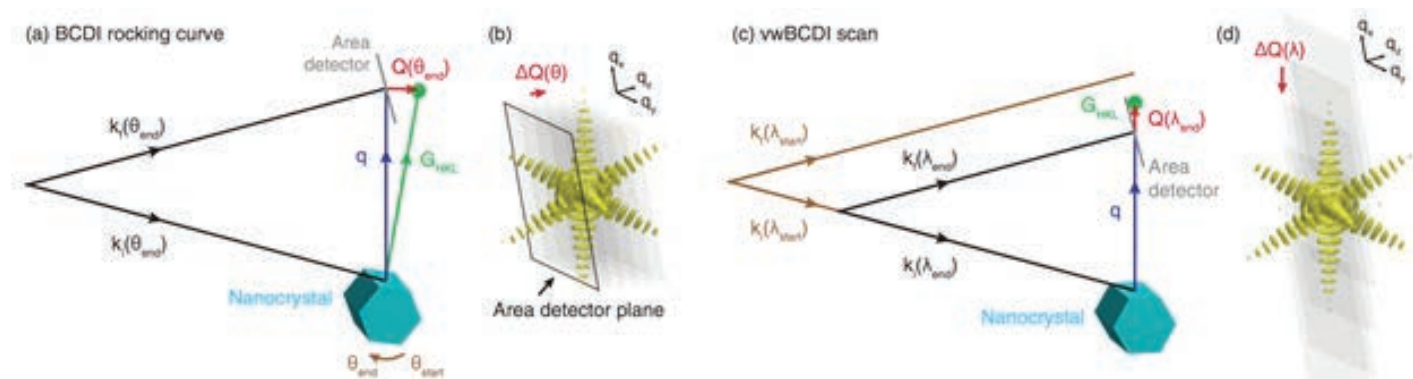


Fig 1. (a) Schematic diagram of rocking-curve-based BCDI. (b) A set of slices collected around the 3-D Bragg intensity distribution with rocking-curve-based BCDI geometry. (c) and (d) Corresponding diagrams for variable wavelength BCDI.

In last decade, Bragg coherent diffractive imaging (BCDI) has been utilized as an emerging nanomaterial characterization tool at modern synchrotron sources. A unique feature of BCDI, namely extremely high sensitivity to nanoscale distributions of strain and lattice distortions in crystals, enables the imaging of local strain distributions in three dimensions with nanoscale spatial resolution. In recent years, *in situ* and *operando* measurements essential for gaining insight into new materials science questions became a major driver for BCDI.

To enable three-dimensional (3-D) strain-sensitive imaging with BCDI, the 3-D Bragg intensity distribution must be measured. This is done with current rocking-curve-based BCDI methods by scanning the sample angle as shown in Fig. 1(a). In this manner, the 3-D Bragg intensity distribution can be collected as a series of two-dimensional slices through the reciprocal space volume with an area detector. Alternately, in a Bragg diffraction experiment, the reciprocal space volume about a Bragg peak can be measured by finely scanning the wavelength of incident x-rays, which requires no sample motion (Fig. 1(c)). Such a scan will result in an equally valid 3-D Bragg intensity data set obtained by different means (Fig. 1(d)) that requires the development of a new image reconstruction approach.

A team led by researchers from Ar-

gonne and Aix-Marseille University has demonstrated how to overcome this challenge, opening the door to new strain imaging studies of materials in environments where sample manipulation is difficult and the details of nanoscale strain distribution and evolution remain elusive. These researchers introduced a new phase retrieval algorithm designed to handle x-ray wavelength variability in BCDI.

The algorithm takes advantage of the Fourier slice projection theorem and considers the relationship between spatial sampling and array size in a two-dimensional discrete Fourier transform.

The researchers demonstrated the new method on a (111) Bragg peak of gold nanocrystal by scanning the energy of coherent x-rays from 8.85 to 9.15 keV with 6-eV increments at the

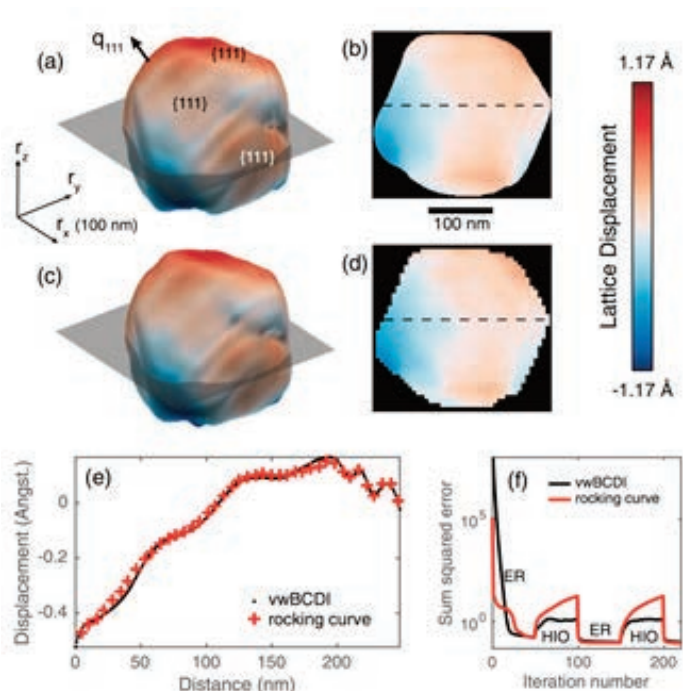


Fig. 2. (a) The 3-D shape and near-surface lattice displacement of the gold nanocrystal reconstructed from variable wavelength BCDI. (b) The lattice displacement within a gray plane is shown in (a). (c) and (d) Corresponding images of the same crystal from rocking-curve-based BCDI. (e) Comparison of linecuts of lattice displacement along the dotted line in (b) and (d). (f) Error metrics from rocking-curve-based BCDI and variable wavelength BCDI.

XSD 34-ID-C beamline of the APS. Using the new algorithm, a 3-D image of a gold nanocrystal was reconstructed as shown in Fig. 2(a). Figure 2(b) displays the lattice displacement within a gray plane in Fig. 2(a). The coloring corre-

"Bragg" cont'd on page 218

### "Bent" cont'd from page 216

to take away the low-energy radiation in order to reduce the heat load on the Bragg crystal, which is cooled by house water through the two cooper brackets holding its legs. The old optics contained a collimating mirror and a vertical focusing mirror that are no longer used with the new monochromator. Because of this simplified optics, the beam stability has been greatly improved so that realignment is rarely needed when continually operating at the same energy for weeks.

Contact: Wenqian Xu,  
wenqianxu@aps.anl.gov;  
Andrey Yakovenko  
ayakovenko@aps.anl.gov

Details of the monochromator design and ray tracing results were included in a recent submission to the Journal of Applied Crystallography, titled "Bent Bragg-Laue monochromator for high-energy X-rays." Peter Chupas, Xianbo Shi, Charles Kurtz, Gregory Halder, Zunping Liu, Lynn Ribaud, Guy Jennings, Karena Chapman, and Kevin Beyer among other staff in the SRS group contributed to the design, construction and installation of the new monochromator. Special thanks to Xianrong Huang and the optics group for cutting the crystals, Jun Qian for the metrology measurement, and Stanislav Stoupin for help in testing the monochromator at XSD beamline 1-BM.

### "Bragg" cont'd from page 217

sponds to lattice displacement along a {111} crystallographic direction. Comparison of the new method, entitled variable-wavelength BCDI, with standard BCDI measurements show excellent agreement (Fig. 2(c) and 2(d)).

This research demonstrates that variable wavelength BCDI preserves the strain-sensitive 3-D imaging capability of current BCDI without any sample motion. This capability will enable certain *in situ* and *operando* strain measurements in environments that are currently incompatible with current BCDI methods because of the difficulty of accurately rotating the sample about the center of rotation of a diffractometer system.

Contact: Wonsuk Cha, wcha@anl.gov

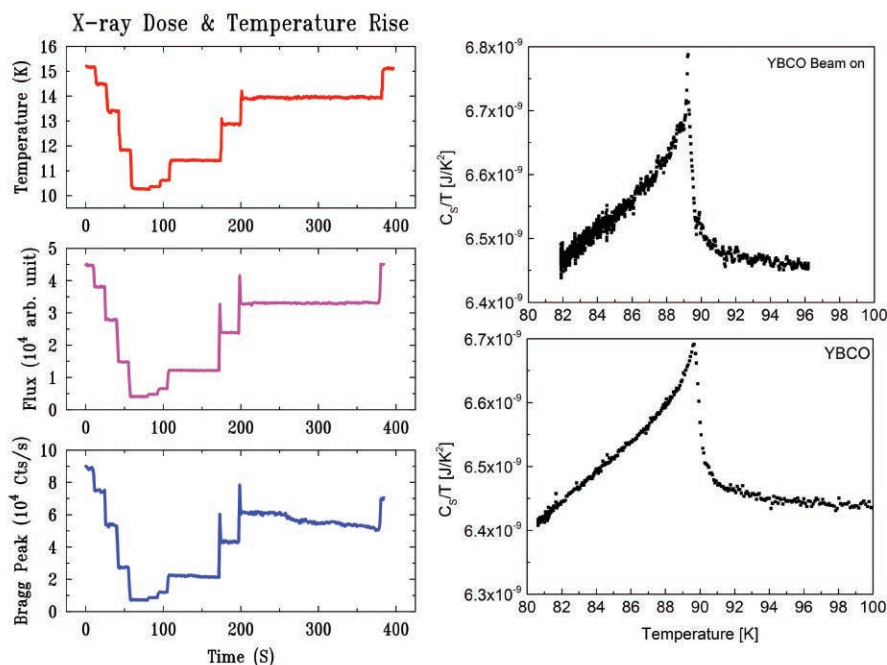


Fig. 2. Left: Sample YBCO temperature changes as the amount of incident flux is varied using attenuators. On increasing flux momentary rises are observed while foils are being removed and inserted to obtain a set attenuation of the beam. Right: Specific heat measured with and without a full x-ray beam on a YBCO crystal.

### "States" cont'd from page 215

with a structural transition. As shown, the use of a nano-calorimeter enables one to control sample temperature with a 10-ppm precision, determine intrinsic transition width as a function of magnetic field, and exactly correlate structural changes with specific heat through a hysteretic transition.

At cryogenic temperatures, x-ray beam heating has a spectacular effect on YBCO sample temperature and Bragg-peak intensity in direct correlation with incident flux (Fig. 2, left panels). This change in temperature as a function of absorbed dose has been utilized to measure x-ray resonant features (not shown). The right panels in Figure 2 display specific heat measured with and without a full x-ray beam impinging on the sample, clearly identifying the superconducting transition with a high fidelity.

Looking forward, as the proposed APS Upgrade is poised to enable sub-micron spot sizes of intense coherent beams, the need for *in situ* determination of the exact thermodynamic state of a sample seems greater than ever. Some salient benefits of nano-calorimetry include, first a precise control of sample temperature to eliminate artifacts due to thermal fluctuations in co-

herent scattering studies as well as to enable one to reach smaller reduced temperature,  $t=|T/T_c|$ , for better observation of critical phenomena. Second, local control of sample temperature translates into a fast cycling of sample temperature over hundreds of degrees in seconds for order parameter measurements and quenching in disorder, if desired. Preliminary measurements also demonstrated that by modulating incident x-ray flux, one can induce sample-temperature oscillations for specific-heat determination, which can eliminate the need for an AC heater in the nanocalorimeter.

With cutting-edge nano-technology at our disposal, nano-calorimetry lends itself to tailoring in order to exactly meet the thermal and geometric demands of specific x-ray experiments.

Contact: K. Willa, kwilla@anl.gov;  
U. Welp, welp@anl.gov; and  
W.-K. Kwok, wkwok@anl.gov (all Argonne MSD) D. Campanini,  
Donato.Campanini@fysik.su.se; Z. Diao,  
zhu.diao@fysik.su.se; and A. Rydh,  
andreas.rydh@fysik.su.se (all Stockholm University) Z. Islam,  
zahir@aps.anl.gov (Argonne APS)

### REFERENCE:

S. Tagliati, V.M. Krasnobov, and A. Rydh, "Differential membrane-based nanocalorime-

# MODELING WAVE PROPAGATION THROUGH NON-IDEAL OPTICS

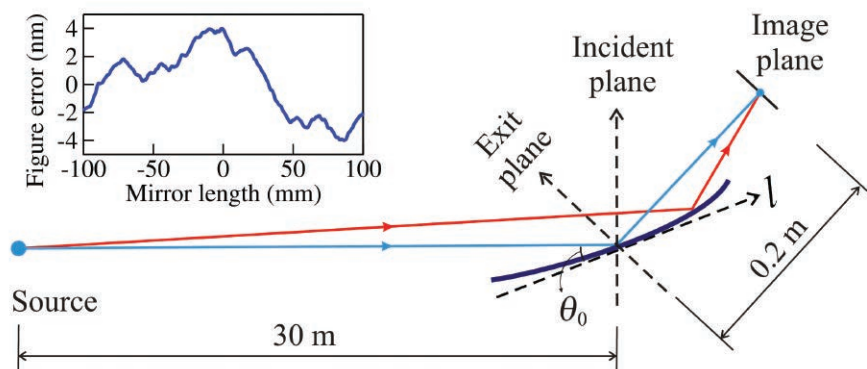


Fig. 1. Schematic layout of MOI propagation through a mirror. Insert is the figure error profile of the mirror.

Coherence-and wavefront-preserving optics are central elements for the APS beamlines that will take full advantage of the APS Upgrade. Knowledge of the coherence properties of the beamlines in different optical layouts and arrangements is of great importance for beamline and experiment design. Therefore, a simulation program that analyzes beamline coherence with effects of non-ideal optics is essential. An advanced simulation code was developed [1] based on the mutual optical intensity (MOI) model, and extended [2] to propagate the MOI function through non-ideal x-ray optics.

The MOI function is a four-dimensional function that fully describes the wavefront and coherence of a partially coherent beam. In the MOI model, the wavefront is separated into small elements within which the beam is assumed to be fully coherent with constant complex amplitude. The figure errors on reflecting mirrors are dealt with by path-length calculations through local ray-tracing. Figure 1 is a schematic layout of a focusing elliptical cylinder mirror. The Gaussian source with a sigma size of 2  $\mu\text{m}$  and divergence of 30  $\mu\text{rad}$  is focused by a 200-mm-

long mirror with a grazing angle of 2.5 mrad. The source-to-mirror and mirror-to-image distances are 30 m and 0.2 m, respectively. The simulated intensity profiles at the image plane with and without figure errors [cf. Fig. 1 insert] are shown in Fig. 2(a). The multiple maxima near the central peak are the results of the low spatial frequency figure errors. The MOI model also provides the local degree of coherence [Fig. 2(b)] and the wavefront [Fig. 2(c)]. Even though the figure errors do not change the global degree of coherence, they redistribute the local coherence and could severely distort the wavefront.

The MOI model has been benchmarked against the Synchrotron Radiation Workshop" (SRW) open source computer code [3], and the HYBRID [4] code, an efficient code combining ray tracing and wavefront propagation for calculating beam intensity profiles along the beamline. The MOI model can provide accurate results in different coherence conditions. Since the full MOI function is stored, sequential simulation of beamline optics can be carried out, which is its main advantage over SRW.

Compared to HYBRID, the MOI model can provide much more information on beam coherence and wavefront. Furthermore, the accuracy and efficiency of the MOI model can be balanced by changing the number of elements within the wavefront. These merits make the MOI model a promising tool for advanced beamline simulation, especially for coherence related beamlines. Further development will include extending the MOI model to two-dimensional simulation and implementing real source calculations.

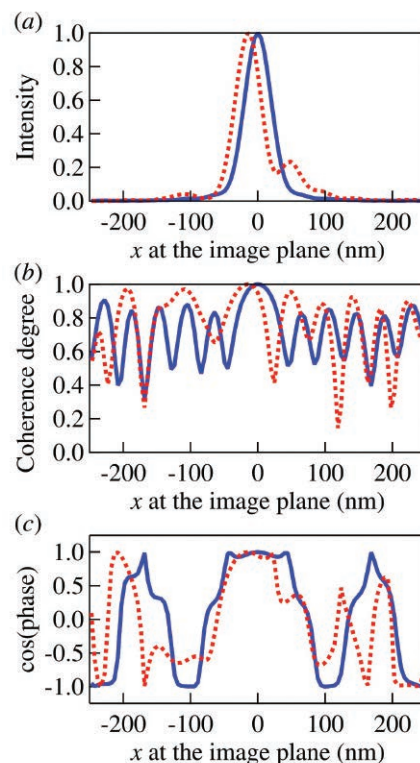


Fig. 2. (a) Intensity profiles, (b) local coherence degree, and (c) wavefront calculated at the image plane by the MOI model through an elliptical cylinder mirror with (dotted lines) and without (solid lines) figure errors (cf. Fig. 1).

Contact: Xianbo Shi  
[xshi@aps.anl.gov](mailto:xshi@aps.anl.gov); Ruben Reininger  
[rreininger@aps.anl.gov](mailto:rreininger@aps.anl.gov); Lahsen Assoufid  
[assoufid@aps.anl.gov](mailto:assoufid@aps.anl.gov)

## REFERENCES

- [1] X. Meng, C. Xue, H. Yu, Y. Wang, Y. Wu, and R. Tai, *Opt. Express* **23**, 29675 (2015).
- [2] X. Meng, X. Shi, Y. Wang, R. Reininger, L. Assoufid, and R. Tai, to be submitted.
- [3] O. Chubar, *Proc. SPIE.* **9209**, 920907 (2014).
- [4] X. Shi, R. Reininger, M. Sanchez del Rio, L. Assoufid, *J. Synchrotron Rad.* **21**, 669 (2014).



# STREAMING IMAGES TO POWDER PATTERNS AND PAIR DISTRIBUTION FUNCTIONS WITH GSAS-II

Modern powder diffraction and total scattering experiments are frequently collected as a series of two-dimensional images that reflect structural changes within the sample as a function of time, temperature, or other experimental stimuli. It is difficult to track reaction progress directly from the inspection unless each of these images are converted to a one-dimensional powder diffraction pattern and associated pair distribution function (PDF), the first step in data analysis.

In the past, this data processing required a series of programs, each with idiosyncratic input and output and invoked image-by-image to produce data in a desired format necessary for plotting or crystallographic analysis. Often, users did not complete many of these operations until they returned to their home institutions, making it impossible to determine data quality in time to make changes.

This has changed with GSAS-II, an open source Python project that addresses all types of crystallographic studies, from simple materials through macromolecules, using both powder and single-crystal diffraction and with both x-ray and neutron probes. Measurements can be constant wavelength or TOF (thanks to support from Oak Ridge National Lab.) GSAS-II replaces an earlier crystallographic package, GSAS/EXPGUI that is cited ~500 times/year, but GSAS-II also handles all the steps in diffraction analysis, such as data reduction, peak analysis, indexing, Pawley fits, small-angle scattering fits, stacking fault simulations and structure solution, in addition to the structure refinement of

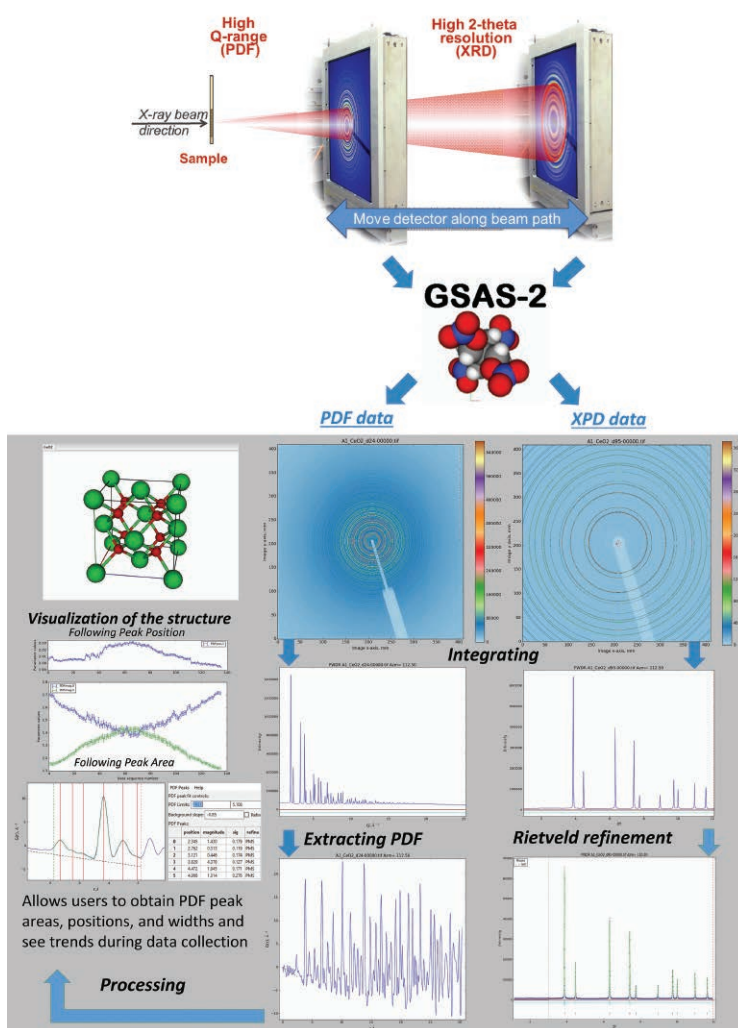


Fig 1. Varying the detector distance allows for optimizing the high Q-range for PDF or 2-theta resolution for x-ray diffraction. Images collected at both distances are automatically integrated within GSAS-II using all the necessary parameters and with all corrections applied.

GSAS/EXPGUI. Most recently, GSAS-II has been expanded to handle PDF extractions and PDF peak fitting analysis. It can be used with large collections of related datasets for repeated (sequential) refinements and for parametric fitting to these results.

The GSAS-II web site, with tutorials, installation and update information, is at <https://subversion.xray.aps.anl.gov/trac/pyGSAS> and source code is found at <https://subversion.xray.aps.anl.gov/pyGSAS/trunk/>.

In a cooperative effort between

beamline scientists in the XSD Structural Science Group and the computational scientists in the XSD Computational X-ray Science Group, the GSAS-II package has been adapted to automate data reduction. This has allowed it to be deployed at APS beamlines 17-BM, 11-ID-B, and 11-ID-C, where streamed diffraction images are converted directly to powder patterns and pair distribution functions as they are acquired (Fig. 1). The advanced visualization capabilities of GSAS-II help users to better assess and improve the progress of their experiments. This significantly improves the likelihood of beam-time success and ensures that experimenters return home with completely processed data, enhancing the likelihood for complete analysis.

The proposed APS Upgrade will result in greatly increased flux increase at insertion device beamlines, significantly increasing data collection rates. The development and implementation of the automatic data reduction and visualization methods, such as what has now been added to the GSAS-II environment, is an important step in preparation for the APS-Upgrade.

Contact: Kamila M. Wiaderek,  
[kwiaderek@aps.anl.gov](mailto:kwiaderek@aps.anl.gov)  
 Robert B. Von Dreele,  
[vondreele@anl.gov](mailto:vondreele@anl.gov)  
 Andrey A. Yakovenko,  
[ayakovenko@aps.anl.gov](mailto:ayakovenko@aps.anl.gov)

Wenqian Xu, Olaf Borkiewicz, and Brian Toby contributed to the design, testing and implementation of the auto-integration and PDF extraction techniques in GSAS-II.

# AERODYNAMIC LEVITATOR FOR HIGH-ENERGY X-RAY SCATTERING FROM HIGH-TEMPERATURE NUCLEAR MATERIALS

At 16,000 reactor-years of civil operation and counting, nuclear power from fission currently accounts for about 10% of the global electricity supply. Because the majority of currently operating nuclear reactors use either UO<sub>2</sub> or mixed oxide fuel (typically 90% UO<sub>2</sub>), understanding and predicting the behavior of UO<sub>2</sub> at extreme temperatures is of great importance to improved safety and optimization of this low-carbon electricity source.

To facilitate the study of radioactive samples at these extreme temperatures, an aerodynamic levitator with laser-beam heating has been integrated with a hermetically sealed chamber on the XSD high-energy x-ray beamline 6-ID-D. Laser heating from above enables temperatures from 2000 C to 3500 C to be attained. Integral safety features include a pressure monitored double-laser window and a gas cross purge to a HEPA filter. Containerless levitation techniques eliminate the possibility of chemical reactions with surrounding materials at high temperatures and the gas mixing provides control of the process atmosphere chemistry. A built-in remote sample handling mechanism enables up to 25 samples to be interchanged during a single installation.

High-energy x-rays (typically 100 keV) can penetrate the bulky chamber, allowing radioactive samples, including nuclear fuel materials, to be studied using Pair Distribution Function analysis. Powder diffraction experiments are also feasible using a rotating levitation nozzle that creates a gas vortex to spin the sample. The laser power, levitation gas flow, and pressure are remotely controlled using a LabVIEW GUI interface, which also logs the pyrometer temperature data. Diffraction patterns are typically measured from the top few hundred microns of the levitated sample, co-incident with the laser spot and focal point of the pyrometer to minimize temperature gradient effects.

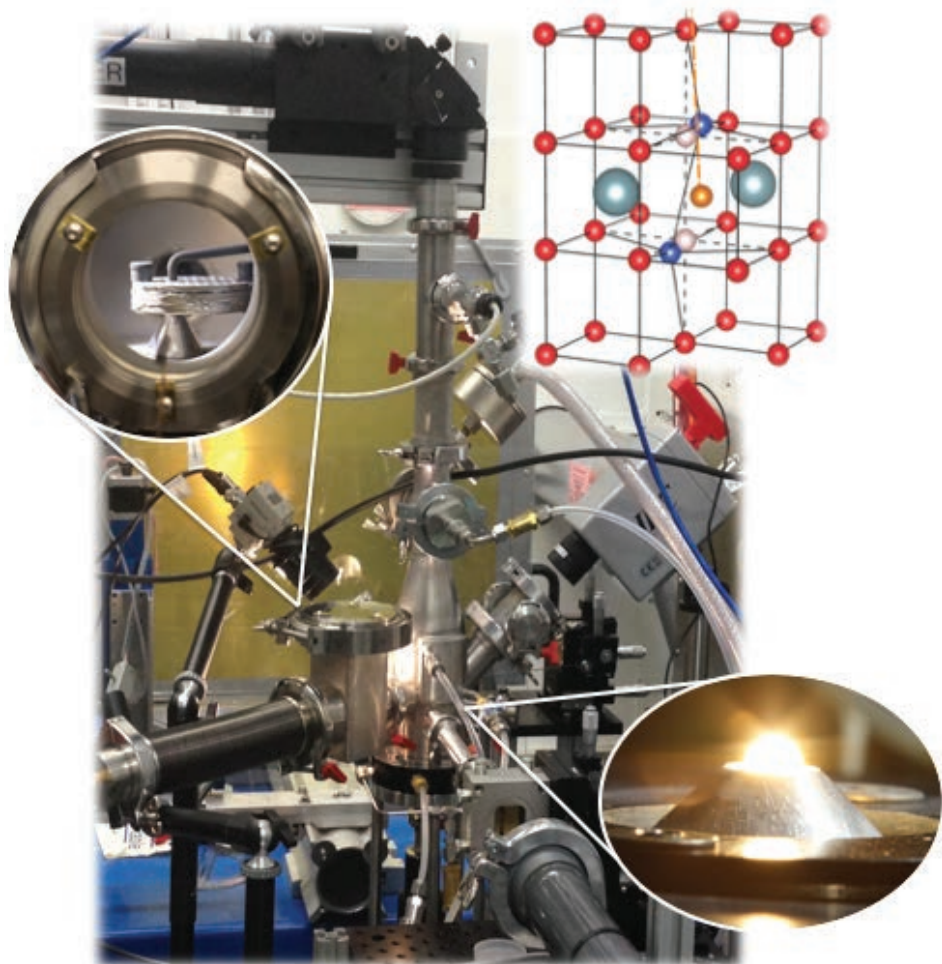


Fig. 1. The nuclear material is levitated from below on a gas jet and heated from above by a 400-W CO<sub>2</sub> laser. The scattered x-ray beam is measured with a large, a-Si flat plate area detector. The sample manipulator is operated outside the chamber using a bellows system.

The chamber was fabricated by Materials Development, Inc., and technical resources were provided by the Argonne Nuclear Engineering Division.

**See:** J.K.R. Weber<sup>1,2</sup>, A. Tamalonis<sup>2</sup>, C.J. Benmore<sup>2</sup>, O.L.G. Alderman<sup>1,2</sup>, S. Sendelbach<sup>1</sup>, A. Hebden<sup>2</sup>, and M.A. Williamson<sup>1</sup>, "Aerodynamic levitator for *in situ* x-ray structure measurements on high temperature and molten nuclear fuel materials," *Rev. Sci. Instr.* **87**, 073902 (2016).

DOI: 10.1063/1.4955210

**Author affiliations:** <sup>1</sup>Materials Develop-

ment, Inc., <sup>2</sup>Argonne National Laboratory

Work was supported under the following contracts: MDI, Contract Nos. DE-SC0007564 and DE-SC0015241 from the U.S. Department of Energy (DOE) and Contract Nos. 6F-30221, 6F-30241, and 6F-30581 from Argonne National Laboratory. APS, U.S. DOE, Argonne National Laboratory was supported under Contract No. DE-AC02-06CH11357. We thank Douglas Robinson for helping with the beamline experiments at APS and John Vacca and Bruce Glagola for their advice about radiation safety for the beamline installation.



# A NEW ERA FOR X-RAY FLUORESCENCE MICROSCOPY: FASTER, BETTER, MORE-AUTOMATED ANALYSIS

X-ray fluorescence (XRF) data can be analyzed using different techniques from quick region-of-interest (ROI) summing to more precise curve fitting. The faster ROI method provides a quick view of the data but can give incorrect results (e.g., due to cross-talk between fluorescence lines from different elements). A per-pixel Gaussian fit gives a more accurate representation of the data but takes significantly longer in terms of computation time. Argonne researchers recently inaugurated a new implementation in C++ for significantly improved robustness, better performance (4x), and better scaling compared to previous versions. To further accelerate the performance of per-pixel Gaussian fitting, the team took advantage of the C++ framework to implement a robust optimization algorithm—non-negative least squares (NNLS)—for an additional speedup of 30x (Fig. 1).

A website was created to allow APS beamline scientists and users to submit analysis jobs to a cluster of computers for processing. The web page displays the current status of each analysis computer showing CPU, system RAM, and swap hard drive memory utilization. There are three informative lists for the status of each job, displaying which jobs are queued, processing, and finished. Meta information saved for each job records when the job processing was started and finished (Fig. 2).

The engine running the web page is a python application. It exposes a REST web interface that allows other python scripts to submit jobs or get information concerning which jobs are queued. A python script at XSD beamline 2-ID-E checks for completed scans and submits jobs to the web site. The web site then checks to see what analysis computer is free to process the jobs and sends it accordingly. The architecture makes it possible to perform additional tasks when the analysis is complete. For example, users can choose to receive automatic emails with pre-an-

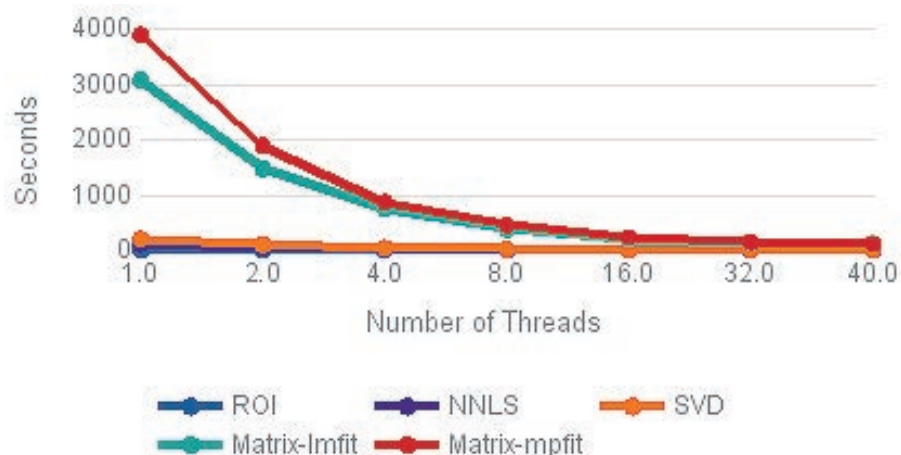


Fig. 1. Performance in seconds of five XRF-MAPS elemental mapping algorithms for increasing numbers of processing cores. The data set is 291 x 331 x 2048 in size. The software is processing the following elements: Al, Si, P, S, Cl, Ar, K, Ca, Cr, Mn, Fe, Co, Ni, Cu, Zn.

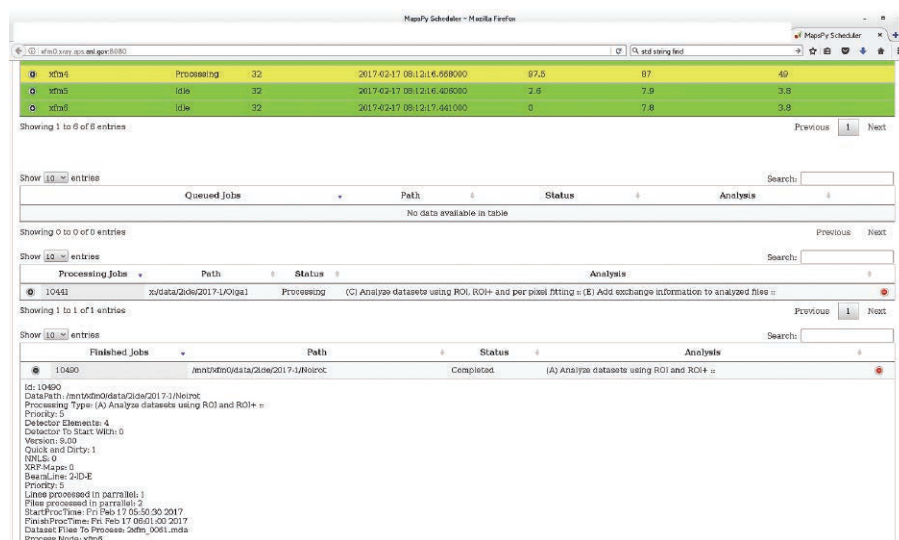


Fig. 2. User view of the job submission web page, which extends an API for jobs to be automatically submitted when acquisitions is done to automate data analysis

alyzed images as scans finish.

XRF data captured using a tomographic scan protocol can be used to reveal the three-dimensional internal elemental composition of a given sample. However, the resulting reconstruction problem typically is ill-posed and does not have a unique solution because of insufficient measurements. By adding x-ray transmission as a modality to the dataset, one can obtain the spatial distribution of the absorption coefficient inside the sample. To take advantage of

the complementary information from different modalities to this limitation, we integrated both modalities, which are concurrently captured during experiment to formulate an optimization approach called “joint inversion.” This simultaneously reconstructs the elemental composition and overall absorption of the sample. The joint inversion can provide a dramatically improved reconstruction result. In particular, the challenges in XRF tomography arising mainly from the effects of self-absorption in the >>



> Fig. 3. Numerical results on synthetic Phantom sample composed of elements K, Ga, and Fe. The first row is the ground truth elemental maps, the second row is the initial guess set up as 0 everywhere, then compared to the reconstruction results obtained from single XRF (3rd row), single XRT (4th row), and joint inversion (last row) separately, where the last column shows the overall reconstruction error. As demonstrated, joint inversion dramatically outperforms the other two schemes.

<< sample are greatly mitigated (Fig. 3 and Fig. 4).

XRF data analysis involves multiple parameters and in-depth knowledge of equipment. Providing a simple interface can help researchers minimize mistakes and concentrate more on their experiments. Collaboration between the XSD Scientific Software & Data Management, Computational X-ray Science, and Microscopy groups allows us to streamline the data analysis with integrated tools, and faster, yet precise, data analysis techniques.

Contact: Arthur Glowacki,  
[aglowacki@aps.anl.gov](mailto:aglowacki@aps.anl.gov);  
 Zichao Di, [wendydi@mcs.anl.gov](mailto:wendydi@mcs.anl.gov);  
 and Stefan Vogt, [svogt@anl.gov](mailto:svogt@anl.gov)

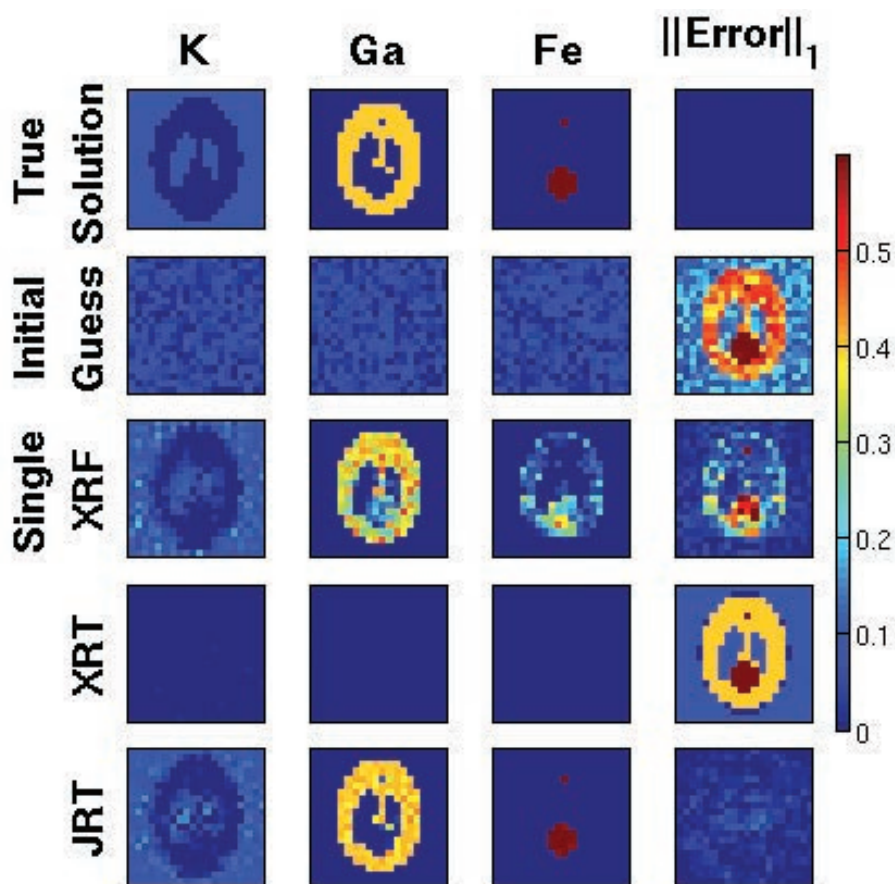
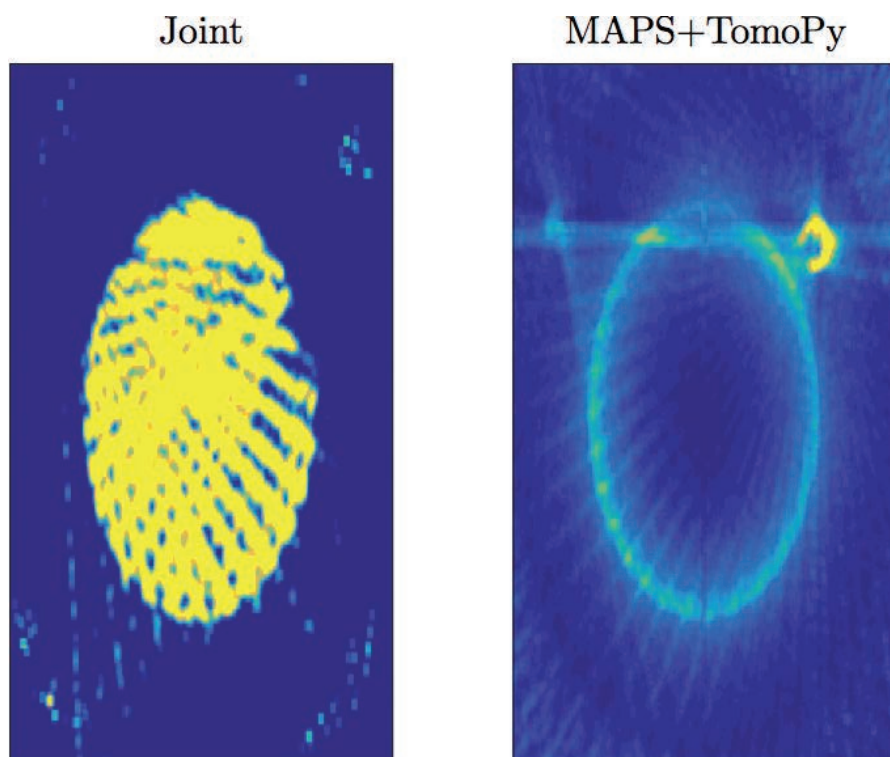


> Fig. 4. Numerical results on real data where the sample is a silicon solid rod. Due to the thickness of the rod, XRF data suffers heavily from the well-known self-absorption scheme. Using the standard single modality reconstruction scheme (TomoPy+MAPS), the reconstructed rod appears to be hollow, while joint inversion is able to recover the solid nature of the rod.



# GENERAL-PURPOSE RECIPROCAL SPACE MAPPING SOFTWARE FOR USE AT THE APS

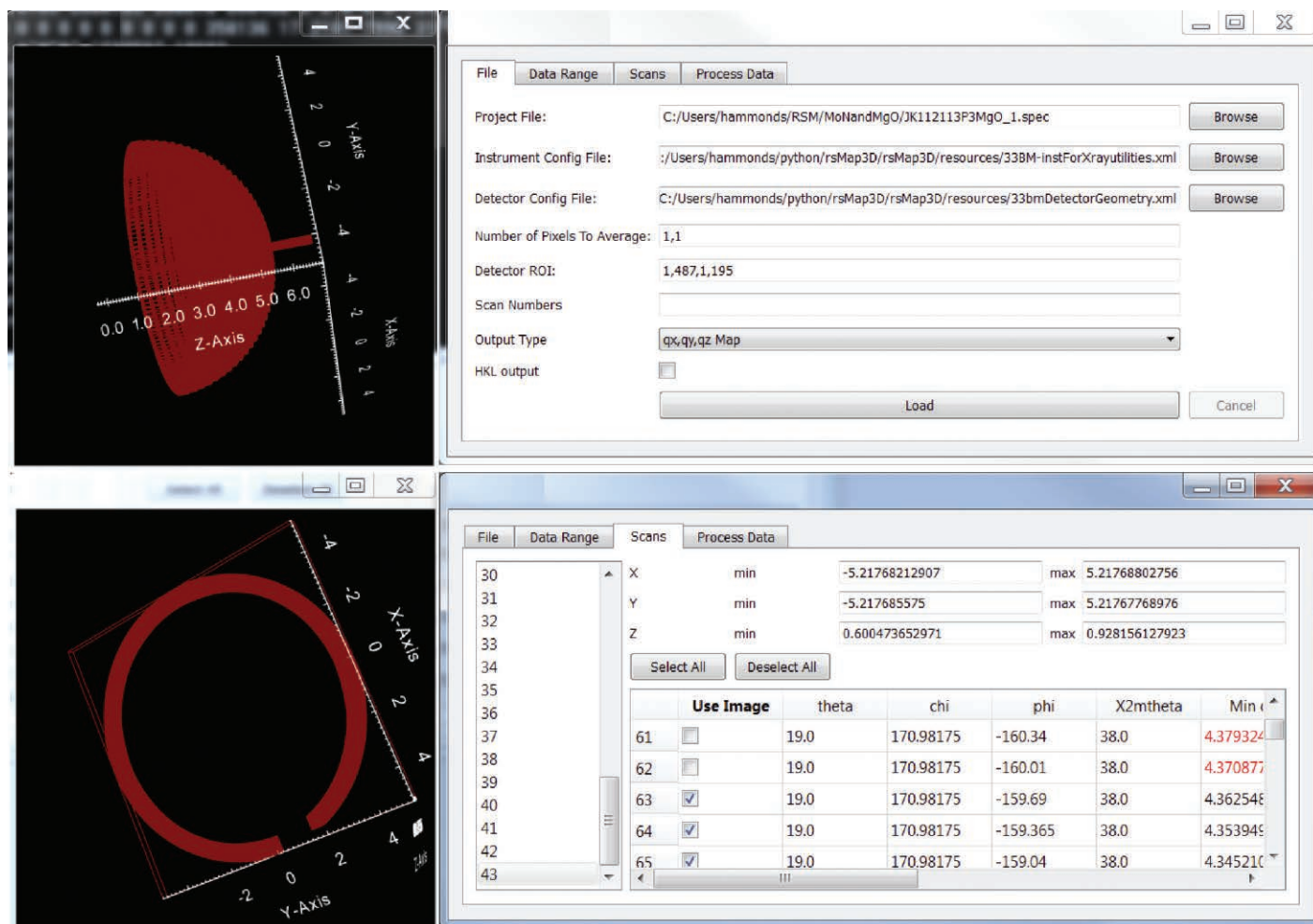


Fig. 1. RMap3D user interface. Top: An interactive 3-D view of the full scan space imported from acquisition data specified in the dialog to the right. Via the interface users can select scan geometry and image data files, and instrument configuration settings. Bottom: 3-D view of a smaller scan space selected based on parameters in the adjacent dialog. Users can set the bounding region of the scan area to map, select individual images to include or exclude from space-mapping, and view scan parameters associated with individual images.

Data analysis software is fundamental to scientific discovery at the APS. The impressive variety of world-leading techniques performed at the APS coupled with the facility's diverse user-base naturally leads to a demand for a variety of different software tools. Despite this variety, some analysis techniques are of common interest to many APS beamlines, either as a primary form of analysis, or through use as a data processing step performed as a part of a larger analysis workflow.

An example of such a common data analysis technique is found in reciprocal space mapping (RSM) tools. RSM tools are used to transform data from diffractometer-space (images collected at a set of angles) into reciprocal-space (scattered intensities at  $q^{\rightarrow}$ ) or in terms of the related Miller Indices ( $h, k, l$ ). The output from this mapping

often forms the basis of further data analysis. For example, they are used as a part of general-purpose scattering and diffraction (including microdiffraction) beamlines. Additionally, these tools are used for techniques that study dynamics, such as time-dependent diffraction, to provide reciprocal-space input to wide-angle x-ray photon correlation spectroscopy (WA-XPCS) reduction software, or to assist in the discovery of spectroscopic features associated with particular lattice sites, which can then be studied further.

As with many other techniques at the APS, the development and application of higher frame-rate detectors enables novel science in a wide range of diffraction based areas. A consequence of these detector advancements is the creation of greater amounts of image data that must be

processed, making parallel computation necessary.

In this area, the APS continues to develop the RSMa3D software package, a general-purpose tool for reciprocal-space mapping. The tool allows users to examine a volume of data and select portions on which to apply transformations that convert detector pixel locations from diffractometer geometry to reciprocal-space units, and then map pixel data on to a three-dimensional (3-D) reciprocal-space grid. RSMa3D can map data acquired using 4- and 6-circle diffractometers, and with scans taken over angles or energy. The application presents a graphical interface for selecting the relevant parts of data to process via a 3-D representation of the acquired data volume (Fig. 1).

Scan angle or energy data is usually read from data files generated by spec, while image data is often read from TIFF or HDF5 files. The core mapping routines utilize the OpenMP programming API to parallelize operations across multiple cores on a workstation for increased performance. Data too big to fit entirely into memory at one time is processed in smaller chunks and re-assembled to form the final output volume, allowing users to process arbitrarily large input datasets.

Once data is processed it may be used as input to further analysis workflows. Additionally, visualization is often an important part of the data analysis process. Data generated by RSMa3D is easily read by ParaView, an open-source, high-performance tool for 3-D data visualization and manipulation. ParaView allows the user to easily produce 3-D contour plots and make slices through the data using plane cuts or cuts on the surface of a defined sphere, for constant  $|\vec{q}|$  cuts, for example. Using RSMa3D in combination with sophisticated visualization tools enables APS staff and users to study large diffraction data quickly and effectively (Fig. 2).

RSMa3D is written in Python and relies heavily on the xray utilities, spec2nexus, and VTK libraries. It is easily installed using the pip package management system, and runs on the Linux, OS X, and Windows platforms. RSMa3D is now in regular use for scattering and diffraction experiments at

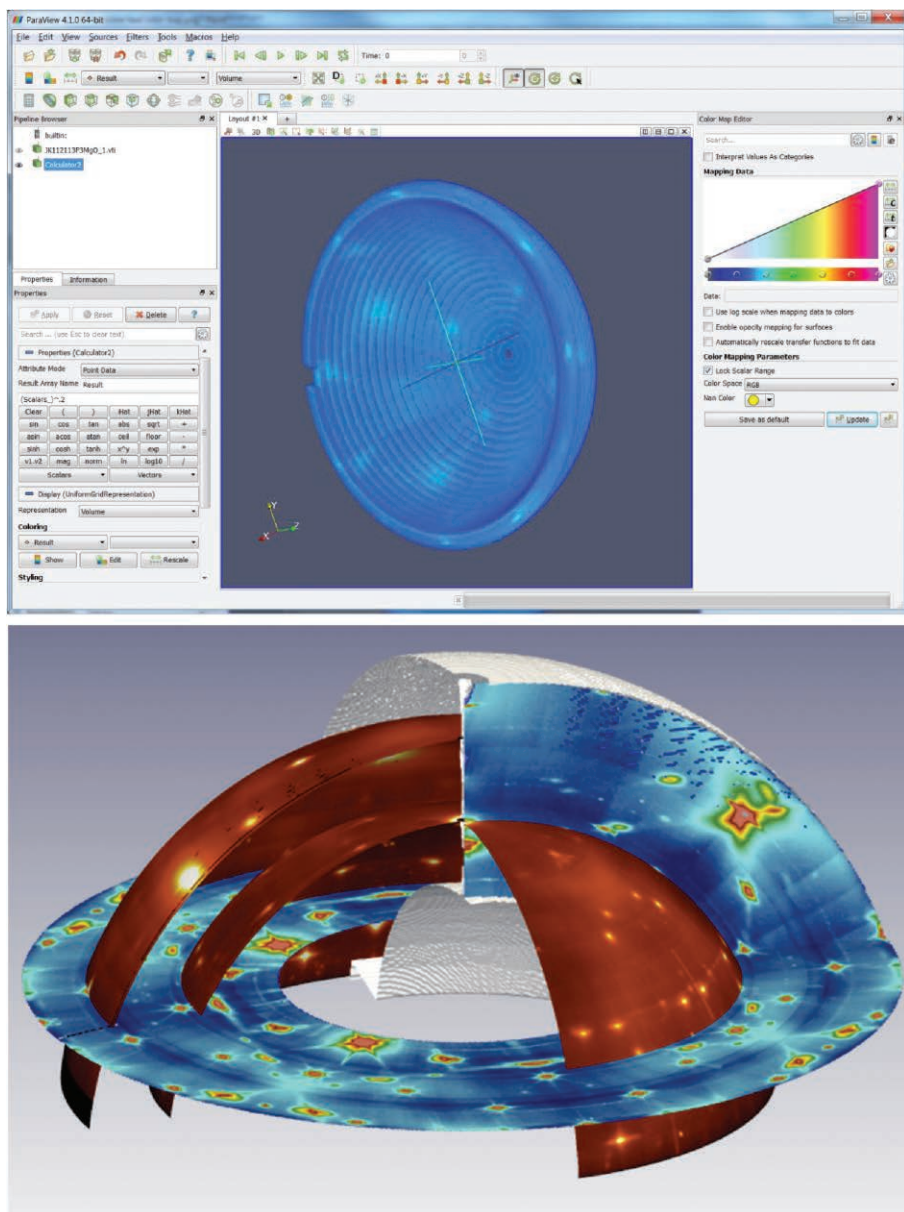


Fig. 2. Top: ParaView visualization of a diffraction dataset composed of a series of phi scan scans at various chi values. The dome thickness represents a range of  $|\vec{q}|$  values at each of the chi/phi values. Bottom: 3-D view of reciprocal-space map showing multiple cuts through the data.

the XSD 33-BM and 33-ID beamlines, for microdiffraction analysis at 34-ID, and for time-resolved diffraction work at 7-ID. Development is underway for WAXPCS analysis at 8-ID, and for data exploration with inelastic x-ray measurements at XSD 30-ID.

Contact: John Hammonds,  
jphammonds@anl.gov; Jonathan  
Tischler, tischler@aps.anl.gov;  
Christian Schlepütz,  
christian.schlepuetz@psi.ch;  
Nicholas Schwarz,  
nschwarz@aps.anl.gov

The RSMa3D software package was developed, and is supported and maintained by the XSD Scientific Software Engineering & Data Management Group in collaboration with Jonathan Tischler (XSD-SSM) with funding from the U.S. Department of Energy Office of Science under Contract No. DE-AC02-06CH11357.



## TYPICAL APS MACHINE PARAMETERS

### LINAC

Output energy	375 MeV
Maximum energy	500 MeV
Output beam charge	0.3–3 nC
Normalized emittance	5–20 mm-mrad
Frequency	2.856 GHz
Modulator pulse rep rate	30 Hz
Gun rep rate (1–6 pulses, 33.3 ms apart every 0.5 s)	2–12 Hz
Beam pulse length	8–15 ns
Bunch length	1–10 ps FWHM

### PARTICLE ACCUMULATOR RING

Nominal energy	375 MeV
Maximum energy	450 MeV
Circumference	30.66 m
Cycle time	500 ms or 1000 ms
Fundamental radio frequency (RF1)	9.77 MHz
12th harmonic RF frequency (RF12)	117.3 MHz
RMS bunch length (after compression)	0.34 ns

### INJECTOR SYNCHROTRON (BOOSTER)

Nominal extraction energy	7.0 GeV
Injection energy	375 MeV
Circumference	368.0 m
Lattice structure	10 FODO cells/ quadrant
Ramping rep rate	2 Hz or 1 Hz
Natural emittance	69 nm-rad (actual) 92 nm-rad (nominal)
Radio frequency	351.930 MHz

### STORAGE RING SYSTEM

Nominal energy	7.0 GeV
Circumference	1104 m
Number of sectors	40
Length available for insertion device	5.0 m
Nominal circulating current, multibunch	100 mA
Natural emittance	2.5 nm-rad
RMS momentum spread	0.096%
Effective emittance	3.1 nm-rad
Vertical emittance	0.040 nm-rad
Coupling (operating)	1.5%
Revolution frequency	271.555 kHz
Radio frequency	351.935 MHz
Operating number of bunches	24 to 324
RMS bunch lengths	33 ps to 25 ps
RMS bunch length of 16 mA in hybrid mode	50 ps

## APS SOURCE PARAMETERS

### UNDULATOR A (29 INSERTION DEVICES [IDs])

Period: 3.30 cm  
 Length: 2.1 m in sectors 16, 21, 23, 24, 34; 2.3 m in Sector 6;  
 2.4 m in others  
 Minimum gap: 10.5 mm  
 $B_{\max}/K_{\max}$ : 0.892 T/2.75 (effective; at minimum gap)  
 Tuning range: 3.0–13.0 keV (1st harmonic)  
 3.0–45.0 keV (1st–5th harmonic)  
 On-axis brilliance at 7 keV (ph/s/mrad<sup>2</sup>/mm<sup>2</sup>/0.1%bw):  
 4.1 x 10<sup>19</sup> (2.4 m), 4.0 x 10<sup>19</sup> (2.3 m), 3.3 x 10<sup>19</sup> (2.1 m)  
 Source size and divergence at 8 keV:  
 $\Sigma_x$ : 276  $\mu$ m  $\Sigma_y$ : 11  $\mu$ m  
 $\Sigma_x$ : 12.7  $\mu$ rad (2.4 m), 12.8  $\mu$ rad (2.3 m), 12.9  $\mu$ rad (2.1 m)  
 $\Sigma_y$ : 6.7  $\mu$ rad (2.4 m), 6.8  $\mu$ rad (2.3 m), 7.1  $\mu$ rad (2.1 m)

### 2.30-CM UNDULATOR (2 IDs IN SECTORS 11, 14)

Period: 2.30 cm Length: 2.4 m  
 Minimum gap: 10.5 mm  
 $B_{\max}/K_{\max}$ : 0.558 T/1.20 (effective; at minimum gap)  
 Tuning range: 11.8–20.0 keV (1st harmonic)  
 11.8–70.0 keV (1st–5th harmonic, non-contiguous)  
 On-axis brilliance at 12 keV (ph/s/mrad<sup>2</sup>/mm<sup>2</sup>/0.1%bw): 6.9 x 10<sup>19</sup>  
 Source size and divergence at 12 keV:  
 $\Sigma_x$ : 276  $\mu$ m  $\Sigma_y$ : 11  $\mu$ m  
 $\Sigma_x$ : 12.3  $\mu$ rad  $\Sigma_y$ : 5.9  $\mu$ rad

### 2.70-CM UNDULATOR (5 IDs IN SECTORS 3, 12, 14, 35)

Period: 2.70 cm  
 Length: 2.1 m in Sector 12; 2.4 m in sectors 3, 14, and 35  
 Minimum gap: 10.5 mm  
 $B_{\max}/K_{\max}$ : 0.698 T/1.76 (effective; at minimum gap)  
 Tuning range: 6.7–16.0 keV (1st harmonic)  
 6.7–60.0 keV (1st–5th harmonic, non-contiguous)  
 On-axis brilliance at 8.5 keV (ph/s/mrad<sup>2</sup>/mm<sup>2</sup>/0.1%bw):  
 5.7 x 10<sup>19</sup> (2.4 m), 4.7 x 10<sup>19</sup> (2.1 m)  
 Source size and divergence at 8 keV:  
 $\Sigma_x$ : 276  $\mu$ m  $\Sigma_y$ : 11  $\mu$ m  
 $\Sigma_x$ : 12.7  $\mu$ rad (2.4 m), 12.9  $\mu$ rad (2.1 m)  
 $\Sigma_y$ : 6.7  $\mu$ rad (2.4 m), 7.1  $\mu$ rad (2.1 m)

### 3.00-CM UNDULATOR (9 IDs IN SECTORS 12, 13, 16, 21, 23, 27, 34, 35)

Period: 3.00 cm  
 Length: 2.1 m in sectors 12, 13, 16, 21, 23, 34; 2.4 m in sectors 27 and 35  
 Minimum gap: 10.5 mm  
 $B_{\max}/K_{\max}$ : 0.787 T/2.20 (effective; at minimum gap)  
 Tuning range: 4.6–14.5 keV (1st harmonic)  
 4.6–50.0 keV (1st–5th harmonic)  
 On-axis brilliance at 8 keV (ph/s/mrad<sup>2</sup>/mm<sup>2</sup>/0.1%bw):  
 4.8 x 10<sup>19</sup> (2.4 m), 3.9 x 10<sup>19</sup> (2.1 m)  
 Source size and divergence at 8 keV:  
 $\Sigma_x$ : 276  $\mu$ m  $\Sigma_y$ : 11  $\mu$ m  
 $\Sigma_x$ : 12.7  $\mu$ rad (2.4 m), 12.9  $\mu$ rad (2.1 m)  
 $\Sigma_y$ : 6.7  $\mu$ rad (2.4 m), 7.1  $\mu$ rad (2.1 m)

### 3.50-CM SMCo UNDULATOR (SECTOR 4)

Period: 3.50 cm Length: 2.4 m  
 Minimum gap: 9.75 mm  
 $B_{\max}/K_{\max}$ : 0.918 T/3.00 (effective; at minimum gap)  
 Tuning range: 2.4–12.5 keV (1st harmonic)  
 2.4–42.0 keV (1st–5th harmonic)  
 On-axis brilliance at 7 keV (ph/s/mrad<sup>2</sup>/mm<sup>2</sup>/0.1%bw): 3.7 x 10<sup>19</sup>  
 Source size and divergence at 8 keV:  
 $\Sigma_x$ : 276  $\mu$ m  $\Sigma_y$ : 11  $\mu$ m  
 $\Sigma_x$ : 12.7  $\mu$ rad  $\Sigma_y$ : 6.7  $\mu$ rad

### 3.60-CM UNDULATOR (SECTOR 13)

Period: 3.60 cm

Length: 2.1 m

Minimum gap: 11.0 mm

$B_{\max}/K_{\max}$ : 0.936 T/3.15 (effective; at minimum gap)

Tuning range: 2.2–11.8 keV (1st harmonic)

2.2–40.0 keV (1st–5th harmonic)

On-axis brilliance at 6.5 keV (ph/s/mrad<sup>2</sup>/mm<sup>2</sup>/0.1%bw):  $2.8 \times 10^{19}$

Source size and divergence at 8 keV:

$\Sigma_x$ : 276  $\mu\text{m}$      $\Sigma_y$ : 11  $\mu\text{m}$

$\Sigma_x$ : 12.9  $\mu\text{rad}$      $\Sigma_y$ : 7.1  $\mu\text{rad}$

### 1.72-CM UNDULATOR (SECTOR 30)

Period: 1.72 cm

Length: 4.8 m (2 x 2.4 m)

Minimum gap: 10.6 mm

$B_{\max}/K_{\max}$ : 0.330 T/0.53 (effective; at minimum gap)

Tuning range: 23.7–26.3 keV (1st harmonic)

On-axis brilliance at 23.7 keV (ph/s/mrad<sup>2</sup>/mm<sup>2</sup>/0.1%bw):  $1.0 \times 10^{20}$

Source size and divergence at 23.7 keV:

$\Sigma_x$ : 276  $\mu\text{m}$      $\Sigma_y$ : 11  $\mu\text{m}$

$\Sigma_x$ : 11.6  $\mu\text{rad}$      $\Sigma_y$ : 4.3  $\mu\text{rad}$

### 1.80-CM UNDULATOR (SECTOR 32)

Period: 1.80 cm

Length: 2.4 m

Minimum gap: 11.0 mm

$B_{\max}/K_{\max}$ : 0.244 T/0.41 (effective; at minimum gap)

Tuning range: 23.8 - 25.3 keV (1st harmonic)

71.4 - 75.9 keV (3rd harmonic)

On-axis brilliance at 23.8 keV (ph/s/mrad<sup>2</sup>/mm<sup>2</sup>/0.1%bw):  $2.8 \times 10^{19}$

Source size and divergence at 23.8 keV:

$\Sigma_x$ : 276  $\mu\text{m}$      $\Sigma_y$ : 11  $\mu\text{m}$

$\Sigma_x$ : 11.9  $\mu\text{rad}$      $\Sigma_y$ : 4.9  $\mu\text{rad}$

### IEX 12.5-CM QUASI-PERIODIC POLARIZING UNDULATOR (SECTOR 29)

Period: 12.5 cm

Length: 4.8 m

*Circular polarization mode:*

Max. currents: horizontal coils 34.4 A, vertical coils 20.7 A

$K_{\max}$ : 2.73 (effective; at max. currents)

$B_{\max}$ : 0.27 T (peak; at max. currents)

Tuning range: 0.44–3.5 keV (1st harmonic)

On-axis brilliance at 1.8 keV (ph/s/mrad<sup>2</sup>/mm<sup>2</sup>/0.1%bw):  $1.4 \times 10^{19}$

*Linear horizontal polarization mode:*

Max. current: vertical coils 47.6 A

$K_{\max}$ : 5.39 (effective; at max. current)

$B_{\max}$ : 0.54 T (peak; at max. current)

Tuning range: 0.24–3.5 keV (1st harmonic)

0.24–11.0 keV (1st–5th harmonic)

On-axis brilliance at 2.1 keV (ph/s/mrad<sup>2</sup>/mm<sup>2</sup>/0.1%bw):  $1.1 \times 10^{19}$

*Linear vertical polarization mode:*

Max. current: horizontal coils 50.3 A

$K_{\max}$ : 3.86 (effective; at max. current)

$B_{\max}$ : 0.37 T (peak; at max. current)

Tuning range: 0.44–3.5 keV (1st harmonic)

0.44–11.0 keV (1st–5th harmonic)

On-axis brilliance at 2.1 keV (ph/s/mrad<sup>2</sup>/mm<sup>2</sup>/0.1%bw):  $1.1 \times 10^{19}$

Fast polarization switching not required

Source size and divergence at 2 keV:

$\Sigma_x$ : 276  $\mu\text{m}$      $\Sigma_y$ : 13  $\mu\text{m}$

$\Sigma_x$ : 13.9  $\mu\text{rad}$      $\Sigma_y$ : 8.8  $\mu\text{rad}$

### 12.8-CM CIRCULARLY POLARIZING UNDULATOR (SECTOR 4)

Period: 12.8 cm

Length: 2.1 m

*Circular polarization mode:*

Max. currents: horizontal coils 1.34 kA, vertical coils 0.40 kA

$K_{\max}$ : 2.85 (effective; at max. currents)

$B_{\max}$ : 0.30 T (peak; at max. currents)

Tuning range: 0.4–3.0 keV (1st harmonic)

On-axis brilliance at 1.8 keV (ph/s/mrad<sup>2</sup>/mm<sup>2</sup>/0.1%bw):  $3.1 \times 10^{18}$

*Linear horizontal polarization mode:*

Max. current: vertical coils 0.40 kA

$K_{\max}$ : 2.85 (effective; at max. current)

$B_{\max}$ : 0.30 T (peak; at max. current)

Tuning range: 0.72–3.0 keV (1st harmonic)

0.72–10.0 keV (1st–5th harmonic)

On-axis brilliance at 2.1 keV (ph/s/mrad<sup>2</sup>/mm<sup>2</sup>/0.1%bw):  $2.3 \times 10^{18}$

*Linear vertical polarization mode:*

Max. current: horizontal coils 1.60 kA

$K_{\max}$ : 3.23 (effective; at max. current)

$B_{\max}$ : 0.34 T (peak; at max. current)

Tuning range: 0.58–3.0 keV (1st harmonic)

0.58–10.0 keV (1st–5th harmonic)

On-axis brilliance at 2.1 keV (ph/s/mrad<sup>2</sup>/mm<sup>2</sup>/0.1%bw):  $2.3 \times 10^{18}$

Switching frequency (limited by storage ring operation): 0–0.5 Hz

Switching rise time: 50 ms

Source size and divergence at 2 keV:

$\Sigma_x$ : 276  $\mu\text{m}$      $\Sigma_y$ : 12  $\mu\text{m}$

$\Sigma_x$ : 16.7  $\mu\text{rad}$      $\Sigma_y$ : 12.7  $\mu\text{rad}$

### 1.80-CM SUPERCONDUCTING UNDULATOR (2 IDs IN SECTORS 1, 6)

Period: 1.80 cm

Length: 1.1 m

Gap: 9.5 mm (fixed)

Max. current: 450 A

$B_{\max}/K_{\max}$ : 0.962/1.61 (effective; at maximum current)

Tuning range: 11.2–24.7 keV (1st harmonic)

11.2–150.0 keV (1st–13th harmonic, non-contiguous)

On-axis brilliance at 13 keV (ph/s/mrad<sup>2</sup>/mm<sup>2</sup>/0.1%bw):  $3.2 \times 10^{19}$

Source size and divergence at 13keV:

$\Sigma_x$ : 276  $\mu\text{m}$      $\Sigma_y$ : 11  $\mu\text{m}$

$\Sigma_x$ : 13.2  $\mu\text{rad}$      $\Sigma_y$ : 7.5  $\mu\text{rad}$

### APS BENDING MAGNET

Critical energy: 19.51 keV

Energy range: 1–100 keV

On-axis brilliance at 16 keV (ph/s/mrad<sup>2</sup>/mm<sup>2</sup>/0.1%bw):  $5.4 \times 10^{15}$

On-axis angular flux density at 16 keV (ph/s/mrad<sup>2</sup>/0.1%bw):  $9.6 \times 10^{13}$

Horizontal angular flux density at 6 keV (ph/s/mradh/0.1%bw):  $1.6 \times 10^{13}$

Source size and divergence at the critical energy:

$\Sigma_x$ : 92  $\mu\text{m}$      $\Sigma_y$ : 31  $\mu\text{m}$

$\Sigma_x$ : 6  $\mu\text{rad}$      $\Sigma_y$ : 47  $\mu\text{rad}$

# ACKNOWLEDGMENTS

## **APS Science 2016 Editorial Board:**

Mark A. Beno (ANL-XSD), John P. Connolly (ANL-AES), Robert Fischetti (ANL-XSD), Jonathan C. Lang (ANL-XSD), Dennis M. Mills, (ANL-PSC), George Srajer (ANL-PSC), Stephen K. Streiffer (ANL-PSC), Stefan Vogt (ANL-XSD), Alexander A. (Sasha) Zholents (ANL-ASD)

## **Unless otherwise noted, the research highlights in this report were written by:**

Mary Alexandra Agner (marymary@gmail.com)  
William Arthur Atkins (waarc@grics.net)  
Christen Brownlee (christenbrownlee@gmail.com)  
Erika Gebel Berg (erikagebel@gmail.com)  
David Bradley (david@sciencebase.com)  
Vic Comello (ANL-CEP, vcomello@anl.gov)  
Dana Desonie (desonie@cox.net)  
Sandy Field (sfield@fieldscientific.com)  
Joseph E. Harmon (harmon@anl.gov)  
Jenny Morber (jenny.morber.business@gmail.com)  
Emma Nichols (emma@nascentmc.com)  
Philip Koth (philkothe@comcast.net)  
Kim Krieger (mskrieger@gmail.com)  
David Lindley (dxlindley@gmail.com)  
Tien Nguyen (tmnguyen5@gmail.com)  
Chris Palmer (crpalmer2009@gmail.com)  
Nicola Parry (nicola@parrymedicalwriting.com)  
Neil Savage (neil@stefan.com)  
Michael Schirber (mschirber@gmail.com)  
Mark Wolverton (exetermw@earthlink.net)

**Photography:** Wes P. Agresta, Mark L. Lopez (both ANL-CEP)

**Aerial photograph of the APS:** John Hill (Tigerhill Studio, <http://www.tigerhillstudio.com>)

**Publications, contracts, rights and permissions, circulation:** Jessie L. Skwarek (ANL-PSC)

**Printing oversight:** Gary R. Weidner (ANL-CEP)

**CD production:** Lorenza M. Salinas and Janet Barrett (both ANL-CEP)

**Editorial, project coordination, design, photography:** Richard B. Fenner (ANL-PSC)

Our thanks to the corresponding authors and others who assisted in the preparation of the research highlights, to the users and APS personnel who wrote articles for the report, and our apologies to anyone inadvertently left off this list. To all: your contributions are appreciated.

Panorama of the APS particle accumulator ring. Left to right in the photo are Aaron Lopez, Guy Harris, and Debra Curry (all AES).